Haase, Frerk

The investigation and design of a piezoelectric active vibration control system for vertical machining centres

The Investigation and Design of a Piezoelectric Active Vibration Control System for Vertical Machining Centres

A thesis submitted to the University of Huddersfield in partial fulfilment of the requirements for the degree of Doctor of Philosophy

By
Frerk Haase

School of Computing and Engineering
The University of Huddersfield

July 2005

University of
HUDDERSFIELD

Abstract

The presented thesis documents the successful investigation and design, of a novel active vibration control system for milling machines. To the authors knowledge this has never been tried before on conventional milling machines. It is important to realize that most work on machine tool vibration control is based on process control, which is optimizing the parameters of the machining process, such as spindle speed and feederate. Compared to active vibration control, which changes the structural dynamics actively through the energy supplied by the actuators, it does not increase the Maximum Metal Removal Rate (MMRR) of the machine. Examples of active vibration control systems on machine tools are very rare and usually done on simpler single cutting operations such as boring.

The developed system was able to demonstrate that active vibration control reduces the vibration level of an intermittent time varying, non-linear, cutting process and improve the surface finish. Furthermore the system demonstrated that the unstable cutting process (chatter or self-excited vibrations), which reduces the MMRR on machine tools, could be stabilized. Improvements in the vibration level by about 23dB (92.9%) and 24.5dB (93.9%) at the main structural resonance frequencies of 339Hz and 1024Hz have been achieved. As a result the surface finish has been improved significantly. The vibration control system is universal and can be easily implemented onto a variety of vertical machining centers.

Different control methods have been explored, by simulation and evaluation on a simple test rig. The time invariant nature of machine tool structures led to a deeper investigation of adaptive control algorithms. It was found that compared to the continuous methods, discrete adaptive filters are ideal for this application, since they are able to track and adjust in real time to the change in machine tool dynamics.

This prototype system leaves much potential for further work. The presented work has already attracted the attention of the machine tool industry and it is planned to develop an industrial version of an active control system, which is going to be integrated into the spindle head of a conventional machining center.

Acknowledgements

First of all I would like to thank my supervisors Dr. Stephen Lockwood and Professor Derek Ford, who both have made this project possible. I also wish to thank, without naming anyone in particular, the whole Ultra-Precision Engineering Centre (UPEC) at the University of Huddersfield, from the research fellows to the technicians. Their help and support, which always gave me a lot of encouragement, has motivated me to finish the presented work successfully. Further, I would like to give thanks to the EPSRC and collaborating companies of the CAPM- and STRUCTURES/REDUCE projects, of which this work was part.

Finally I would like to give special thanks to my parents Ursula and Reiner Haase and my sister Deike Haase, for their years of support and encouragement.

Content

List of figures

Chapter 1

Chapter 2

Chapter 3

Chapter 4

Chapter 6

Chapter 7

Chapter 8

List of tables

List of equations

Chapter 1

Chapter 2

Chapter 3

Chapter 6

Chapter 7

List of abbreviations and symbols

MMRR	Maximum Metal Removal Rate
a_r	Radial depth of cut (width of cut)
b	Axial depth of cut
c	Chip load
m	Number of teeth on the cutter
n	Spindle speed
b_{limit}	The maximum stable axial depth of cut
K_s	The specific cutting force per unit chip area (specific power) of a material. (Sometimes simply called static cutting stiffness)
$G(f)$	Transfer-function between tool and workpiece
$Re[(G(f)]$	Real part of a transfer-function
$Im[(G(f)]$	Imaginary part of a transfer-function
f	Frequency
$f_{chatter}$	Chatter frequency
f_{tooth}	Tooth pass frequency
ε	Phase shift between the vibrations of a tooth and the wavy surface left by the previous tooth
e	Amount of eccentricity between the spindle axis and the centre line of the workpiece
N	The number of entire waves between two succeeding teeth of the cutter
FRF	Frequency Response Function
FFT	Fast Fourier Transform
FIR filter	Finite Impulse Response filter
IIR filter	Infinite Impulse Response filter
LMS	Least Mean Square algorithm

DSP	Digital Signal Processing
ϕ	Shear plane angle
α	Tool rake angle
β	Wedge angle of the tool
γ	Clearance angle
h_0	Uncut chip thickness
h_{cut}	Chip thickness
F_t	Tangential cutting force vector
F_f	Feed or thrust force vector
F_r	Radial cutting force vector
BUE	Build-up edge
SCEA (σ)	Side cutting edge angle
v	Cutting speed
f	In this contend it is the feedrate of a machine tool
f_r	Feed per tooth (milling) or feed per revolution (turning)
D_w	Workpiece diameter
D_c	Diameter of the cutter
A	Chip area
a_a	Axial depth of cut
b_{cum}	Cumulative chip width for all the teeth cutting simultaneously
m_{cum}	Number of inserts inside the cut
MRR_m	Mean Metal Removal Rate
P_m	Mean Power of the spindle motor
$h(t)$	Instantaneous chip thickness
T	Time period
$F(t)$	Instantaneous cutting force
SDOF	Single degree of freedom system
MDOF	Multi degree of freedom system
$y(t)$	Instantaneous motion (vibration or output of a SDOF system – equation of motion)
$x(t)$	Displacement (input of a SDOF system)

k	Stiffness (spring constant)
c	Damping coefficient
m	mass
ω	Angular frequency
ω_n	undamped natural frequency (angular)
ζ	faction of critical damping
OTF	Orientated Transfer Function
F(s)	LAPLACE transform of f(t)
k_m	Static stiffness of the structure
k_c	Cutting stiffness
LVDT	Linear variable displacement transducer
LTI	Linear time invariant system
x(n)	Input sample of a digital system
y(n)	Output sample of a digital system
$a_0 ... a_n$	Weight coefficients of a digital filter (numerator)
$b_0 ... b_m$	Weight coefficients of a digital filter (denominator)
F(z)	Z-transform of f(t)
H(z)	A digital system in the z-domain (digital filter)
MA	Moving average filter
ARMA	Autoregressive moving average filter
RLS	Recursive Least Square algorithm
MSE	Minimum squared error criterion
E[]	Expectation operator
μ	Adaptation coefficient
ADC	Analogue to Digital converter
DAC	Digital to Analogue converter
FXLMS	Filtered-x LMS algorithm
IMC	Internal Model Control
MEMS	Micro-Electro-Mechanical Systems
IC	Integrated Circuits
CMOS	Complementary metal oxide semiconductor
M	Generally the Torque of a motor

c	In this contend the machine constant of a electrical motor
Φ	Magnetic flux
I_A	Armature current
DC	Direct current
AC	Alternating current
ODS	Operational deflection shape
FEM	Finite Element Method
m	In this contend the modulation index
f_{cs}	Frequency of the carrier signal
f_{ms}	Frequency of the modulated signal
E_{cs}	Peak amplitude of the carrier signal
E_{ms}	Peak amplitude of the modulated signal
CPU	Central Processing Unit
ISA bus	Industry Standard Architecture bus
PCI bus	Peripheral Component Interconnect bus
DOS	Microsoft DOS (disk operating system)
I/O	Input-Output
TTL	Transistor-transistor logic
FORTRAN	Formula Translator (high level programming language)
C	High level Programming language
MATLAB	Commercial mathematic software from MathWorks
MATLAB/SIMULINK	Toolbox of MATLAB
NCDT	Non contact displacement transducer
PID	Proportional Integral Derivative controller
EMI	Electromagnetic Interference
CNC	Computerized Numerical Control
PZT	Lead titanium-zirconate
HVPZT	High voltage PZT
f_0	Resonance frequency
F	Force

n	In this contend the number of PZT layers
d_{33}	Piezoelectric coefficient for stacked design
U	Applied voltage
ΔL	Remaining elongation of the PZT stack actuator
ΔL_0	Nominal displacement of the PZT with no external spring
ΔL_R	Lost displacement cause by the external spring load
$F_{pre\text{-}load}$	Preload force
F_T	Force acting on the actuator
F_S	Force acting on the external spring
k_S	Spring stiffness
k_T	PZT actuator stiffness
$k_{T\,new}$	New pre-loaded actuator stiffness
m_{eff}	Effective mass (about 1/3 of the PZT mass)
M	In this contend the added mass to the PZT actuator
ANEF	American National Extra Fine Standard for threads
HRC 57	Rockwell hardness C57
k_{PZT}	Stiffness of the PZT actuator
k_{DS}	Stiffness of the disc spring
k_{GS}	Stiffness of the guide system
k_{CB}	Stiffness of a single flexure (cantilever bridge)
PF	Pre-load factor of the PZT actuator
F_{stat}	Static cutting force
F_{dyn}	Dynamic cutting force
σ_b	Stress level (due to bending)
ε	Strain of a material
E	Young's modulus
I_{xx}	Second moment of inertia (axial direction of X)
W_b	Second modulus (due to bending)
τ_q	Shearing stress

F_q	Shear forces
S	In the contend of fatigue stress analysis it is a safety factor, which can be found in handbooks
K	In the contend of fatigue stress analysis it is a material and form factor, which can be found in handbooks
R	In the contend of fatigue stress analysis it is the tensile strength of a material
ST37	DIN definition for mild steel ($R=37N/mm^2$)
ICP sensor	Integrated circuit piezoelectric
RH	Relative Humidity
BNC connector	Standard connector for coaxial cables (Bayonet Neill-Concelman)
EPSRC	Engineering and Physical Science Research Council (UK agency for research funding)

Chapter 1

Introduction

1.1 Background and motivation

In today's modern manufacturing industry there always has been an increasing demand concerning the accuracy and productivity of a highly automated manufacturing environment.

The ultimate goal is to produce accurate components, which satisfy the customer level of tolerance with the minimum amount of resources.

Some advantages of producing accurate components are:

- Greater accuracy of each component often increases the performance of the assembled part (e.g. car engines).
- Greater accuracy of each component often accelerates assembly time.
- Greater interchangeability.
- Reduction of scrap rates.

The invention of numerical control in the early 1960's and later, computer numerical control has improved the productivity and consistency of accurate parts that a manually controlled machine would find difficult to achieve. This has reduced, the possibilities for human error in the machining process, but the limitation, in terms of accuracy of each machine tool still remains. The optimisation of the machine tool performance using advanced control strategies has therefore become the motivation of many researchers [1].

The improvement of machine tool accuracy is the aim for the Ultra-Precision Engineering Centre (UPEC) at the University of Huddersfield. This group led by Professor Ford has had much success by improving the geometric and thermal [2] machine tool accuracy. The correction systems can be retrofitted to any already installed machine and update to the machine capabilities.

The purpose of this research is to follow the strategy of the group by developing and designing a general-purpose vibration compensation system, which can be fitted to any existing conventional milling machine in order to improve its dynamic performance.

It is well known that vibration problems on machine tools are related to the dynamic stiffness of the machine structure. It therefore has a significant impact on the tool life, surface finish and productivity. To avoid this, an experienced machine tool operator will try to change the cutting parameters or the work-piece clamping. In the past many researchers have used the cutting parameters such as spindle speed, feedrate and the depth of cut as variables for their vibration control systems. Active control of machine tool vibration is a relatively new and totally different solution to this problem. It is becoming popular and very promising results have already been reported on turning operations [3]. Secondary vibrations are introduced by an actuator system near the cutting process, which can reduce the amplitude of the primary vibrations (forced or self-excited). To achieve this, the control strategy must model the machine tool structures adaptively in the digital domain in order to control machine tool vibrations. The advantage is that the stiffness and damping of the most important part of the machine tool structure, the tool/work-piece interface, can be changed actively during operation. It is therefore not just a passive method of optimising the machine tool structure, but more a method of changing its mechanical properties (e.g. stiffness) actively depending on the output of the adaptive controller without redesigning the machine.

1.2 Inaccuracies of the machine tool structure

The precision of a machine tool is affected by the positioning accuracy of the cutting tool with respect to the work-piece. There are 3 major sources of machine tool errors, that affect the accuracy of machine tools and which will directly relate to the machined component:

- Geometric or rigid body errors, caused by the geometric inaccuracies of the machine itself
- Non-rigid body errors (load errors)
- Thermal errors

However machine tool accuracy is just one of several inputs affecting the workpiece accuracy, which need to be controlled in order to achieve the ultimate goal [4].
Figure 1.1 shows the various factors, which influence the work-piece accuracy.

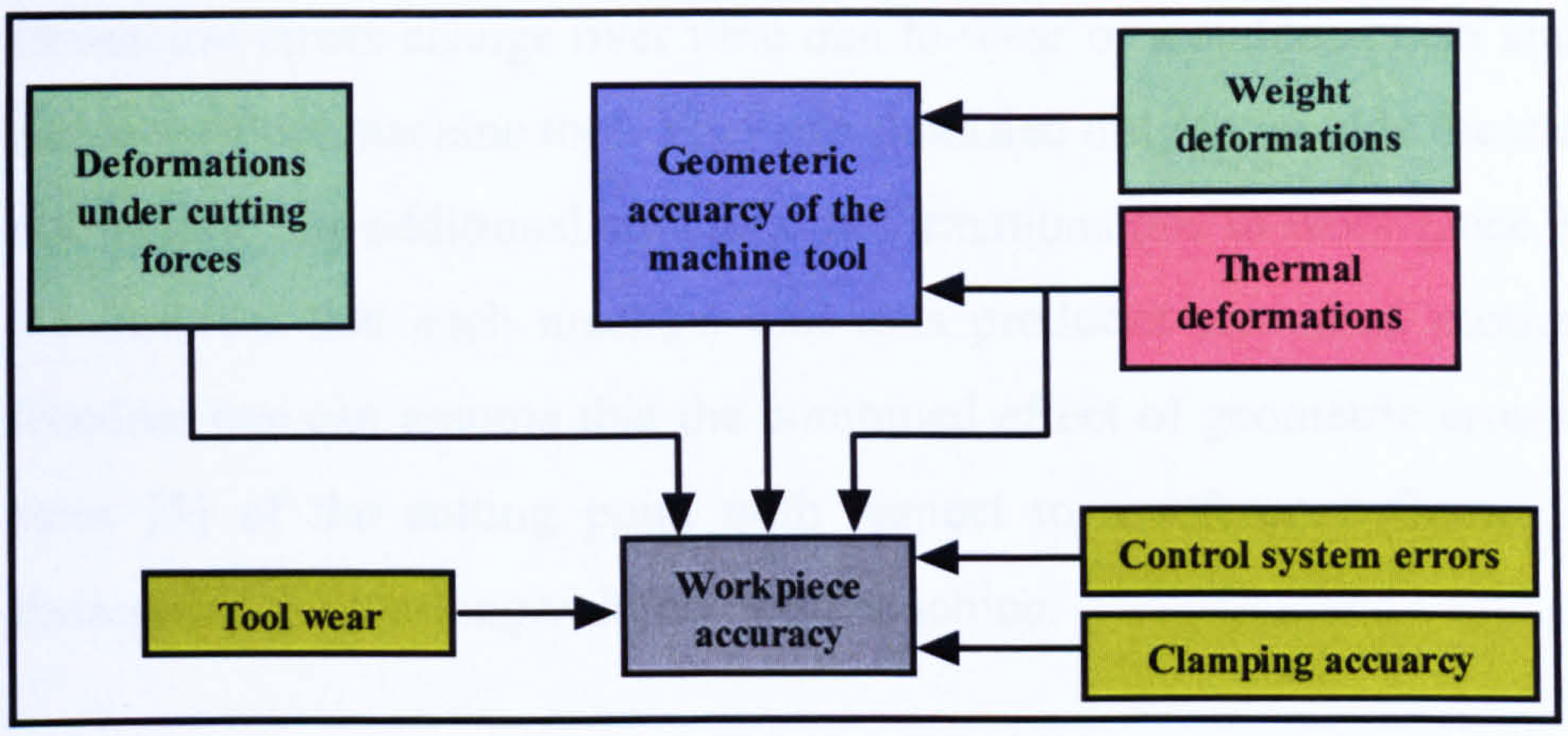

Figure 1.1: Factors influencing the accuracy of the work-piece

1.2.1 Geometric inaccuracies

The concept of geometric accuracy was historically established in the 1930's, when Professor Schlesinger in Berlin undertook tests in accuracy specifications for machine tool acceptance on the manufacturers and customers behalf [4]. He established a system to define the geometric accuracy of machine tool structures. His tests have been adapted as the basis of many national and international standards. They are non-machining tests designed to isolate the accuracy of machining motions.

Geometrical errors result from imperfections of the machine tool structure due to misalignments of individual machine tool parts. It is for example impossible, to produce a mechanically perfect slide. When the slide with its rigid body (cutting tool or work-piece) is moving along the axis it will produce small, unwanted motions in all six possible degrees of freedom. The small unwanted motions are the geometric errors of a machine tool and are inherent in its production. Geometric errors for a single linear axis are known as linear positioning error, horizontal and vertical straightness error, and roll, pitch and yaw errors (Figure 1.2).

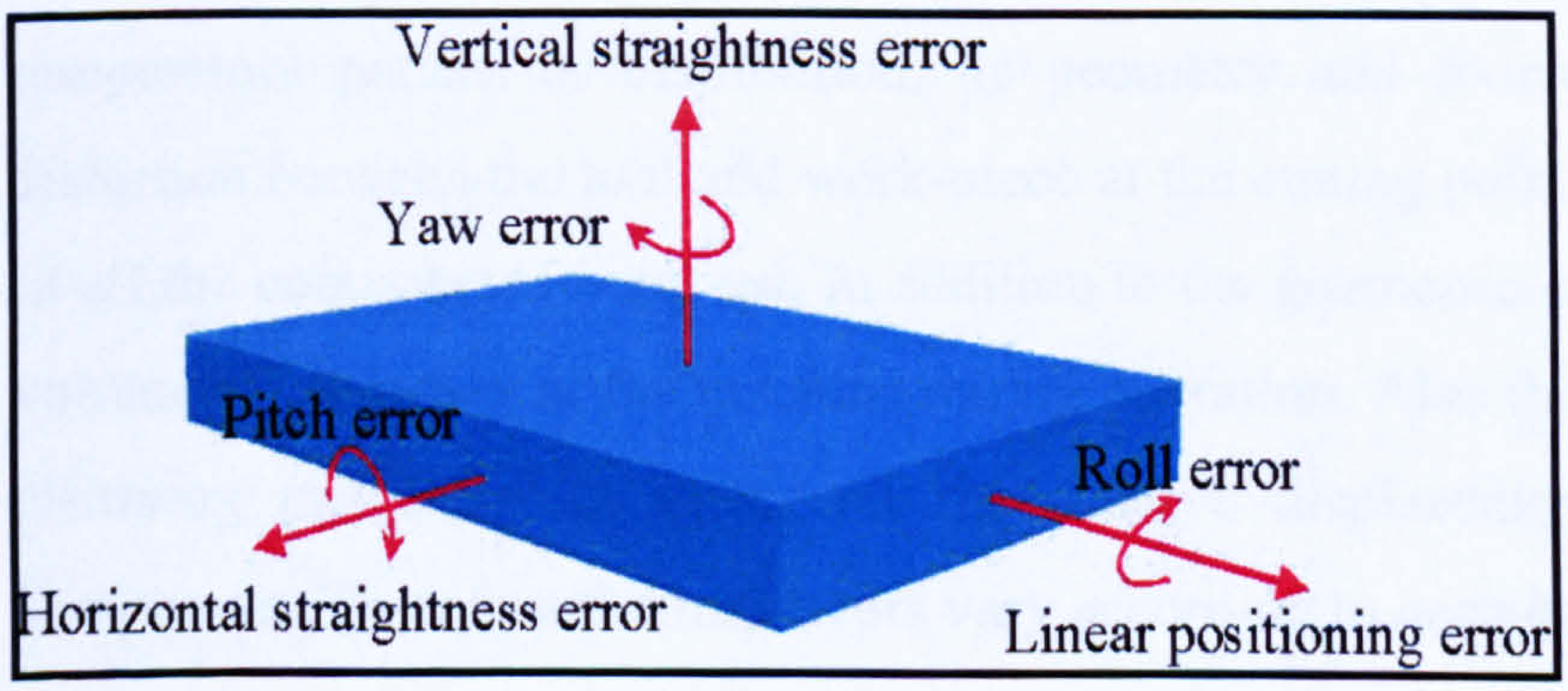

Figure 1.2: The geometric errors of a single linear axis

Geometric errors change over time due to wear or a sudden crash and depend on the quality and size of the machine tool. They are classified only to include the machine tool itself and do not include any additional structural deformations due to work-piece mass or cutting loads. If we consider that each machine tool axis produces unwanted motion in all six degrees of freedom one can assume that the combined effect of geometric errors results in a volumetric error [5] of the cutting point with respect to a reference frame. This error will change throughout the working volume of the machine.

1.2.2 Thermal errors

There are a number of heat sources present, when a machine tool operates in a general workshop environment. They cause changes in the temperature distribution (isothermal lines i.e. lines with the same temperature potential), within the machine tool structure and machine components depending on loading and time.

Heat sources can be classified into two groups [6]:

-Internal heat sources

-External heat sources

The heat sources, cause thermo-elastic deflections of the machine tool structure and result in geometric inaccuracies. The effect of the various heat sources on the machine tool and work-piece accuracy differ. The shop floor temperature variation, radiation caused by the sun or heating of neighbouring machines are examples for external heat sources. The energy dissipation in bearings, motors, gear boxes, guide-ways, drive system, hydraulic system and the cutting process, are heat sources generated by the machine itself and defined as internal. The effect of these heat sources on the machine or machine part deformations is determined by its design, the material properties (temperature gradient) and heat transfer mechanism. The thermal deformations that the machine tool structure and work-piece undergo, depend on the temperature pattern or distribution, its geometry and fixing or clamping conditions. The distortion between the tool and work-piece at the cutting point are the sum of the deformation of all the components involved. In addition to the geometric errors, thermal errors change the volumetric accuracy of the machine during operation. Also the deformation of the work-piece clamping can have an effect on the relative displacement between tool and machine component. Therefore thermal errors vary according to each operation of the machine tool.

1.2.3 Load errors

Loads or forces during machining operations result in deformations, which disturb the accuracy of machining. These forces may be due to the weight of the moving parts in the machine, which affect its geometric accuracy. More significant however, are forces due to the cutting process.

In general load errors can be divided into 5 classes:

- Deformation caused by weight forces
- Deformations caused by cutting forces
- Random vibrations
- Forced Vibrations
- Self-excited vibrations

1.2.3.1 Deformations caused by weight forces

Moving masses such as the travelling headstock and table affect the positional error between tool and work-piece. The moving masses are constantly changing the form of the structure and the machine must be designed so as to minimise these effects. Such structural deformations have such a large time constant that they are normally assumed to be static. Or to illustrate this differently, the force-displacement function (Force = f (displacement)), whether it is linear or non-linear, slowly changes its point of operation, so that it does not produce dynamic effects (i.e. resonances).

Ford et al [7], identified sources of non-rigid errors in particular for moving slides and work-piece weight and their effect on the machine tool accuracy on a wide range of machines.

1.2.3.2 Deformation caused by cutting forces

The cutting forces deform the machine tool structure, which in turn, results in geometric errors between the tool and workpiece.

Furthermore as the cutting tool travels along a tool path, the magnitude and direction of the cutting force, at the point of contact may vary and the resulting deformations of the frame will change, causing deviations of the form of the machined surface. These deviations from the desired dimensions of the workpiece are called “dimensional form errors”.

The deformation X depends on the cutting force F and on the stiffness k between tool and workpiece:

$$X = \frac{F}{k}$$

Eq. 1.1: The deflection between tool and workpiece

Also, the stiffness is a variable during cutting operations and will change depending on the position of the tool and machine tool geometry. In an end milling process for example, the tool can be considered as the most flexible part in the machine tool system, since the ratio of diameter over the tool length is very small. This kind of structure can be considered as an elastic cylindrical beam, cantilevered to the spindle. In practice the cutting force varies during the cut and therefore the deformation between tool and work-piece also varies. This form error caused by the flexibility of the end mill transfers onto the machined surface. To avoid form errors the cutting process is terminated with a final "light cut". This results in an more accurate work-piece, because the cutting forces are low minimising the cutter deformation.

1.2.3.3 Structural vibrations in machining

Machine tool vibration plays an important role in precision machining, because it is a function of speed, feed and depth of the cut (cutting parameters), which have to be controlled in order to achieve acceptable vibration levels. Excessive vibration accelerates tool wear, causes poor surface finish and may damage the cutter or spindle bearings.

Machine tool structures are multi-degree-of-freedom systems that can not easily be described mathematically [8] and therefore, experimental modal analysis, (structural testing) is often used to identify the transfer-functions of existing systems.

There are 3 main types of mechanical vibrations in machine tools, (see figure 1.3):

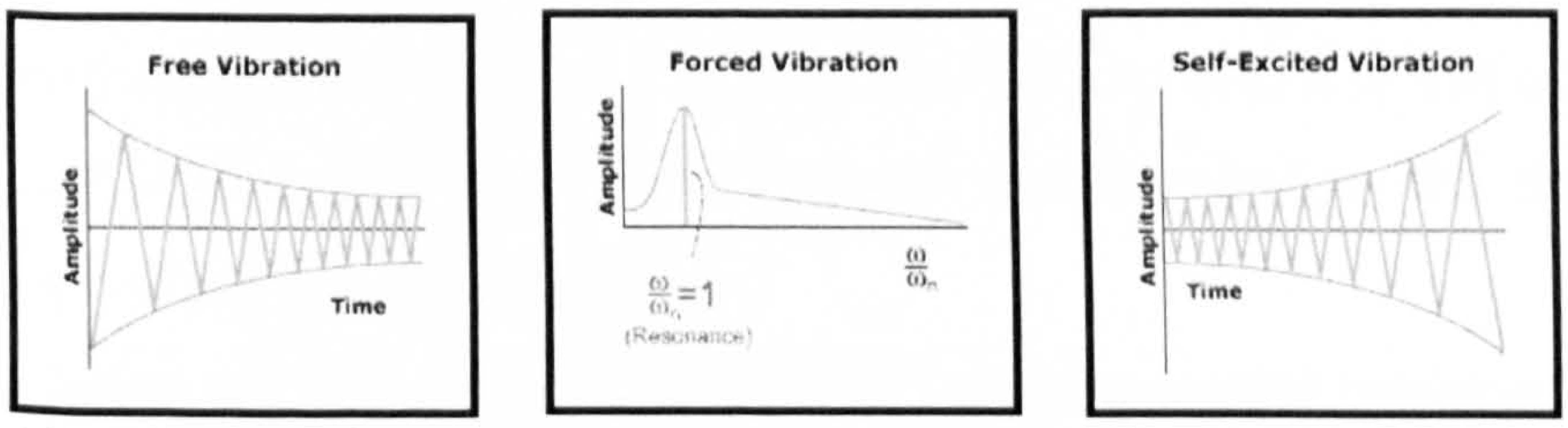

Figure 1.3: The main types of mechanical Vibrations in machine tools

1.2.3.3.a Random or free vibrations

Shock or impulsive loading of the machine tool causes random or free vibrations. An example is when the tool strikes a hard grain in the work-piece during the cutting operation. When the damping is assumed to be zero the structure will oscillate at its natural frequency because the potential energy will be converted without loss (friction-damping) into kinetic energy. In practice however real systems always have damping, which decays the oscillation amplitude with time. In machine tools, this kind of vibration is often neglected since forced or self-excited vibrations play a more important role.

1.2.3.3.b Forced vibrations

Forced vibrations are caused by periodic excitation, such as spindle imbalance, gear drive irregularities, electric motors, pumps, the periodic break of the chip due to the build up edge or shear angle variations, and the tooth entry impact. The machine system will oscillate at the frequency of the excitation force. These excitation forces can be amplified through the structure of the machine when a resonance frequency of the structure is excited. This kind of vibration can be reduced by removing the source, by changing the exciter frequency so that is not close to the natural frequency of the system or the excitation force can be de-coupled by passive or active dampers [1].

1.2.3.3.c Self-excited vibrations

In processes where a large amount of energy is transmitted as a steady input and mechanical damping of the system is low, a small amount of transient energy can be enough to bring the system out of balance. This can then be modulated into vibrations.

Initially the system will be stable (figure 1.4) and no excitation force will be significant. At some critical depth of cut, the static cutting forces become so large, that even a small transient force (may be caused by a hard grain in the work-piece), can "trigger" a self-excitation mechanism called chatter. Forces then build up over a period of time, depending on damping and in turn, this leads to the generation of variation in the chip thickness which results in further varying cutting forces.

Chatter leads to the excitation of one of the structural modes of the machine tool-work-piece system (figure 1.5) and this results in a relative displacement between tool and work-piece. A wavy surface finish left during the previous revolution in turning or by a previous tooth in milling will be removed by the following revolution or tooth period. If the phase between previous cut and current cut is 180^{o}, the varying cutting forces can grow and oscillate at the chatter frequency (close to the resonant frequency of the excited mode of the structure, see figure 1.6) [9].

The cutting process and the vibratory system of the machine form a closed loop, where the cutting force (F) and the relative displacement between tool and work-piece (Y) are the variables, (figure 1.7) [4]. This closed-loop characteristic of self-excited vibrations becomes unstable when the closed loop gain, rises above a certain value.

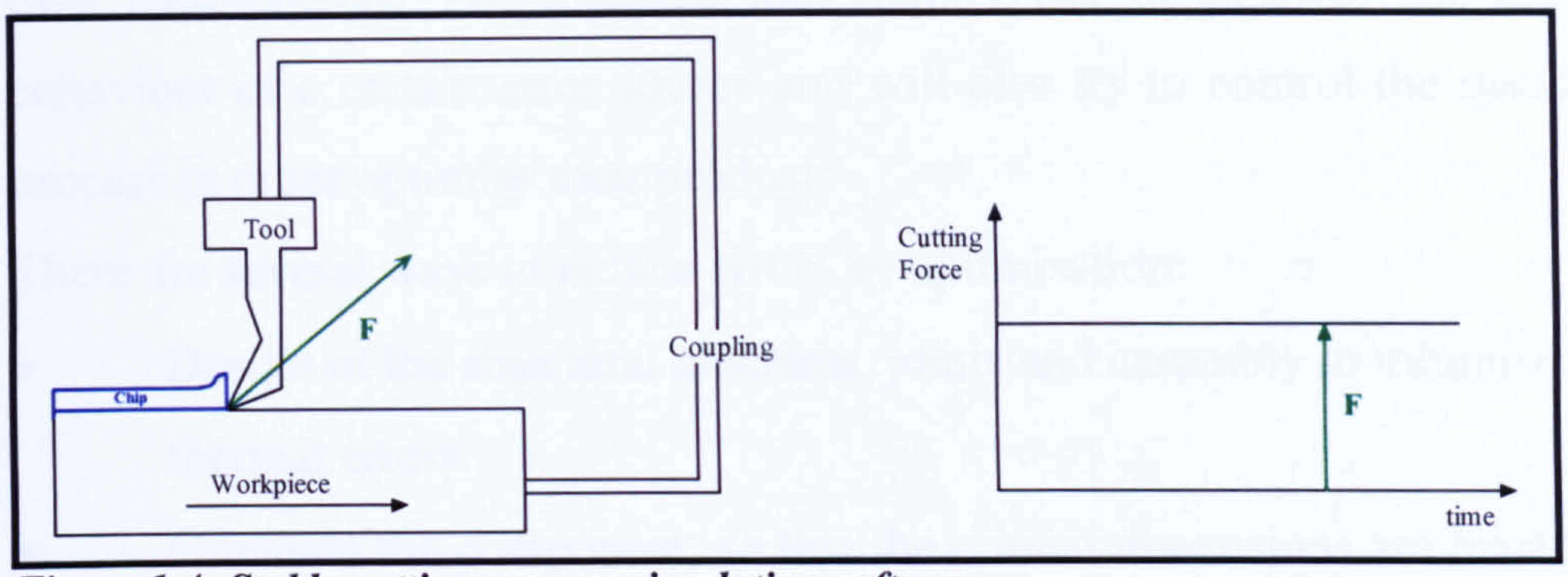

Figure 1.4: Stable cutting process simulation software

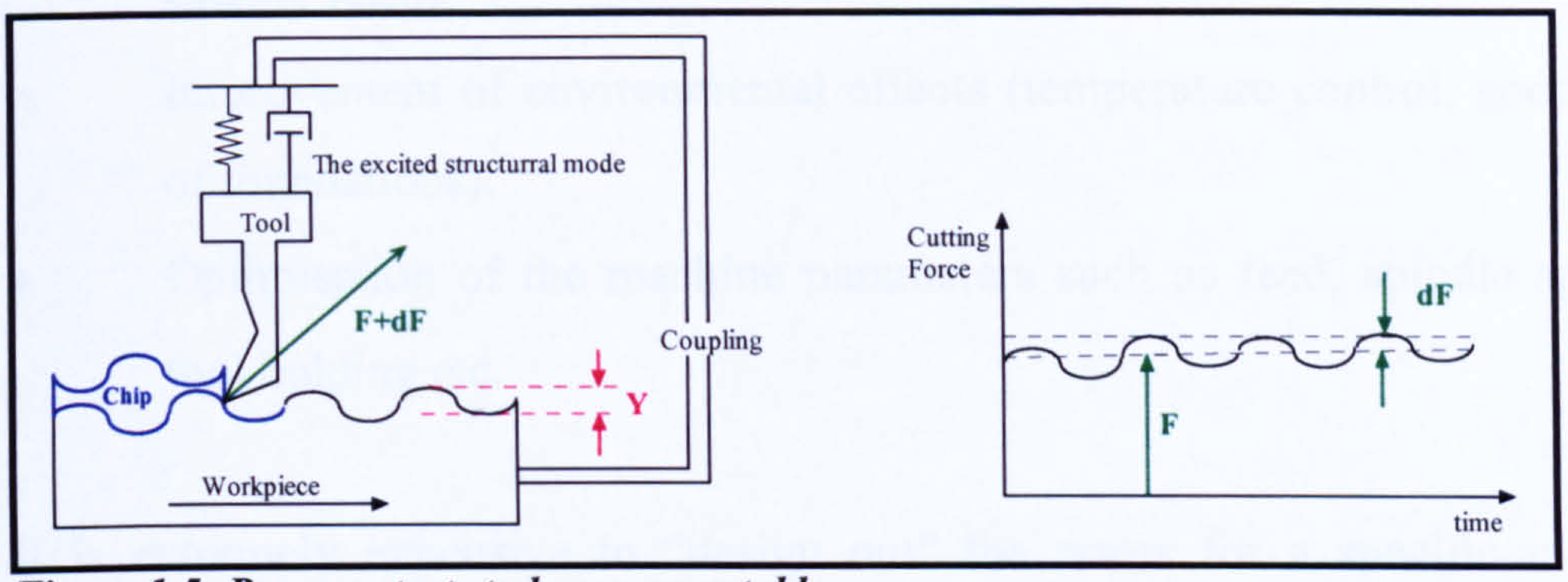

Figure 1.5: Process starts to become unstable

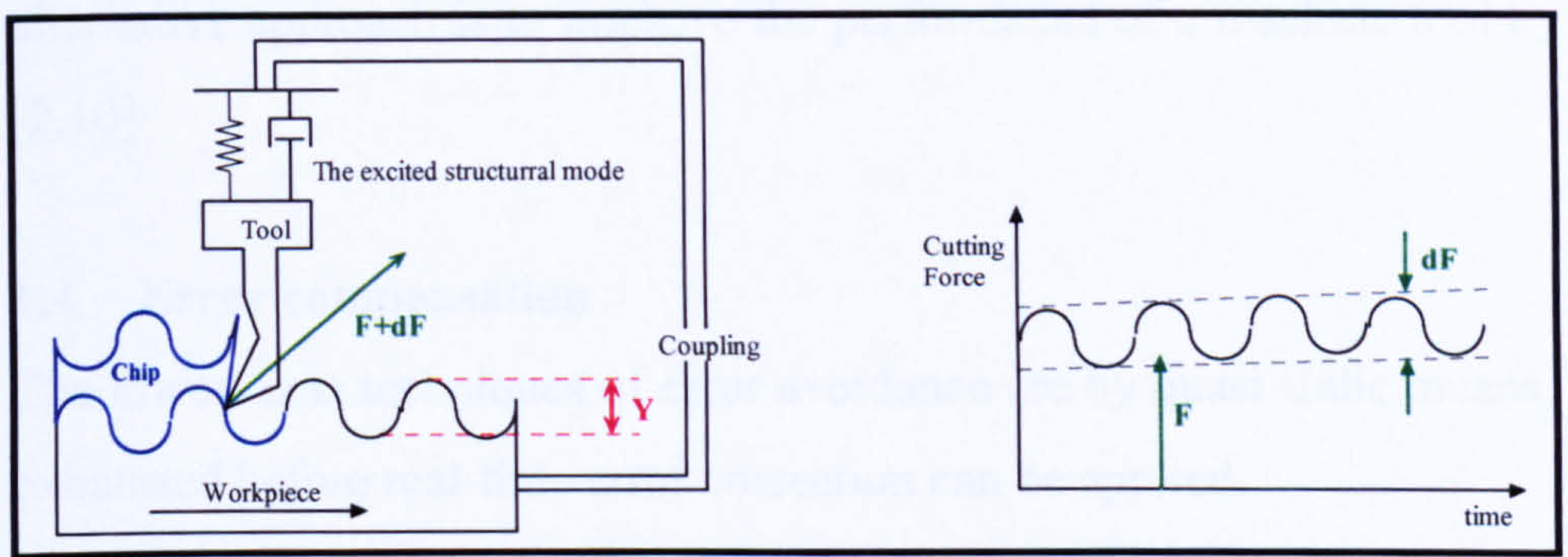

Figure 1.6: Vibration grows until saturation

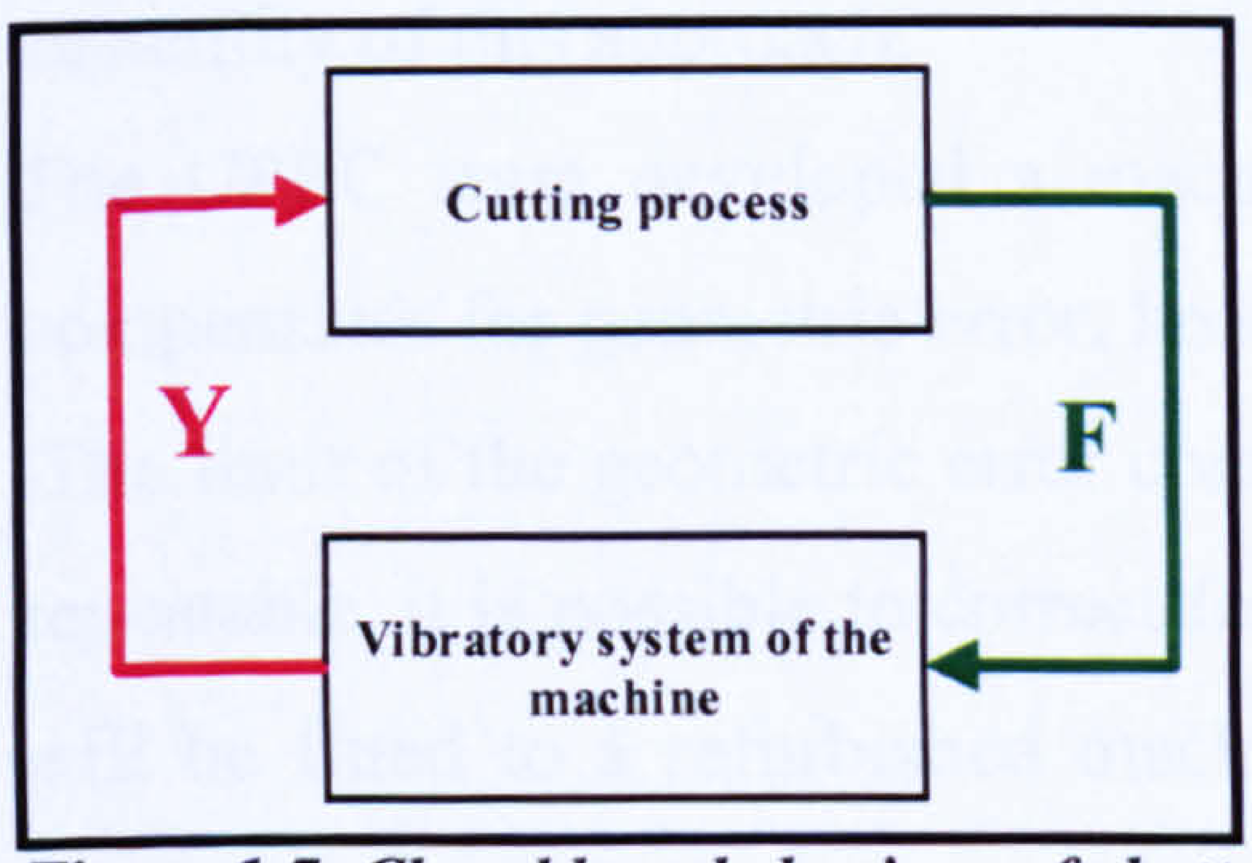

Figure 1.7: Closed loop behaviour of chatter

1.3 Error avoidance

One way of reducing errors is to avoid them in the first place. Each machine type will have its own specification or tolerances. The customer will then decide whether the machine meets his own requirements. The machine tool builder has to consider the cost of improving the behaviour of a certain error source and will also try to control the machining and assembly process in order optimise their product.

There are several ways to reduce errors by optimisation:

- Design of the structural elements, joints and assembly to minimize geometric load and thermal errors.
- Orientate the component, so that the critical dimensions are machined by an axis with smaller errors.
- Improvement of environmental effects (temperature control, good vibration isolation of foundations).
- Optimisation of the machine parameters such as feed, spindle speed, tool wear and tool holding etc.

It is extremely expensive to "design out" the errors for a specific machine type and an alternative approach is to improve the performance of a machine tool by error compensation. [2,10]

1.4 Error compensation

The lowest cost techniques of error avoidance are by quasi static means, and these need to be exhausted before real-time error correction can be applied.

Previous research in the Ultra-Precision Engineering Centre (UPEC), has already shown the capability of this approach.

The UPEC team developed a machine tool error compensation system [11,12,13], which compensates for geometric error, head-slide thermal error and work-piece distortion.

The limit of the geometric error compensation lies in its repeatability. As long as the error is repeatable, it is possible to correct for it. In a current UPEC project, the compensation system will be fitted to a refurbished machine to establish if the error correction performance can reach the standard of a new machine.

1.5 Summary

There is an ever-increasing demand in high precision machine tools to optimise and improve the machine tool performance using advanced control techniques. This is the key strategy of the UPEC at the University of Huddersfield. This is done through error compensation and error avoidance and systems have been developed to compensate for geometric and thermal errors. The purpose of this research is to find new ways to compensate for structural vibration (self-excited and forced) at the cutting point in order to improve surface finish, productivity and tool wear. The intended control approach should be based on adaptive algorithms in order to change the mechanical properties of the cutting process, such as stiffness and damping, actively, during operation.

1.6 Aim

To investigate vibrations in CNC machine tools and design a universal active control system to compensate for vibration effects at the tool/work-piece interface.

1.7 Objectives

a.) Review current state of the art vibration control techniques for machine tools.

b.) Design/select appropriate sensors to measure vibrations in machine tools.

c.) Derive a greater understanding of measured vibrations on the machine under investigation by analysing the sensor signals and comparing these with the surface finish of the component.

d.) Identify low cost passive techniques (e.g. optimisation of the cutting operation) in order to reduce the vibration level.

d.) Design and build a test rig, in order to prove that active vibration control can reduce the vibration of machine tool structures.

e.) Investigate adaptive algorithms through simulation methods and identify those techniques that are suitable for machine tools by use of the test rig.

f.) Select appropriate actuators and sensors that can be used for active vibration control on machine tool structures.

g.) Design an active work-piece holder, which can be integrated to a vertical milling machine.

h.) Test the active work-piece holder statically and dynamically and perform cutting tests.

i.) Draw conclusions from the work and make recommendations for future studies.

1.8 Thesis organisation

The thesis is divided into 11 chapters, which are outlined below:

- Chapter 2 reviews previous research done on vibration control of machine tools and explains the novelty of this research
- Chapter 3 analyzes the basic mechanics of metal cutting operations
- Chapter 4 overviews the theory of vibration control
- Chapter 5 describes the investigation of the structural behaviour of a vertical machining centre
- Chapter 6 investigates how active vibration control can be implemented on a test rig in order to demonstrate its potential
- Chapter 7 describes the design and development of an active work piece holder for milling machines
- Chapter 8 describes the testing phase of the vibration compensation system
- Chapter 9 concludes the work and suggests further developments

Chapter 2

Previous research and literature survey

2.1 Introduction to methods for preventing chatter

The value of a machine tool is usually directly proportional to the speed at which it can perform machining operations. The speed of cutting is often limited by chatter and machine vibrations induced by the cutting process. Regenerative chatter occurs when a steady input force is modulated into larger amplitude vibrations at the natural frequency of the system (compare with self-excited vibrations in a violin where the steady pull of bow across the string produces a tone depending on the acoustic system of the body). A quantitative measure of the productive capacity of a machine tool is the Maximum Metal Removal Rate (MMRR). The MMRR is limited by dynamic stiffness of the machine and tool.

$$MMRR = a_r \times b_{limit} \times c \times m \times n$$

Where a_r is the radial depth of cut (width of cut), b is the axial depth of cut, c the chip load, m the number of teeth on the cutter, and n the spindle speed. One way of controlling chatter therefore would be to change the cutting parameters and another, to improve the dynamic stiffness of the machine or tool. The table 2.1, introduced by Weck [14], shows a summary of factors influencing the chatter behaviour, and therefore gives a good overview.

Machine		**Work-piece/Tool**	**Cutting process**
Operating conditions	**Directional orientation**		
1 Foundations, installation conditions 2 Positioning of machine components 3 Spindle speed 4 Slide and Table movement 5 Slack, backlash, non-linearity, pre-stressing, clamping conditions 6 Operating temperature	Geometric influence in a given machining operation 1 Direction of the dynamic cutting force due to setting angle and rake angle 2 Work-piece/tool configuration	1 Work flexibility 2 Work mass 3 Work clamping 4 Work or tool diameter 5 Tool flexibility 6 Tool mass 7 Tool clamping	1 Work material 2 Cutting geometry 3 Tool wear conditions 4 Point radius 5 Cutting velocity 6 Feed rate 7 Hysteresis determine the limiting chip width 8 Tool and work-piece combination 9 Uneven distribution on multi cutting-edge tools 10 Cooling and lubrication medium

Table 2.1:Factures influencing self-exiting vibrations on machine tool chatter control [14]

For machine tool chatter control and therefore the improvement of the MMRR of an already existing machine tool, there are 3 different approaches, which attract researchers:

- Process Control (Changing the cutting parameters)
- Passive vibration control
- Active vibration control

All the other methods involve the physical re-design or modification of the machine tool structure and therefore do not fall within the category of chatter control.

Most reviewed literature refers to traditional process control and passive vibration control, examples of active systems to alter the dynamics during machining are relatively few.

2.2 Process control

During the last decade, there has been an increased need in the industrial market, to use a so called high speed machining technology. This decade has seen the development of machining centres capable of spindle and slide speeds that are a magnitude higher than those available on conventional machining centres. For example a number of different machine tool suppliers have recently introduced reliable machining centres with feed rates that exceed 40 meters per minute and spindles that deliver more than 20 KW of power at spindle speeds greater than 20,000 RPM [15]. While these machining centres have the possibility of much higher material removal rates, chatter is one of the most difficult phenomena to deal with in high speed machining. By choosing the "right" cutting conditions the machine tool stability can be optimised.

For example speeding up the spindle or increasing the overhang of the tool may actually eliminate chatter from the system.

Especially the correct choice of the spindle speed for a particular tool is critical because under some conditions a spindle speed change of only 10% can result in a magnitude change of achievable material removal rates [16].

Because of its simplicity and effectiveness various researchers have chosen the method of process control as the chatter control solution. But it has nothing to do with structural vibration control, whether it is active or passive, since it does not alter the nominal stiffness and therefore does not increase the MMRR capability of a machine [17,18].

Over the next few pages several very different examples of dynamic control are chosen to show the effectiveness of this approach in order to control chatter.

J. Tlusty [19] was one of the first researchers, to model the cutting process, by assuming a linear transfer function between the vibration and the force. The structure was assumed to be a vibratory system that is characterised by individual modes of vibration, each representing a degree of freedom of the relative motion between tool and work-piece with a particular direction. The resulting amplitude of vibration of all modes normal to the cut surface create a variation in chip thickness. This is because the magnitude and phase shift of this vibration are then copied onto the work-piece surface. The variation in the chip thickness then generates a dynamic cutting force, which excites the vibrating system even further (chip thickness variation or regenerative effect – figure 2.1). This closed loop feedback of force and vibration provides the mechanism for regenerative chatter. The assumption was made that this mainly is influenced by the elasticity of the machine tool frame rather than the dynamics of the cutting process itself [19,20].

Merrit [20] has shown that self-excited vibration can be represented by a feedback loop. In practice the system is always non-linear and therefore the chatter amplitude only grows to a finite value [21]. But since the stability question is of more importance than the maximum vibration amplitude the linear models are generally considered to be adequate.

Using classical feedback theory the limit of stability of the cutting system (stability threshold of the cutting process) can be obtained with the open-loop transfer function and the Nyquist criterion (explained in more detail in chapter 4).

This leads to 3 independent basic equations:

The limit of system stability ("structural equation"):

$$b(f_{chatter})_{limit} = -\frac{1}{2K_s \operatorname{Re}[G(f)]_{neg}}$$

Eq. 2.1:The structural equation

where:

b_{limit} = The maximum stable axial depth of cut

K_s = The static cutting stiffness (dynamics of the cutting process are neglected) of the material (Steel $\approx$ 2000N/mm^2, aluminium $\approx$ 800N/mm^2)

Re [G(f)]$_{neg}$ = The real part of the transfer function between tool and work-piece, where the function is negative

Note: Since the depth of cut is a physical quantity, the solution is only valid for the negative values of the real part of the transfer function G(f).

The relationship between the chatter frequency and the tooth pass frequency is the "drive equation":

$$n(f_{chatter}) = \frac{60 \times f}{m \times \left(N + \frac{\varepsilon}{2\pi}\right)}$$

Eq. 2.2:The drive equation

where:

n = The rotational seed of the spindle in RPM

60 = The conversion factor 60 sec/min since the spindle speed n is in RPM

m = The number of teeth so that nm is the tooth pass frequency

f = The frequency, at which chatter should occur

ε = The phase shift between the vibration of a tooth and the wavy surface left by the previous tooth

N = The number of entire waves between two succeeding teeth of the milling cutter

The phase shift between the vibration of a tooth and the surface left by a previous tooth has been derived as (chip thickness variation):

$$\varepsilon(f_{chatter}) = 2\pi - 2\arctan\left(\frac{\mathrm{Re}[G(f)]}{\mathrm{Im}[G(f)]}\right)$$

Eq. 2.3:The chip thickness variation

where:

Re [G(f)] = The real part of the transfer function between tool and work-piece

Im [G(f)] = The imaginary part of the transfer function between tool and work-piece

These equations lead to stability charts presented by Tobias [22] indicating chatter free spindle speeds and critical axial depths of cut. Stability lobes allow the selection of larger depth of cut at high spindle speeds, because large stable gaps occur at spindle speeds, where the rotational frequency of the work-piece (turning) or the tooth passes frequency in milling (or one of its harmonics) is equal to the natural frequency of the dominant mode of the structural system. Therefore chatter can not occur at the tooth pass frequency (or any of its harmonics) in milling or at the rotational frequency in turning [23]. In simple terms:

Stability lobes separate stable machining from chatter. If the transfer function of the tool/work-piece is known, either through structural simulation or through measurement the stability lobes can be calculated. For example the transfer function of the structure is obtained by a modal test (Figure 2.2).

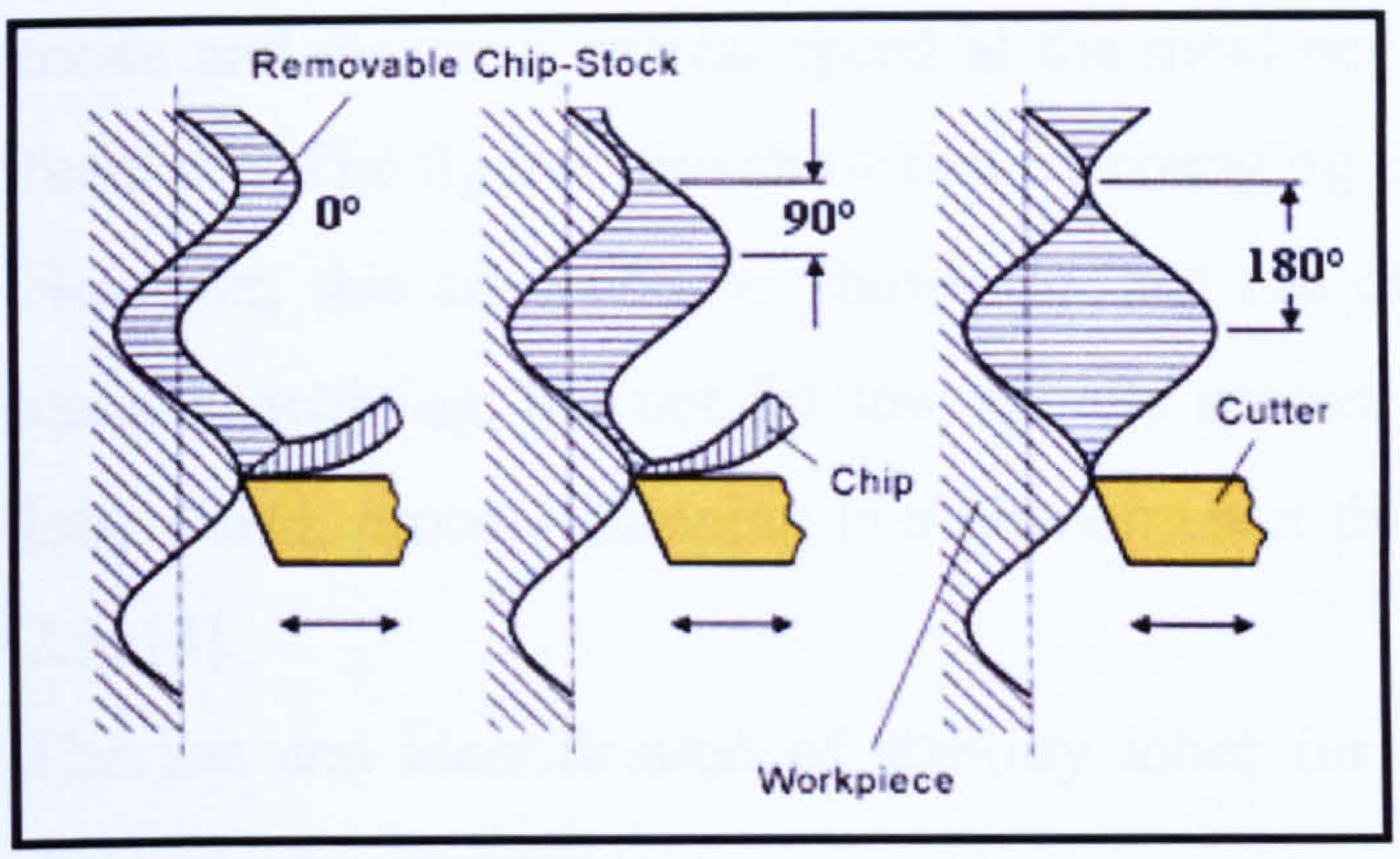

Figure 2.1:The chip thickness variation [23]

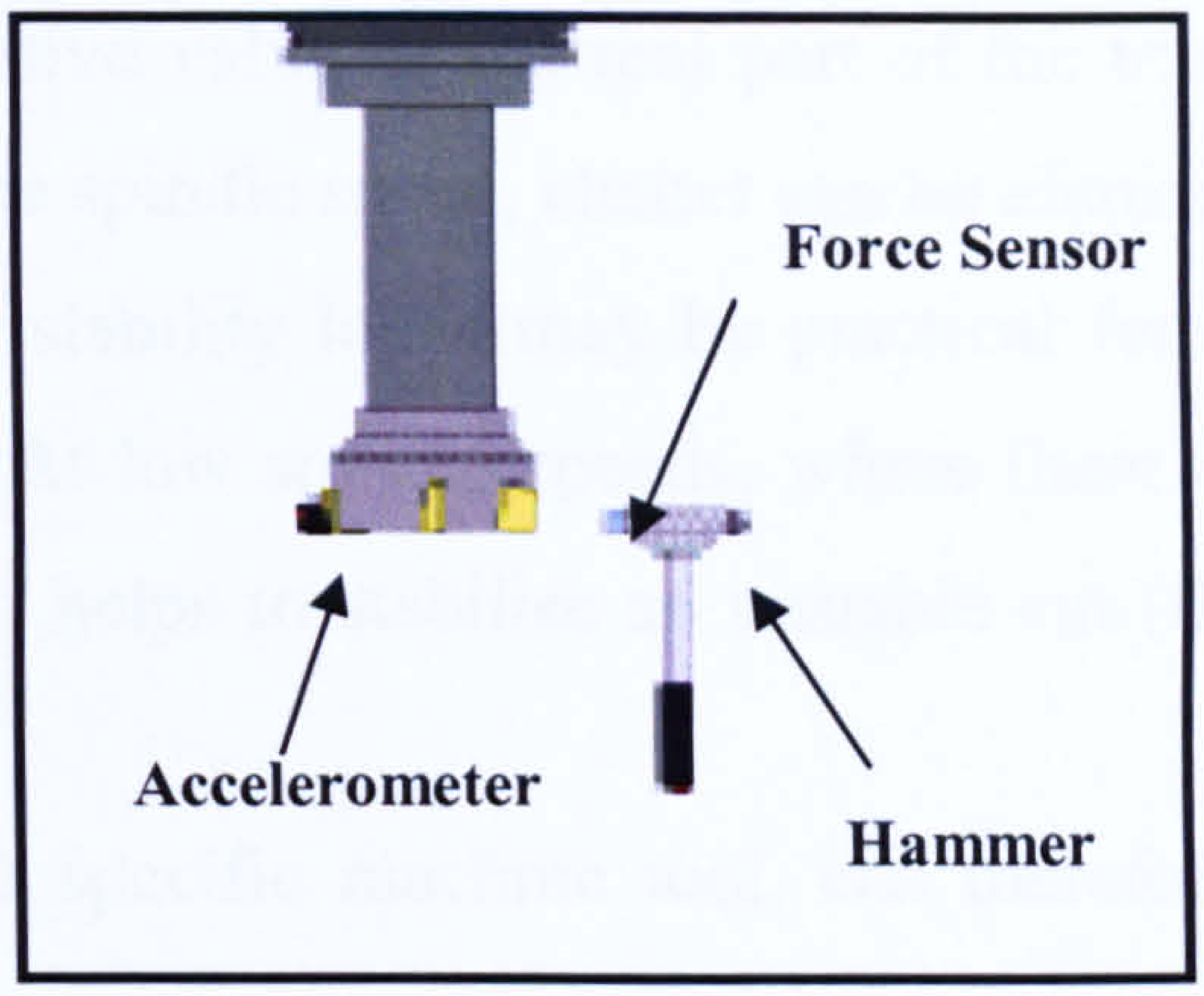

Figure 2.2:Modal test (hammer test) on the tool structure

The stability lobes of the most dominant mode (single degree of freedom) are numerically generated by dividing the chatter frequency into a vector of small steps. For each frequency the critical axial depth of cut is calculated (equation 2.1). Then the phase lag angle ε, using equation 2.3. The spindle speed at which the stability limit is reached can then be calculated using equation 2.2. Standard software like Microsoft EXCEL® or Math Works MATLAB® can be used for the computation, since the modal test results can normally be converted into ASCII format. Figure 2.3 shows such a stability chart.

The relationship between the spindle speed, a single stability lobe, and the real part of the most dominant mode of the frequency response function of the tool work-piece interface is shown in figure 2.4.

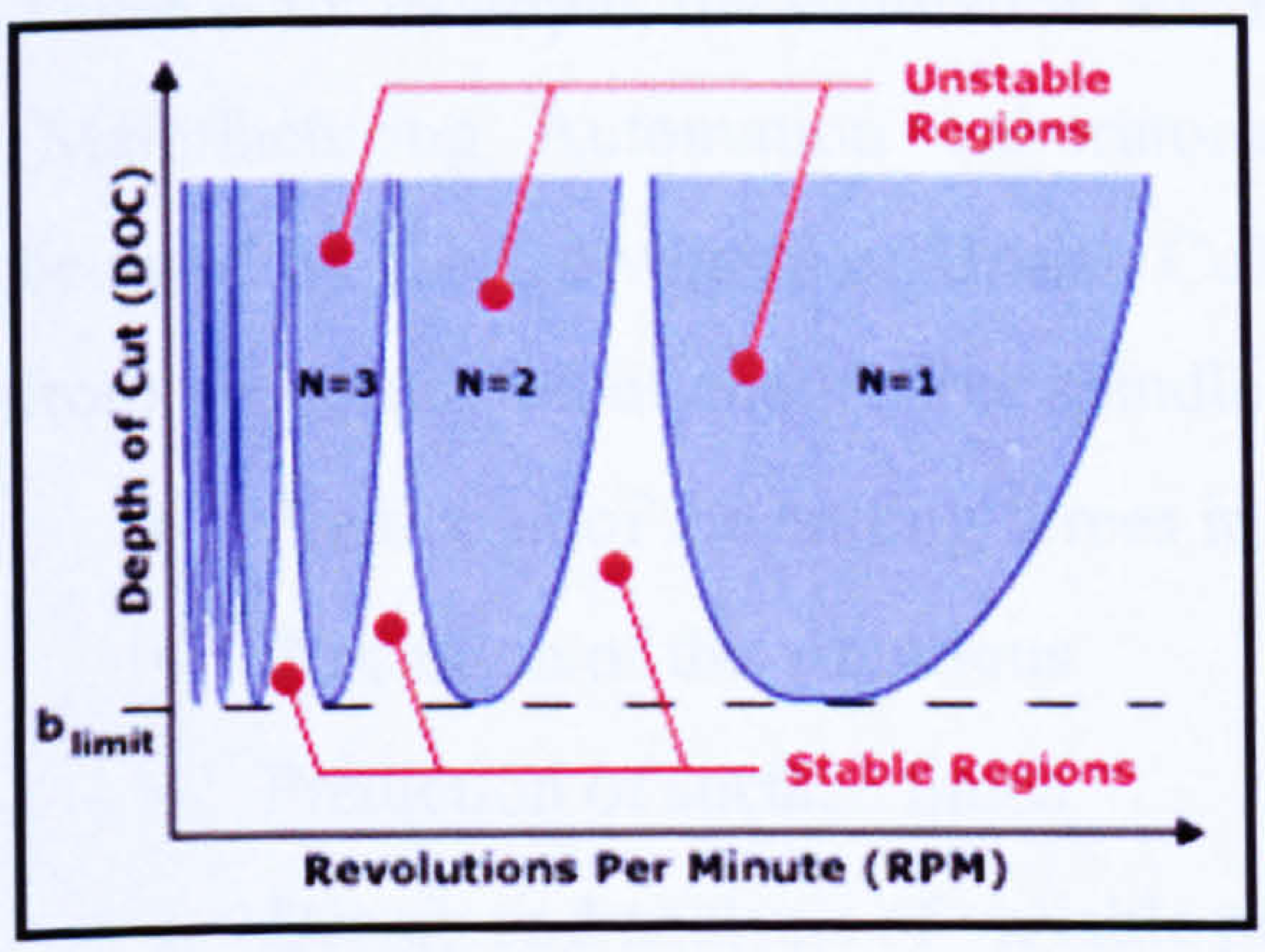

Figure 2.3:Stability Lobe of a SDOF system [23]

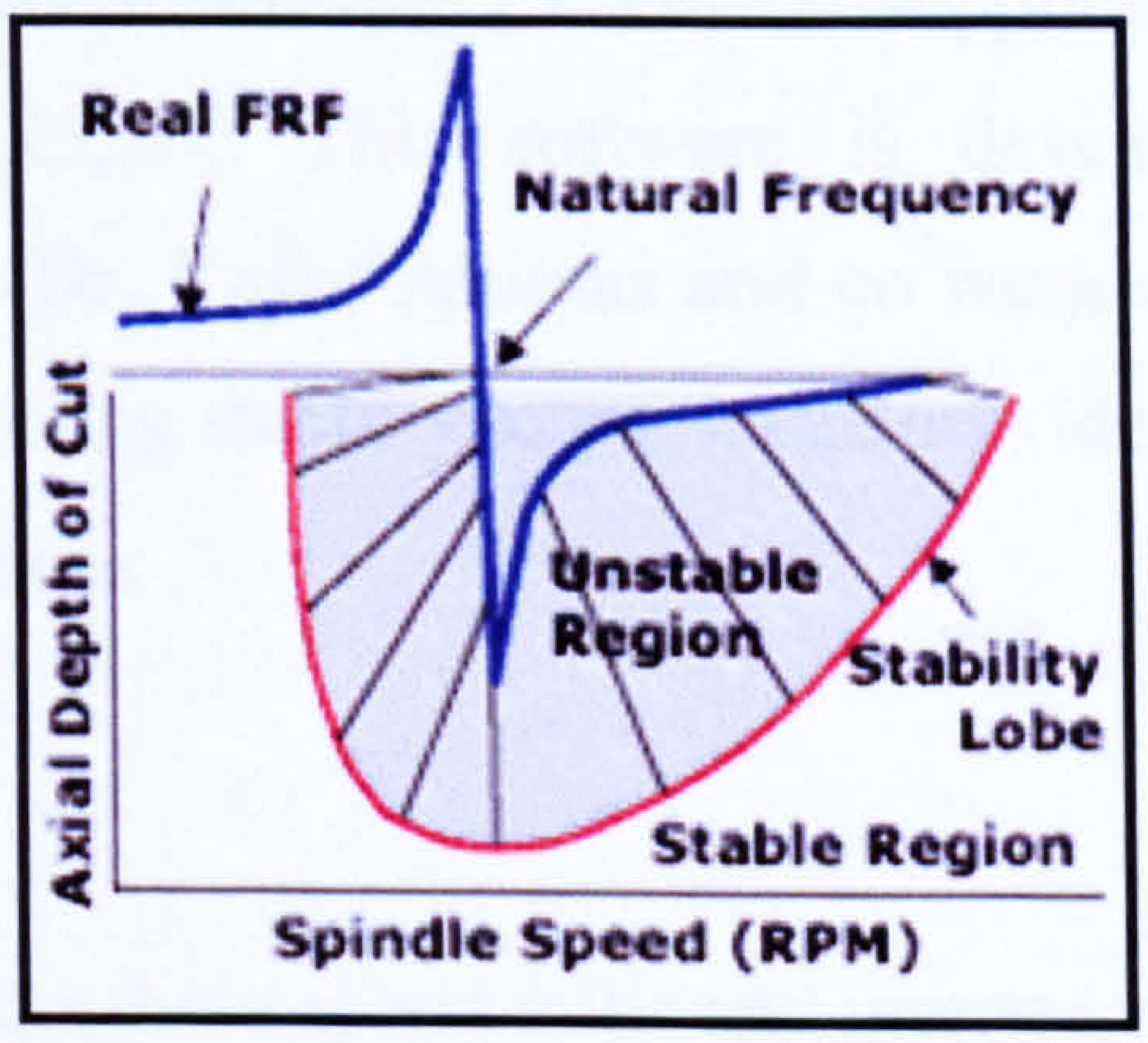

Figure 2.4:Generation of a lobe from the transfer function of the vibrating structure [23]

All conditions above the line of stability result in chatter, while the ones below do not. It very clearly shows that the most stable spindle speed is at the resonance of the most dominant mode and the most critical speed at the most negative value of the real part of the transfer function. The figures also show that by changing the spindle speed, chatter can be eliminated. However, this analysis also shows that the use of stability lobes may be practical for high speed machining, but not for low spindle speeds. At low spindle speeds, where there is no lobe effect, process damping is a phenomenon that helps to stabilise an unstable cut (figure 2.3) [4].

The use and identification of stability lobes for a specific machine tool, can therefore be divided into categories:

- Off-line approaches (Finite element modelling or modal testing of the dynamics of the tool/spindle structure)
- On-line approaches, where the dynamics of the machine structure are unknown, but the stable pockets are identified by measuring the chatter frequency under cutting conditions using a suitable sensor

2.2.1 Off line techniques

There are already chatter avoidance packages commercially available. Most of them are based on the prediction of the stability lobes using the machine conditions and the frequency response function (FRF) of the vibrating structure obtained by a modal test. Although it is possible to write software (eg. MATLAB) to solve the stability equations, as shown earlier, these packages offer much more.

There is for example, the simulation and measurement software CUTPRO© supplied by MAL (Manufacturing Automation Laboratories) [24,25,26]. This software is developed and licensed by the University of British Columbia (Dr. Yusuf Altintas and co workers). Apart from the prediction of chatter free spindle speeds using stability lobes, it can provide:

- Prediction of the cutting forces in 3 directions
- Prediction of the vibrations
- Prediction of surface finish
- Design and analysis of variable pitch cutters, helical end mills and inserted cutters
- Finite element based design and optimisation of machine tool spindles
- Incorporated experimental modal analysis software, which automatically obtains the modal parameter of a frequency response function (FRF)

Even with these facilities, the main function for chatter prediction of an existing machine tool is still the stability lobes. This allows the software to identify stable spindle speeds and large depths of cut, which do not lead to chatter. Figure 2.5 shows a typical graphical user interface of this software.

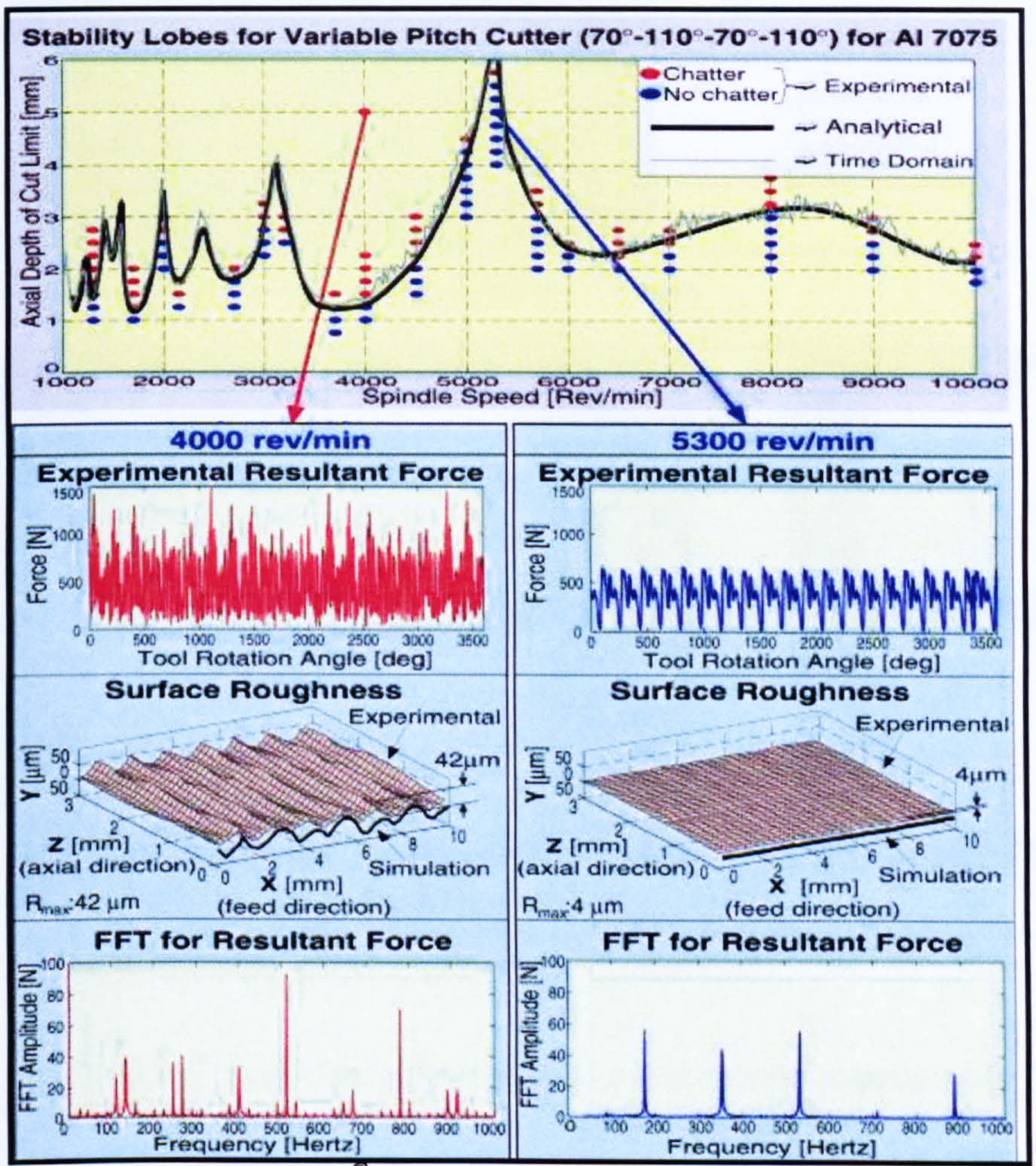

Figure 2.5:The CUTPRO© measurement and simulation software [26]

The researchers of the University of Florida (Tlusty, Smith, Delio), who were probably the first offering a commercial simulation package based on the stability theory derived from Tlusty's work in vibration and high speed machining, have formed the Manufacturing Laboratory Inc. (MLI) 1987. They offer the MetalMax™ system [27]. Again this software optimises the spindle speed without cutting tests by analysing the stability of the machine tool structure under cutting conditions and predicting the stable pockets. The hardware consists of an impact hammer with a force sensor to excite the tool/spindle structure and an accelerometer to pick up the response of the system (figure 2.6).

Through charge amplifiers both sensors are linked to a PC based data acquisition system. A visual programming software has been used for the additional computation to create the stability lobes on a practical user interface (figure 2.7).

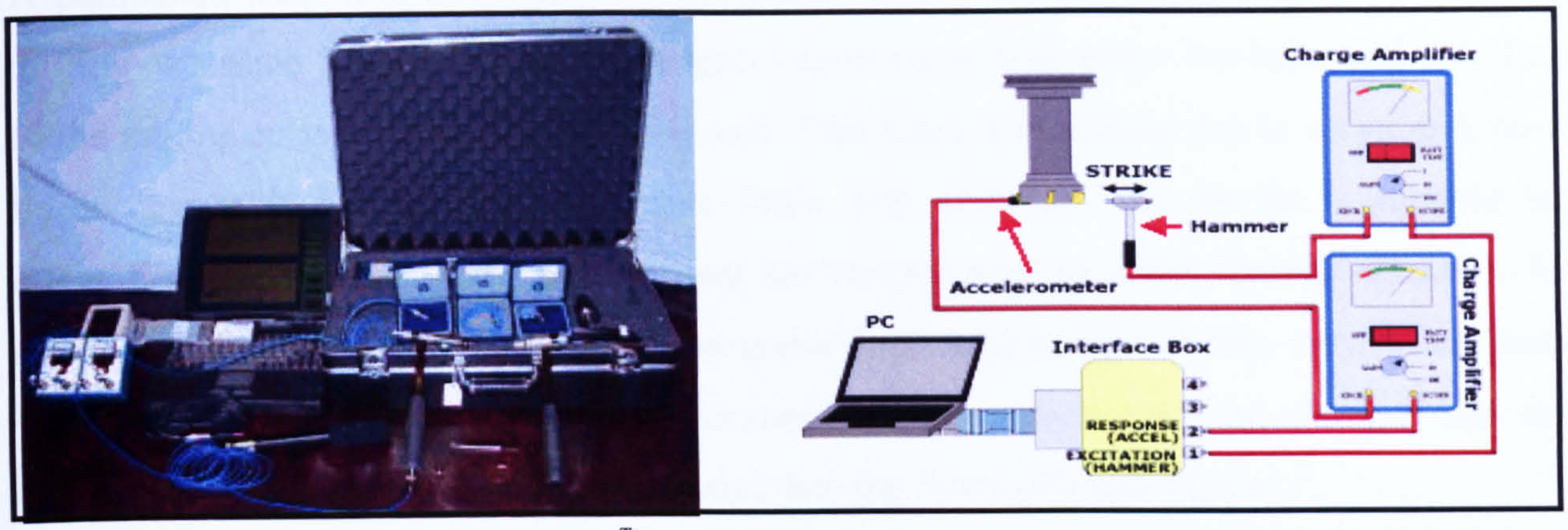

Figure 2.6:The hardware of the MetalMax^{Tm} system

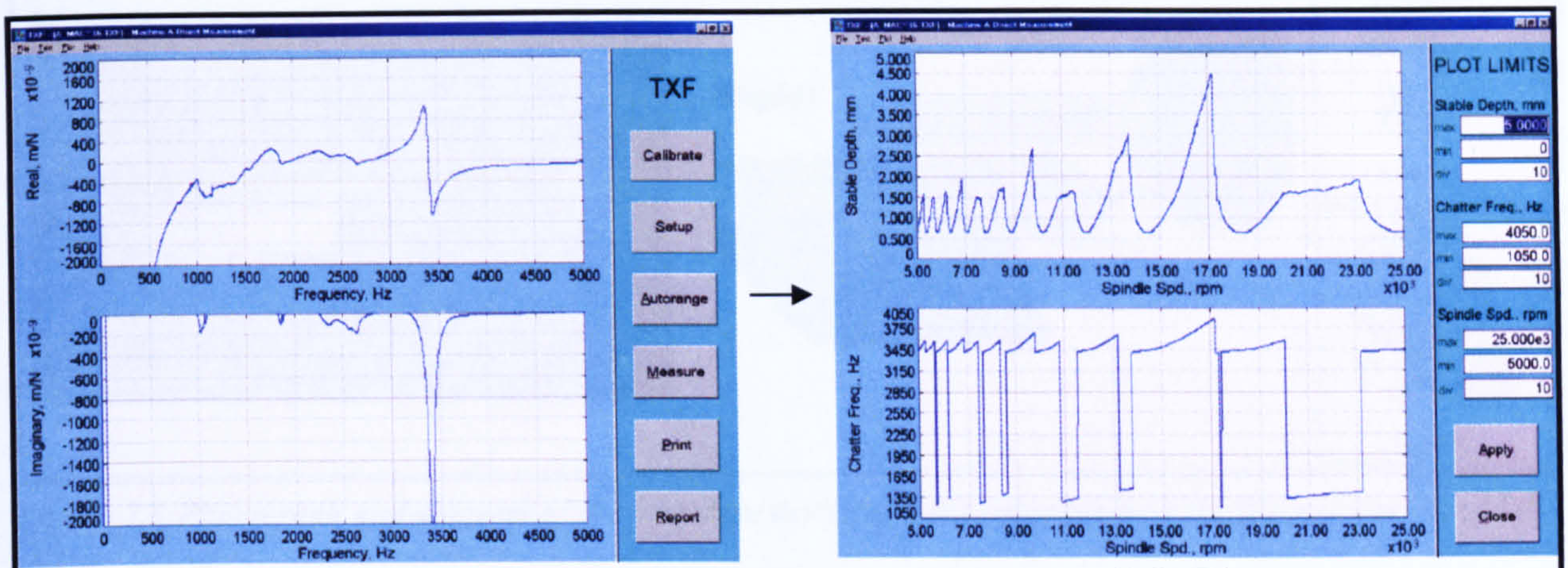

FRF: Frequency Response ***Lobe Diagram***

Figure 2.7:The software of the MetalMax^{TM} system [27]

MetalMax^{TM} is proven software and has been used successfully in both industry and research [28].

Another very similar software package has been developed and licensed by Boeing [29]. It is called MPS (Machine Prediction Software) and again predicts the stability lobes from a Nyquist or stability plot of the machine tool structure. The disadvantage of both the above systems is that they require a certain amount of expertise in modal testing in order to operate them correctly.

Snyder et al, took a different approach [15], again, without the need for exhaustive cutting tests. They used a "magnetic non-contact force actuator" and non-contact displacement sensor to excite the spindle tool structure at various spindle speeds and measured the structural response. The force actuator is fed by an impulse train, which excites the tool structure. As the spindle speed is ramped from zero to its maximum speed, those speeds that maximise the dynamic response of the tool are the speed that minimise regenerative chatter at the measured frequencies. Figure 2.8 shows the principle of how the impact force is generated.

A permanent magnet is positioned either on tool or work- piece depending whether it is a milling or turning application. As the magnet comes close, with either the lathe tool or a flute of the milling cutter, a large force is produced. This force is impulsive due to very rapid, non-linear change in the magnetic attractive force with distance. The device is suitable for integration into the machine controller and has the potential to allow optimal speeds to be downloaded and stored for later CNC programming. A prototype of this system has been designed and built (figure 2.8). The experimental set up uses a steel rod clamped into the spindle, flat sections at the end of the rod simulate the flutes of a milling tool.

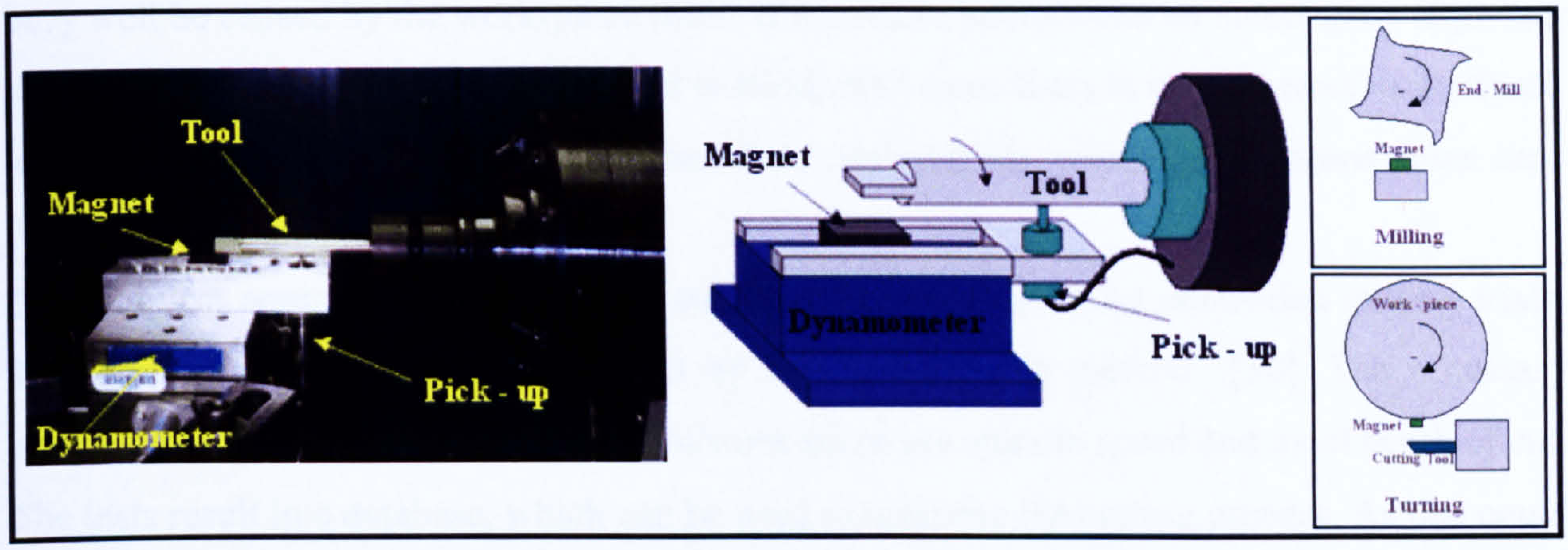

Figure 2.8:Photograph and diagram of the prototype device and the principle how the force is generated [15]

The results are encouraging but more work especially concerning the quality of the excitation force needs to be done.

2.2.2 On line techniques

In many cases production is a cyclic process between the part programmer and the shop floor. The part program is normally written by a programmer, who has little knowledge about the dynamic characteristic of the machine tool or work-piece. As a result he may specify cuts which are well within the available power and torque range of the machine, but which result in self excited vibrations. The machine operator then has to override the program (normally decrease the axial depth of cut) or the programmer has to re-write his program. An ongoing dialog between the part programmer and the shop floor then is necessary. If the axial depth of cut is used to stabilize the process it is at the expense of the fact that the machine is not being used to its full capability and production time and cost increase. If off-line techniques are used to allow the use of the whole machine capability, the programmer needs knowledge about the dynamic characteristic of each tool, even each tool/work-piece configuration. This again increases the production time.

On line techniques take data during the machining process and attempt to make corrections to the process parameters to guide the machine to stable cutting conditions. So again they use stability lobes indirectly, but instead of the time consuming off line identification procedures they are done on-line during cutting. This saves time for the off line identification. Another advantage is that most on line techniques identify the stable pockets of the whole tool/work-piece interface, where the off-line modal testing is normally only done on the tool itself, which is assumed to be the most flexible part in this system. If for example thin walled aluminium parts for the aerospace industry are to be machined, the problematic dynamics may very well be caused by the work-piece itself. If the stable pockets can be detected by adjusting the spindle speed, the regenerative effect is eliminated since there is no regenerative feedback loop. But some off line techniques are based on cutting trials, which again means down time for the machine.

The simplest approach to measure the stability lobes on-line is by controlled cutting trials. The stability lobes are simply recorded by this "cutting test method" [30]. The necessary parameters for a certain machine and tool/work-piece are spindle speed and axial depth of cut. The tests result in a database, which can be used to optimise the cutting process. As one could imagine this is a very expensive and time-consuming exercise

One of the first research exercises not requiring cutting trials was carried out by Weck et al, [31,32]. They developed an adaptive control system for face milling operations. The system is capable of exploiting the available machine capacity to its limit at any moment in time.

The basic structure of this process monitoring and optimisation system is shown in figure 2.9. The most important feature of this system is the use of adaptive control approach to automatically suppress chatter vibrations. This was thought to be one of the major factors in optimising the cutting capability of the machine. A torque sensor for the spindle was developed using strain gauges and a special telemetry system used in order to transmit the sensor signals from the rotational part to the non-rotating part of the machine, by a carrier signal. A chatter detection unit then separates the chatter vibrations from the forced vibrations. All this was done electronically without the use of a computer. The vibration signal was divided into a discrete frequency spectrum using a very narrow adjustable bandpass filter, whose window could be shifted over the frequency range of interest.

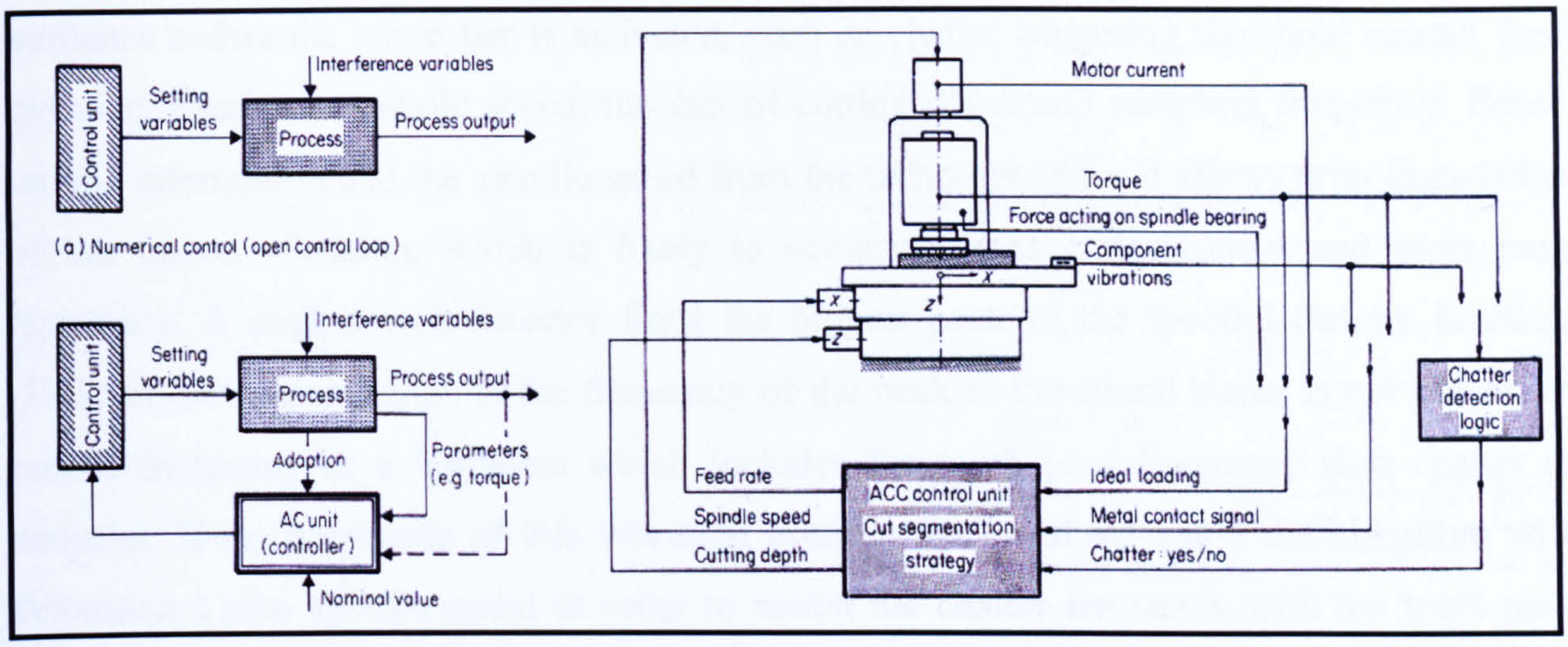

Figure 2.9: The comparison between conventional and intelligent CNC's (left)
The limit control system for milling (right) [31]

The amplitude of individual vibrations was then measured using a peak detector. If the vibrations exceeded a certain threshold value, a frequency comparator determined whether the vibration originated from forced vibration or not. This is usually related to the spindle speed (gear, tooth-pass, run-out). Since the spindle speed and the number of teeth are known, the chatter detection unit can distinguish between the externally forced vibrations and chatter vibrations. If chatter occurs during operation, the process computer records the chatter frequency and determines a stability minima in a certain range of spindle speeds. With the variation of the spindle speed, the target or ideal spindle speed is approached. This means that the system tries to find a stable pocket. If no spindle speed is found which stabilises the system, the axial depth of cut will be reduced automatically. If the system decides to change the speed and passes through a stability minimum, the feed is briefly stopped. This avoids the increase in chatter vibrations.

The first commercial system has been introduced by Manufacturing Laboratory Inc. (MLI) and again is based on the expertise of Tlusty and co workers.

Their Harmonizer^{TM} system [33] uses a unidirectional microphone to collect acoustic emissions from the tool/work-piece interface. Fourier analysis of the data produces a frequency spectrum that indicates the presence of chatter. With the knowledge of the spindle speed and cutter (number of teeth) the system can differentiate between chatter and forced vibrations (tooth pass and bearing frequencies relating to the spindle speed). When a minimum amount of chatter is detected, the cutting process is interrupted using the feed override, while a controller computes a new cutting speed based on the detected chatter frequency. The system is very well explained by Smith [34,35]. The user has to input several variables before the controller is activated, such as chatter triggering threshold current feed override, maximum spindle speed, number of cutting edges and sampling frequency. Based on this information and the spindle speed from the tacho-generator it allows prior knowledge of the forced vibration, which is likely to occur, such as cutter runout and tooth pass frequency. A peak search detector finds the highest peak in the spectral density function (FFT) of the sensor signal. If the frequency of the peak in the sound signal is not the cutter runout frequency or a harmonic which includes the tooth pass frequency then chatter is detected. If the amplitude of this vibration exceeds the threshold value the algorithm will determine a new spindle speed in order to match the chatter frequency with the tooth pass frequency.

The algorithm (equation 2.4) is based on equation 2.2 when $\varepsilon/2\pi$ is 1 ($f_{tooth\,pass} = f_{chatter}$):

$$n = \frac{60 \times f_{chatter}}{m \times \left(N + \frac{\varepsilon}{2\pi} \right)},$$

(refer to equation 2.2)

$$n = \frac{60 \times f_{chatter}}{m \times (N+1)}$$

Eq. 2.4: The algorithm used by Smith

Where n is the spindle speed in rotations per minute (RPM), m the number of teeth, $f_{chatter}$ the measured chatter frequency and N an integer presenting the stability lobe number. If it finds this stable pocket where ε equals 2π then there is no regenerative feedback loop. It does the iterative calculation, from the first stability pockets onwards, to the higher order pockets, if it falls within the initialised maximum range. This way the system can find the highest stability pockets, which are at higher speeds. The feedrate is reduced to zero using the feed override until the new spindle speed is found. If a new speed has been found the feed is increased to a defined value in order maintain maximum chip load. By doing this, the algorithm monitors the sound level in order to check whether chatter has exceed the threshold. If it has, it carries out another adjustment. This iteration can be performed up to 5 times before the feed is interrupted and an error message indicates that the algorithm is unable to find stable cutting conditions. As a result the operator knows that he has to decrease the axial depth of cut, since it is too much for the machine. The time delay before this algorithm can react to chatter vibration, is the processing time to collect one frame for the FFT calculations (e.g. 1024 samples). This can be changed but a longer time frame means better resolution in the frequency domain. The authors make use of the feedrate parameter, which is effectively a direct parameter for the maximum chatter amplitude [32]. Figure 2.10 shows the Harmonizer™ system implemented to a vertical-milling machine.

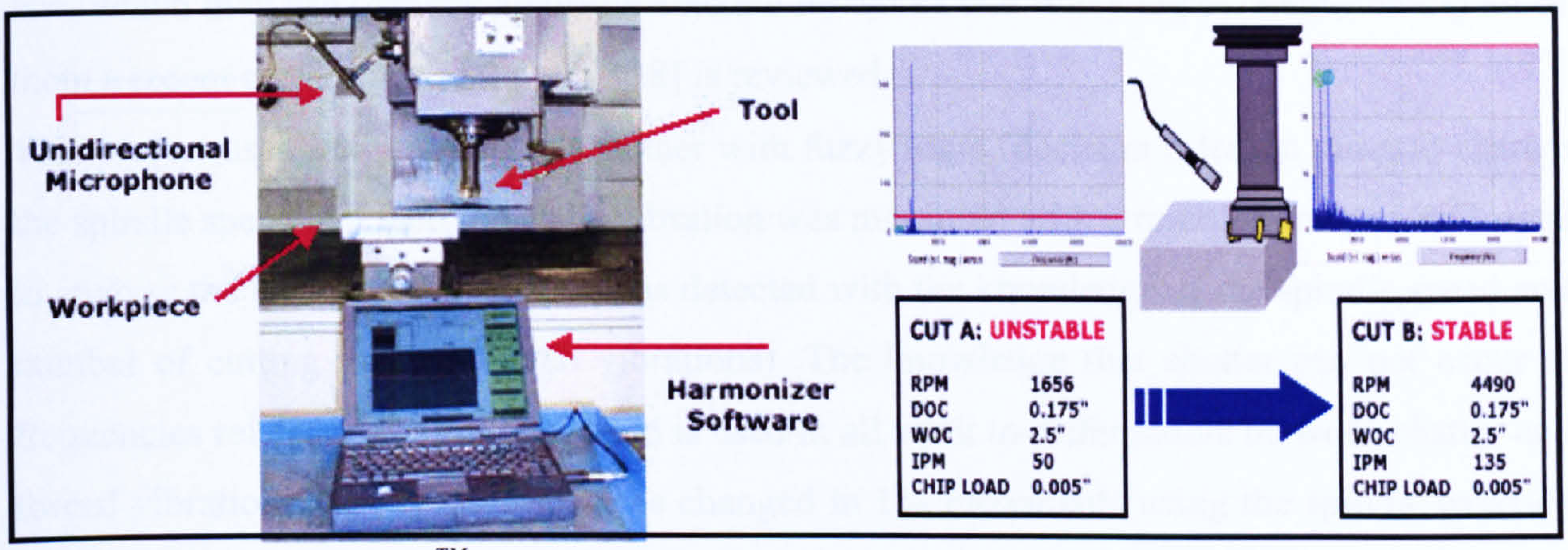

Figure 2.10: The Harmonizer™ system [33]

To date this system is the best-known chatter control package and therefore has been discussed in more detail. It is implemented in several companies across the US [28].

A similar solution to the previous one is offered by the toolmaker Kennametal [36]. It is called "BestSpeed" and is a hand held analyser with a built in microphone. It can isolate the distinct frequencies in the sound signal and calculates the optimum speed for a smooth cutting operation. The only input the user has to make is the number of cutting edges of the tool.

With the knowledge of the stable lobes, a greater axial depth of cut is possible. It has been reported that it even works over the telephone line in order to diagnose a remote work shop chatter problem. But again, it just works for regenerative chatter vibration and not for forced vibration, which may be caused by some interrupted cutting operation.

Another approach based on the principle of consuming chatter energy by the best vibrating phase using speed regulation techniques is described by Lio and Young [37]. They determined that the largest amount of energy extracted from the tool-vibration system in each period is when the phase shift ε between the vibration of the tooth and the wavy surface left by the previous tooth is 90° (π/2). Again equation 2.2 is used to calculate the new stable spindle speed. Another difference from the previous approaches is that the feed is not interrupted. The disadvantage is that chatter first has to develop before the controller can react and even then when the spindle speed is altered the feed remains the same. Their simulation and experimental prototype is again a good demonstration for the spindle speed regulation technique in order to avoid chatter. In the experiments the cutting force obtained from a table dynamometer are used to record the cutting process and detect chatter.

There is much work published for on-line chatter control using the spindle speed and feed rate as control parameter in order to stabilise the cutting process. The difference is the control law, which they use (genetic algorithms neural networks and fuzzy logic). Representing all of them a recent project from Sim et al [38] is reviewed.

This project uses weighting rules together with fuzzy logic (decision rules) in order to change the spindle speed and feed rate. The vibration was measured with a microphone and FFT used to analyse the signal. Again chatter was detected with the knowledge of the spindle speed and number of cutting inserts (forced vibrations). The knowledge that chatter can not occur at frequencies related to the spindle speed is used in all work to differentiate between chatter and forced vibrations. The spindle speed is changed in 1% increments using the spindle override up to 10%. If chatter increases when the spindle speed is increased by 1%, the decision unit decreases the spindle speed. This iterative approach stops when a stable speed is found.

Again the, system needs to detect chatter before it can do anything about it. Also this system as all the other reviewed systems uses process control. As such it does not increase the MMRR capability since it does not alter the nominal stability of the machine. Second, the sensitivity of the microphone to environmental noise can make it difficult to recognize the chatter vibrations. Although this problem can be minimized by adjusting the location of the microphone.

2.2.3 Other approaches

There are other interesting and more practical techniques, which are not related to the variation of spindle speed or feedrate as a parameter, but still rely on operator control. Most of them assume the proper clamping of tool and work-piece.

There are, for example, different types of tool holder on the market, which affect the stability in high speed machining [39]. Set-screw holders, which do not clamp the tool in all directions can be replaced by collet holders or even shrink fit holders. Shrink fit holders are preferred since the tool is clamped very rigidly after heating up the tool holder. Unfortunately these devices are also very expensive. Another important factor is to make the right choice of work-piece holder. The clamping design of the hydraulic types is preferred, where the screw arrangement of some fast clamping "carrousel" types are often insufficient.

Tobias [22] has also found that the chatter behaviour of the machine depends on the position of the work related to the spindle.

Figure 2.12 shows the chatter amplitudes for various amounts of eccentricity (*e*), defined as the distance between the centre line of the work and the spindle axis (figure 2.11).

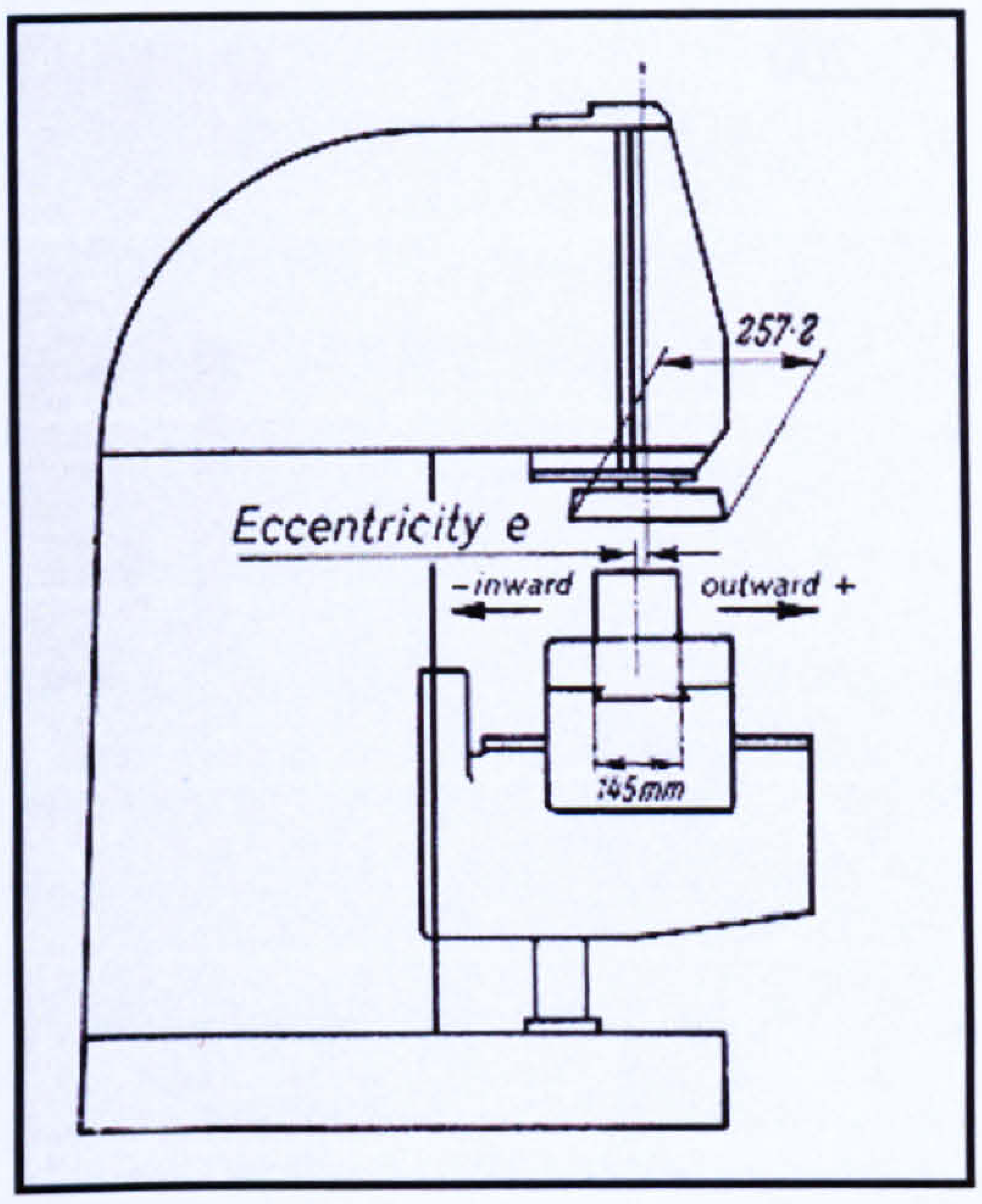

Figure 2.11:Schematic diagram of the machine used in the experiment [22]

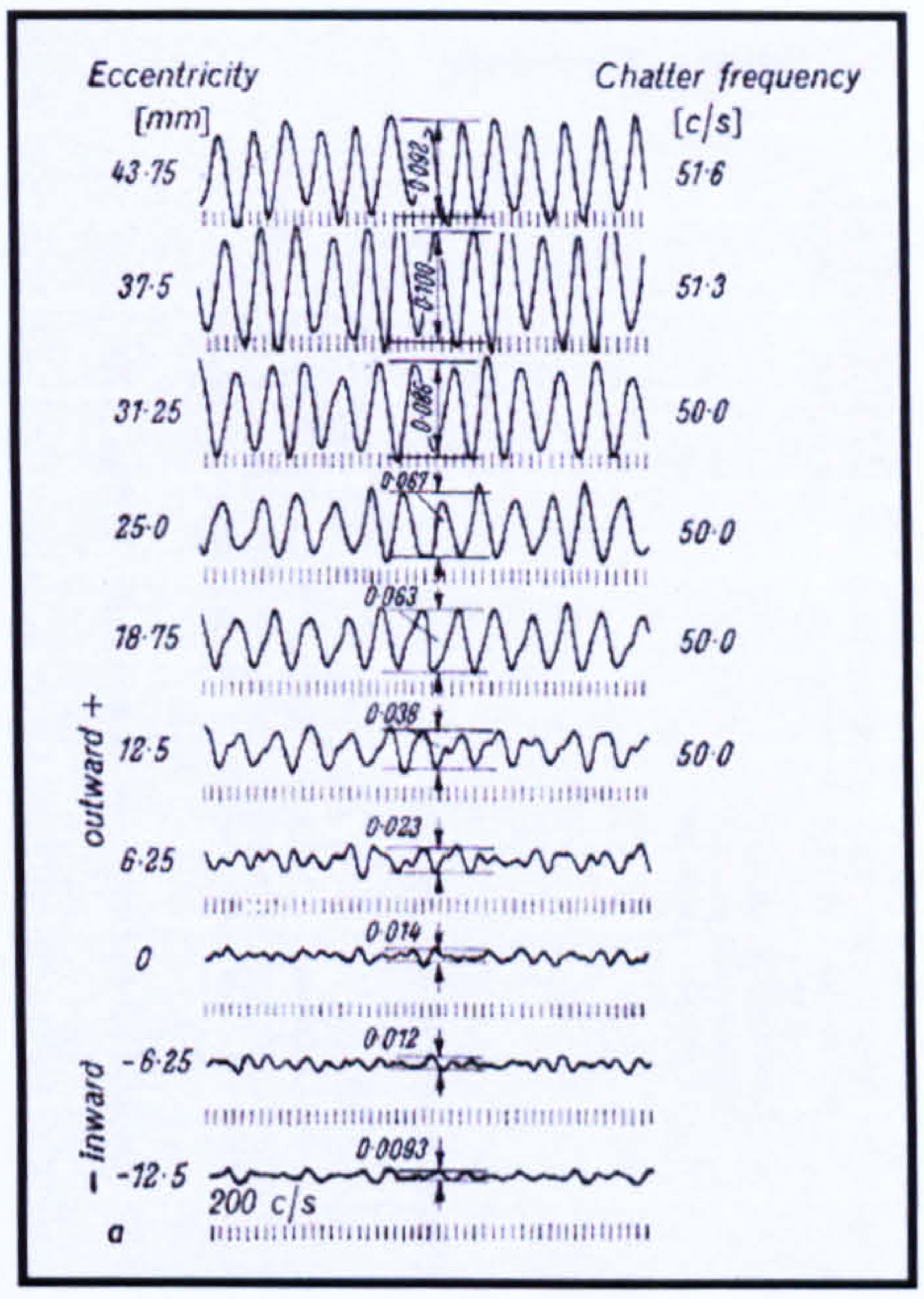

Figure 2.12:Chatter vibrations for various values of eccentricity [22]

From this it can be seen that the chatter amplitude increases, as the workpiece moves away from the central position towards the outer edge of the table, whilst the chatter vibrations assume a more or less harmonic character due to the fact that the machine structure vibrates at one of its natural modes. Shifting the work-piece towards the column has the opposite effect. The chatter amplitude varies in an approximately linear manner with eccentricity, as shown in figure 2.13.

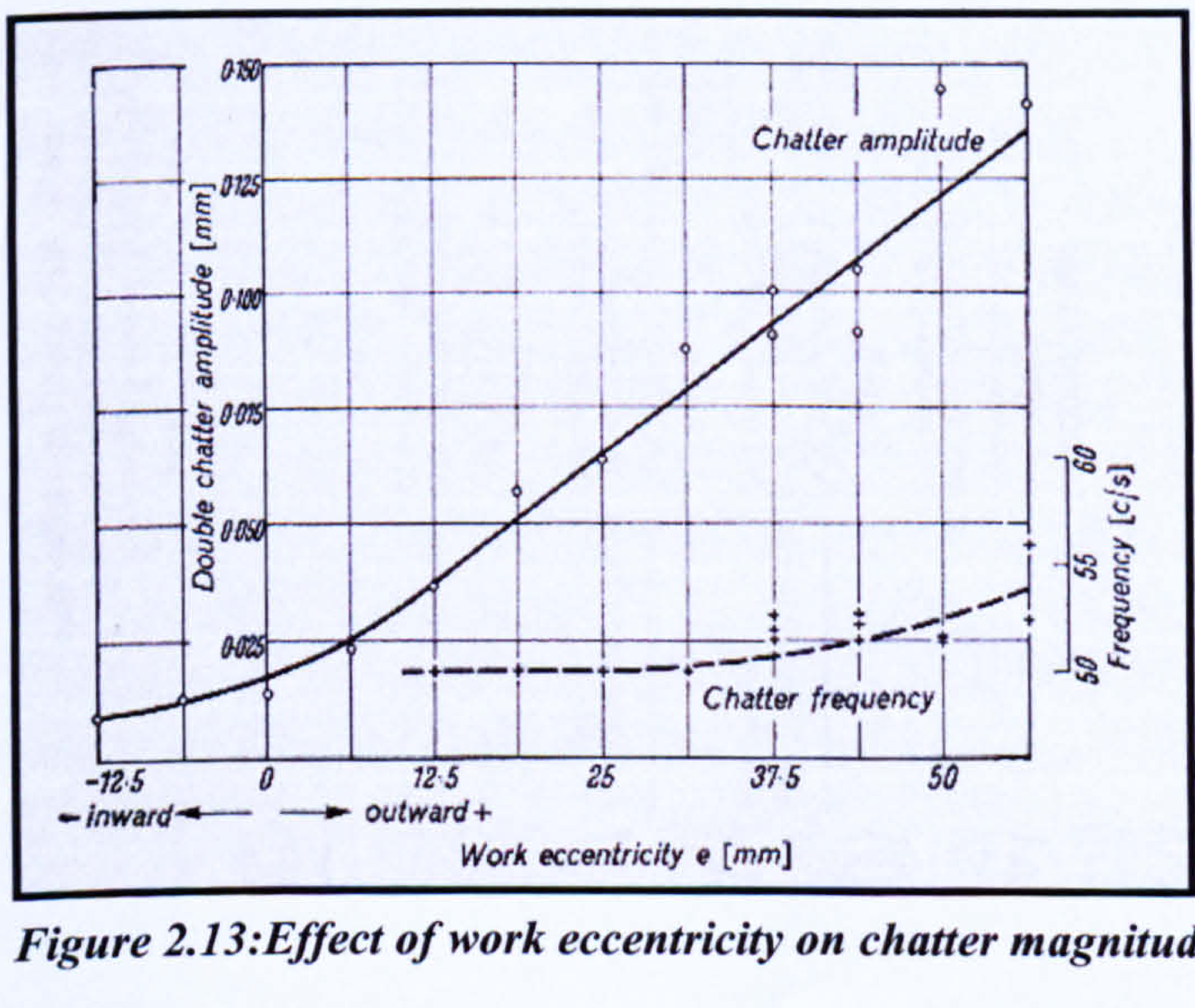

Figure 2.13:Effect of work eccentricity on chatter magnitude and frequency [22]

This figure also shows the variation in chatter frequency as a function of workpiece eccentricity. With increasing eccentricity, the chatter frequency also increases.

Another very practical approach is referred to as tool tuning [40]. This is simply a method that adjusts the dynamics of the spindle/tool/workpiece structure using the overhang of the tool as the control parameter, which is easy accessible. The tool overhang is defined as the length by which the tool extends from the holder. Collet and shrink fit holders (among others) offer some freedom to vary the overhang length. This variable can allow greater productivity for high speed machining. Schmitz and Davis [41] with the aid of the University of Florida's machine tool research centre has developed a method of systematically tuning the machining process using the overhang effect. To determine the optimal tool overhang for a given application a "tap test", as described earlier, is performed on the tool holder first, with a second test carried out on the tool clamped in the tool holder. Having evaluated the stiffness and damping from the frequency response functions this can be modelled mathematically. With this information the right length of tool overhang can be obtained through simulation in order to take deep cuts without chatter near the spindle maximum speed. This method has been validated through experimental testing. The tests have shown that a shorter tool is usually more stable but in some cases stability improvement can come from a longer tool. The disadvantage again is that workshops normally do not have the expertise or instrumentation required to do "tap testing" or simulating structural dynamics.

Choudhury and Mathew [42], have investigated another very popular approach to controlling machine tool vibration through process control. In order to suppress vibration, the tooth spacing is a very useful parameter for achieving higher productivity. The purpose of their work was to design a face mill cutter with an odd number of teeth, which are unevenly spaced along the cutter periphery. They obtained the optimum spacing by minimising the total power and relative cutter-work-piece vibrations with the aid of a standard optimisation program. The new face mill cutter with uneven teeth spacing has been designed and fabricated based on a standard SANDVIK mill. The newly designed cutter has reduced vibration significantly within a certain range of cutting conditions. The reduction is caused by uneven tooth impacts and hence the avoidance of excitation at the machines natural frequencies.

2.3 Passive vibration control

Initially vibration control was accomplished using passive elements. This means that no power source was used to add energy to the system. The level of vibration was controlled by making the mechanical system stiffer or by adding damping. But this is usually very difficult to achieve on existing machine tools without major changes to the structure of the whole machine.

Batrakov and Tikhomirov [43] used a tool holder made from powder material with increased porosity that possessed vibration-damping properties. They were able to reduce the vibration by 50% compared to vibrations observed during operation without the vibration absorbing material. It should be noted that the frequency ranges are not mentioned in their paper. However it is well known that one of the major limitations of applying passive vibration control is the limitation of the effectiveness in narrow bandwidths. Also the tool holder needs high rigidity in order to withstand the static cutting forces. They did not mention whether that (high rigidity) was still the case after the integration of the new tool holder. Also the new tool holder will not have the same thermal conductivity as a standard steel type, and therefore will not be able to dissipate the thermal energy of the cutting process as a standard tool holder can.

On existing machine tools, the integration of additional damping in the vibratory system especially in the form of a damped vibration absorber, can help to prevent self-excited vibrations.

Successful use has been reported in boring, milling and turning operations [44,45]. These vibration absorbers introduce additional damping into the vibratory system, which reduces the magnitude of the resonant peak. Figure 2.14 shows the realisation of this technique on a turning tool, boring bar and horizontal-milling machine.

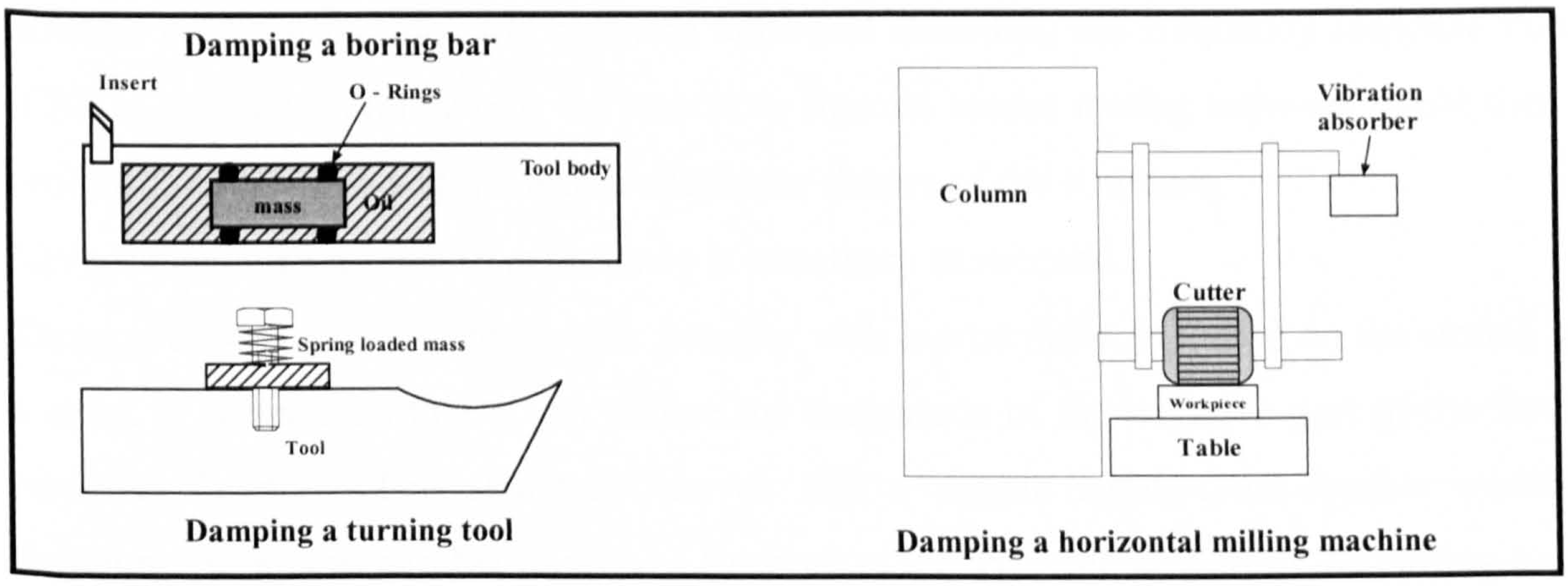

Figure 2.14:Passive vibration control using damping absorbers on various tool configurations

In the case of turning, the damping effect is realised through a spring-loaded mass, which dissipates the energy of the vibrating tool.

Hardwick [45] has also shown that increasing the damping, next to increasing the stiffness, has the greatest effect on reducing or eliminating the effects of vibrations on machine tools.

Hardwick and his team have developed much expertise over many years in "trouble shooting" unstable machine tools, by using a specially designed tuned vibration absorber in order to introduce damping into machine tool structures (figure 2.15).

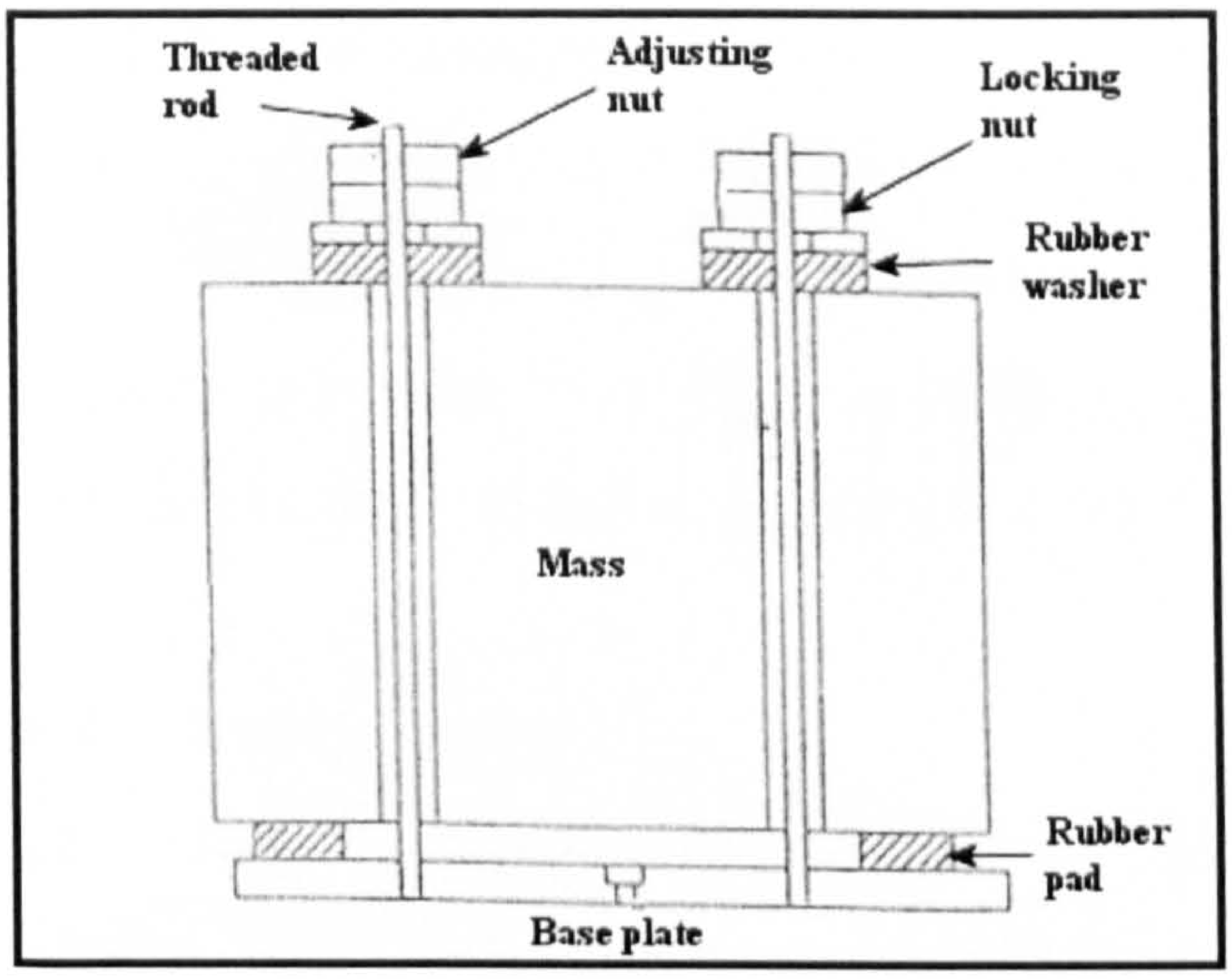

Figure 2.15: The commercial tuned damper [45]

The system consists of spring elements (rubber feet), which are adjustable so that the frequency can be tuned to match the problematic modal frequency of the primary machine tool structure.

Hardwick recommended that the secondary mass of the absorber must be at least 10% of the primary structure and located at the point of maximum vibration amplitude. The position of maximum vibration amplitude was determined by simulating chatter using a hydraulic actuator between the tool and machine table and recording the frequency response functions (FRF's) at many points along the structure. Special modal testing software could then post-process the FRF data and determine the mode shapes of the structure.

Nevertheless a great deal of experience is necessary to succeed.

Tarng et al [46], use a piezo-electric actuator with inertia mass, mounted on the cutting tool of a lathe. It is tuned so that it can reduce the magnitude of the negative part of the frequency response function. The actuator behaves like a simple spring-mass-damper system and therefore introduces another degree of freedom to the dynamic system of the cutting tool. The initial frequency response function of the cutting tool is recorded using an accelerometer mounted on the cutting tool and a PC data acquisition system records the data. The initial mass of the actuator acts as a tuned vibration absorber and the natural frequency of the system can be adjusted by adjusting the inertia mass. It is claimed that experimental cutting tests have shown that the stability was increased by six times using this technique.

The first major disadvantage of passive control is that if the structural parameters change, then the damper, which is designed for a particular frequency, needs re-tuning, to suit the new dynamics. Secondly the additional mass, which depends on the machine tool structure, can be significant and stands in opposition to the machine tool specifications (higher speeds lighter structure with maximum rigidity). Thirdly, the tool fixtures need to have high rigidity, which makes it difficult to add meaningful passive damping elements to the tool system. As will be shown in the next chapter, active elements are even stiffer than the steel structure of a machine tool. The only major advantage of passive vibration control, compared to active control, is that it is easy to implement, low cost and does not need external energy.

2.4 Active Control

In the past traditional, "passive" approaches, whether process control or passive vibration control, have been used to prevent chatter. Having applied these techniques to their full practical extent with limited success, the machine tool industry is now looking forward to active solutions. This becomes more and more important as recent advances in miniature actuators (smart-materials), sensors and digital systems have been made.

Active vibration control is an alternative way to alter the dynamics of a dynamic system. In active control systems actuators, sensors, computers and software replace the mechanical components to provide the desired dynamic response characteristics. Effectively, secondary vibrations are introduced into the machine tool structure by secondary force actuators. These are driven in such a way that the generated secondary vibrations interface with the tool vibration induced by the cutting process (primary vibrations). An effective control algorithm is able to modify the structural response of the tool in real time, and thereby reducing the vibrations.

Examples of active systems to alter the dynamics during machining are rare. In general, most of the work reported addresses turning operations rather then milling.

2.5 Active control in turning and boring

In turning applications a single-point-cutting tool is continuously in contact with the work-piece, and the direction of both the main and the thrust cutting force components are fixed with respect to the structure. The formulation of the stability problem therefore results in a characteristic equation with constant coefficients and time delays, which can be studied using well-known control theory.

J. Rojas, and C. Liang [47] use magnetostrictive (Terfenol-D) actuators with an industrial horizontal lathe. This initial research successfully showed the feasibility of active machine tool vibration using readily available sensors, actuators and control algorithms. The sensor (accelerometer) and actuator are attached to the boring bar. Figure 2.16 shows the experimental set up.

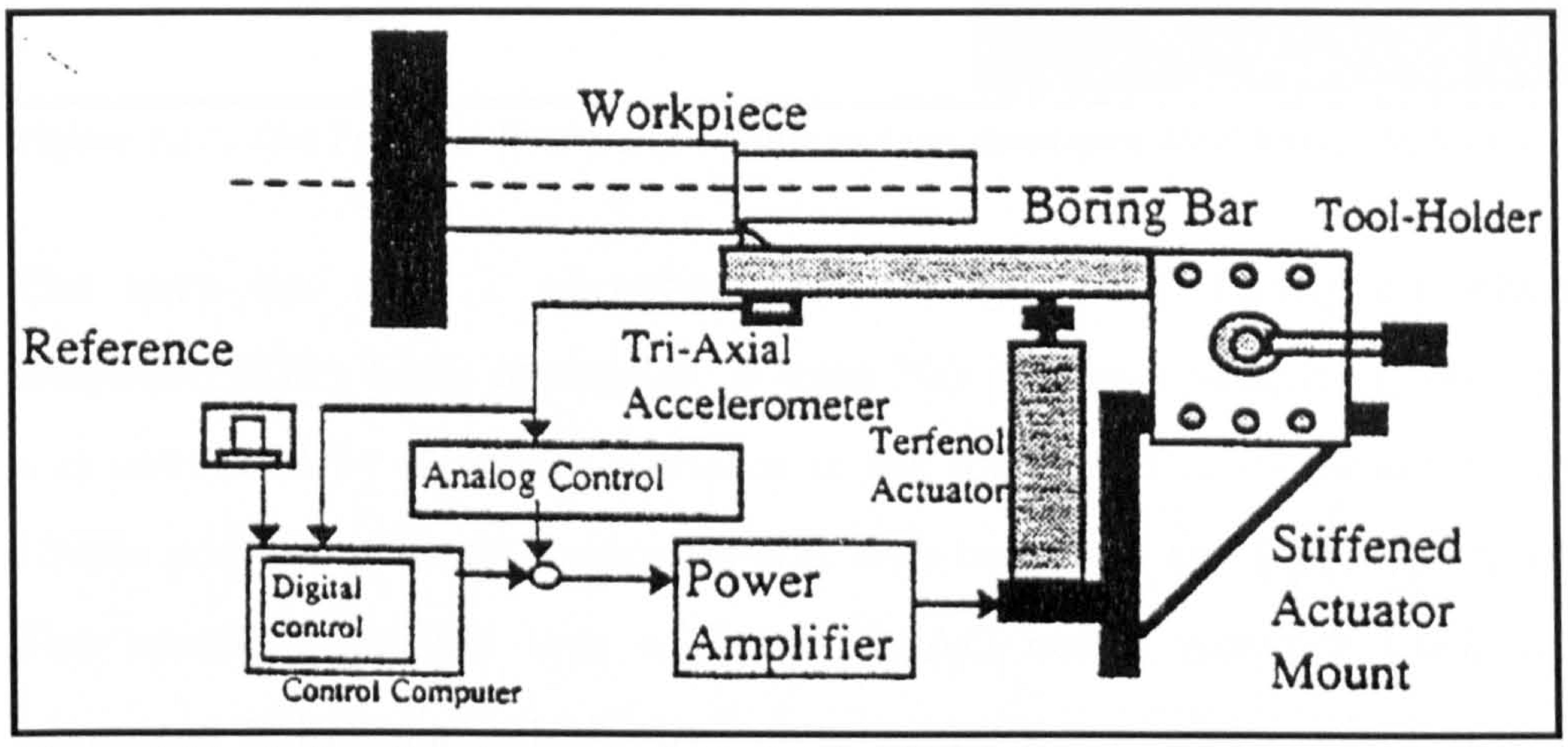

Figure 2.16: Active vibration control of a Boring Bar [47]

Extensive vibration testing has been conducted to understand the system dynamics. This includes the measurement of the transfer functions of the boring bar both with and without contact with the work-piece. To do this the actuator was used as an exciter and the accelerometer as a sensor to identify the structural system to be controlled. The boring bar system was mathematically modelled as a three-degree of freedom system (lumped parameter model of a cantilever beam). Two different controllers (analogue PI controller and digital Least Mean Squares (LMS) adaptive filter) were tested and the results showed that machine tool vibration can be significantly reduced using active vibration control.

The work done by Pan et al [48] is a continuation of this. They also use a customised magnetostrictive alloy terfenol-D actuator. The same test rig as the previous one has also been used, where the actuator was attached to the boring bar. This paper also described the digital controller itself. It is a customised powerful Digital Signal Processor board (DSP) developed by Pan [49]. The mother- and all of the daughter boards have an independent TMS320C31 processor since the system was designed for maximum processing power (figure 2.17). An industrial collaborator built and supplied several Terfenol-D actuators in order to suit the application (figure 2.17)

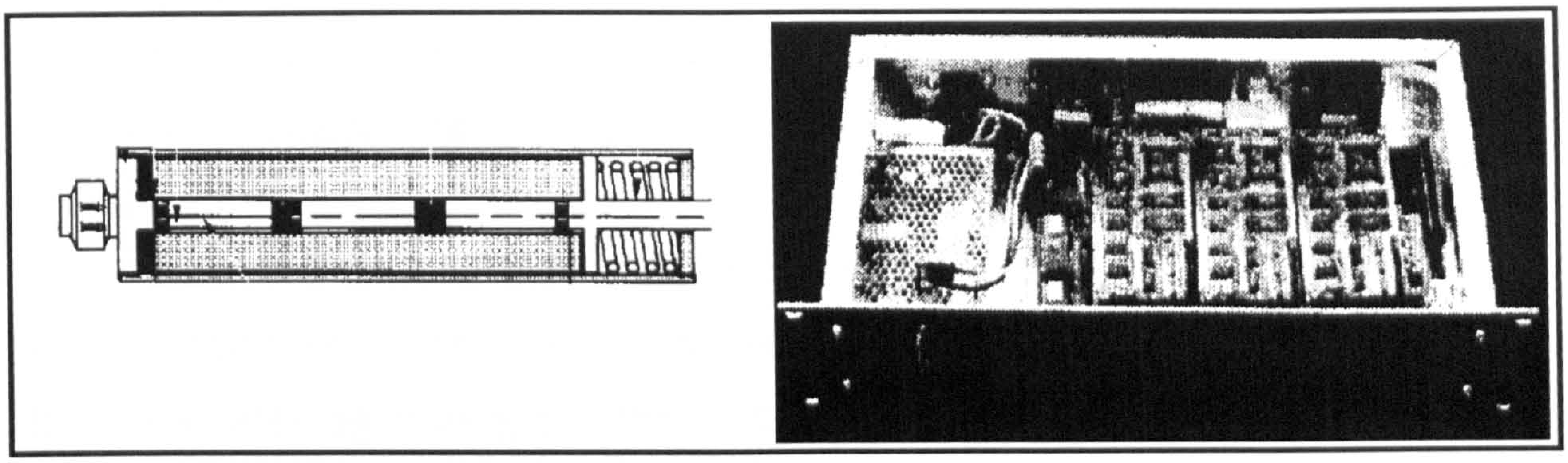

Figure 2.17: The Terfenol-D actuator (right) and the developed DSP board (left) [48]

The team has used 2 advanced control algorithms. Firstly an adaptive Finite Impulse Response (FIR) LMS controller. It uses 300 previous samples (300 tap FIR filter). Chatter was simulated by attaching a shaker to the tool tip. The harmonic excitation frequency was 180Hz and the adaptive controller was able to reduce the forced vibration by about 70-80%. The second algorithm was a fuzzy CMAC neural network [48], which has the major advantage of being able to "learn" about non-linear systems. It's disadvantage is that it needs a lot of computing power to calculate the new output sample within the sampling time. Even with the very fast DSP board this controller was just able to reduce the forced vibrations by about 50%. This was due to the fact that they could only use 5 previous samples in order to predict the next controller output sample (it was 300 samples for the FIR LMS controller). The shaker test was the only test conducted (no cutting tests) and future work aimed to find a more powerful DSP board in order to implement the potential fuzzy CMAC algorithm.

O'Reagan at al, [50], have applied active structural control on a Vertical Turning Lathe. The study has proved that active damping can reduce regenerative chatter. An actuator (active damper) attached to the end of the ram introduced additional vibration, which counteracted the relative vibration between tool and work-piece. These vibrations were sensed by an accelerometer on the ram and fed to the controller. They used an active damper control concept (refer to chapter 6.8). The sensor signal was integrated and multiplied with a pre-defined gain and then passed through a bandpass filter, which determined the main chatter frequency. The modified velocity signal then drove the actuator on the ram, providing the secondary force. Again a digital signal processor was used as processing hardware. The system reduced the surface roughness by approximately 60%, but because of their control scheme (bandpass-filter and gain) it needed tuning for individual machines.

General Dynamics [51], group members Kennametal and machine tool builder Cincinnati, have developed a prototype system, which can be used in real machine tool environments.

They designed an active boring bar system. This consists of an active clamp, (which is lathe-mountable) instrument bar and electronics. The clamp supports the boring bar and houses piezoelectric actuator motors, which physically move the bar in opposition to cutting vibrations. An accelerometer is embedded into the boring bar and digital control functions, based on the principles of adaptive filters, are achieved using 2 DSPs (figure 2.18). The device is capable of extending the existing chatter threshold up to 400 percent for deep boring applications while maintaining precision surface finish.

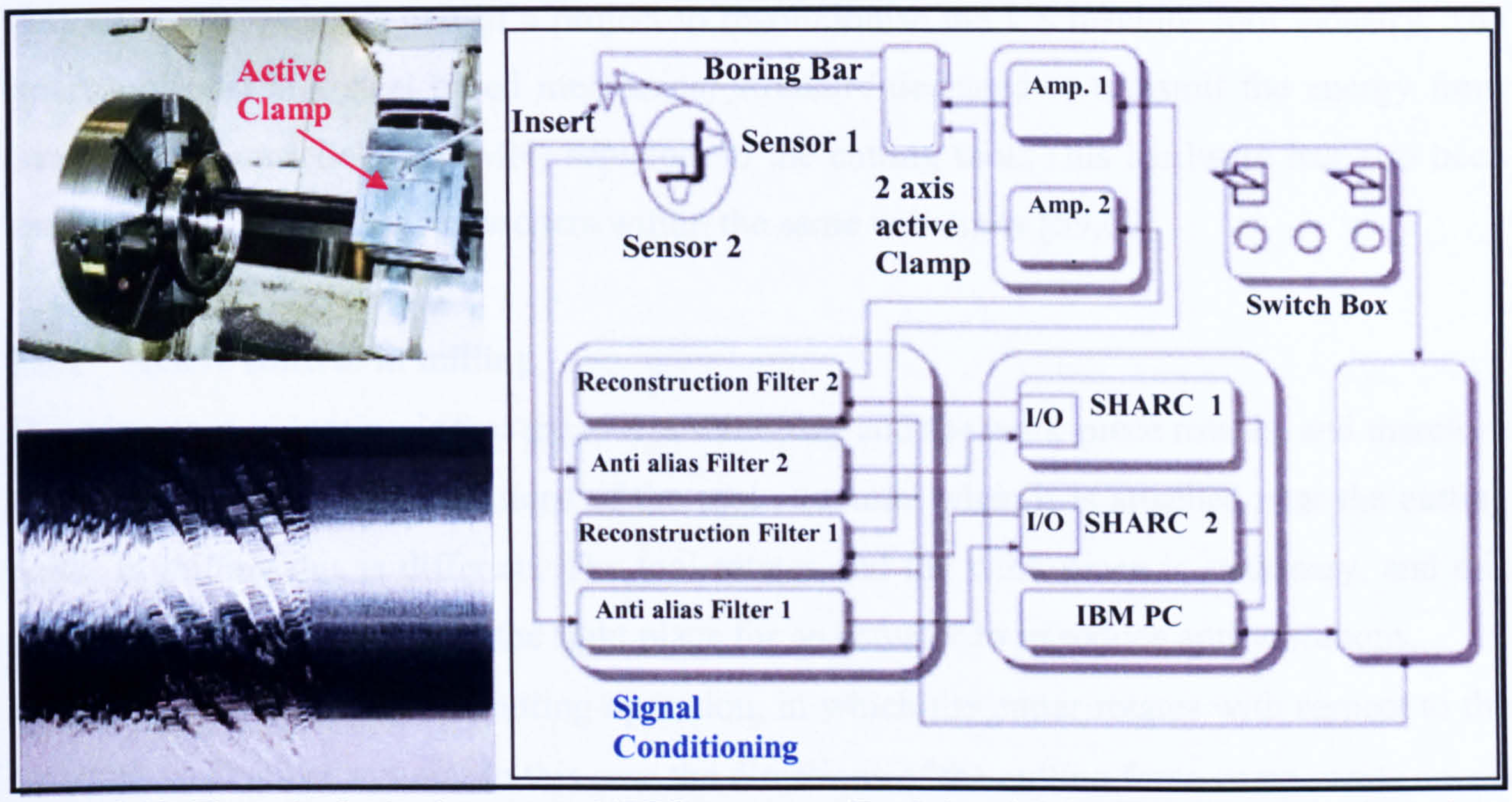

Figure 2.18: The active boring bar system (ABBS) prototype (Top left and right).The improvement in surface finish (Bottom left) [51]

Håkansson et al [52,53], have also developed an active tool holder system. The tool holder is constructed with embedded piezo ceramic actuators. They use an adaptive FIR controller based on the Filtered-X LMS algorithm [54] and FIR filters to model the dynamics of the actuator (secondary path), which was an initial off-line identification procedure. Even though their system was non-linear (hysteresis of the piezo actuators) it was still able to reduce the tool vibration of an unstable cut up to 35dB at 1.7kHz and 30dB at 3.1 kHz. This went along with a significant improvement in the surface finish and reduction of acoustic noise. This work has led to the development of a system called Acticut™. This was designed by Active Control Sweden AB [55] and its prototype is currently undergoing more testing in a real machine tool environment.

A different approach of active damping was achieved by Olgac and Holm-Hansen [56]. The active damping of a spring-mass-damper was achieved with a technique called a delayed resonator. The idea was to select a gain and time delay in real time, so that the two dominating roots of the vibrating system lie on the imaginary axis while the rest were in the left half of the s-plane. This pole-placement design was chosen so that the absorber of the spring-mass-damper system displayed 180 degrees out of phase with a harmonic disturbance input. This concept of 180 degrees out of phase was also used by Dold [57]. The downside of this approach is the assumption that the disturbance is harmonic. A smart tool post structure [58] was used, which is part of a project to revolutionise the US machine tool industry. The smart tool post is a steel based mechanical structure designed to transmit the energy from Lead Magnesium Niobate (PMN) actuators to the cutting tool. This hardware has also been used by a variety of other researchers within the same university [59,60].

2.5.1 Active control in milling

The advantage in turning is that the tool is stationary and the work-piece rotates, and therefore an actuator can suppress vibrations of the tool structure, when it is attached near the cutting point. In milling this is different. The tool rotates and the work-piece is stationary, and this makes it more difficult to find the right place for an actuator to introduce anti-vibrations.
Also milling is a multi-point cutting operation, in which the cutter rotates with respect to the structure-work-piece system. In this case the directions of the cutting force components are no longer fixed and rotate with respect to the structural coordinate system. This makes it far more difficult to control than the turning operations, where the cutting force vector is fixed. Because of this there is only one known work on the subject, where an industrial team has tackled the problem with very promising results.
Jang and Tarng [61] have studied active vibration control on a cutting tool. However they did not describe whether their system was for milling or turning operations since the objective of their work was a systematic approach for the analysis of the piezoelectric actuator to act as an active vibration damper on a cutting tool. The actuator was attached to a cutting tool and a modal shaker used to produce a harmonic disturbance (figure 2.19). The vibration was sensed by an accelerometer and fed back via the amplifier to the piezo actuator.
It is believed that the location of sensor actuator has been tuned in order to get the right phase to damp the vibration of the primary force of the shaker. The forced vibrations at 737Hz have been reduced by abut 90% (figure 2.19).

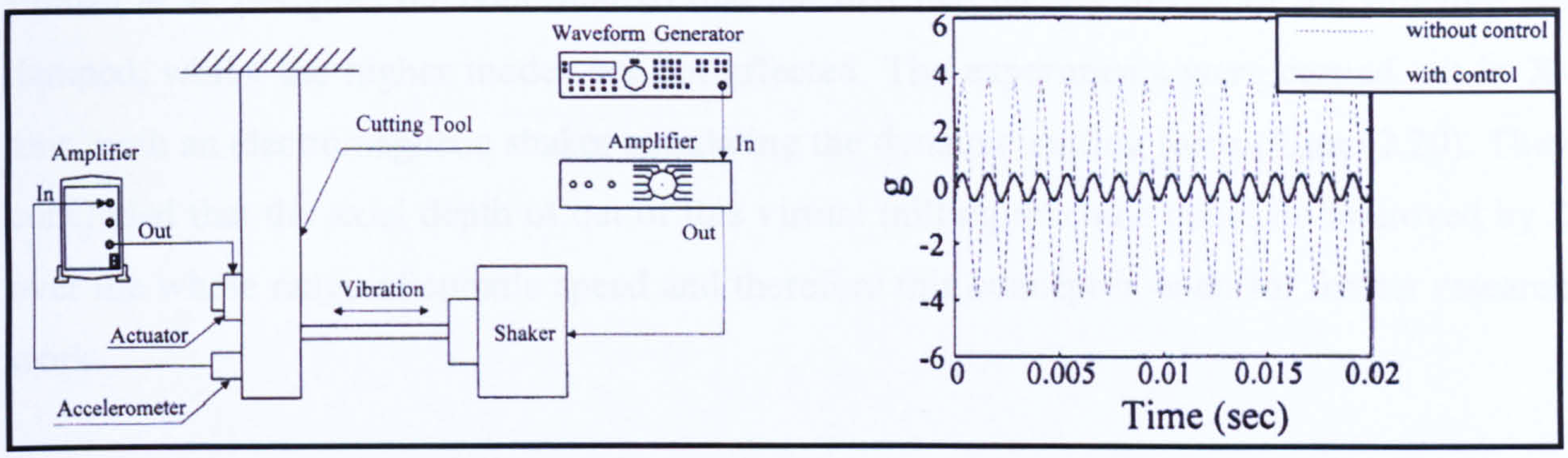

Figure 2.19:Schematic diagram of the experimental set up (right) and forced vibration response with and without active vibration control (right) [61]

This work has not been more than a general case study for active vibration control for machine tools. No cutting tests have been performed, since the system was not designed to do so. Also the principle only has been proven for forced harmonic excitation but not for a more complex vibration under cutting conditions.

A similar approach was taken by Ehman et al [62]. Their approach was to show that piezo-electric actuators can improve the dynamics of milling machines. The laboratory results show the potential of this approach and have led to further research work on real milling machines. The machine tool structure was a gantry robot type and since their structure is not very stiff it is very sensitive to self-excited vibrations. It was therefore a good vehicle to show the potential of active vibration control. They used an μ-synthesis control algorithm [63], implemented in a digital signal processor, DSP, board. Figure 2.20 shows the laboratory model of the gantry milling machine. It was designed to have a very flexible structure in order to show the principle of active vibration control. Figure 2.20 shows the embedded piezo actuators.

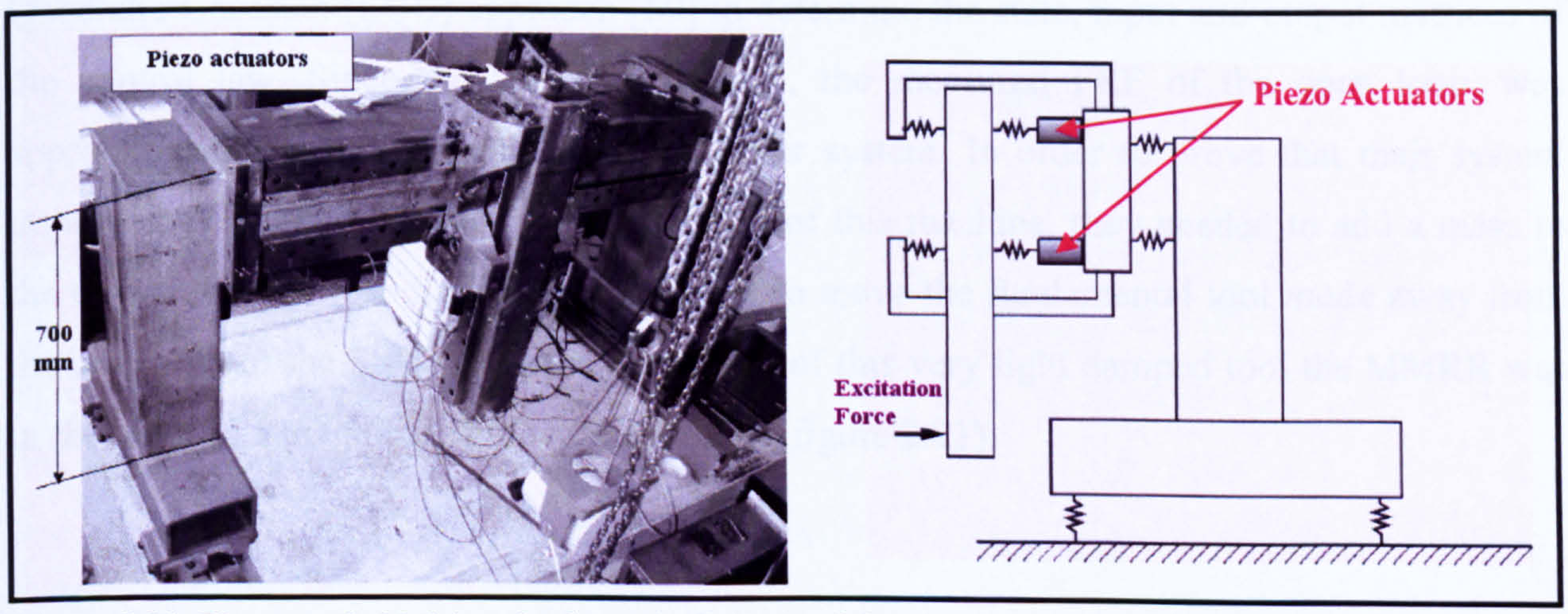

Figure 2.20: Photograph (right) and schematic diagram of the gantry prototype (left) including actuators [62]

Ehman et al, designed the controller so that the first two natural modes of the structure are damped, whilst the higher modes are not affected. The experiments were carried out in X-axis, with an electromagnetic shaker simulating the dynamic cutting force (figure 2.20). They concluded that the axial depth of cut of this virtual milling machine could be improved by 2 over the whole range of spindle speed and therefore this concept is open for further research work.

Recently Dohner et al [64] and Lauffer et al [65], developed an active feedback compensation system for Ingersoll's Horizontal Octahedral Hexapod Machine (HOHM) used for machining aeroplane structures. The team, lead by Lockheed Martin Space Systems Co., identified, by using a Finite Element model, that the most flexible structure was the spindle unit with its tool, and made the assumption that the rest of the structure is rigid for this type of milling machine [66]. Vibration in the two lateral directions is picked up at the root of the rotating tool by strain gauge sensors. The power is supplied by magnetic coupling between the stationary and rotating part. One of their collaborators went on to develop a telemetry system, which was used to transmit the strain data to the stationary receivers. In order to translate the data from the rotating coordinate system to the stationary coordinate system the angular position was measured using a Heidenhain encoder [67]. Other, stationary chatter sensor's have been tested, but these were not sensitive enough to pick up the tool dynamics [68]. The actuators were constructed using PMN-based electrostrictive ceramics. The hardware, consists of the spindle, the tool holder, the cartridge, the actuators and the telemetry system were given a special name – the Smart Spindle Unit (SSU) – figure 2.21.

The digital state-space controller was designed by another collaborator and used a Linear Quadratic Gaussian (LQG) approach [69] to determine the state, input and output matrices of the control law. Since the tool was flexible, the measured FRF of the open loop, was approximated and modelled by a second order system. In order to prove that their system improves the Maximum Metal Removal Rate of this machine, they needed to add a mass to the end of the tool (see figure 2.21), in order to move the fundamental tool mode away from the dynamics of the SSU. After the "creation" of this very light damped tool the MMRR was in the order of a magnitude higher then before (figure 2.21).

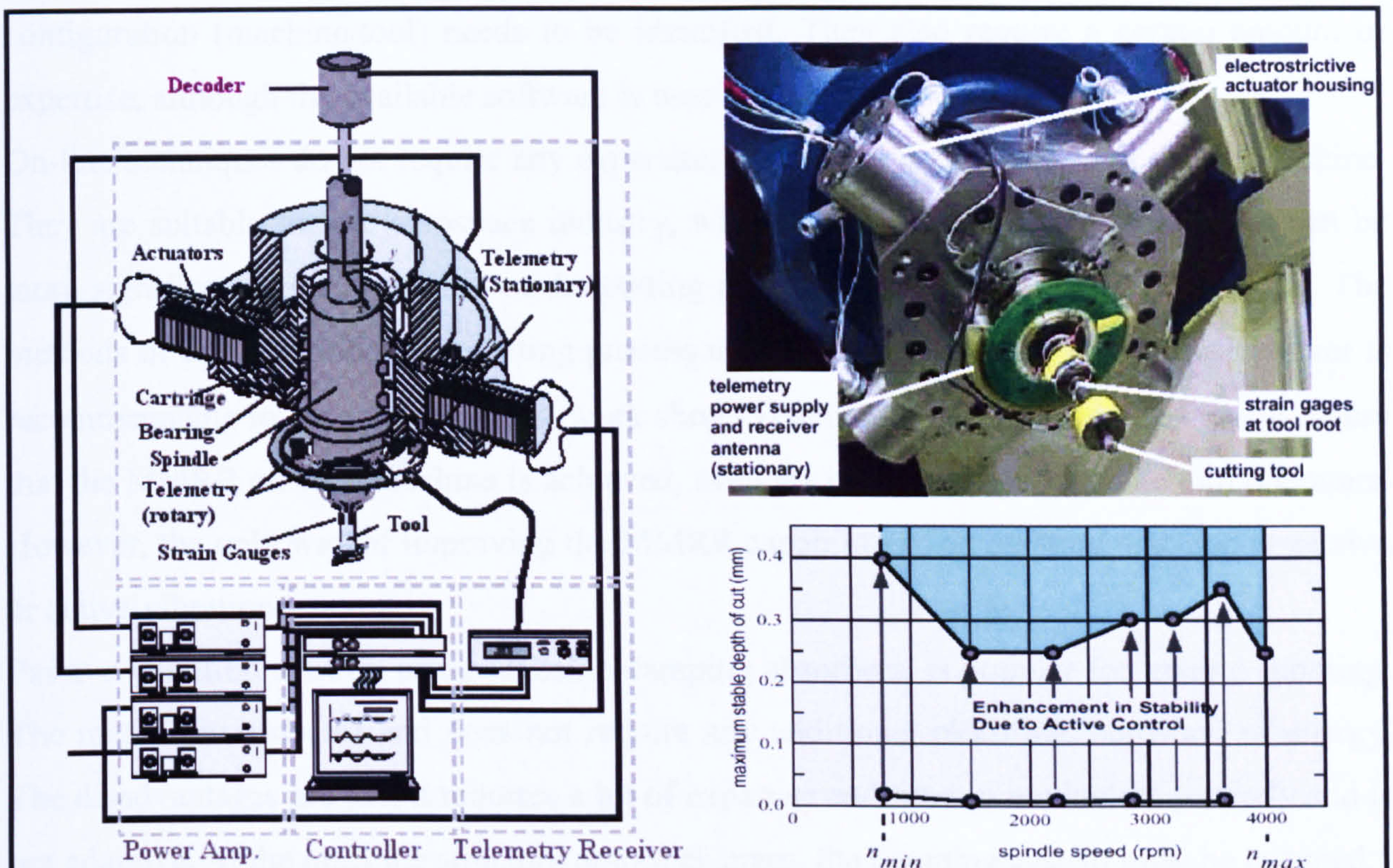

Figure 2.21: Schematic diagram (left) and photograph of the SSU (top right). Stability lobes for the machine with controller on and off (bottom left)

The team concluded that active control of milling machines using a standard cutting tool is possible. However better control and design methods are required to produce a working solution in the absence of any added mass to the cutting tool. For the future, the team will pay particular attention to the development of control algorithms that allow adaptability [64].

2.6 Summary of the literature review

It has been seen that chatter instabilities force vibration energy into the tool to eject the insert from its path. At the ejection the forces on the tool are relieved and bounce back into the metal. This cyclic process results in vibration in the machine and poor surface finish. Chatter therefore sets a limit to the productive capability of the machine and tool. Since the dynamics of machine tools are complex, each individual machine is expected to behave differently. Proper design and operation of the machine tool can ensure that the maximum metal removal rate of each machine is optimised.

Process control, especially the variation of spindle speed, is a common technique used to optimise the machining process, but it does not improve the dynamics of the system and therefore its MMRR capability. Furthermore, off-line techniques used to calculate the best spindle speed are usually time consuming, since the dynamic system of each machine tool configuration (machine/tool) needs to be identified. They also require a certain amount of expertise, although the available software is user-friendly.

On-line techniques do not require any expertise, and do not need down-time on the machine. They are suitable for the aerospace industry, where the dynamics of the work-piece can be more significant for the stability of the cutting process than the machine tool structure. The methods of optimisation of the cutting process using a process control technique, however is recommendable to each machine tool work shop. Systems like the Harmonizer™, will assure that the MMRR on each machine is achieved, even for inexperienced machine tool operators. However, the only way of improving the MMRR capability of an existing machine is passive or active vibration control.

Passive vibration control, using tuneable damping absorbers, is popular for trouble shooting. The method is low-cost and does not require any additional electronic hardware or energy. The disadvantages are that it requires a lot of expertise and time to implement properly and is not adaptive. If the machine structure or tool changes, the damping system must be re-tuned. However, since passive techniques have reached their full potential, there seems to be an increasing tendency not just for the machine tool industry, to develop new active control systems. This is even more valid since significant improvements in the field of smart materials can be expected over the next years [70]. Active vibration control can be adaptive depending on the controller as shown by General Dynamics [51] and Active Control Sweden AB [55] and can also work for low frequencies. Since the technique is relatively new, there is a high potential for research. But much of the work reported to date has focused on turning and boring operations because of the relative simplicity of these processes. It seems there is no system, or even a prototype available, which demonstrates active vibration control for milling machines using standard cutting tools.

2.7 Novelty of the research project

Active and passive vibration control is the only way to increase the dynamic stiffness and damping of a machine tool without major changes to the existing machine. In the literature, chatter control of a machine tool has really been process control, and not vibration control. Active vibration control has a lot of potential due to recent advances in material technology. The relatively few examples of active control on machine tools have been in turning not in milling. Most the control algorithms used, are also not adaptive and therefore need to be redesigned when the dynamics of the system (machine and tool) change.

Therefore the novelties of this research project are:

- A demonstration system for 2 axis active control on a standard milling machine (vertical machining centre).
- The designed active control system is universal and portable in that it can be used for any vertical machining centre. This also assures that no major changes to each machine have to be made.
- The system described in this work uses "off the shelf" actuators, which are lower cost than customised types. It also uses a new type of silicon accelerometer (MEM technology), which is less expensive than traditional piezo types.
- The active vibration device can measure cutting forces in 2 directions and measure the displacement directly. It therefore serves as a "built in" table dynamometer.
- The control algorithms are adaptive in order to follow any changes in the machine tool dynamics. The proposed algorithm has not been used in machine tool applications so far.
- The active system is able to introduce defined vibration into the cutting process in order to achieve a certain surface waviness, this may be used for the automotive industries for machining the parts of a combustion chamber, where the exact shape of the surface is crucial.
- The system also introduces another 2 degrees of freedom to the machine tool for very accurate tool positioning. The system is more direct and accurate than the existing ballscrew drive systems. It therefore also can be used to compensate for static cutting forces, since it measures the cutting forces and tool displacement.
- The adaptive algorithms and estimators allow identification and modelling of machine tool structures or the cutting process off line. This will lead to digital simulation systems of machine tool structures.

Chapter 3

Mechanics of metal cutting

3.1 Introduction

The mechanics of metal cutting has been studied for many years. The process itself is complex, due to the many factors that influence it. This chapter takes a practical approach to explaining the fundamentals of the cutting process and the parameters which affect vibration. The static and dynamic cutting forces for milling and turning are derived, and a method of predicting and estimating the static cutting forces and power requirements for turning and milling using simplified formulas is provided. These formulas are important since they will later be used for the design of the active work-piece holder (chapter 7). The dynamics of the cutting process and their effect on chatter vibrations will also be explained with a stability analysis to derive the stability lobes using traditional control theory in the frequency domain. With this knowledge it will be possible to develop the different approach taken in this project to model machine tool chatter vibrations in the digital domain.

3.2 The chip formation

Cutting operations are often referred to as "chip removing" and represent the largest class of manufacturing activities in production engineering. The most common cutting operations are:

- Turning
- Milling
- Drilling
- Boring
- Grinding

Normally cutting processes are those in which soft bodies are cut by a tool such as a knife. The wedge shaped tool is forced symmetrically into the body having a very small included or wedge angle of the tool edges. If the tool is sharp, the body may be cut cleanly with very little force into two pieces, which is gently forced apart by the faces of the tool. Metal cutting is different. Metals and alloys are hard, so that no tool materials are strong enough to withstand the stresses they impose. If both faces, which form the tool edge, act to force apart the two newly formed surfaces, very high stresses are imposed and heat is generated so that both tool and surfaces are damaged. Because of this, it is necessary for a metal cutting tool to take the form of a large angled wedge (normally over 60°), which is driven asymmetrically into the work material to remove a thin layer from a thicker body, (figure 3.1) [71].

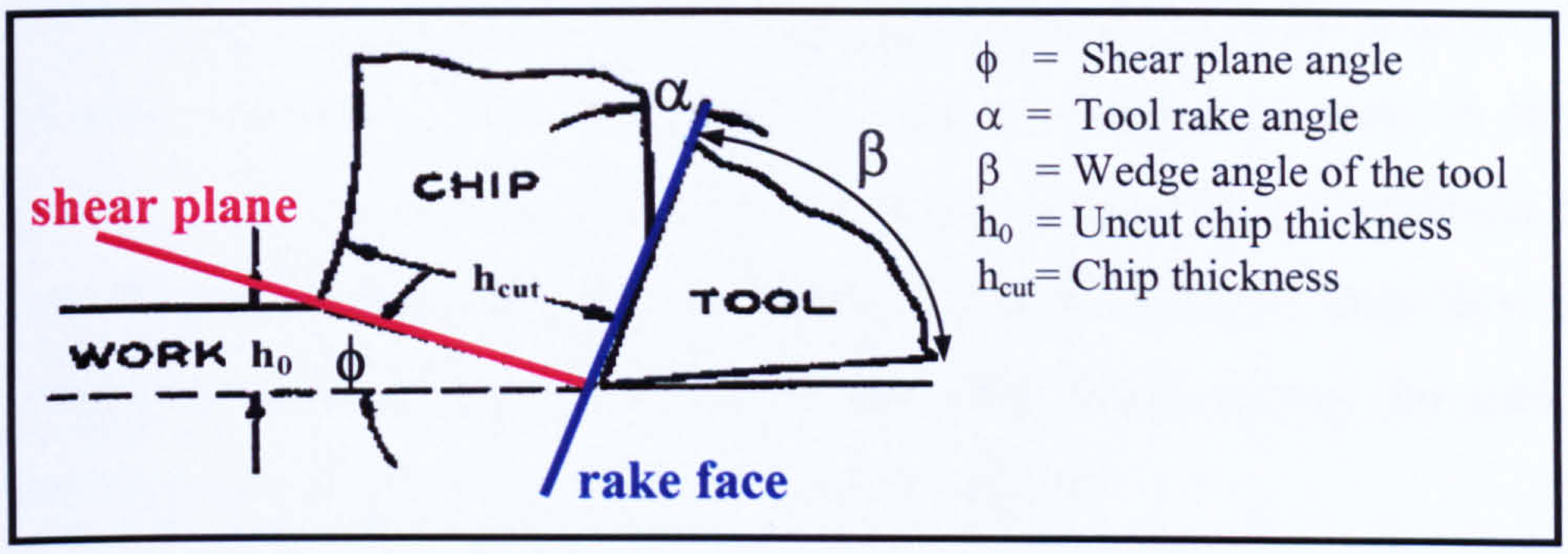

Figure 3.1: The metal cutting process

Although all metal cutting operations share the same principles of mechanics, their geometry and kinematics differ from each other. However, all different machining processes can be classified into two categories:

- Orthogonal cutting (2 dimensional)
- Oblique cutting (3 dimensional)

Orthogonal cutting is a special case of oblique cutting, where the tool is perpendicular to the cutting velocity vector (figure 3.2), and a metal chip with the width of cut b and thickness h, is sheared away form the work-piece.

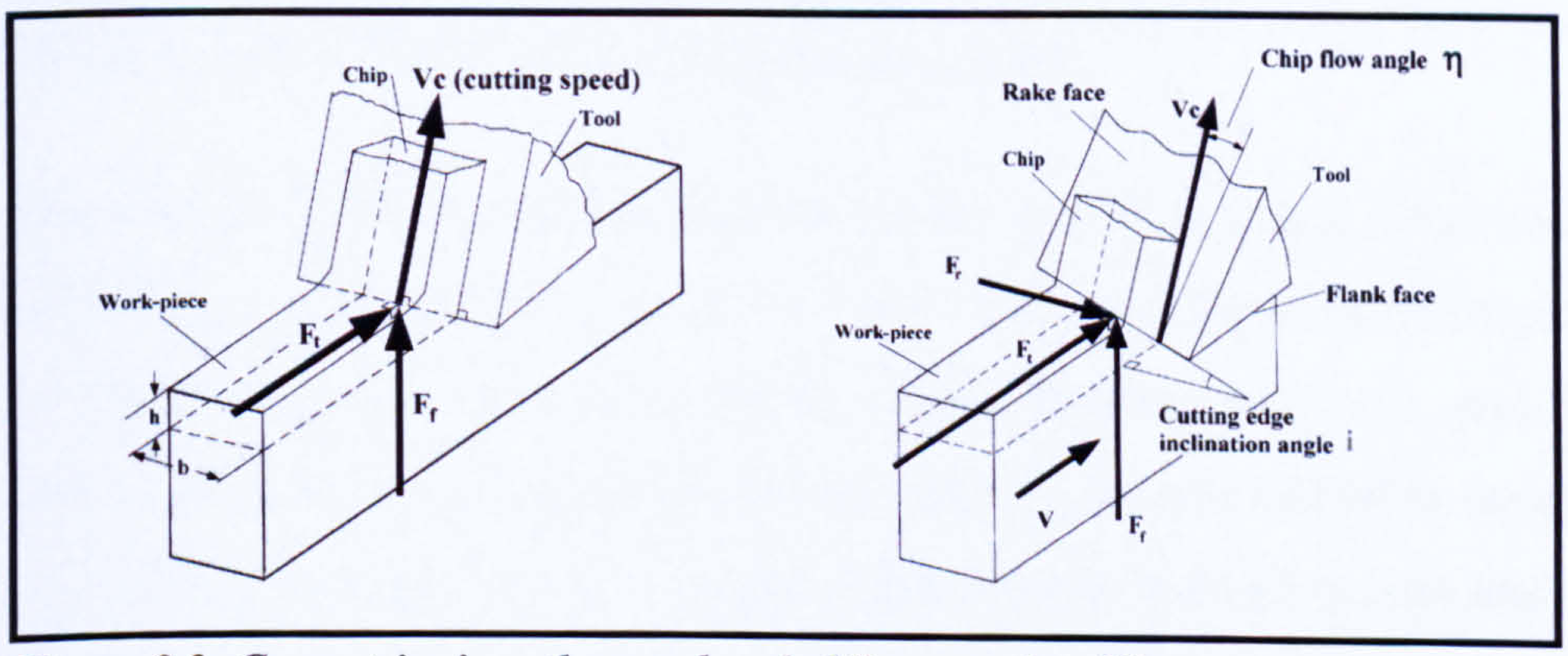

Figure 3.2: Geometries in orthogonal and oblique cutting [8]

Since in orthogonal cutting, the strain is uniform along the cutting edge, the cutting forces only act in the directions of the velocity and uncut chip thickness. These forces are called the tangential or primary cutting force forces (F_t) and feed or thrust forces (F_f). In oblique cutting the cutting edge is orientated with an inclination angle (i) and the third force acts in the radial direction (F_r). The resulting force vector is the geometric or vector sum of all three.

All machining processes involve the formation of chips by deforming the work material on the surface of the object being machined using the cutting tool. Because of the deformation on the surface, the quality of the cutting process can be judged not only by the surface itself but also by the type of chip. Therefore the type of chip formed is a direct indication of the surface quality. Chip formation is simplest when a continuous chip is formed using orthogonal cutting. In oblique cutting a single, straight cutting edge is inclined in the direction of tool travel. This inclination causes changes in the direction of chip flow up the face of the tool. When the cutting edge is inclined, the chip flows across the tool face with a sideways movement that produces a helical form of chip [4].

Metal cutting chips can be classified as three basic types [4,44]:

- Discontinuous
- Continuous
- Continuous chip with Built-up Edge (BUE)

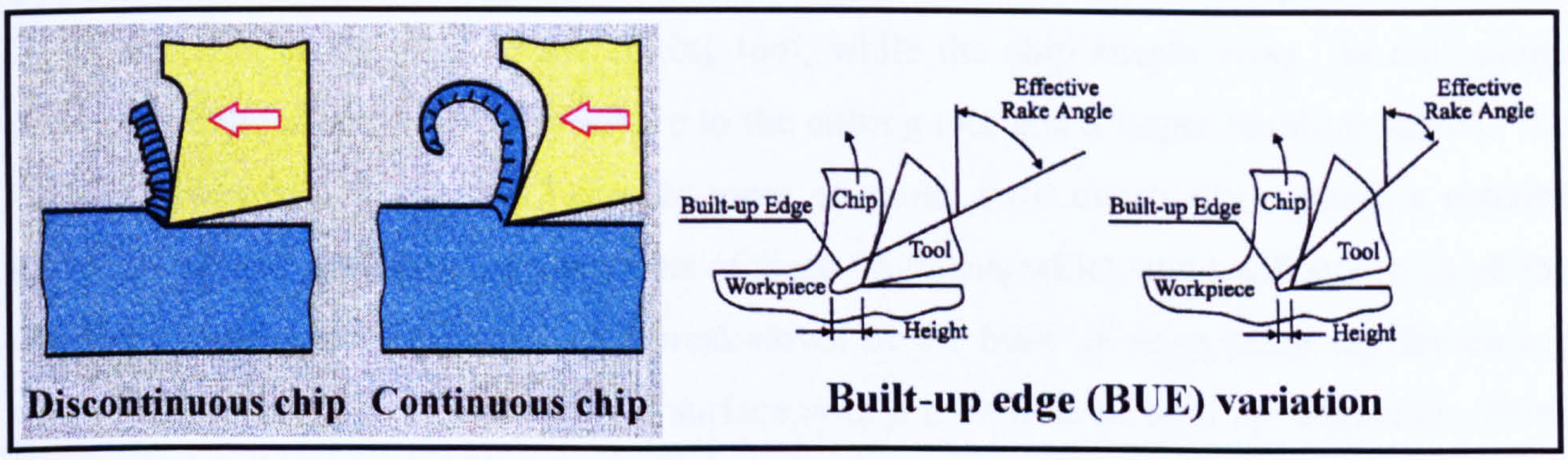

Figure 3.3: The 3 different types of chip formation [150]

Discontinuous or segmented chips are produced when brittle metal such as cast iron and hard bronze are cut or when some ductile metals are cut under poor cutting conditions. As the point of the cutting tool contacts the metal, some compression occurs, and the chip begins flowing along the chip-tool interface. As more stress is applied to brittle metal by the cutting action, the metal compresses until it reaches a point where rupture occurs and the chip separates from the un-machined portion. This cycle is repeated indefinitely during the cutting operation, with rupture of each segment occurring on the shear plane (figure 3.3). Segmented chips are the easiest to remove from the working space area, although the segmented parts are partly welded together again because of the heat the chip is carrying away. Generally, as a result of these successive ruptures, a poor surface finish is produced on the work-piece.

Many materials provide a continuous chip (figure 3.3). This kind of chip runs almost straight like a long ribbon and gets entangled around the tool holder and other parts of the working space. This continuous ribbon is produced when the flow of metal next to the tool face is not restricted by a build up edge or friction at the chip tool interface. In order to clear the working area the cutting process must be interrupted, so that the chip breaks and can be cleared away. This is the general procedure for manual turning or drilling. In automatic cutting processes however, this approach becomes a problem. In automatic processes, it is desirable to form the chip into tight curls that break into short pieces. This can be achieved by the use of chip breakers and chip forming grooves [4]. However, the continuous ribbon chip is considered ideal for efficient cutting action to produce better surface finishes, since unlike the segmented chip, fractures or ruptures do not occur due to the ductile nature of the metal.

Another phenomena that is important in the chip formation process is a "built-up edge" (BUE), which is formed by highly strained material adhering to the tool tip. In this case the metal ahead of the cutting tool is compressed and forms a chip, which begins to flow along the chip tool interface. As a result of the high temperatures produced and the high frictional resistance against the flow of the chip along the chip-tool interface, small particles of metal begin adhering to the edge of the cutting tool, while the chip shears away. As the cutting process continues, more particles adhere to the cutting tool and a larger build-up results. The build up increases in size and becomes more unstable, until eventually a point is reached where fragments are torn off. Proportions of these fragments which break off, stick to both the chip and work-piece. The build-up / break-down of the built up edge occur rapidly during cutting action and cover the machined surface with a multitude of built up fragments. These fragments adhere to and score the machined surface, resulting in a poor surface finish. Moreover BUE also generates forced vibrations generated internally through the cutting process itself [4,44]. The random process of the BUE produces a change in the "effective rake angle" through the different sizes in the built-up edge (figure 3.3). As the result is a variation in the rake angle the cutting forces vary (α increases and therefore F decreases, or if α decreases F increases) and vibrations are produced.

3.3 Single point operations

A single point operation is normally a continuous cutting process using tool with a single cutting edge. Turning, boring planning and shaping are all examples where single point cutting is used (figure 3.4).

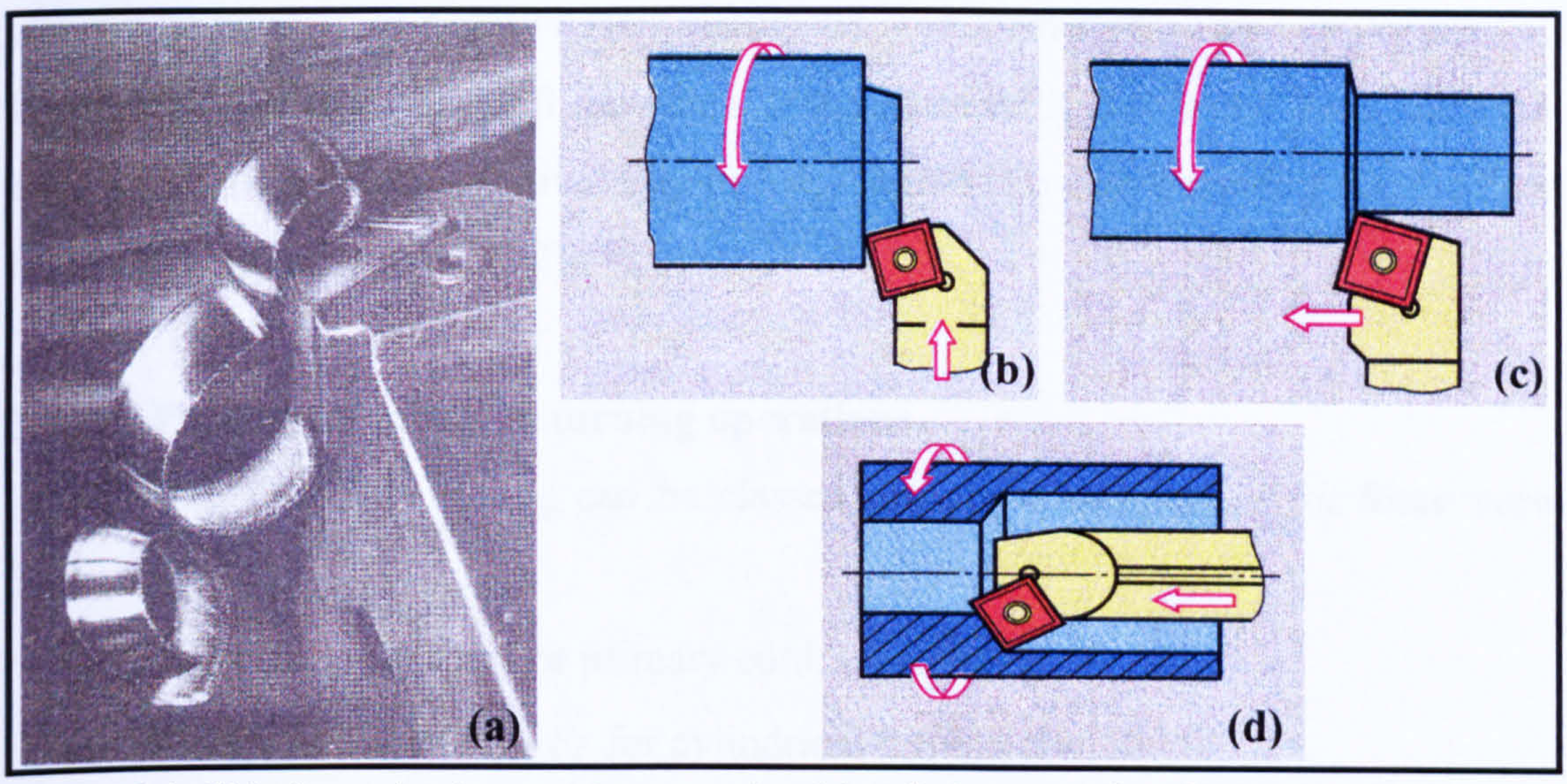

Figure 3.4: Chip formation in a turning operation (a), a facing operation (b), a cylindrical turning operation (c) and a boring operation [4,150]

The figure 3.4.a shows a chip being cut in a turning operation. The tool is a triangular carbide insert mechanically clamped in a tool holder and the tool moves parallel with the axis of the cylindrical work-piece. Marks of the feed per revolution of the work-piece can be seen both on the surface previously machined and on the just-generated surface (figure 3.4.a). This operation is called cylindrical turning. If the tool moves perpendicular to the axis it removes material from the flat face of the work-piece, the operation is called facing. The combination of both cylindrical and facing operations allows complex profiles to be machined (e.g. chamfering).

3.3.1 Tool geometry in turning

The main features of a turning tool are shown in figure 3.5.

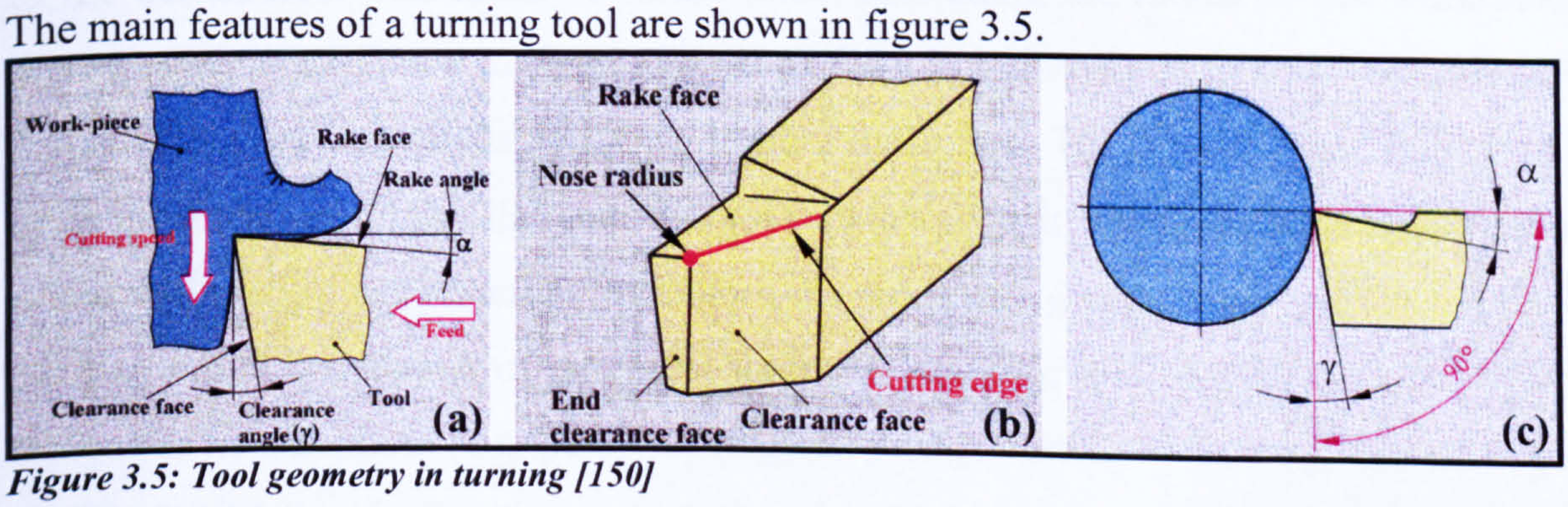

Figure 3.5: Tool geometry in turning [150]

The surface of the tool over which the chip flows is known as the rake face. The cutting edge (wedge angle) is formed by the intersection of the rake face with the clearance face or flank of the tool. The tool is designed so that the clearance face does not rub against the freshly cut metal surface. The rake face is inclined depending on the work-piece material and rake angle (α) can be positive or negative (this affects the chip formation). Rake angles over 10° are only appropriate for relatively soft materials. If the material is brittle and hard, the rake angle can be very small or even negative. Figure 3.5.c shows the tool geometry for medium hardened materials (e.g. mild steel) [72].

3.3.2 Power and forces in turning operations

The cutting forces in turning can be classed into three components or force vectors (figure 3.6):

- The tangential force or primary cutting force (F_t)
- The axial force ($F_a = F_f$ for cylindrical turning operation)
- The radial force or thrust force ($F_r = F_f$ for facing operation)

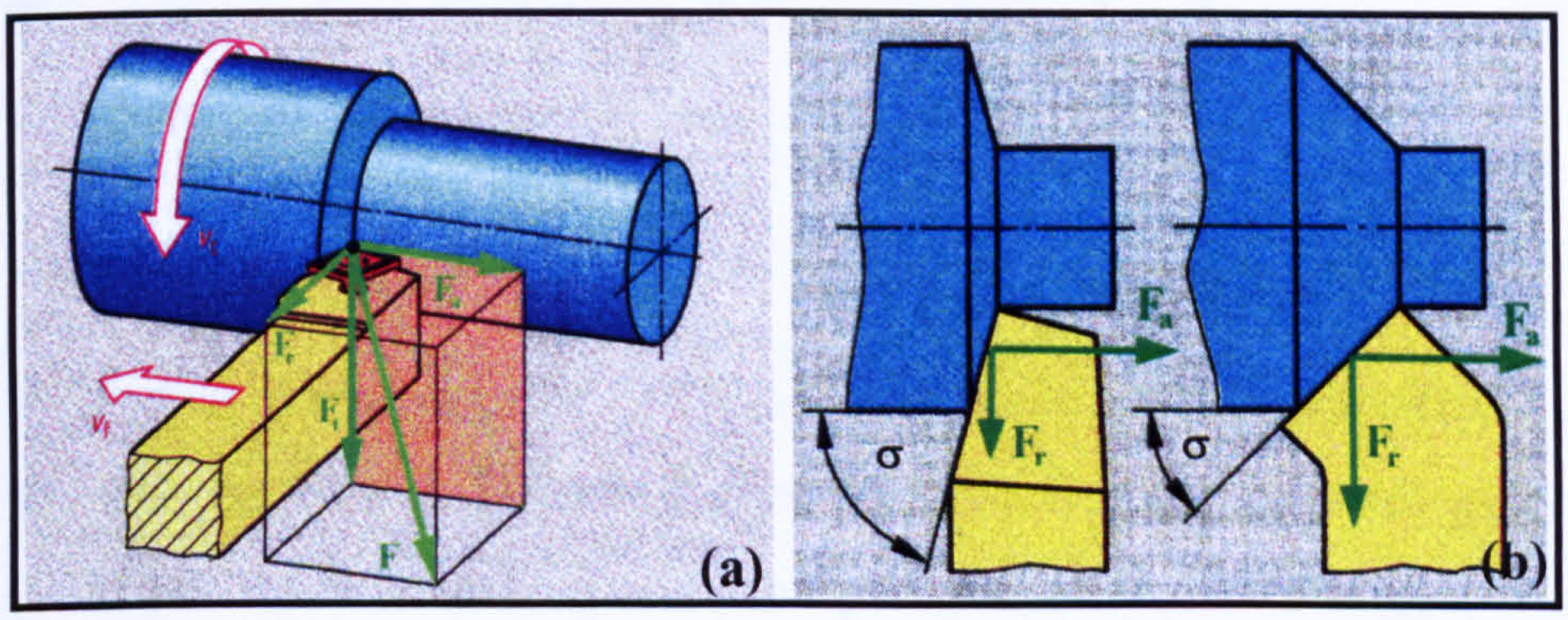

Figure 3.6: Cutting forces in turning

The tangential force has the same direction as the cutting speed, which is the rate at which the uncut surface of the work passes the cutting edge of the tool and has the direction tangential to the cut surface. The radial or thrust force, acts along the radius of the work-piece and therefore is perpendicular to the machined surface. This force acts to push the tool out of the cut and therefore is responsible for work-piece deflection. The direction and amount of radial force is critical for minimising machine tool chatter since it acts in the most flexible direction of the tool/work-piece structure. Therefore the side cutting edge angle (SCEA - σ) in figure 3.6.b is a direct parameter of the radial force and machine tool chatter [72]. At 0° the radial force is at its maximum (e.g. purely orthogonal plunge cutting operation). The work-piece or shaft is flexible in this direction and may bend and lead to vibration. When the SCEA is at 90°

the radial force would in theory be zero, but because of the nose radius of the tool (figure 3.5.b) a radial force is always present, although small. The axial force acts in the axial direction of the shaft, which is the work-piece in turning or the tool in milling. In turning it is also called longitudinal force. The feed force in turning is equivalent to the axial force, where in milling it is equivalent to the radial force (chapter 3.4.2). In both operations it acts in the direction of the feed and therefore determinates the direct load on the feed drive.

Figure 3.7 shows the different machine operations in turning.

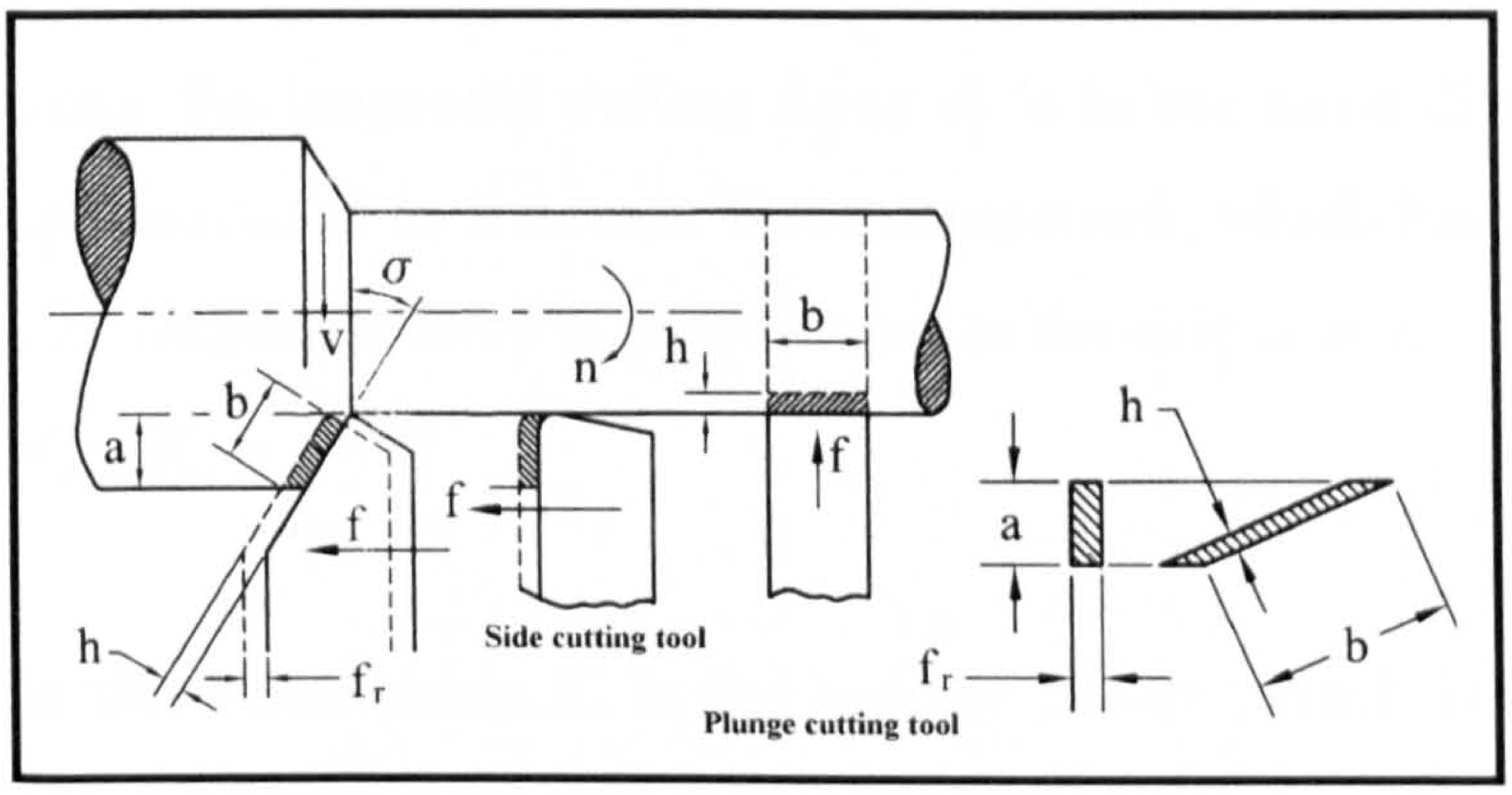

Figure 3.7:The constant chip thickness in turning [4]

The peripheral speed of the work-piece is defined as the cutting speed v.

$$v = \frac{Workpiece\ diameter\ D_w\ [mm] \times \pi \times n\ [RPM]}{60\,\mathrm{sec}/\mathrm{min}} \left[\frac{mm}{\mathrm{sec}}\right]$$ ***Eq. 3.1:The cutting speed***

This is an averaged value since the work-piece diameter reduces in a facing operation. With the feedrate f the tool moves f_r after one revolution of the work-piece. This is called chip load (feed per tooth in milling and feed per revolution in turning) and leaves the distinguishing *feed per revolution* marks on the surface.

$$f_r = \frac{f\left[mm/\mathrm{min}\right]}{n\left[RPM\right]}\left[mm\right]$$ ***Eq. 3.2: The chip load in metal cutting***

The shaded area in figure 3.7 is called the chip area A and can be calculated by:

$$A = a \times f_r = b \times h\left[mm^2\right]$$ ***Eq. 3.3: The chip area***

Where a is the depth of cut measured in radial direction of the cut surface, b the chip width and h the chip thickness. For turning, the chip thickness is a constant value, whereas for milling it varies with the rotational angle (see later). The depth of cut a depends on the *side* *cutting edge angle* (SCEA), which therefore also determines the type of cutting operation [e.g. plunge cutting).

$a = b \times \cos\sigma \; [mm]$ ***Eq. 3.4: The depth of cut***

The metal removal rate (*MRR*) is obtained as the product of chip area and cutting speed:

$MRR = A \times v = a \times f_r \times \pi \times D_w \times n = \pi \times D_w \times f \times a \; \left[{mm^3}/{\text{min}} \right]$ ***Eq. 3.5: The Metal Removal Rate***

Since the tangential cutting force F_t is in the same direction as the cutting speed, it can be approximated as the main force component, which has to be delivered by the spindle motor. The tangential force is proportional to the chip area A:

$F_t = K_s \times A \; [N]$ ***Eq. 3.6: The tangential cutting force***

In this relationship K_s is the *specific power* ,which is primarily determined by the material being cut. For mild steel it is about 2500 N/mm^2 and can be found in machine handbooks. The main cutting power delivered by the spindle motor is:

$P = F_t \times v = K_s \times A \times v = K_s \times MRR$ ***Eq. 3.7: The main cutting power***

In turning it can be approximated that the vector sum of F_a and F_r is about 30% of F_t [4].

3.4 Multi-point tool operations

A Multi-point tool operation is an intermittent cutting process using a cutter with several teeth. An example is milling where the cutter is held in a rotating spindle, whilst the work-piece is clamped on the machine table moving linearly towards the cutter (figure 3.8).

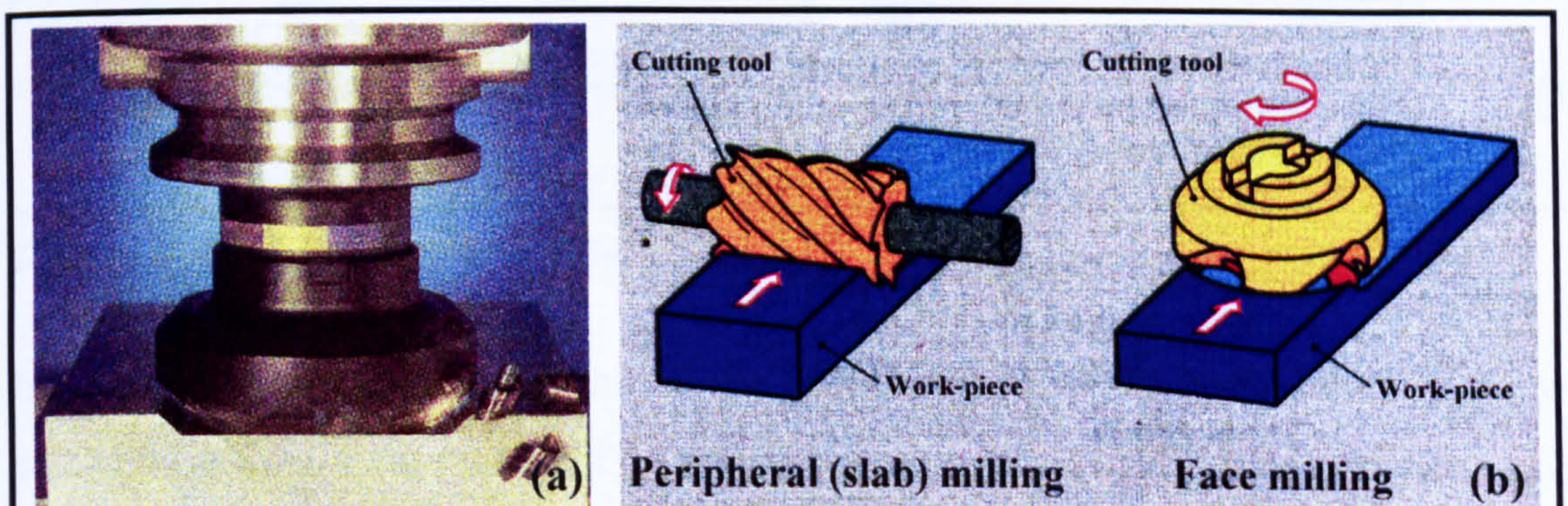

Figure 3.8: Chip formation in a milling operation (a) [150]
Tool work relationship in peripheral and face milling (b) [150]

The figure illustrates that there are two types of milling process [73,74]:

- Peripheral or slab milling
- Face milling

The names of the milling processes refer to the fact that it is the face or the periphery of the cutter which generates the machined surface. In peripheral cutting the surface is parallel to the rotational axis of the cutter. Both flat and formed surfaces can be produced by this method. The cross section of the resulting surface corresponds to the axial contour of the cutter. A very common type of peripheral milling is end milling, where the cutter has a small diameter clamped in overhang (Tool overhang is the length of the tool that extends unsupported from the tool holder). Since the length of an end mill is several times its diameter it is very flexible and therefore can produce form errors on the work-piece and also chatter vibrations. In face milling the generated surface is at right angle to the cutter axis and is a combined result of both the periphery and face of the cutter teeth.

Both peripheral and face milling depend on the relationship between feed motion and cutter rotation. This results in two different arrangements, which are known as up- and down milling. In up milling (conventional milling), the cutter rotates against the direction of the feed of the work-piece, whereas in down milling (climb milling) the rotation is the same as the feed direction. As shown in figure 3.9 the chip formation and therefore the surface generation in both cases is completely different.

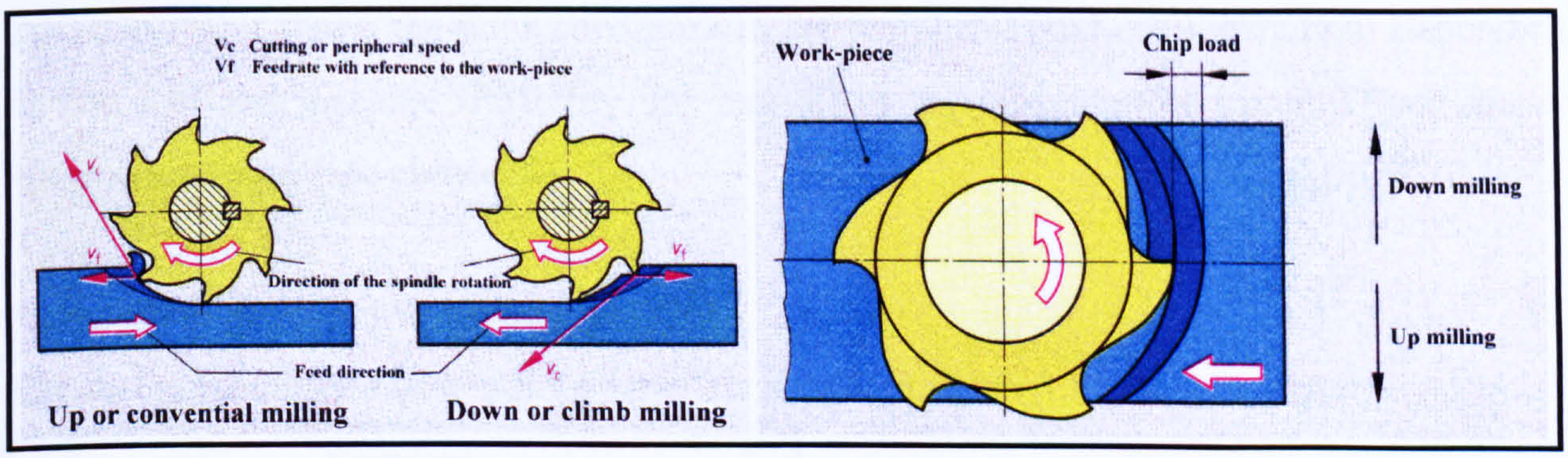

Figure 3.9: Up- and down milling [150]

In up milling the chip is very thin at the beginning, where the tooth contacts the work-piece and becomes maximum where it leaves. The cutter tends to push the work-piece along and lift it upwards from the table. This tends to eliminate any effect of looseness in the feed-screw and nut of the machine table and therefore guaranties a smooth cut. Conventional milling is normally done on lower cost machines with a lead screw, which has a large amount of backlash and also for machining hard materials. In down or climb milling, maximum chip thickness occurs close to the point at which the tooth leaves the work-piece. Because of the relative motion it tends to pull the work-piece into the cutter, which suddenly increases the chip load and can result in breakage of the cutter or inserts, depending on the amount of looseness in the screw and nut of the table. Down milling is therefore only appropriate for more modern and more expensive machines with ballscrews instead of leadscrews. A significant advantage of down milling is the surface quality as there is less tendency for tooth marks to show at the end of tooth engagement as the work-piece moves in the tangential cutting direction. Figure 3.10 shows the form error on the work-piece, generated through the fact that up milling pulls the cutter into work and down milling pushes it away from it.

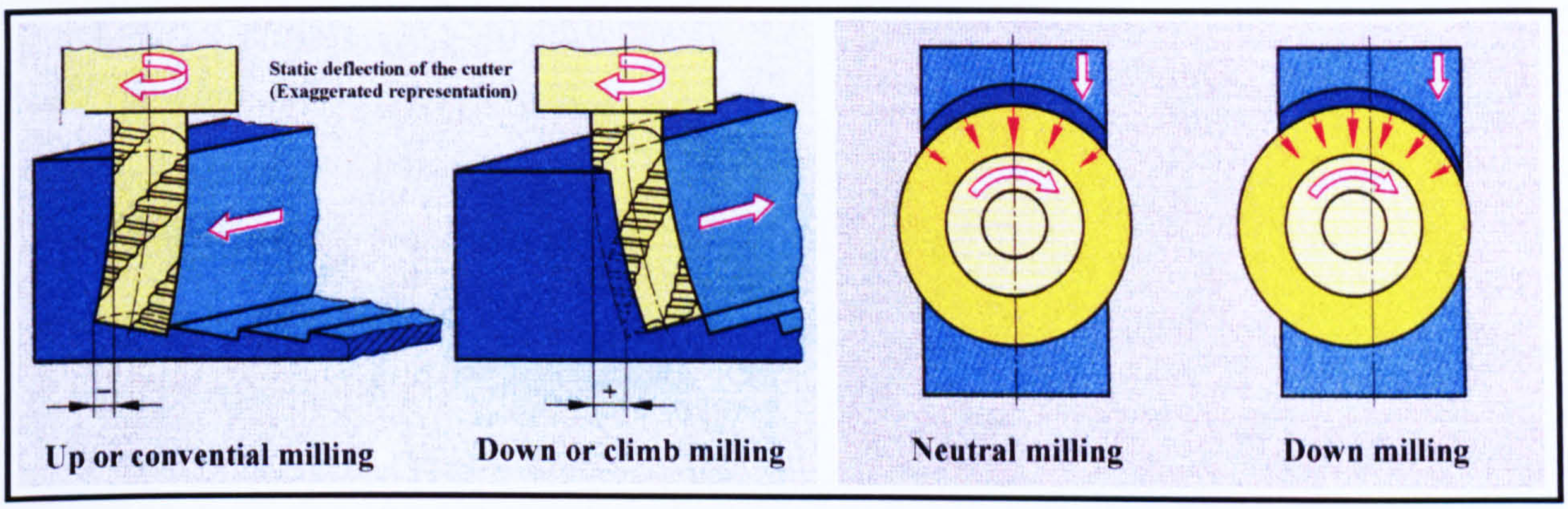

Figure 3.10: Form errors in up- and down milling [150]

In the special case of face milling with symmetrical location of the cutter to the work-piece (neutral milling), the effects of up and down milling can be neglected. However, if it is asymmetrical it shows the same conditions as the peripheral (end-mill) operation. Depending on the tool and machine flexibility this can affect the tendency for machine tool chatter vibrations to arise (see chapter 5).

3.4.1 Tool geometry in milling

The main features of a face milling cutter are shown in figure 3.11.

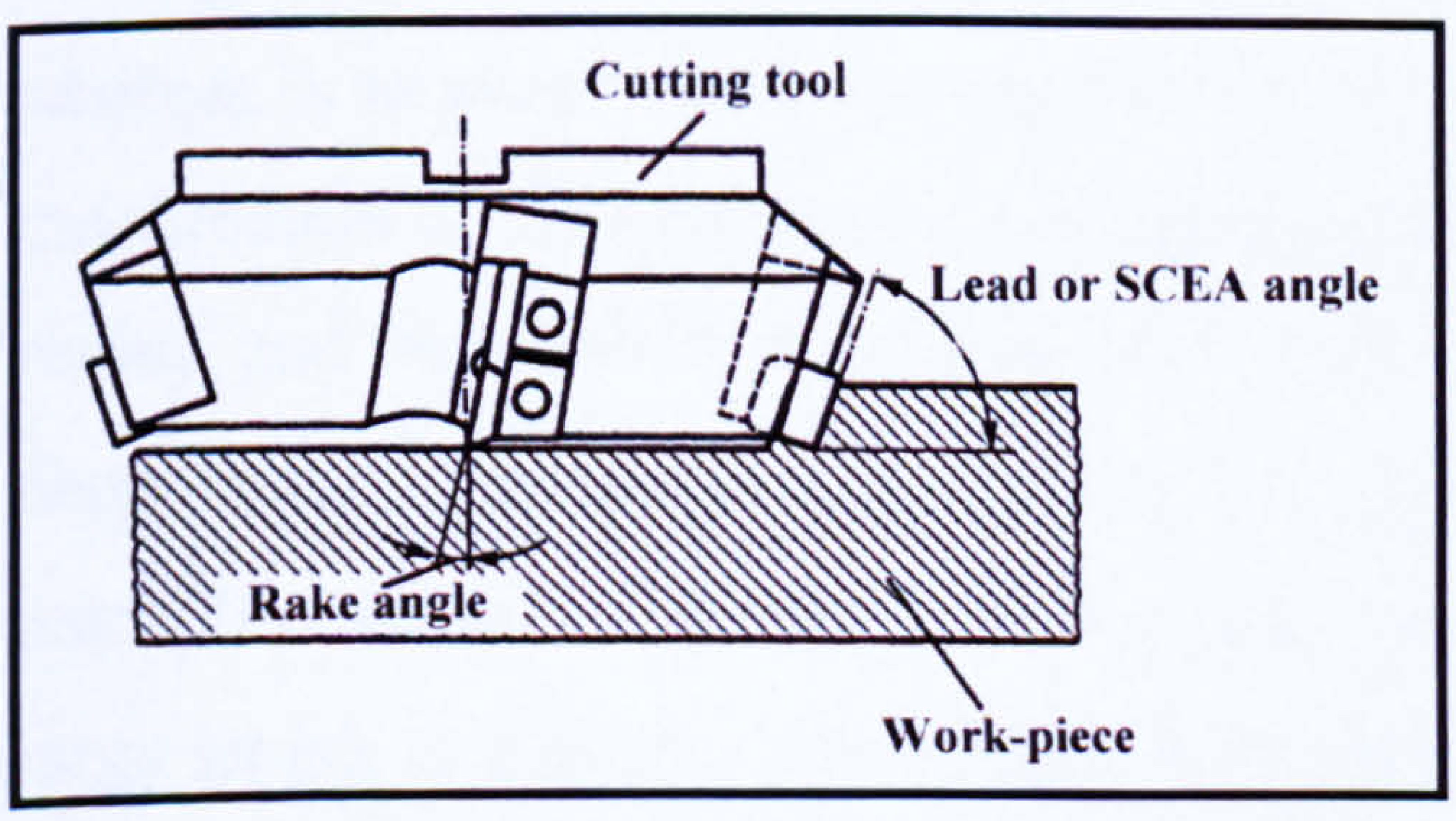

Figure 3.11: Tool geometry of a face mill cutter [73]

Face mill cutters are most commonly constructed as bodies with mechanically clamped carbide inserts (some end mills are also made in the same way). Just as it was for turning, the rake angle (axial rake angle) can be positive or negative. A positive rake angle cuts the work-piece with the cutting edge first (figure 3.11), whereas a negative rake angle directs the chip back to the surface. The larger the positive rake angle the lower the cutting forces will be [73]. This is an advantage for machining thin walled aluminium parts. The larger the negative rake angles the bigger the cutting forces, spindle power and temperature generation. Negative rake angles are normally used for hard materials like cast iron. The lead angle is equivalent to the side cutting edge angle and just as in turning the SCEA affects the chip thickness and chatter vibration possibilities.

3.4.2 Power and forces in milling

As with turning, the cutting forces can be divided into 3 components (figure 3.12):

- The tangential force or primary cutting force (F_t)
- The axial force (F_a)
- The radial force (F_r)

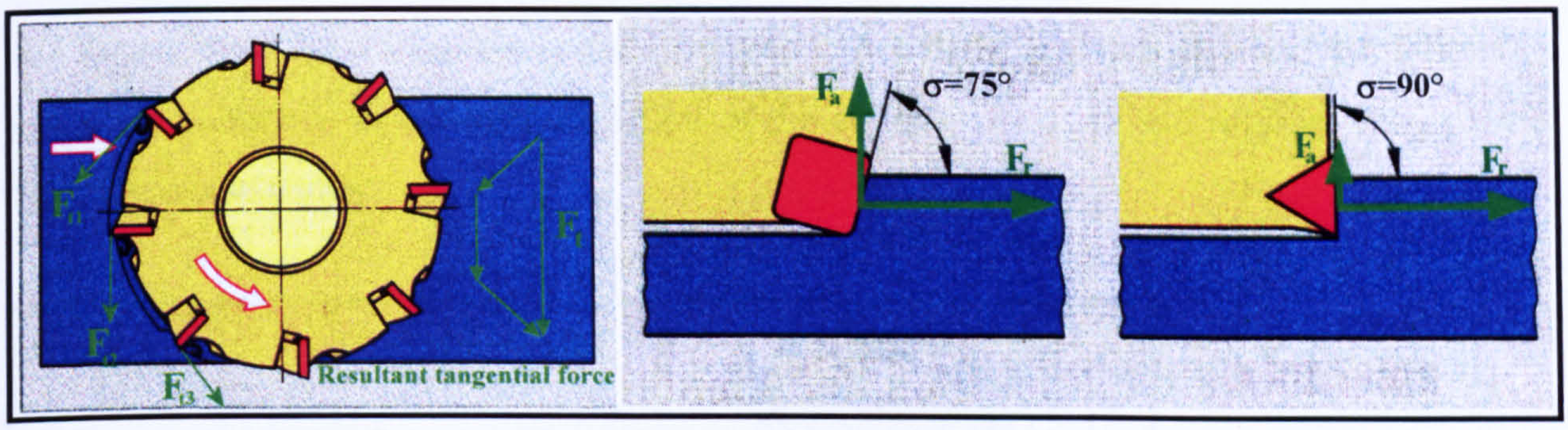

Figure 3.12: The cutting forces in milling [150]

The notation is similar to that used for turning, with the difference that the radial force in turning is the axial force and vice versa. This is because the rotating axis holds the tool, whereas in turning it holds the work-piece. The primary cutting force is the tangential force in the direction of the cutting speed, tangential to the cut surface. The radial force acts along the radius, and the axial force in axial direction of the cutting tool (spindle axis). Both forces are dependent on the side cutting edge angle σ. Again the radial force acts along the most flexible part of the cutter and chatter vibration can be a significant problem for long cutting tools with large length to diameter ratio. Since in milling usually several cutting teeth are in the cut, at the same time, the tangential force vector of each tooth in the cut must be added together. The resultant tangential cutting force can then be used to calculate the required power for the spindle motor. Figure 3.13 and 3.14 show the variation in chip thickness for face and end (peripheral) milling operations, where v is the cutting speed and f the feedrate between the cutter and the work-piece.

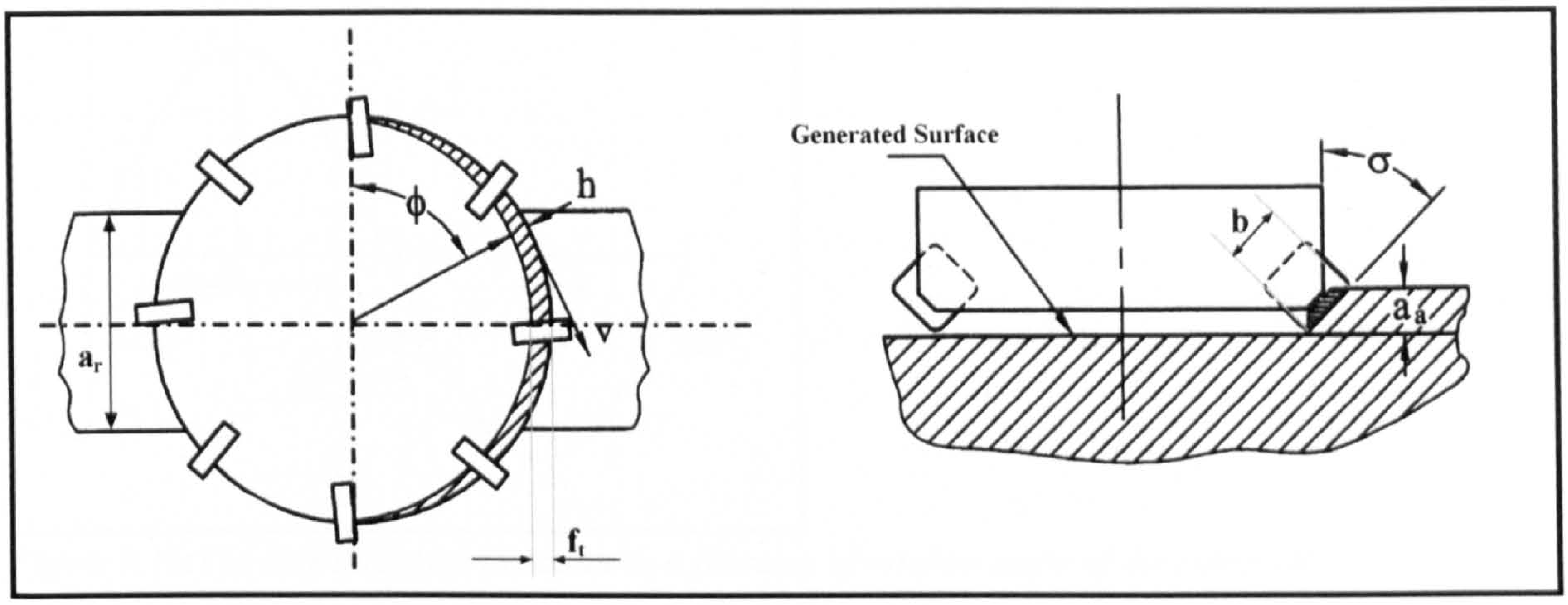

Figure 3.13: The chip thickness variation in face milling [4]

In face milling, the depth of the layer removed from the work-piece is the axial depth of cut a_a, the width of the chip is b and the chip thickness h. The width of cut a_r is the width of the work-piece and determines how many teeth are in the cut. In peripheral milling it is the other way round. The layer removed from the work-piece is now called the radial depth of cut a_r and the width of the work-piece is the axial depth of cut a_a. This is because in face milling the generated surface is in the axial direction of the cutter whereas in end milling it is in radial direction of the cutter.

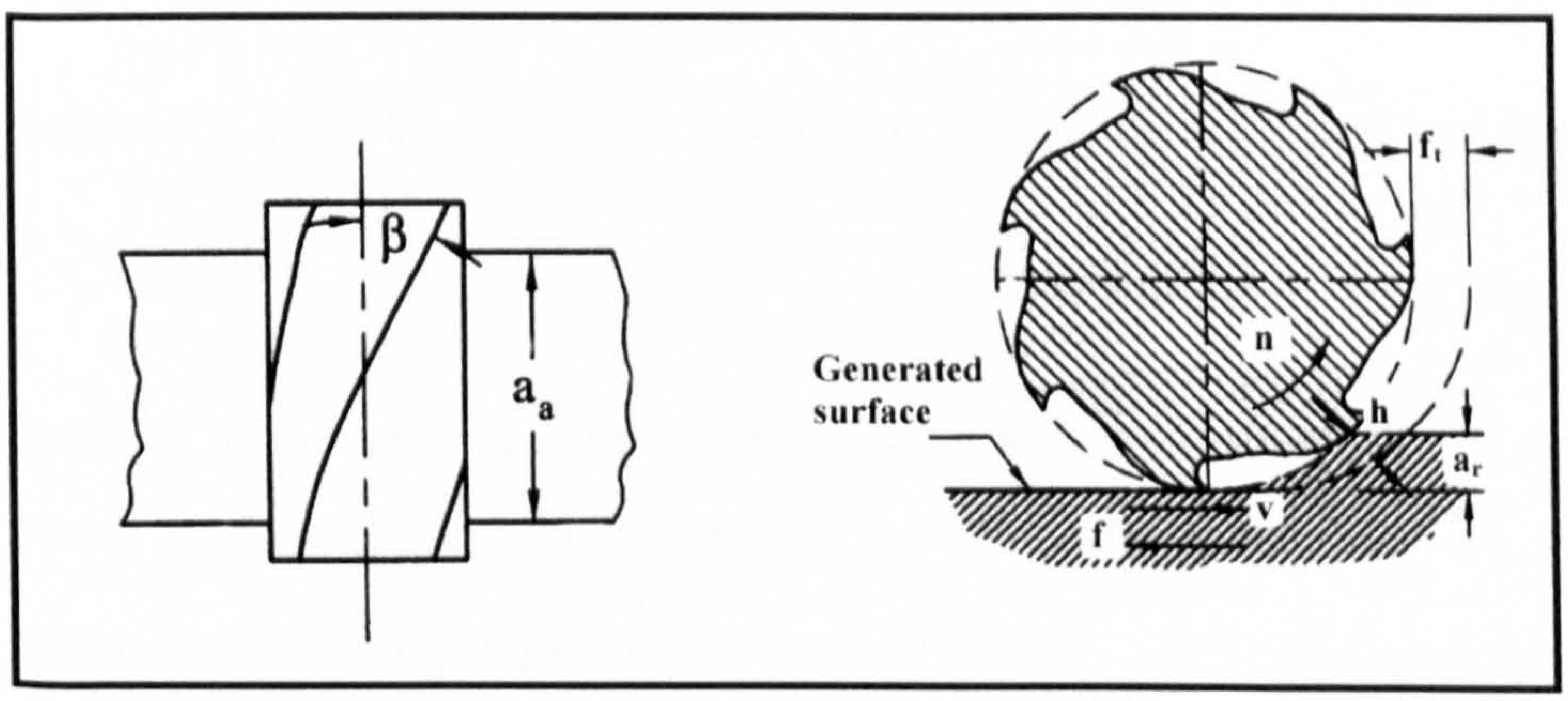

Figure 3.14:The chip thickness variation in end milling [4]

The teeth of the end mill are helical and the angle is called the helix β. Geometrically this angle can be compared with the rake angle α in face milling. The figure also shows that the path resulting from the rotation of each insert and translation of the work-piece is a cycloid.

The chip thickness h varies with the angle ϕ of cutter rotation. It can be expressed as a sine function between the moment the tooth is entering in the workpiece and when it is leaving (figure 3.15).

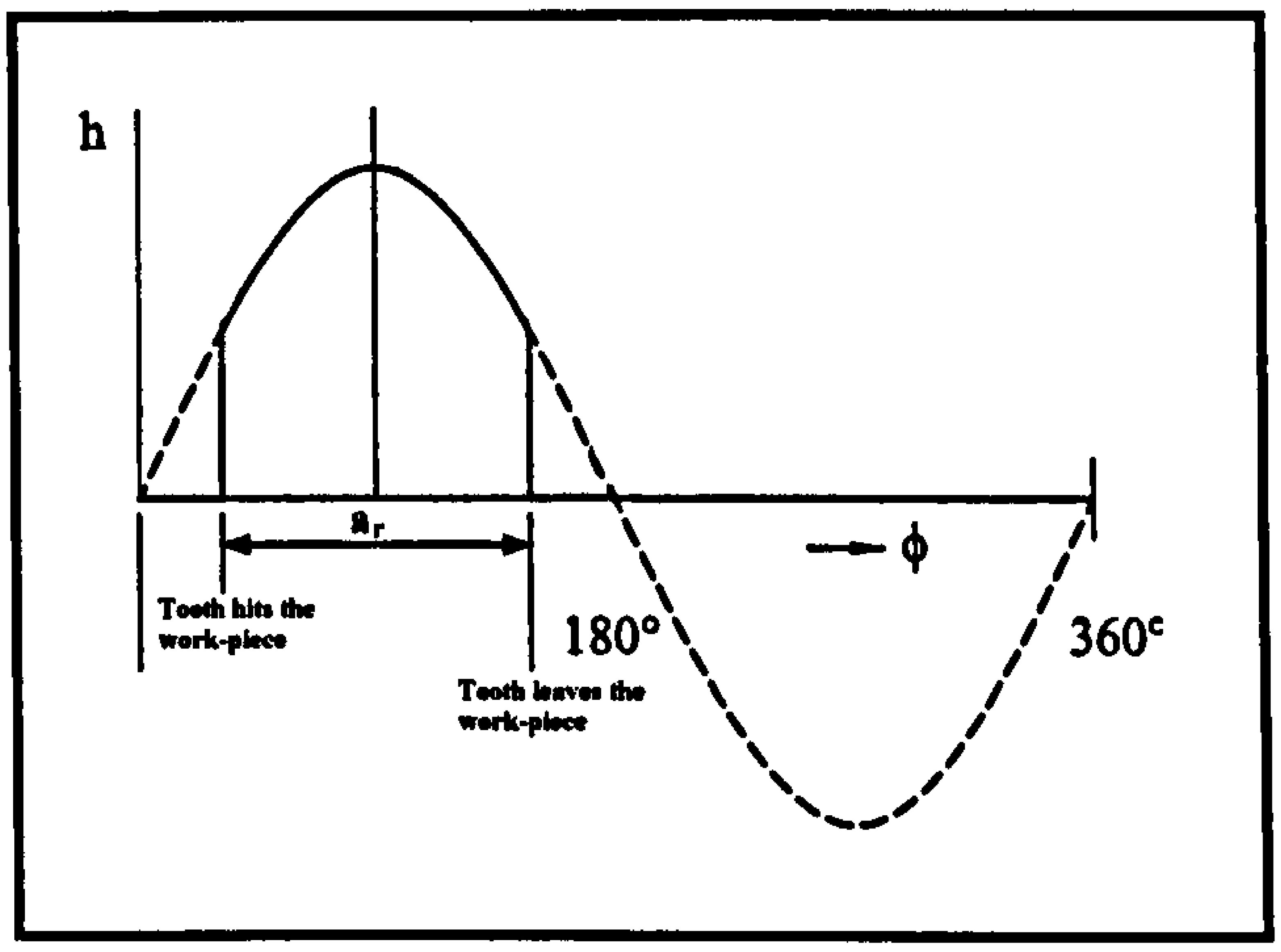

Figure 3.15:The chip thickness variation as a function of rotation angle of the cutter [4]

In milling the cutting speed is the peripheral speed of the cutter, whereas in turning it was the peripheral speed of the work-piece.

$$v = \frac{Cutter\ diameter\ D_c\ [mm] \times \pi \times n\ [RPM]}{60\,\mathrm{sec}/\mathrm{min}} \left[\frac{mm}{\mathrm{sec}}\right]$$

Eq. 3.8:The cutting speed in milling

The chip load is called feed per tooth in milling (m is the number of teeth).

$$f_t = \frac{f\ \left[mm/\mathrm{min}\right]}{m \times n\left[RPM\right]}\ [mm]$$

Eq. 3.9: The feed per tooth in milling

As already seen, the chip thickness h is not constant in milling and can be calculated by:

$$h = f_t \sin\phi\ \left[mm^2\right]$$

Eq. 3.10: The chip thickness in milling

Because of this chip thickness variation the Metal Removal Rate is approximated to the Mean Metal Removal Rate (MRR_m) and can be obtained from:

$$MRR_m = a_r \times a_a \times f_t \times m \times n = a_r \times a_a \times f\ \left[mm^3/\mathrm{min}\right]$$

Eq. 3.11: The Mean Metal Removal Rate

The axial depth of cut a_a in face milling depends on the *side cutting edge angle* (SCEA) or lead angle:

$$a_a = b \times \cos\sigma\ [mm]$$

Eq. 3.12:The axial depth of cut

The mean power of the spindle motor in order to achieve the MRR_m is:

$$P_m = \frac{MRR_m \left[cm^3/\min \right] \times K_s \left[W_{sec}/cm^3 \right]}{60 \left[\sec/\min \right]} \left[W \right]$$

Eq. 3.13: The mean power of the spindle motor

Again K_s the *specific power*, which is the approximate power required at the spindle in order to remove 1 cubic centimetre of a particular material.

Since the tangential force has to be delivered from the spindle motor it can be obtained from:

$$F_t = \frac{P}{v} \left[N \right]$$

Eq. 3.14: The tangential force in milling

The radial force can be approximated to about 30% of the tangential force [4]. Because of the SCEA (face milling) and helical angle (peripheral milling) the axial force then is:

$$F_a = F_r \tan\sigma \ (face\ milling)$$
$$F_a = F_r \tan\beta \ (peripheral\ milling)$$

Eq. 3.15: The radial force for milling operation

3.5 Cutting process dynamics

Milling and turning are dynamic, time-varying, processes and the structural dynamics of the machine play an important role. Chatter during cutting is due to the dynamic feedback between the tool inserts. As an insert cuts through metal it lays down a pattern that affects the cut of the next inserts. This interaction creates a dynamic feedback path between successive cuts and as in many feedback systems can lead to instability. During cutting, energy is fed into well coupled modes of the structure's dynamics. If the chip thickness variation or pattern on the surface of the machine part is so big that energy gain is not balanced by energy loss, energy storage will increase. This dynamic instability is known as regenerative chatter. Chatter is not only recognised by distinguishing surface pattern (chatter marks) but also by the noise associated with this type of vibration.

The most significant parameter, for the generation of chatter, is the chip width *b*. Chatter will start at a certain chip width b_{limit}, when the cutting energy becomes so big that it reaches the stability limit of the structure. In milling the cumulative chip width also has to be considered (figure 3.16).

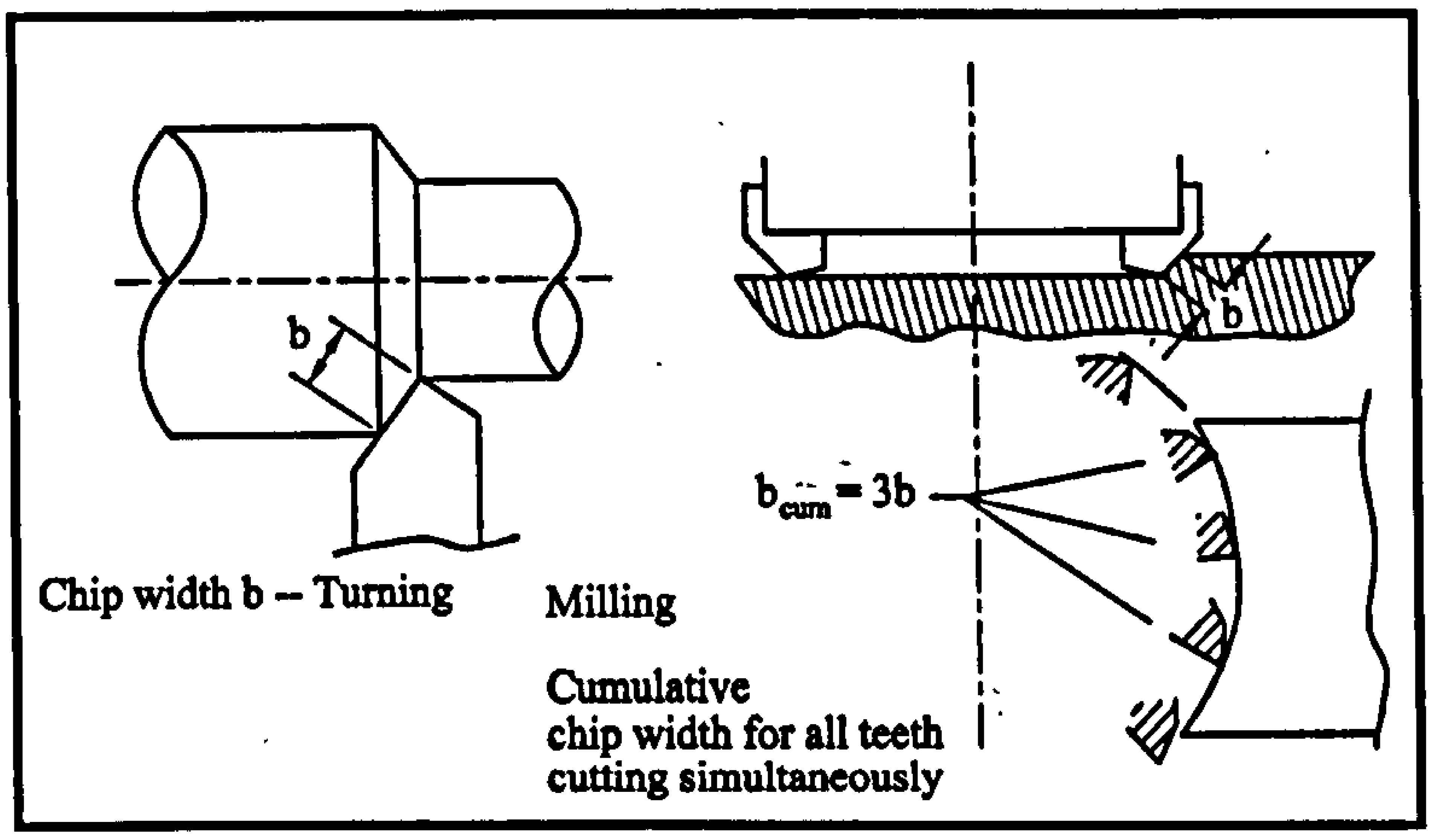

Figure 3.16: The chip width b as the decisive parameter for chatter [4]

The more teeth that are simultaneously in the cutting process, the bigger the cutting force will be. Therefore, the sum of the chip width of each tooth in the cut needs to be considered.
In milling, the cumulative chip width is often defined as the axial depth of cut, since it is in the axial direction of the cutting tool and therefore a direct CNC programming parameter, similar to the depth of cut a in cylindrical turning (figure 3.7). More precisely the axial depth of cut depends also on the SCEA σ (see equation 3.12).

3.5.1 Derivation of the chatter loop

As already discussed chatter is the result of the interaction between the cutting process and the machine tool dynamics. Tlusty and Polacek [19] were among the first researchers to derive theories to explain the occurrence of chatter. They drew attention to the machine tool dynamics but neglected the dynamics of the cutting process. Merritt [20] has shown that self-excited vibrations can be illustrated as a feedback loop; he also showed that traditional feedback control theory can be used to calculate the stability limit.
The main assumptions of this theory are:

- The behaviour of the vibratory system, between the tool and work-piece is linear.
- The direction of the time dependent component of the cutting force is constant.
- The dynamics of the cutting process are neglected.
- The cutting force depends only on vibration in the direction to normal to the cut.

The closed loop input/output relationship of the relevant transfer functions are discussed next.

Assuming an orthogonal plunge operation in turning (figure 3.17a, b, and c). The flat faced tool is fed perpendicular to the axis of a cylindrical shaft, which is held between the chuck and the tail stock centre of a lathe. The tool is mounted rigidly and the feed rate is adjusted to obtain a steady state of chip thickness *h(t)*.

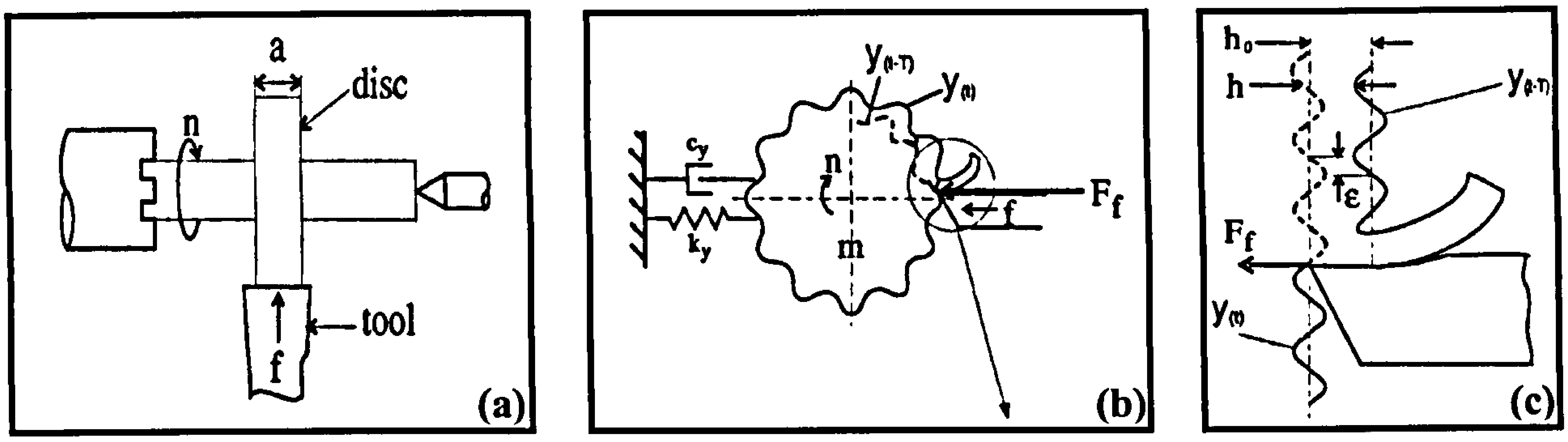

Figure 3.17: Regenerative chatter in orthogonal cutting [8]

3.5.1.1 Transfer function of the uncut chip thickness

Since the shaft is flexible in the direction of the feed, the feed cutting force (F_f) causes it to vibrate. The initial surface of the shaft is smooth, so there is no wave or surface pattern during the first revolution. But because of the bending vibrations in the feed direction y, which for this cutting operation is also the direction of the radial cutting force ($F_f = F_r$), the tool starts to leave a wavy surface pattern behind. When the second revolution starts, the surface has waves both inside where the tool is cutting (inner modulation, $y(t)$) and on the outside surface of the cut, from the vibrations during the previous revolution of cut (outer modulation $y(t-T)$). Hence the resulting dynamic chip thickness is no longer constant but varies as a function of vibration frequency and speed of the work-piece. The dynamic chip thickness can be written as:

$$h(t) = h_0 - (y(t) - y(t-T)),$$

Eq. 3.16: The dynamic chip thickness

where h_0 is the intended or mean uncut chip thickness, which is proportional to the feed rate of the machine, and ($y(t) - y(t-T)$) is the dynamic chip thickness produced by the vibrations at present time and on one spindle revolution before (time period T).

For milling operations the period T is the time from one insert to the next.

The dynamic chip thickness expressed using the LAPLACE operator is:

$$\begin{aligned} h(s) &= h_0 - y(s) + e^{-sT} y(s) \\ &= h_0 + (e^{sT} - 1) y(s) \end{aligned}$$

Eq. 3.17: The dynamic chip thickness in the LAPLACE domain

3.5.1.2 Transfer function of the cutting process

The resolved cutting force *F(t)* is related to the instantaneous uncut chip thickness, *h(t)*, and affected by the dynamics of the cutting process. Merchant [75] suggested that a steady cutting process can be characterized by a parameter to represent the proportionality between the cutting force and the chip thickness.

$$F(t) = K_s \times b \times h(t)$$ *Eq. 3.18: The dynamic cutting force*

This parameter is called specific power of the work-piece material (compare with equation 3.6 and 3.7). But it actually not only depends on the work-piece material, but also on the tool geometry. It either can be found in machining data handbooks [4] or experimentally by measuring cutting force and chip thickness. The proportionality factor between the cutting force and chip thickness is sometimes simply called the cutting stiffness.

$$k_c = K_s \times b$$
$$\Rightarrow F(t) = k_c \times h(t)$$ *Eq. 3.19: The cutting stiffness*

The direct proportionality between the cutting force and uncut chip thickness is the simplest approximation that can be made for the cutting process. The model has been widely accepted by the machine tool industry despite its limitations [59]. The two deviations from the accurate model are that the uncut chip thickness depends on the cutting dynamics, and that the cutting stiffness varies with spindle speed.

3.5.1.3 Transfer function of the vibratory system

The dynamics of the machine structure play a significant role for machine tool vibrations. The structure can be modelled as a frame with the work-piece at one end and the tool at the opposite end (figure 3.18.c). This vibratory system is characterised by individual modes of vibration, each representing a degree of freedom of the relative motion between tool and work-piece in a particular direction (mode shape). For machine tool chatter, the vibratory system normally can be approximated by only a few degrees of freedom. Assuming the vibratory system is approximated as a single degree of freedom system in the radial direction (figure 3.17.b), the structural system can then be described by a 2nd order differential equation (equation of motion):

$$m\,\ddot{y}(t) + c\,\dot{y}(t) + k\,y(t) = F(t)$$ *Eq. 3.20: The equation of motion*

In the frequency domain, the relationship between the excitation force and the relative motion or vibration is:

$$\frac{y(s)}{F(s)} = \frac{\omega_n^{\,2}}{k_m(s^2 + 2\zeta\omega_n s + \omega_n^{\,2})} = \frac{1}{k_m} G_m(s)$$ ***Eq. 3.21: The equation of motion in the frequency domain***

G_m represents the normalised dynamic compliance (measured displacement versus excitation force) and k_m the static stiffness of the structure. This transfer function is sometimes called *orientated transfer function (OTF)* since it is the sum of direct transfer functions of each mode multiplied by a directional factor, which takes the amplitude normal to the cut surface into account [4,19]. This transfer function of the vibratory system is best obtained experimentally (figure 3.18) [14,76,77].

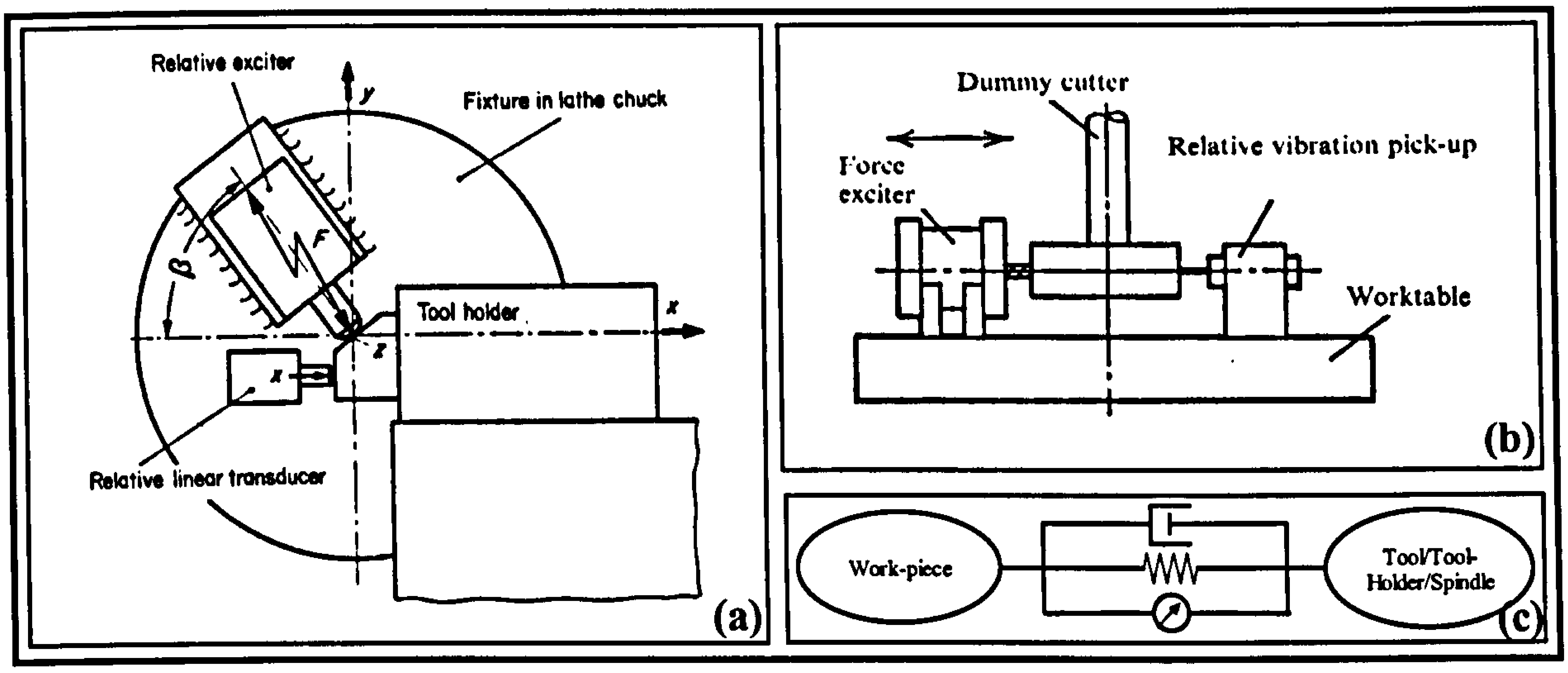

Figure 3.18:Measuring the orientated transfer function (OTF) on a lathe and vertical milling machine [76]

For example a relative exciter can be mounted between the table and spindle (milling) or work-piece and tool post (turning). This simulates the dynamic cutting force and the relative motion (vibration) between the work-piece and tool and can be measured using a displacement sensor. If the machine tool structure is relatively stiff in comparison to the tool and spindle then an impact hammer test on the tool can provide a quicker answer about the relevant structural dynamics. Since the exciting force is a space vector, a dynamic compliance exists for each possible orientation of the cutting force. In turning for example most flexibility is found on the work-piece, perpendicular to the spindle axis. If the side cutting edge angle σ is 0° (plunge cutting), then the radial forces are high and stability is low. In comparison, for a side cutting tool ($\sigma \approx 90°$) the radial force is very low, which means high stability. In milling the direction of the resultant force is time variant and depends on how many teeth are in the cut at a particular moment in time. This direction is normally assumed to be stationary for a particular mill and work-piece. The direction of relative displacement *y(t)* is measured normal to the cut surface, since this vibration effects the uncut chip thickness (figure 3.17.b and c).

3.5.1.4 Block diagram of the chatter loop

Equations 3.16, 3.18 and 3.20 are the three basic equations required to define the vibrating system. The cutting process is directly coupled to the structure and the uncut chip thickness equation provides the necessary feedback for the possibility of chatter. The independence of the equations can best be seen in the block diagram of figure 3.19.

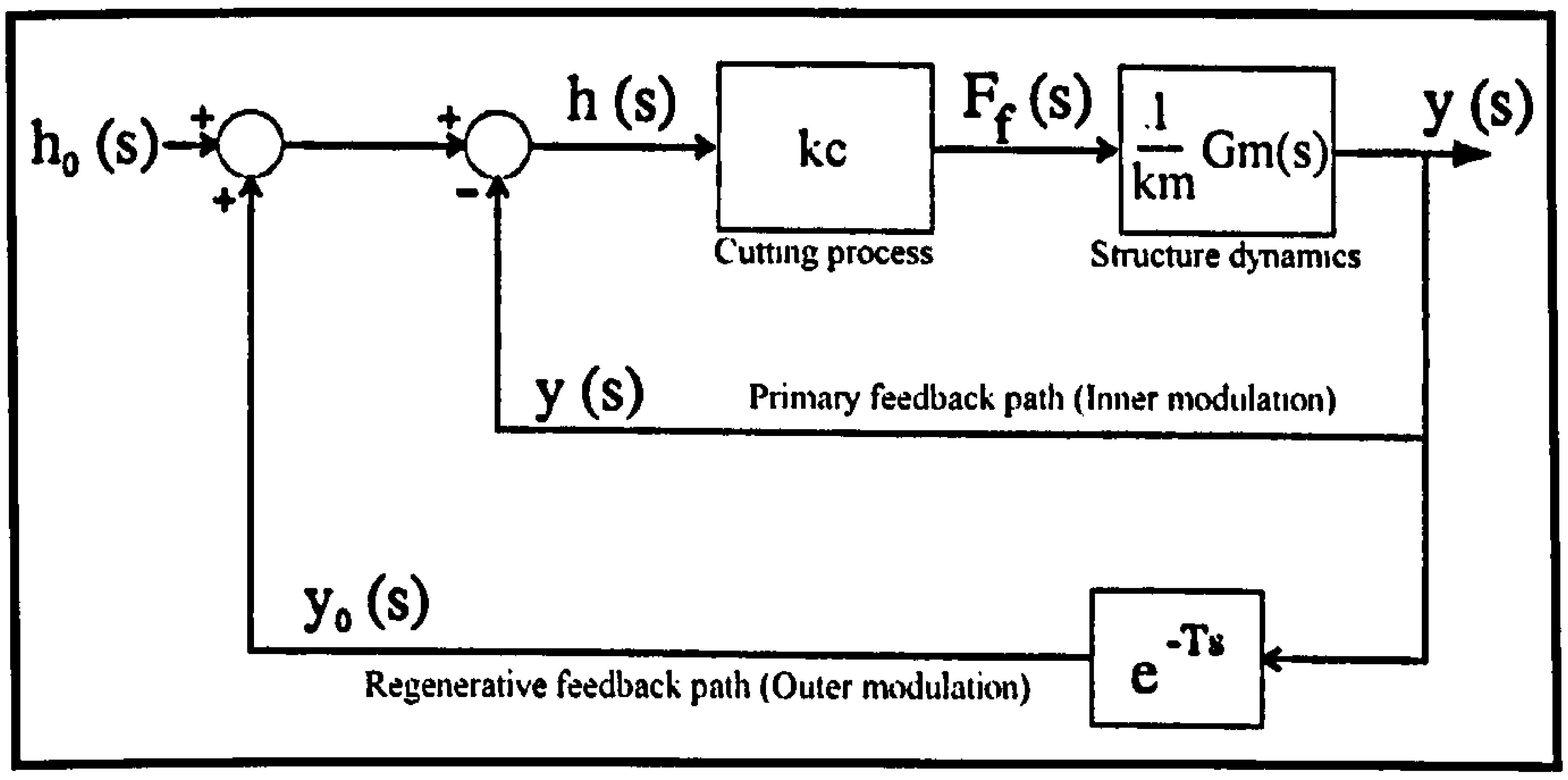

Figure 3.19:The chatter block diagram [8]

There are two position feedback loops, the inner one negative (primary feedback path), the outer one positive (regenerative feedback path – delayed position). The dynamic chip thickness *h(s)* is produced by the intended chip thickness $h_0(s)$, the inner modulated cut surface *y(s)*, and the outer modulated work-piece surface $y(s)e^{-Ts}$, where *T* is the time delay between the inner and outer modulated surface. The dynamic chip thickness is fed into the cutting process to produce the cutting force $F_f(s)$ acting on the cutting tool. The cutting force then excites the machine tool structure to generate the displacement y(s) between tool and work-piece.

The resulting transfer function between the dynamic and reference chip load can be obtained from the block diagram using traditional block diagram algebra [e.g. 78] – figure 20,21 and 22.

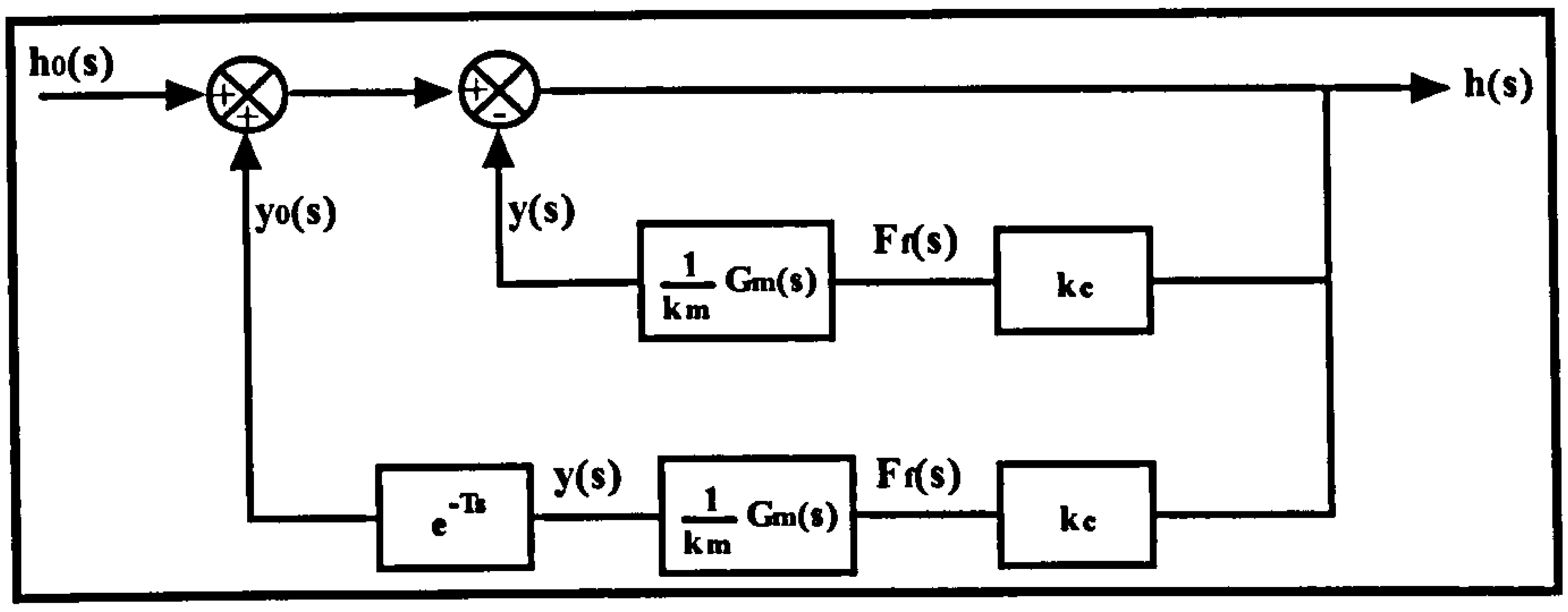

Figure 3.20:Inner and outer feedback of the chatter model

⇒

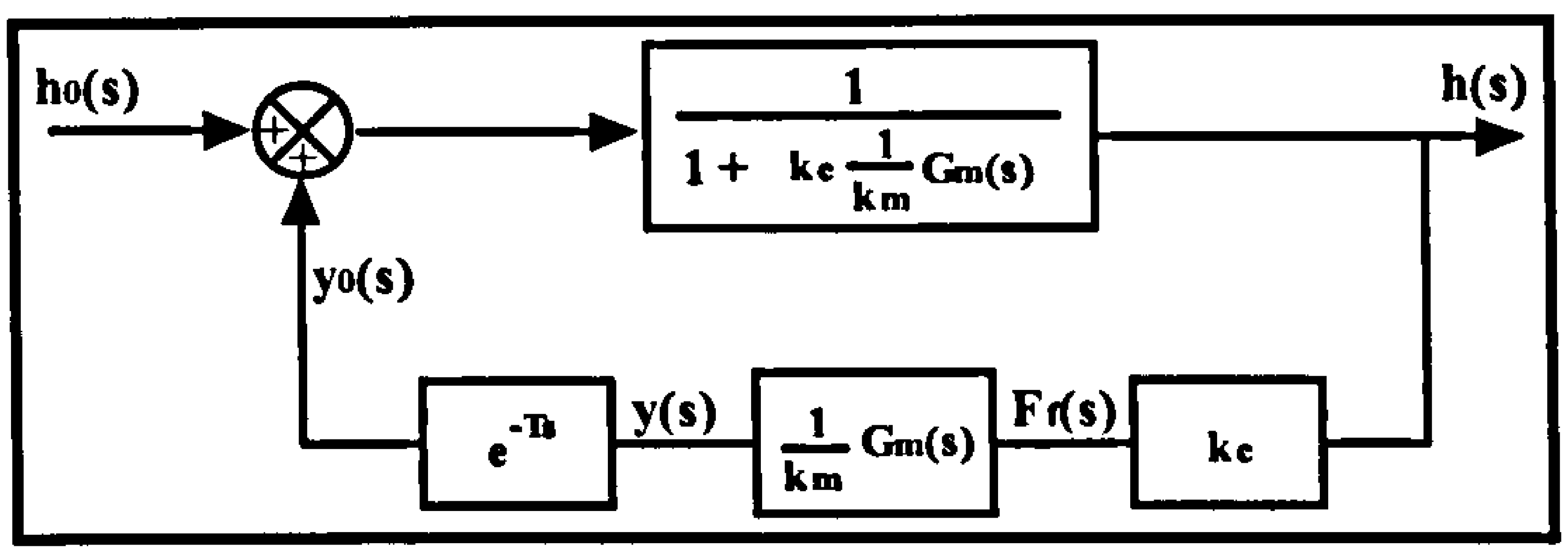

Figure 3.21:Chatter model simplified to a simple feedback system

⇒

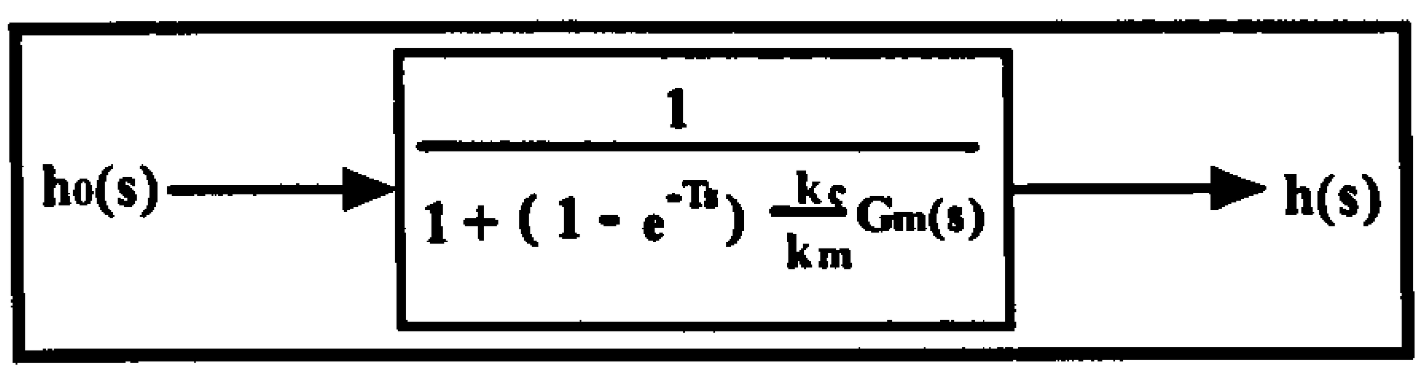

Figure 3.22:Resulting chip thickness transfer function

This results in the required relationship between the dynamic chip thickness and static chip load being:

$$\frac{h(s)}{h_0(s)} = \frac{1}{1 + (1 - e^{-Ts})\frac{k_c}{k_m} G_m(s)}$$

Eq. 3.22: The chip thickness transfer function

The advantage of modelling chatter in this way is, that the chatter loop can be treated as a closed-loop and that classical control theory can be used to analyse the performance of the machine tool, such as stability and bandwidth.

3.5.1.5 Stability of the chatter loop

From the chatter loop (figure 3.19) it can be seen that the chip width b ($k_c = K_s\, b$) expresses the gain of the self excited process. Increasing the gain always results in a change from stable machining to chatter. By analysing the border line of stability (Nyquist criterion), the maximum axial depth (milling) and maximum chip width (turning) can be calculated.

The stability of the closed loop transfer function of equation 3.22 (figure 3.22), is characterised by the roots of its characteristic equation.

$$1+(1-e^{-Ts})\frac{k_c}{k_m}G_m(s)=0$$

Eq. 3.23: The open loop transfer function

where,

$$(1-e^{-Ts})\frac{k_c}{k_m}G_m(s)=G_{open\,loop}(s)$$

$$= \text{The open loop of the transfer function } \frac{h(s)}{h_0(s)}$$

From the frequency characteristics of the open loop the nyquist criterion is used to determine the stability of the closed loop system [32,79]. This leads to the derivation of the *structural equation*, *drive equation* and the *variation of chip thickness* (equations 2.1, 2.2, 2.3)

The *Structural equation* can be more generalized for both turning and milling (refer also to equation 2.1):

$$b_{cum_{limit}}=\frac{-1}{2K_s m_{cum}\operatorname{Re}\{G_m(j\omega_c)\}}$$

Eq. 3.24: The generalised "structural equation"

where m_{cum} is the number of inserts for all inserts inside the cut and b_{cum} the cumulative chip width (figure 3.16).

3.6 Summary

The basic mechanics of the cutting process have been studied. It is evident that it can be very complex to model the cutting process for 3 dimensional oblique cutting operations. Nevertheless, averaged static cutting forces and power can be predicted relatively easy, even for complex time varying milling operations. This knowledge will be used later in order to predict the static cutting forces for the design of the active work-piece holder (chapter 7). The traditional methods of modelling chatter in the LAPLACE and frequency domain have been studied. Most research carried out in machine tool chatter modelling and control relies on these fundamentals. This project tries out different and more unusual ways of doing this which can be more appropriate for modern digital controllers. Using the results of the foregoing analysis the next chapter will show the different approaches taken to modelling machine tool chatter in the digital domain.

Chapter 4

Theory for adaptive active vibration control

4.1 Introduction to vibration control

The goal of vibration control is to reduce the vibration of a mechanical system. It either can be active or passive. Traditional vibration control uses passive elements in order to control the system by increasing its stiffness or damping. The major limitation of this technique is that the vibration attenuation is only effective in a narrow bandwidth and is not capable of adjusting itself automatically if the structural response or the system changes.

The goal of adaptive active vibration control is to reduce the vibration of the mechanical system by modifying the system's structural response automatically.

The main components are:

- A sensor to detect the vibration
- An electronic or digital controller to manipulate the measured vibration in a certain way
- An actuator to influence the mechanical response of a system

The actuators can be classified into two categories:

- Semi-active actuators
- Fully-active actuators

The semi-active actuators behave like passive elements in order to control the vibration. They can only store or dissipate the oscillating energy. Therefore they effectively convert the vibration energy into heat. The performance of such actuators is dependent on the efficiency of this conversion process. Fully-active actuators are used to supply mechanical energy to the system, ideally in such a way that the disturbance vibration will be cancelled. Examples are electro-dynamic shakers, piezoelectric ceramics and electro-hydraulic devices.

Two main control schemes for active vibration control are discussed. These are:

- Feedback control
- Feed forward control

In general, the performance of a feed forward controller is better since it is theoretically possible to drive the vibration down to zero [80].

The whole concept of using energy (supplied by the actuators) to add stiffness and damping to a structural system in order to replace mass, is often referred to as being a discipline of *smart materials and structures* or *adaptronic structures* [81].

4.2 Smart materials and adaptronic structures

4.2.1 Background

For decades researchers and scientist have used nature as the inspiration for designing advanced systems. In recent years this inspiration has lead to an entirely new class of materials: Intelligent or smart materials and structures, which are based on biological analogies and nature's ability to adapt a material's structure to accommodate its changing environment. These new classes of structure have functions allowing them to change their shape, monitor their own "health", control vibrations and behave like materials they are not [81].

These new materials are described as structures that contain multifunctional parts by integrating their own sensors, actuators, real time control algorithms and memory capabilities composed with a material structural component as a skeleton (figure 4.1) [70,81,82].

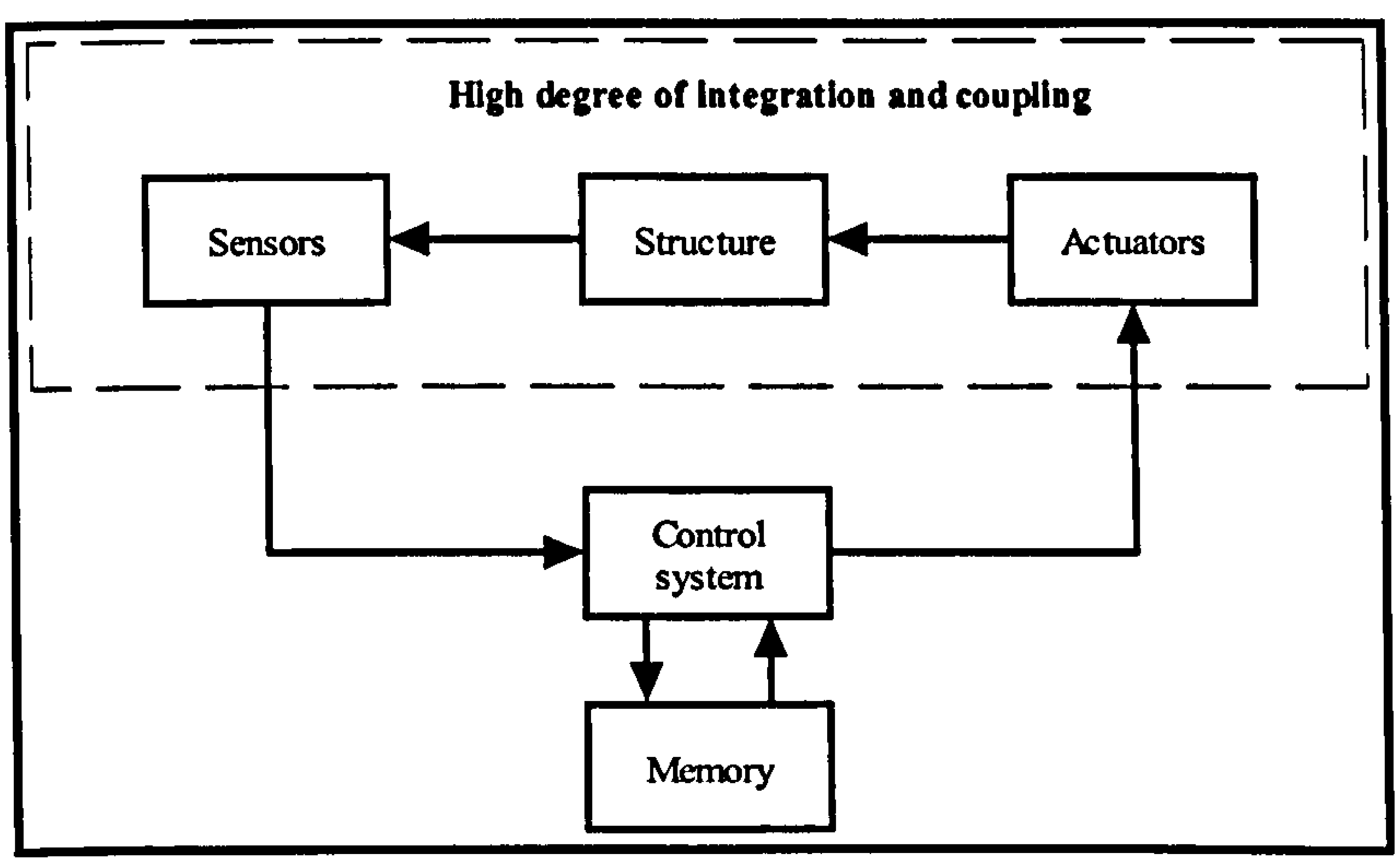

Figure 4.1: The technical definition of a smart material and structure

Today, several smart systems or structures are in various stages of development for civil and military applications [83,84]. An example is the shape control of propellers, which can provide vehicles of the air and sea with the ability to increase their efficiency, manoeuvrability and their structural life through vibration control. Aircraft designers are working on smart planes that continuously change the wing's shape to increase altitude and range of supersonic flights and even to evade radar detection. The health of structures such as bridges and aircraft wings can be monitored by integrating sensors into the structure. Such "passive smart sensors" deliver an accurate robust way to remotely monitor the structure's health on command, without expensive time consuming inspections.

4.2.2 Actuators

In general an actuator is an element that produces a physical quantity directly proportional to its electrical input. A network of embedded actuators can dynamically tune the global mechanical properties of a structure and therefore link the control system with the structure itself. Because of this they are often referred as artificial muscles.

Electrodynamic or electromagnetic shakers, pneumatic and hydraulic actuators are traditional types of actuators. But because of their size, mass, and energy consumption, they are not suitable for integration into a smart structure. In comparison to these traditional types, "smart" actuators" consist of one material only which, after being integrated into the structure, has the ability to change its shape, stiffness, position, natural frequency, damping or other mechanical characteristics. It could respond for example, to changes in temperature, electric and magnetic field. These "active" materials do not have the disadvantage of moving parts such as the armature in electrodynamic shakers for example. Table 4.1 gives an idea of the characteristic's of some actuator materials [83].

Actuator / **Characteristics**	Electro-strictive materials	Electro-Rheological Fluids	Nitinol Shape Memory Alloy	Magneto-strictive Materials	Piezoelectric Ceramics
Cost	Moderate	Moderate	Low	Moderate	Moderate
Technical Maturity	Fair	Fair	Good	Fair	Good
Networkable	Yes	Yes	Yes	Yes	Yes
Embedability	Good	Fair	Excellent	Good	Excellent
Linearity	Fair	Fair	Good	Good	Good
Bandwidth (Hz)	1-20 000	0-12 000	0-5	1-20 000	1-20 000
Maximum Mircostrain	200	---	5000	200	200
Maximum Temperature	300	300	300	400	300

Table 4.1: Comparison between different smart materials [83]

Recently, Weismüller et al [85], have found a way to make metal expand and contract like piezoceramics. This interesting approach may have a huge impact for the future of *Smart Materials*.

4.2.3 Sensors

Broadly speaking, a sensor or transducer is a device which transforms one type of energy into another. In smart structures, however a sensor is in general, an element that produces an electrical signal (for measuring and control purposes) relating to the physical quantity to be measured. A network of embedded sensors in a smart material is often referred to as the artificial nerves of the system. They have the ability to feedback the current state of the structure, which may be stimulated by the environment. They should be able to sense or "feel" every joule of energy (e.g. temperature or vibration), which the structure has been forced to accept through the environment. An important feature of these sensors is the possibility of integrating them into a structure. Most of the already discussed smart materials can be used as both sensors and actuators (table 4.2).

	Capacitive Devices	Strain Gauges	Piezo-electric Materials	Electro-, Magneto-Rheological Fluids	Shape Memory Materials	Magneto-strictive Materials	Electro-strictive Materials	MEMS	Fiber-Optice Devices
Actuators			X	X	X	X	X		
Sensors	X	X	X		X	X		X	X

Table 4.2: Active and passive materials used for smart structure applications [82]

The smart materials of table 4.2 are referred as *active sensors* since they do not need any additional energy. The energy of the stimuli is directly transformed into the energy of the electrical signal. Traditional sensors such as strain gauges, LVDT's, thermocouples and many others do not have that feature and are therefore regarded as *passive sensors*. They mainly consist of materials that convert physical energy into a change of electrical capacitance, inductance or resistance, which then can be detected and converted into electrical energy using additional signal conditioning [86,87,88].

The compact, commercially available, sensors used in this project for measuring force, vibration and precision positioning are:

- Strain gauges (strain) [87,89,90]
- Piezoelectric sensors (force and acceleration) [86,91,92]
- Micro Electrical Mechanical Systems – MEMS (acceleration) [93,94]

4.2.4 Control algorithm and memory

An ideal smart structure would be capable of sensing its environment and also being aware of its current state and conditions. It would be capable of diagnosing itself and taking actions to minimise the consequences and be capable of adapting its static and dynamic behaviour through a control algorithm, in response to changes in the structure, measured by sensors. It would then apply correction forces through actuators. Neural networks in control systems for example, mimic the human brain, where approximately 12×10^9 nerve cells or neurons, with dendritic connections, pass the signal from one neuron to another. The idea is to use many neurons as "simple" processing elements to perform very complicated tasks (e.g. control of non-linear systems). The strategy is to use very simple algorithms in a "this works better than that (or trial and error)" control methodology [95]. Unfortunately this involves a lot of computational power as already discovered by Pan et al [48]. However neural networks seem to offer a very encouraging solution for the future, since computing power is increasing.

Other feedback algorithms, which use much less computational power, are based on *classical feedback control theory* or *modern optimal control theory*. The plant is described either by an n^{th} order differential equation (classical theory) or in the case of *optimal control* by a set of first order differential equations describing the "state" of the system (based on the state variable concept). The classical approach uses the system output as a feedback signal, whereas modern control uses the system states as feedback. The controller design can be done either in the frequency domain (classical – bode diagram method), time domain (optimal control) or both as used in H_∞ *optimal control theory* [96].

The classical approach is based on open-loop measurements, where the frequency response is adjusted in order to achieve a certain closed loop performance. Based on the nyquist stability criterion the gain and phase margins are adjusted through the controller parameters, until the specification is met and before the feedback loop is closed [97].

In optimal control, feedback is used to minimize a cost function or performance index, which is proportional to the required system response. The objective is to reduce the response (e.g. vibration error) to the greatest possible extent. These synthesis techniques allow the "optimal" controller to be found analytically without trial and error. The control objective becomes an optimisation problem. By weighting the cost functions in *Linear Quadratic (H_2)* and H_∞ *optimal control*, the controller becomes more robust against system and noise uncertainty. For more information on optimal control the reader is referred to the literature [96,97,98].

The idea for the control algorithm used in this project stems from adaptive feed-forward control theory used in active noise control. Digital feed-forward control is especially useful when controlling the sound propagation in ducts (Figure 4.2 a).

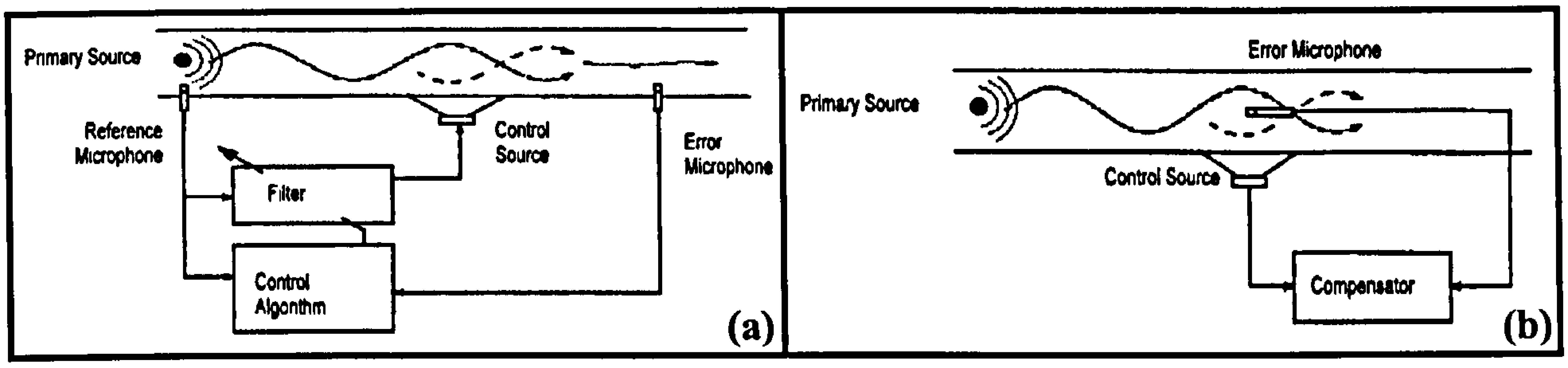

Figure 4.2:Feedforward- and feedback control in active noise control applications

Here the system between the reference sensor and control source (actuator) is controlled by a digital filter [80]. In feed-forward systems the error sensor is only used to monitor the performance of the controller. The impulse response of the digital filter may be adjusted by "hand" in response to the error signal, or the tuning may be done by a control algorithm automatically. It has been shown that digital feed-forward controllers can attenuate narrow-band noise, whereas analogue feedback controllers (Figure 4.2 b) are better suited for random noise [80]. For periodic narrow-band noise, where the signal consists of a repeating pattern of complex sinusoidal components, however, digital feed-forward systems achieve much better performance than traditional feedback controllers even when the disturbance is time varying (non stationary). Another very important advantage is that it is far easier to change the coefficients of a digital controller, even in real time, than those of an analogue one. *Hybrid control systems* combine both advantages, where the broad band performance is achieved by analogue feedback systems and time varying narrow band noise is tackled by the adaptive digital feed-forward system.

Because of the ability to attenuate periodic, deterministic signals even when the disturbance is time varying (machine tool chatter), the control algorithm used in this project is an adaptive digital feedback controller, since the reference signal is not directly available. But as we will see later it is possible to derive the reference signal from the error signal. Because of that the control algorithm shares its characteristic with the adaptive digital feed-forward controller.

Next the basic theory about digital filters, and how they can be used to model and control continuous mechanical systems are discussed in more detail. This work has also been published by Lockwood, et al [99] and gives more theoretical background for the control algorithm being used.

4.3 Mechanical system modelling using digital filters

4.3.1 Traditional methods of modelling mechanical systems

Vibrations are the response of dynamic systems to force. Systems are capable of storing kinetic and potential energy, which can be converted from one into the other. This results in oscillations or relative movement of objects around a reference frame or coordinate. In mechanical systems the kinetic energy is due to the velocities of mass elements (inertia) and the potential energy is due to spring elements or mass elements against gravity.

The study of vibration is concerned with the oscillatory motion of these elements or bodies and the force associated with them.

A goal of vibration analysis or modelling is to predict the response or motion of a vibrating system. Two basic approaches are being used:

- Newton's second law of motion based on momentum considerations
- Methods based on the consideration of kinetic and potential energy

Each model or equation uses the mechanical parameters:

- Mass (m)
- Stiffness (k)
- Damping (c)

This leads to the equation of motion of a simple single degree of freedom (*SDOF*) system (figure 4.3).

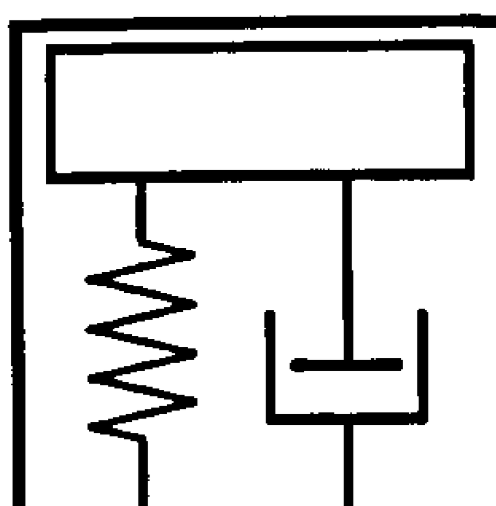

$$m\ddot{x} + c\dot{x} + kx = f(t)$$
$$(\rightarrow 0 \; for \; free \; vibration)$$

Figure 4.3:A mechanical SDOF system

This linear ordinary differential equation (*ODE*) can be solved in the time domain either analytically or through numerical integration.

If the structure is a multi degree of freedom system, then the structural dynamic model will become a set of differential equations in matrix from. Each degree of freedom will have its own resonant frequency (eigenvalues) and its associated mode shape (eigenvectors).

Even if the structure is an elastic body, it can still be assembled discretely as a rigid body system, also called a lumped parameter model. Elastic bodies are normally modelled analytically using wave equations or if more complex, discretely using the finite element method. [100,101]

Another possibility to obtain a model of the single degree of freedom system is to use the LAPLACE transform to solve the problem in the complex frequency domain ($s = j\omega$). This has the advantage that the differential equation is transformed into an algebraic equation (Equation 4.1).

$$\frac{1}{ms^2 + cs + k} X(s) = F(s)$$

Eq. 4.1: A simple mass, spring and damper system in the LAPLACE domain

After this algebraic equation has been solved, the inverse LAPLACE transform is used to transform it back to the time domain. The algebraic equation is also called the transfer-function of the vibration system *H(s)*. Again the transfer function is an "analytic" model, valid for a *SDOF*. To model an elastic body it will yield into a transfer function matrix [102].

If the mechanical parameters are known we have a parametric model and the vibration response can be calculated or predicted. If the system is unknown a vibration measurement will lead to a non-parametric model (*Frequency response function – FRF*), in which parameters need to be identified. This process is called curve fitting or parameter estimation and is illustrated in figure 4.4.

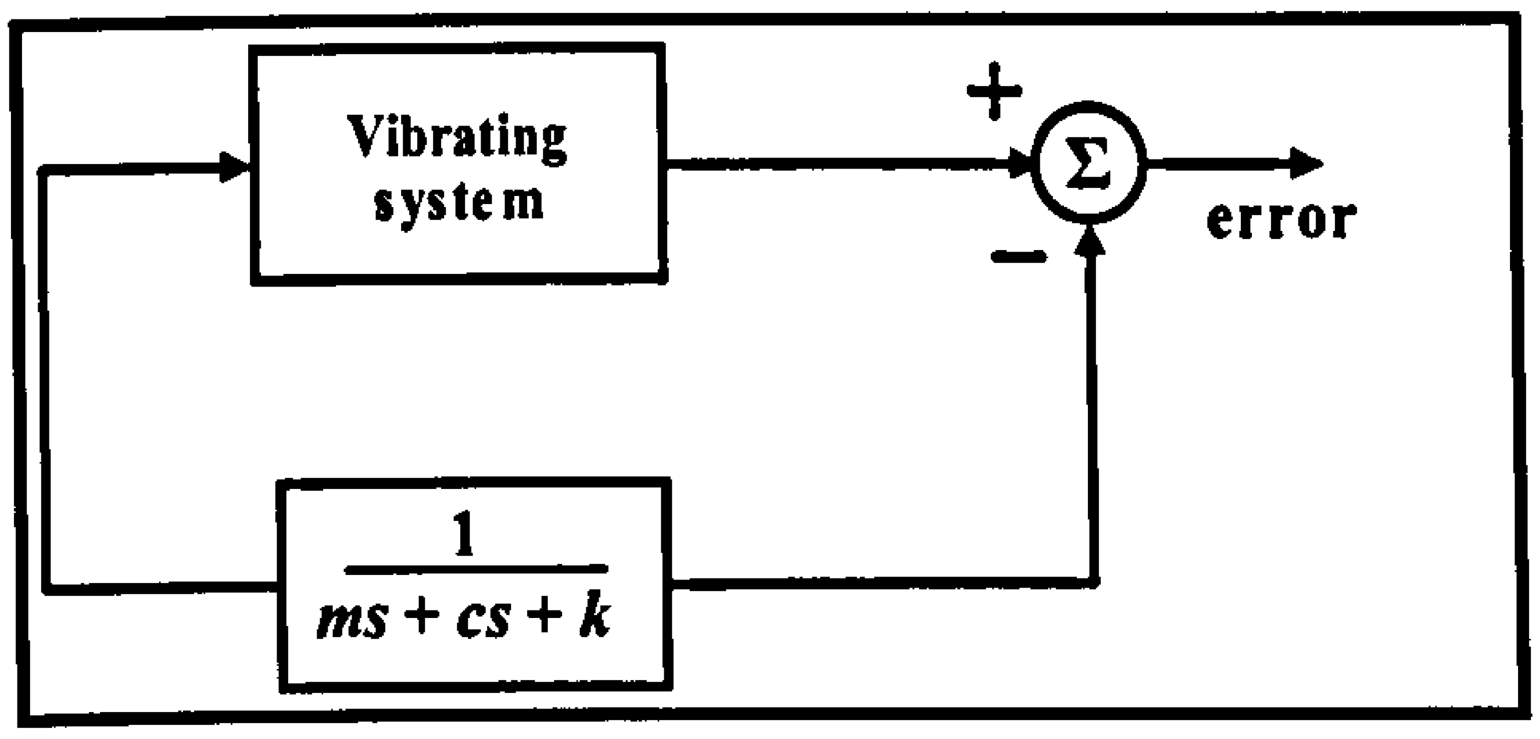

Figure 4.4: Parameter estimation method of a mechanical system

The goal is to reduce the error between the plant and the model in order to find the right parameters (if the system is more complex then the model will be higher order).

The identification process also reduces the large number of experimental values from the non-parametric model into a much smaller number of parameters for the parametric model.

It is also important to note that the curve fitting is done in the frequency domain and therefore it is an off line process after the experimental data (*FRF's*) are taken [103].

This method helps to design, re-design and improve a structural system since it is based on the mechanical parameters but it is not suitable for real time applications.

4.3.2 The digital approach of modelling mechanical systems

Digital filters on the other hand are based on the difference equation, which is the digital equivalent of the differential equation. If the sampling time is small enough these digital filters can represent any frequency response. Originally digital filters were used in signal processing, in order to extract certain information from a received signal (e.g. low-pass filters or band pass filters). But there is no restriction that a frequency response function from a modal test can not be modelled or synthesised as a digital filter.

The parameters of the filter are given by the filter kernel [95] along with its filter coefficients. Since the "vibration controller" will be implemented using a digital device (e.g. DSP based data acquisition card) digital filters are the ideal method of modelling a frequency response function and controlling the associated mechanical structure.

4.3.2.1 Difference equations and digital filters

As described in the previous section, the relationship between the input and output of a linear time invariant system (*LTI*), consists of elements which are able to store kinetic and potential energy, and this can be described as a linear differential equation with constant coefficients [104]. For discrete systems the differential equation will become the difference equation:

$$a_0x(n)+a_1x(n-1)+...+a_Nx(n-N)=b_0y(n)+b_1y(n-1)+...+b_My(n-M)$$
$$\rightarrow \quad y_n=a_0x(n)+a_1x(n-1)+...+a_Nx(n-N)\;-(b_1y(n-1)+...+b_My(n-M))$$

$$\Rightarrow \quad y(n)=\sum_{i=0}^{N}a_ix(n-i)\;-\;\sum_{i=1}^{M}b_iy(n-i)$$

Eq. 4.2:The difference equation

Therefore the output signal is a linear combination of the previous input and output samples weighted with the coefficients a and b. It can also be seen that difference equations have delays, where differential equations have derivatives. The integers *N* and *M* represent the order of the difference equation and just as for the differential equation, correspond to the number of energy storage devices in the system. As discussed earlier, for continuous systems the LAPLACE transform is used to solve differential equations. Therefore analog filters for traditional signal processing are designed using the LAPLACE transform. The equivalent for discrete systems is the z-transform. Just as the relationship between a system input and output is called a transfer function for continuous systems the name remains the same for discrete systems [95].

For example using the most simple approximation for derivatives, the second order differential equation from the spring mass system would become:

$$M\left(\frac{dx(t)}{dt}\right)^2 + C\frac{dx(t)}{dt} + Kx(t) = f(t)$$

Eq. 4.3:Differential equation for modelling continuous systems

$$\Leftrightarrow M\left[\frac{x(n)-x(n-1)}{T}\right]^2 + C\left[\frac{x(n)-x(n-1)}{T}\right] + Kx(n) = f(n)$$

Eq. 4.4:Difference equation for modelling discrete systems

$$Conversion\ to\ the\ z-domain\ where: \frac{d}{dt} = s \approx \frac{1-z^{-1}}{T}$$

$$\Rightarrow M\left[\frac{1-z^{-1}}{T}\right]^2 X(z) + C\left[\frac{1-z^{-1}}{T}\right]X(z) + KX(z) = F(z)$$

$$\Rightarrow (M + CT + KT^2)X(z) - (2M + CT)z^{-1}X(z) + Mz^{-2}X(z) = F(z)T^2$$

$$and\ back\ to\ the\ time\ domain\ where: X(z) = x(n);\ z^{-1}X(z) = x(n-1);\ z^{-2}X(z) = x(n-2)$$

$$\Rightarrow (M + CT + KT^2)x(n) - (2M + CT)x(n-1) + Mx(n-2) = f(n)T^2$$

Let

$$a_0 = \frac{T^2}{(M + CT + KT^2)}, \qquad b_1 = \frac{(2M + CT)}{(M + CT + KT^2)}, \qquad b_2 = -\frac{M}{(M + CT + KT^2)}$$

Then

$$x(n) = a_0 f(n) + b_1 x(n-1) + b_2 x(n-2)$$

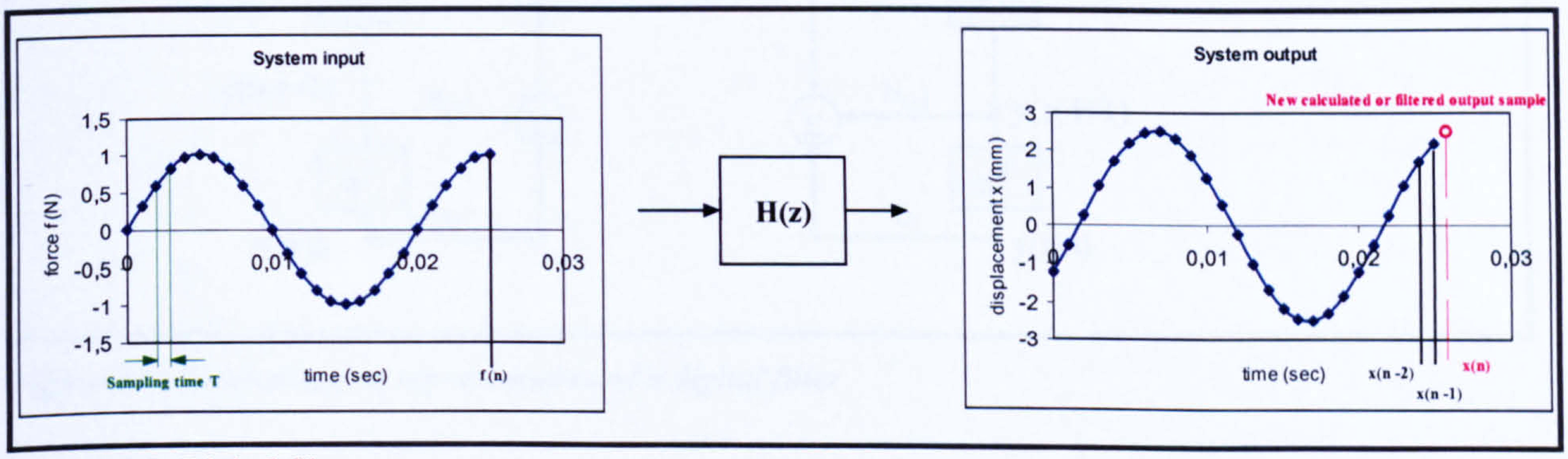

Figure 4.5: Digital filters

Figure 4.5 shows that if the sampling frequency becomes too low in comparison with the frequency components of the sampled signal than it is not possible to produce an accurate filter output signal. Which means that the difference equation is only valid if the frequency components produced by the system are much lower than the Nyquist frequency.

The transfer-function or block diagram, can be obtained by transforming the difference equation into the z-domain (replacing the unit delays with the appropriate z operator- equation 4.5 and 4.6).

$$y(n)=\sum_{i=0}^{\infty}h_i\,x(n-i)=\sum_{i=0}^{N}a_i\,x(n-k)\;-\;\sum_{i=1}^{M}b_i\,y(n-i)$$

Eq. 4.5:Digital filter representation in time domain (general differential equation)

$$H(z)=\frac{\sum_{i=0}^{N}a_iz^{-i}}{\left(1+\sum_{i=1}^{M}b_iz^{-i}\right)}$$

Eq. 4.6:Digital filter representation (transfer function) in the z-domain

The described transfer-function or filter is called an infinite impulse response filter (IIR) since the recursive form in theory makes its impulse response *h(n)* of infinite duration (equation 4.5). The impulse response *h(n)* is the equivalent of the transfer function *H(z)* in the time domain. By convolving the digital filter kernel, with an input signal, the output sequence can be calculated. Figure 4.6 shows the block diagram of the digital filter.

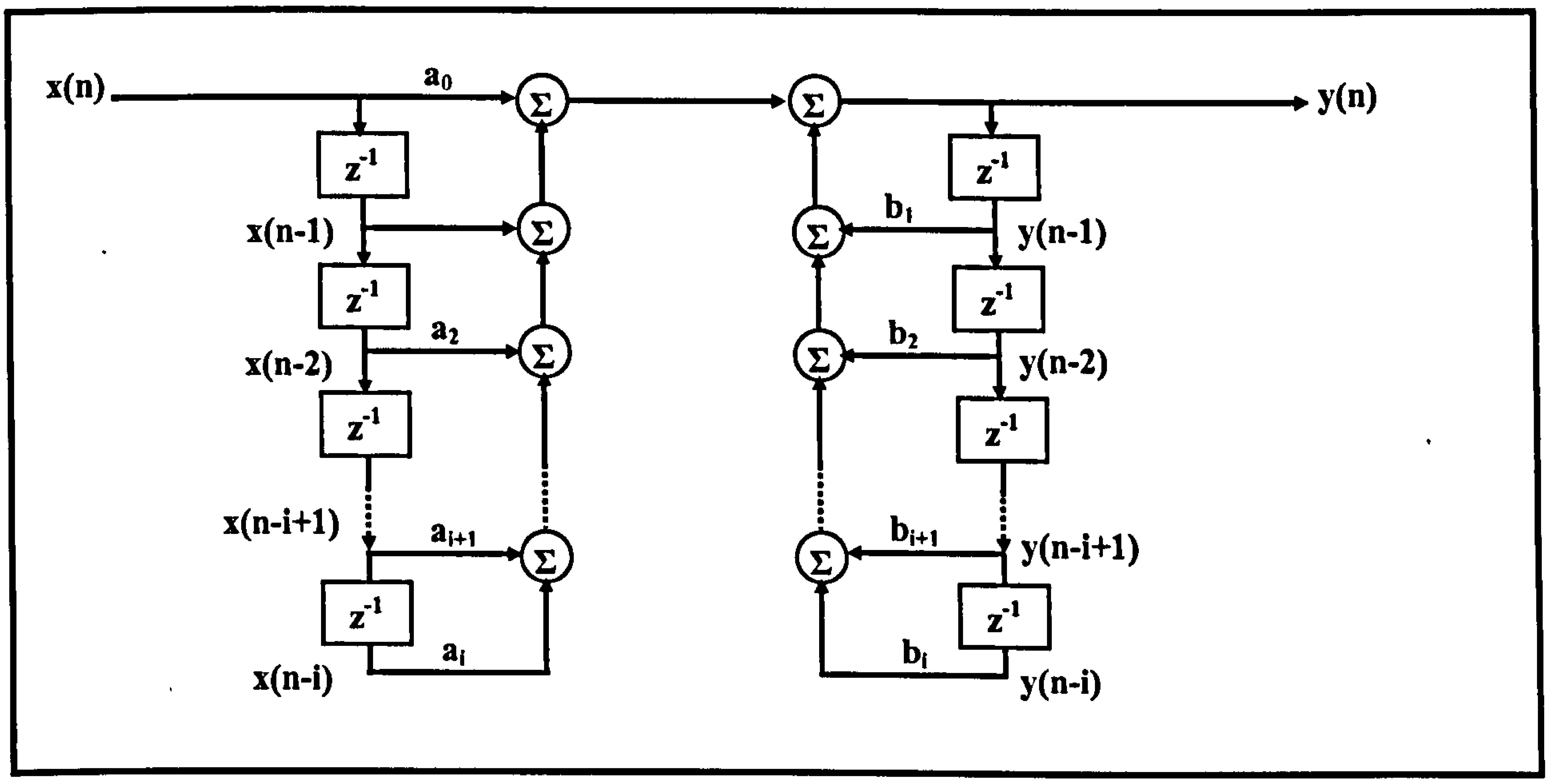

Figure 4.6: Block diagram representation of a digital filter

Other standard names for filters reflecting the number of filter coefficients *a* and *b* include:

- *Infinitive Impulse Response (IIR)-, all-pole-, recursive-,* or *autoregressive (AR) filters* when N=0
- *Finite Impulse Response (FIR)-, all-zero, non-recursive, transversal,* or *moving average (MA) filter* when M=0
- *Infinitive Impulse Response (IIR)-, pole-zero, recursive-,* or *autoregressive moving average (ARMA) filter* when N and M $\neq 0$

Especially interesting is the *FIR* filter, since its impulse response is of finite duration and because it does not use feedback, this type of filter can not become unstable, but requires a long filter kernel compared to an equivalent *IIR* filter. It is also interesting to note that *FIR* filters have no equivalent in the "continuous" world [105].

4.4 Adaptive filters

4.4.1 Introduction

An adaptive filter is a digital filter with self-adjusting characteristics. It means that its filter kernel with the filter coefficients adapts or adjusts itself in order to satisfy a certain criteria. For signal processing for example, the task is to filter a certain observed signal in order to extract certain information from it. In conventional signal processing this is done in an open loop manner, which means that the filter remains static. If the observed signal changes and it is decided to extract different information from it, the filter needs to be re-designed. In other words the system or filter is time invariant.

Adaptive filters on the other hand operate in a closed loop (feedback) arrangement, where the impulse or frequency response of the filter kernel is controlled by the feedback algorithm.

This means that they can be adjusted to cope with non-linear and time variant systems, where the frequency response or linear transfer function can be altered (adapted) in order to pass desired components of a signal through the filter and attenuate the undesired signal components. There might be also unforeseen changes in the statistical properties of the input signal (non-stationary signals). In general, adaptive filters have the ability to operate in a time-varying, non-stationary environment [106]. Figure 4.7 shows the general adaptive filter configuration.

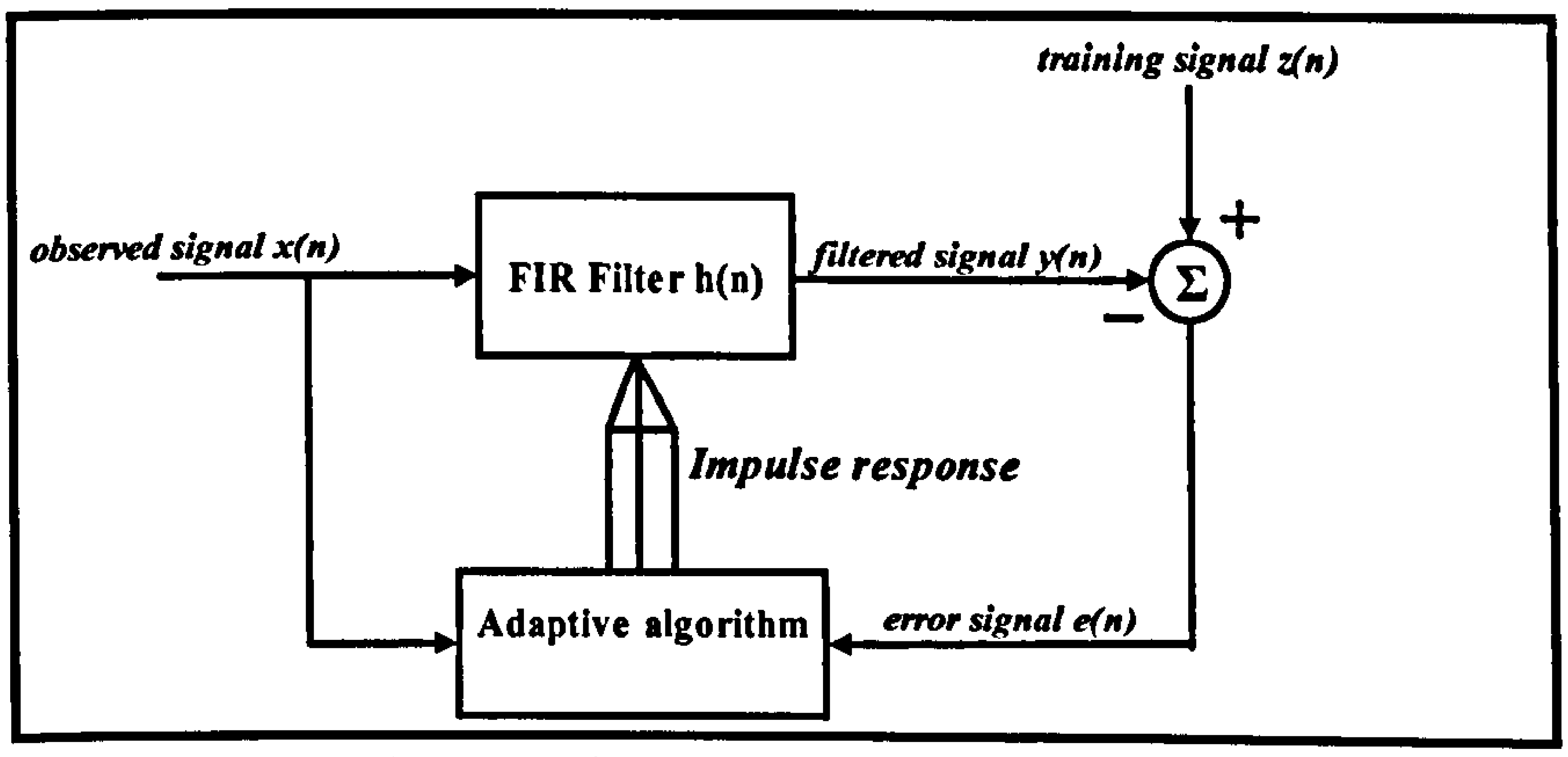

Figure 4.7: Adaptive filters in digital signal processing (here FIR filter)

Adaptive filters may be both infinitive impulse response (*IIR*) or finite impulse response (*FIR*) in nature. Often the *FIR* filter is preferred because of its inherent stability.

Figure 4.7 shows the general adaptive *FIR* filter. The observed signal or sequence *x(n)*, because it is discrete, is convolved with the *FIR* filter kernel *h* to obtain the filtered sequence *y(n)*.

$$y(n) = \sum_{i=0}^{N-1} h_i(n)\, x(n-i)$$ ***Eq. 4.7:The discrete convolution of a FIR filter kernel***

The weights of the FIR filter, or its impulse response *h(n)* are altered in such a way as to reduce the error signal *e(n)*. To take the time variation into account, the impulse is written as *h(n)* rather than simply *h*. The training sequence *z(n)* is subtracted from the filter output signal to yield a scalar error signal (equation 4.8).

$$e(n) = z(n) - y(n)$$ ***Eq. 4.8:The scalar error signal***

The optimum filter has been found when *e(n)* is zero and the training sequence matches the filtered signal. The solution is called the *optimum Wiener filter*, whose objective is to minimise the mean-square-error (*MSE*). This is done in the time domain, whereas other *optimum filters* are found in the frequency domain (e.g. *McClellan-Parks/Remez algorithm* – [107]). The *MSE performance index* or function has only one global minimum point, and finding it is also the objective of many current adaptive control algorithms. *Optimum Wiener solutions* can not be obtained in real time, since they require knowledge of the associated *autocorrelation* of the input signal and *cross-correlation* between the input and desired output signal. This means that many previous samples would have be taken into account. Nevertheless optimum wiener filters are often used to provide an optimum performance benchmark for other adaptive (real time) filter algorithms. Adaptive filters in comparison work on a sample by sample basis and do not have the auto- and cross-correlation function available. Instead they have the training or desired signal sequence, which is the representation of the expected or desired output of an optimal filter. There are 2 major classes of control algorithms used in conjunction with adaptive digital filters:

- *Recursive least square (RLS)*
- *Least mean square (LMS)*

A useful application of adaptive filters is in system identification, and this is discussed next in more detail since it has been used in this project.

4.4.2 Adaptive filters for system identification using the LMS algorithm

One of the main applications for adaptive filters is direct system modelling or system identification. Three major issues are involved in adaptive system identification:

- The excitation or training signal
- The filter structure
- The adaptive algorithm

If the excitation signal is rich in frequency content in order to excite all modes of the system and if the internal noise of the plant is small, the adaptive filter will converge to a good model of the unknown system. The filter can be an all-pole or pole-zero (*IIR*) filter, or may be an all-zero (*FIR*) filter with a large number of taps. The adaptive mechanism used here is the *LMS* algorithm (presented by Widrow) [108]. The objective of the adaptive filter *h(n)* is to minimize the residual error *e(n)*.

By taking for example the second order system of the spring mass damper model, whose mechanical parameters may be unknown, an adaptive *IIR* filter can be used to find the optimal filter coefficients directly in time domain. Figure 4.8 shows an adaptive *FIR* filter using the *LMS* algorithm.

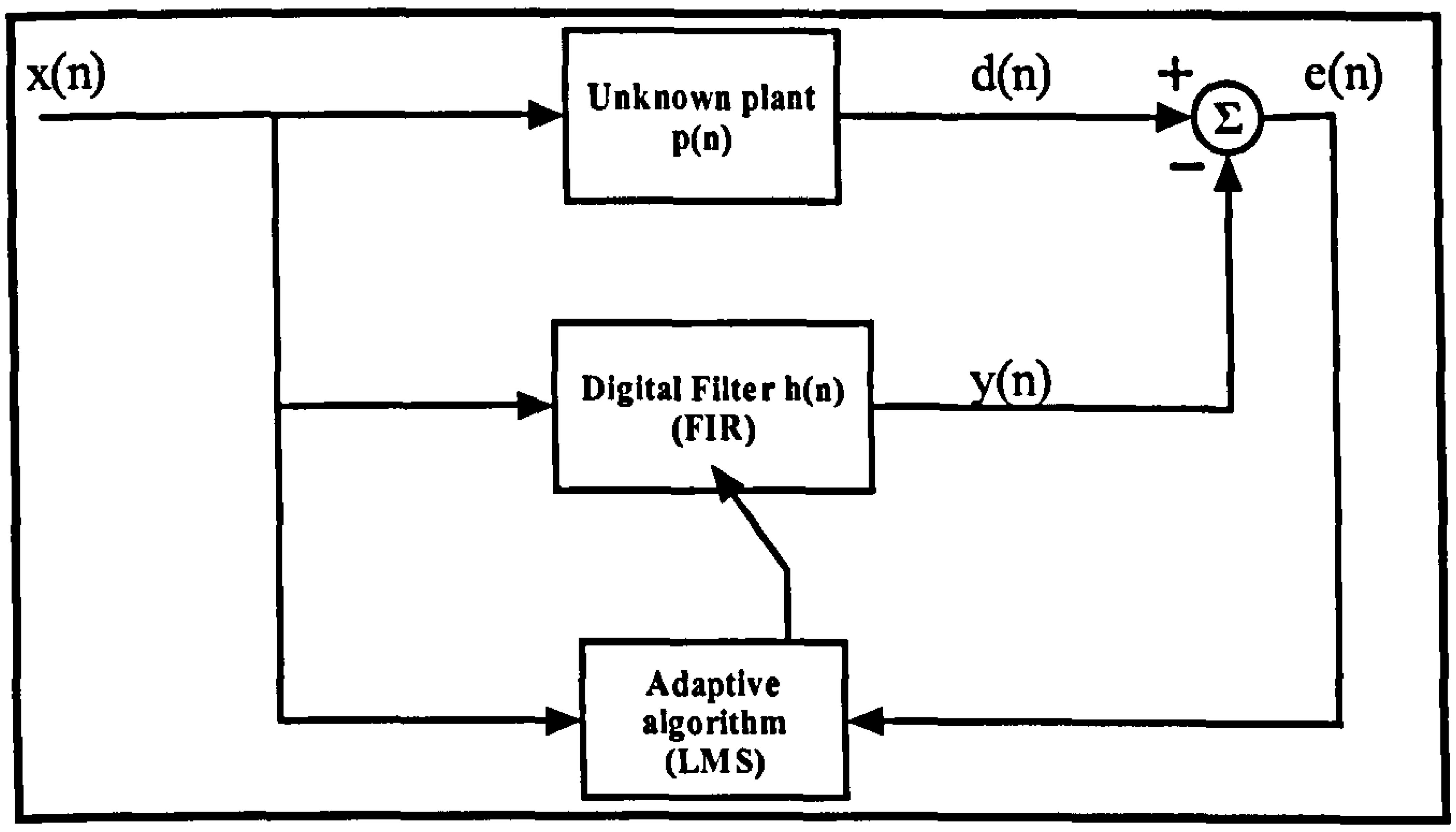

Figure 4.8: Adaptive FIR filter using the LMS

Assuming that the excitation signal is sinusoidal, it will pass through the plant *p(n)* with some gain and phase shift. It is desired to adapt the filter in such a way that the error signal will be minimised. The filter *h(n)* needs at least 2 coefficients to provide the desired gain and phase shift. A least mean square algorithm tries to minimise the mean-square (rms) value of the error by adjusting the filter coefficients. If the error signal is squared it will only have one global minimum. This function is sometimes also called a *cost-function* or *objective function.*

A typical 3 dimensional mean square *error surface* is shown in figure 4.9 (higher order filters have more than 3 dimensions).

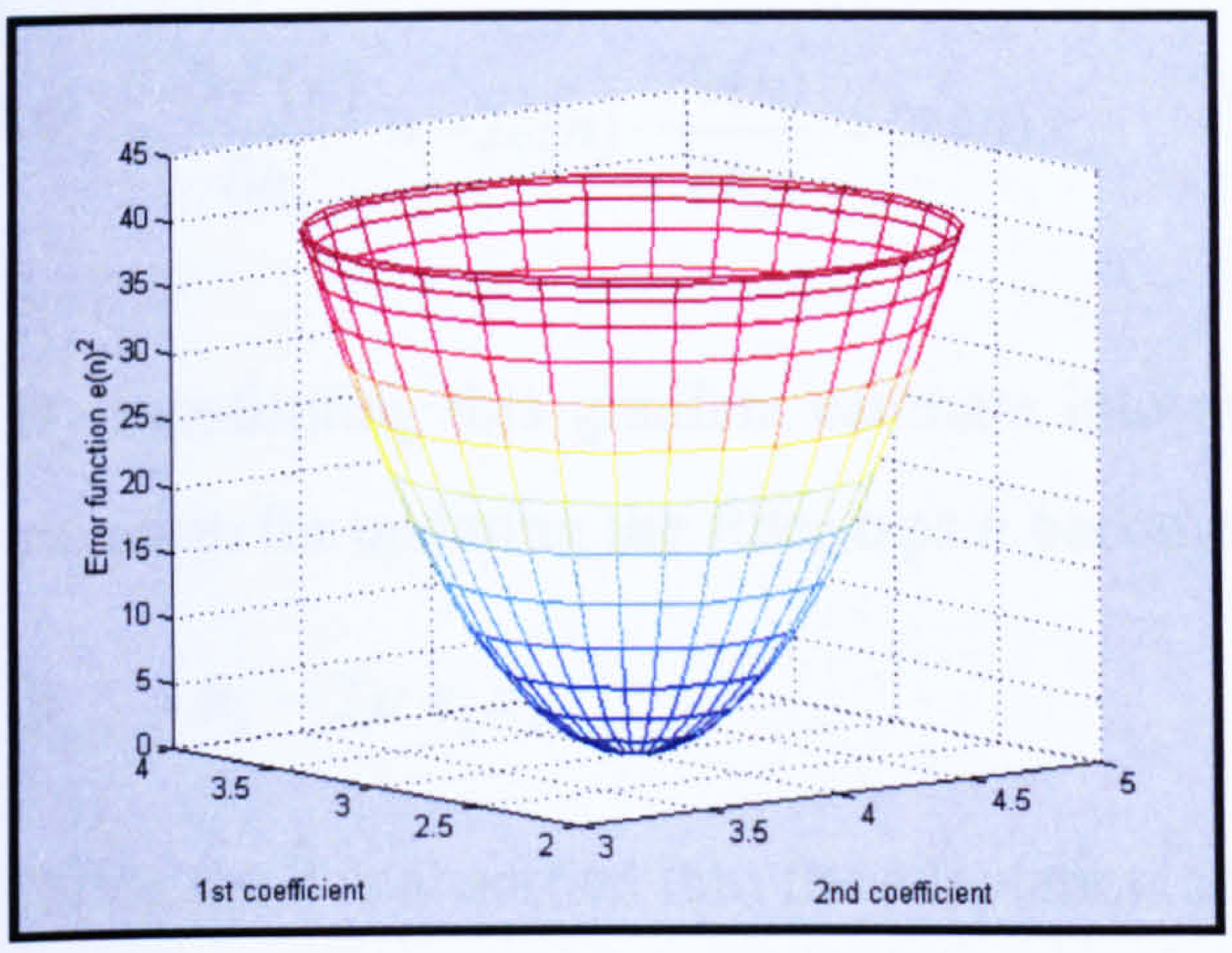

Figure 4.9: Error surface of a filter with 2 coefficients (taps)

The task is now to find the minimum of this function [108], since this will provide the optimum filter coefficients to drive the error signal down to zero (this is when the gain and phase shift of the unknown plant *p(n)* and the model *h(n)* are the same). Various gradient based methods algorithms such as *Newton's method* [108] and the *steepest decent* are available to make local estimates of the gradient of the *MSE* and move incrementally downwards to the "bottom of the bowl". The method of steepest decent for example, takes the following iterative approach to update each coefficient in order to find the minimum point of the mean squared error:

$$\boldsymbol{h}_{n+1} = \boldsymbol{h}_n - \mu \nabla_n$$

Eq. 4.9:The method of steepest decent

Where h_{n+1} is the new coefficient value, h_n the previous coefficient value, ∇_n the gradient of the cost-function and μ the adaptation coefficient. The adaptation coefficient determines the step size used for each iteration, which must be set small enough to obtain stability of the adaptation algorithm. The gradient after the differentiation of the cost function with respect to the filter coefficients becomes:

$$\nabla_n = \frac{\partial E[e^2(n)]}{\partial \boldsymbol{h}_n} = -2E[e_n \boldsymbol{x}_n]$$

Eq. 4.10:The calculation of the gradient

Here E[] is the expectation operator, e_n the current error signal and x_n the current input or excitation signal. The disadvantage here is that the whole error surface must already be known in order to find the minimum, where the gradient is zero. Since the filter taps (weights or coefficients) are updated sample by sample in order to find the minimum the assumption is made that the instantaneous values will on average adjust the coefficients in such way as to reduce the mean square error. This assumption makes real time application possible:

$$\nabla_n = \frac{\partial e^2(n)}{\partial h_n} = -2e(n)\cdot\frac{\partial e(n)}{\partial h_n} = 2e(n)x_n$$

Eq. 4.11:The real time estimation of the gradient used by Widrow [108]

By substituting this gradient estimate into the steepest descent algorithm (equation 4.9), the equation for updating the filter taps *h* becomes:

$$h_{n+1} = h_n - 2\mu\, e_n x_n$$

Eq. 4.12:The LMS or stochastic gradient

(often the 2 is absorbed into the adaptation coefficient μ.)

This is the well known *LMS algorithm* or *stochastic gradient algorithm.* If the filter is an infinite impulse response filter (*IIR*) the *IIR LMS algorithm* of Feintuch [109] can be used as a computationally simple algorithm to update the feed-forward and feed-back filter weights (figure 4.10).

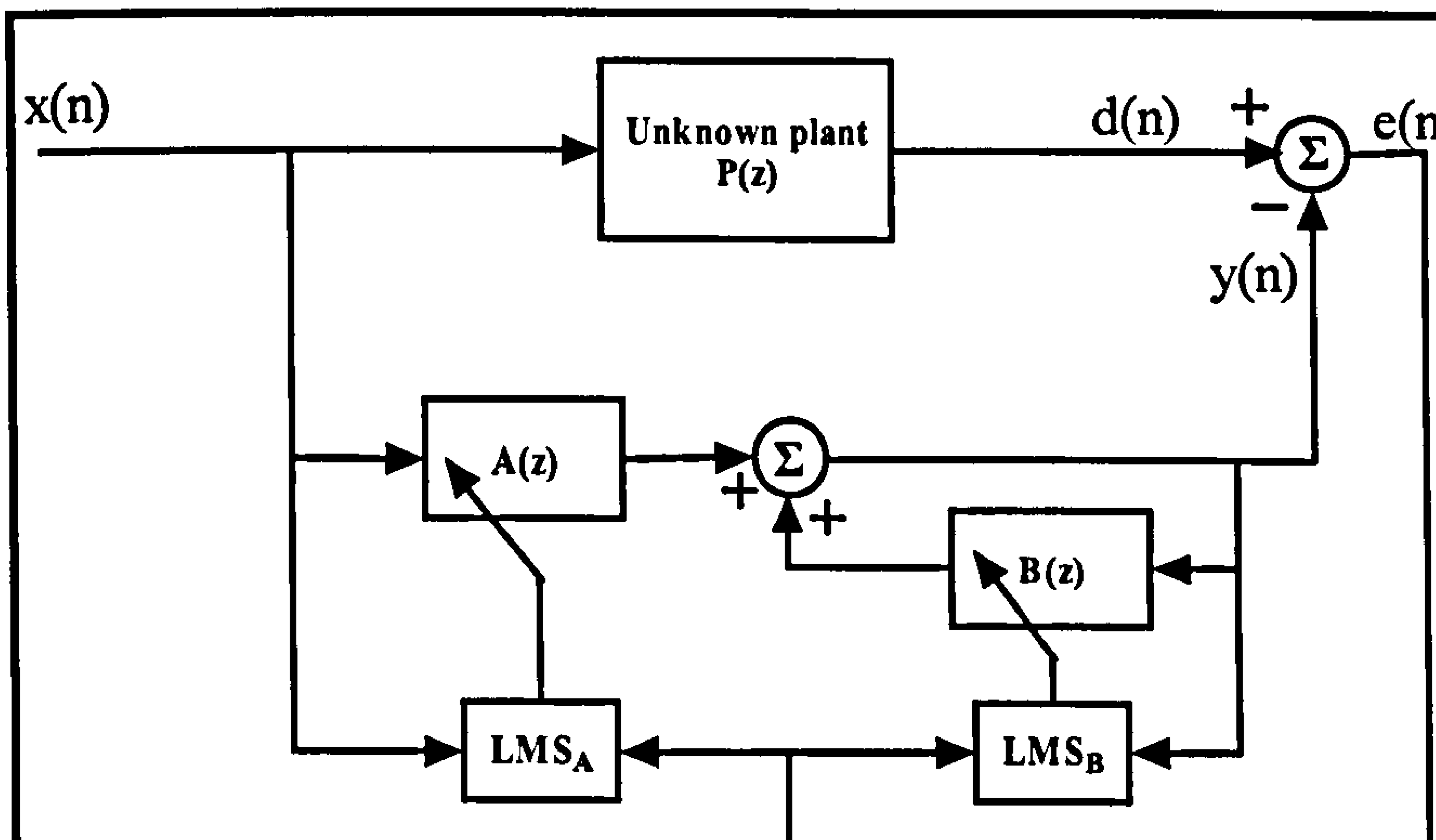

The Feintuch IIR LMS algorithm:

$$a_{l+1} = a_l - 2\mu_a\, e_l x_l$$
$$b_{l+1} = b_l - 2\mu_b\, e_l x_{l-1}$$

Figure 4.10: Adaptive IIR filter updated using Feintuch's IIR-LMS algorithm

Another more competent adaptive algorithm using an *IIR* filter has been discussed by Lockwood et al [99]. They used *Plackett's algorithm* (Recursive Least Squares algorithm) [110] to identify the cutting process of a milling machine under unstable machine conditions (chatter). Because of its complexity a very fast data acquisition board or DSP board is needed for real time implementation.

4.5 Adaptive control

Adaptive control uses adaptive filters in order to control a plant or dynamic system. The most important difference between adaptive control and traditional system identification schemes is that the summing junction is not digital any more. In adaptive control the summing junction is an acoustic summing point or for mechanical vibration control a mechanical summing point. In mechanical structures forces can be superimposed as long as the structure is linear or linearised for small perturbations around a point of operation, which is the assumption made here, and for vibration testing (modal testing) in general.

Figure 4.11 shows a LMS adaptive feed-forward controller for mechanical vibration control.

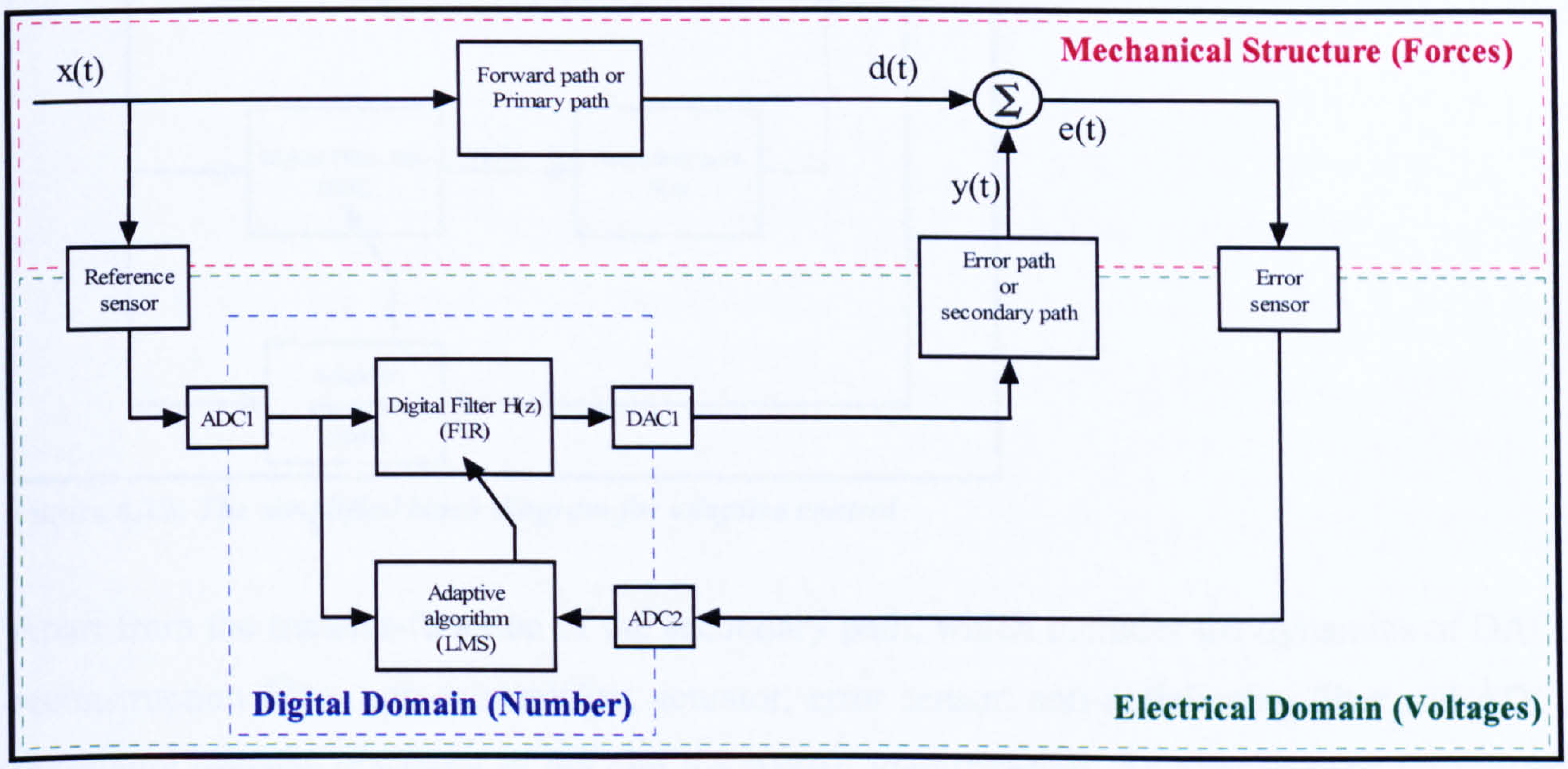

Figure 4.11: Parts of an adaptive control scheme

It is important to note that the signals need to be converted between 3 different domains:

- Digital Domain
- Electrical Domain
- Domain whose units needed to be controlled (e.g. mechanical or acoustical domain)

Actuators are used to convert from the electrical domain to the domain where the controller should perform actuation (electro-dynamic shakers or loudspeakers), where sensors are used for the other way round (force sensors, vibration sensors e.g. accelerometers, microphones etc.). The conversion from the digital domain to the electrical domain and vice versa is done by analog to digital converters (ADC) or digital to analog converts (DAC) respectively. It also

can be seen that the summation point, in comparison to the adaptive system identification arrangement has moved from the digital domain to the mechanical domain, in this case.
To improve the quality of the signal smoothing filters and anti-aliasing filters are often added. Figure 4.12 shows a simplified arrangement, since the dynamic characteristics of the sensors and ADC/DAC are not frequency dependent (normally a constant gain or calibration factor), in order to convert from one unit to a different one. They can also can become part of the remaining blocks by applying block algebra to them and by moving them over the summation and connection points into the other blocks [54].

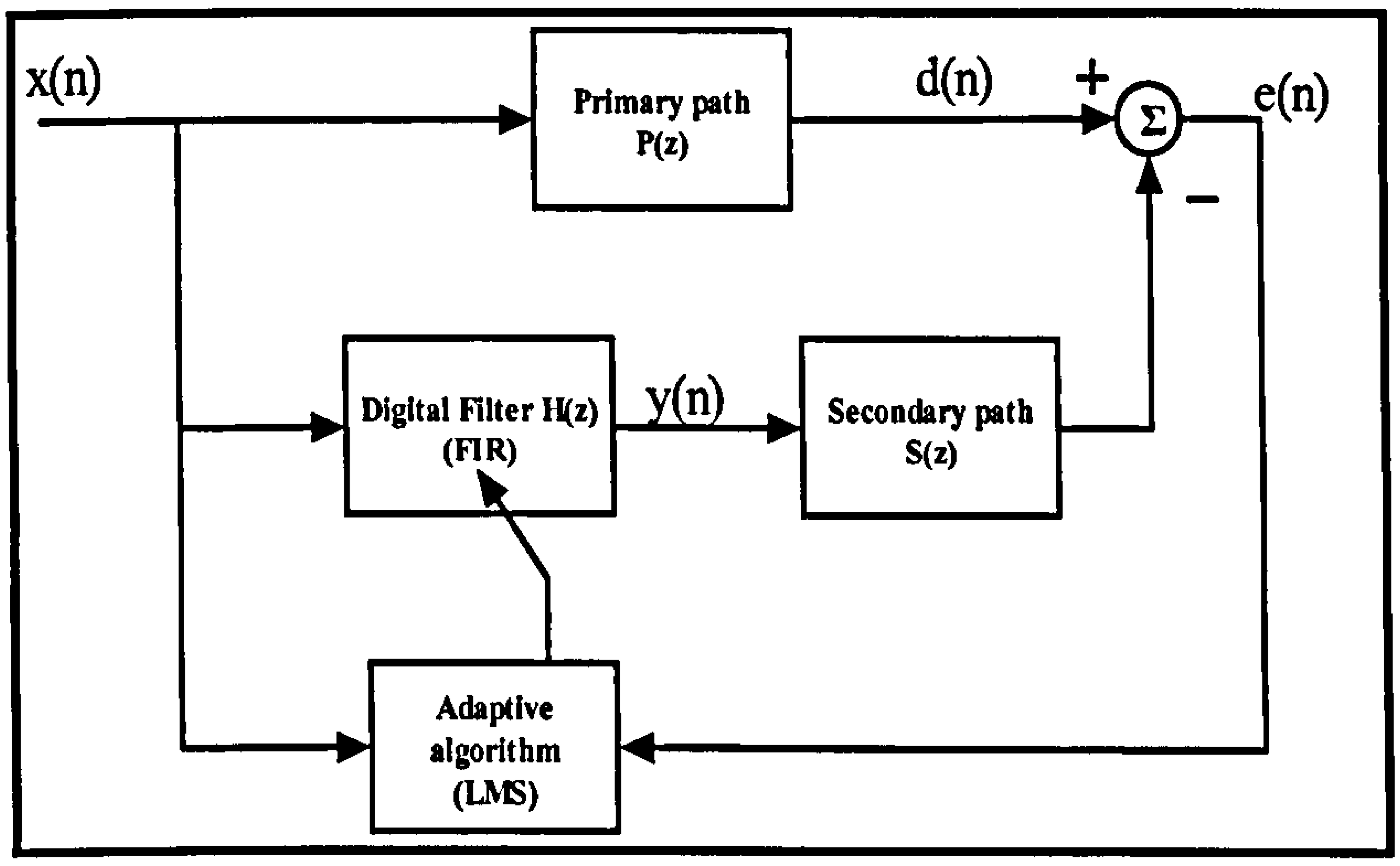

Figure 4.12: ***The simplified block diagram for adaptive control***

Apart from the transfer-function of the secondary path, which includes the dynamics of DAC, reconstruction filter, power amplifier, actuator, error sensor, anti-antialiasing filter and ADC, the model remains the same as the one for system identification. As already seen for system identification the error becomes zero if the digital filter converges to the same transfer-function as the primary path (equation 4.13).

$$e(n) = d(n) - y(n)$$
$$E(z) = P(z)X(z) - H(z)X(z)$$
$$For\,the\,optimum\,filter\,solution\;e(n)\,converges\;to\,zero \;\Rightarrow\; H_{optimum}(z) = P(z)$$

Eq. 4.13:The optimum filter solution in direct system identification using adaptive filters

For adaptive control, which includes the dynamics of a secondary path, the optimum filter solution will be:

$$e(n) = d(n) - s(n) * y(n)$$
$$E(z) = P(z)X(z) - H(z)S(z)X(z)$$
$$For\,the\,optimum\,filter\,solution\;e(n)\,converges\;to\,zero \;\Rightarrow\; H_{optimum}(z) = \frac{P(z)}{S(z)}$$

Eq. 4.14:The optimum filter solution in adaptive control

In other words the optimum filter $H_{optimum}(z)$ has to model $P(z)$ and an inverse model of $S(z)$. This requires an *IIR* filter or high order *FIR* filter. For the adaptive filter using the standard LMS algorithm the presence of the secondary path means that the difference between the filter output $y(n)$ and desired signal $d(n)$ is no longer available to update the filter coefficients. According to equation 4.14 the LMS algorithm uses an instantaneous estimate of the cross correlation $(e(n) * x(n))$ to update the filter coefficients. For adaptive control applications the phase characteristics of the secondary path would distort this cross-correlation estimate, since the reference signal $x(n)$ is not correctly "aligned" with the error signal $e(n)$. In practical terms this means that the LMS algorithm will generally cause instabilities for adaptive control, because of the presence of the secondary path.

However, one way of taking the transfer-function of the secondary path into account is to implement an inverse model of it in cascade, as shown by Widrow and Stearns [108]. This obviously only works if the inverse model of the secondary path is stable (minimum phase characteristic). Another much better possibility of "aligning" the reference signal with the error signal is to use the same secondary path, which has separated the adaptive filter output $y(n)$ and the error signal $e(n)$ and also to modify the reference signal $x(n)$. Proposed by Morgan in 1981 [54], the *filtered-reference LMS or filtered-x LMS* (FXLMS) algorithm pre-filters the reference signal with an estimated digital model of the secondary path, so that the error signal and filtered reference signal are again aligned in time to give a valid cross-correlation estimate. Figure 4.13 illustrates this for adaptive control updating algorithm.

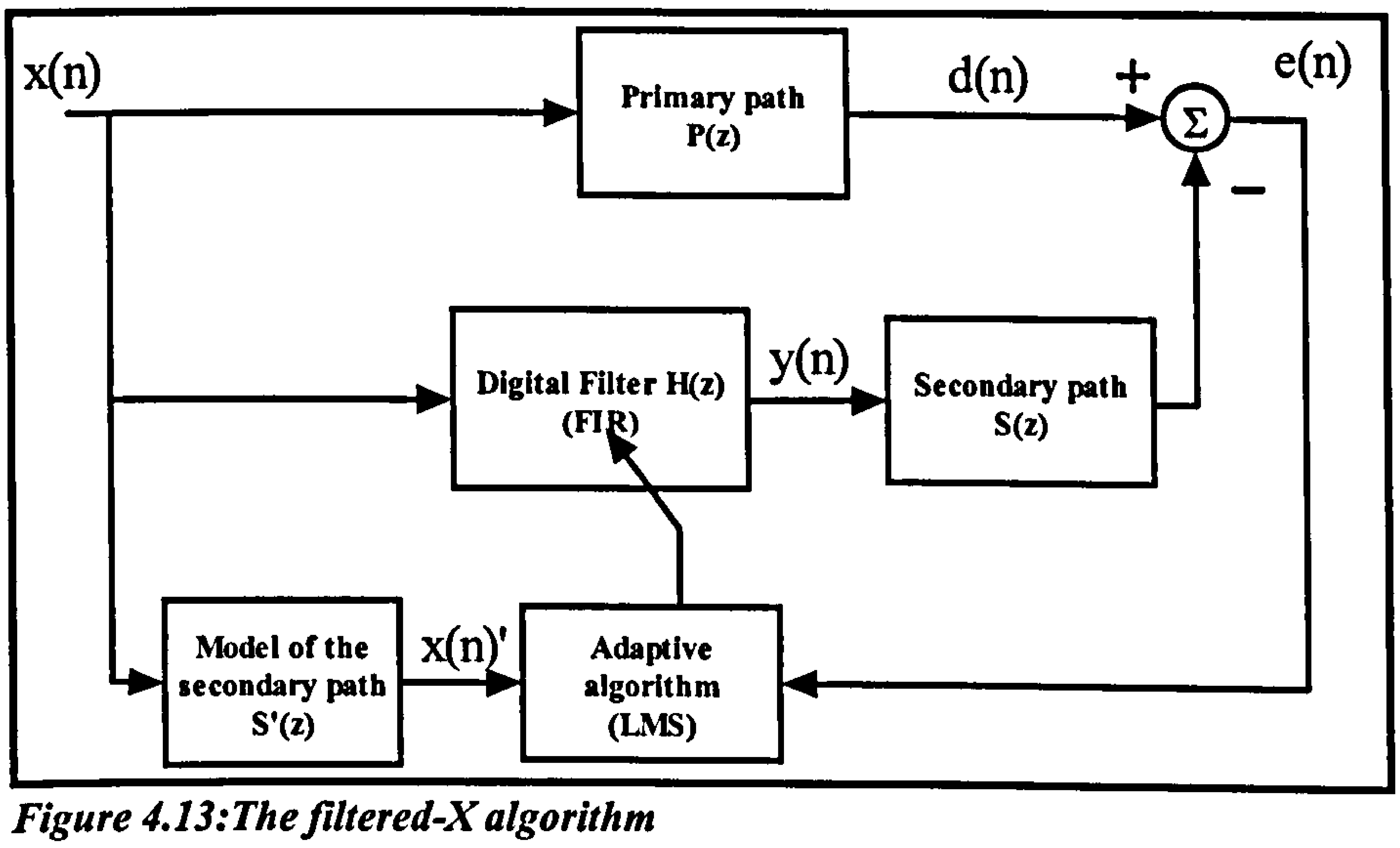

Figure 4.13: The filtered-X algorithm

$$h_{n+1} = h_n - 2\mu\, e_n x_n'$$

Eq. 4.15: Filtered x LMS algorithm

Morgan [54] and also Boucher et al [111] showed that if the adaptation coefficient μ is small enough the coefficients of the adaptive filter will converge to the optimal values, even with phase errors between the secondary path and its model of up to +/-90 degrees. It is also very important to realize that the additional secondary path model requires additional computational power for the controller, but only needs to be accurate for the disturbance frequencies of interest. For a single frequency only, a two tap FIR model, which is very fast, would be enough.

Both, the LMS and the FXLMS algorithms require a reference sensor, which is part of any feed-forward control system. Feedback systems in comparison do not have a reference sensor to give time advanced information about the disturbance being controlled. The primary source, which generates the disturbance, can not be directly observed. Furthermore, a feedback system always needs a signal to be measured. A digital feedforward system in comparison, has the theoretical potential to cancel a harmonic signal down to zero, since the error signal only monitors the performance of the controller, whereas the reference signal is used as a controller input. For many feedforward systems the error signal can be reduced to almost zero without affecting the amplitude of the reference signal (weak feedback path). Feedback systems in comparison use the error signal as the controller input. By taking a harmonic excitation for example, the controller may go unstable when the error is reduced to such as extent that the controller is only supplied with the uncorrelated noise of the vibration sensor. Practical examples are given in chapter 6, where a simple beam structure is controlled using both feedforward and feedback control.

A simple adaptive feedback controller could use the error measurements for both error- and reference signal. Because of the correlation between reference and error signal care must be taken with the fact that there is no guarantee that the error surface will be unimodal (only one global minimum) as it was in the feedforward case. In order to add robustness to such systems a leakage factor can be introduced to the FXLMS algorithm (equation 4.16), to weight the filter coefficients [112].

$$h_{n+1} = \gamma h_n - 2\mu\, e_n x_n$$
$$\textit{with the leakage factor}: 0 < \gamma < 1$$

Eq. 4.16: Leaky FXLMS algorithm

Practically the leakage prevents the adaptive filter reducing the error signal down to zero. The amount of leakage determines the amount of vibration left in the system. This algorithm is very practical for possible instabilities in adaptive feedback systems [53,113], as will be seen later.

Another very interesting feedback approach has been presented by Morani [98,114]. He has introduced a method of transforming the feedback design problem into a feedforward one with all its associated advantages.

The differences between the classical feedback structure and the new *Internal Model Control (IMC)* structure approach can be seen in figure 4.14.

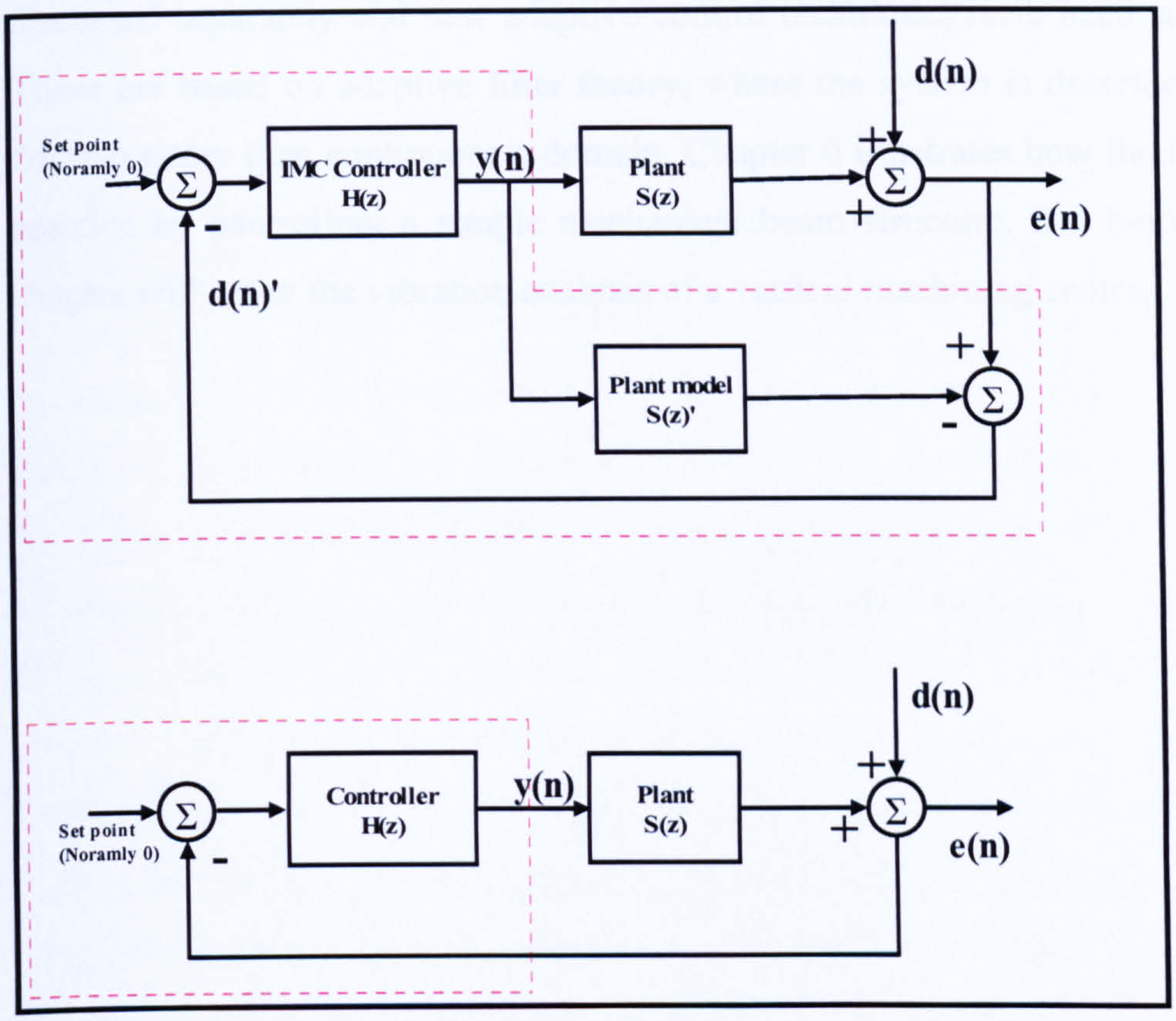

Figure 4.14:Digital feedback controller using the IMC structure (top)
Digital feedback controller using the classical feedback structure (bottom)

The figure shows that the IMC estimates the disturbance signal *d(n)*, which is then used as the reference signal. The huge advantage is that the IMC controller is now a feedforward controller, which can also cancel the influences of unmeasured disturbances. It has a reference signal as the control signal and an error signal to monitor the controller performance. This means that the error could the reduced down to a level (zero), which the classical feedback controller would not be able to achieve. Practical results can be seen later in chapter 6.

4.6 Summary

The theory of adaptive active vibration control has been studied. Today, the use of *smart materials,* in active vibration control are of great interest since they allow the integration of sensors and actuators into the same structure skeleton. This new science is called *smart materials-* or *adaptronic structures*. The sensors or "nerves" of the system are linked through the control system (incl. memory) to the actuators or "muscles" to compensate for any changes in the environment (disturbance). Actuators, sensors and control strategies have been discussed separately and new adaptive control techniques have been studied in more detail. These are based on adaptive filter theory, where the system is described discretely in the z-domain rather than continuous s-domain. Chapter 6 illustrates how the theory can be put into practice by controlling a simple mechanical beam structure. But before that the following chapter will cover the vibration analysis of a vertical machining centre.

Chapter 5

Vibration analysis of a vertical machining centre

5.1 Introduction

It is clear from the literature research that there is a great need for structural vibration control on machine tools, especially because these machine errors can affect the surface finish of the component more than any others.

The identification of the effect of vibration on Machine tools, together with research into active vibration control techniques to reduce this, are the main aims of this research project.

In the first section a 3-axis vertical milling machine is introduced. This is followed by the design of the MEM's accelerometers, which have been used for most of the vibration measurements. Then all possible vibration sources of the milling machine have been investigated. An experimental modal analysis of this machine was conducted by AMTRI [115], which was then confirmed and extended to a wider more interesting frequency band. stable and unstable cutting tests revealed the true vibration levels of this machine under real cutting conditions. The unstable chatter tests also confirmed the theory covered in chapter 3. A very interesting observation regarding the frequency development of self-excited vibration (chatter) has been made and the surface finish has been analysed and correlated with the vibration readings from the vibration sensors.

Part of this chapter has already been published by Haase et al [116].

5.2 Practical structural investigation of a vertical milling machine

The Beaver VC35 is a vertical 3 axis-milling machine built in 1983. The tool moves in one direction (z-axis) and the machining table moves in two directions (X and Y-axis) on planar guide-ways. The spindle speed can be controlled from 63RPM to 5500RPM and the maximum axis feed-rate is 10 m/min. The feed drive system is by SIEMENS, whereas the spindle drive system and DC motors for feed and spindle are from CONTRAVES. The CNC controller is from FANUC.

Figure 5.1 shows the analysed milling machine.

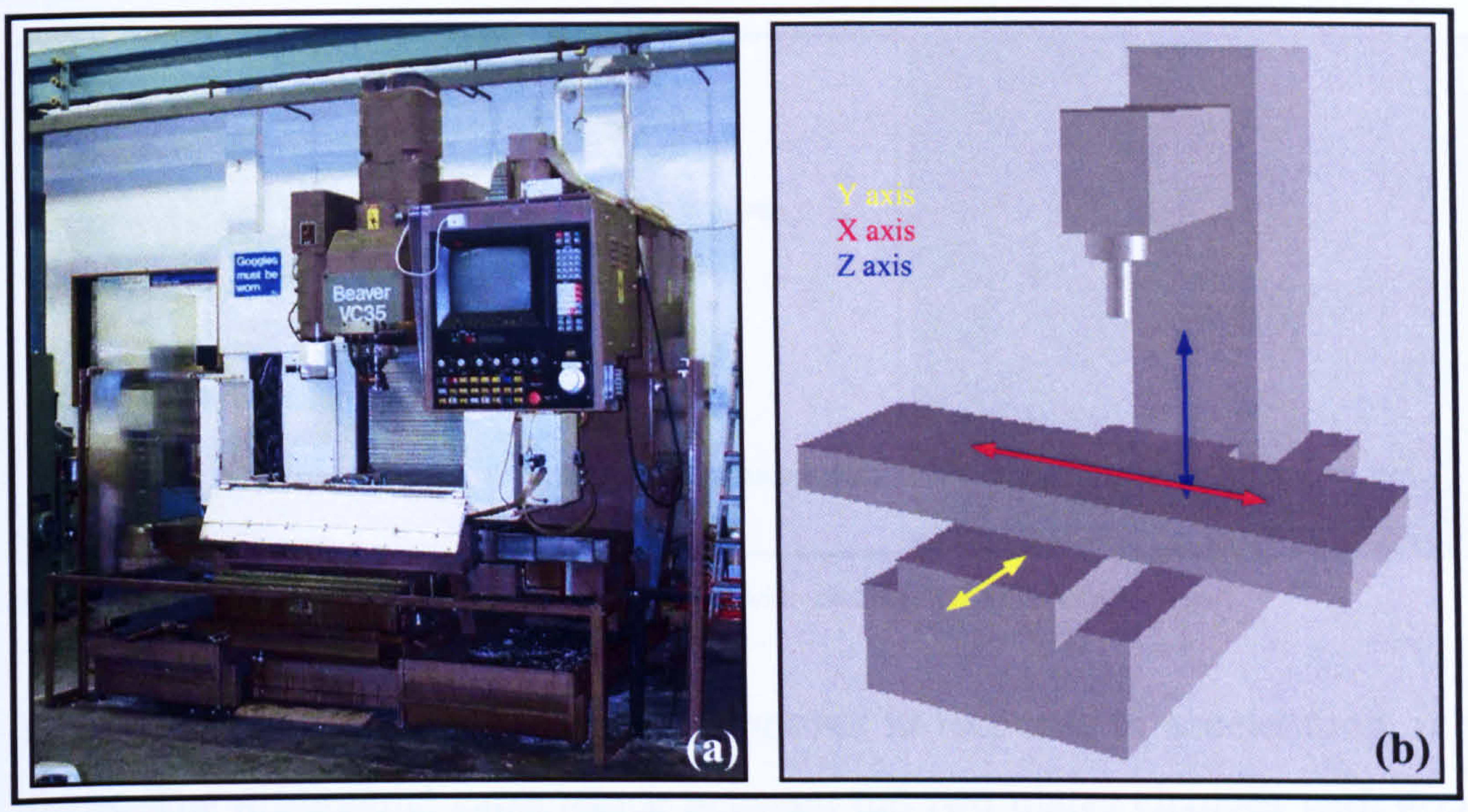

Figure 5.1: 3-axis machining centre (Beaver VC35): Physical machine (a), Schematic machine structure (b)

5.3 The sensor design

The most appropriate physical quantities to measure and use to evaluate the cutting process are the energising cutting force and the resulting relative displacement between tool and work-piece. The cutting force can be measured using a dynamometer and displacement sensors can measure the relative vibration.

The most convenient sensor to measure vibration however is the accelerometer. It measures absolute vibration and the most common type is based on the piezo-effect. The cost of measuring acceleration using these accelerometers is relatively high, because of the need for expensive signal conditioning units such as charge amplifiers. In these experiments several points need to be considered simultaneously and therefore an investigation of lower-cost sensors was carried out.

5.3.1 MEMS sensors

In general Micro-Electro-Mechanical Systems (*MEMS*) is the integration of mechanical elements, sensors, actuators and electronics on a common silicon chip [93,94]. In Europe the new technology is sometimes called Microsystems Technology (MST). While the electronics are fabricated using integrated circuits (IC) e.g. CMOS or Bipolar, the micro-machined components are fabricated using "micro-machining" processes that selectively etch away parts of a silicon wafer and add new structural layers to form a mechanical and electromechanical device.

Figure 5.2 shows the principles and sensor structure of an MEM accelerometer.

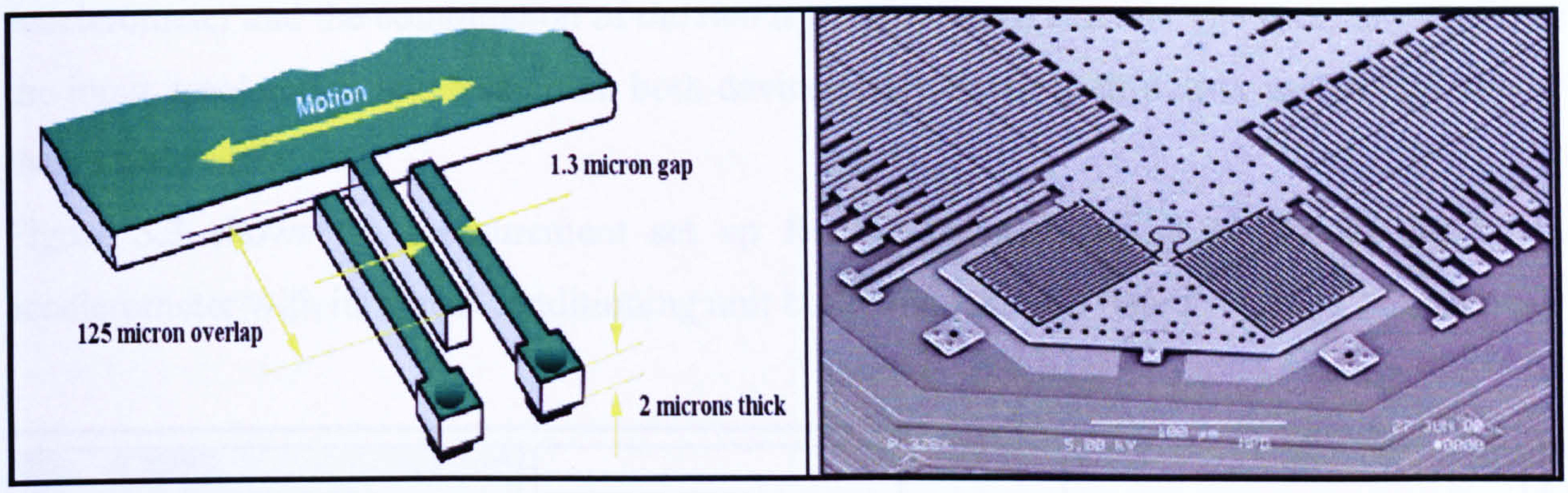

Figure 5.2: Principle and beam structure of micro-machined accelerometers

They are made from a beam plate that moves in response to acceleration, relatively to fixed plates. The differential capacitance between the two plates changes with acceleration and is measured with the on chip circuitry.

The big advantage of MEMS accelerometers over piezoelectric sensors is their low cost. The major disadvantage is the resolution, which is limited by the noise-floor. Although continuously improving, it is still in the range of *mg*, compared to μg for high quality piezoelectric devices.

Today every new car being sold has micro-machined sensors on board. They are used in applications ranging from MAP (Manifold Absolute Pressure) engine sensors to accelerometers for active suspension, stability-control (rollover), anti-lock braking and airbag systems. But the field is widening fast in applications such as diagnostics or machine monitoring. [94]. Pitter et al [117], for example, describe the advantages of these silicon vibration sensors on machine tools.

5.3.2 The AD XL 105 accelerometer

The AD XL 105 [94] was used in this research, because it has a good resolution and the range is +/- 5g. Apart the low cost of the sensor, it also is low in weight, which is an advantage for structural testing of light structures. For machine tool applications the small size also make it possible to mount them near the process to be observed [117]. The accelerometer chip also incorporates a temperature sensor and an integrated operational amplifier, which can be used for signal conditioning. In this case it was configured as a second order Bessel filter [118], which cuts off signals over 3kHz. This gives a calibrated and known frequency response.

The sensor was calibrated using the back-to-back method. The calibration was carried out according to an established Brüel & Kjær procedure [86]. The accelerometer, whose sensitivity is to be measured, is mounted in a back-to-back arrangement with a reference accelerometer and the combination of the two is mounted on a suitable vibration source. Since the input acceleration is the same on both devices the ratio of their output is also the ratio of their sensitivities.

Figure 5.3 shows the measurement set up for the back-to-back method and the MEM accelerometer with its signal conditioning unit built onto a circuit board.

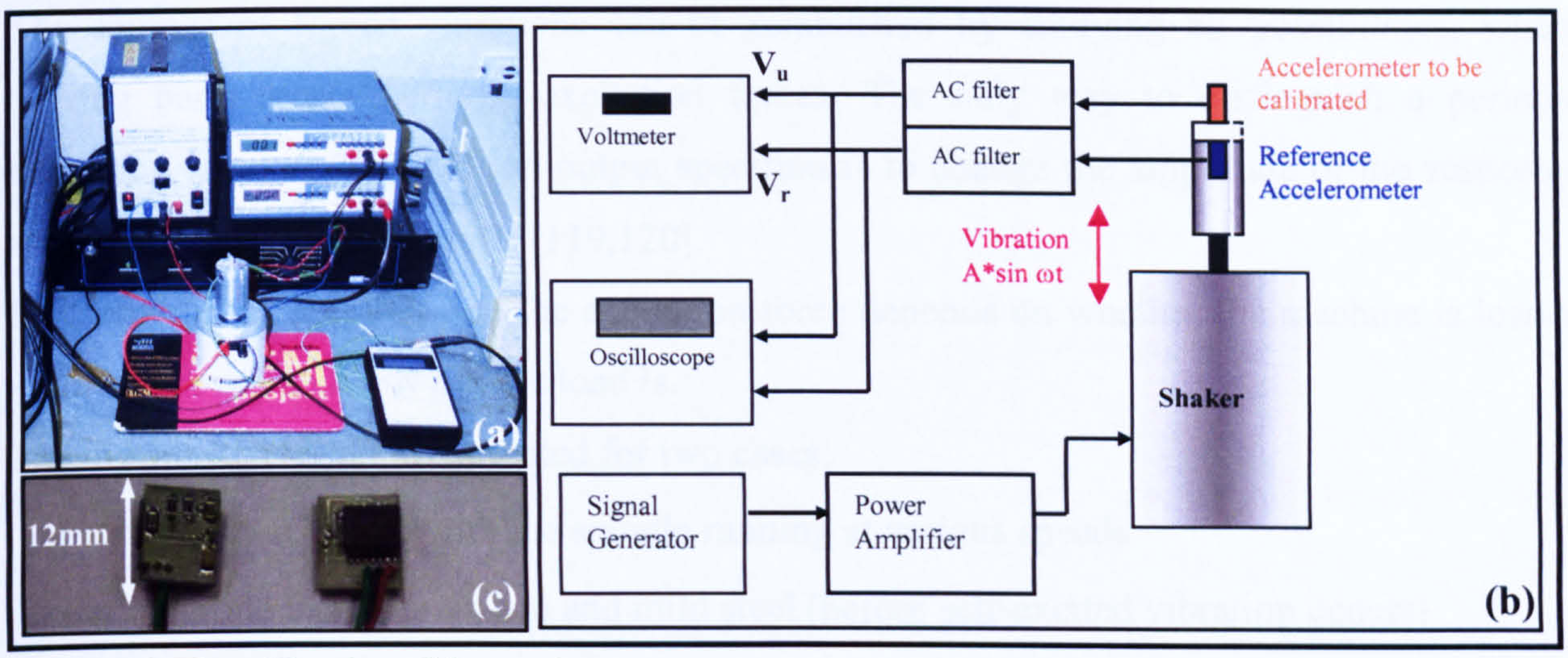

Figure 5.3:The calibration of the accelerometer:
- ***Experimental set up (a)***
- ***Schematic set up (b)***
- ***AD XL 105 including signal conditioning unit (c)***

The accelerometers were excited with a sinusoidal acceleration signal at a constant frequency and a constant amplitude and their outputs then passed through signal conditioning units and measured individually by a high quality voltmeter. For a linear sensor with flat frequency response it makes little difference at what level or frequency the accelerometer is calibrated (usually between 50-200Hz) as long as it lies within the normal working range of the accelerometer [86].

The following equations were used to calculate the sensitivity of the MEM accelerometers:

$$g_r = g_u$$
$$\frac{V_r}{S_r} = \frac{V_u}{S_u}$$
$$S_u = S_r \cdot \frac{V_u}{V_r}$$

Eq. 5.1:Calculation of the unknown sensitivity of the accelerometer

Further "static" and "dynamic" tests at different vibration levels have confirmed a linear frequency range and flat frequency response of the MEM accelerometers.

5.4 The vibration sources of the Beaver machine

It is important to know the sources of forced vibration before cutting tests are carried out since the output of any vibration sensor is the sum of all excitation forces, whether they are random, forced or self-excited. These forced vibration sources can be amplified through the structure of the machine, when the excitation frequency matches with one of the structural resonance frequencies. Experience has shown that even small excitation forces at the right frequency can dominate the vibration frequency response.

The sources of forced vibrations can be established by studying all possibilities, where moving parts create periodic excitation forces. The only way to distinguish a periodic excitation force in the vibration output spectrum is to change the amplitude of the suspected source and compare the results [119,120].

Furthermore the amplitude of the excitation force depends on whether the machine is loaded (cutting) or not and how big the load is.

The machine has been investigated for two cases:

- Machine switched on with the spindle running at various speeds
- Light cutting tests aluminium and mild steel (before self-excited vibration occurs)

The first series of tests were carried out to identify and show the differences in the vibration amplitude of the vibration sources without any cutting.

The results showed that the tool or spindle had slight imbalance. The imbalance of the spindle can be calculated by:

$$f_{run-out} = \frac{Spindle\ Speed\,[RPM]}{60\left[{}^{\text{sec}}\!/_{\text{min}}\right]}$$

Eq. 5.2:Calculation of the spindle run out

However, the effect of this was overshadowed by a vibration amplitude at exactly 300 Hz. No evidence of other significant vibration sources such as spindle bearing or hydraulic pump problems were found.

Figure 5.4 shows the frequency spectrum of the acceleration signal, measured at the spindle housing with the spindle running at 3000RPM (no cutting).

By investigating the armature current of the spindle drive the 300Hz vibration was found to be caused by the DC drive of the spindle motor.

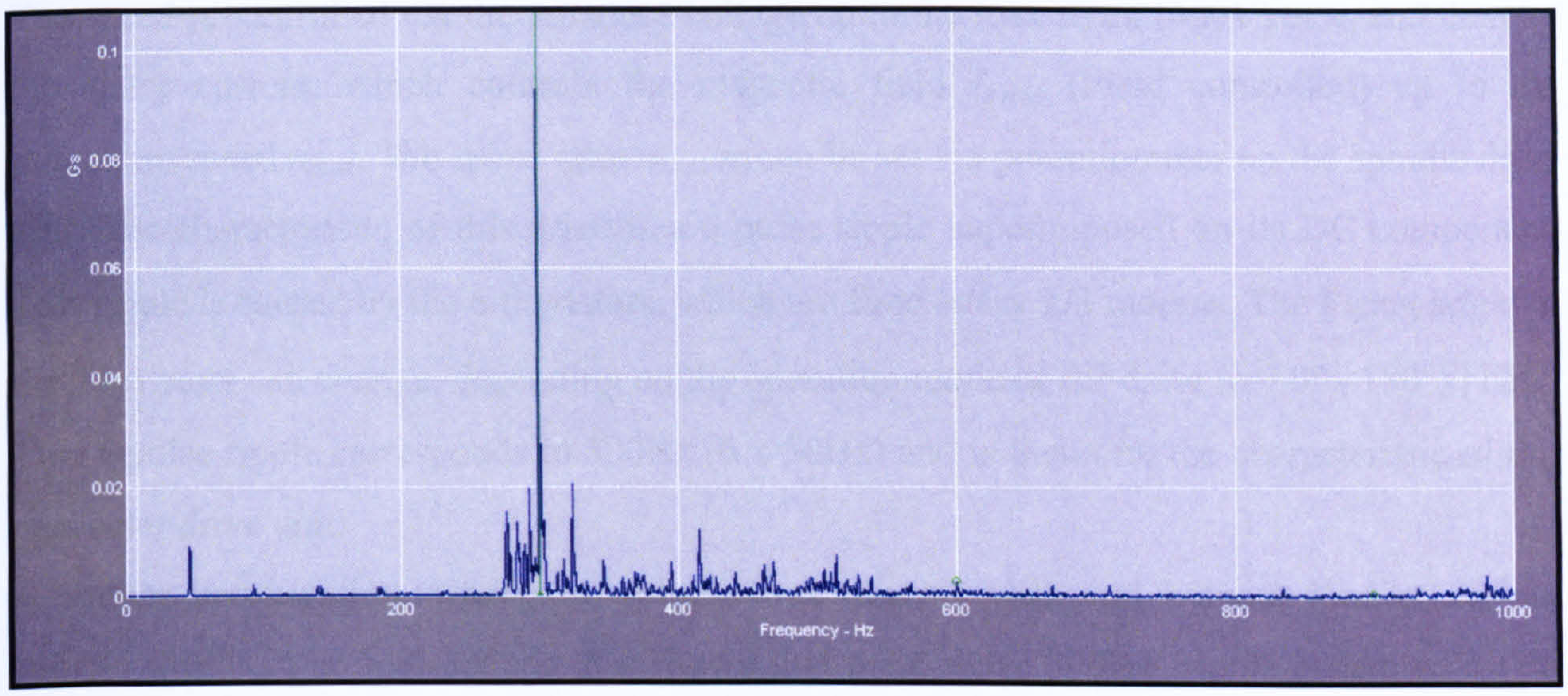

Figure 5.4: The spectrum of the acceleration at 3000 RPM measured on the spindle housing (no cutting)

This particular machine is fitted with a separately excited DC Motor, which is driven by a fully controlled double bridge rectifier [121]. This allows a four-quadrant operation, which is essential for machine tool spindle drive since the tool needs to be able to rotate in both directions and also to brake in both directions. Figure 5.5 shows the characteristics of the Contraves® Spindle Drive Unit [122].

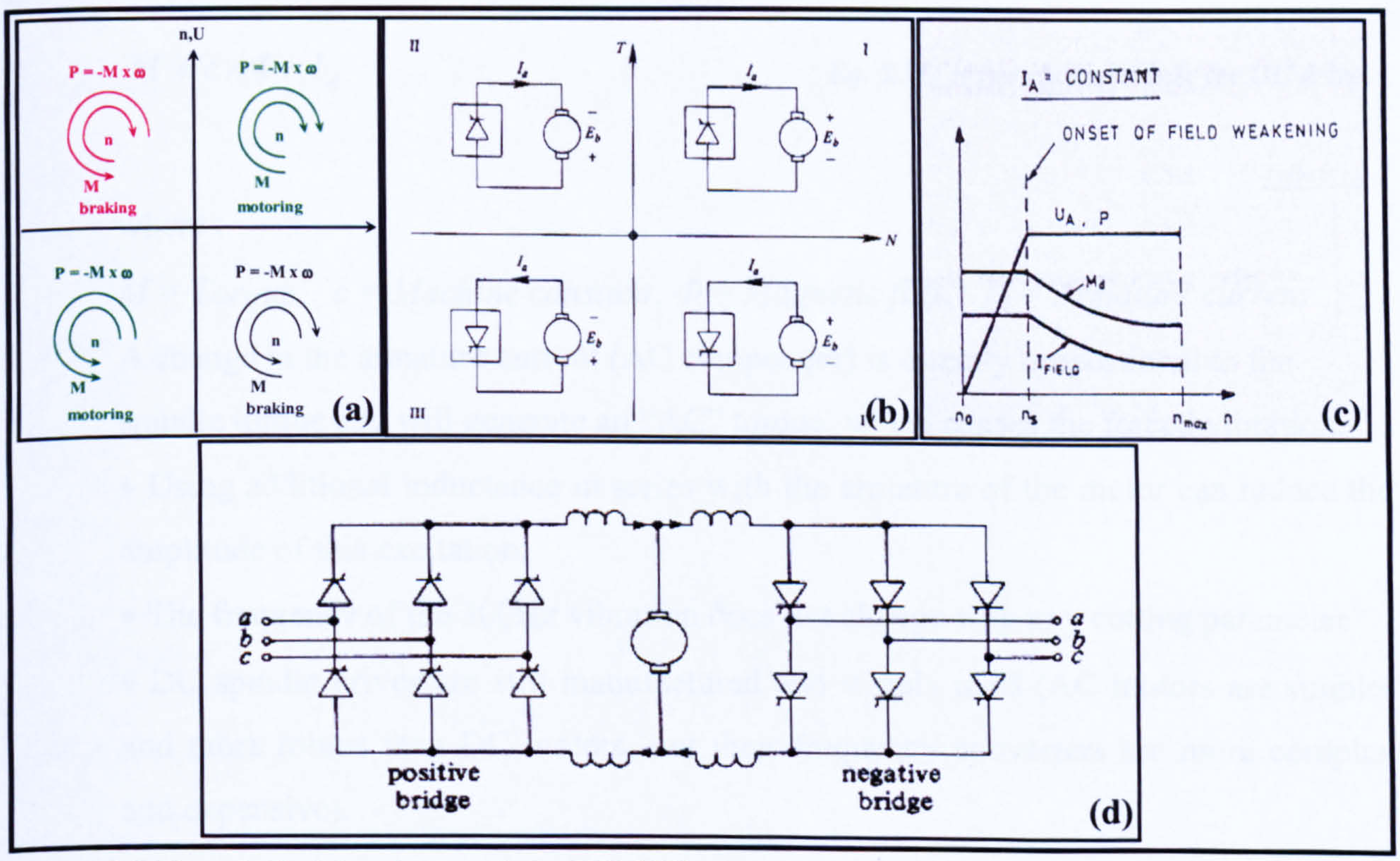

Figure 5.5: The spindle drive characteristics [121,122]:

- ***Four Quadrant operation servo drive (a,b)***
- ***Load characteristics of the Contraves® Spindle Drive (c)***
- ***Fully controlled double converter bridge rectifier including armature current chokes (d)***

The speed is controlled via the armature voltage up to the maximum (400V) at n_s and then by the stator current, which controls the magnetic field I_{Field} (Field controlled) up to the maximum speed n_{max}. The speed ratio n_{max}/n_s can be set via potentiometer on the spindle drive unit. The characteristic of this drive is a 6 pulse ripple superimposed on its DC component. This ripple is caused by the 6 thyristors, which are fired every $\pi/3$ radians. The Firing angle of the Thyristors can change, depending on the operation mode of the drive (α= 0° - 180°) [121]. This 6 pulse ripple corresponds to 300Hz (6 x 50Hz) and is therefore the characteristic of this particular drive unit.

A further investigation, where the spindle was running with and without load at various spindle speeds in both directions, has shown that the 6 pulse 300Hz ripple generated by the thyristor drive does in fact cause significant mechanical vibrations. The voltage applied to the DC motor and the AC content of the armature current cause this mechanical vibration at 300Hz.

The conclusions made here include:

- The 300Hz vibration increases with load on the spindle. If the load or torque increases (e.g. due to the depth of cut), the AC component of the armature current also increases. This leads directly to an increase of the vibration level.

$$M = c \times \Phi \times I_A$$ ***Eq. 5.3: Torque characteristic for DC drives***

where :

M = Torque, c = Machine constant, Φ = Magnetic flux, I_A = Armature current

A change in the armature current (AC component) is directly proportional to the spindle torque and will generate an "AC" torque, which causes the forced vibration.

- Using additional inductance in series with the armature of the motor can reduce the amplitude of this excitation.
- The frequency of the 300Hz vibration does not change with any cutting parameter
- DC spindle drives are still manufactured and widely used (AC motors are simpler and more robust than DC motors, but their frequency converters are more complex and expensive).

The second series of tests consisted of light cutting on aluminium and mild steel. Most periodic energy is likely to be caused by the cutting tooth impact force, which is dependent on the depth of cut and work-piece material.

The tooth pass frequency can be calculated by:

$$f_{tooth} = \frac{Spindle\ Speed\,[RPM] \times (\sum Teeth)}{60\ [\mathrm{sec}/\mathrm{min}]}$$

Eq. 5.4:Calculation of the tooth pass frequency

Figure 5.6 shows the vibration during a light cut of mild steel using a 100mm Face Mill (8 cutting edges). The vibration was measured in the cutting direction on the spindle housing. The rotational speed of the spindle was 410rpm, which resulted in a tooth pass frequency of 54.5 Hz. Figure 5.6 (a) shows the fundamental and the harmonics of the tooth pass frequency. The result also shows the significant vibration at 300Hz, which is not a harmonic of the tooth-pass frequency. Figure 5.6 (b) shows the spindle current, which caused this periodic excitation force. The armature current of the spindle motor was measured with a LEM Hall effect sensor [123] fitted to the machine (figure 5.6 c).

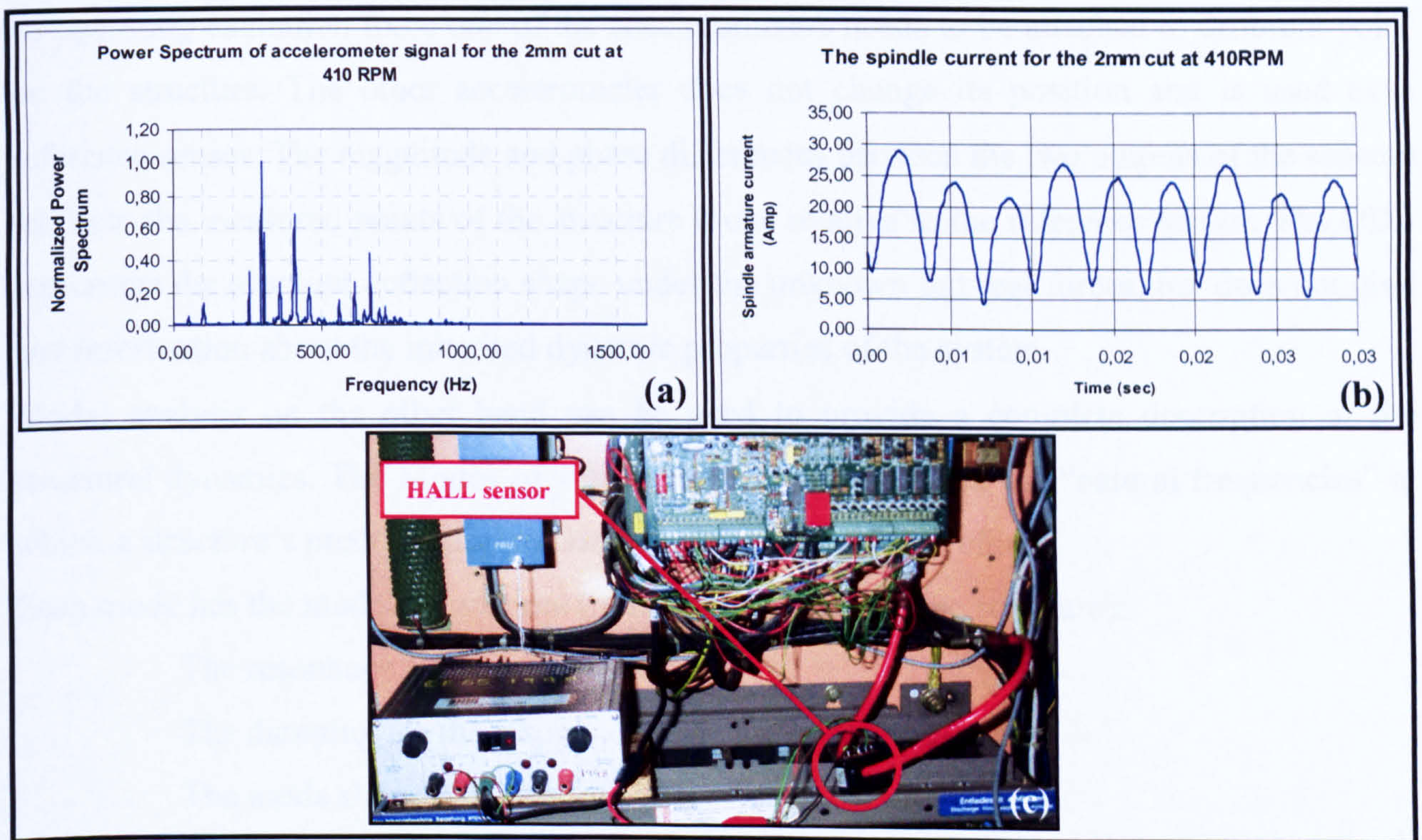

Figure 5.6: Light cutting tests:

- ***Power spectrum of the acceleration signal (a)***
- ***Spindle current measured with the HALL sensor (b)***
- ***The HALL sensors fitted to the spindle drive unit of the milling machine (c)***

Other potential forced vibration sources such as spindle imbalance and bearing irregularities were again, not significant in the frequency spectrum and have therefore not been considered any further.

5.5 Experimental modal analysis

Since chatter always involves excitation of a dominant mode of the structure, the first step of chatter analysis on a machine tool is to measure the frequency response of the structure.
Structural testing can be divided into 2 different techniques:

- Signal Analysis = Operational deflection shape (ODS)
- System Analysis = Modal Testing

The goal of ODS measurements is the determination of the dynamic deformations of a mechanical structure during operation. It tells how the structure actually reacts to the real forces applied to it, when in operation. Attaching two accelerometers on the structure under operation can do this. The magnitude- and phase difference between them can be recorded with a simple 2-channel spectrum analyser. To get an idea of how the structure vibrates under its operating excitation force one of the accelerometers needs to be attached to different point on the structure. The other accelerometer does not change its position and is used as a reference sensor. The magnitude and phase differences between the two outputs of the sensors tell how the measured points of the structure move relative to the reference sensor. The ODS represents the absolute deflection shape under the unknown but real forces, but does not give any information about the inherited dynamic properties of the system.
Modal analysis on the other hand can be used to provide a complete description of the structural dynamics. The Modes of vibration of the structure are the "natural frequencies" at which a structure's predominant motion has a well defined waveform.
Each mode has the modal parameters (inherent properties of the structure):

- The resonance or modal frequency
- The damping for the resonance – the modal damping
- The mode shape

Modal analysis is the process of determining all modal parameters within the frequency range of interest to formulate a mathematical dynamic model. This can be done either analytically (FEM) or experimentally (modal testing). Experimentally modal analysis, determines the modal parameters by artificially exciting the structure so that the different resonance frequencies, damping and mode shapes can be identified. The structure can be excited using an instrument hammer or a shaker (e.g. electro-dynamic shaker). The most popular method of obtaining the modal parameters is the *Transfer Function Method*. This method measures the frequency response function (FRF) between two points of the structure. The reference or input force is measured with a force transducer and the vibration output at a number of points along the structure with a displacement, velocity or acceleration transducer. The modal frequencies and damping can be found from all FRF's, except those for which the excitation or response is in a nodal position. To extract the modal parameters form the experimental data, special software can be used (e.g. STAR MODAL®). If such software is not available, the *Normal Mode Method* has been found to be more practical to obtain the mode shape, whereas the damping and resonance frequency can be obtained best from the FRF's (*Transfer-Function Method*). A proper modal analysis on a simple structure has been done in chapter 6, whereas AMTRI, who are a leading institution of vibration analysis on machine tools performed a modal analysis on this vertical milling machine [115]. This included cutting test and frequency response measurements in all 3 axes using an electro-hydraulic shaker. AMTRI used STAR MODAL® to obtain the mode shapes of the machine. A huge disadvantage of the AMTRI test was the restriction of the highest frequency to 200Hz, as the light cutting tests (figures 5.4 and 5.6) and the following cutting tests have shown that the interesting dynamic effects on this machine are above 200Hz. The restricted frequency bandwidth in the AMTRI tests might have been due to the frequency limitations of the electro-hydraulic shaker, which they used. Nevertheless the results of this analysis were used as a reference for the tests carried out for this research. Figure 5.7 shows the experimental set up, to validate the AMTRI tests (for clarification the AMTRI test and its results, have not been published in this thesis).

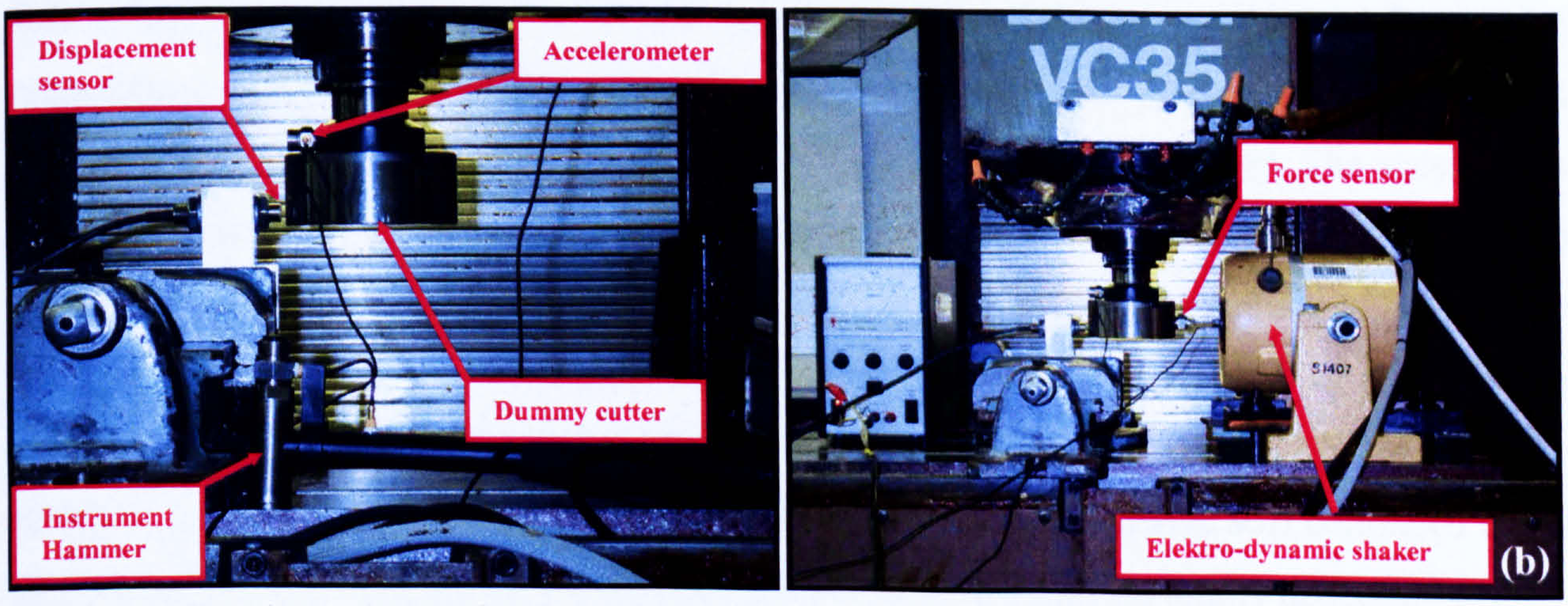

Figure 5.7: Experimental set up for the modal testing using an instrument hammer (a) and shaker (b)

A special dummy cutter was designed, which had the same dimensions as the SANDVIK face mill used for the cutting tests, to attach the electro-dynamic shaker to the machine. This simulates the cutting forces, which act on both the cutting tool and the work-piece with equal but opposite amplitudes. The resulting relative displacement between the two structures was measured using a displacement transducer, whereas the force was measured using a piezo-electric force transducer. As already explained in chapter 3 the resulting transfer-function between tool and work-piece provides information about the static and dynamic stiffness. In addition to this, the machine was dismantled in order to gain access to all important structural elements, such as ballscrew nut and machine column. Here the vibration response was measured with accelerometers, which were moved along the structure to get an idea about the absolute movement of various parts of the machine structure. Figure 5.7.a also shows an instrument hammer, which can be used as an alternative to excite the tool tip.

Figure 5.8.a shows the FRF (compliance), where the relative vibration between tool and machine table was measured with the displacement transducer. Figure 5.8.b shows the accelerance (acceleration / force), where the vibration was measured at the tool tip.

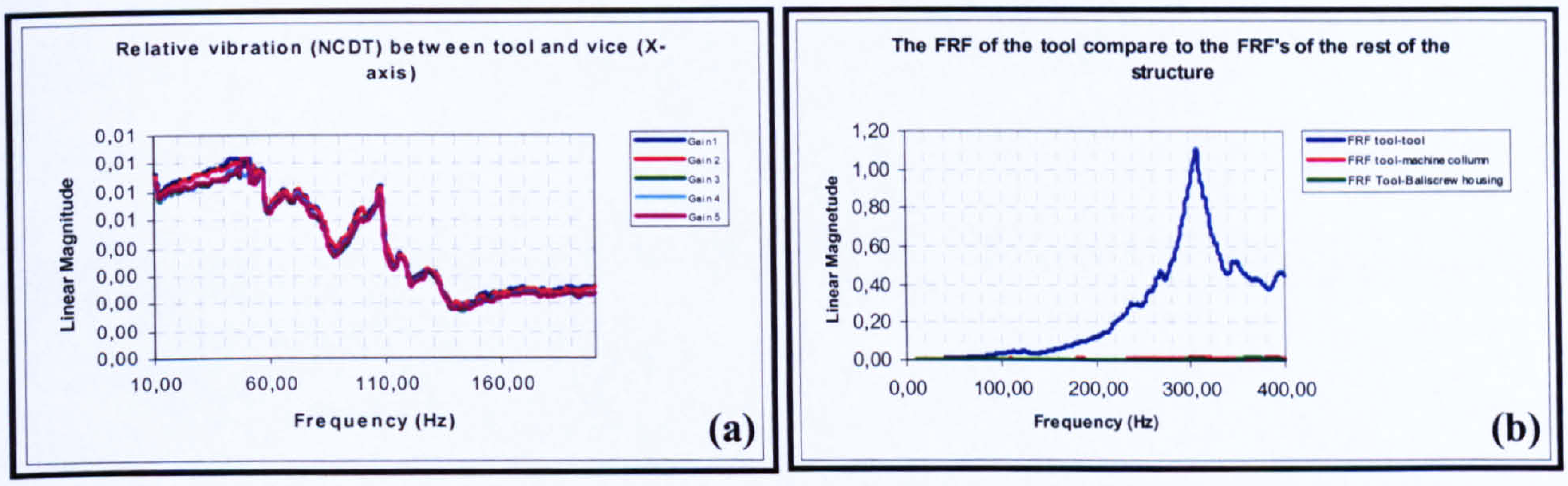

Figure 5.8: FRF (compliance) between machine table and tool tip (a), Tool FRF (accelerance) comparison with other FRF' s of the structure (b)

The compliance (displacement / force) between tool and machine table confirmed the measurements made by AMTRI. The measurement set up was the same and the results showed good correlation with all the resonance frequencies determined here. The accelerance of the tool tip however showed that as already suspected the dynamics of the spindle were above 200 Hz. This confirms the fact that the previously identified vibration source of the spindle drive at 300 Hz was amplified through the structure. Figure 5.7.b also shows the difference in vibration amplitude between the spindle/headstock and the rest of the machine structure (e.g. ballscrew nut). The planar guideway seemed to be relative stiff compared to the spindle/headstock. On a machine with linear guide ways, this may be totally different [45].

In another test the FRF of the tool spindle structure was measured, since the spindle housing is the nearest place to the cutting process whose sensor can be attached without practical difficulties. This particular static test was done because it would be expensive to measure excitation force or relative displacement of the tool during cutting (on line). A further discussion about the most suitable vibration sensor for machine tools is included in chapter 7. Figure 5.9 shows a simplified model of the cutting process, and the measured tool-spindle housing FRF in X and Y directions.

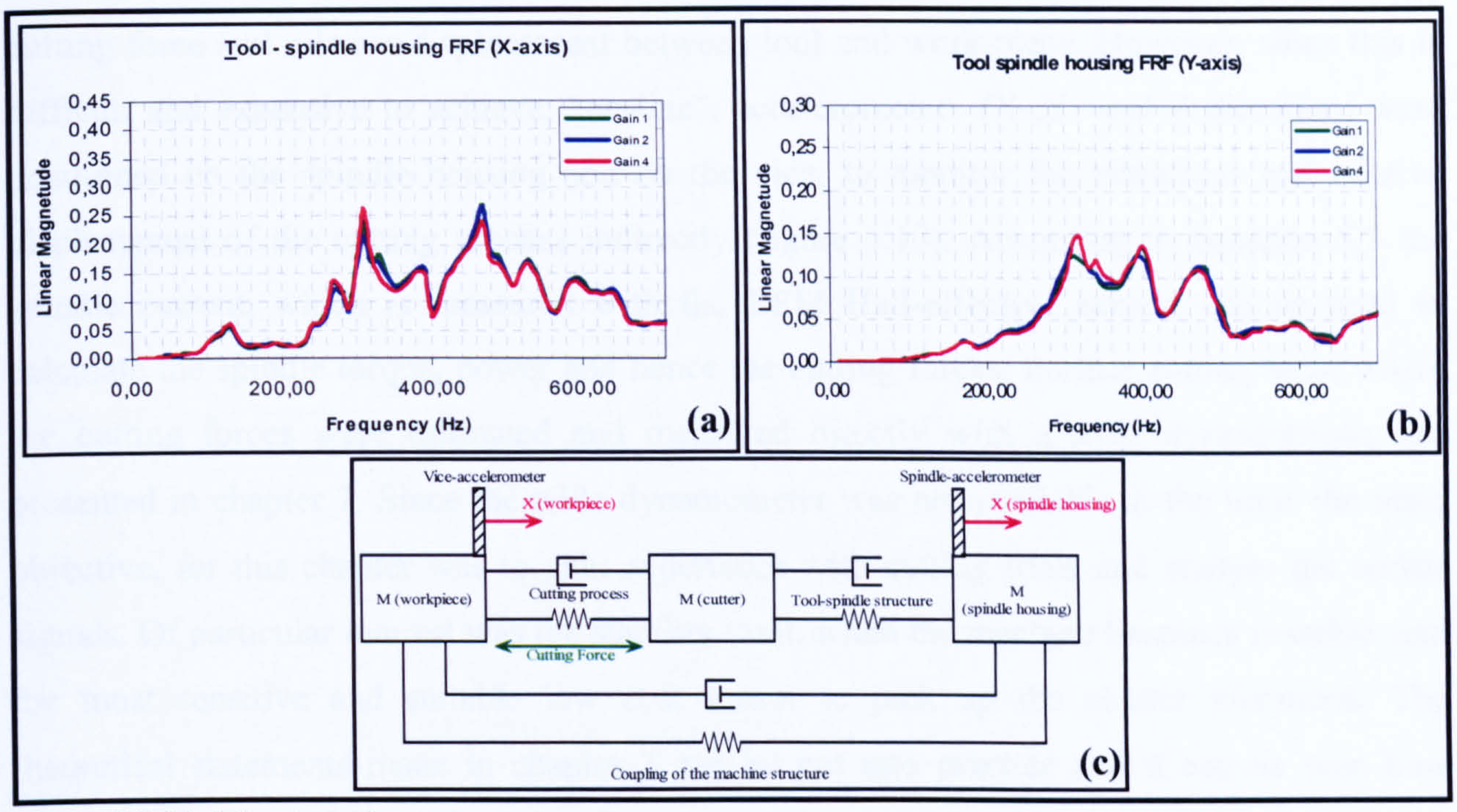

Figure 5.9:Modal test results:
- ***Tool-spindle housing FRF X-axis (a)***
- ***Tool-spindle housing FRF Y-axis (b)***
- ***Block diagram of cutting process dynamics (c)***

In order to measure the linearity of the structure, the input excitation force on the tool-tip was increased by up to 4 times, through gain adjustments of the power amplifier of the shaker. Figure 5.8 (a) and 5.9 (a and b) show no difference in the resulting FRF's, which indicates that the mechanical structure is behaving in a linear fashion. It should also be mentioned that the input signal to the shaker needs to excite every frequency with the same energy. The spectrum analyser used here (HP 3566A) could generate white noise and swept sine in order to identify an unknown system (more on system identification in chapter 6). For all FRF measurements done here the coherence function, which is a statistical procedure for assessing the quality of the impact testing and random noise tests, was used to validate the data.
For more detailed information on modal analysis the literature of Brüel & Kjær [119,120] Evans [92] and Richardson [102,103] is highly recommended.

5.6 Cutting tests

To see what effect load errors have, the machine must operate under cutting conditions. The varying loads (forces) applied to a machine tool structure during the cutting operation provide the main source of this error. The effect of this load on machine accuracy will depend on the machine resistance to elastic deformation or stiffness.

The task was to measure and interpret forced- and self-excited vibrations using different sensors. The most appropriate variables for investigating the cutting process would be the cutting force and relative displacement between tool and work-piece. However, since this is difficult and expensive to achieve, "on-line", accelerometers (X-,Y- and Z direction) were positioned on the spindle housing and on the vice, to monitor the vibrations and relative displacement of the cutting process indirectly (figure 5.10). According to equation 5.3 the spindle current, which is measured with the LEM Hall-effective sensor, can be used to calculate the spindle torque, power and hence the cutting forces. Further cutting tests, where the cutting forces were estimated and measured directly with a table dynamometer, are presented in chapter 7. Since the table dynamometer was not available at the time, the main objective, for this chapter was to gain experience with cutting trials and analyse the sensor signals. Of particular interest was the stability limit, when the machine becomes unstable, and the most sensitive and suitable low cost sensor to pick up the chatter vibrations. The theoretical statements made in chapter 3 can be put into practice and it can be seen how effective the process parameters feedrate and spindle speed are for chatter control. This will confirm the theoretical and experimental statements made by the researchers in chapter 2.

Figure 5.10 shows the experimental set up (spindle current sensor is not shown).

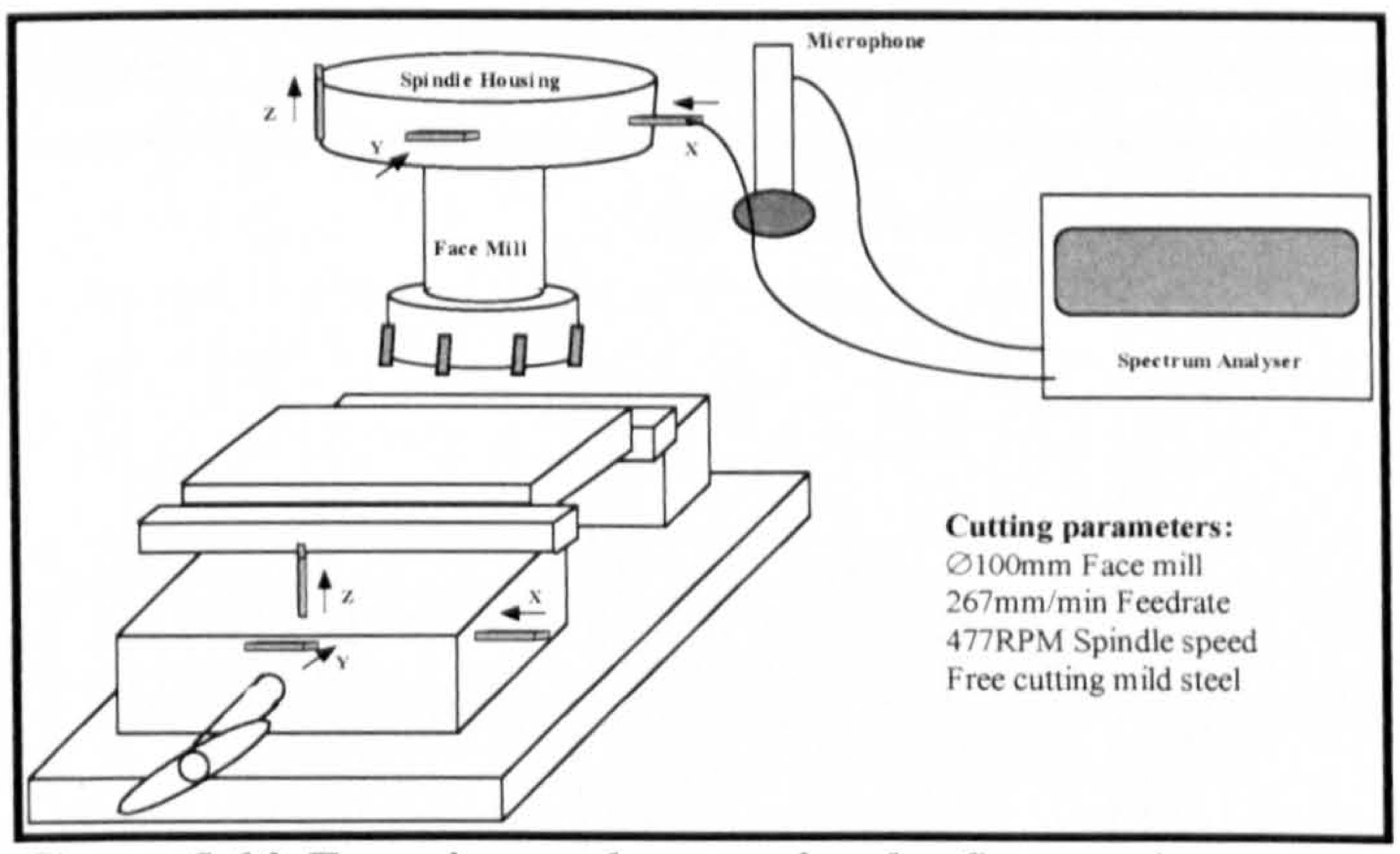

Figure 5.10:Experimental set up for the first cutting tests

The figure also shows a microphone, located near the cutting process to measure the sound pressure. In comparison to the spindle current sensor the microphone seems to be a very popular choice for chatter detection [33,34,35,36,37,38].

The sensors investigated were:

- 6 Accelerometers (attached to spindle housing and vice in three orthogonal directions)
- Hall sensor to measure spindle current
- Microphone to measure the sound pressure of the cutting process

Cutting tests were carried out for mild steel and aluminium with adequate feed and spindle speed. A ∅100mm face mill with 8 cutting edges and the same work-piece, in material and dimensions (width of work-piece is the width of cut – see figure 3.13) has been used for all the tests. For each set of parameters (feedrate, spindle speed) the axial depth (a_a) of cut was increased until chatter occurred. Up to then, the process was stable and the sensor signals showed forced vibration due to the tooth pass frequency and the spindle drive. Figure 5.11 – 5.16 show a comparison of the sensor signals for a stable cut (a_a = 2mm) and unstable cut (a_a = 4mm). The cutting parameters were 410RPM spindle speed and 267mm/min feedrate.

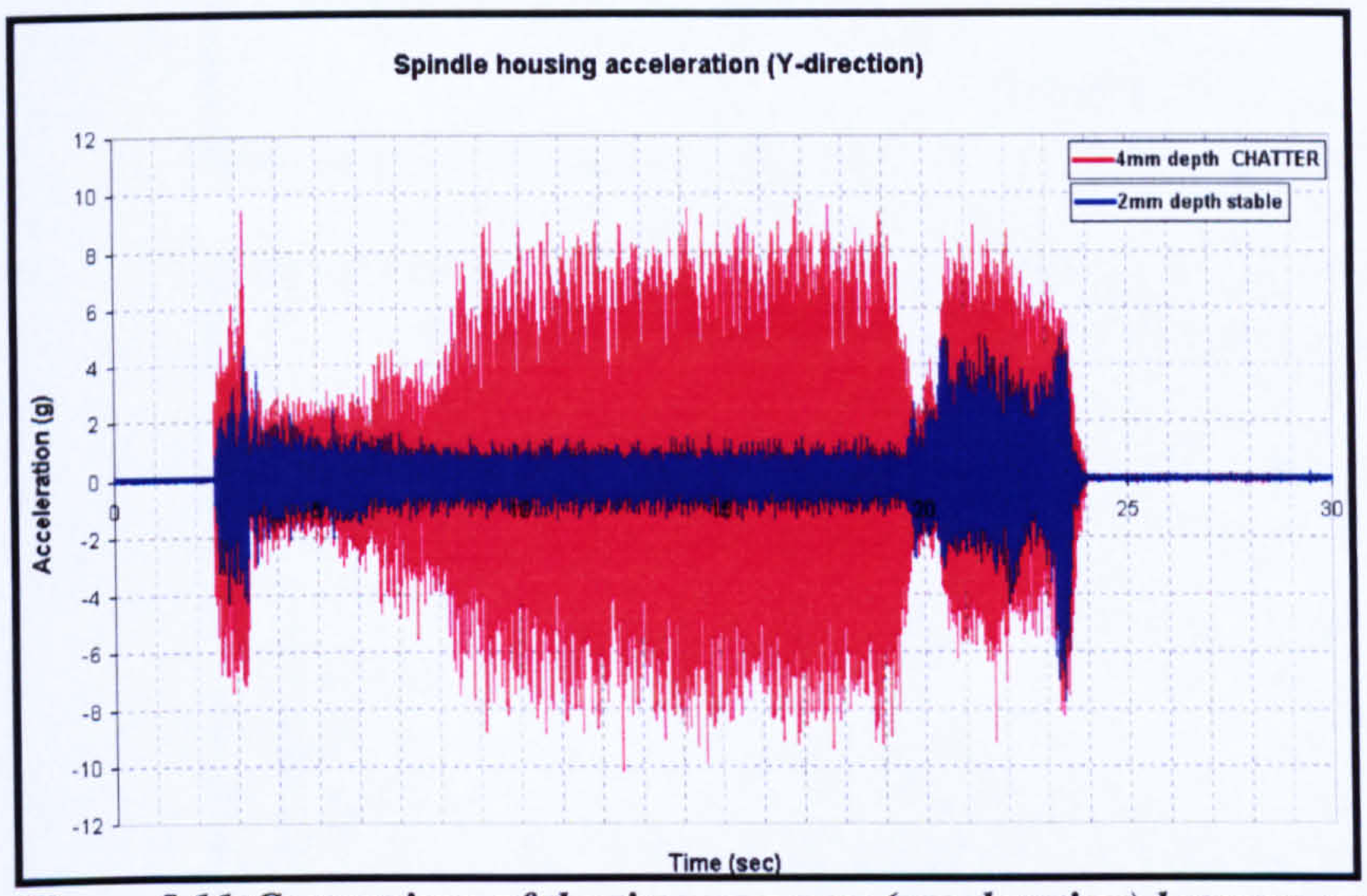

Figure 5.11:Comparison of the time response (acceleration) between a stable cut and a unstable cut

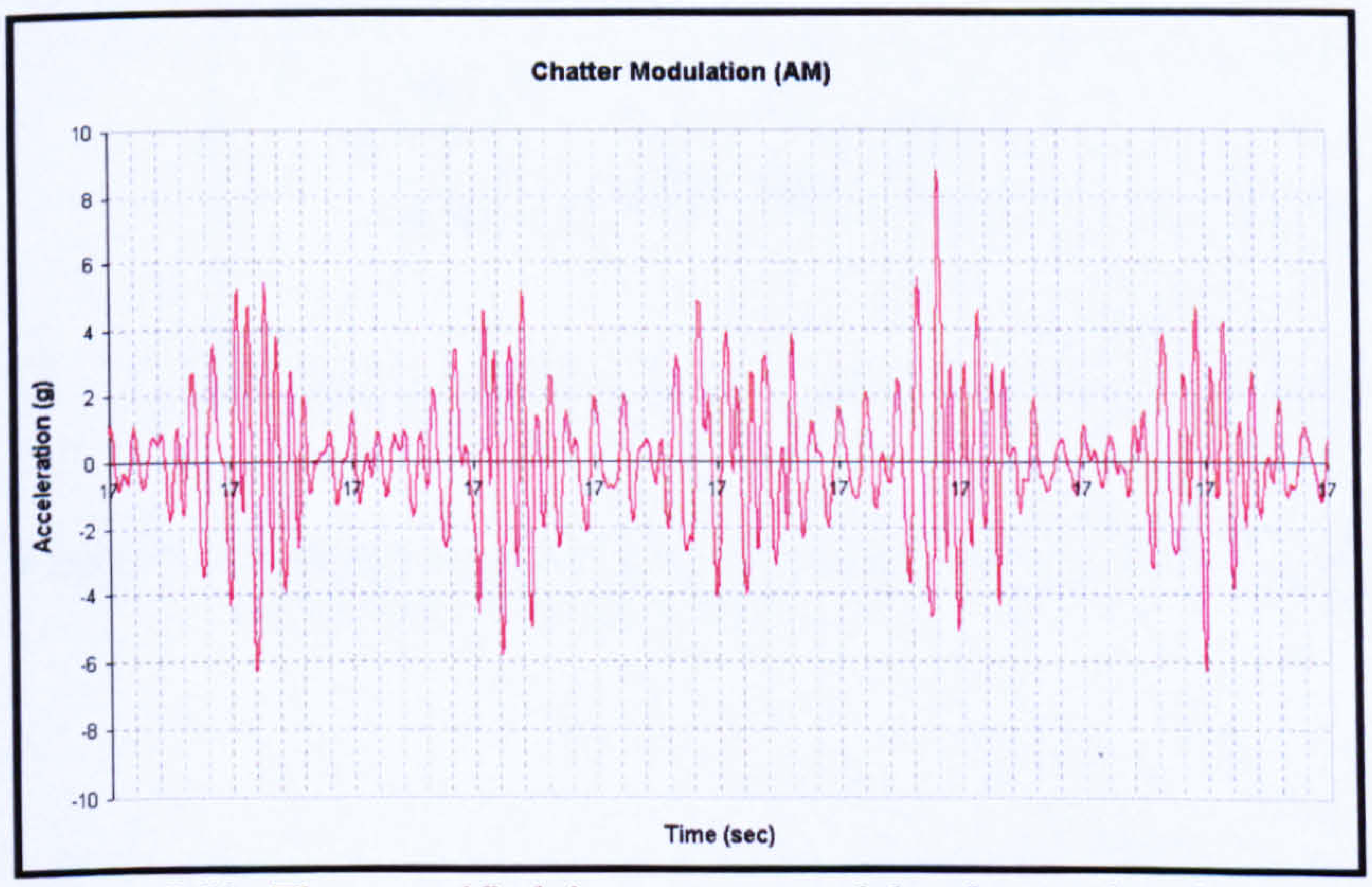

Figure 5.12: The magnified time response of the chatter signal

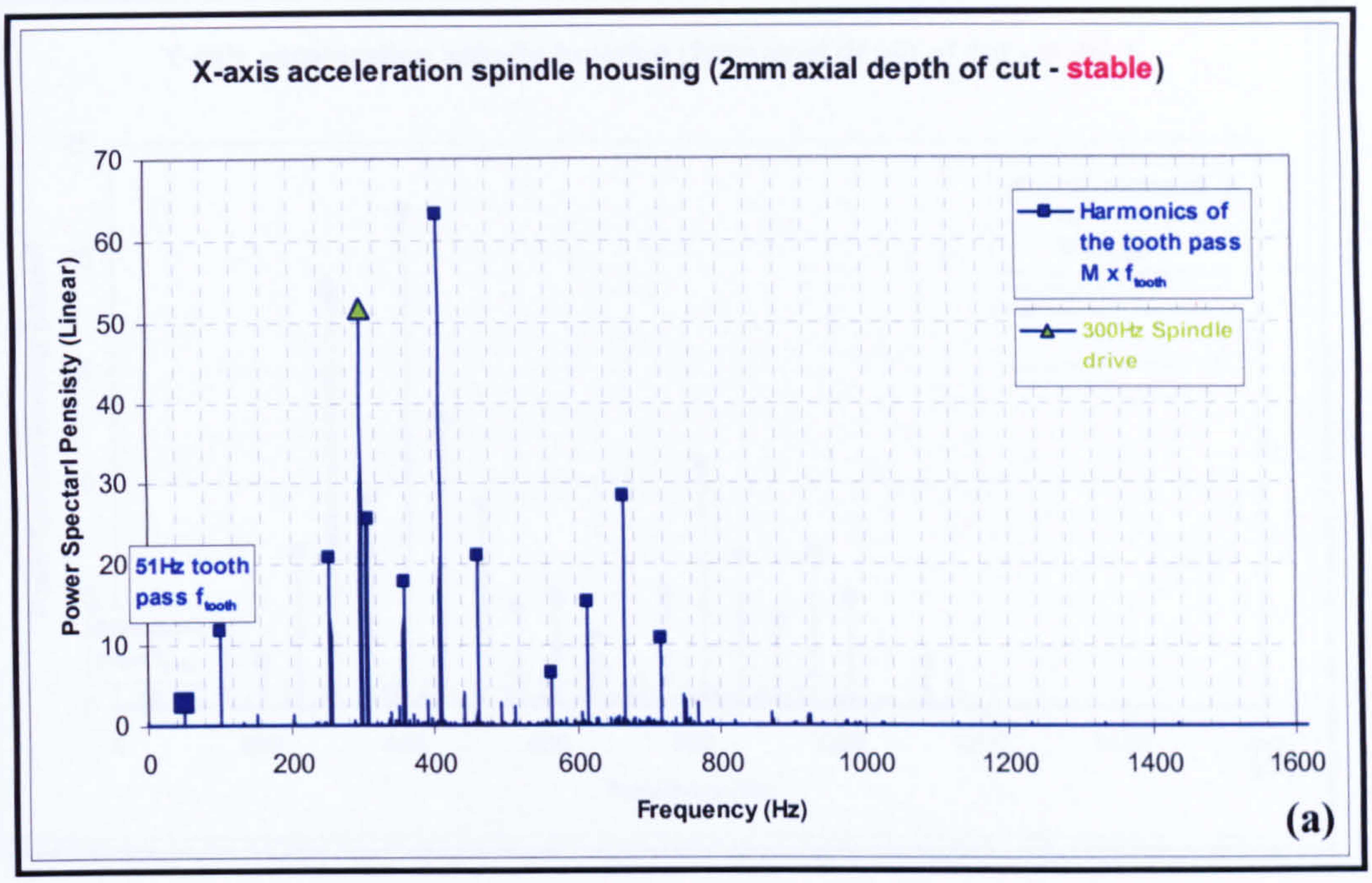

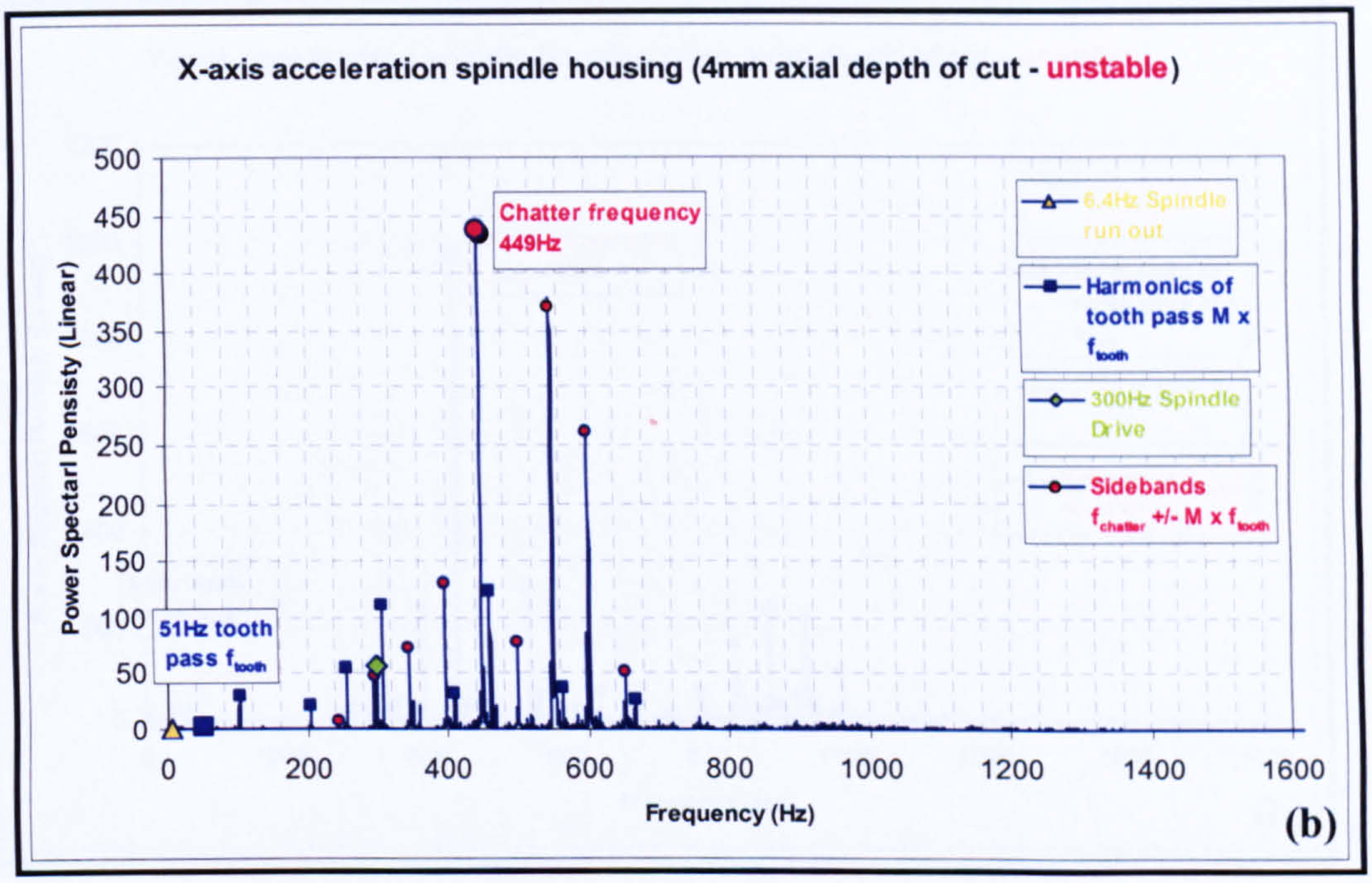

Figure 5.13: Comparison of the frequency response (spindle housing acceleration – X axis) between a stable cut (a) and a unstable cut (b)

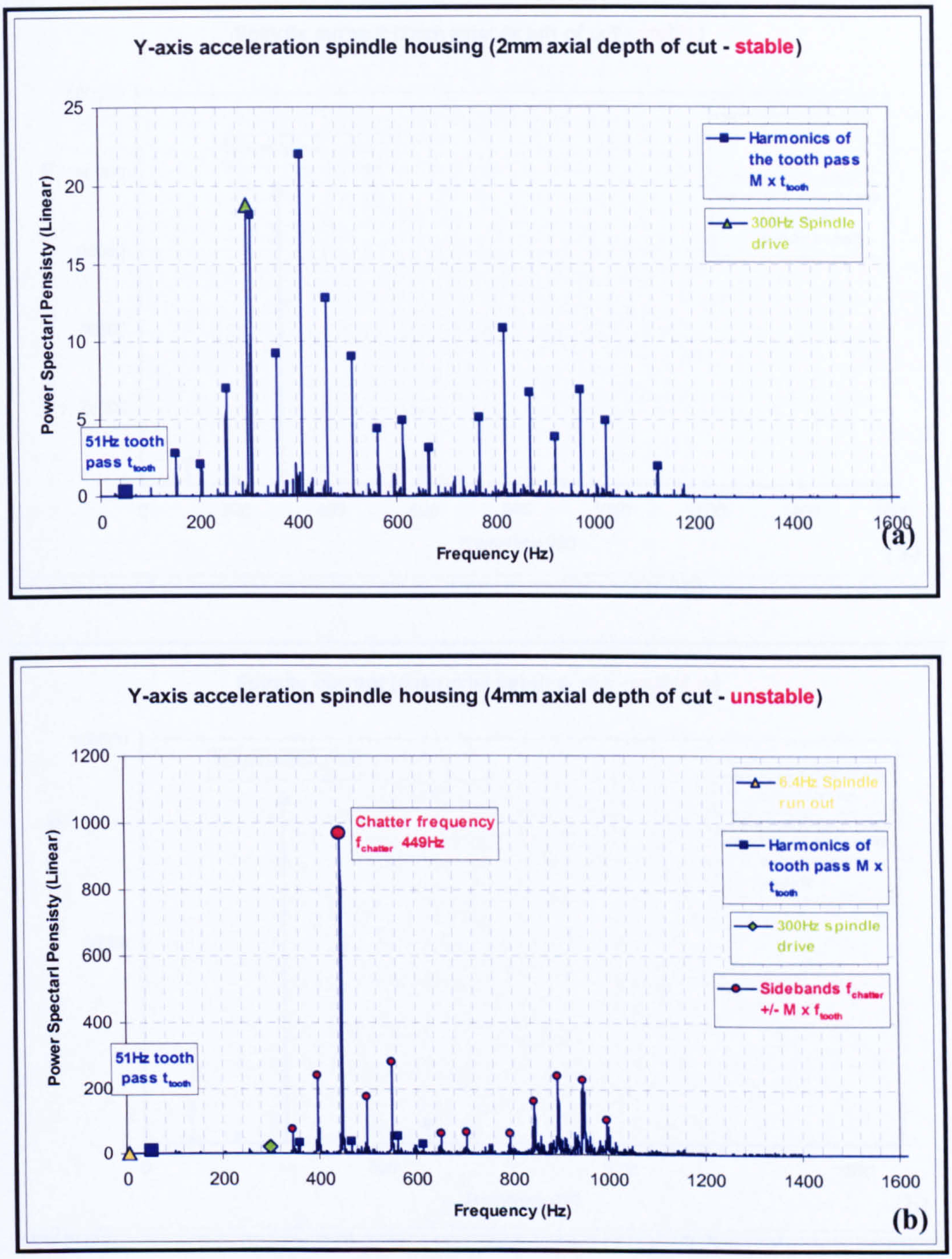

Figure 5.14: Comparison of the frequency response (spindle housing acceleration – Y axis) between a stable cut (a) and a unstable cut (b)

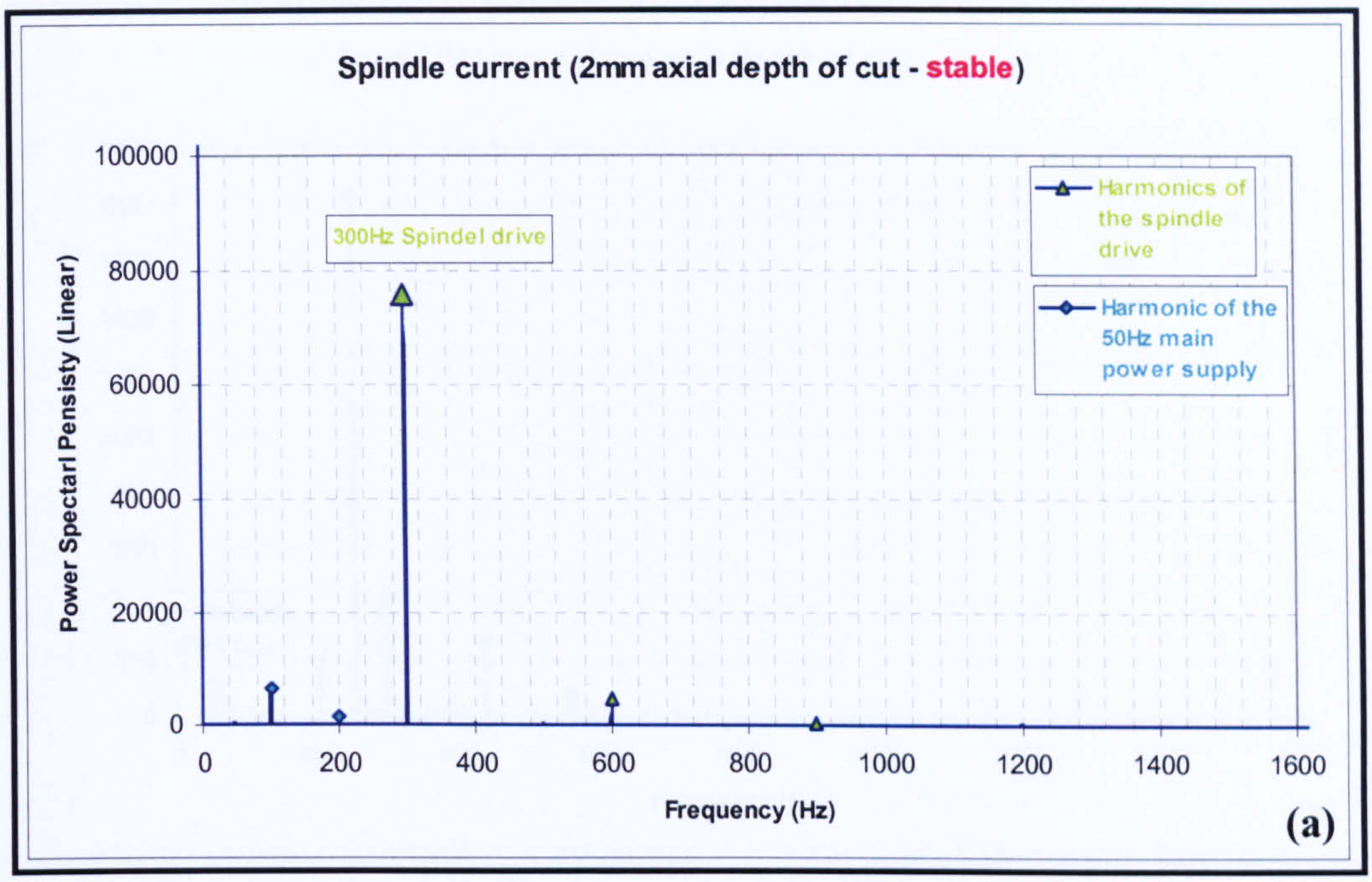

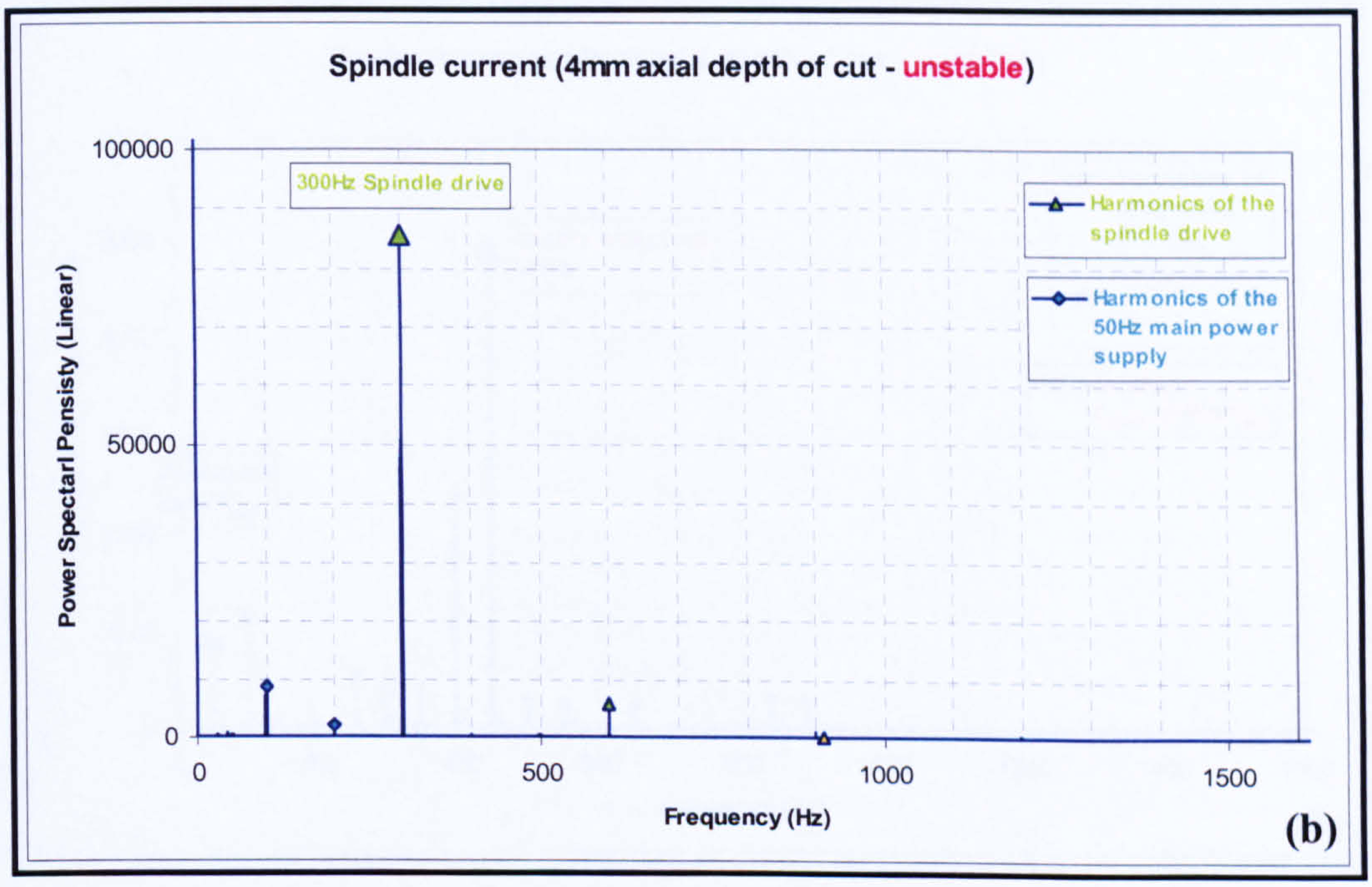

Figure 5.15: Comparison of the frequency response (spindle current) between a stable cut (a) and a unstable cut (b)

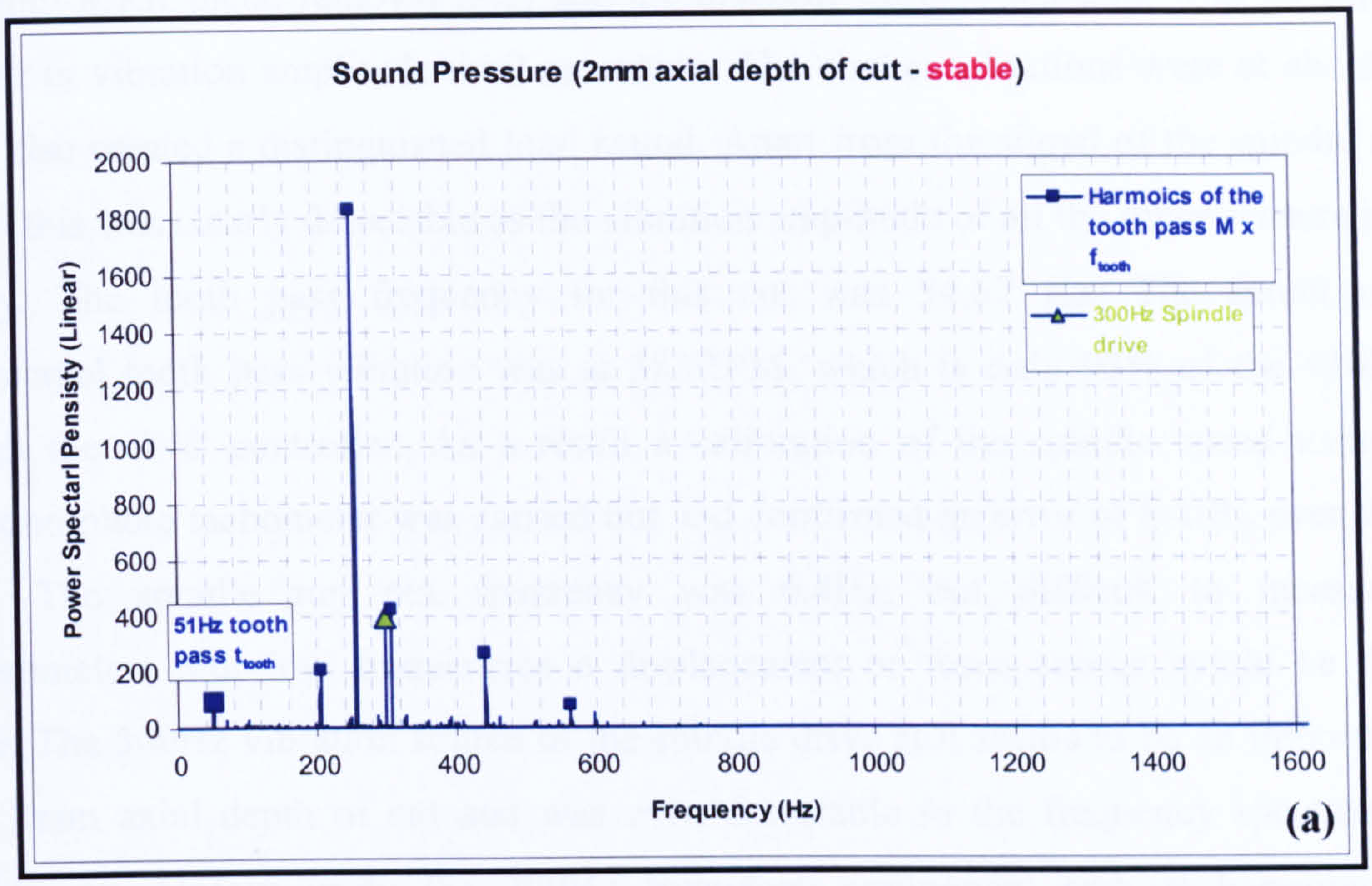

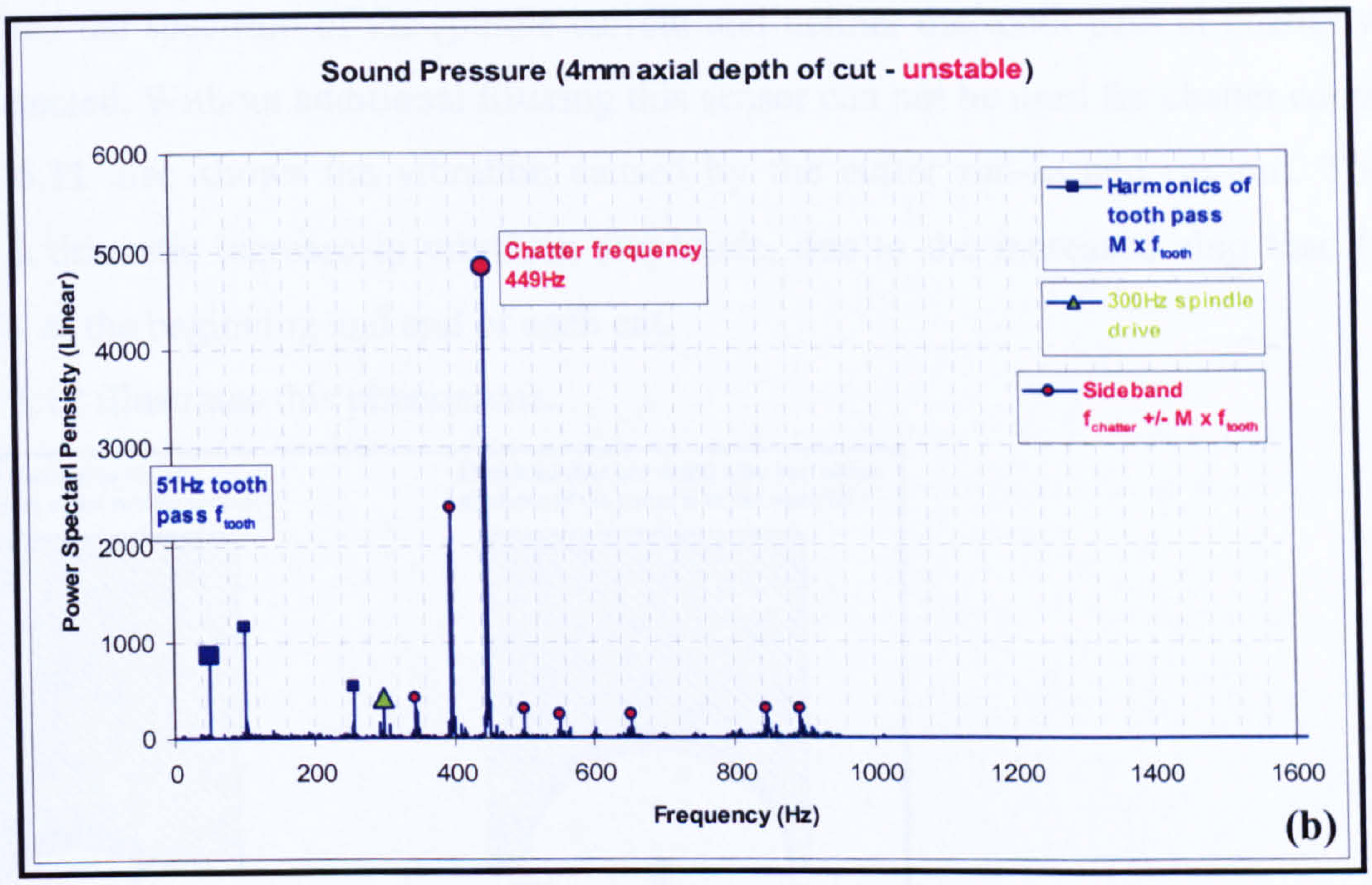

Figure 5.16: Comparison of the frequency response (sound pressure) between a stable cut (a) and a unstable cut (b)

Figure 5.11 shows that chatter did not develop until the whole diameter of the cutter entered the work-piece. It was then that the dynamic cutting force reached its stable limit (at the maximum MRR metal removal rate) and the machine became unstable with an exponential increase in vibration amplitude until saturation. The chatter vibrations were at about 450Hz, which also created a distinguished loud sound. Apart from the signal of the spindle armature current this was clearly detectable as the vibration amplitude of all the other sensors increased sharply. The tooth pass frequency for this cut was 54.67 Hz. The actual measured fundamental tooth pass vibration was at 383RPM, which is only 93% of the 410RPM set through the CNC controller. As a result a calibration of the spindle speed using a high resolution photo tachometer was carried out and confirmed an error of 8-10% over the whole range. The spindle run out frequency was 6.4Hz, but difficult to measure using accelerometers. For low frequencies a displacement or force sensor would be the better choice. The 300Hz vibration source of the spindle drive still seems to be an important factor up to 3mm axial depth of cut and was even detectable in the frequency spectrum for the unstable cut. Unfortunately the 300Hz frequency component and its harmonics totally dominated the spectrum of the spindle current and neither the tooth pass or chatter vibration were detected. Without additional filtering this sensor can not be used for chatter control.

Figure 5.11 also shows the vibration caused by the cutter run-in and run-out. This effect causes a dramatic increase in vibration amplitude, due to the increased chip load (feed per tooth f_t), at the beginning and end of each cut.

Figure 5.17 illustrates this phenomena.

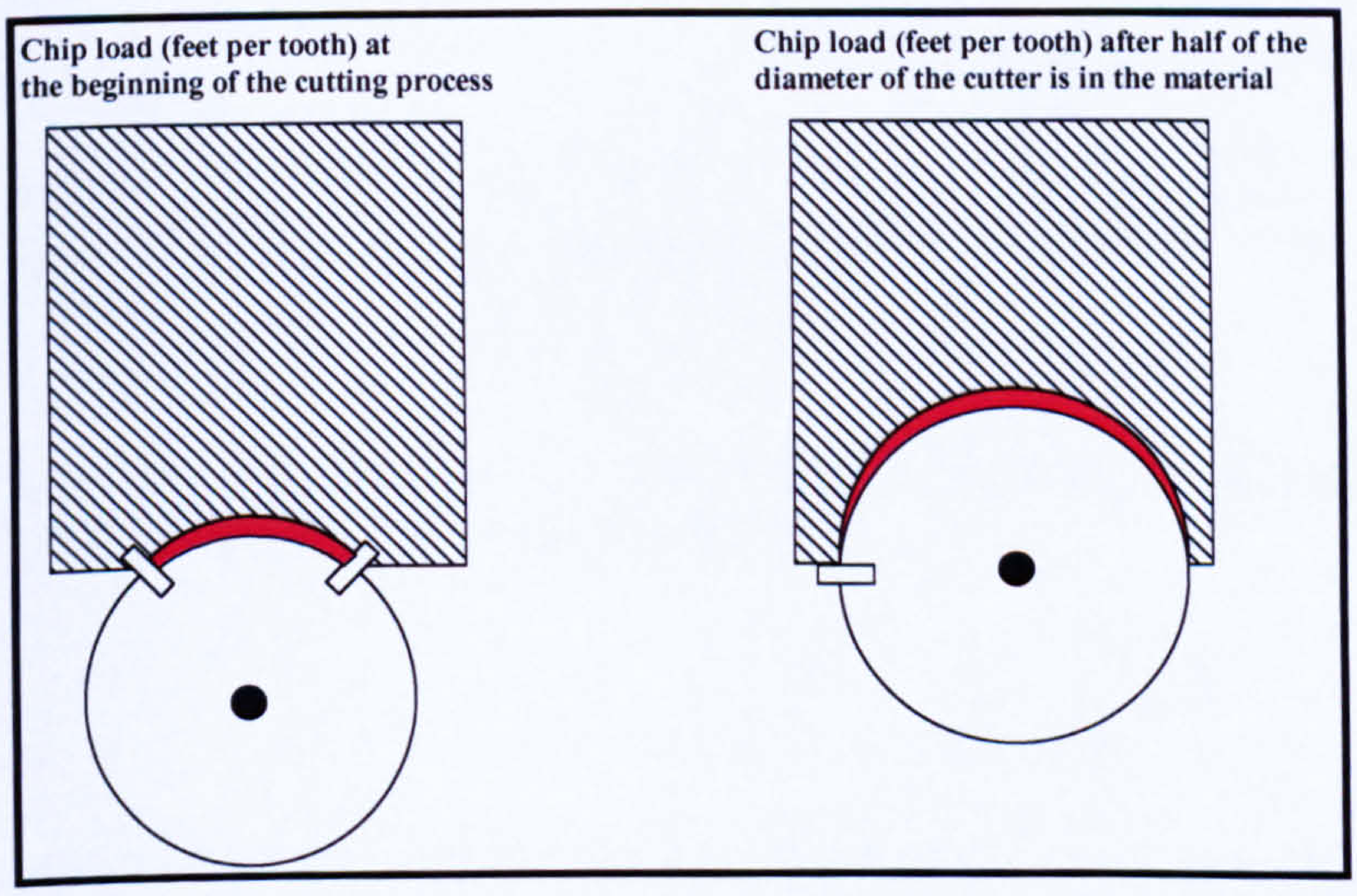

Figure 5.17: Cutter run-out - the increased chip load at the beginning and end of the cut

Chatter does not occur until the cutting forces reach the stability limit of the machine structure (b_{limit} - chip width), in the middle section of the cut when the whole width of the cutter is penetrating into the work-piece. Figure 5.11 shows that on a small time scale the chatter vibration looks like an Amplitude Modulated (AM) signal. The spectral density functions of the chatter vibrations also reveal frequency components that are not related to the harmonics of the tooth pass or chatter frequency. They show upper and lower sidebands of the main 450Hz chatter frequency component, which are 51Hz (tooth pass frequency) or a multiple of 51Hz (harmonics of the tooth pass frequency) apart. The chatter frequency (Carrier signal) seems to be modulated by the tooth pass frequency (Modulating signal). The spectrum of the "AM" chatter signal suggests non-linearity, since the signal should only contain tooth pass frequency components, its harmonics and the chatter frequency itself. But a fraction of the power generated by the dynamic cutting forces seems to be converted into the sidebands of the vibration output signal. Mathematically the non-linear process of modulation means multiplication of the modulating signal with the carrier signal (equation 5.5) [124]. In radio communications for example the modulated signal and carrier are first added together through a linear device (resistor) and then a non-linear device (diode or transistor) is used to modulate the signal. Figure 5.18 is shows the generation of an AM signal from carrier- and modulating signal and equation 5.5 illustrates its mathematical description.

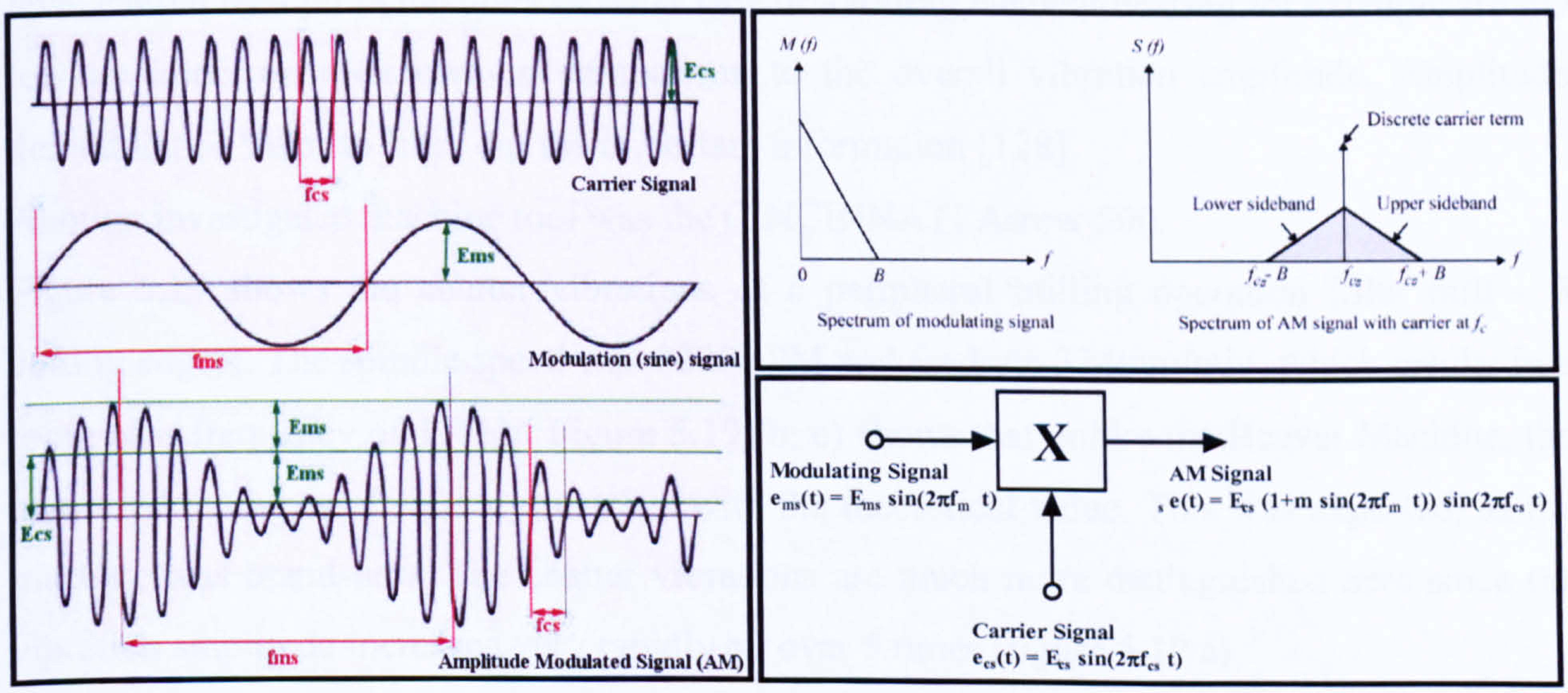

Figure 5.18: Amplitude Modulation (AM)

$$e(t) = E_{cs}(1 + m\ \sin(2\pi\ f_{ms}\ t))\ \sin(2\pi\ f_{cs}\ t)$$ ***Eq. 5.5:Mathematical description of the AM signal***

where:

E_{cs} = Peak Amplitude of the carrier signal

E_{ms} = Peak Amplitude of the modulated signal

f_{cs} = Frequency of the carrier signal

f_{ms} = Frequency of the modulated signal

$m = E_i/E_c$ = modulation index

This observation also explains the theory that chatter can not develop if the chatter frequency matches a harmonic of the tooth pass frequency (equation 2.2 and figure 3.17).

The only references found on the subject chatter modulation in machine tools are the work from Jemielniak and Widota [125], who investigated the case of "beating" in machine tool vibrations (lathe), where two close vibration modes are excited. The addition (linear) of these result in interference (beats), which is a form of amplitude modulation observed frequently in common vibration analysis. Tarng and Lee [126] also supported this theory.

The phenomena of Amplitude Modulation is commercially used in condition monitoring. The *Envelope analysis* [127] is a well known signal processing technique, which originates from the field of telecommunications. This amplitude demodulation technique helps in the investigation and monitoring of bearing and gear defects at an early stage since the vibration level caused by a pit in the inner or outer race of a rolling element bearing for example are too low to detect on their own in comparison to the overall vibration amplitude. Amplitude demodulation helps to filter out the important information [128].

Another investigated machine tool was the CINCINNATI Arrow 500.

Figure 5.19 shows the chatter vibrations of a peripheral milling operation (Slot mill – 3 cutting edges). The spindle speed was 2228RPM and feedrate 334mm/min, which results in a tooth pass frequency of 111Hz. Figure 5.19 (b, c) shows that unlike the Beaver Machine, the measured tooth pass frequency matches with the theoretical value. This was expected, as the machine was brand-new. The chatter vibrations are much more distinguished here since the vibration amplitude increased very rapidly by over 5 times (figure 5.19 a).

Figure 5.19 also confirms the more dominant chatter frequency of 700Hz, since the amplitude of the modulating tooth pass frequency was small in comparison to the amplitude of the chatter carrier signal (spectrum only shows 1 upper and lower sideband of small amplitude).

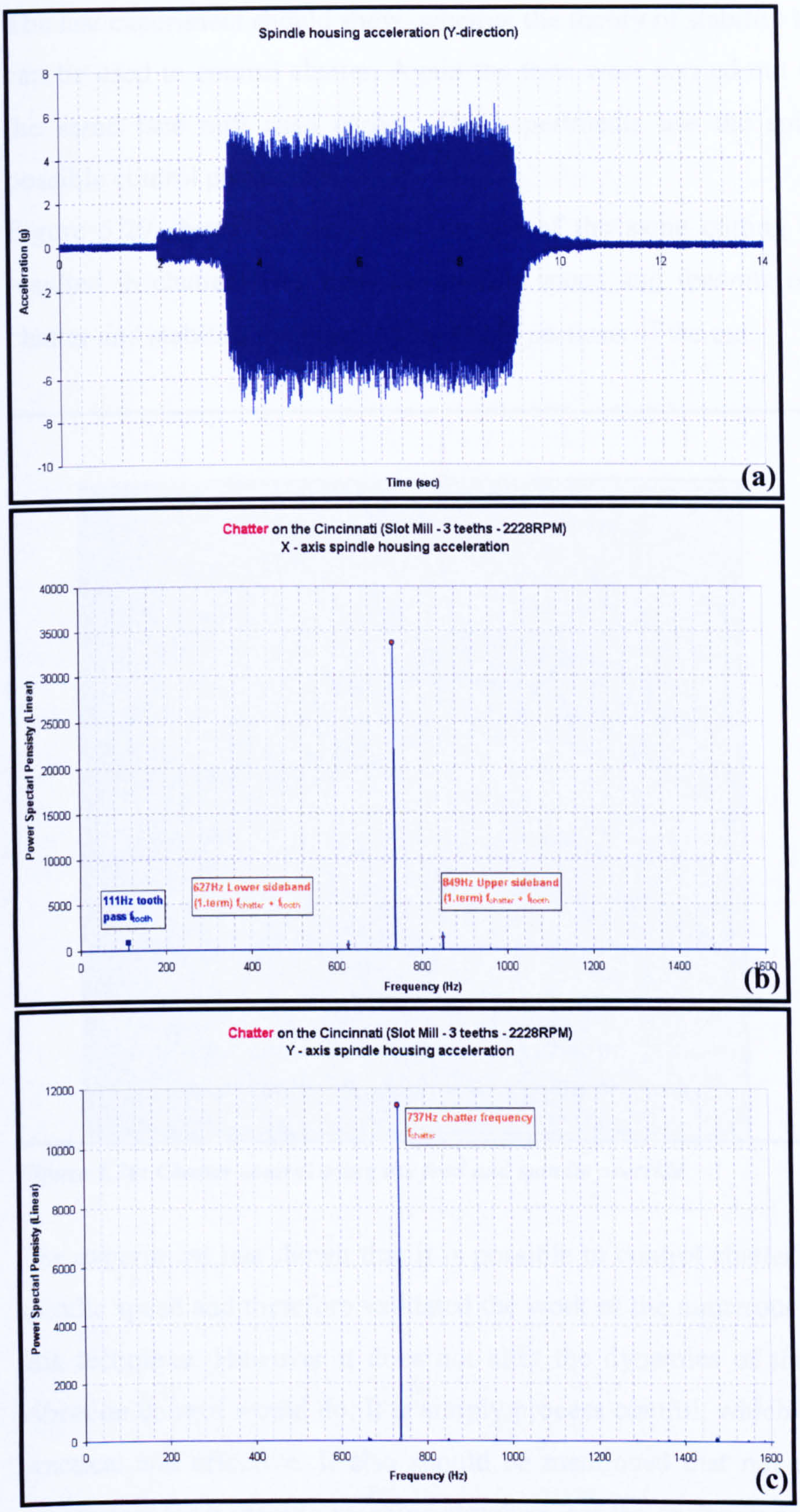

Figure 5.19: Chatter on the Cincinnati Arrow 500:

- ***Time response of Y-axis spindle housing acceleration (a)***
- ***Spectrum of the X-axis spindle housing acceleration (b)***
- ***Spectrum of the X-axis spindle housing acceleration (c)***

The last experiment should show, whether the theory of stability lobes, explained in chapter 3, can be used to control chatter. Again the tests were carried out on the Beaver machine with the same face mill used earlier. The experiments use the spindle speed and feedrate as possible control parameters.

Figure 5.20 shows the generated surface of the same cutting operation, which previously resulted in chatter. This time the spindle speed and feedrate override was used to control chatter and stabilise the machine at certain sections of the cut.

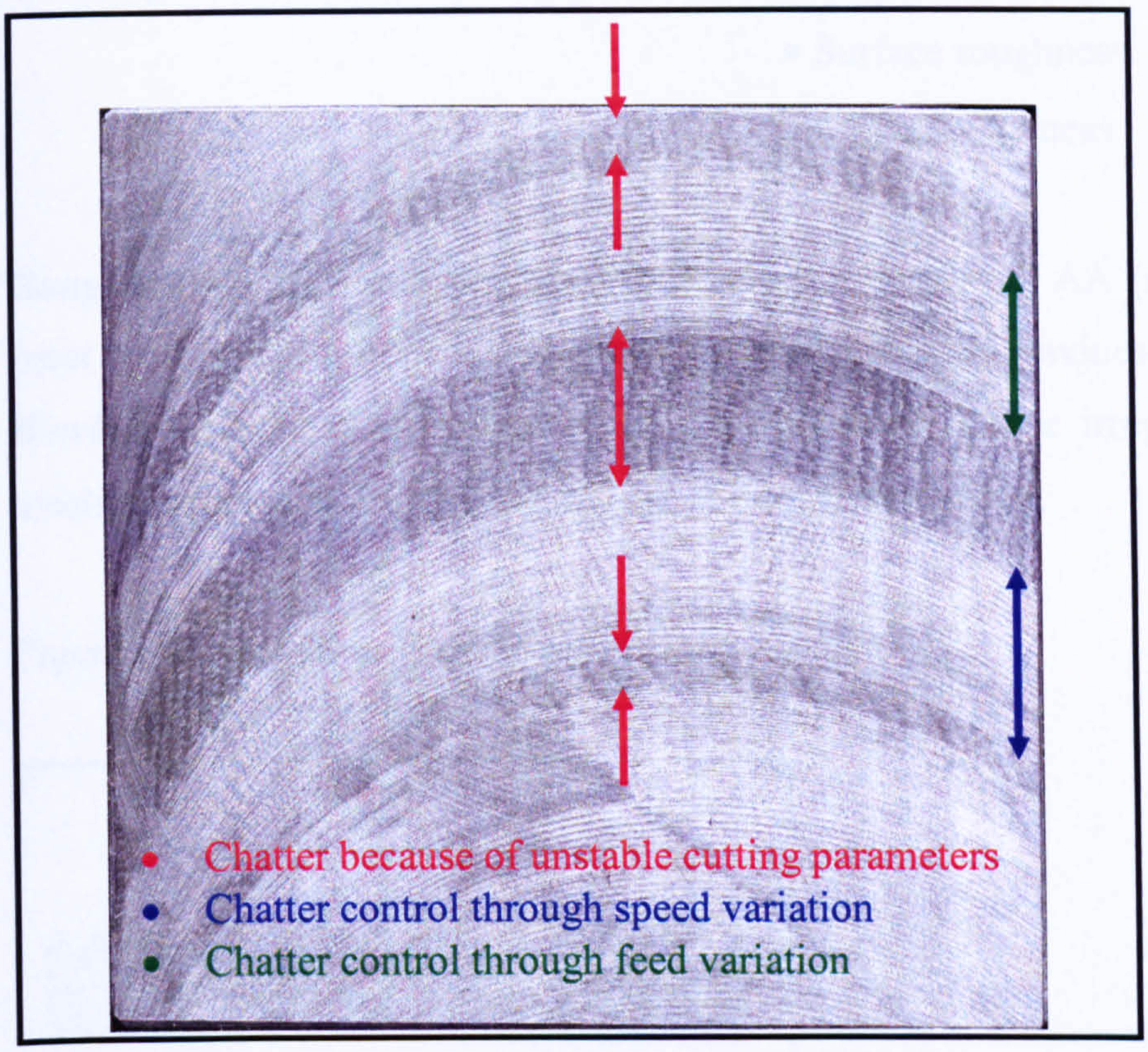

Figure 5.20: Chatter control using the feed and spindle override

The experiment has shown that it is possible to control chatter by changing the feedrate and spindle speed and therefore validated the work of the numerous of researchers who have used this technique. However it does not alter the dynamics of the machine structure as active vibration control would do. It is simply process control, which nevertheless seems to be very practical and effective. It also should be mentioned that not every optimum set of process parameters for a specific machine structure, are the optimum set of parameters for the cutting tool. The manufacturers of cutting tools recommend a certain range of spindle speed and feedrate for their tools. This range of parameters sets a limit on this chatter control technique, since it may interfere with the optimal parameters for a specific machine tool structure.

5.7 Investigation of the surface-finish

The vibrations of the investigated milling machine can be better understood by comparing the signals of the vibration sensors with the surface finish of the work-piece. The surface finish is arguably the best sensor to see the effect of vibration on machine tools, because it "stores" all the important information of the cut.

The surface finish in milling operations is the result of tool marks. These are the irregularities created by the cutting edges of the milling cutter.

The irregularities are defined as [129]:

- Surface roughness
- Surface waviness

Roughness is the measurement of tool marks in terms of AA (arithmetic average), or rms (root mean square). In doing roughness measurements the waviness is filtered out.

Waviness describes irregularities of the roughness. These irregularities are the result of machine-work-piece vibrations and are periodic in character.

Figure 5.21 illustrates the difference.

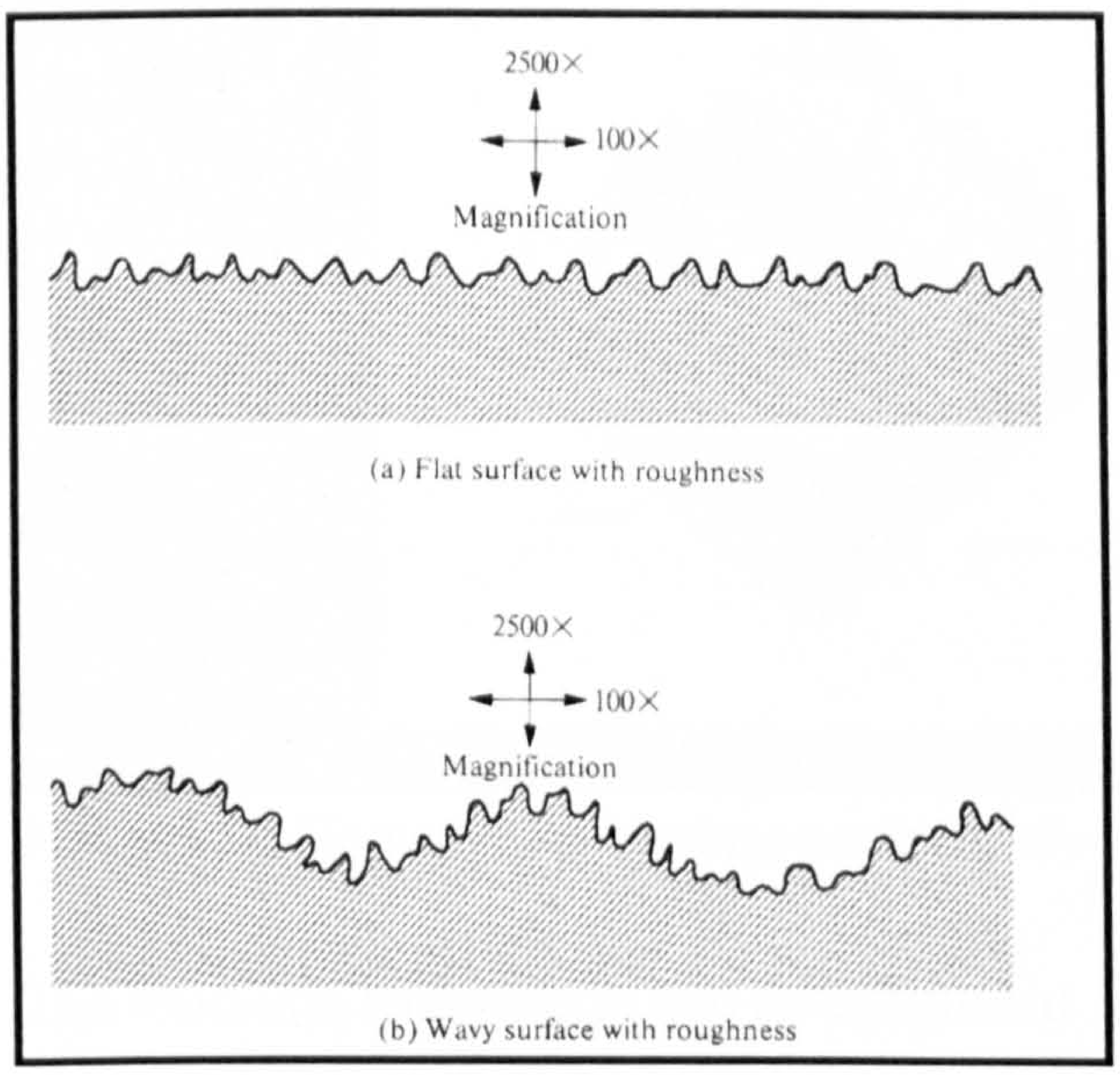

Figure 5.21: The difference between roughness and waviness [71]

Figure 5.22 and 5.23 shows the whole surface of a mild steel-test piece which was machined with a 100mm face mill (8 cutting edges). The cutting parameters were 477rpm spindle speed, 267 mm/min feed rate.

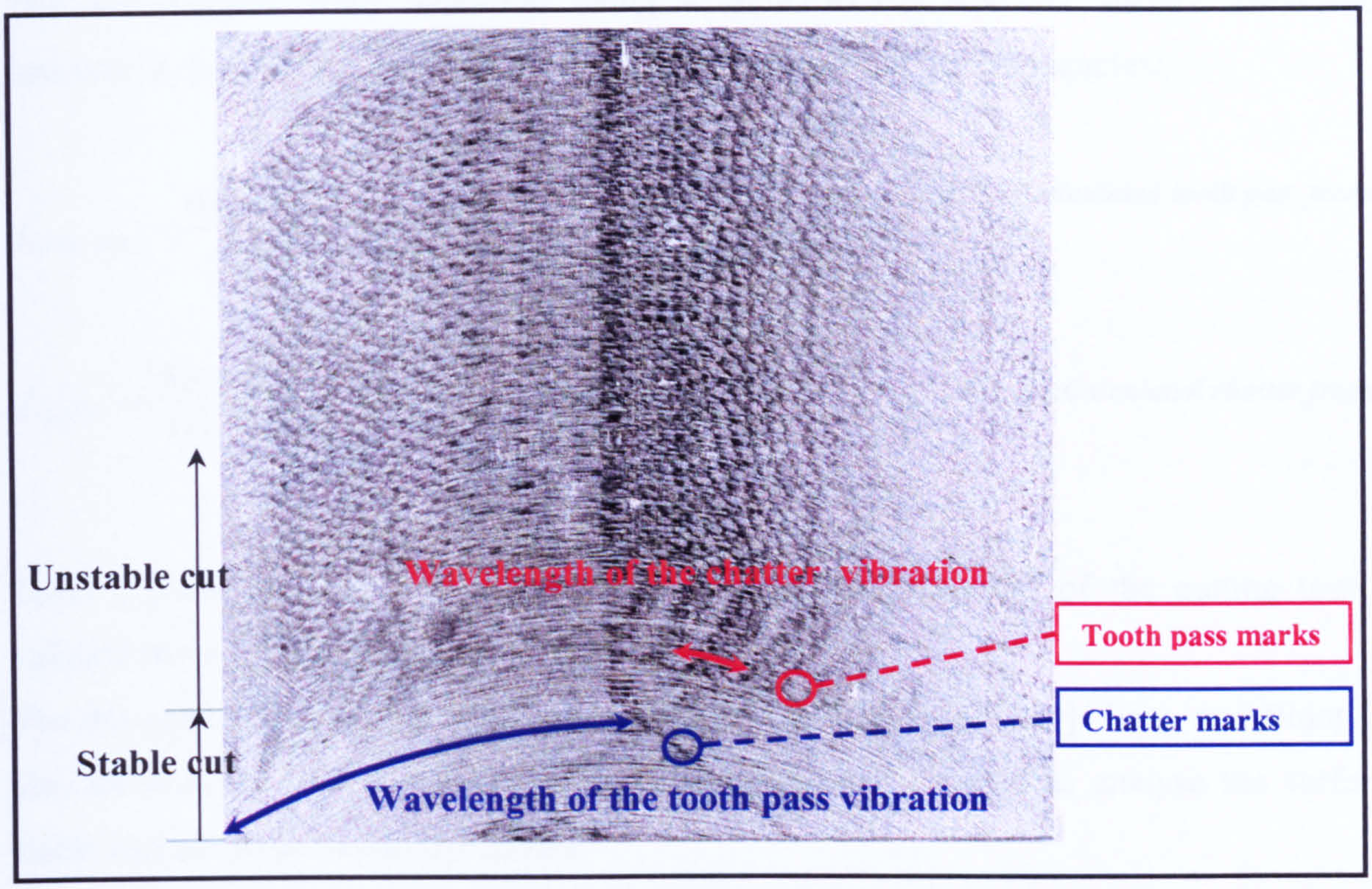

Figure 5.22: Image of the work-piece surface after the 4mm cut (axial depth of cut)

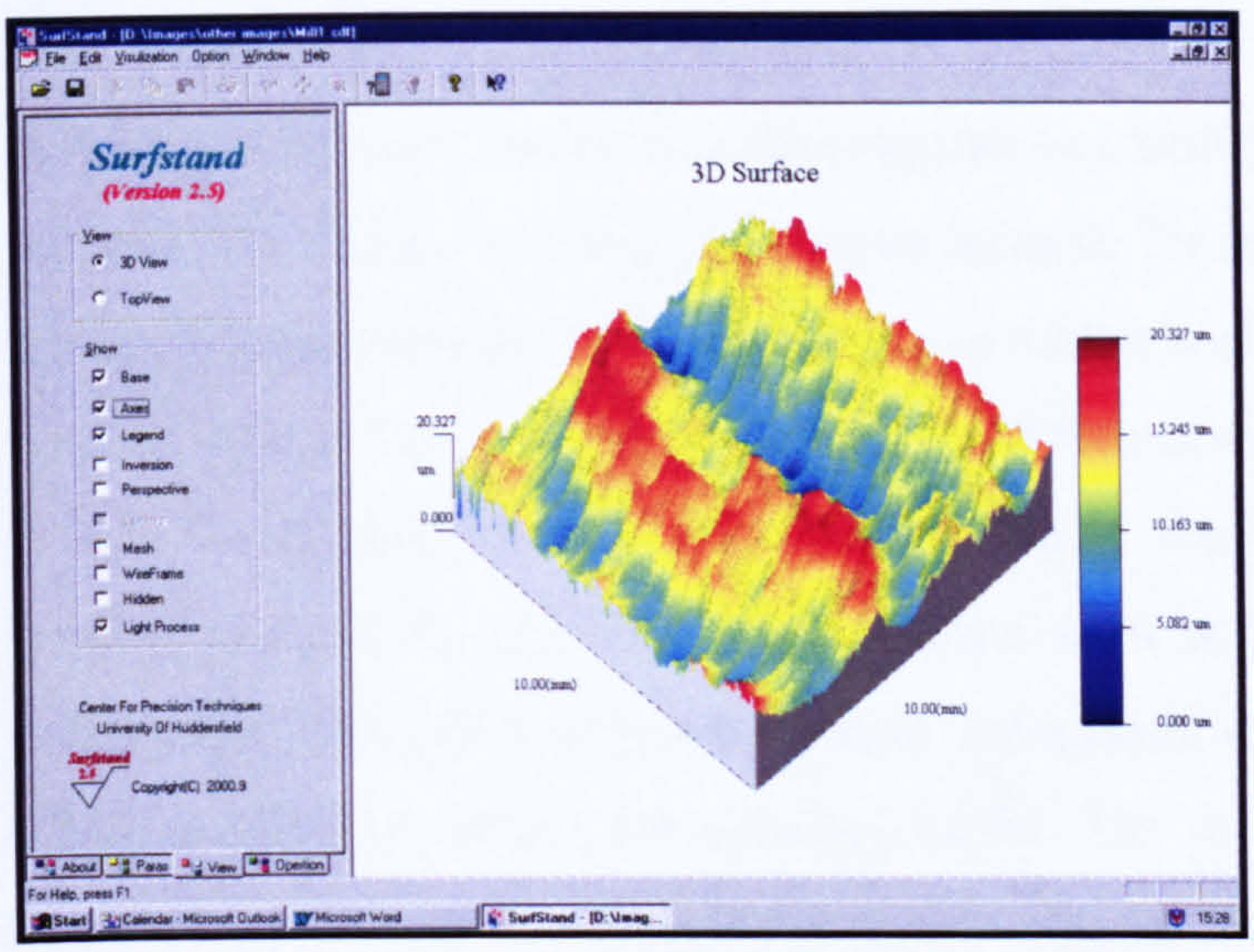

Figure 5.23: 3D scan of the waviness caused by the chatter vibrations

The vibration frequencies can be calculated from the surface scan using the following formula [74]:

$$f = \frac{tool\ diameter\ x\ spindle\ speed}{wavelength\ of\ the\ vibration}$$

Eq. 5.6: Calculation of the vibrations from the measured surface

The wavelengths were measured using a SURFACESCAN 3D surface measurement instrument, (see figure 5.23) and these resulted in the following frequencies:

$$f_{tooth-pass} = \frac{100\pi x 477}{60 x 39} = 64Hz$$ *Eq. 5.7:Calculated tooth pass frequency*

$$f_{chatter} = \frac{100\pi x 477}{60 x 5.5} = 454Hz$$ *Eq. 5.8:Calculated chatter frequency*

These figures correspond well with the vibration measurements of the cutting tests and validate the whole experimental procedure.

The 3D scan software used here was developed by Jiang et al [130]. Jiang and Blunt [131] also showed how 3D surface metrology techniques can be used to analyse the surface of stable and unstable cutting operations.

5.8 Summary

A 3-axis machining centre was investigated to identify its dynamic characteristics. This also included the design of a low cost sensor suitable for integrating onto the machine. The MEM accelerometers include signal conditioning which was built onto the same circuit board. The modal analysis done by AMTRI has been confirmed and extended to a wider frequency range. It was found that between 200Hz and 800Hz, the headstock and spindle were the most flexible parts of the machine. The vibration sources of the machine have been identified by performing light and heavy cutting tests. Additional sensors included a microphone and Hall-effect sensor to measure the spindle current. The tooth impact force and a 300Hz periodic force were the dominant frequency components in the sensor spectrum of a light cutting test. The 300Hz vibration was due to the spindle drive system and amplified through a structural resonance. The heavy cutting tests revealed the stability limit of the machine structure. It was found that the chatter frequency of about 450Hz was Amplitude Modulated with the tooth-pass frequency. The chatter frequency of a second machining centre was more dominant, but again the 700Hz chatter frequency was Amplitude Modulated with the tooth pass frequency. A search was done to find the most sensitive process parameters for controlling chatter vibrations. It was found that it was possible to stabilise the cutting process by optimising the feed and spindle speed, using the override of the CNC controller. This has confirmed some of the theory presented in chapter 2 and 3. Other sensitive parameters were the spindle – work-piece eccentricity and location inside the working volume of the machine. Although the process parameters changed the stability limit of the machine the chatter frequency itself seemed to be almost unchanged. It also was found that without additional signal conditioning the spindle current sensor can not be used for chatter control. An investigation of the surface finish showed a good correlation to the sensor signals.

These initial tests allowed a better understanding of the dynamic behaviour of the machine. They also showed the effectiveness of choosing the optimal cutting parameters, which nevertheless do not alter the structural dynamics as active vibration control would achieve.

The next chapter demonstrates the effectiveness of active vibration control on a simple beam structure.

Chapter 6

Implementation and results on a test rig

6.1 Introduction

Following the study of active vibration control theory in chapter 4, this chapter presents an experimental study of active vibration control on a simple beam structure.

It will show the process of building up the digital adaptive controllers eventually used to control a mechanical structure and also discuss the practical difficulties that were encountered. Traditional electronic controllers were also built and compared to the digital adaptive controllers. Furthermore the optimal type and location of the sensors and actuators on the vibrating structure are discussed.

First the mechanical structure to be controlled is introduced by identification, simulation and extraction of its mechanical parameters. Then the first step of controlling the structure is taken by designing an electronic feed-forward controller with "static control parameters". In order to implement an adaptive controller a suitable digital platform needed to be built. Static and adaptive digital filter routines have been designed for simulation under MATLAB-SIMULINK and for the digital real time control platform.

These models were used to identify the frequency response functions of the mechanical structure in order to simulate an adaptive controller to control the mechanical structure. This was then validated through the implementation of the adaptive controller to the mechanical plant. An interesting investigation was undertaken in the type and optimised location of the vibration sensors and actuators and finally traditional active vibration controllers (e.g. active damping) were developed in order to compare their performance with the digital adaptive controllers with regard to their use on machine tool structures.

After gaining experimental knowledge about active vibration control and developing the controller hardware and software, a system to control vibrations on milling machines was designed (chapter 7). The work presented in this chapter has partly being published by Haase, et al [132].

6.2 The mechanical structure for adaptive control

A standard cantilever beam was chosen for the experiments. The advantages are that we do not have to use Finite Element Analysis in order to simulate its dynamic behaviour and that the size of the beam matches the power capabilities of readily available actuators. Furthermore the shape of the structure is representative of a cutting tool in a tool post or spindle and therefore very common for this kind of research. The modal frequencies of the cantilever beam were also in the same range as the ones measured on the vertical milling machine, discussed in the previous chapter.

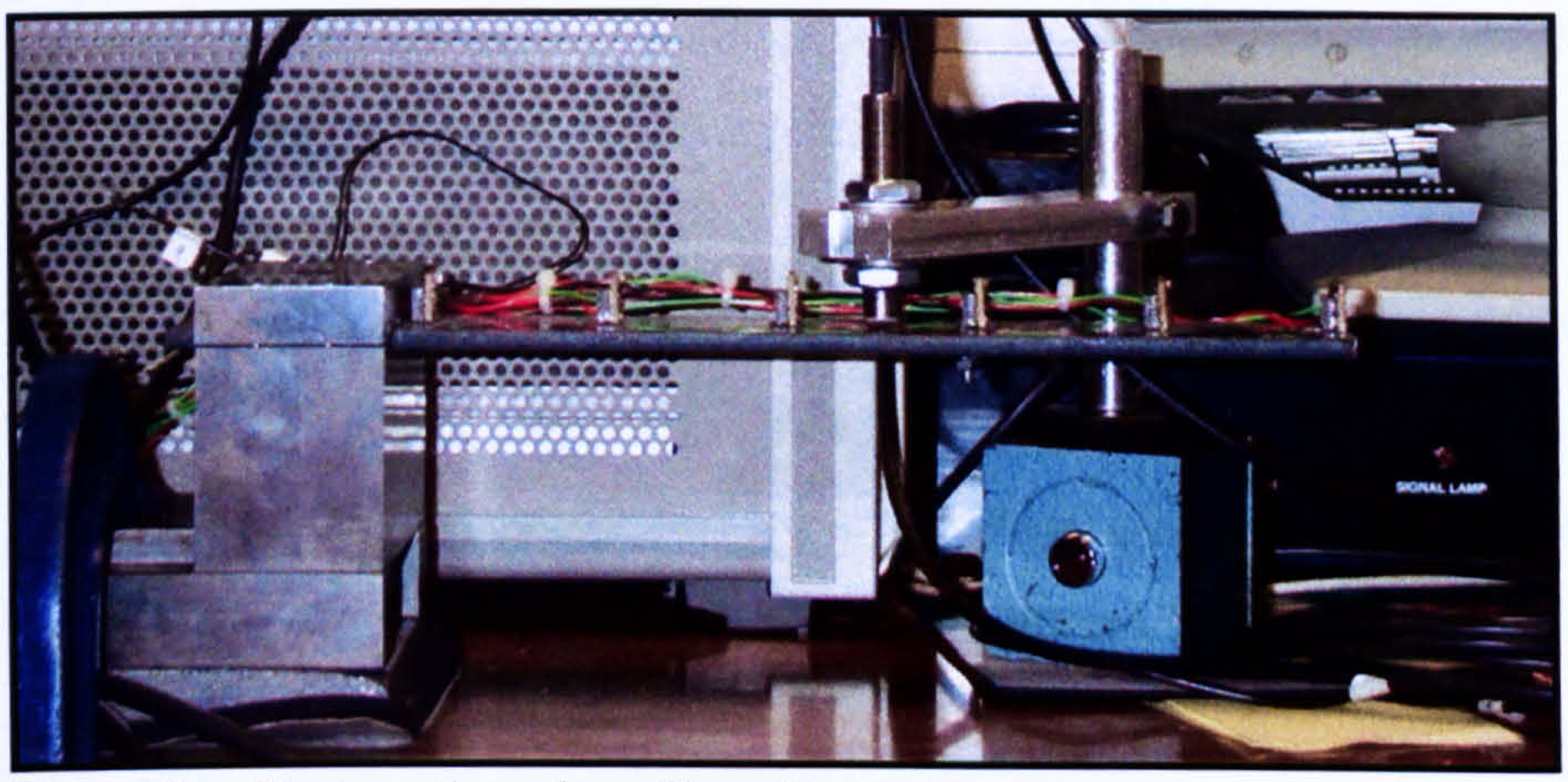

Figure 6.1: The investigated cantilever beam structure

6.2.1 Identification of the mechanical parameters of the beam structure

The first experiment was a modal test on the beam to identify its frequency response functions (FRF's).

There are two different ways of doing this:

- Normal Mode Method
- Transfer Function Method

Both methods have been explored here. The *Normal Mode Method* is the "traditional " method of modal testing, which aims to extract the modal parameters (modal frequency or resonance frequency, mode shape and damping) from a structure.

The procedure for the *Normal Mode Method* is:

1. Determine the modal frequencies by applying a wide band sine sweep using a shaker and a vibration sensor with an oscilloscope to monitor the response.
2. Excite or tune in on one mode at a time using one or more shakers and record the instantaneous amplitude of several sensors along the structure (modal dwell).

3. Determine the damping by shutting off the shakers after a particular mode has been excited in order to simulate an impulse response.

The *Transfer Function Method* makes use of digital signal processing techniques (FFT) in order to extract the modal parameters.

The procedure here was:

1. Measure the frequency response function (FRF) at several points of the structure by using a spectrum analyser, vibration output sensor, force input sensor and either shaker or impact hammer to excite the whole frequency range of the mechanical structure.
2. Transform the FRF's into a parametric model using curve fitting.

The second technique is much quicker than the *Normal Mode Method* and the FRFs can be measured one after the other, which means one vibration sensor is enough. The curve fitting can be done using sophisticated algorithms and software such as Star Modal [133]. A measure for mode shape is the value of imaginary part of the transfer-function at resonance, where the real part is zero [119, 120].

Figure 6.2 shows the FRF taken at the end point of the beam. Since the measured output is acceleration the FRF is called accelerance (acceleration/force).

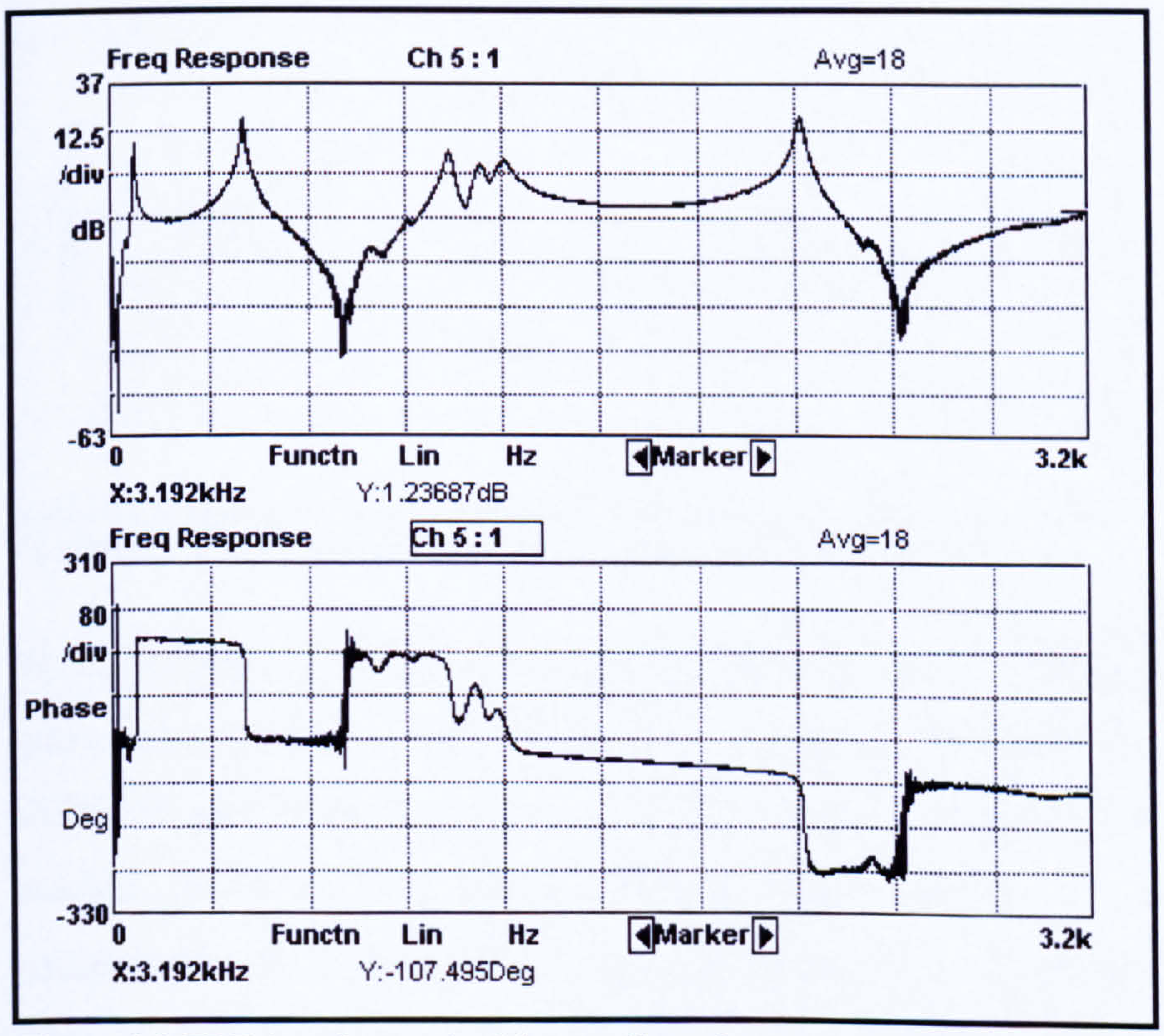

Figure 6.2:FRF (accelerance) of the cantilever beam

Other FRFs are compliance (displacement/force) or mobility (velocity/force) depending on which sensor is used to measure the vibration response of a structure to a recorded force input. Whether the FRF is measured using an impact hammer or shaker did not make any significant difference. The coherence function [119,120] for all these measurements was almost unity throughout the whole frequency span (the coherence function provides a statistical measure of the quality of the modal measurements). It should also be mentioned that the right choice of sensor is important for modal testing [92]. Depending on the frequency of interest an accelerometer is suitable for high frequencies and the displacement sensor for low frequencies. Because of the integration of acceleration the sensor signal decreases by $1/\omega$ for velocity and $1/\omega^2$ for displacement (–20 dB/dec and –40 dB/dec. for logarithmic scale). From this the modal frequencies can directly be seen:

1. Mode at 70 Hz
2. Mode at 428Hz
3. Mode at 1150Hz

Figure 6.3 shows the identified modal shape (modal dwell) of the second mode.

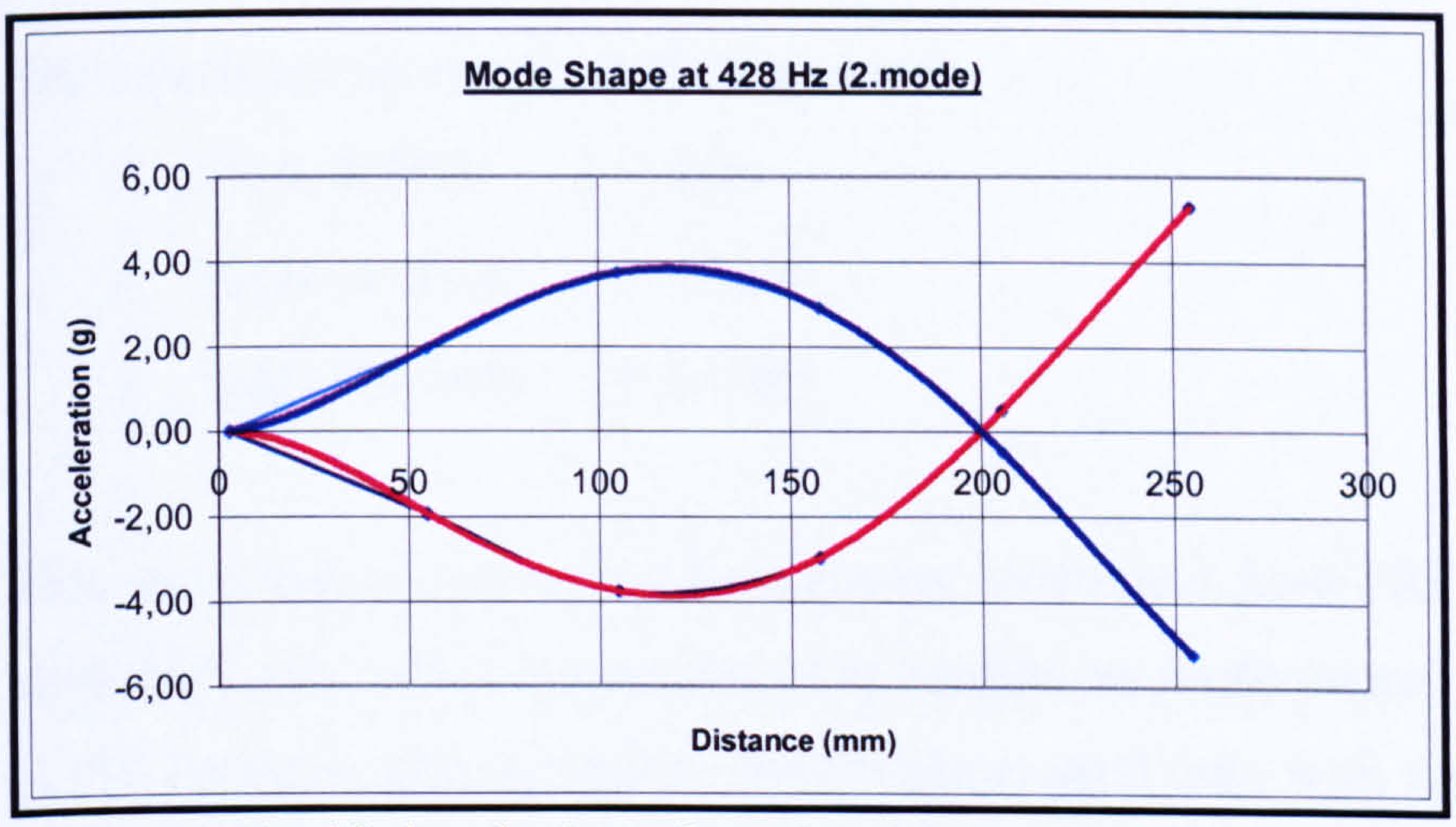

Figure 6.3:Identified mode shape (2. mode) of the beam structure

To identify the damping for each mode the bandwidth method [100] was used. This method allows the damping parameter from the frequency domain to be identified by measuring the width of each resonance peak at –3dB. A MATLAB routine was written to carry out this analysis. Here the frequency resolution, which depends on the number of data points to compute the FFT, can also be improved by an optional interpolation between the frequency lines if the resonance peak is narrow (low damping). More information on frequency resolution, leakage error and windowing can be found in the literature [100, 119].

Figure 6.4 shows the graphics produced by the MATLAB program for the second mode.

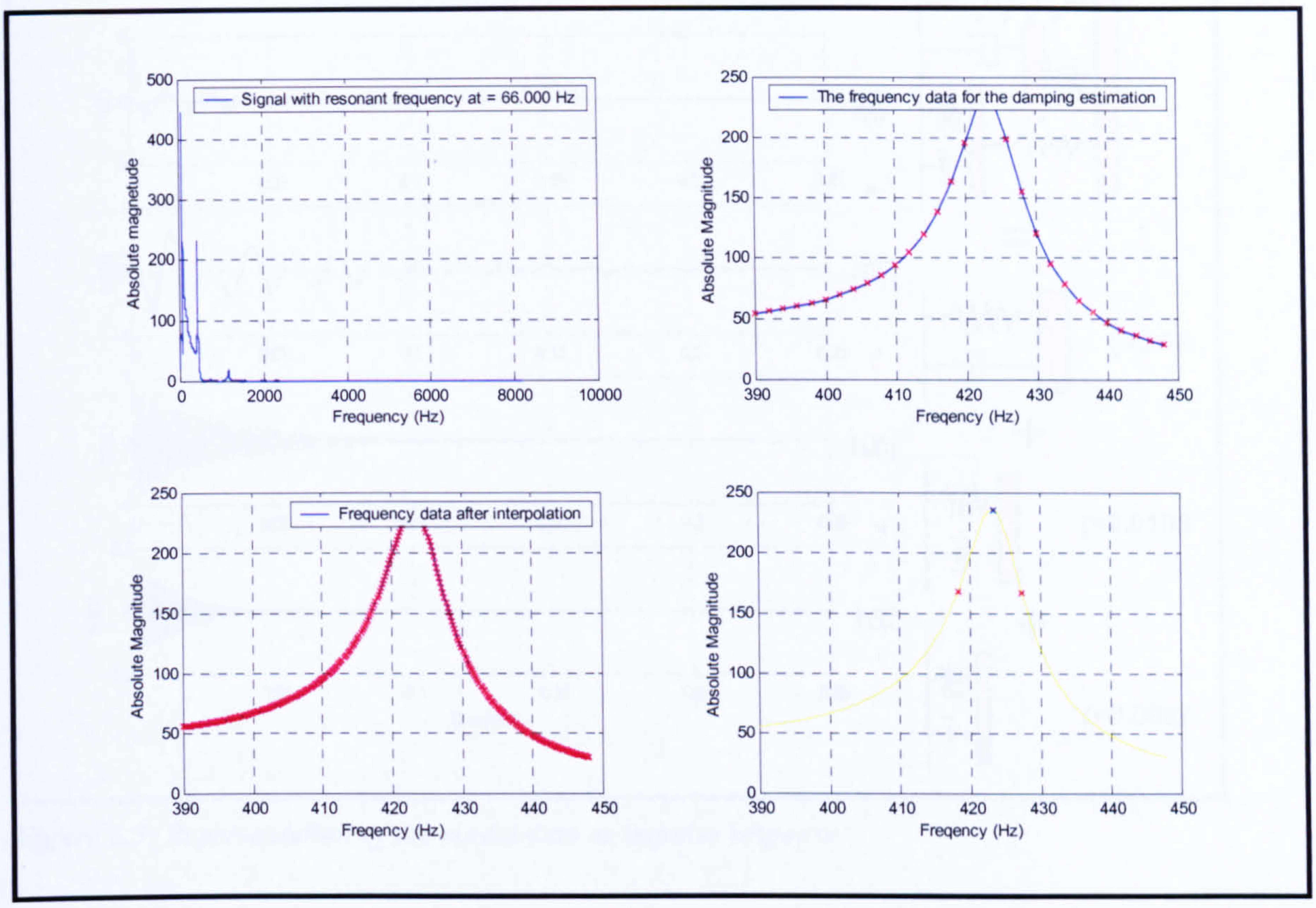

Figure 6.4: Graphical display of the MATLAB routine estimating the damping in the frequency domain

The calculated damping coefficients were:

1. Mode (66Hz) $\zeta = 0.04$
2. Mode (423Hz) $\zeta = 0.0108$
3. Mode (1156Hz) $\zeta = 0.0087$

This technique of estimating the damping coefficient from FRF's has been calibrated against simulated data with a known damping coefficient implemented as a digital filter by Freeman [133]. Freeman also compares the technique used here with the wavelet analysis and STAR MODAL. When the structure has two coupled modes with heavy damping, the –3dB points of the less dominant modes can not be identified since the peak is too small.

For completion, figure 6.5 shows a different view of the measured data. Instead of the usual FRF's the impulse response in time is shown here. The reason why this representation is interesting is because the parameter estimation of adaptive filters looks very similar, since it is also done in the time domain. The figure not only shows the impulse response of the whole system, but also the impulse response of each single beam mode, using wavelet analysis [133].

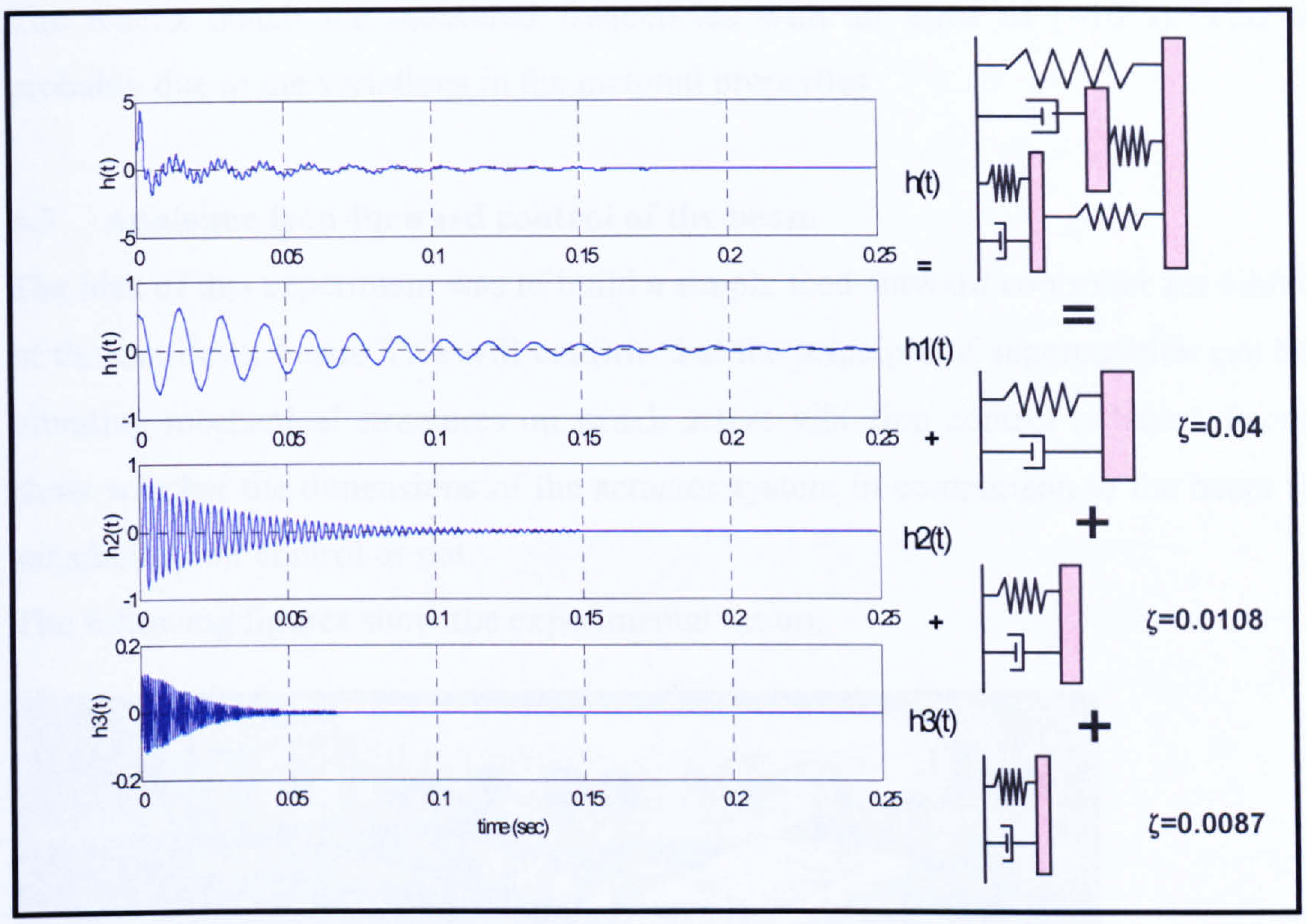

Figure 6.5: Representation of the modal data as impulse response

6.2.2 Simulation of the beam structure

In order to predict the dynamic behaviour of the mechanical structure a mathematical model based on the properties of the beam was developed and its response compared with the measured results.

As discussed in chapter 4, a mechanical system can be either a rigid body system or an elastic body system. Rigid body systems are "mass-spring-damper" systems or an assembly of those (lumped parameter models). They are solved analytically using ordinary differential equation (ODE) based on Newton's second law. A simple homogenous elastic body, such as the cantilever beam, has to be solved using a partial differential equation instead of an ODE. For homogenous structures this is not too difficult and solutions exist.

A MATLAB routine was written to calculate the modal frequencies. The function input parameters are the properties of the beam (Young Modulus, Moment of Inertia, Cross section of the structure and length).

The calculated modal frequencies were:

- 71.2 Hz (1.mode)
- 445Hz (2. mode)
- 1249 Hz (3. mode)

The results match the measured frequencies with an error of (~10%). This variation is probably due to the variations in the material properties.

6.3 Analogue feed-forward control of the beam

The idea of this experiment was to build a simple feed-forward controller for vibration control of the cantilever beam. This will confirm that the principle of superposition can be applied to vibrating mechanical structures on which active vibration control is based. Secondly it will show whether the dimensions of the actuator system in comparison to the beam structure are satisfactory for control or not.

The following figures show the experimental set up.

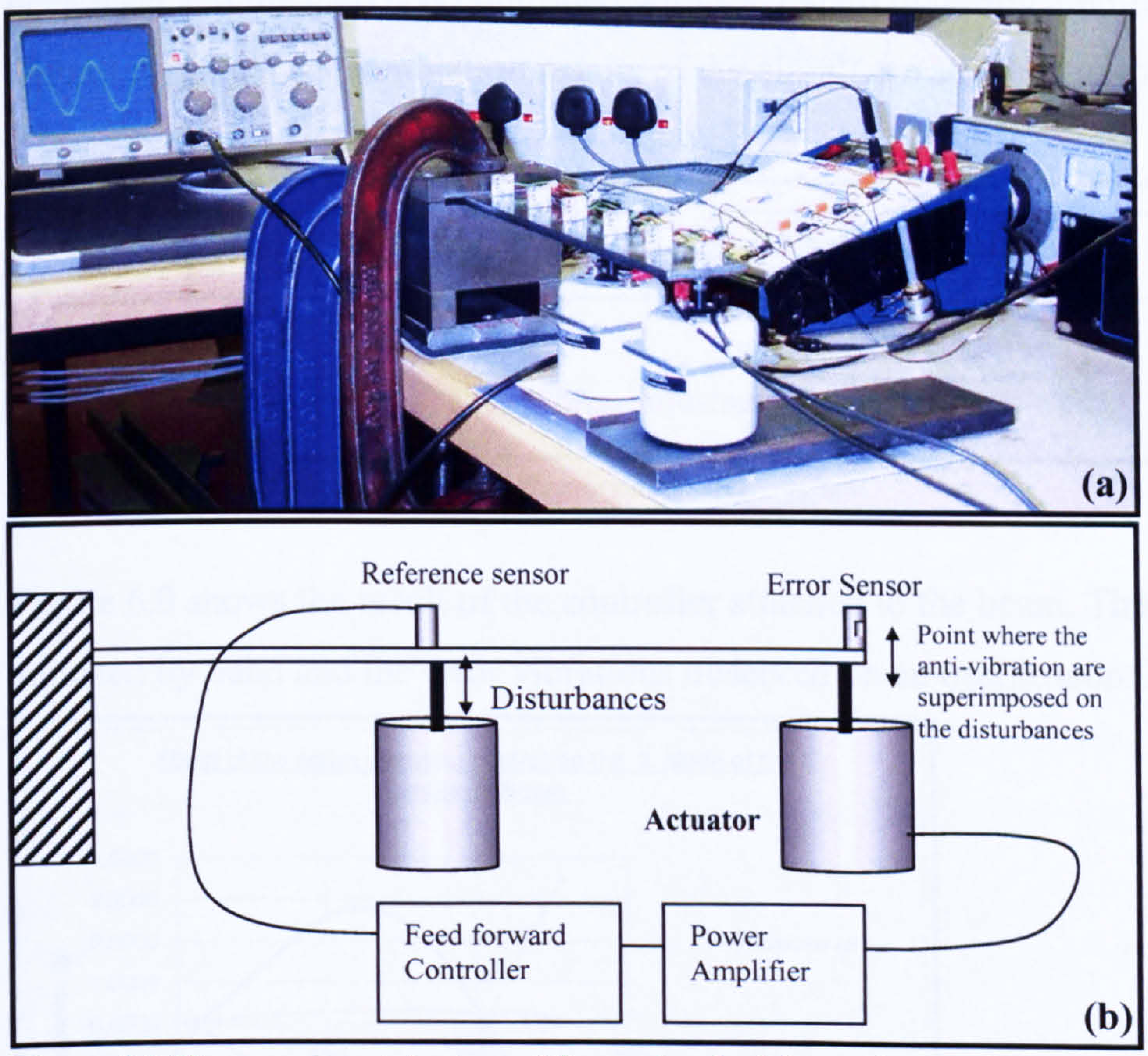

Figure 6.6: The experimental set up of the analog feed-forward controller

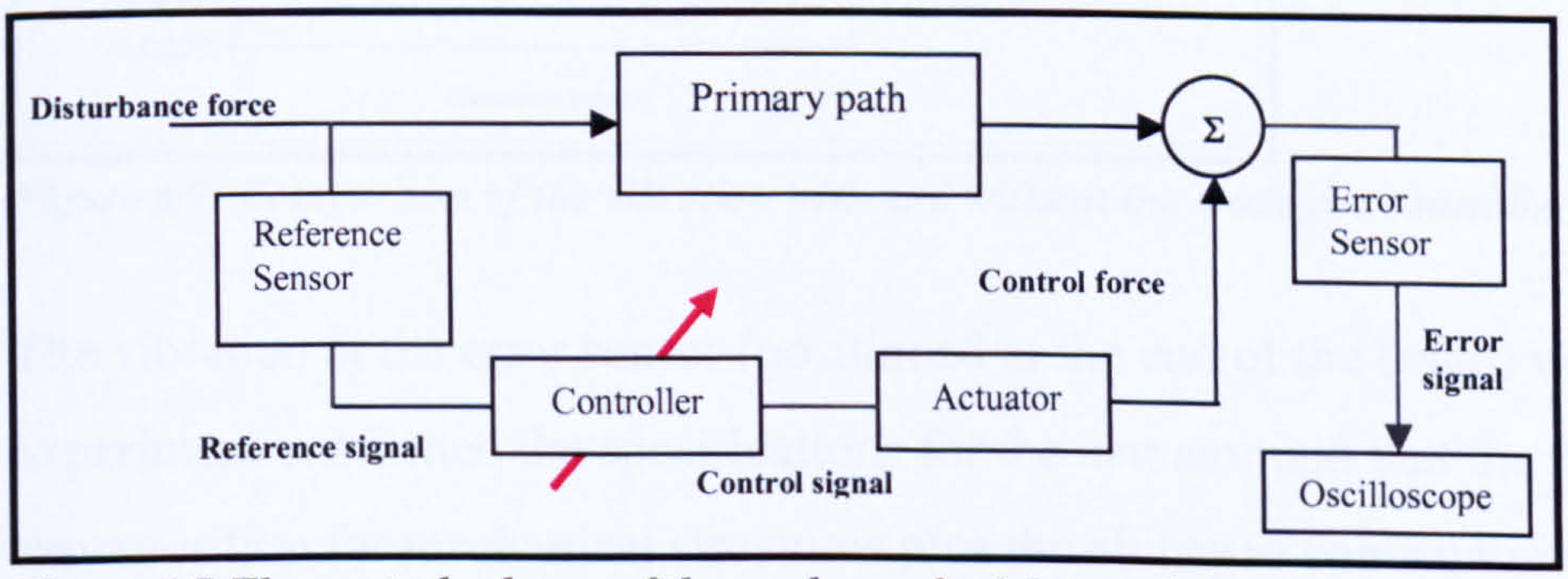

Figure 6.7: The control scheme of the analogue feed-forward controller

The harmonic disturbances are produced somewhere along the beam and the reference sensor measures the disturbances at a certain point (from that point to the point where the compensation is applied, will be a certain gain difference and phase shift). First the phase of the controller needed to be adjusted so that the vibration produced by the actuator was in opposite phase to the vibrations produced by the disturbance source. Secondly the controller gain can be increased so that the control force reduces the disturbances. If the error signal reaches its minimum (observed on the oscilloscope) the vibration is cancelled. In order to work, the analogue controllers must be able to produce a phase shift of at least 360 degrees and also provide a gain adjustment. It is important that these two parameters can be controlled separately from each other. In order to adjust the phase, two first order all-pass filters have been used and the gain was controlled with a standard inverting amplifier (figure 6.8).
Circuit diagrams and simulation results of the circuit are attached in the Appendix C.

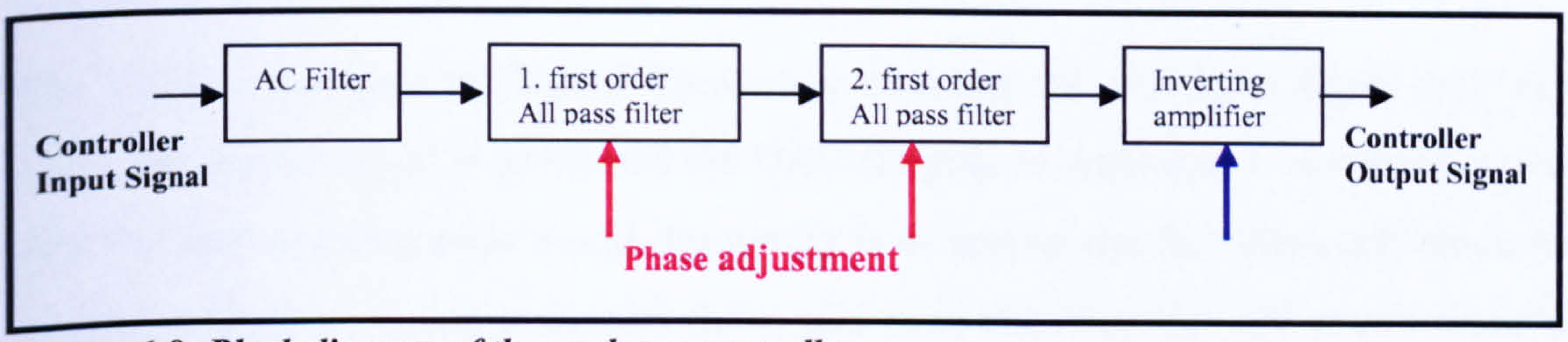

Figure 6.8: Block diagram of the analogue controller

Figure 6.9 shows the result of the controller attached to the beam. The parameters were adjusted by hand and the error vibrations observed on an oscilloscope.

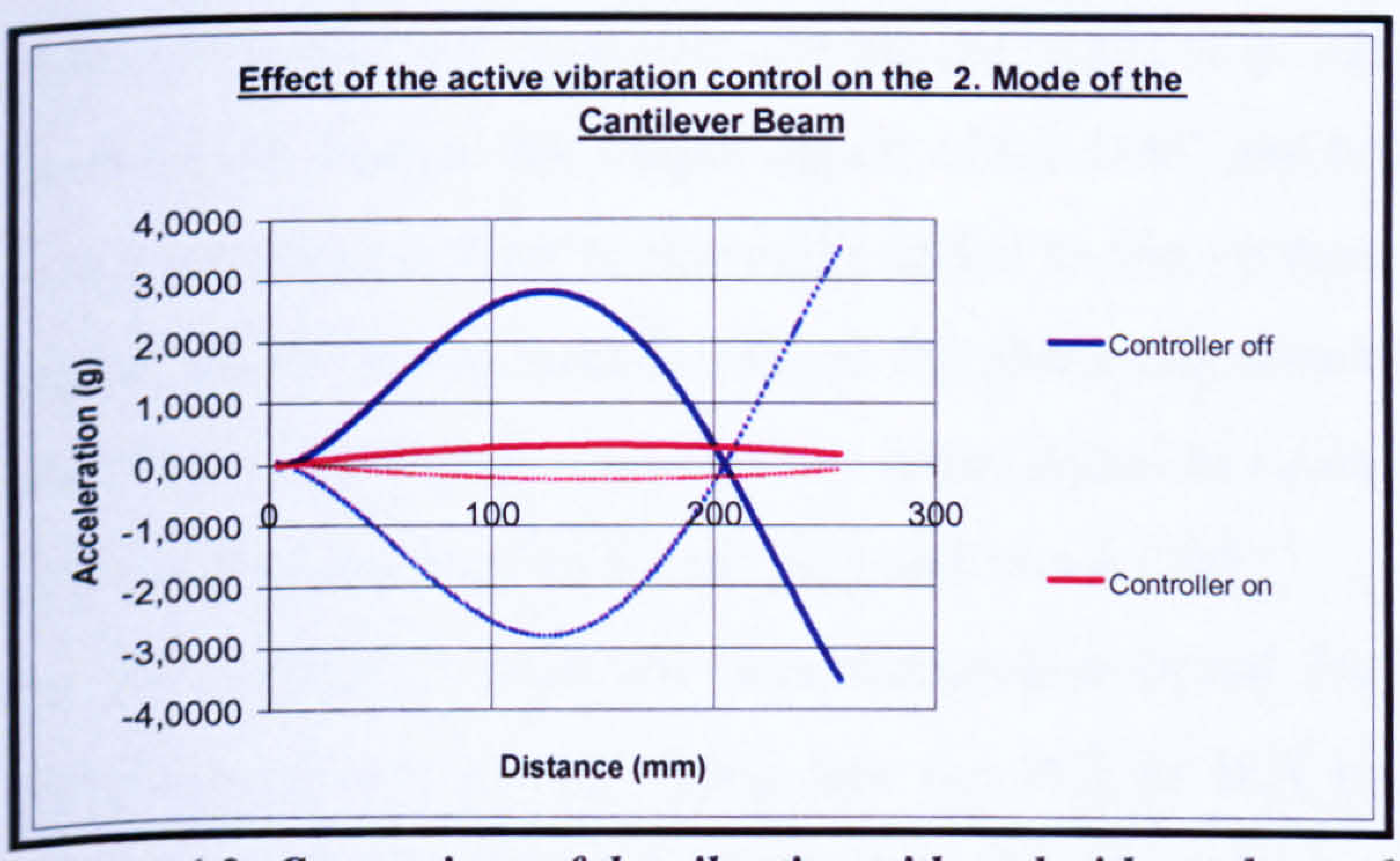

Figure 6.9: Comparison of the vibration with and without the analogue controller

The vibration at the error sensor (positioned at the end of the beam) was reduced by 97%. The experiment confirmed the specifications for the actuator and that the principle of superposition for mechanical structures plus the ability to control these is valid.

The next section describes how the controller tuning process was automated, using adaptive algorithms.

6.4 The real time data acquisition platform for the digital controller

To apply any form of Digital Signal Processing, such as the adaptive algorithms to an analogue signal, a data acquisition platform or DSP system is required. For control purposes this system needs to operate in real time in order manipulate and modify the analogue signals. Figure 6.10 shows a typical real time DSP system.

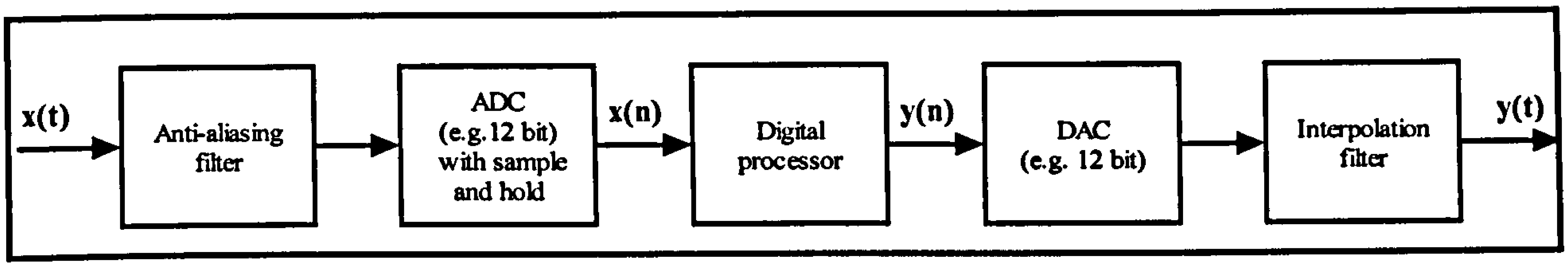

Figure 6.10: Block Diagram of an typical real time DSP

The ADC (Analogue to Digital Converter) converts the analogue signal into digital form. After the digital signal is processed the DAC (Digital to Analogue Converter) converts it back into the real or continuous world. Important is of course the fact that each block has to work in real time. For vibration control these real time requirements are much more demanding than for example, in temperature control. The sampling frequency needs to be at least twice the highest frequency component, of the signal to be controlled. The anti-aliasing filters prevent signals with higher components than half the sampling frequency entering the ADC. Another possibility is to over sample the signal (e.g. 10x over sampling).

In order to smooth the output signal of the DAC and remove any high frequency components a reconstruction filter is normally added to the system. It should however be noted that any signal conditioning already affects the phase response of the controller. Much information on DSP systems such as quantisation error, signal to noise ratio and dynamic range, is contained within the reference by Smith [95] and Jervis [105].

In this project a standard data acquisition board for the PC was used as digital control platform. It can be connected into the PCI or ISA bus of the motherboard of the PC and therefore uses the main PC CPU as processor. The advantage is that no additional software has to be used in order to compile and debug the programs. It also has no additional signal conditioning filters, which gives the option to design our own if needed.

The chosen card is from BLUE CHIP Technology has 16 single ended and 8 differential ADC's and two DAC's. It can be programmed at a register level under MS DOS and uses the

16 bit ISA bus. The system is programmed using on older version of the Borland C++ compiler (version 4.5) since new compilers (e.g. Microsoft C++ - Version 6) can only create Win32 projects (for Windows 95 and later). Tests with using Microsoft NT as an operational system failed since the non-deterministic interrupts were causing serous problems for real time control.

To explore the speed limitations of this DSP system, it was used to perform a static FIR filter operation (for the theory on digital filters refer to chapter 4.3). The PC had a 90MHz Pentium processor. Figure 6.11 shows the experimental set up.

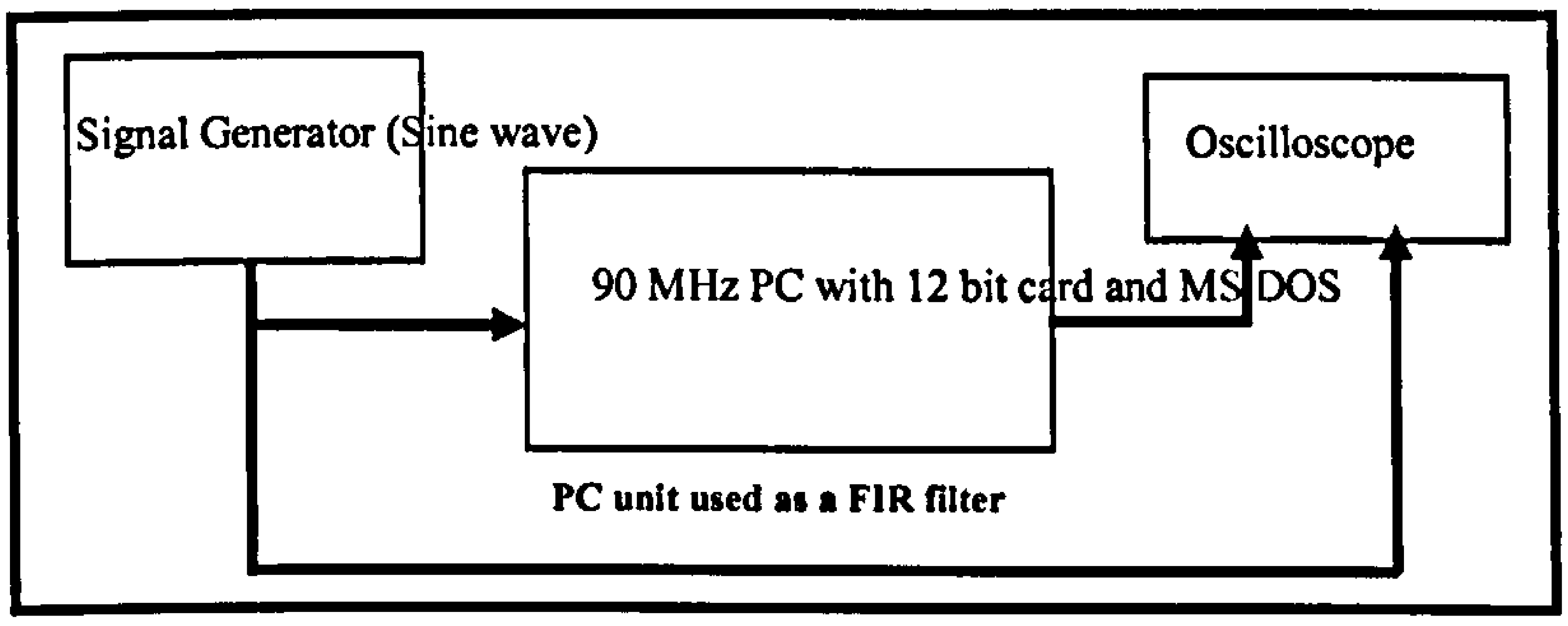

Figure 6.11:The PC and data acquisition card used as a digital filter

The maximum available speed for a 60 tap FIR filter was about 6kHz, which was sufficient for the adaptive controller. It was also found that it made a difference, which version of Microsoft DOS was used. Three different versions were tested:

- DOS Version 6.22
- DOS shell of Windows
- Win 98 DOS

Figure 6.12 shows the difference in speed between DOS Version 6.22 and Win 98 DOS.

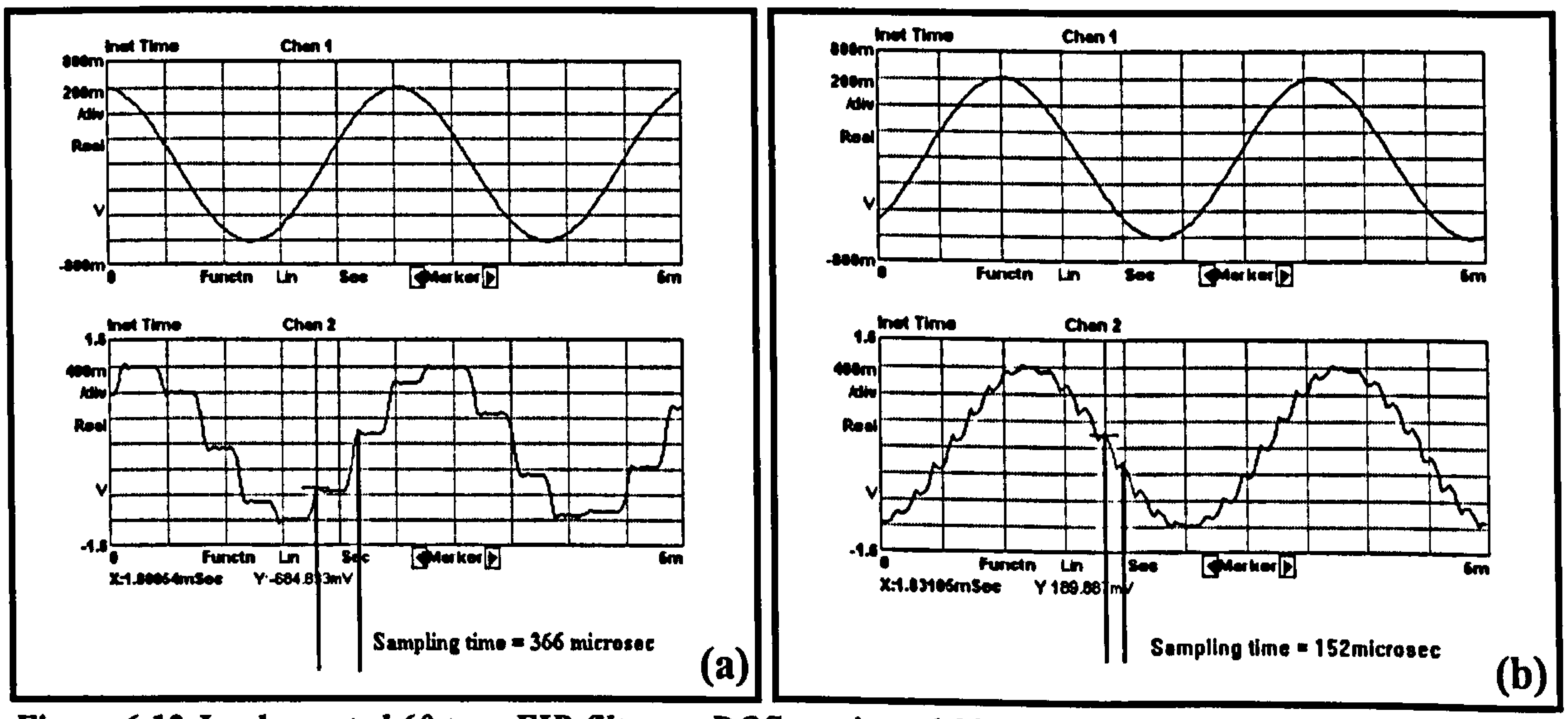

Figure 6.12:Implemented 60 taps FIR filter on DOS versions 6.22 (a) and Win 98 DOS (b)

This clearly shows that Win 98 version is the fastest DOS version. Next the output of this digital filter was connected to the actuator system, in order to vibrate the cantilever beam. As expected, DOS didn't cause any uncontrolled interrupts.

But there was one further problem. In order to sample the reference signal and the error signal for the feed-forward controller two BLUE CHIP cards had to be used, because the multiplexer of these cards caused a "bouncing" effect. (Even by having 1msec time delay between ADC1 and ADC2). Figure 6.13 illustrates this.

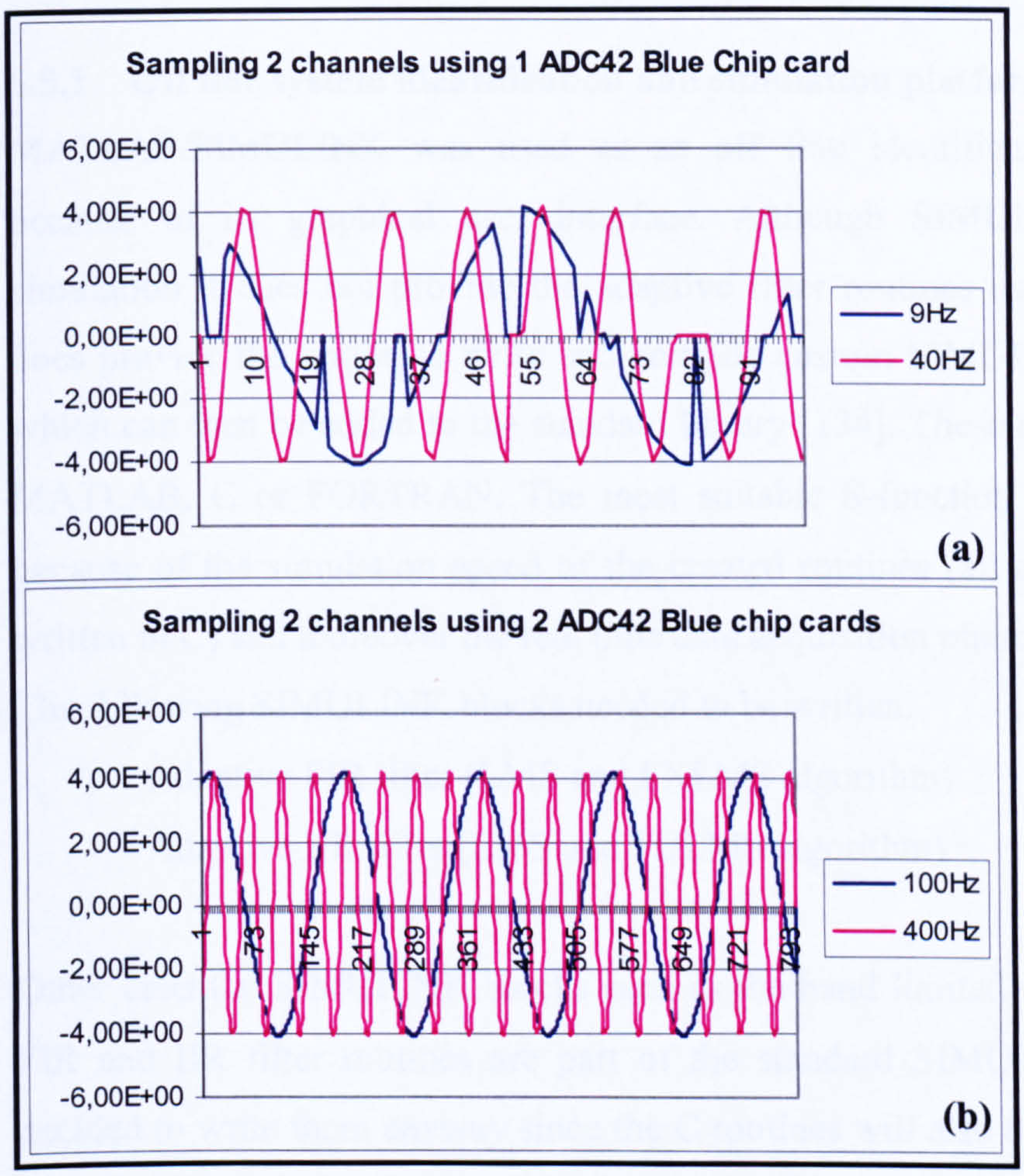

Figure 6.13:Two analog signals sampled over 2 ADC channels using:
- ***1 Blue chip card (a)***
- ***2 Blue chip cards (b)***

With this, a suitable data acquisition units for the adaptive controller had been found, and the programs optimised with an option to select the sampling frequency. This was done by synchronising the filter algorithm to a TTL signal from a frequency generator, which was read in via one of the boards digital I/O's. The sampling frequency could then be set on the TTL generator up to the maximum sampling frequency of the board. This was an essential option for the filtered-X algorithm since an incorrect sampling frequency has the effect of shifting the FRF's resonances.

6.5 Adaptive digital filters

The main objective of this work was to design digital filters, which have the same frequency response as the measured FRF's of the modal test from the beam. The theory of the adaptive filters was covered in chapter 4.4. After the adaptive filter routines for system identification were programmed, they were used to identify the relevant transfer-function of the cantilever beam, which then led onto a simulation program for the beam structure, in order to control the vibrations adaptively.

6.5.1 Off line system identification and simulation platform

MATLAB/SIMULINK was used as an off line identification and simulation platform, because of its graphical user interface. Although SIMULINK is very convenient for simulation it does not provide the adaptive filter routines used in this project. However, it does provide the option to write and compile custom SIMULINK blocks using S-functions, which can then be added to the standard library [134]. These custom blocks can be written in MATLAB, C or FORTRAN. The most suitable S-function compiler was the C compiler, because of the simulation speed of the created routines (all existing SIMULINK blocks are written in C) and moreover the real time data acquisition platform also is programmed in C.
The following SIMULINK blocks needed to be written:

- Adaptive FIR filter (LMS and FXLMS algorithm)
- Adaptive IIR filter (LMS and FULMS algorithm)

Other essential SIMULINK blocks such as the band limited white noise generator and static FIR and IIR filter routines are part of the standard SIMULINK library. However, it was decided to write them anyway since the C routines will also be required later for the real time DSP system. It also should be mentioned that all included SIMULINK blocks are only available as a compiled versions and therefore it is not possible to access the code itself. Nevertheless the provided MATLAB routines were used to calibrate the customised ones.

6.5.1.1 Adaptive FIR filter (LMS and FXLMS algorithm)

The objective here was to write a SIMULINK function, which executes an adaptive FIR filter using either, the LMS or FXLMS algorithm. The theory can be reviewed in chapter 4 figure 4.13 (LMS) and 4.18 (FXLMS).
The CS_FCT_LMSFIR.dll has 3 input parameters:

- The FIR filter order
- The sampling time (**-1** for inherited sampling time from the driving block)
- The adaptive algorithm (**0** for the LMS and **1** for the FXLMS algorithm)

In order to test the new SIMULINK block, a FIR filter was designed using MATLAB's filter design tool (*fdatool.m)*. The filter was a 10^{th} order low pass FIR windowed-sinc filter (figure 6.14.c). The adaptive FIR filter routine was then used to re-identify this low pass filter. Ideally the results should be that both filter kernels are identical. Figure 6.14.a shows the graphical user interface of this SIMULINK routine.

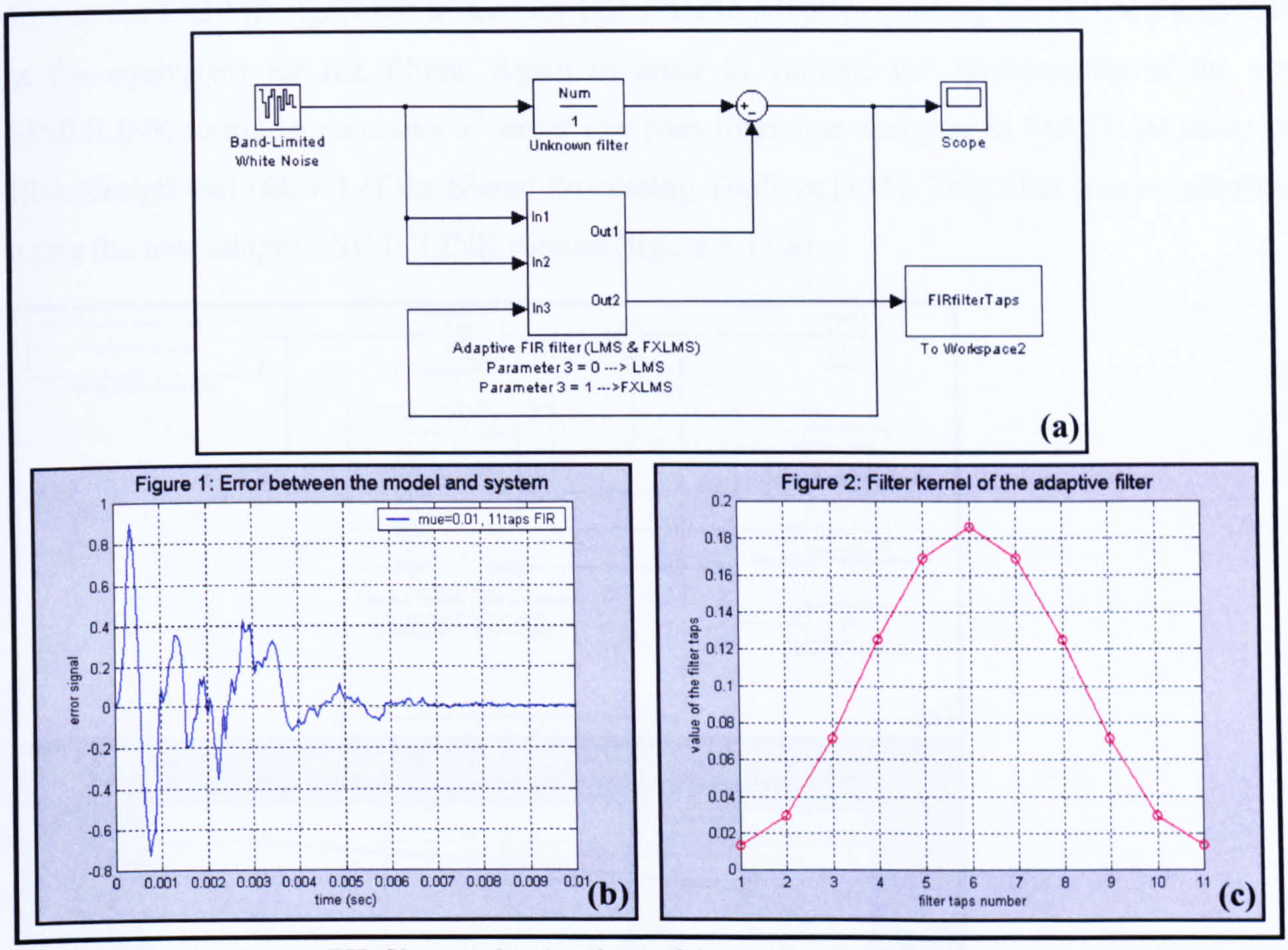

Figure 6.14:The adaptive FIR filter routine (a), the model error (b), the re-identified filter kernel (c)

The re-identification process of the digital FIR filter was successful, since the modelling error reduced to zero (figure 6.14.b) and both filter kernels matched (figure 6.14.c). This SIMULINK routine also tested against more complicated models such as the dynamics of the cantilever beam. It also showed a good match between the unknown system and the identified FIR filter model. However, since the filter has no feedback (non-recursive) it required a long filter kernel (1400 taps) for a good identification on the beam. A recursive adaptive IIR filter would be much more efficient for the requirements for system modelling.

6.5.1.2 Adaptive IIR filter (LMS and FULMS algorithm)

Adaptive recursive filters are more efficient and suitable for the system identification process. But because of the feedback there is always the danger of instability if the adaptive step size is too large (the theory of the adaptive IIR LMS filter of Feintuch was reviewed in chapter 4 – see figure 4.15). The new SIMULINK routine CS_FCT_LMSIIR.dll, has 3 input parameters:

- The IIR filter order
- The sampling time (**-1** for inherited sampling time from the driving block)
- The adaptive algorithm (**0** for the LMS and **1** for the FULMS algorithm)

Just as the FXLMS algorithm is used for FIR filter in adaptive control, the FULMS algorithm is the equivalent for IIR filters. Again in order to validate the functionality of the new SIMULINK routine a recursive 5^{th} order low pass filter was designed in MATLAB using the filter design tool (*fda.m*) of the Signal Processing Toolbox [135]. This filter was re-identified using the new adaptive SIMULINK routine (figure 6.15.a).

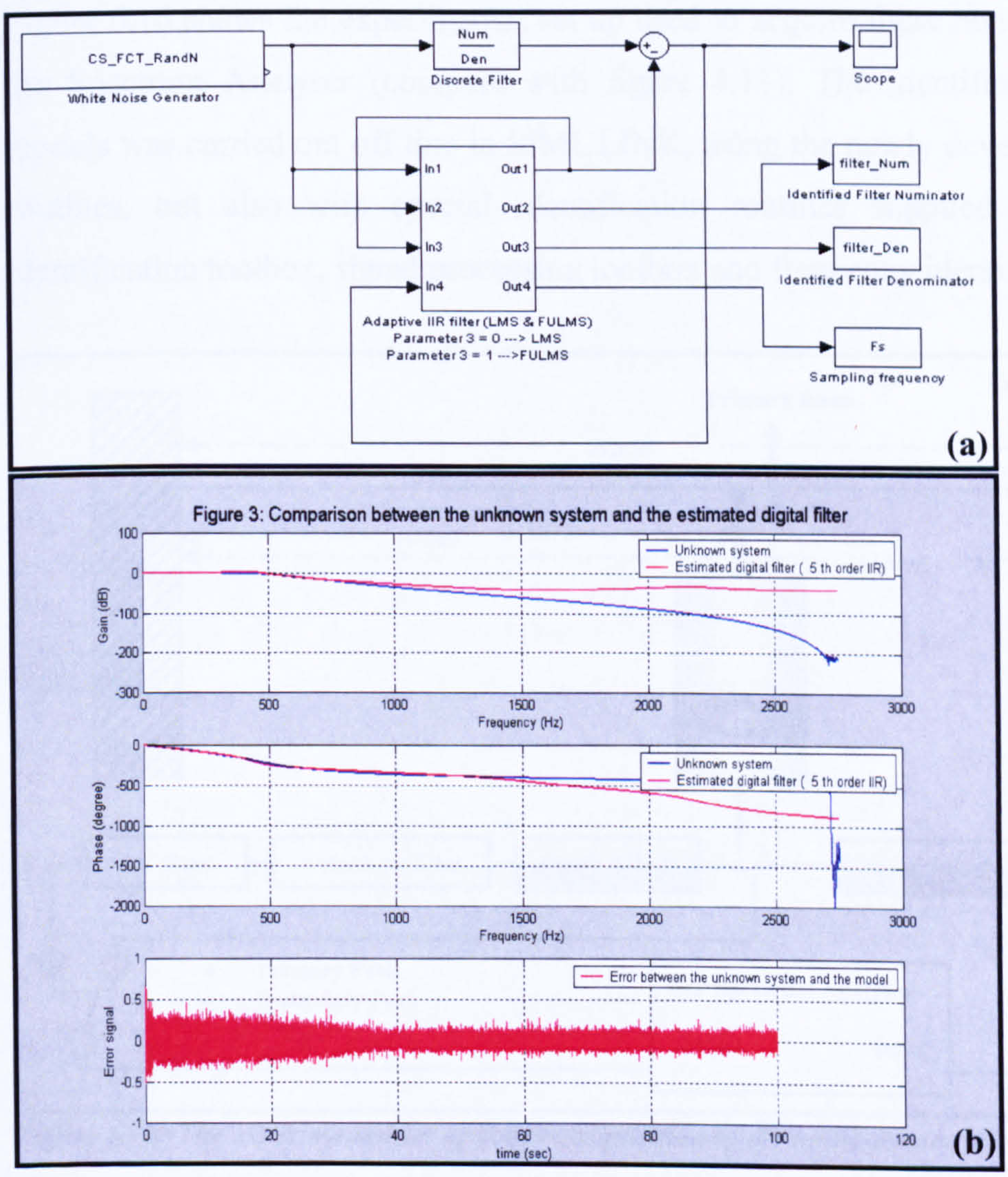

Figure 6.15: The adaptive Feintuch IIR filter routine (a), the re-identified 5^{th}order filter (c)

Unlike the adaptive FIR filter the model error was not reduced down to zero (figure 6.15.b). The reason for that is that the cost function of an adaptive IIR filter has more than just one global minimum, unlike the adaptive FIR filter, which is unimodal. To improve this the IIR filter order could be increased or a different adaptive algorithm (e.g. *Plackett's algorithm*) could be used. Nevertheless the estimated parametric model was a good fit with the non-parametric model and there were no signs of instability encountered even for higher adaptive step sizes. The next section will show how these functions were used for this project.

6.5.2 System identification of the FRF's of the cantilever beam using digital filters

In order to construct the MATLAB/SIMULINK simulation model two relevant transfer functions of the beam test rig needed to be identified:

- Primary or feed-forward path
- Secondary or error path

Figure 6.16 shows the experimental set up used to acquire these non-parametric models with the Spectrum Analyser (compare with figure 4.11). The identification of the parametric models was carried out off line in SIMULINK, using the newly developed adaptive IIR filter routines, but also with special identification routines supplied by MATLAB (system identification toolbox, signal processing toolbox and frequency identification toolbox).

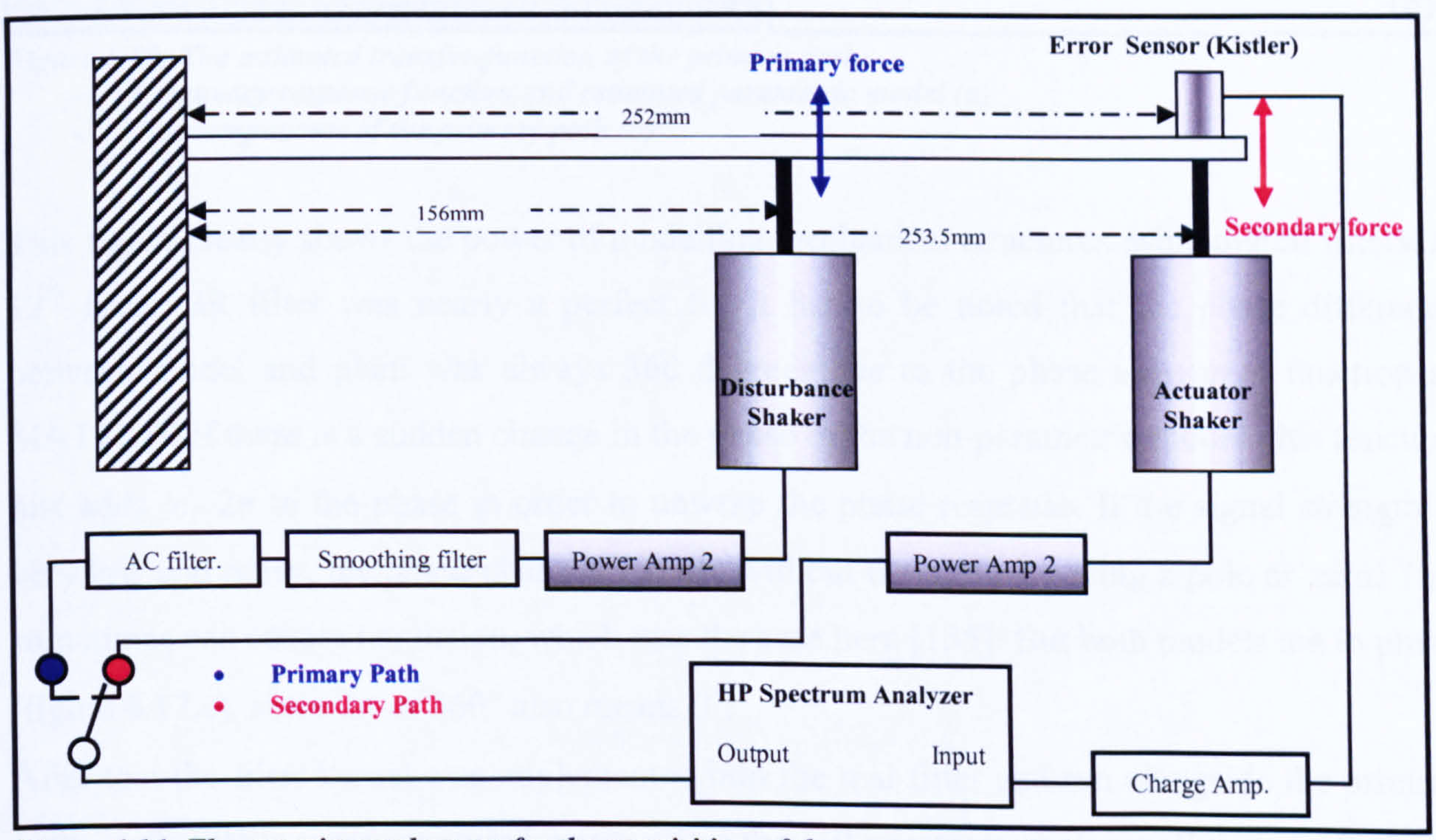

Figure 6.16: The experimental set up for the acquisition of the non-parametric beam models

The only components not shown in the figure are the ADC's and DAC's of the digital controller, which can not be identified externally (chapter 4 – figure 4.16). But since they do not have any dynamic effects, only a constant gain (see appendix C.7 – the calibration of the ADCs) the tests were appropriate. The high pass filter was designed in order to make the BLUE CHIP cards bipolar since the outputs of the DAC's are only positive or uni-polar.

6.5.2.1 System identification of the primary path

The first transfer-function to be identified was the primary path (6.17.b). Figure 6.17.a shows the difference between the measured FRF and the estimated model (12th order IIR). The parameter estimation was done in the time domain, using the MATLAB signal processing toolbox.

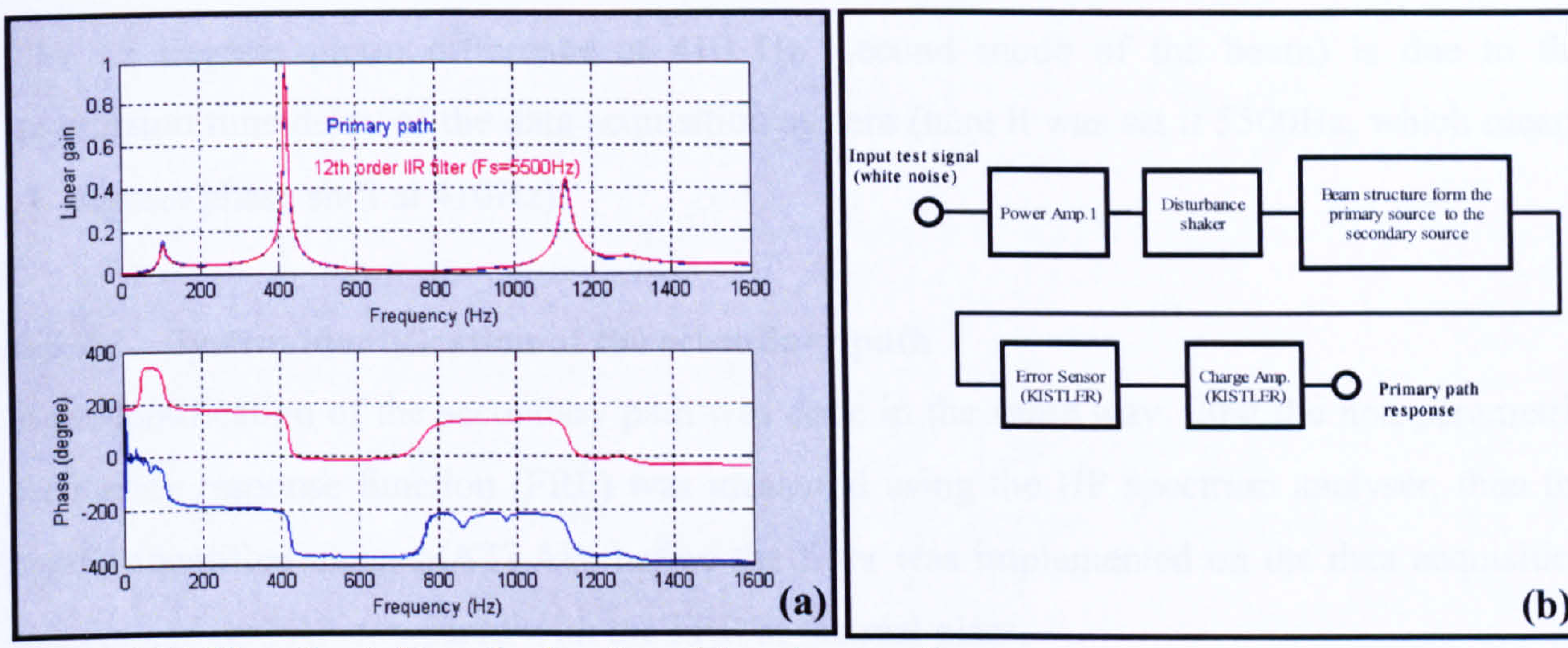

Figure 6.17: The estimated transfer-function of the primary path:
- ***Frequency response function and estimated parametric model (a)***
- ***The components of the primary path (b)***

This figure clearly shows the power of modelling mechanical structures using digital filters. A 12th order IIR filter was nearly a perfect fit. It has to be noted that the phase difference between model and plant was always 360 degrees due to the phase *unwrap.m* function of MATLAB. If there is a sudden change in the phase of the non-parametric model, this function just adds +/- 2π to the phase in order to unwrap the phase response. If the signal strength is very low and noisy, the phase changes rapidly without the system having a pole or zero. This sometimes can causes confusion, which was the case here [135]. But both models are in phase (figure 6.17.a), since 2π or 360° also means 0°.

After that the filter kernel was implemented into the real filter and run alongside the primary path. Both FRF's were measured again using the HP spectrum analyser. Figure 6.18 shows the result of that validation experiment.

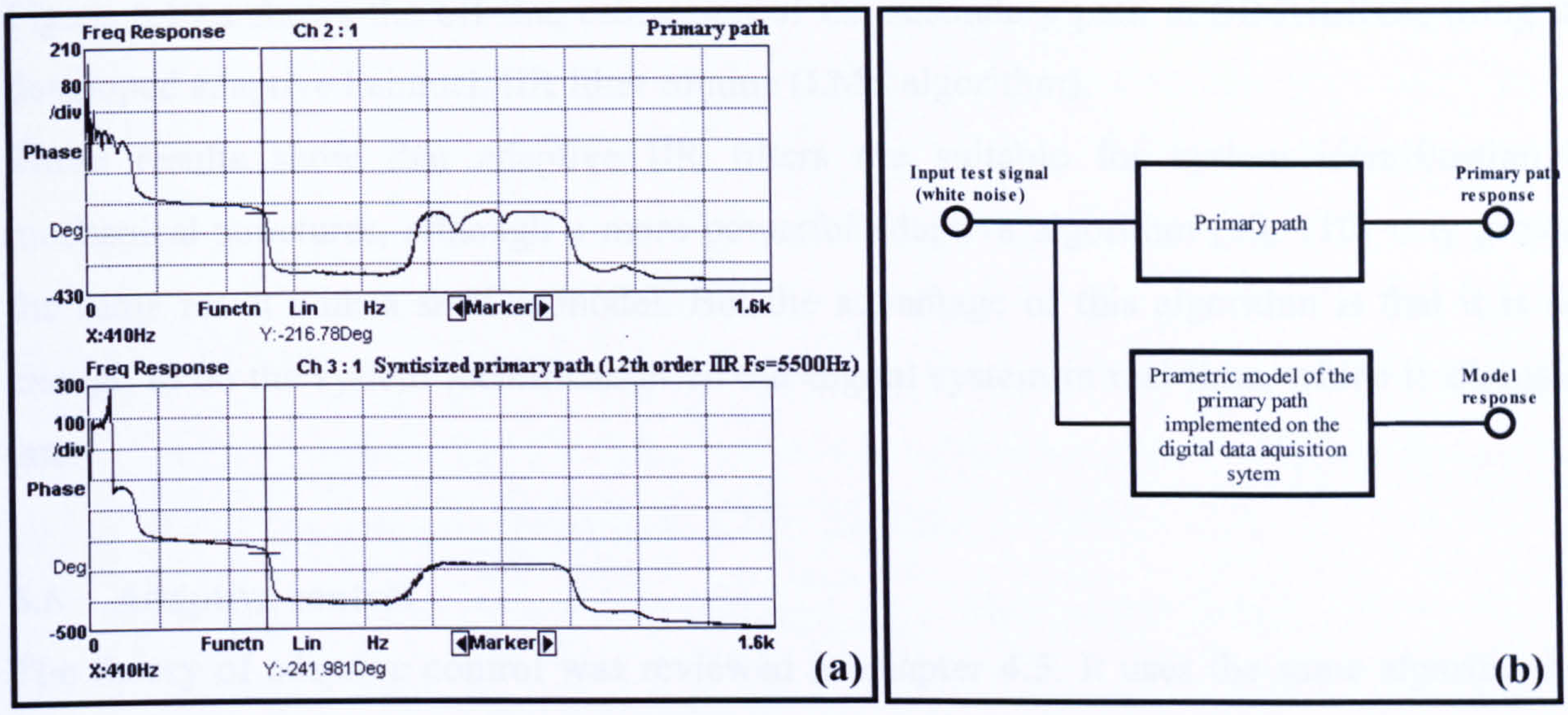

Figure 6.18: FRF's of the primary path and its model, Phase response (a), Experimental set up (b)

The 25 degrees phase difference at 410 Hz (second mode of the beam) is due to the conversion time delay of the data acquisition system (here it was set it 5500Hz, which means 26 degrees phase shift at 410Hz).

6.5.2.2 System identification of the secondary path

The identification of the secondary path was done in the same way. First the non-parametric frequency response function (FRF) was measured using the HP spectrum analyser, then the model identified using MATLAB, before the filter was implemented on the data acquisition system and its FRF compared with the FRF of the real plant.

Figure 6.19.b shows the block diagram of the unknown secondary path.

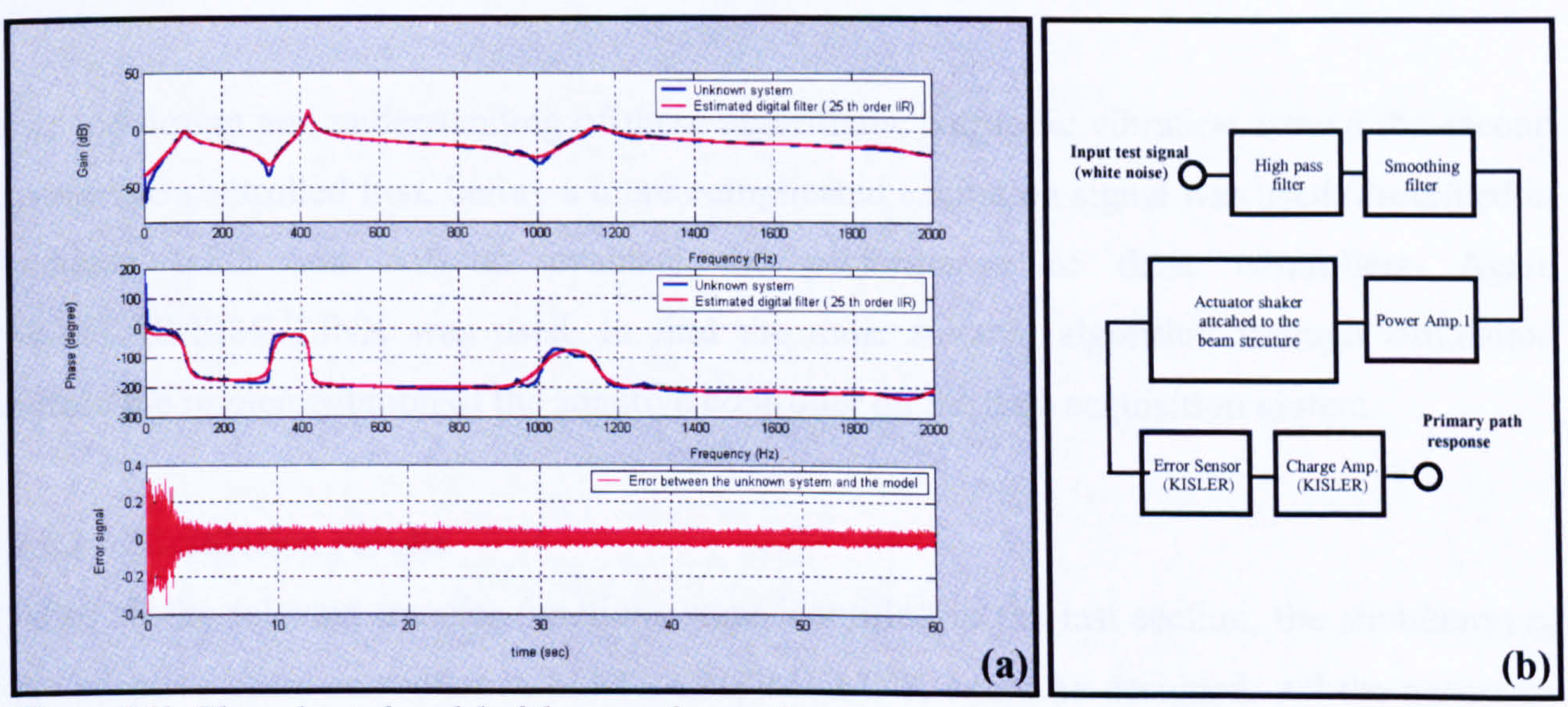

Figure 6.19: The estimated model of the secondary path:
- ***Frequency response function and estimated model (a)***
- ***Block Diagram (b)***

Figure 6.19.a shows the off line estimation of the secondary path in SIMULINK, using the developed adaptive Feintuch IIR filter routine (LMS algorithm).
These results show that adaptive IIR filters are suitable for system identification of mechanical structures, although a more powerful adaptive algorithm [99, 110] may provide the same result with a smaller model. But the advantage of this algorithm is that it is fast enough to do the system identification on our digital system in real time, which is discussed later.

6.6 Adaptive control

The theory of adaptive control was reviewed in chapter 4.5. It uses the same algorithms as adaptive filters for direct system identification. As already mentioned the only difference is the fact that the summing point is in the mechanical domain (the domain where the controller applies correction) rather than in the digital domain (figure 4.11). Therefore the dynamics of all the relevant transfer-functions need to be taken into account.
Four different adaptive control algorithms were tested in order to cancel the forced vibrations on the beam test rig:

- Adaptive FIR feed-forward controller using the LMS algorithm
- Adaptive FIR feed-forward controller using the filtered-x LMS algorithm (FXLMS)
- Adaptive FIR feedback controller using the error signal as reference signal (FXLMS algorithm) and classical feedback structure
- Adaptive FIR feedback controller using IMC (Internal Model Control) as feedback structure to derive the reference signal (FXLMS algorithm)

For the design and understanding of these algorithms, harmonic vibration around the second mode was controlled first, before a more complicated excitation signal was used (described in sections 6.8.2 and 6.9) to evaluate the performance of these controllers. Again MATLAB/SIMULINK was used, to find the most suitable algorithm through simulation before the implementation of the adaptive controller on the data acquisition system.

6.6.1 Simulation results

After all the relevant transfer-functions were identified in the last section, the simulation of the adaptive beam controller in MATLAB/SIMULINK could be designed. All the necessary SIMULINK blocks have already been written and only the adaptive FIR filter routine was updated to the adaptive FIR controller routine, with an optional leakage factor (leaky FXLMS algorithm – equation 4.16). All the newly developed S-function blocks were added to the standard SIMULINK library.

6.6.1.1 Initial simulation and experimental validation

The first controller to be tested was the adaptive feed-forward FIR controller filter using the LMS algorithm (figure 6.20). The beam excitation through the primary source was at 415Hz and 425Hz, just before and after the 2nd modal frequency (420Hz).

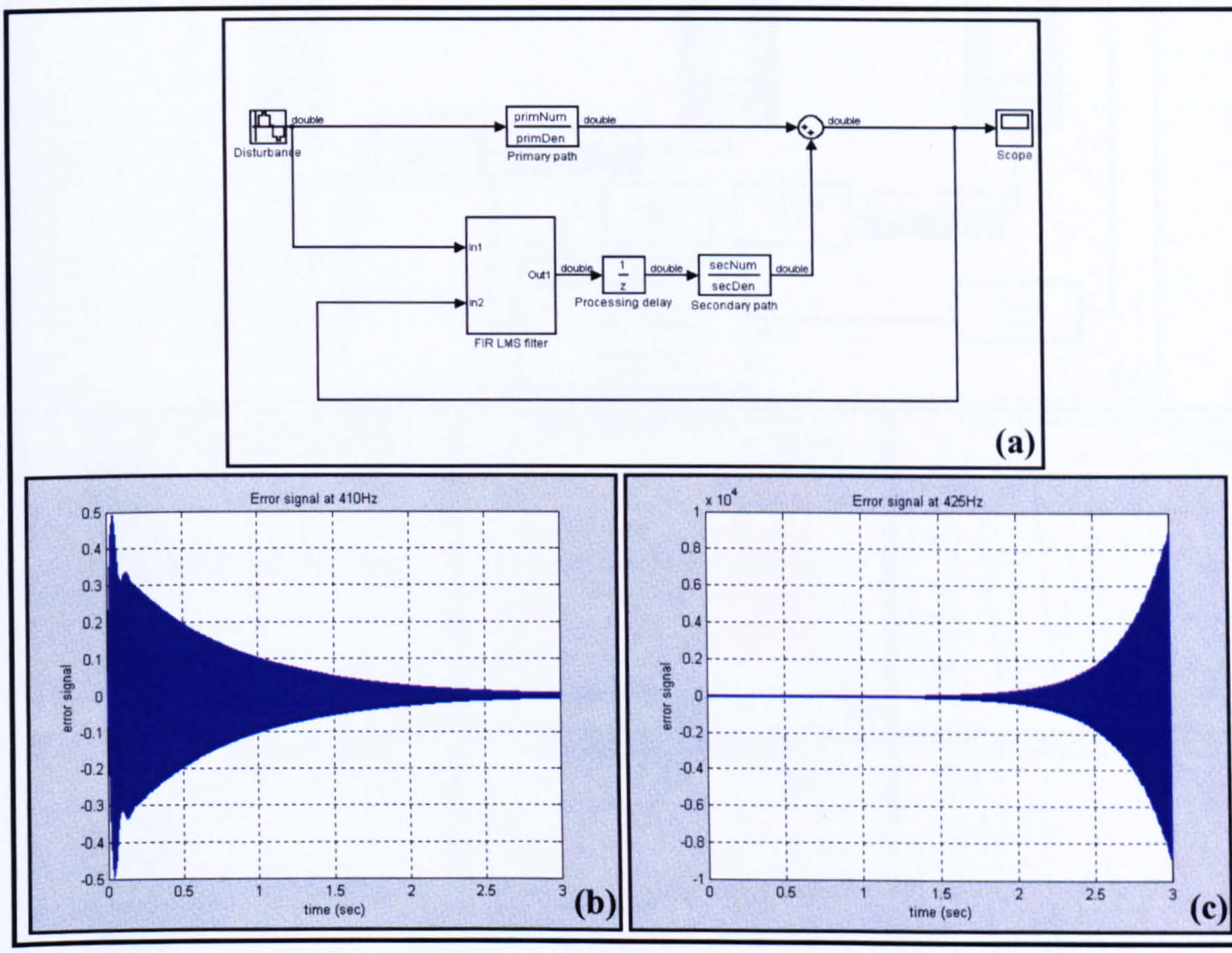

Figure 6.20: Simulation of the adaptive FIR feed-forward controller using the LMS algorithm:
- ***SIMULINK simulation (a)***
- ***Harmonic excitation at 410Hz (b)***
- ***Harmonic excitation at 425Hz (c)***

This shows that the controller was able to cancel the vibration, but it also shows that it does go unstable at the at the second mode (420Hz). More tests were done and revealed that the controller was stable between 340Hz and 418Hz.

An experimental validation of the simulation on the real beam test rig was carried out first, before the more complicated algorithms were simulated. Figure 6.21 shows the experimental arrangement. The frequency range around the second mode (420Hz) was tested.

According to the simulation the controller should be stable between 340 and 418Hz. Figure 6.21 shows 2 different cases:

- 400Hz excitation (figure 6.21.b-d)
- 340Hz and superimposed 400Hz excitation (figure 6.21.e-g)

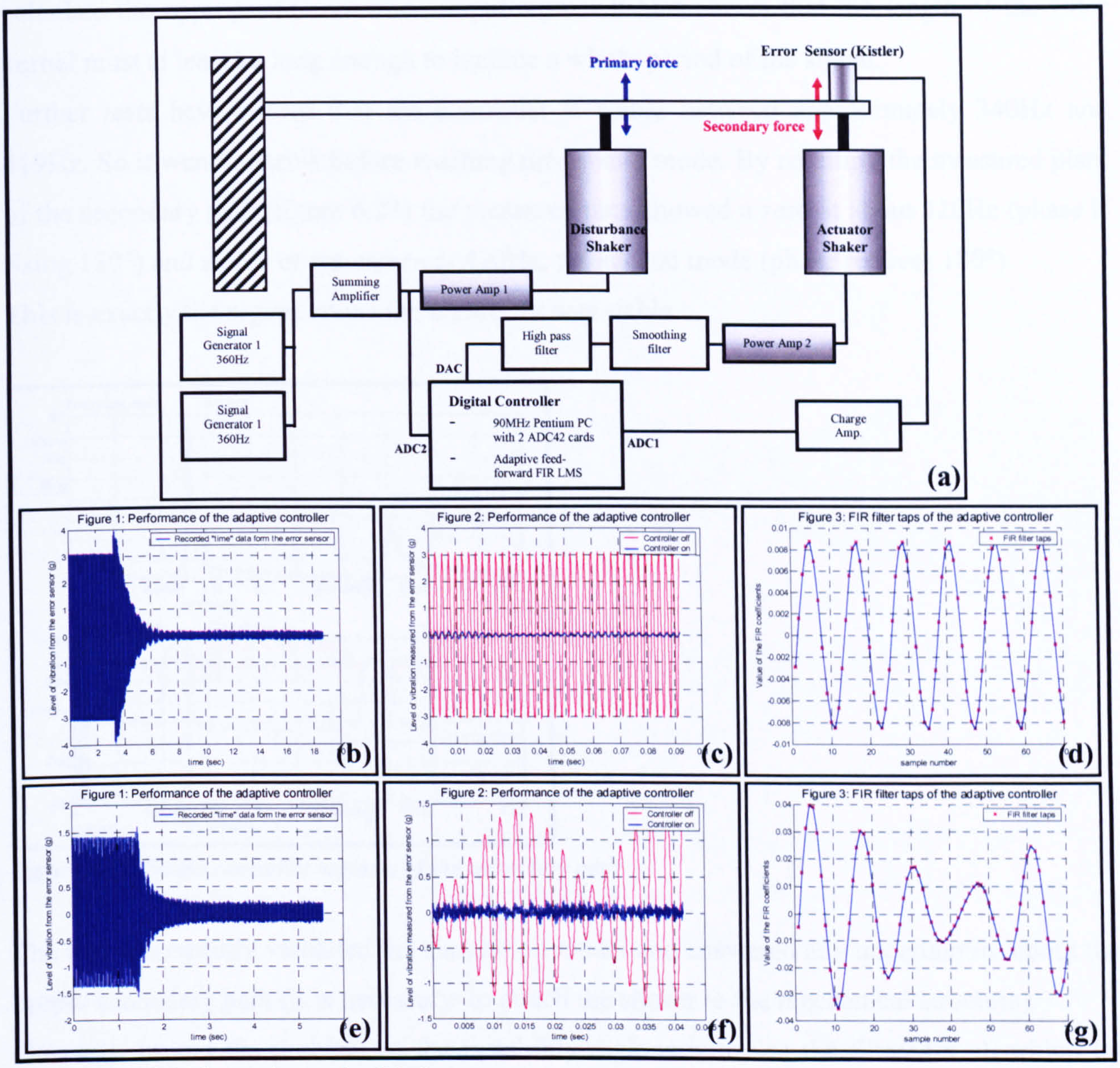

Figure 6.21: Initial experimental validation:

- ***Experimental set- up (a)***
- ***400Hz error vibration***
- ***400Hz error vibration before and after control (b)***
- ***400Hz FIR filter kernel (c)***
- ***360Hz + 400Hz error vibration (d)***
- ***360Hz + 400Hz error vibration before and after control (e)***
- ***360Hz + 400Hz FIR filter kernel (f)***

For both cases the C controller program (adaptive FIR-LMS) was updated with an option to save the filter kernel onto floppy disk after the adaptation process. A simple summing amplifier was designed to superimpose the 340Hz signal onto the 400Hz signal.

The results validate the simulation model. The filter kernels for both cases (figure 6.21.d and 6.21.g) show how the controller input signal is weighted by the FIR filter taps in order to calculate the appropriate controller output signal. It also shows that the length of the filter kernel must at least be long enough to include a whole period of the signal.

Further tests have shown that the controller is stable between approximately 340Hz and 419Hz. So it went unstable before reaching the second mode. By recalling the measured plant of the secondary path (figure 6.22) the measured data showed a zero at about 320Hz (phase is rising 180°) and a pole or resonance at 420Hz, the second mode (phase reduces 180°). This is exactly the region where the controller was stable.

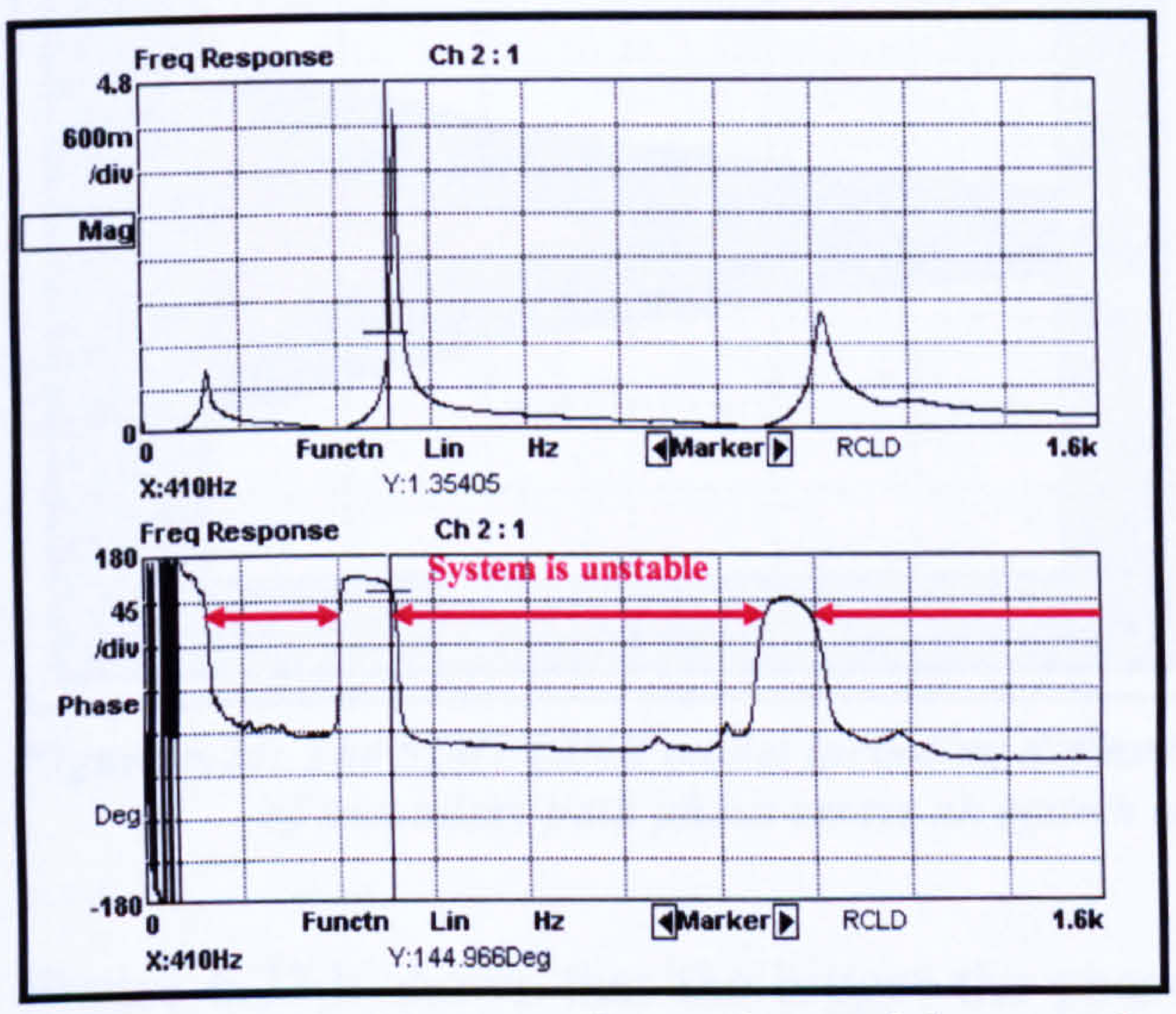

Figure 6.22: Stable controller regions, of the secondary path

The test successfully validated the simulation model and answered any uncertainties about the proper secondary path (it is necessary to attach the shaker to the mechanical structure).

One way around the problem of the instability regions is to use the filtered-x algorithm by Morgan [54], covered in chapter 4, where a model of the filter is used to filter the reference signal (called filtered-x, because the reference, x, signal is filtered).

The next experiment was done in order to understand the problem, that caused the instability and also the statement made by Morgan [54,111] that the adaptive controller would find the optimal filter coefficients for phase shifts up to 90° degrees caused by the secondary path. Figure 6.23.a shows the SIMULINK model of the adaptive FIR controller using the simple

LMS algorithm. The phase shift was introduced by additional time delays (a time delay is always present due to the fact that the controller is digital).

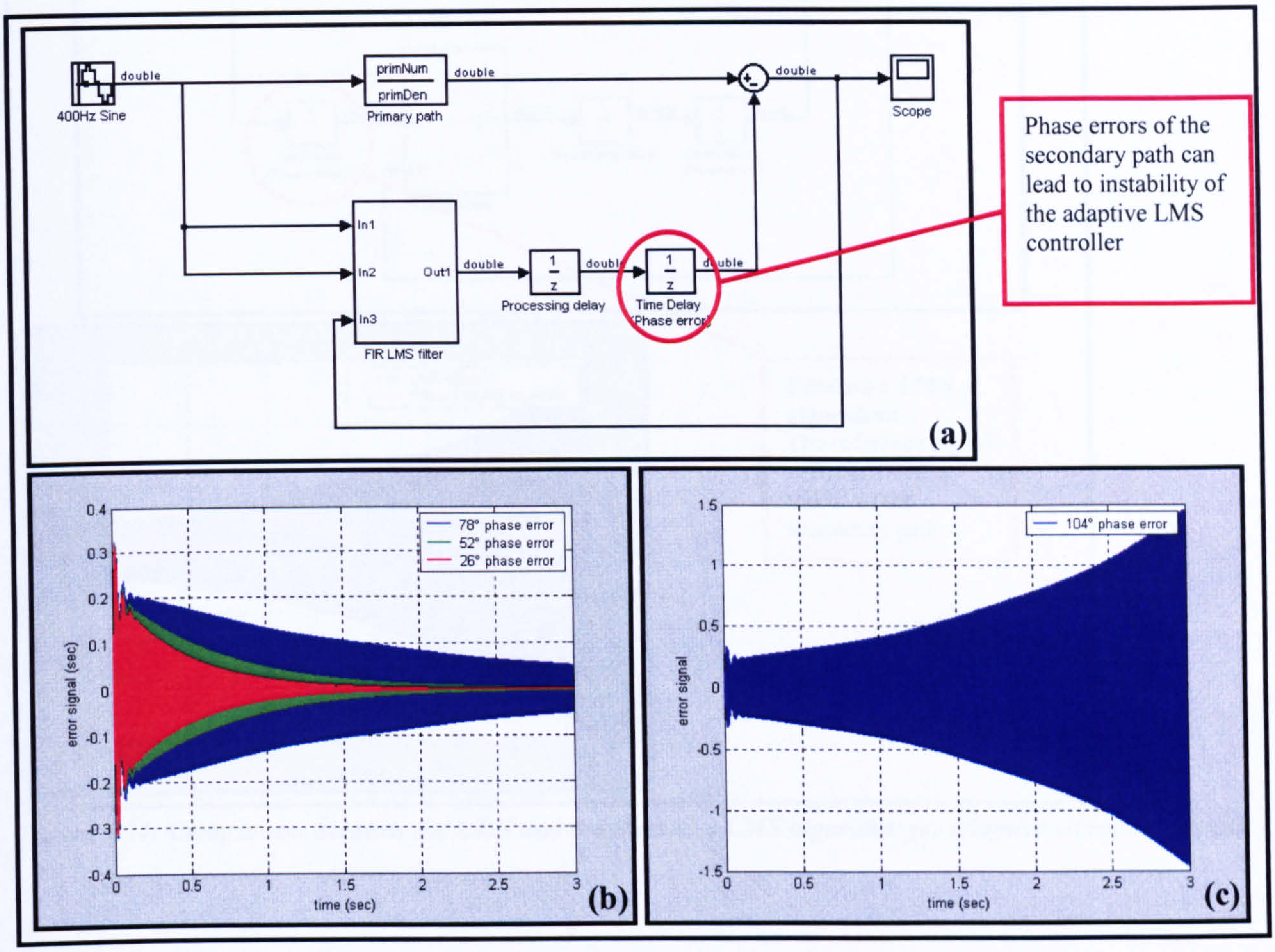

Figure 6.23: The SIMULINK model including defined phase errors for the secondary path (a) and the effects of secondary path phase errors on system stability (b,c)

Figure 6.23.b shows that the bigger the phase lag, of the secondary path the more time the controller needs to adapt. Further tests also have shown that at about 89° the controller goes unstable (figure 6.23.c). This confirms the statement made by Morgan.

The next simulation used the filtered-x controller in order control the previously unstable case, where the secondary path has a phase error of 104° (figure 6.24). This simulation shows that the controller with the filtered-x LMS algorithm compensates for the dynamics of the secondary path. The adaptation time is now the same as in the case where the phase error of the secondary path was only 26°, which is the processing delay of the digital controller.

The fact that the simulation model now matches the real controller on the beam structure and the knowledge that the filtered-x LMS algorithm allows the control of any system adaptively, the simulation of the possible adaptive algorithms on the beam structure was continued.

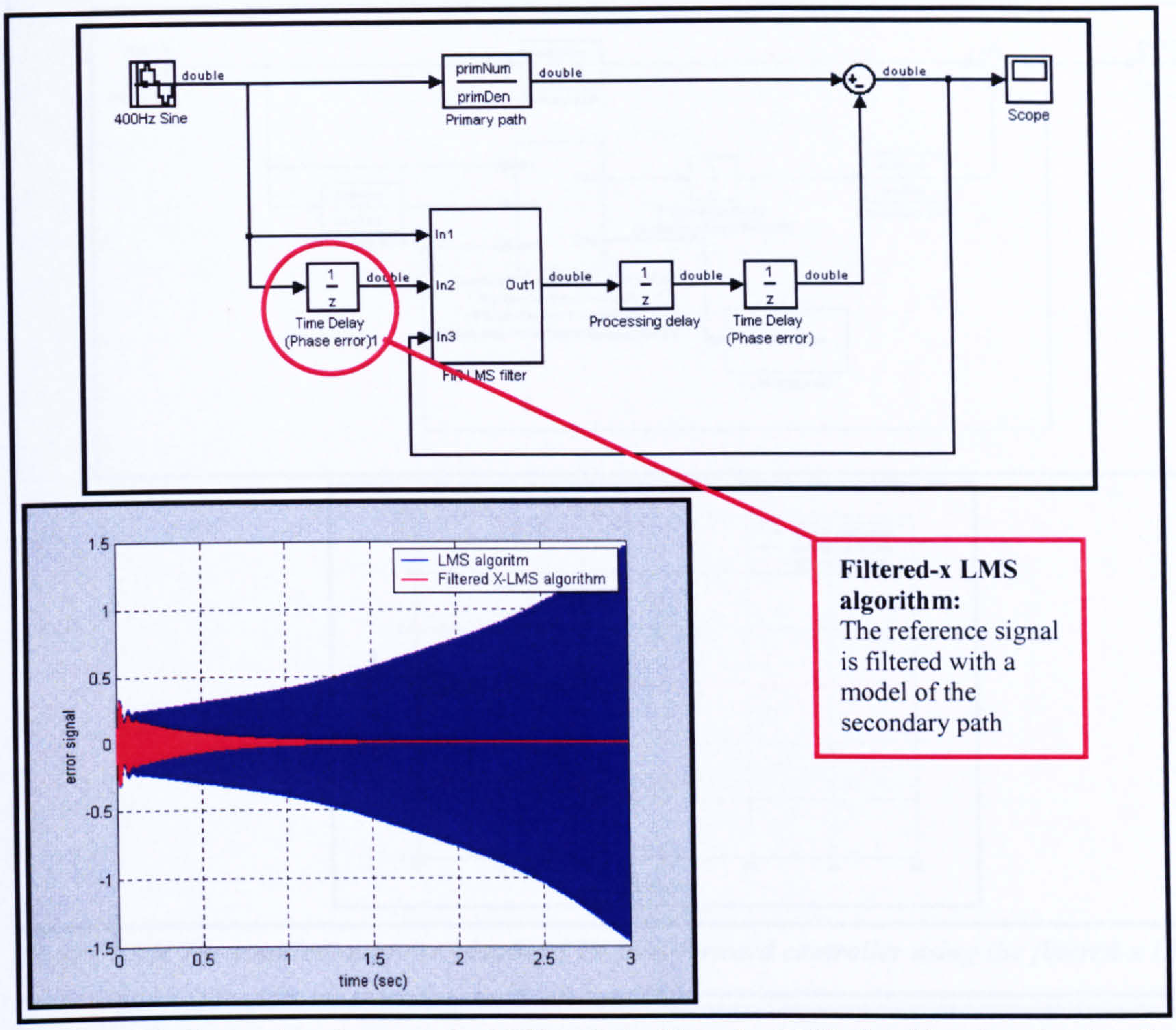

Figure 6.24: Comparison between the LMS and the filtered-x LMS algorithm for adaptive vibration control

6.6.1.2 Simulation of suitable adaptive control algorithms

Since the simple LMS is not suitable for active control, the remaining three adaptive control algorithms tested all use the FXLMS algorithm in order to cancel the forced vibrations on the beam test rig (see 6.6).

The excitation is around the second mode of the beam structure (400Hz – 435Hz). This gives a good indication about the controller performances (figures 6.25 - 6.27). It also should be noted that more sophisticated controllers, were not tested since they exceed the available processing power of our digital signal processing platform.

The simulation showed that the filtered-x LMS algorithm works over the whole frequency range. Since the reference signal will not be available on machine tool structures a feedback structure needs to be chosen. As already mentioned in chapter 4.5 the problem with classical feedback structures is that if the feedback signal becomes so low that it reaches the noise level of the sensor, the system becomes unstable. This problem can be seen on figure 6.26.a, where the error signal is also used as reference signal.

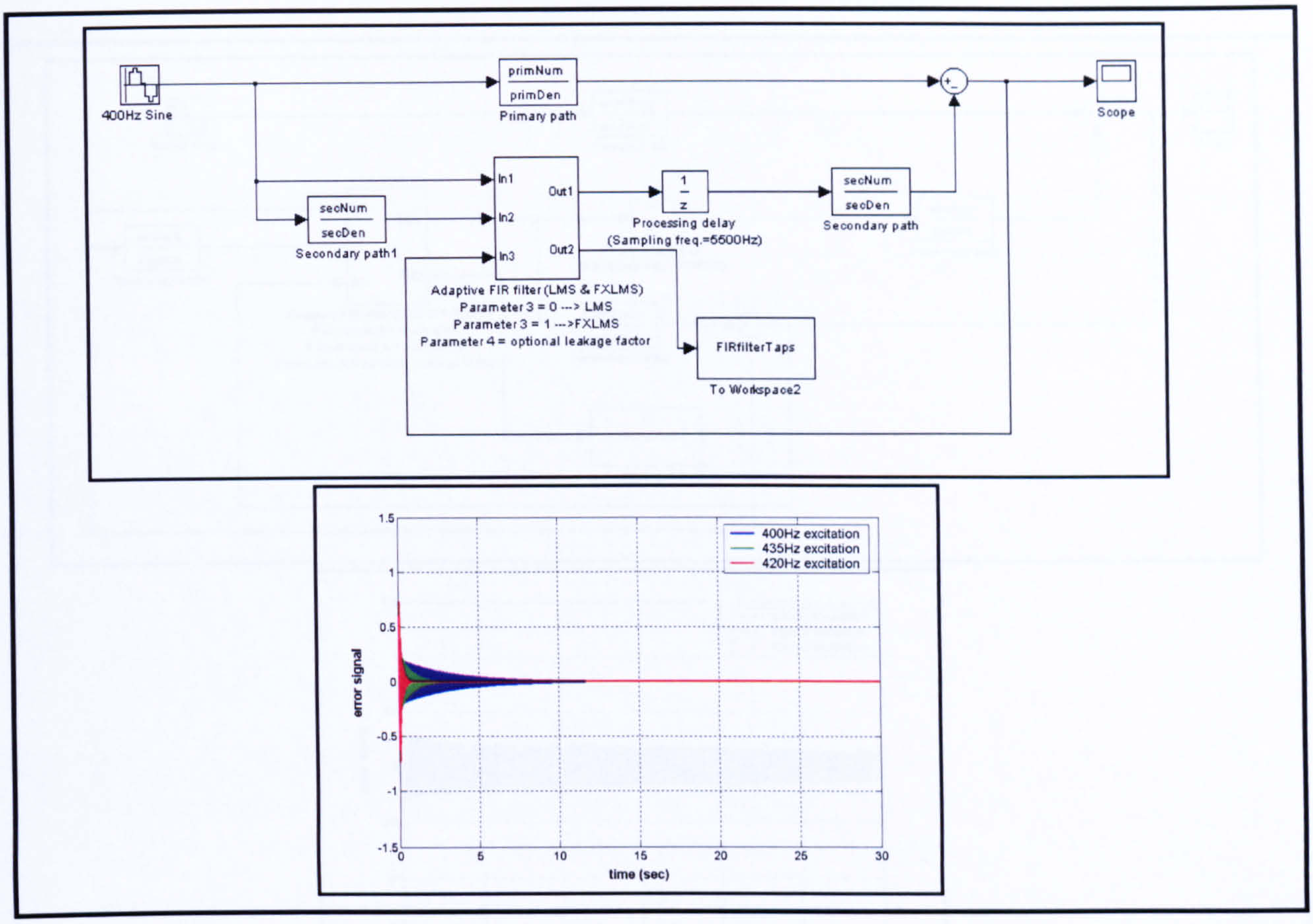

Figure 6.25: The simulation of the adaptive FIR feed-forward controller using the filtered-x LMS algorithm

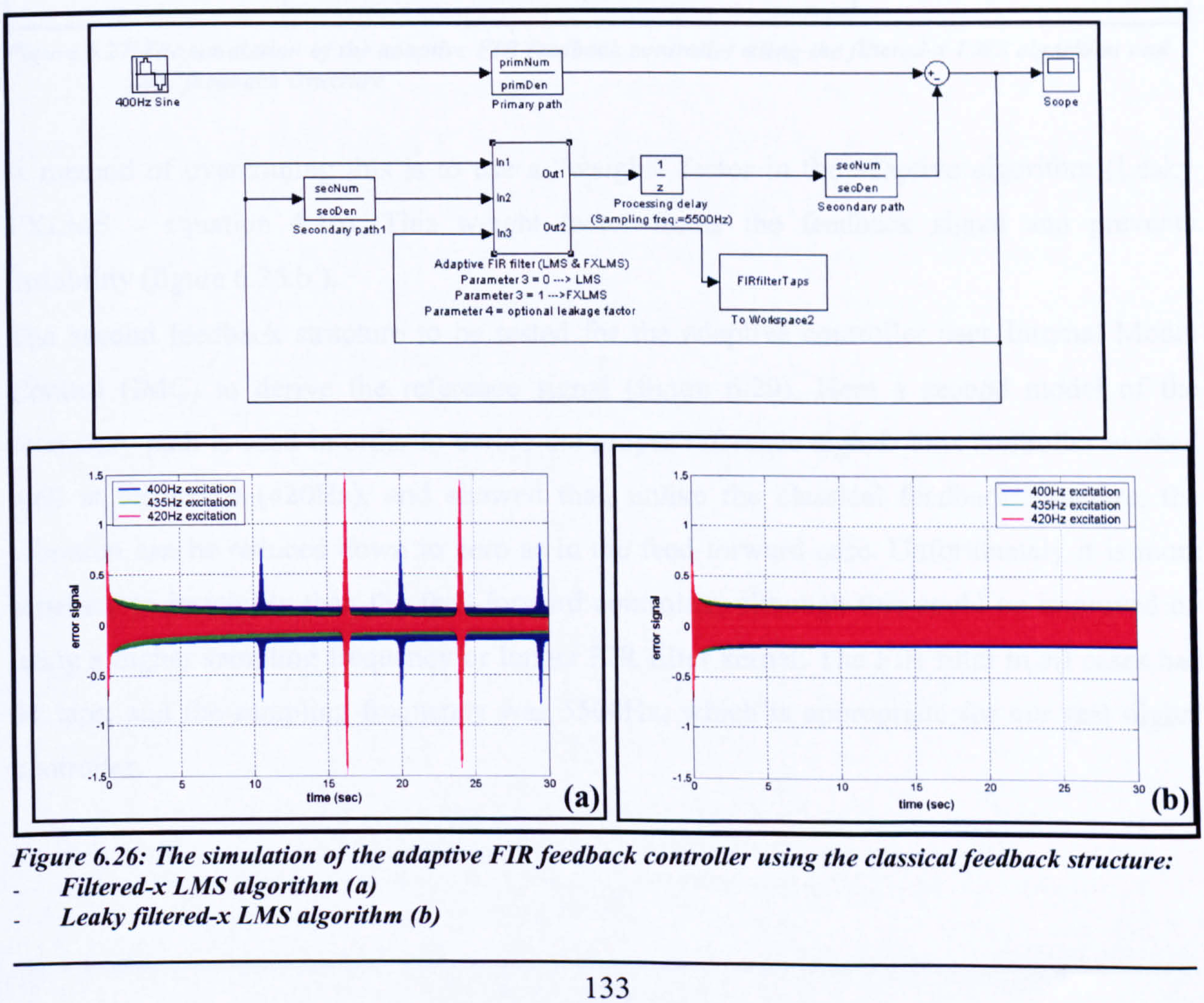

Figure 6.26: The simulation of the adaptive FIR feedback controller using the classical feedback structure:
- *Filtered-x LMS algorithm (a)*
- *Leaky filtered-x LMS algorithm (b)*

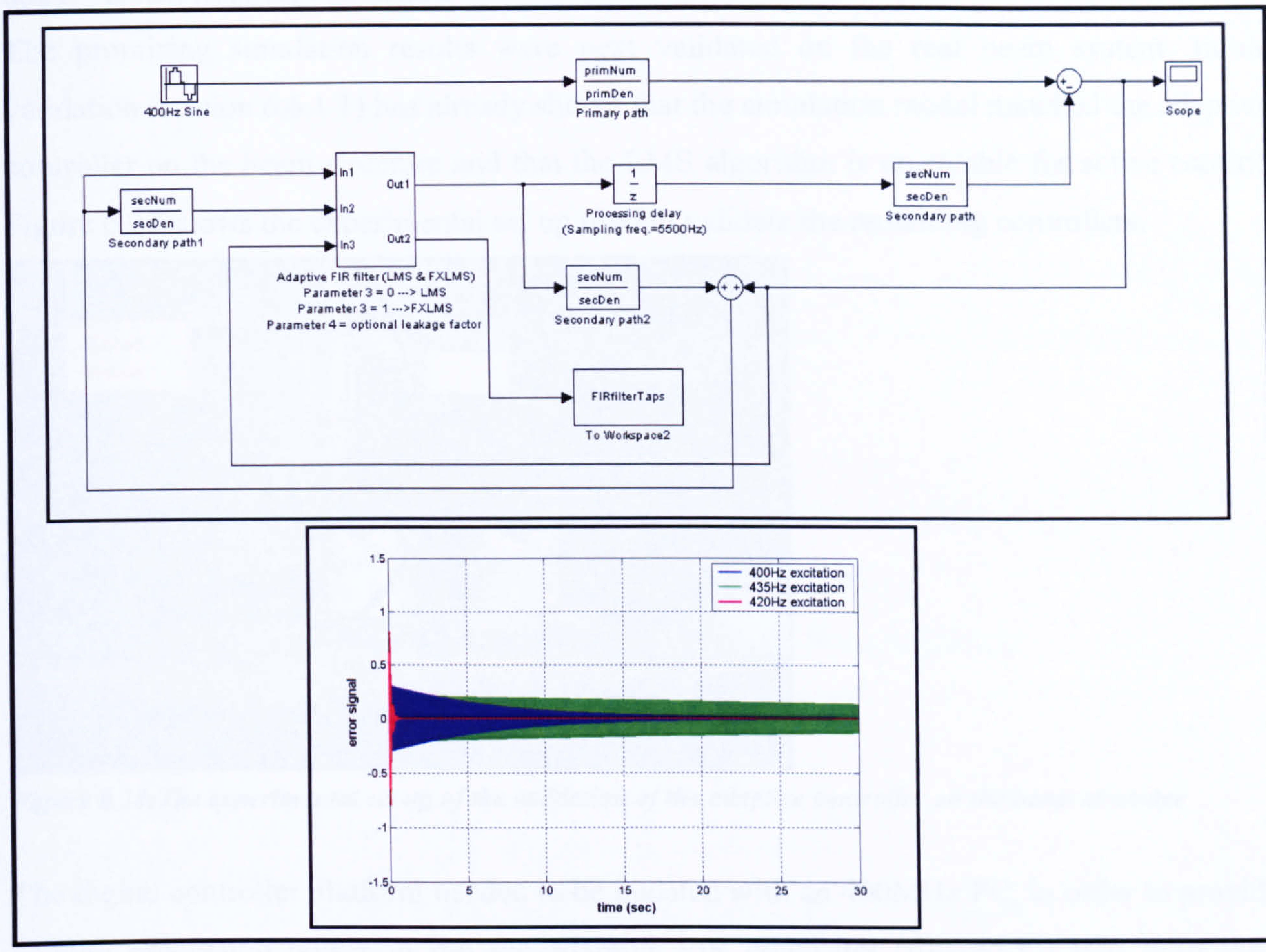

Figure 6.27:The simulation of the adaptive FIR feedback controller using the filtered-x LMS algorithm and IMC feedback structure

A method of overcoming this is to use a "weight" factor in the adaptive algorithm (Leaky FXLMS – equation 4.16). This weight factor limits the feedback signal and prevents instability (figure 6.26.b.).

The second feedback structure to be tested for the adaptive controller uses Internal Model Control (IMC) to derive the reference signal (figure 6.29). Here a second model of the secondary path is used in order to derive the proper reference signal. This controller worked well at resonance (420Hz), and showed that, unlike the classical feedback structure, the vibration can be reduced down to zero as in the feed-forward case. Unfortunately it is more sensitive to instability than the feed-forward controller, although this could be improved by using a higher sampling frequency or longer FIR filter kernel. The FIR filter in all cases had 31 taps, and the sampling frequency was 5500Hz, which is appropriate for our real digital controller.

6.6.2 Experimental validation

The promising simulation results were next validated on the real beam system. Initial validation (section 6.6.1.1) has already shown that the simulation model matched the adaptive controller on the beam structure and that the LMS algorithm is unsuitable for active control. Figure 6.28 shows the experimental set up used to validate the remaining controllers.

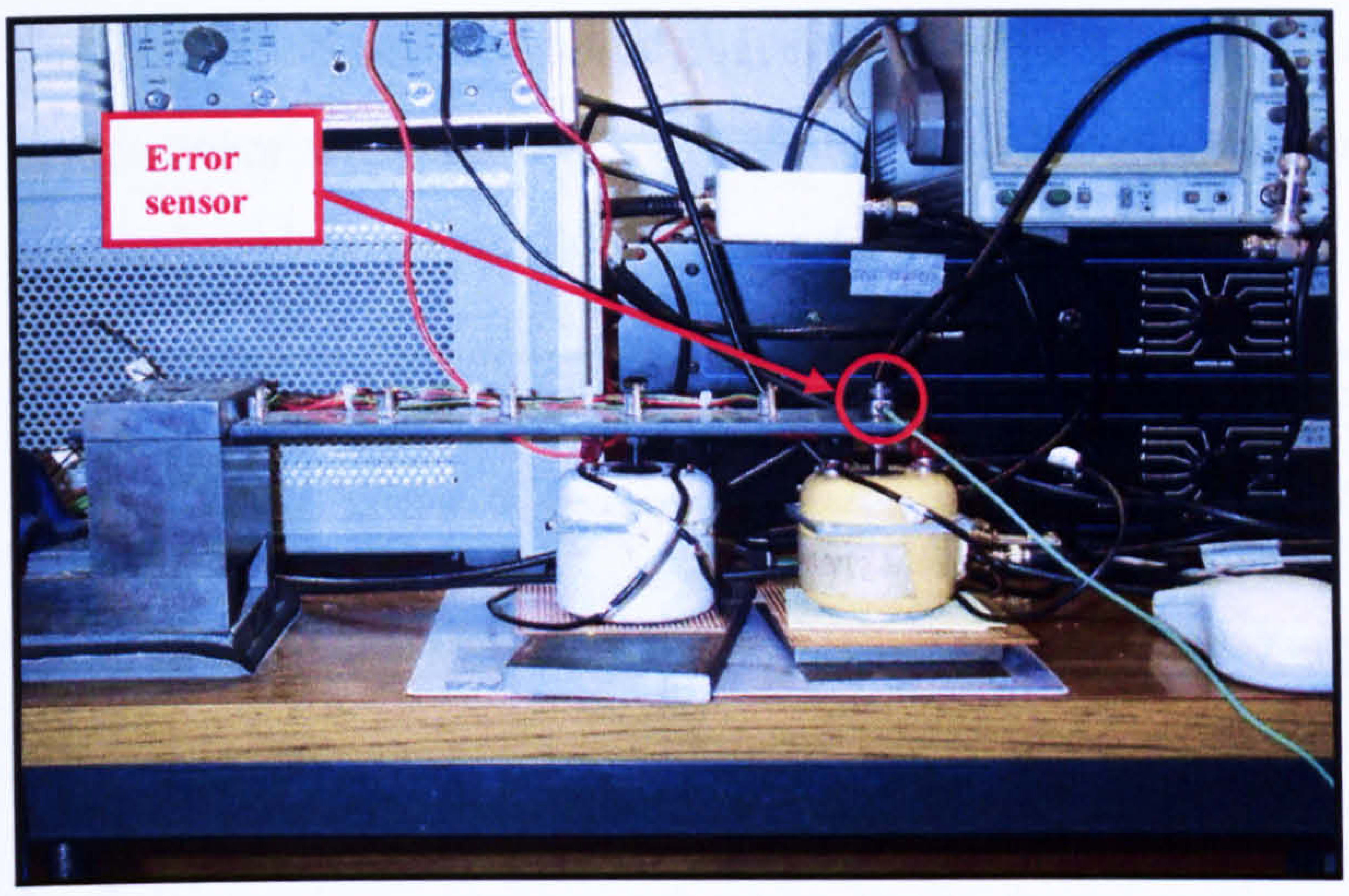

Figure 6.28:The experimental set up of the validation of the adaptive controller on the beam structure

The digital controller platform needed to be updated with an 400MHz PC, in order to provide enough processing power to run the adaptive FIR controller (filtered-x LMS) with IMC feedback structure at a sufficient sampling frequency. The adaptive FIR LMS controller routines written in BORLAND C were updated for the filtered-x LMS algorithm, feed-forward and feedback (classical and IMC feedback structure), and the secondary path model, which needed to be identified off-line, was loaded into the algorithm via floppy disk.

Figure 6.29 shows the error vibration of the adaptive feedback controller (leaky FXLMS) with the classical feedback structure.

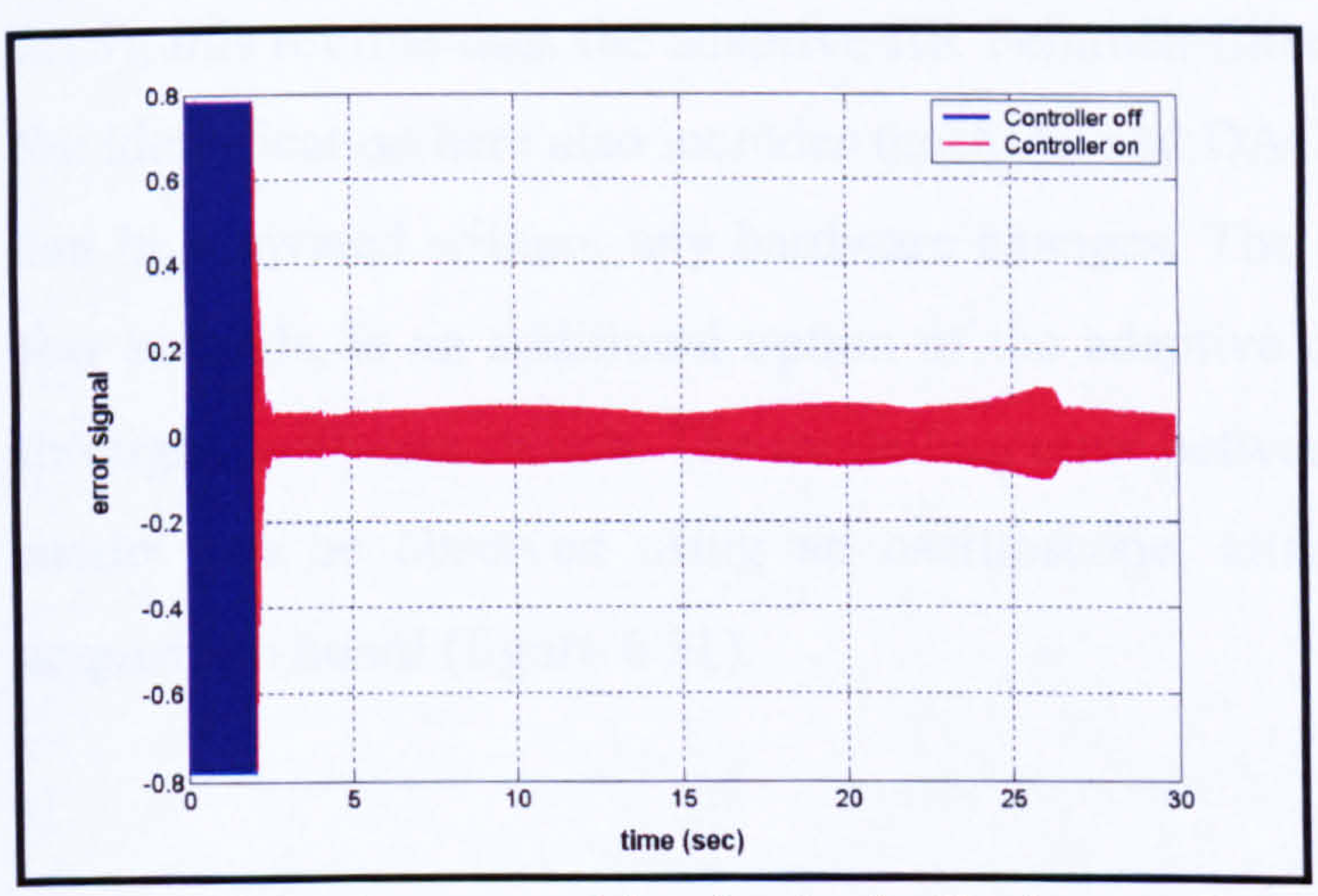

Figure 6.29:Performance of the adaptive feedback controller (classical feedback structure) with the excitation signal changed from 200Hz to 500Hz

The excitation frequency was changed between 200Hz and 500Hz, while the controller was active in order to show any instability.

No instability was observed. The controller performed well and tuned quickly around the high vibration levels at resonance, but slower at lower levels of vibration. This does not matter since only the resonance causes vibration problems.

Further experiments showed that not only the *local vibration response* at the location of the error sensor was reduced by 97%, but also the *global vibration response* along the structure was reduced to at least 80% (figure 6.30).

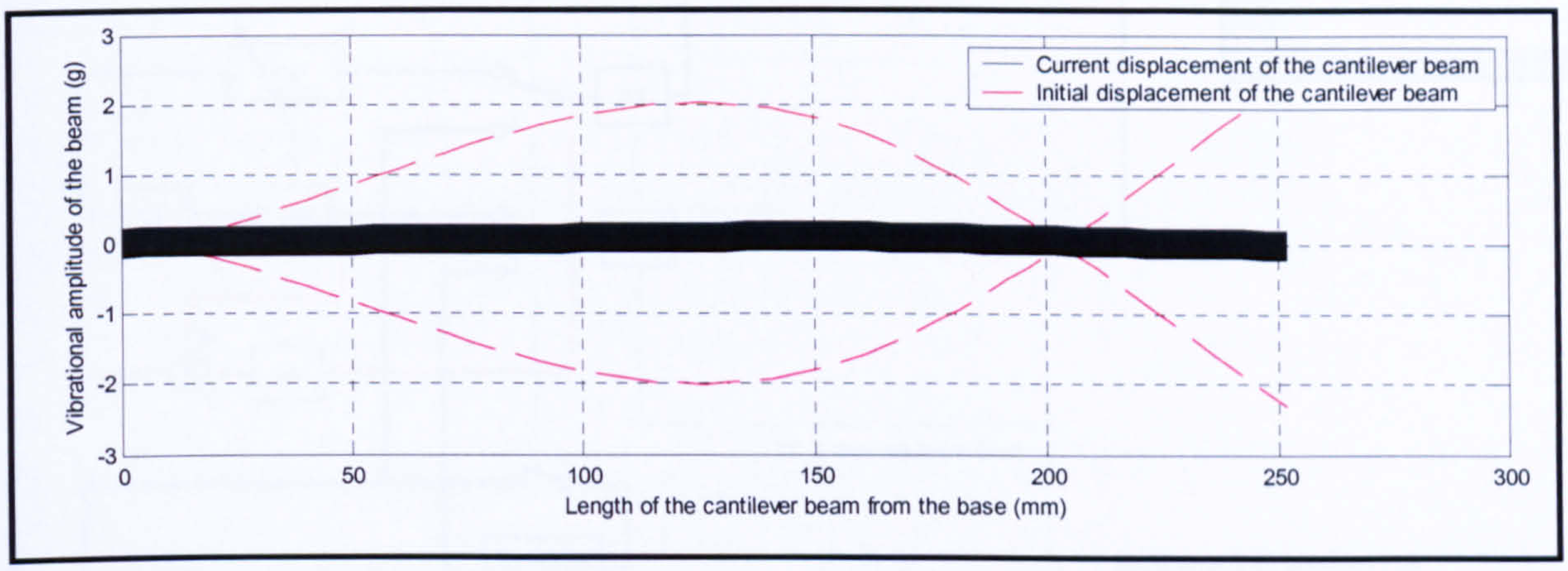

Figure 6.30: The global vibration response of the structure before and after compensation

The last algorithm to be tested and validated was the adaptive controller using Internal Model Control (IMC) as the feedback structure. In order to automate the identification of the secondary path, the controller program was updated with an on-line identification and calibration routine (figure 6.31).

Just as the off line identification routine written in C using MATLAB-S-functions (figure 6.15), this routine uses the adaptive IIR Feintuch filter. In comparison to the off-line routine, the identification here also includes the ADC and DAC converters of the digital controller and can be activated without any hardware changes. The calibration routine, which only takes a few seconds, is an additional option of the adaptive controller, and can be activated simply through a software switch. The modelling error between the secondary path and the identified model can be observed using an oscilloscope, attached to the second DAC of the data acquisition board (figure 6.31).

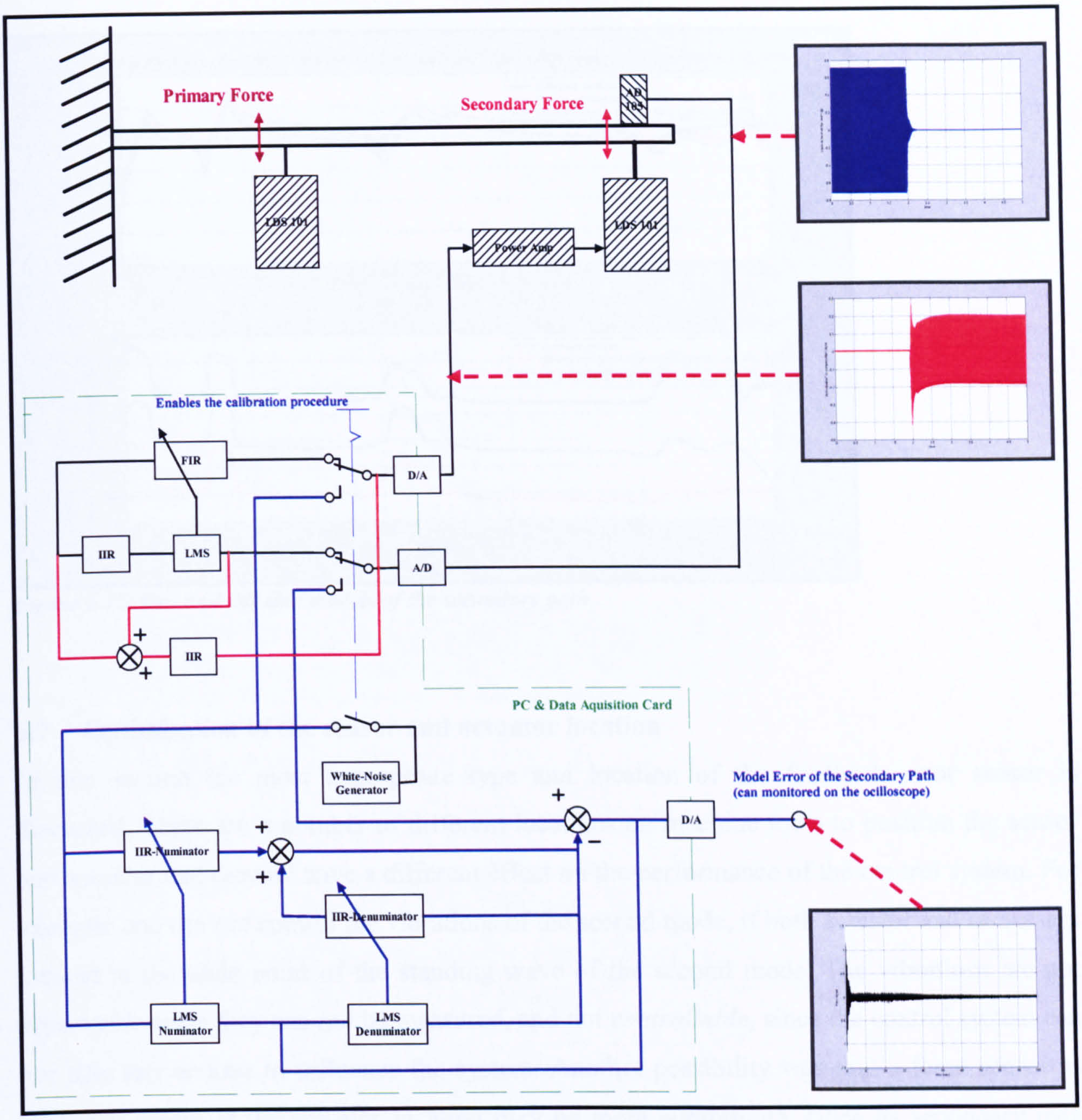

Figure 6.31: The adaptive feedback controller the beam structure:

- ***Adaptive filtered-x LMS FIR controller***
- ***IMC feedback structure***
- ***On-line identification routine using the adaptive Feintuch IIR filter***

Figure 6.32 shows the comparison of the secondary path, between the off-line and on-line identification methods.

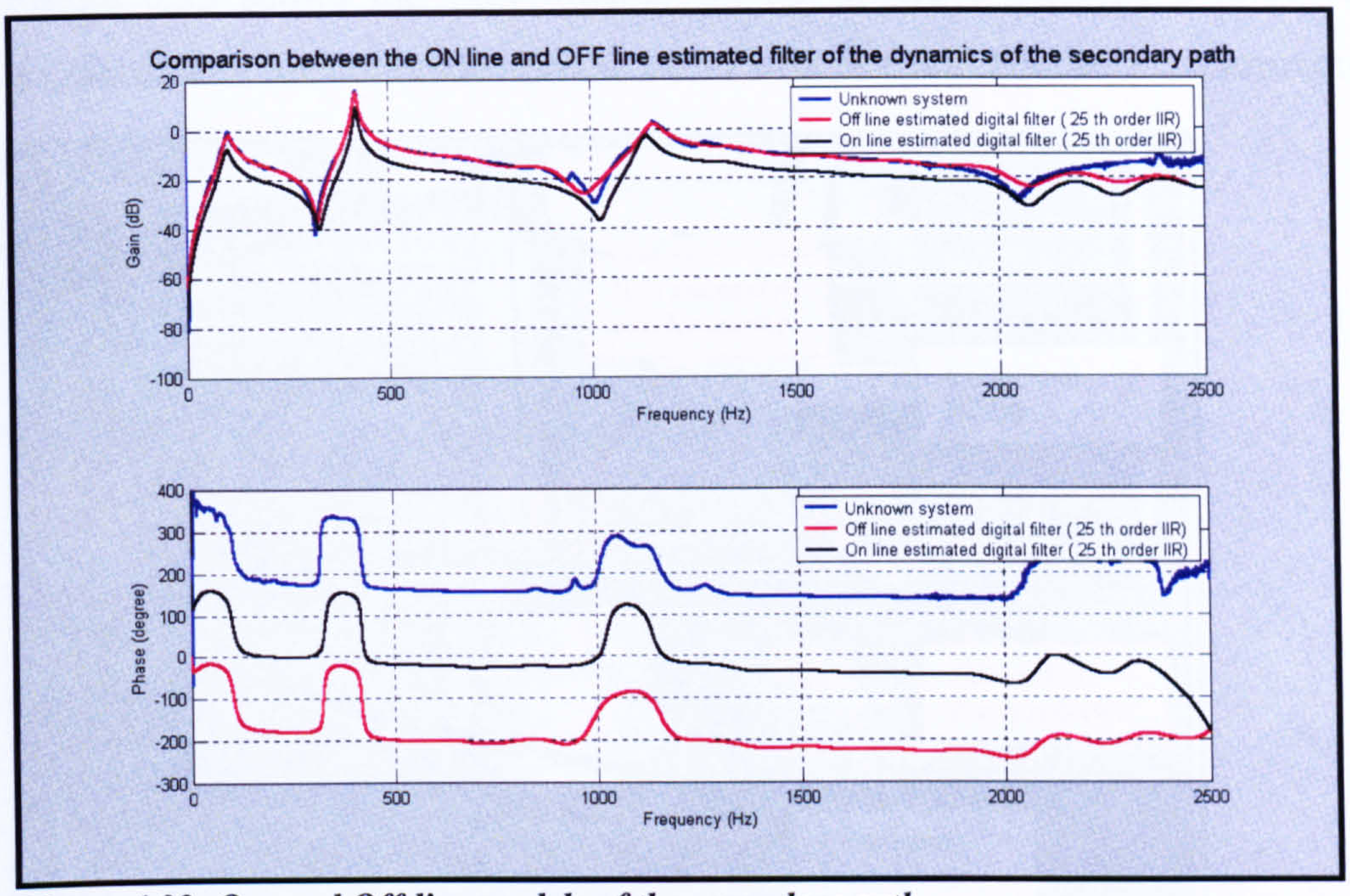

Figure 6.32: On- and Off-line models of the secondary path

6.7 Optimisation of the sensor and actuator location

In this section the most appropriate type and location of the feedback error sensor is discussed. There are a number of different locations on machine tools to position the sensor and actuator and they all have a different effect on the performance of the control system. For example one can not control the vibrations of the second mode, if both actuator and sensor are located at the node point of the standing wave of the second mode. The vibrations are not *observable* since they can not be measured, and not *controllable*, since the control system can not take any actions to influence the system. Another possibility was that a force sensor as feedback sensor at the actuator location may be more appropriate, since its secondary path would not have as much dynamic effect as a vibration sensor (e.g. accelerometer). This would make the control system more robust, since any changes in the secondary path due to structural changes of the system under control, would not necessary lead to a re-identification of the secondary path. It should also be noted that the secondary path response is in fact the open loop response of a traditional feedback control system.

If the sensors are located at the same location as the actuator, the system is called a *collocated* sensor/actuator pair if not it is *non-collocated* [70]. Force feedback, where a load cell was attached on top of a piezo-actuator (collocated), has recently been used by Karkosch et al [136] and Preumont et al [137]. They also compared the force feedback with direct velocity feedback or active damping (see next section), which relies on collocated sensors.

Figure 6.33 shows the experimental set up, where 3 sensors, a force sensor, NCDT and accelerometer are collocated on the beam structure and another accelerometer non-collocated.

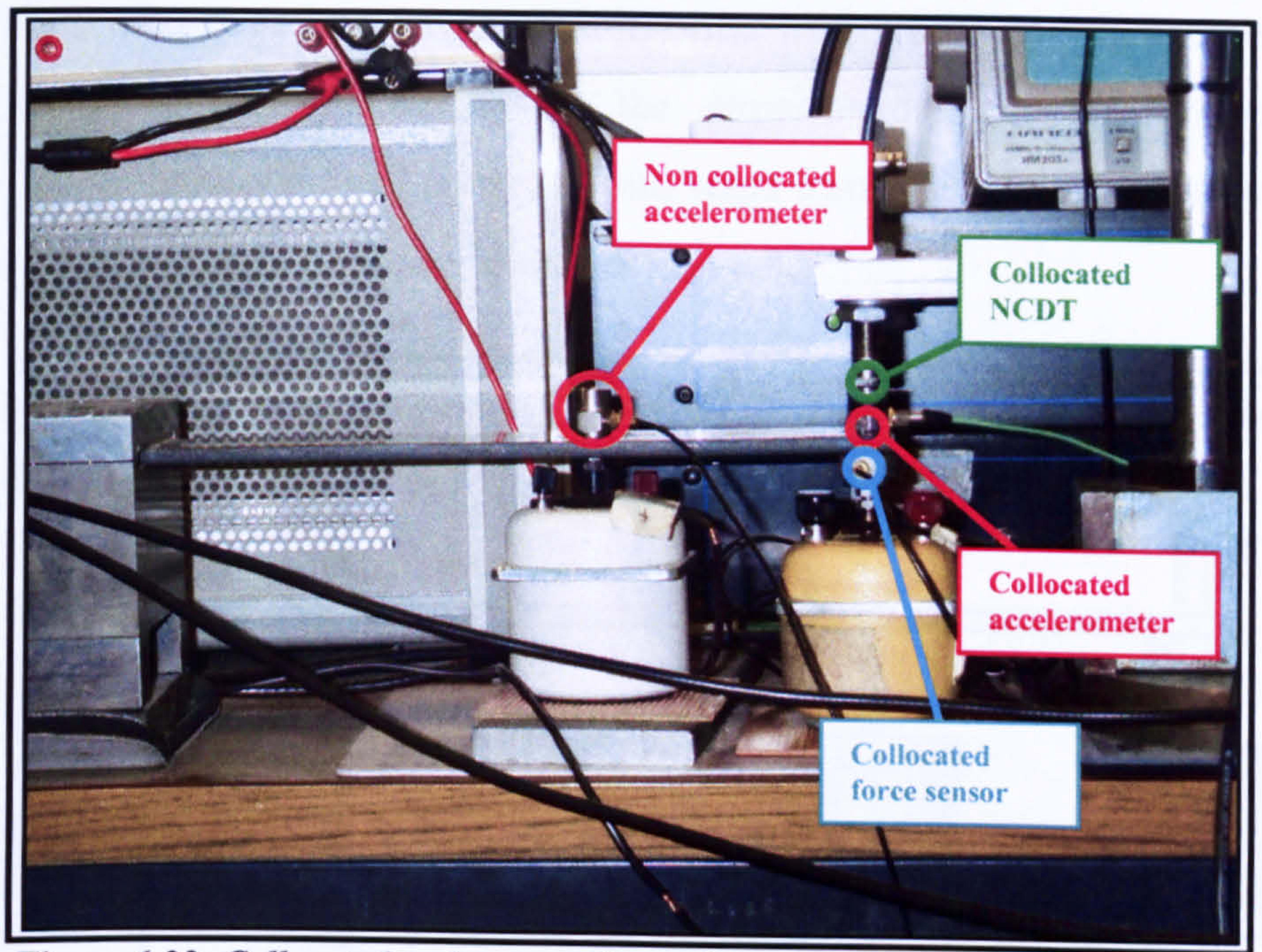

Figure 6.33: Collocated and non- collocated sensors on the beam structure

Figure 6.34 shows the Frequency Response Functions of the secondary path of the 2 accelerometers and the major difference between collocated and non-collocated sensors.

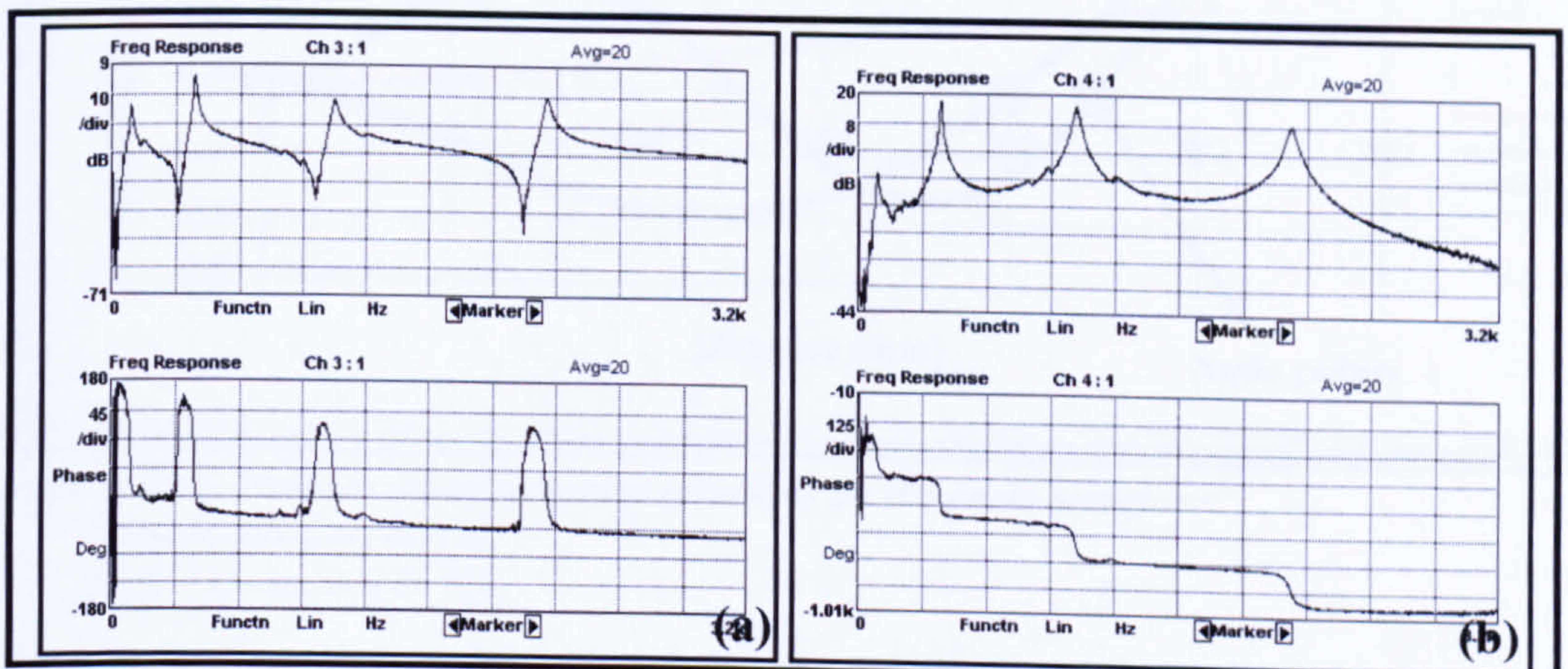

Figure 6.34: Secondary path FRF:
- *Collocated accelerometer (a)*
- *Non-collocated accelerometer (b)*

The FRF of the non-collocated accelerometer (6.34.b) only shows poles and no zero, where the collocated accelerometer (6.34.a) has a repeated pole zero pattern (a zero is always followed by a pole and vice versa). From a control point of view the collocated case is of interest since the phase only changes between 0° and 180°, where for the non-collocated case no zero is present in order to lift the phase up again (every pole results in a –180° phase shift). Collocated and non-collocated control is covered in the following section.

The next experiment was done in order to examine and understand this phenomena in more detail. Figure 6.35.a shows the experimental set up, where the accelerometer was incrementally moved away in 8mm steps from the actuator location and figure 6.35.b the first 3 mode shapes obtained under section 6.2.1.

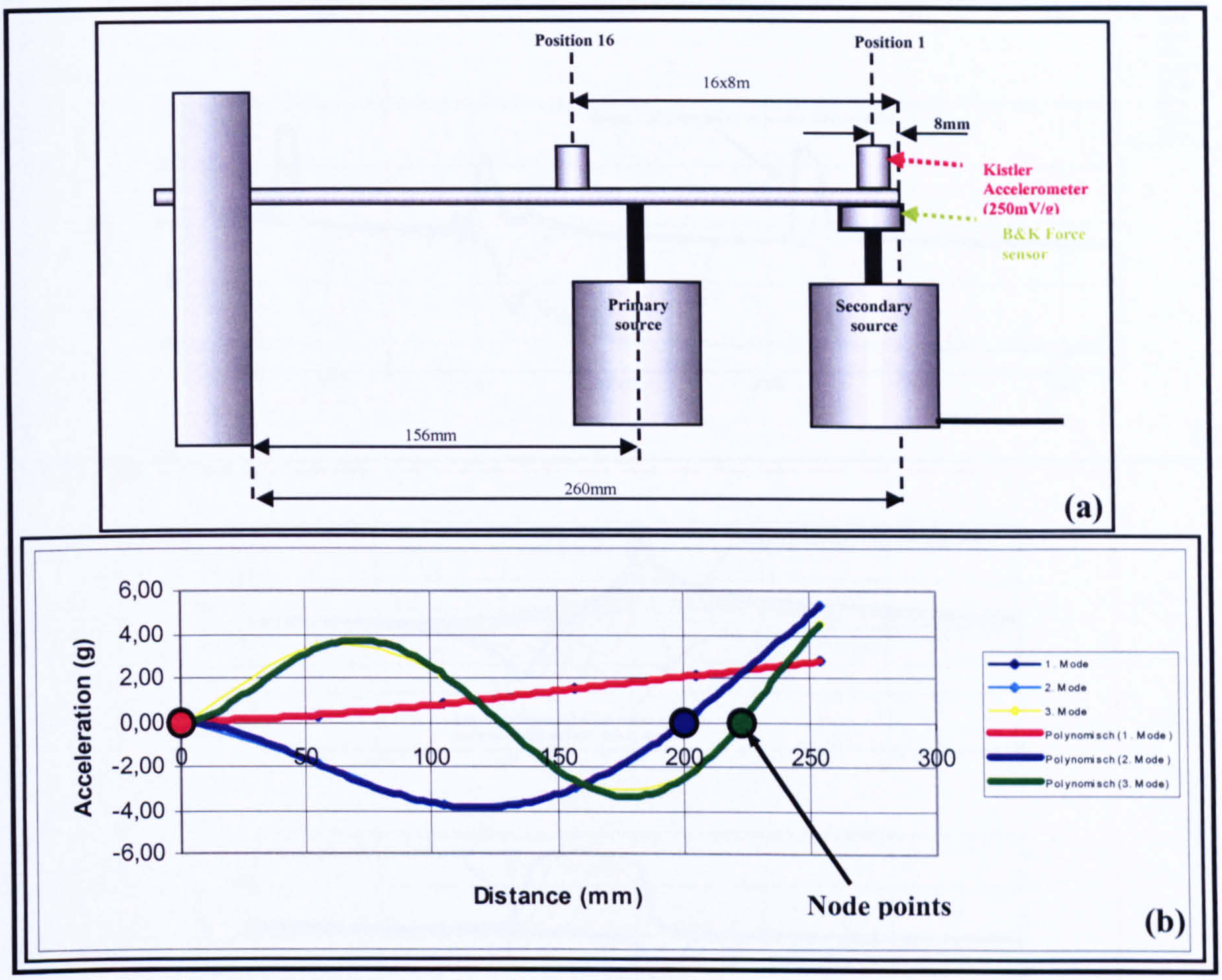

Figure 6.35: Various sensor/actuator locations on the beam structure:
- ***Experimental set up (a)***
- ***First 3 mode shapes (b)***

Figure 6.36.a, shows the measured FRF of the secondary path of the first 11 sensors. Clearly the location of the poles do not change, no matter how far the sensor is moved away from the actuator. But the characteristic of non-collocation is that the further the sensor is moved away, the further the location of the zero moves on the frequency axis of the FRF of the secondary path. The higher the modal frequency, the more the zero actually moves away (figure 6.36.a). The non-collocation of the actuator starts, when the zero overtakes the pole on the frequency axis. Then a pole will follow a pole and result in a -360° phase shift (-180° for each pole), which is a major disadvantage for control.

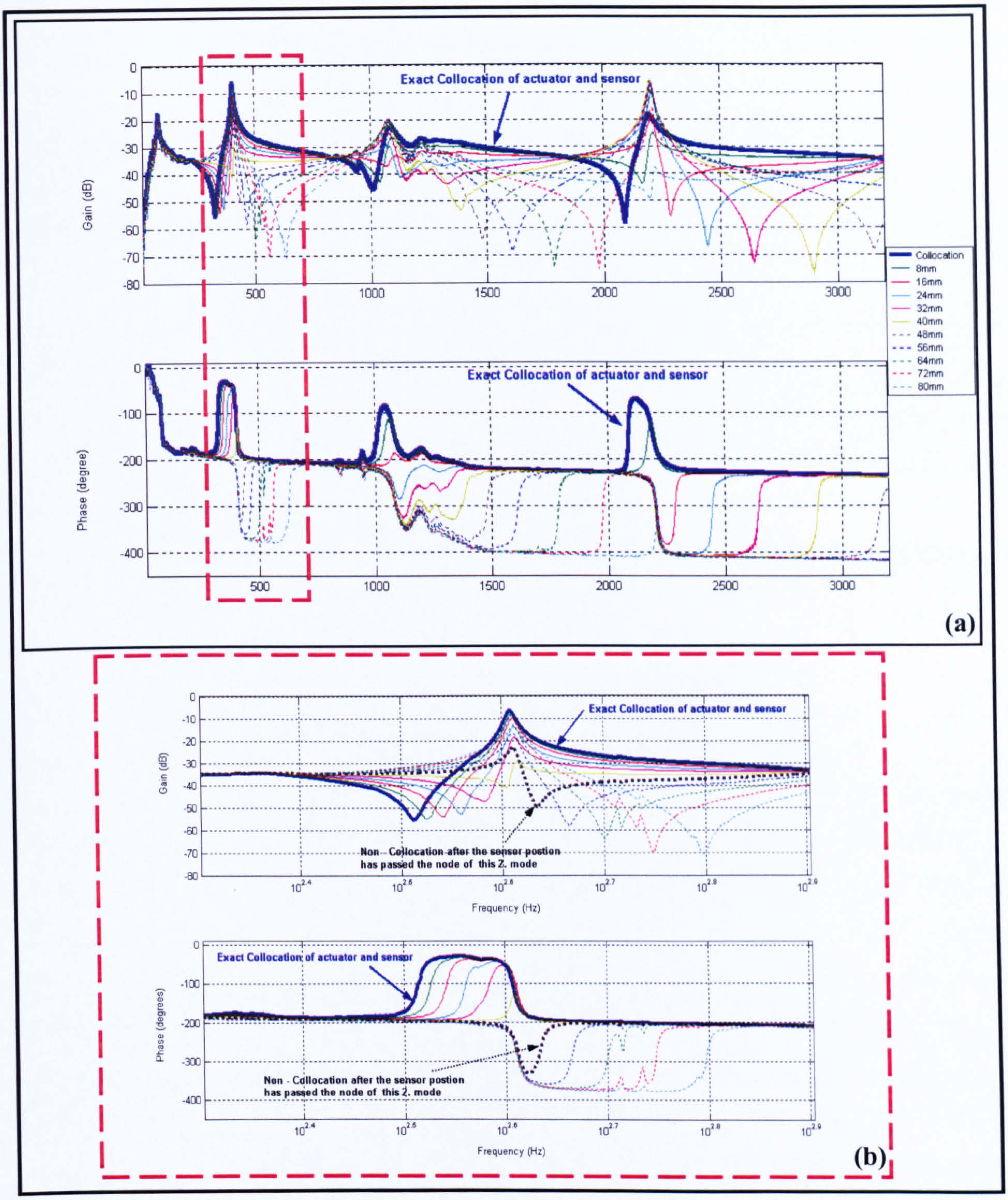

Figure 6.36: Frequency response functions of the secondary path:
- *For the first 11 sensor positions (a)*
- *Zoomed in to the 2. modal frequency (b)*

If the zero only moves to the same pole location on the frequency axis, they both will cancel each other out, with no vibration amplification and 0° phase shift. Practically this means that no vibration can be measured or observed at that frequency. Even more interesting is that the location of the sensor, where this happens is the node of the particular mode shape. A structure is infinitely stiff at the node points and no vibration can be measured. In order to make this clearer figure 6.36.b only shows the frequency range of the second mode. The zero cancels the pole at about 55mm from the beam end (node point of second mode figure 6.35.b and figure 6.36.b). This explains the observation made earlier, that the zeros of the higher modal frequencies change more. By looking at the mode shape in figure 6.35.b, the first mode is always collocated, since the first (from the actuator location) and only node point is the base of the cantilever beam. For the 2nd mode the collocation of sensor and actuator ends at about 55mm sensor distance from the actuator. For the 3rd mode this reduces to 30mm. The higher the mode the smaller this distance gets. Therefore collocated control only works, for the frequencies or modes, where the sensor is located between the position of the actuator and the first location of the node of that particular frequency which should be controlled. In order to optimise the location of the feedback sensor one only needs to measure the mode shape of the structure under control with the actuator as exciter.

The next section discusses why in traditional active vibration control, a collocated control system is desirable.

6.8 Traditional vibration control vs. adaptive vibration control

6.8.1 Theoretical background to traditional active vibration control

Active vibration control on structures can easily be realised using a simple PID controller. Unfortunately most authors do not mention or explain the importance of collocated and non-collocated sensor/actuator positions, on which this control technique relies. As already mentioned in the last section the FRF of the collocated secondary path has a distinguished pattern, where a pole follows a zero and vice versa (e.g. figure 6.34.a). This means that over the whole frequency range the phase is always between 0° and -180°, where for the non-collocated case it can be much bigger depending how far away the sensor is placed from the actuator (figure 6.34.b). It is also important to realise that the secondary path for adaptive control is the open loop transfer-function for traditional control. This also appears not to be mentioned by many authors, since they either only explain traditional and modern control theory or only adaptive control theory. After the reader has worked through this chapter it should become clear that the secondary path actually is the open loop transfer-function of a traditional closed loop feedback system and that from a control point of view both traditional and adaptive control are not that different after all.

Next the modified response of a simple single degree of freedom system is explained using traditional active vibration control. Although this example does not explain the importance of collocated control in terms of closed loop stability (the system only has one pole), it should theoretically explain 3 different control cases:

- Active or virtual stiffness (direct displacement feedback)
- Active or virtual damping (direct velocity feedback
- Active or virtual mass (direct acceleration feedback)

Figure 6.37.b shows a simple SDOF mass-spring-damper system, which represents a passive isolation system, excited by the primary force f_p. Examples are car or bicycle suspension systems, where vibrations are generated through an uneven road, or machine tool foundations where vibrations are generated through the machine itself or ground vibrations generated by other heavy machinery near by. The absolute vibration of the body is measured through an accelerometer and this signal can be integrated to give velocity and displacement.

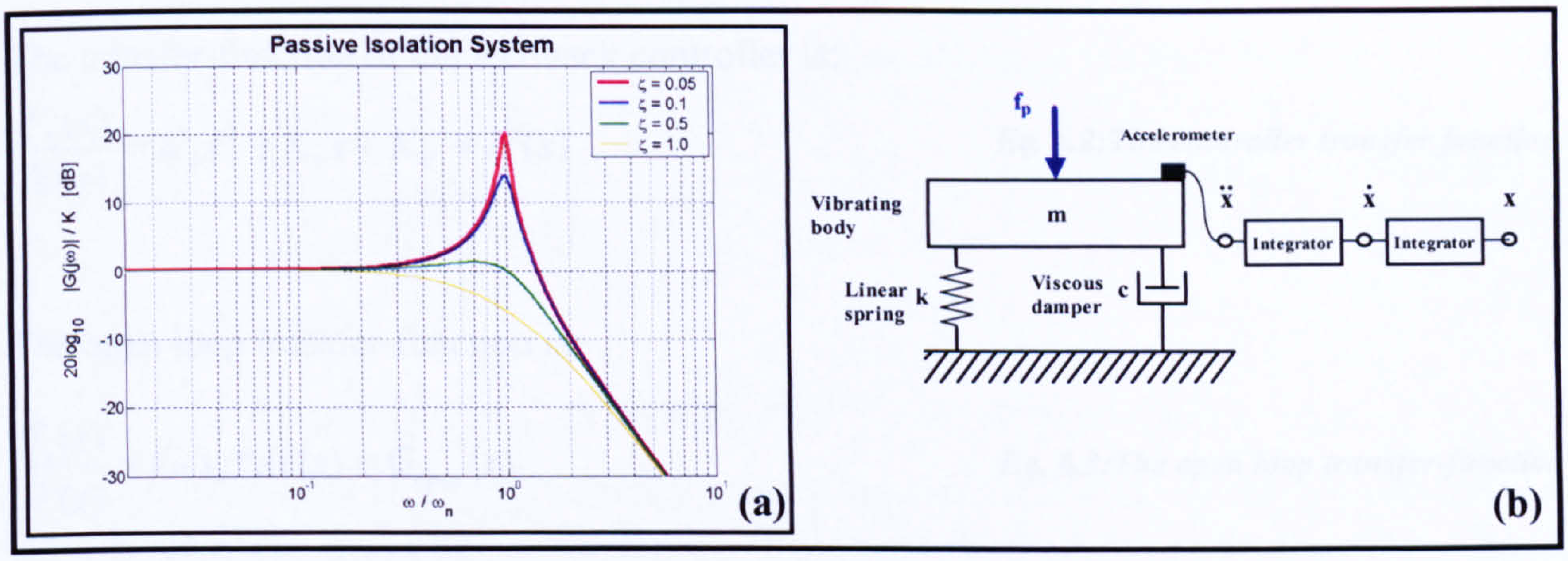

Figure 6.37: Passive vibration isolation system: Physical system (a) and the normalized parametric FRF (b)

The transfer-function and normalized parametric FRF of the system are:

$$\frac{X(s)}{F_p(s)} = \frac{1}{ms^2 + cs + k} \quad ; \; where \;\; w_n = \sqrt{\frac{k}{m}} \;\; and \;\; \zeta = \frac{c}{2m\omega_n}$$

$$\frac{G(j\omega)}{K} = \frac{1}{1 + j2\zeta\dfrac{\omega}{\omega_n} - \dfrac{\omega^2}{\omega_n^{\,2}}} \; ; where \;\; K = \frac{1}{m\omega_n^{\,2}}$$

Eq. 6.1: Transfer-function, natural frequency, damping ratio and normalized parametric FRF

Figure 6.37.a shows the gain of the normalised parametric FRF. A variable viscous damper could change the passive damping of the system (semi-active systems), with no additional energy supplied (e.g. active engine mounts or shock absorbers).

Figure 6.38 shows a fully-active system, where an actuator generates secondary vibrations in order to cancel the primary vibrations.

The feedback signal can be either:

- Displacement
- Velocity
- Acceleration

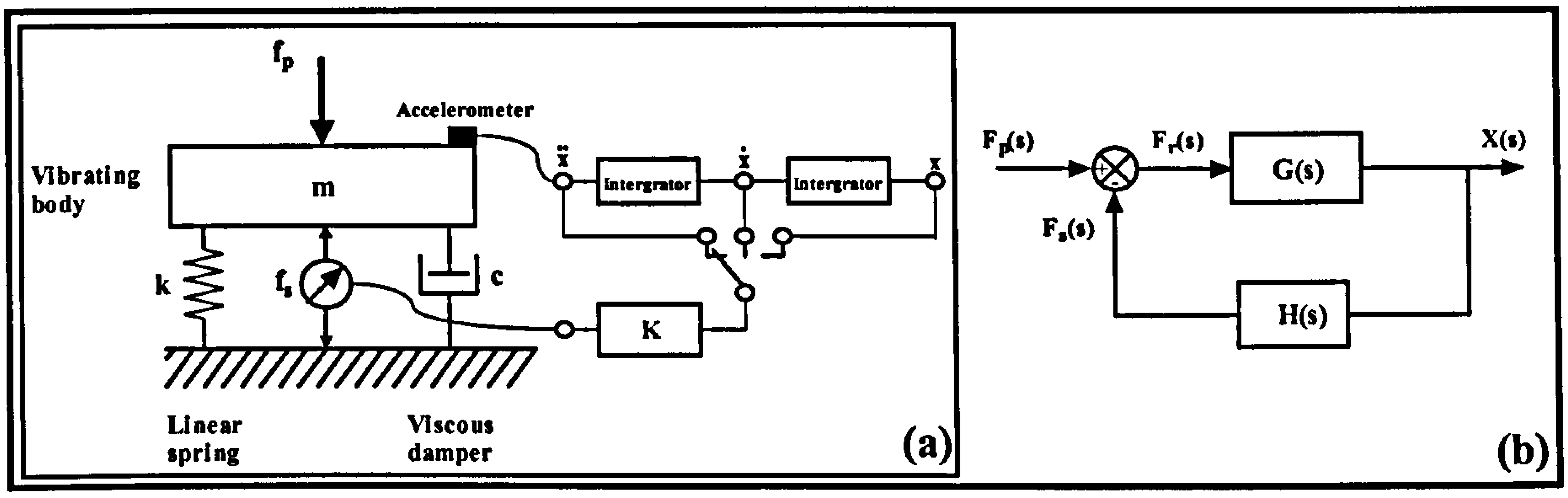

Figure 6.38: Active vibration isolation system: Physical system (a) and the block diagram (b)

The transfer-function of the feedback controller is:

$$\frac{F_s(s)}{X(s)} = K_a s^2 + K_v s + K_d = H(s)$$

Eq. 6.2:The controller transfer function

The open loop transfer-function is:

$$\frac{F_s(s)}{F_r(s)} = G(s) * H(s) = G_{open}(s)$$

Eq. 6.3:The open loop transfer-function

The transfer-function of this closed loop feedback system is given by:

$$\frac{X(s)}{F_p(s)} = \frac{G(s)}{1 + G_{open}(s)}$$

Eq. 6.4:The closed loop transfer-function

$$G_{closed\ loop}(s) = \frac{1}{(m + K_a)s^2 + (c + K_v)s + (k + K_d)}$$

For displacement feedback only, the modified natural frequency ω_n' and damping ζ' become:

$$\omega_n' = \omega_n \sqrt{1 + \frac{K_d}{k}} \quad ; \quad \zeta' = \zeta \sqrt{\frac{k}{k + K_d}}$$

Eq. 6.5: Modified natural frequency and damping for displacement feedback

The normalized parametric FRF for direct displacement feedback can be written as:

$$\frac{G_{closed\ loop}(s)}{K} = \frac{1}{1 + \frac{K_d}{K} + j2\zeta\frac{\omega}{\omega_n} - \frac{\omega^2}{\omega_n^2}}$$

Eq. 6.6:FRF for displacement feedback

For velocity feedback only, the modified natural frequency ω_n' and damping ζ ' become:

$$\omega_n' = \omega_n \quad ; \quad \zeta' = \zeta \, (1 + \frac{K_v}{c})$$

Eq. 6.7:Modified natural frequency and damping for displacement feedback

The normalized parametric FRF for direct velocity feedback can be written as:

$$\frac{G_{closed\ loop}(s)}{K} = \frac{1}{1 + j2\zeta \, (1 + \frac{K_v}{c}) \frac{\omega}{\omega_n} - \frac{\omega^2}{\omega_n^2}}$$

Eq. 6.8: FRF for velocity feedback

For acceleration feedback only, the modified natural frequency ω_n' and damping ζ ' become:

$$\omega_n' = \omega_n \sqrt{\frac{m}{m + K_a}} \quad ; \quad \zeta' = \zeta \sqrt{1 + \frac{K_a}{m}}$$

Eq. 6.9:Modified natural frequency and damping for acceleration feedback

The normalized parametric FRF for direct acceleration feedback can be written as:

$$\frac{G_{closed\ loop}(s)}{K} = \frac{1}{1 + 2\zeta \frac{\omega}{\omega_n} - (1 + \frac{K_a}{m}) \frac{\omega^2}{\omega_n^2}}$$

Eq. 6.10:FRF for acceleration feedback

Figure 6.39 shows the normalised parametric FRF's with different feedback gains.
Active mass has the effect of "virtually" increasing the mass of the whole system, without actually adding a physical mass to the structure (the active mass is created by the energy supplied to the actuator), since it lowers the mass asymptote, natural frequency and damping ratio (equation 6.9). Active stiffness has the effect of virtually increasing the stiffness of the whole system, since it lowers the stiffness asymptote of the FRF and damping factor but increases the natural frequency (equation 6.5). Active damping, which adds additional "virtual" damping to a structure, seems to be the most suitable solution for lightly damped structures, since it only increases the damping and not the resonance frequency of a structure (equation 6.7). It is now obvious, why a simple PID controller can be used. Direct velocity feedback for example can be implemented using a displacement sensor and PD controller, or accelerometer and PI controller. It also should be noted that feedback control changes the parameters of the system (resonance frequency and damping), where feed-forward control can not change the system properties, since it aims to cancel the primary force. Therefore feedback control will not be able to reduce the vibrations down to zero, where feed-forward has the potential to do so [97].

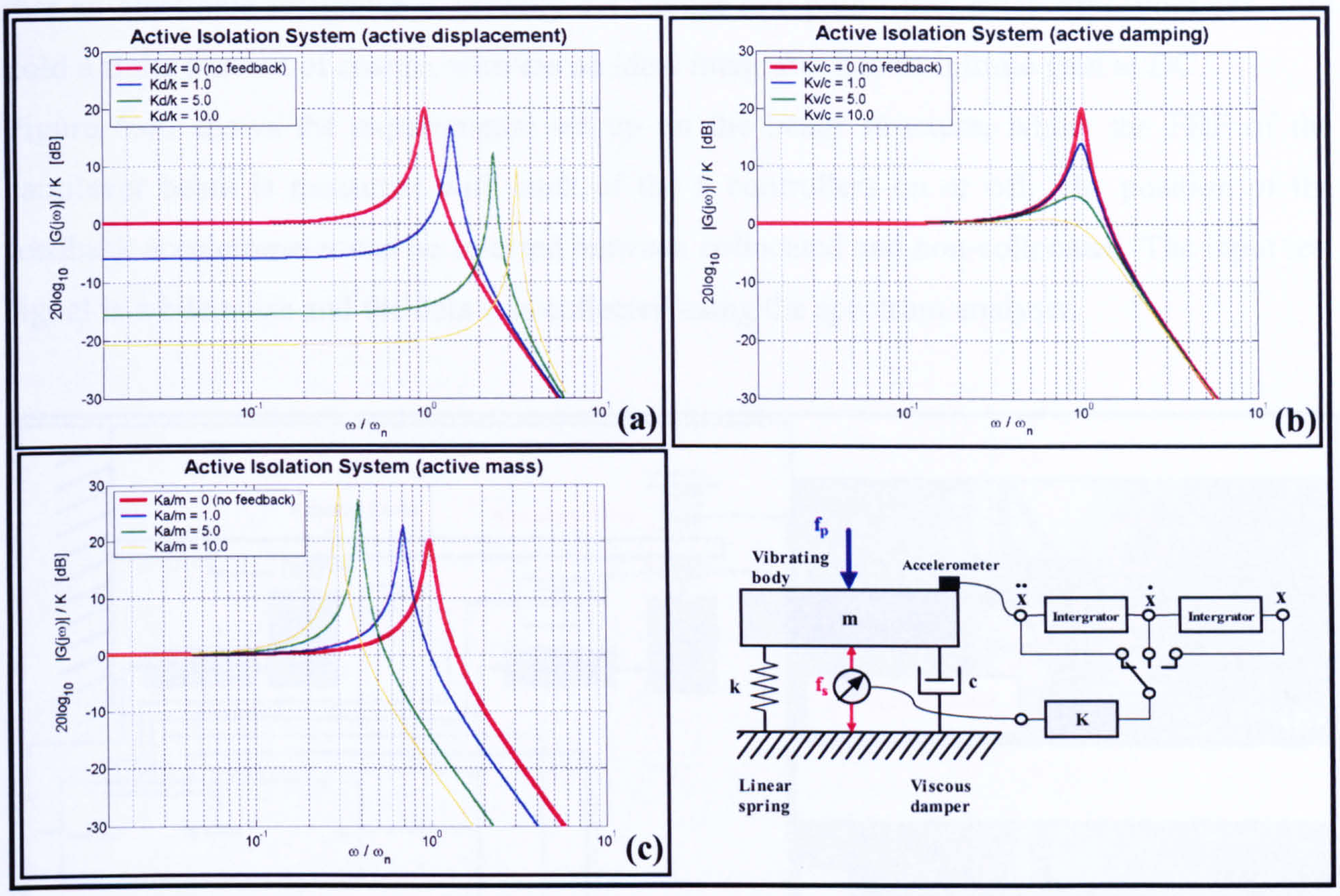

Figure 6.39: Active vibration isolation system characteristics:

- ***Active stiffness using direct displacement feedback (a)***
- ***Active damping using direct velocity feedback (b)***
- ***Active mass using direct acceleration feedback (c)***

6.8.2 Controller comparison on the beam structure

In order to judge the performance of the adaptive controller it has been compared with the traditional controllers explained in the last section. This was done because no qualitative comparison between the methods was found in the literature. The tested controllers are:

- Adaptive FIR feed-forward (FXLMS-algorithm)
- Manual feed-forward controller using an 3rd order all-pass filter and bandpass filter
- Active stiffness
- Active damping
- Active mass

The traditional controllers have been designed using two integrator units and a P-controller (appendix C.3). The manual feedforward controller (refer to section 6.3) has been updated with a bandpass filter to ensure a harmonic reference signal (appendix C4). It should be noted that an electronic integrator is actually a 1^{st} order low pass filter, since capacitors can only hold a finite amount of charge, whereas an ideal integrator has an infinite gain at DC.

Figure 6.40 shows the experimental set up on the beam structure, where the FRF of the cantilever beam is measured with each of the 5 controllers on or off. The position of the feedback accelerometer can be selected between collocated and non-collocated. The input test signal is white noise and the data was collected using the spectrum analyser.

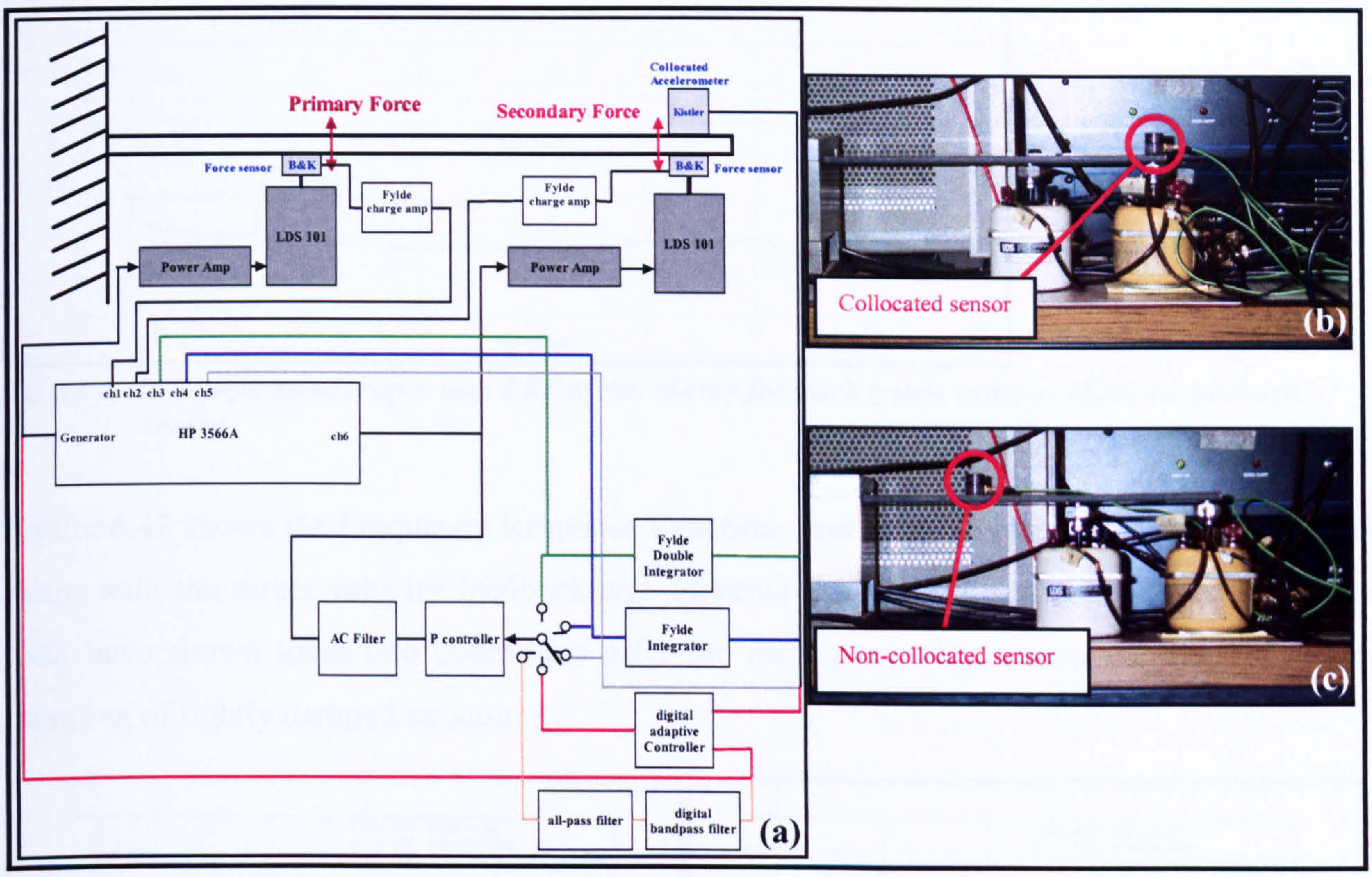

Figure 6.40: Controller comparison on the beam test structure:
- ***Experimental set up (a)***
- ***Collocated control (b)***
- ***Non-collocated control (c)***

6.8.2.1 Vibration control using a collocated sensor

In order to make a stability judgement for the closed loop system and tune the controller parameters, the open loop transfer-function was estimated. The measured non parametric open loop FRF of the velocity feedback system, showed a positive phase margin over the whole frequency range (figure 6.41). According to the Nyquist criterion the control system is stable.

A parametric model (transfer-function – LAPLACE domain) of the open loop system was estimated using MATLAB's frequency identification and signal processing toolbox. The open loop transfer-function made it possible to simulate the control system and optimise its gain. The root locus plot showed an alternating pole zero pattern - the sign of a collocated system.

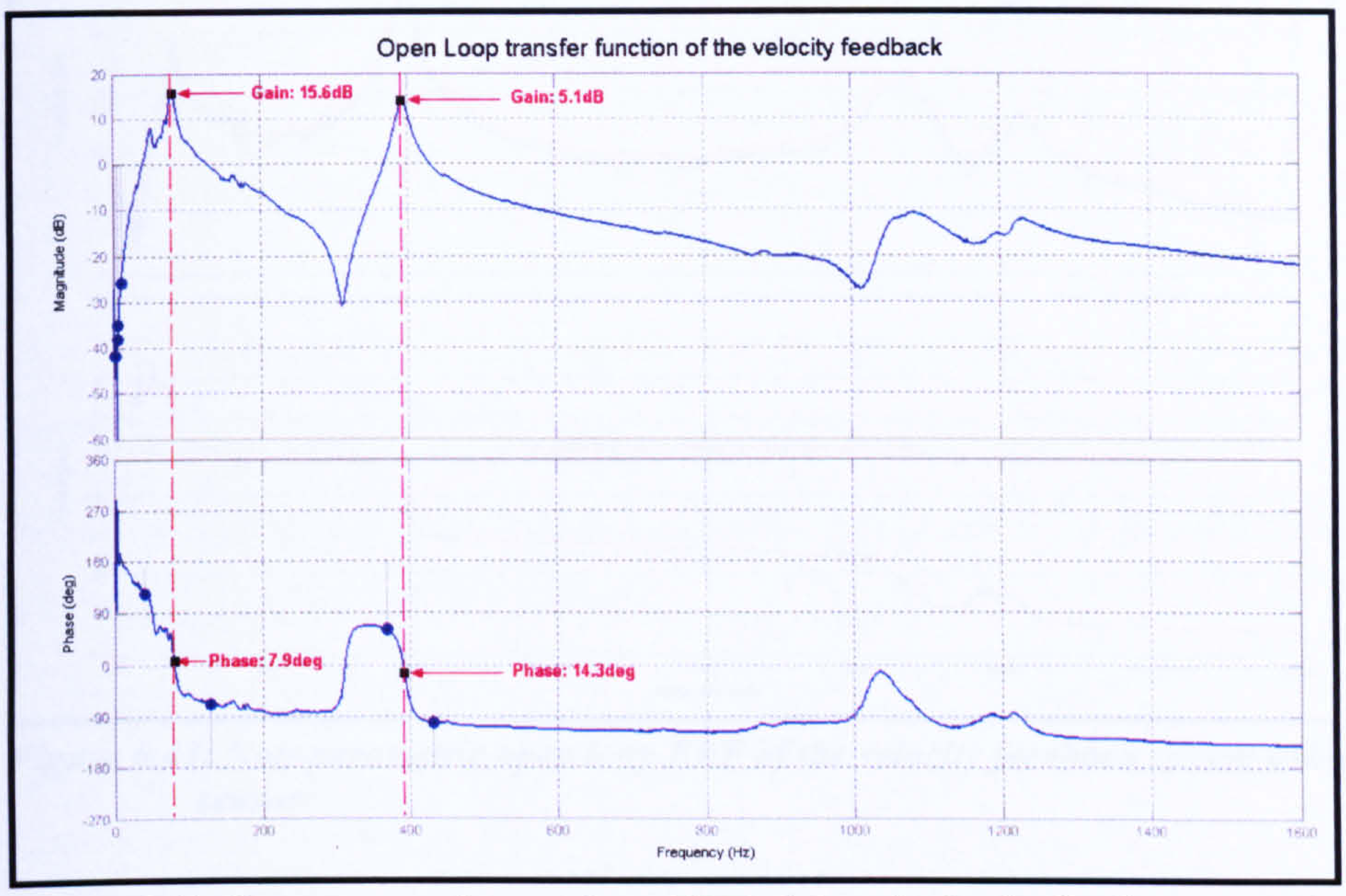

Figure 6.41: Non-parametric open loop FRF of the velocity feedback system using a collocated feedback sensor

Figure 6.42 shows the Frequency Response Functions and Impulse response of the cantilever beam with the direct velocity feedback and adaptive feed-forward controller activated. The tests have shown these two controllers offer the most promising results for increasing the damping of lightly damped structures.

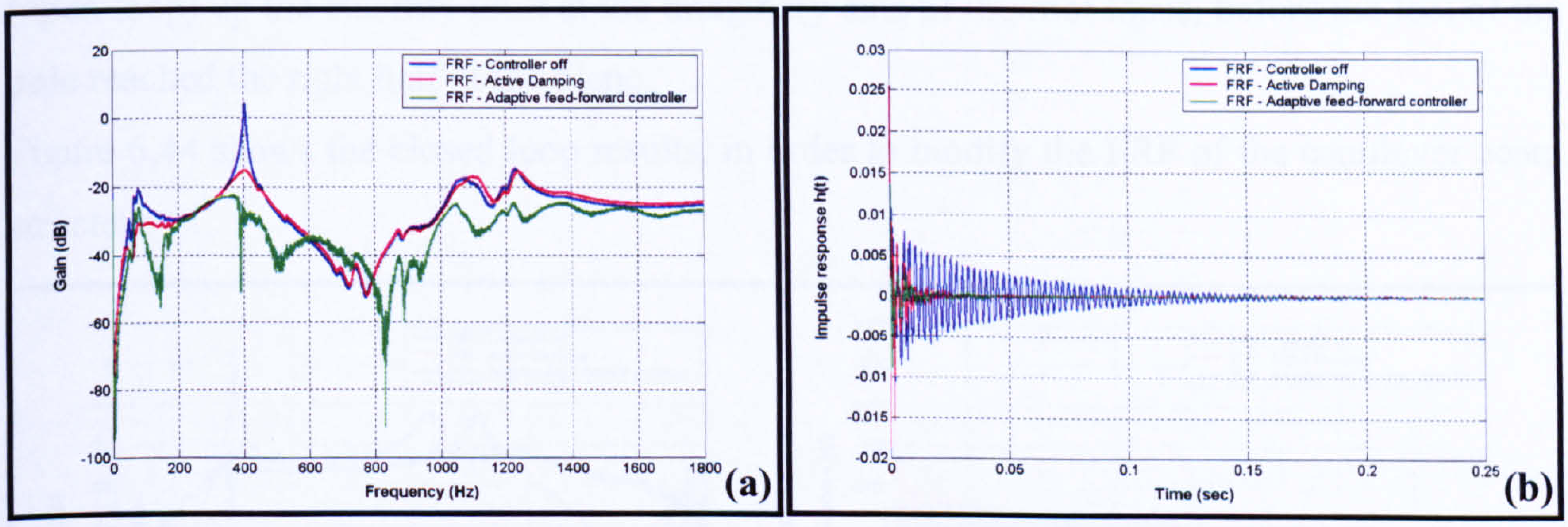

Figure 6.42: Increasing the damping of the beam structure using collocated active vibration control:
- ***The gain of the Frequency Response Function (a)***
- ***Impulse response of the beam structure (b)***

6.8.2.2 Vibration control using a non-collocated sensor

The experiment described in the last section, was repeated with a non-collocated sensor (figure 6.40.c). Again the open loop transfer function was estimated and the controller gain of the direct velocity feedback controller increased up to the stability limit (figure 6.43).

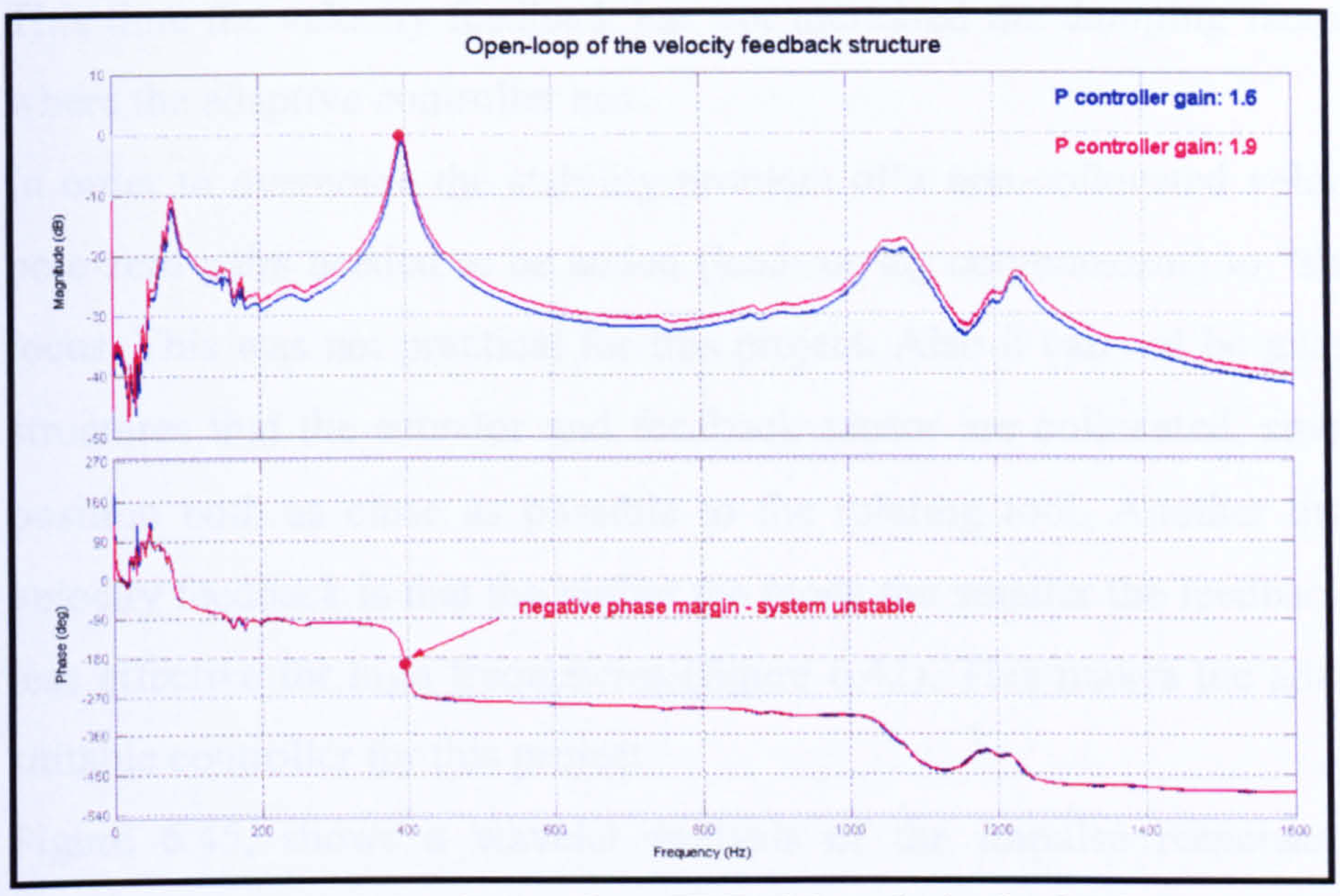

Figure 6.43: Non-parametric open loop FRF of the velocity feedback system using a non-collocated feedback sensor

In comparison to the root locus of the collocated case, where the alternating pole zero pattern prevents a crossing of the loci, (in the root locus the poles are moved towards the zeros by increasing the feedback gain from zero (open loop) to infinity (closed loop)). The non-collocated case however shows no such feature. Here if a pole is followed by a pole on the imaginary axis of the root locus plot, some of the loci must "skip" over a pole by travelling into the right half of the plane (unstable system). The feedback gain was increased from zero (open loop) up the stability limit at the imaginary axis of the root locus, before the loci of the pole reached the right half of the plane.

Figure 6.44 shows the closed loop results, in order to modify the FRF of the cantilever beam structure.

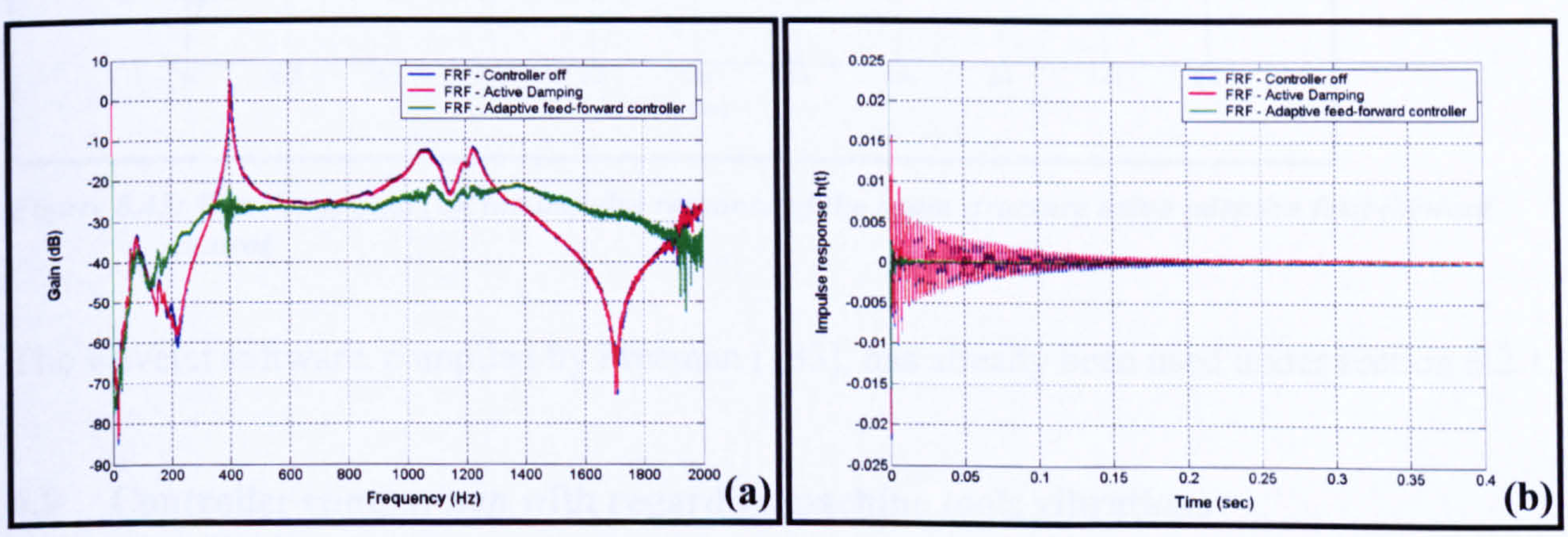

Figure 6.44: Increasing the damping of the beam structure using non-collocated active vibration control:
- ***The gain of the Frequency Response Function***
- ***Impulse response of the beam structure***

This time the velocity feedback has not increased the damping factor of the beam structure, where the adaptive controller has.

In order to overcome the stability problem of a non-collocated velocity feedback controller, pole-zero pairs needed to be added (lead- or lag compensator) to "shape" and repair the root locus. This was not practical for this project. Also it can not be guaranteed on machine tool structures that the actuator and feedback sensor are collocated, since it is very awkward to position both as close as possible to the rotating tool. Another disadvantage of the direct velocity feedback is that the higher the mode the smaller the feedback gain is, which makes it less effective for high frequencies (figure 6.42). This makes the adaptive controller the only suitable controller for this project.

Figure 6.45, shows a wavelet analysis of the impulse response of the beam structure, concludes this section. It illustrates well, the increase of damping for each single mode using active vibration control.

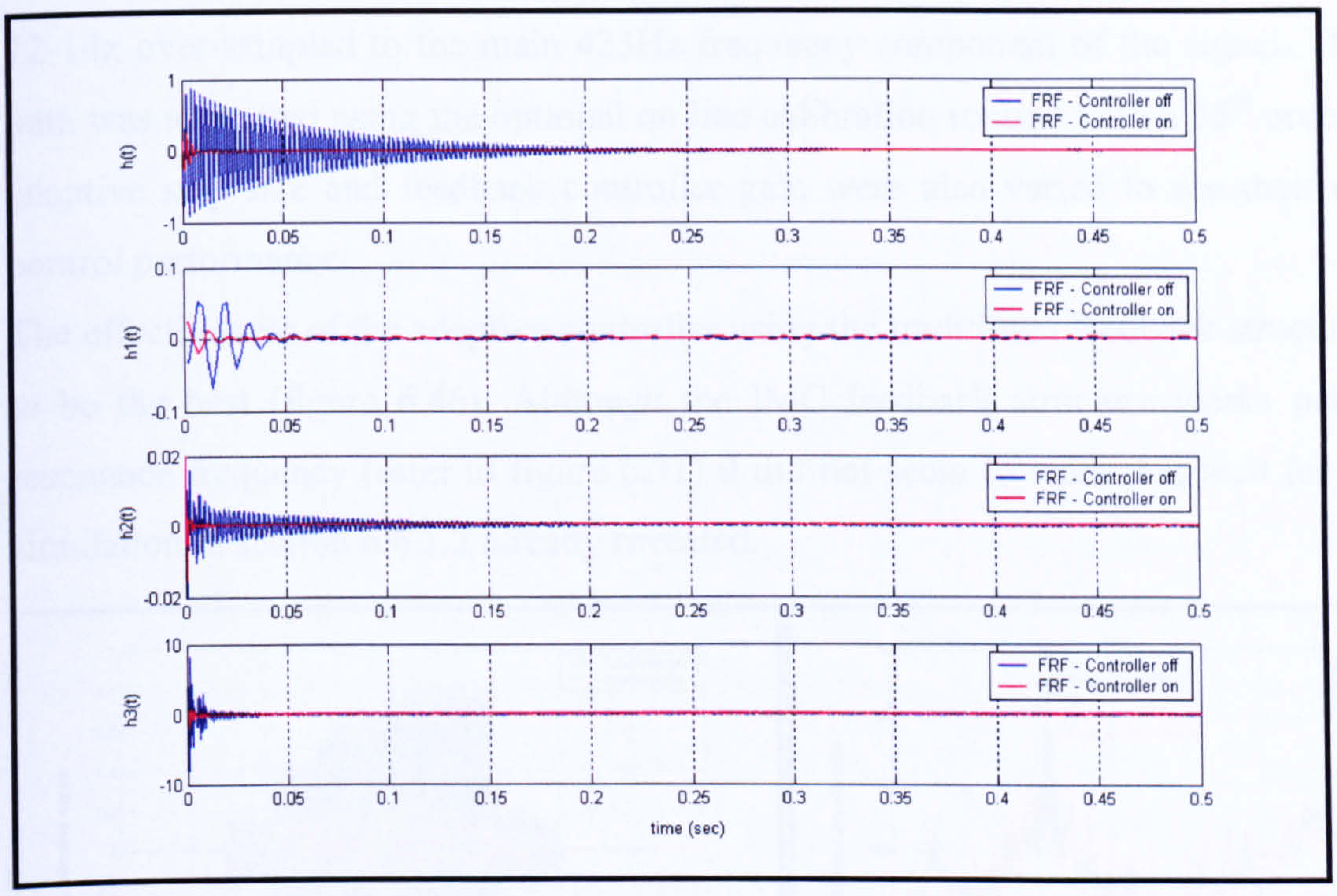

Figure 6.45: Wavelet analysis on the impulse response of the beam structure using adaptive feed-forward control

The wavelet software, compiled by Freeman [133], has already been used under section 6.2.1.

6.9 Controller comparison with regard to machine tools vibrations

In the last experiment the beam structure was excited by the vibration signal from the chattering machining centre in chapter 5 (refer to chapter 5.6 – figure 5.10). The controllers with non-collocated sensor were used to control the chatter vibrations.

The controllers tested here were:

- Adaptive FIR feed-forward controller
- Manual feedback controller using the traditional feedback structure
- Adaptive FIR feedback controller using the traditional feedback structure
- Adaptive FIR feedback controller using the IMC feedback structure

The feed-forward controller was only used as a reference, and can not be used on the machine tool, since the reference signal is not directly available.

The chatter vibration data taken with the spectrum analyser was converted into a "wav" file in order to play the cutting process back using the sound card of the PC using SpectraLAB® software [138]. The data also was re-sampled using MATLAB, so that the main chatter frequency (456 Hz) matched closely the second mode of the beam structure (423 Hz).

The sampling frequency of the digital controller was varied between 5kHz and 6kHz (about 12-14x over-sampled to the main 423Hz frequency component of the signal. The secondary path was identified using the optional on line calibration routine with a 35th order model. The adaptive step size and feedback controller gain were also varied to see their effect on the control performance.

The effectiveness of the adaptive controller using the traditional feedback structure was found to be the best (figure 6.46). Although the IMC feedback structure works perfectly at the resonance frequency (refer to figure 6.31) it did not seem to work that well for others as the simulation in section 6.6.1.2 already revealed.

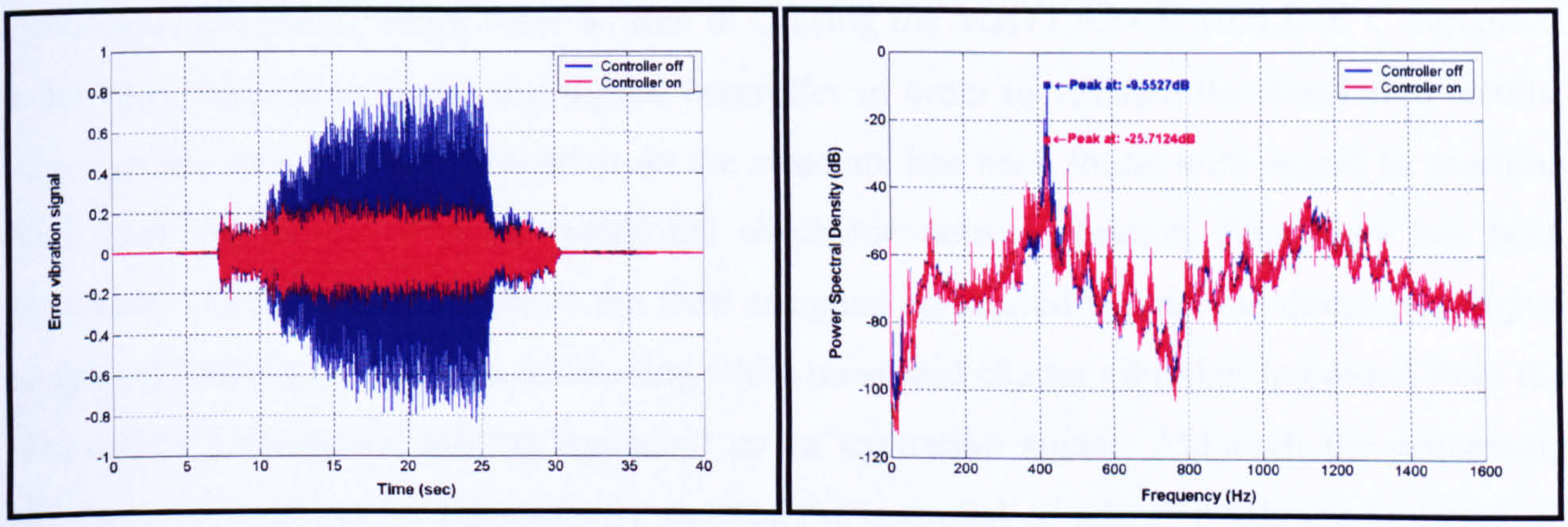

Figure 6.46: The effectiveness of the adaptive controller on the beam structure due to chatter vibrations

It has further been found that performance increases with sampling frequency and controller gain. The controller gain also has the same effect as the adaptive step-size or vice versa in order to make the controller faster. But as in traditional feedback control theory, the faster the system, the less stable it becomes.

Table 6.1 shows the actual vibration reduction for the main chatter frequency for all the tested controllers.

	Manual feedback controller	**Adaptive feedback controller using IMC feedback structure**	**Adaptive feedback controller using classical feedback structure**	**Adaptive feed-forward controller (used as reference)**
Reduction (dB)	**8.13dB**	**9.14dB**	**16.28dB**	**24.01dB**
Reduction (%)	**60.8%**	**65.1%**	**84.9%**	**93.6%**

Table 6.1: The reduction of the chatter vibration on the beam structure for the investigated controllers

6.10 Summary

This chapter showed the investigation into active vibration control systems. It needed to be shown that such a system is able to control machine tool vibrations, such as chatter. The vibrating structure was a cantilever beam, representing the clamped tool in a spindle or tool post, with similar modal frequencies to those of the milling machine investigated in chapter 5. The progress and difficulties that were encountered in building the digital adaptive vibration controllers have been discussed. A suitable low cost digital control platform has been developed and it has been shown through design simulation and actual implementation of digital controllers how it can practically be used. Off line simulation programs to estimate the mathematical, parametric models of the structure were written and based on these, a simulation program for the mechanical beam structure was developed. This program allowed the simulation of various adaptive algorithms in order to find the most appropriate. The simulation programs, which were written in C using the MATLAB- SIMULINK C compiler, were then transferred to the real digital controller in order to validate the simulation results. The optimal sensor actuator location on the structure has been found with regard to machine tool, and the theory of more traditional electronic active vibration controllers has been reviewed. These PID controllers were then designed and tested against the developed digital adaptive controllers. This was done using white noise and chatter vibration (recorded from the previously investigated milling machine) as an excitation signal. Although the processing platform was not fast, it impressively showed the potential of adaptive vibration control, so that the design of a system for machine tools could be considered next.

Chapter 7

The design of an active vibration control system for machine tools

7.1 Introduction

In the previous chapter it was demonstrated that active vibration control is a powerful tool to reduce the vibration level of mechanical structures, by actively increasing their mechanical parameters (stiffness, damping and mass). Practically, this means that an active vibration control system has the potential to change the damping and mass of a machine tool structure, without redesigning it.

Additional mass is replaced with the energy supplied by the actuator system.

This chapter describes the design process of a universal active vibration system for vertical milling machines. The aim was for the prototype system to demonstrate the reduction of the vibration level from the cutting process at the tool/work-piece interface. Sensors were integrated into the system to measure cutting force, acceleration and displacement directly.

The first section of this chapter estimates the cutting force and displacement at the tool/work-piece interface in order to choose appropriate actuators. The theoretical estimation was then validated through cutting tests on the milling machine and the mechanical system design including the chosen actuators and sensors is discussed. The main feature of this design is a high-resolution guide way system with no stiction, friction or backlash. The system needed to be designed for an extreme environment under cutting conditions. Humidity sensors were integrated to monitor and prevent any damage to the instrumentation. Additional instrumentation for analogue signal conditioning was designed, simulated, built and tested. All sensors were calibrated and the whole instrumentation EMI protected. At the end of the chapter static and dynamic testing confirmed the characteristics of the system and showed that the design objectives were met.

7.2 Identification of the sensitive design parameters

The cutting force and maximum displacement of the tool/work-piece interface needed to be estimated in order to design the active vibration control system. The calculation of the cutting forces is based on the face milling operation described in chapter 5. The experimental validation on the machine was done using a table dynamometer [139] and accelerometer. The measured displacement was also compared with the *waviness* of the surface finish and typical vibration levels on vertical milling machines taken from a Japanese contribution to the proposed ISO 230-8 draft [140].

7.2.1 Theoretical estimation of the cutting forces

First the cutting forces were calculated using the theory described in chapter 3.
The main cutting force is the tangential force F_t, which is directly proportional to the required torque and power of the spindle motor.
There are two ways of estimating the tangential cutting forces:

- By using the cutting parameters of a particular cut (MRR_m)
- By using the maximum torque and power allowed by the spindle motor

First the cutting parameters of the unstable face mill cutting operation were used to calculate the tangential cutting force. This was then compared with the maximum spindle power and torque taken from the manual for the machine. The calculated maximum cutting forces were used as a reference for the design of the active work-piece holder.
The cutting parameters were:

- Feedrate (f) = 267mm/min
- Spindle speed (n)= 477 RPM
- Diameter of the face mill (D_c) = 100mm
- Number of teeth (m) = 8
- Axial depth of cut (a_a) = 4mm
- Radial depth of cut (a_r) = 76mm
- Material = Mild Steel – K_s = 2300-2600 Wsec/cm^3 [4]

The mean material removal rate can be calculated using equation 3.11:

$$MRR_m = a_r \times a_a \times f \left[{mm^3}/{\min}\right]$$
$$= 4mm \times 76mm \times 267\, {mm}/{\min}$$
$$= 81168\, {mm^3}/{\min} = 81.168\, {cm^3}/{\min}$$

The power of the spindle motor to achieve the required MRR_m can be calculated using equation 3.13:

$$P_m = \frac{MRR_m\left[{cm^3}/{\min}\right] \times K_s\left[{W_{\sec}}/{cm^3}\right]}{60\left[{\sec}/{\min}\right]}\left[W\right]$$
$$= \frac{81.168\, {cm^3}/{\min} \times 2500\, {W\sec}/{cm^3}}{60\, {\sec}/{\min}}$$
$$= 3382W$$

The tangential cutting force can now be calculated using equation 3.14:

$$F_t = \frac{P}{v}\left[N\right]$$
$$= \frac{3382\, {Nm}/{\sec}}{\dfrac{100mm \times \pi \times 477\, {1}/{\min}}{60\, {\sec}/{\min}}} \times 1000\, {mm}/{m}$$
$$= 1354N$$

The same equation can be obtained by using the common formulas for calculating the power of a rotating disk or shaft (equation 7.1) and its torque (equation 7.2):

$$P = M \times \omega \left[{Nm}/{\sec}\ or\ W\right]$$ ***Eq. 7.1:Power of a rotating shaft***

$$M = F_t \times \frac{D}{2}\left[Nm\right]$$ ***Eq. 7.2:Torque of a rotating shaft***

The instantaneous cutting torque M_c is therefore (equation 7.3):

$$M_c = \frac{P_m}{\omega} = \frac{3382 \, {}^{Nm}\!/_{\sec}}{2 \times \pi \times \dfrac{477 \, {}^{1}\!/_{\min}}{60 \, {}^{\sec}\!/_{\min}}}$$

$$= 68 Nm$$

Eq. 7.3: The instantaneous cutting torque

According to the specification for the spindle motor, the maximum ratings are 4hp (2.98KW) at 416RPM and 10.97hp (8.18KW) at 1140RPM [141]. The load characteristic of the separately excited DC motor can be seen in figure 5.5.c. The slope of the linear part of the function *P=f(n)* up to n_s can be calculated using the given values of 7.18W/RPM. This means that the spindle motor is capable of producing 3425W at 477RPM. Therefore the performed cutting test (3382W) already reached the limitations of the machine, and the calculated cutting forces are appropriate as a reference for the design of the active vibration system.

The design of the milling machine seems to be very well balanced since the maximum cutting forces delivered by the spindle and feed motors, only just reach the chatter stability limit of the machine structure. A very good investigation into machine tool stability, with regard to the spindle torque and tool limits, has been done by Bach [142].

7.2.2 Measurements of cutting forces and displacement

In order to measure the cutting forces of a particular cutting process a dynamometer was needed. Approximately half way through the project a KISTLER table dynamometer became available (figure 7.1.b). This made it possible to evaluate the previous theoretically calculated figures. The relative displacement between tool and work-piece needed to be estimated using an accelerometer attached to the spindle housing (figure 7.1.a).

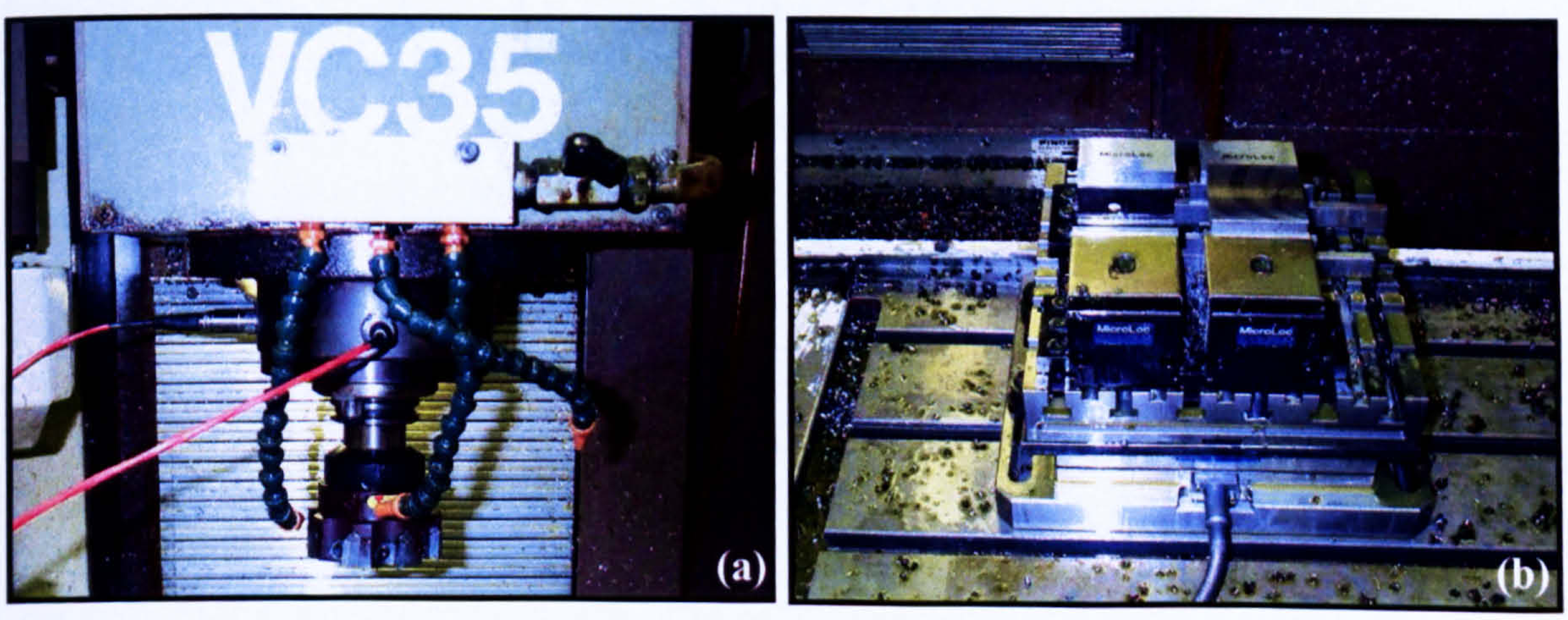

Figure 7.1: Measurement of cutting forces (a) and spindle housing displacement (b) under cutting conditions

The cutting forces and accelerations in the X and Y axis were recorded since it was decided to limit the active vibration system to two axes, because of cost and the complexity of the mechanical design (see section 7.4).

Figure 7.2 shows the recorded cutting forces and spindle housing acceleration.

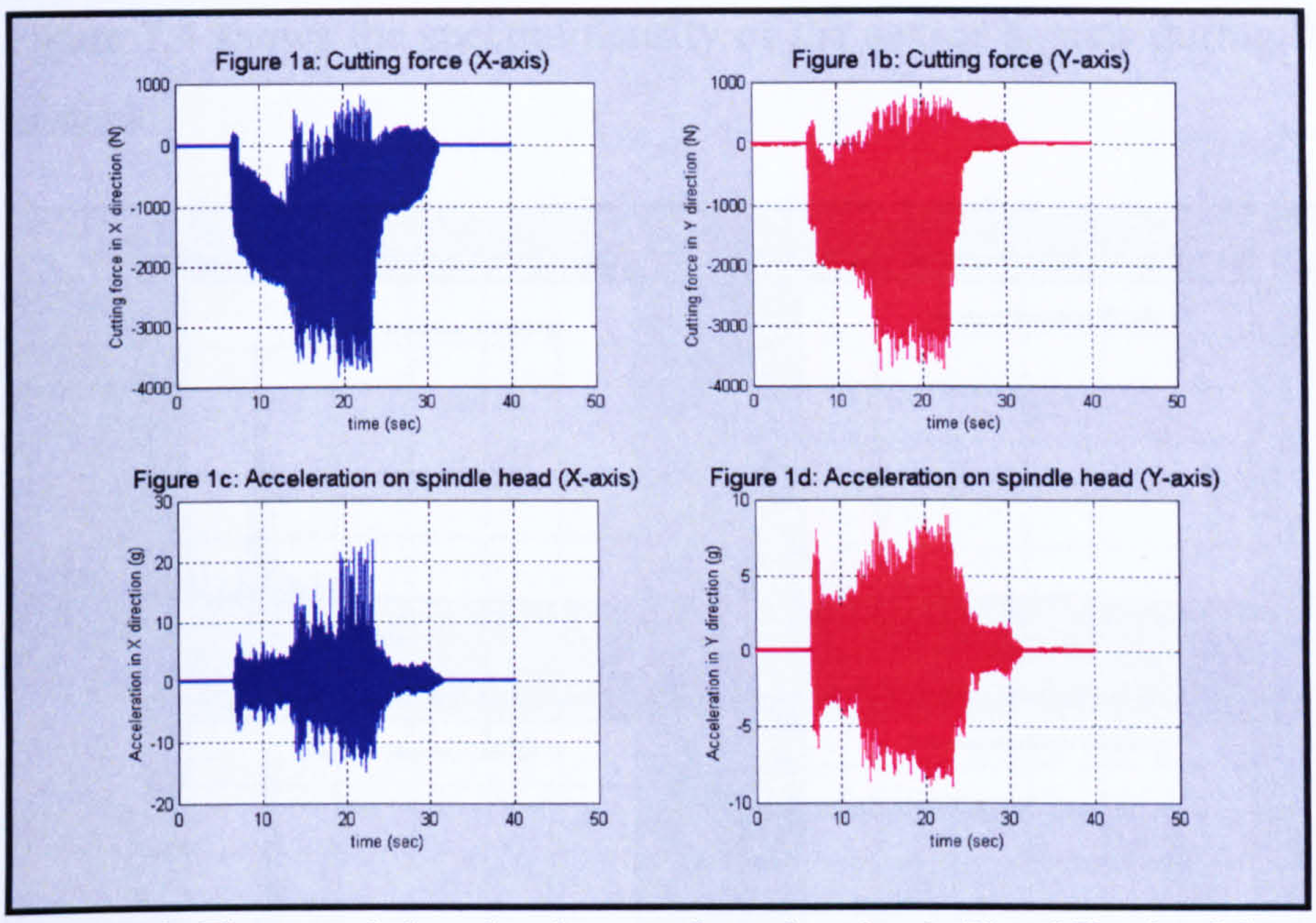

Figure 7.2: The recorded cutting force and acceleration in X and Y axis of the machine for an unstable cutting operation (chatter)

The figure shows that the chatter limit of the machine structure was reached after the whole diameter of the face mill was in the cut. The result of the suddenly increased cutting or excitation force is also a sudden increase in vibration amplitude. This was confirmed by the characteristic chatter sound. After some off line digital signal processing (high and low pass filtering) using MATLAB, figure 7.3.a shows the static- and 7.3.b the dynamic cutting forces.

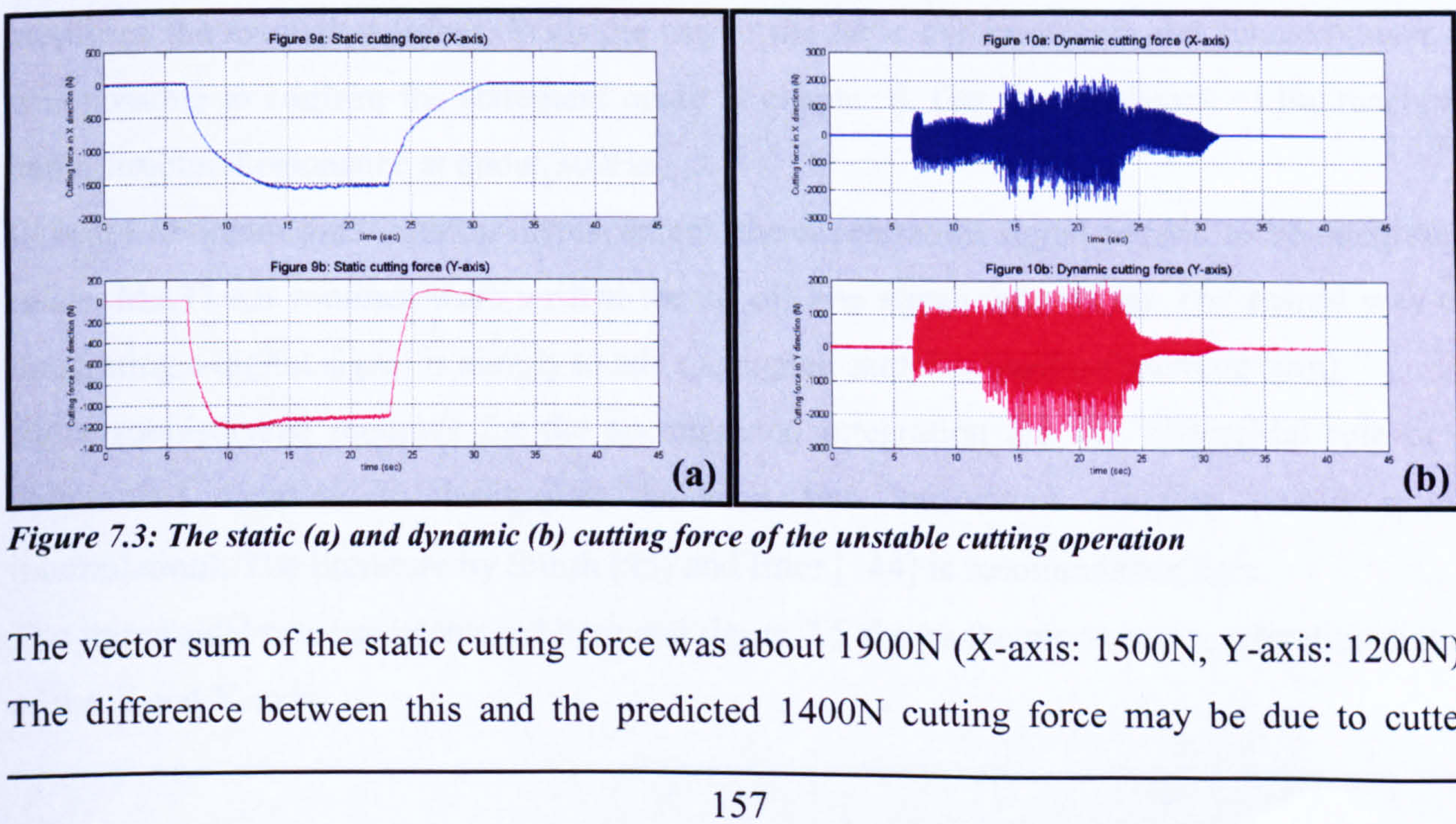

Figure 7.3: The static (a) and dynamic (b) cutting force of the unstable cutting operation

The vector sum of the static cutting force was about 1900N (X-axis: 1500N, Y-axis: 1200N). The difference between this and the predicted 1400N cutting force may be due to cutter dulling (cutting inserts were worn out), which can significantly increase the cutting force [143].

The theoretical calculation and measurements of the cutting force gave a good indication of the forces the active work-piece holder had to withstand.

Figure 7.4 shows the spectral density of the sensor signals during the time the machine was unstable.

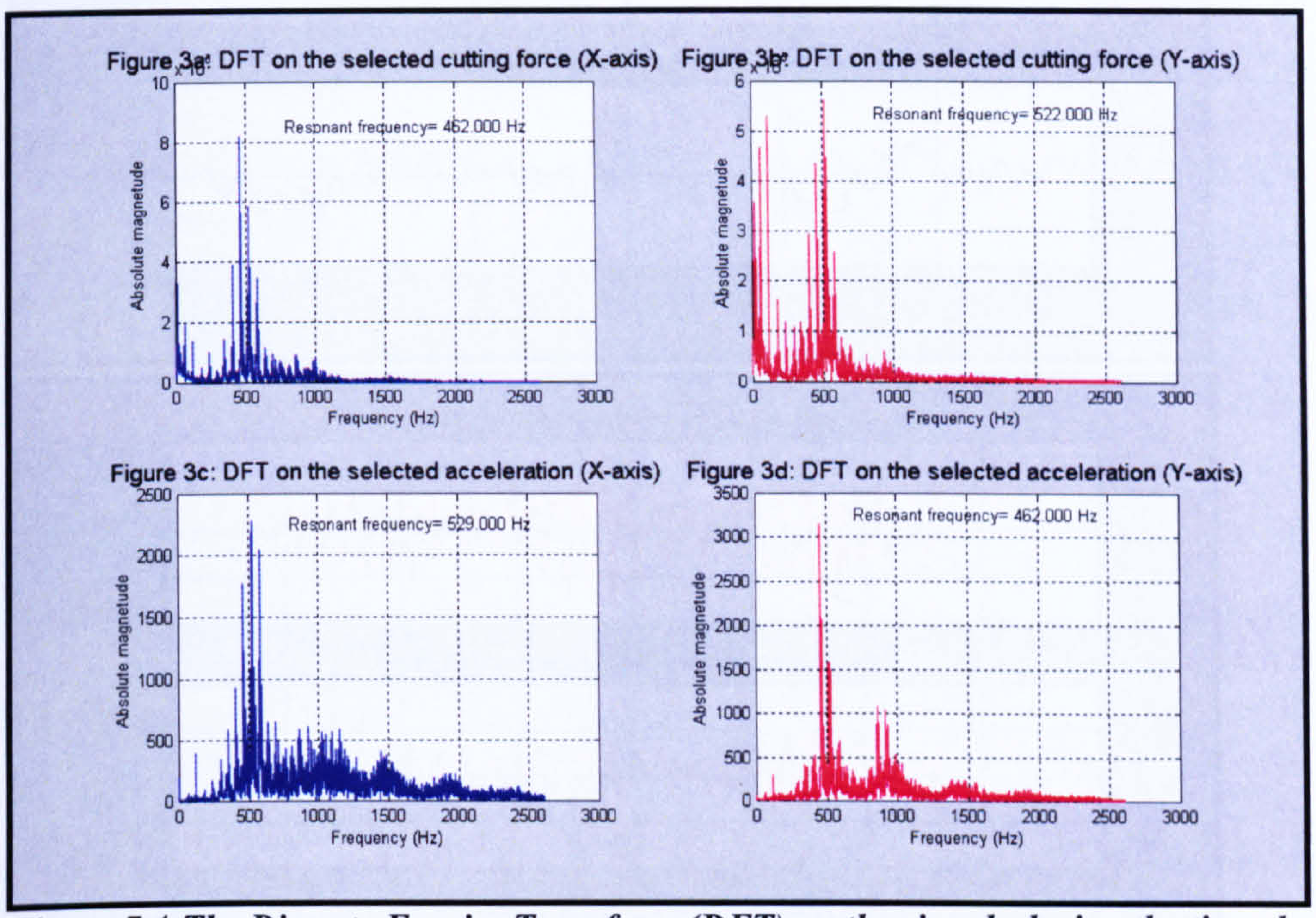

Figure 7.4:The Discrete Fourier Transform (DFT) on the signals during the time the machine was chattering

The chatter frequencies are the same as on the tests recorded earlier during the first cutting trials (refer to chapter 5.6). It is also interesting to see how a comparison between the spectrum of the cutting force and acceleration clearly shows how the mechanical structure amplifies the excitation forces. With the use of the table dynamometer and accelerometer it was possible to confirm the statement made in chapter 6, that the headstock of the machine had a structural resonance at about 300Hz.

In order to obtain the vibration displacement, the acceleration signal needed to be integrated twice. MATLAB routines were written for all off line signal processing. The easiest way of integrating a digital signal is simply to add the signed samples together (running sum).

More sophisticated methods for the accumulated integration are the trapezoidal rule or a polynomial function to interpolate between two successive samples (cubic spline interpolation). The literature by Smith [95] and Etter [144] is recommended here.

The trapezoidal rule has been used here and figure 7.5 shows the processed acceleration signal of the X and Y-axis.

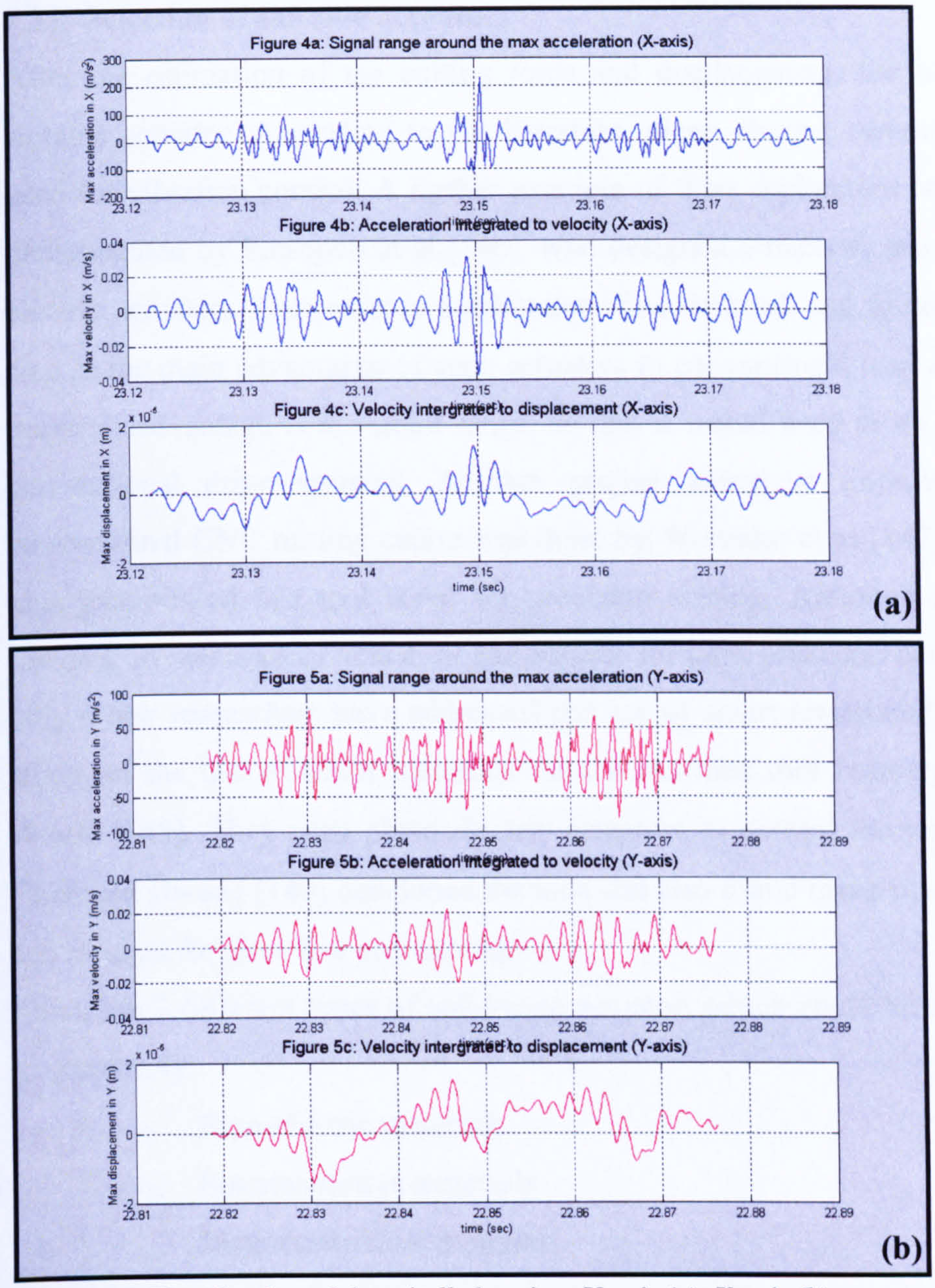

Figure 7.5:The vibration of the spindle housing; X-axis (a); Y-axis (b)

In order to prevent any DC components building up in the accumulator, by the integration of the discrete signal, high pass filters were used (the positive area of a signal with a fixed sampling frequency never exactly the matches the negative area). Another method would be to re-sample the signal again with a random step size or use zero averaging, where all the samples are added together, divided by the number of samples and subtracted to form each new sample value [145]. The higher the sampling frequency or the more sophisticated the integration method is the less important this problem becomes.

The measured maximum displacement during chatter on the spindle housing was about:

- 17μm peak to peak for the X axis
- 10μm peak to peak for the Y axis

7.3 Selection of suitable actuators

After the estimation of the cutting force and displacement, the next task was to select a suitable actuator. According to the literature, piezo electric ceramics have repeatedly been used for vibration control. A further example of their application on machine tools has been demonstrated by Pinsopon et al [146], who designed a nano-metric toolpost based on piezo-electric actuators. They refer to the features of no backlash and friction, large forces and small size as the main advantages of such actuators to conventional lead and ballscrew drives. The major disadvantage is the small range, so that it would need to be used in conjunction with conventional drive systems. Another project aimed at improving the accuracy of a conventional CNC turning centre was done by Woronko et al [147]. They designed a single axis piezo-based fast tool servo for precision turning. Although there has been extensive research in precise tool actuation and control for ultra precision diamond turning machining, only a few researchers have addressed the use of smart materials [147]. Another interesting study on the use of smart materials for the machine tool industry was done by Golz and Weule [148]. They used piezo electric actuators to control the preload of a ballscrew nut. Chen and Dwang [149] developed the idea and also found that a piezo electric active ballsrew can be used for ultra fine positioning.

There are 3 different types of solid-state actuator, which could be used for this project (refer to chapter 4):

- Piezoelectric materials
- Electrostrictive materials
- Magnetostrictive materials

Although the strains, stresses and reaction times are comparable [81], the most traditional and proven actuator for vibration control is the piezoelectric type. These are widely available, linear, temperature stable and low-cost in comparison to the others, and also offer the highest efficiency. They do not need any additional energy to hold their static displacement in comparison to the electrostrictive and magnetostrictive actuators, which rely on a constant electric or magnetic field. But the main reason why piezo-electric actuators was selected in this project is that they are the most established and most commercially available smart actuator.

The use of piezoelectric materials was discovered by Pierre and Jacques Curie in 1880. They found that pressure applied to certain crystalline materials (ceramics) creates an electrical

charge and called it the direct piezo electric effect. The word piezo is derived from the greek word for pressure (piezein – to press). Later they also found that an electrical field applied to a crystal would lead to a deformation of the material. This effect is referred to as the inverse piezo effect. For more than 30 years these effects remained little more than scientific curiosity. Then during World War I, when tools for detecting submarines were needed, quartz plates were used to emit high frequency sound waves under water. Their echo was again received with quartz plates. These ultrasonic submarine detectors represented the beginning of echo sounding, and the first commercial product, which made use of both the direct and inverse piezoelectric effect. The discovery of piezoelectricity in PZT (lead titanium-zirconate) in the late 1960's lead to actuators, which have changed the world of precision positioning.
Materials which exhibit the piezoelectric property are intrinsic piezoelectric monocrystals, such as quartz, Rochelle salt and "man made" artificially polarised ferroelectric ceramics, which contain mixtures of different compounds such as barium titanate, lead zirconate and lead metaniobate [86].
One of the leading suppliers for ultra-precision motion control systems and NanoPositioning technology for more than 30 years is PI (Physik Instrumente) GmbH & Co. They also offered the most powerful piezo electric actuator (High Voltage PZT) and the expertise needed to make the right judgement about the actuator required for this project. Their products are also often used by other researchers [62] and they are referred to in almost any design study of smart structures. The PI catalogue [90] is a good reference for any background reading about the theory of piezoelectric materials and products.
In this project a stack actuator, for producing linear motion, was selected. Figure 7.6.a shows such a PZT actuator and figure 7.6.b an equivalent circuit diagram.

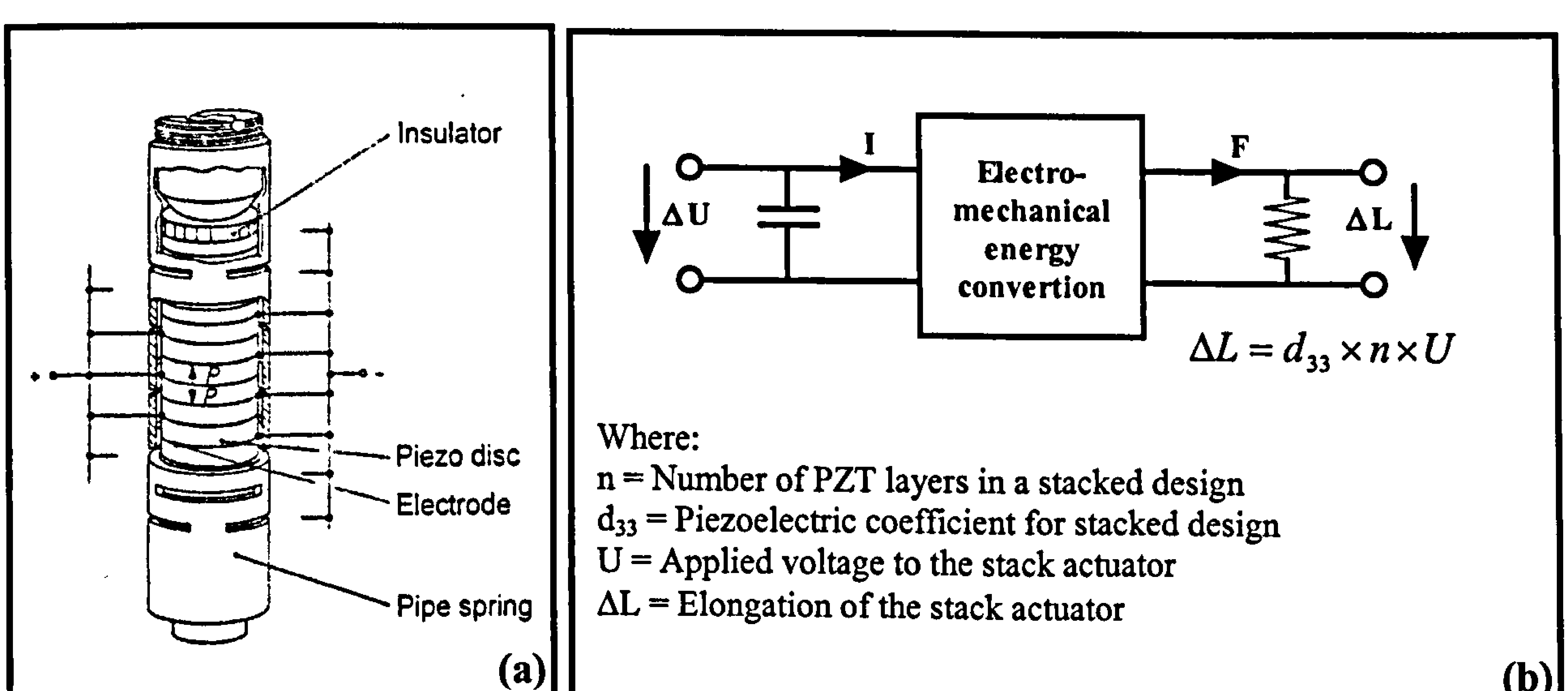

Figure 7.6: A piezoelectric stack transducer (a) and the energy conversion of a PZT

In order to meet the required displacement and bandwidth requirements and also to withstand the estimated cutting forces a High Voltage PZT (HVPZT) with the following characteristics was chosen (it is the best compromise to meet the required specifications):

- 10 μm maximum displacement
- 580N/μm large signal stiffness
- 180 nF electrical capacitance
- Push and pull force capacity 12500/2000N
- 280g of weight
- 11 kHz unloaded resonance frequency (f_0)

Next some fundamental mechanical considerations of PZT actuators are discussed since they played a vital role in the design of the active work-piece holder and the HVPZT selection.
For dynamic applications (push and pull forces) the piezo actuator must be pre-loaded since the ceramic can only resist compression forces - not tensile forces (the selected actuator is already pre-loaded with an internal spring). The stiffness of the ceramic varies depending on the electrical load. The given large signal static stiffness can be used as a reference for the design. Because of this finite stiffness of the piezo ceramic, it depends on the stiffness of the load how much force or displacement the actuator produces. If the ceramic presses against an infinite rigid constraint, then it will produce maximum force (*blocked force*) but no displacement (the ceramic will compress in itself to produce its displacement). If on the other hand the actuator presses against no spring load, it does not generate any force but maximum displacement. It is helpful to think that the piezo ceramic is nothing other than a spring (constant stiffness), whose force and displacement can be controlled by an electrical field (supply voltage).
Figure 7.7 illustrates this on a spring pre-loaded stack actuator.

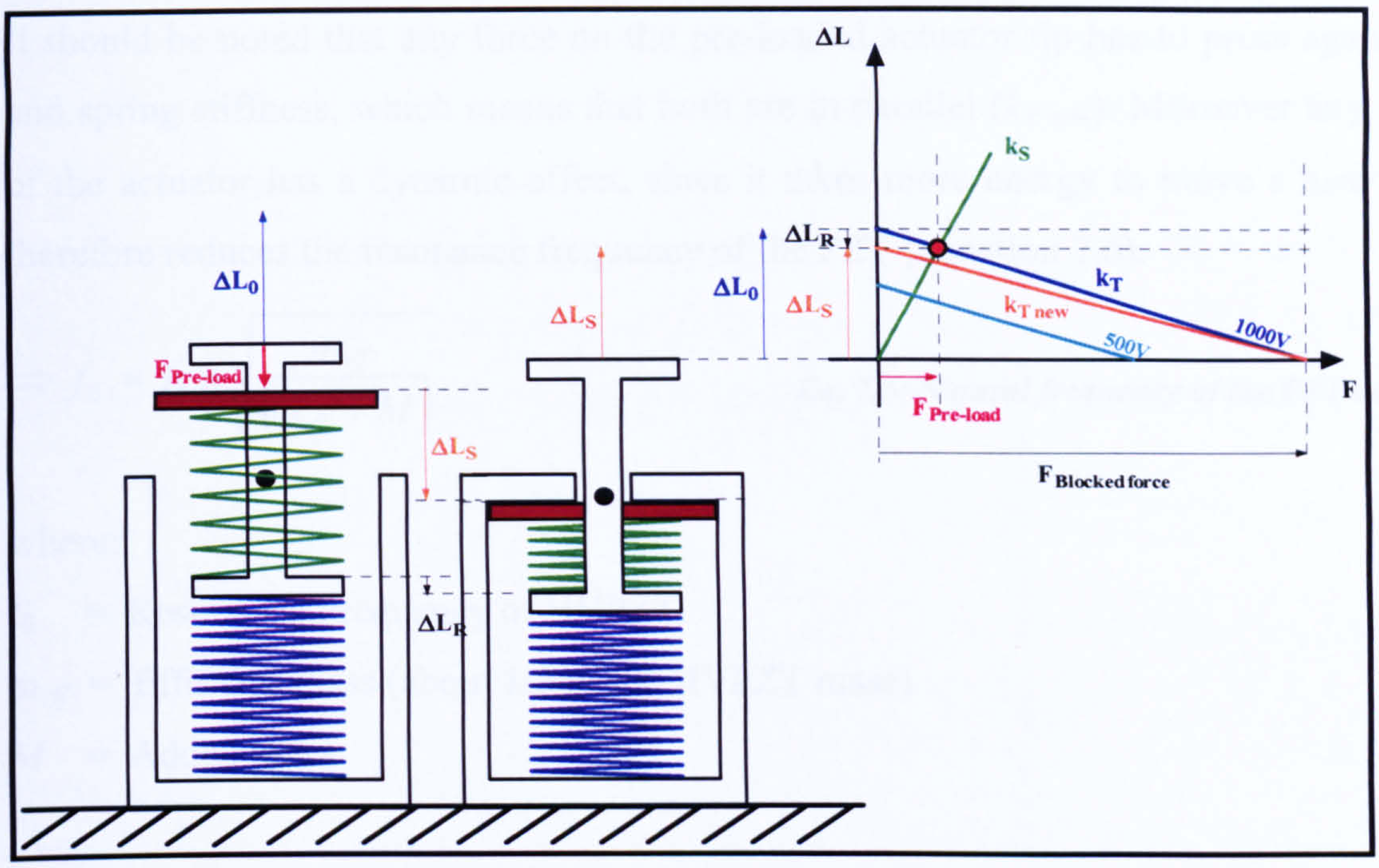

Figure 7.7: Pre-loading the PZT stack actuator with a spring

The applied preload force, acts on both the stiffness of the PZT actuator and pre-load spring and therefore are in a serial arrangement.

$$F_{pre-load} = F_T = F_S$$

$$\Delta L_0 \times \frac{k_T k_S}{k_T + k_S} = \Delta L_R \times k_T = \Delta L \times k_S$$

$$\Rightarrow \Delta L = \Delta L_0 \times \frac{k_T}{k_T + k_S}$$ **_Eq. 7.4: PZT displacement with spring load_**

$$\Rightarrow \Delta L_R = \Delta L_0 \times \left(1 - \frac{k_T}{k_T + k_S}\right)$$ **_Eq. 7.5: Lost displacement caused by the spring load_**

where:

ΔL = Remaining displacement with external spring load

ΔL_0 = Nominal displacement with no external spring load

ΔL_R = Lost displacement caused by the external spring load

$F_{pre\text{-}load}$ = Preload force

F_T = Force acting on the actuator

F_S = Force acting on the external spring

k_S = Spring stiffness

k_T = PZT actuator stiffness

$k_{T\,new} = k_T + k_S$ = New pre-loaded actuator stiffness

It should be noted that any force on the pre-loaded actuator tip has to press against the PZT and spring stiffness, which means that both are in parallel ($k_{T\,new}$). Moreover any added mass of the actuator has a dynamic effect, since it takes more energy to move a heavier mass. It therefore reduces the resonance frequency of the PZT (equation 7.6).

$$\Rightarrow f_0' = f_0 \times \sqrt{\frac{m_{eff}}{(m_{eff} + M)}}$$

Eq. 7.6: Natural frequency of the PZT actuator system

where:

f_0 = Resonance Frequency of HVPZT

m_{eff} = Effective mass (about 1/3 of the HVPZT mass)

M = Added mass

All these considerations have been taken into account for the selection of HVPZT actuators, and the design of the active work-piece holder, which follows next.

7.4 Mechanical design of the active work-piece holder

The system was designed to be universal and relatively easily fitted on a variety of vertical machining centres. This will prevent a major re-design of the machine, which was not an option since the machines in the workshop are regularly used for machining and research. The re-design of a machine headstock for example would have prevented any serious structural and condition monitoring research on the machine over a period of time.

Because of this, the most convenient solution would be a system, which adds the necessary further 2-degrees of freedom to the machine, by allowing the work-piece to move in two directions. This active vibration platform could then be fitted to any existing machining table, without any modifications. The disadvantage of this approach is that the mass of the work-piece varies significantly, whereas the weight of the cutting tool does not. As already seen, any added mass has an effect on the dynamic response of the actuator. For a commercial solution it would be better to integrate the PZT actuator in the headstock. This is more easily done on a turning machine (toolpost), which is the reason why most research on machine tool vibration control was done on lathes and boring bars rather than milling machines. However, the designed system should demonstrate that adaptive active vibration control can not only reduce the vibration level of a single point cutting operation (static) but also of an multi-point cutting operation (time varying). As already mentioned the system would also be useful for research on the cutting process and surface finish of a milling operation, since its integrated sensors also allow the cutting force, displacement and acceleration to be directly monitored. Figure 7.8 shows the finished product of the universal active work-piece holder, which is able to counteract static and dynamic deflections caused by the cutting process. The AutoCAD drawings of the full design are included in the appendix B.

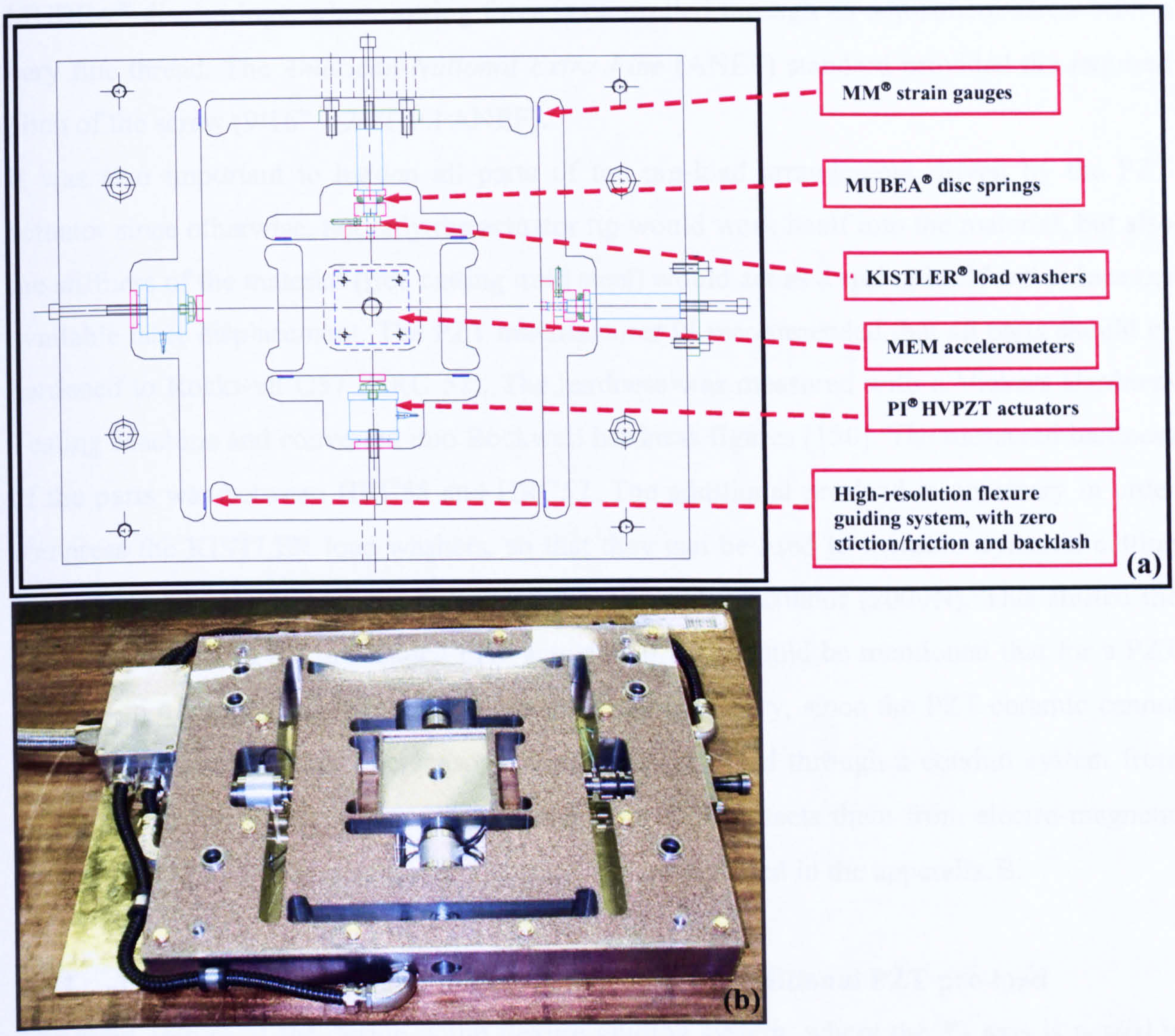

Figure 7.8: The design of the universal active work-piece holder for vertical machining centres (2 degrees of freedom): The design Lay-Out (a) and the actual system after being built (b)

The system is protected from cutting fluid and hot chips through a perspex cover and ground brass base. Each actuator moves its axis through a flexure guide system, which allows high resolution since it does not suffer from any stiction, friction and backlash, like conventional ball- and leadscrew systems. A single axis of the flexure guide system is very flexible in the proposed direction of movement but restricted or very stiff in the other two directions (figure 7.8.a). Both axes are coupled through a sophisticated design, where the inner axis is nested into the outer axis (figure 7.8). This reduces the weight to be moved significantly but also keeps the dimensions much smaller. Therefore the inner table, where the work-piece is mounted, will move in two-axes (X- and Y- axis on the machine), the middle frame only in one axis (X-axis) and the outer reference frame, not at all. In order to allow movement, even under large cutting forces in the Z direction, the outer reference frame rests on shim steel (200μm). The necessary additional preload of the PZT actuators can be provided through MUBEA® disc springs, whose spring force is controlled through an adjustment screw with a very fine thread. The *American National Extra Fine* (ANEF) standard provided the required pitch of the screw (9/16" – 24 T.P.I ANEF).

It was also important to harden all parts of the pre-load arrangement driven by the PZT actuator since otherwise, not only the actuator tip would work itself into the material, but also the stiffness of the material (free cutting mild steel) would act as a spring itself and reduce the available table displacement. The PZT manufacturer PI recommended that all parts should be hardened to Rockwell C57 (HRC 57). The hardness was measured with a Vickers Hardness Testing Machine and converted into Rockwell hardness figures [150]. The measured hardness of the parts was between HRC55 and HRC57. The additional pre-load is necessary in order compress the KISTLER load washers, so that they can be used to measure dynamic cutting forces, and also to increase the pull force capacity of the actuator (2000N). This shifted the operational point of the pre-loaded PZT actuator. It also should be mentioned that for a PZT actuator in a pre-load arrangement, a special tip is necessary, since the PZT ceramic cannot stand any bending forces. The sensor cables were protected through a conduit system from Adaptaflex®, which not only prevents damage but also protects them from electro-magnetic interference (EMI). The most important drawings are included in the appendix B.

7.4.1 High resolution flexure guide way system and additional PZT pre-load

The main feature of the design is the flexure guiding system, where the Y- axis is nested in the X-axis. The small maximum stroke of the PZT, about 10μm, can easily be covered by this approach. This guide system was designed so that:

- The additional guide way stiffness does not exceed an overall pre-load stiffness of 20% of the PZT stiffness [90].
- The flexure, in the constrained directions, is stiff enough to withstand the cutting forces.
- The flexure, in the moving direction is flexible enough so that it does not break due to periodic bending stresses.

7.4.1.1 The mathematical model and given parameters for the flexure guiding system

It was decided to model this flexure analytically, rather than using FEM. Although the configuration is very uncommon a suitable model was eventually found [151].

The guide system of a single axis consists of 4 bridges, which can be seen as a cantilever beam with a thrust bearing on one side and a plain bearing on the other (Figure 7.9.a and b).

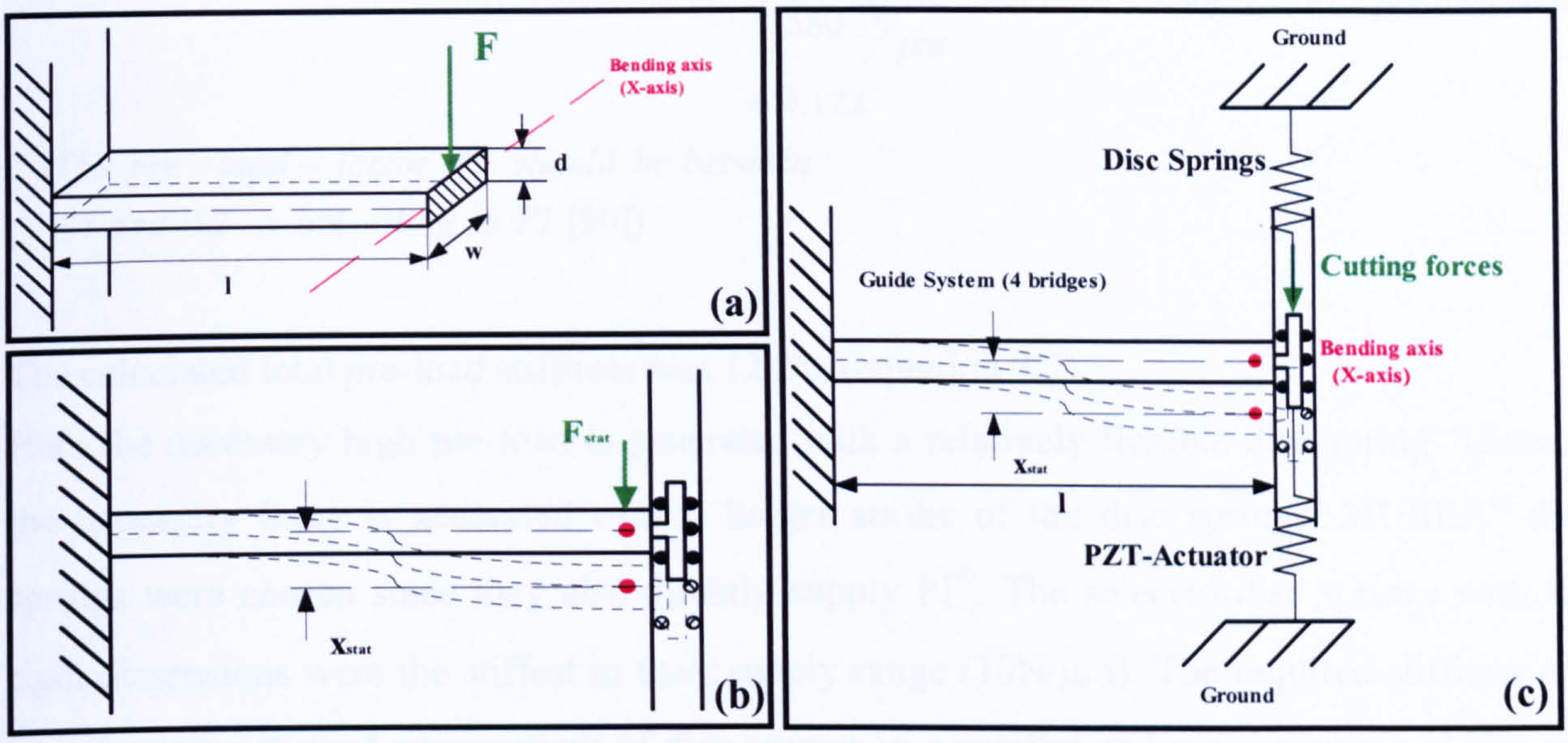

Figure 7.9: The flexure guiding system:

- ***Dimensions of a single bridge (a)***
- ***General simplified model of a single bridge (b)***
- ***Specific simplified model of an assembled single bridge (c)***

Figure 7.9.c shows the assembled arrangement of a single flexure. As explained earlier, if the PZT presses against an elastic load (stiffness of the PZT >> stiffness of the load) the force generation of PZT will be small but its movement maximal. If it presses against an infinitely stiff load (stiffness of the PZT << stiffness of the load), then it will act as a force generator, but without movement. A PZT preload of 20%, of the PZT stiffness, was recommended [90]. This and the fact that the flexure system must be flexible enough to allow for the given motion, but stiff enough not to break under the cutting forces provided the starting point for the design (it can be seen from figure 7.9.c that the stiffness of the guide system and the stiffness of the disc springs are in parallel):

$$- \textit{Stiffness PZT actuator}: \qquad k_{PZT} = 580 \frac{N}{\mu m}$$

$$- \textit{Stiffness disc springs}: \qquad k_{DS} = 10 \frac{N}{\mu m}$$

$$- \textit{Stiffness guide system}: \qquad k_{GS} = 55 \frac{N}{\mu m}$$

$$- \textit{Stiffness per cantilever bridge}: \qquad k_{CB} = \frac{k_{GS}}{4}$$

$$\textit{Stiffness of the total pre-load:}\quad k_{PL} = k_{DS} + k_{GS} = k_{PZT} \times PF$$
$$= 10\frac{N}{\mu m} + 55\frac{N}{\mu m}$$
$$= 65\frac{N}{\mu m}$$
$$PF = \frac{65\ {N}/{\mu m}}{580\ {N}/{\mu m}} \qquad \textit{Eq. 7.7: PZT pre-load factor}$$
$$= 0.122$$

$(\textit{The pre-load-factor PF should be between}$
$0.1 \textit{ and } 0.2 \rightarrow \textit{according to PI}$ [90])

The calculated total pre-load stiffness was 12.2% (equation 7.7).
Here the necessary high pre-load is generated with a relatively flexible disc spring. Thereby the necessary force is generated over a longer stroke of the disc springs. MUBEA® disc springs were chosen since they also directly supply PI®. The selected disc springs with the right dimensions were the stiffest in their supply range (10N/µm). The required stiffness can be set using a stacked arrangement of disc springs in a parallel and serial network [152], and the pre-load force generated within the linear region of the spring (25%-75% of the maximum stroke) [153]. Special lubrication from KLÜBER Lubrication KG was necessary for any combination of stacked disc springs, under dynamic load.
The total spring load on the actuator reduced the maximum stroke to (equation 7.8):

$$\Delta L = Max.\ stroke - PF \times L_0$$
$$= 10\mu m - 0.122 \times 10\ \mu m \qquad \textit{Eq. 7.8: Reduced PZT stroke}$$
$$= 8.88\ \mu m$$

After the pre-loading of about 3000N through the disc springs (which changed the push pull capacity of the PZT actuator to 9500/5000N) the guide system should have zero deflection (initial state). This also means that the initial stress on the guide system also is zero:

$$x_{init} = 0\ \mu m$$
$$\sigma_{init} = 0\ {N}/{mm^2}$$

The maximum displacement of one MUBEA 10N/μm disc-spring is 0.45mm. To achieve 3000N the disc spring will deflect about 0.3mm. This is 50% of its maximum deflection, which is the most linear operating point of a disc spring. However, in order to increase the resolution of the fine threaded pre-load adjustment screw by a factor of 2, a serial stacked arrangement of 2 disc springs was chosen.

The measured maximum cutting forces from the chatter test on the Beaver machine were:

$$\vec{F}_{Stat} = |F_{Stat}| \approx 1900N$$
$$\vec{F}_{Dyn} = |F_{Dyn}| \approx 2800N$$

The dynamic cutting forces may be quite a bit smaller than this, since only the maximum values of the forces in X and Y are added together to form the dynamic force vector. In order to calculate this more precisely the recorded samples of the forces at a certain time needed to be added together to form the dynamic force vector. Therefore the dynamic cutting force estimation taken here already includes a safety factor.

Next the thickness d of each single flexure bridge of the guide system needed to be estimated using the mathematical model and the following dimensions (refer to figure 7.9.a):

$$l = 30\ mm$$
$$w = 45\ mm\ (\textit{given through the the PZT diameter})$$
$$d = \textit{The estimated thickness of each flexure bridge}$$

$$k_{CB} = \frac{12 \times E\, I}{l^3} \left[\frac{N}{m}\right]$$

$$I_{xx} = \frac{w \times d^3}{12} \left[m^4\right]$$

$$= \textit{Second moment of inertia for the beam cross section}$$
$$(\textit{Bending around its most flexible axis})$$

Eq. 7.9: Second moment of inertia of the flexure

$$k_{CB} = \frac{E \times w \times d^3}{l^3} \quad (\textit{E is the Young Modulus of mild steel})$$

Eq. 7.10: Stiffness of a single flexure of the guiding system

$$d = \frac{l}{\sqrt[3]{\dfrac{E \times w}{k_{CB}}}}$$

$$= \frac{30\ mm}{\sqrt[3]{\dfrac{210000\ N/mm^2 \times 45\ mm}{\frac{55}{4}\ N/\mu m \times 1000\ \mu m/mm}}}$$

$$\underline{\underline{d = 3.399\ mm}}$$

The model is valid if the length l is substantially higher than the transverse dimensions d. This means that the bending stresses dominate the shearing stresses (see next section).

7.4.1.2 Prediction of the maximum stresses in the flexure guiding system

In order to carry out a fatigue stress analysis of the flexure guide system, the maximum stress of the guide system under "chatter" conditions (dynamic and static) needed to be estimated. The next step was to calculate the table deflection under the static cutting forces of 1900N. It should be remembered that the initial deflection is zero, so that the initial stress of the guide system is also zero.

Figure 7.10 shows the simplified model and the redundant force after *"freeing"* or *"opening"* the system (the resultant force of any static system is zero - static equilibrium):

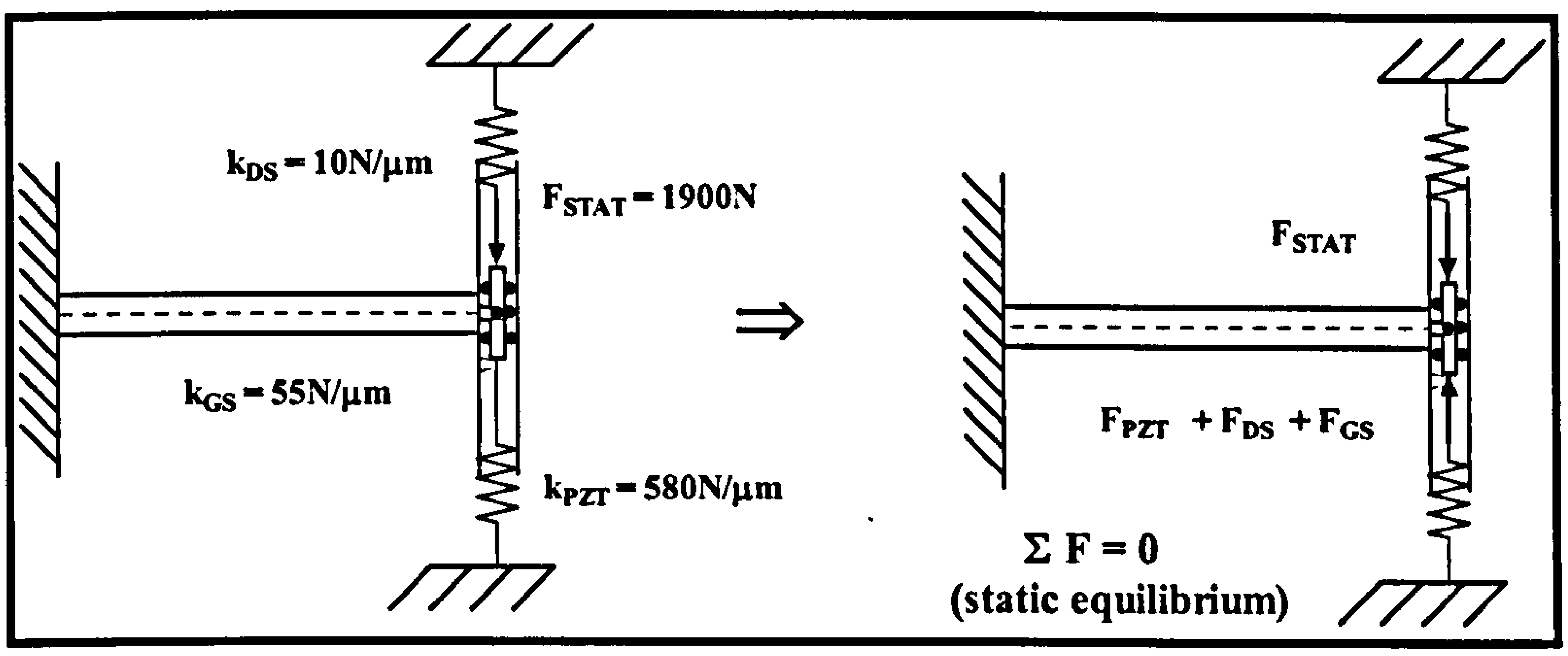

Figure 7.10: The simplified model and redundant forces after freeing or opening the system.

The stiffness of disc springs, guide system and PZT actuator are in parallel, which means the overall stiffness is the sum of the individual stiffness. MATLAB routines were written to calculate the following equations more efficiently.

$$
\begin{aligned}
&\Sigma F_{Stat} = 0\\
&-F_{Stat} + F_{Stat\,PZT} + F_{Stat\,DS}\ F_{Stat\,GS} = 0\\
&x_{Stat} \times k_{PZT} + x_{Stat} \times k_{DS} + x_{Stat} \times k_{GS} = 0\\
&x_{Stat} \times (k_{PZT} + k_{DS} + k_{GS}) = F_{Stat}
\end{aligned}
$$

$$
\begin{aligned}
x_{Stat} &= \frac{F_{Stat}}{k_{PZT} + k_{DS} + k_{GS}}\\
&= \frac{1900N}{(580 + 10 + 55)\ N/\mu m}\\
&= \underline{\underline{2.94\ \mu m}}
\end{aligned}
$$

Eq. 7.11: The estimated static deflections due to the cutting forces

Next the maximum bending stresses in the guide system were estimated. The highest stresses occur at the support end of each cantilever bridge as figure 7.11 illustrates.

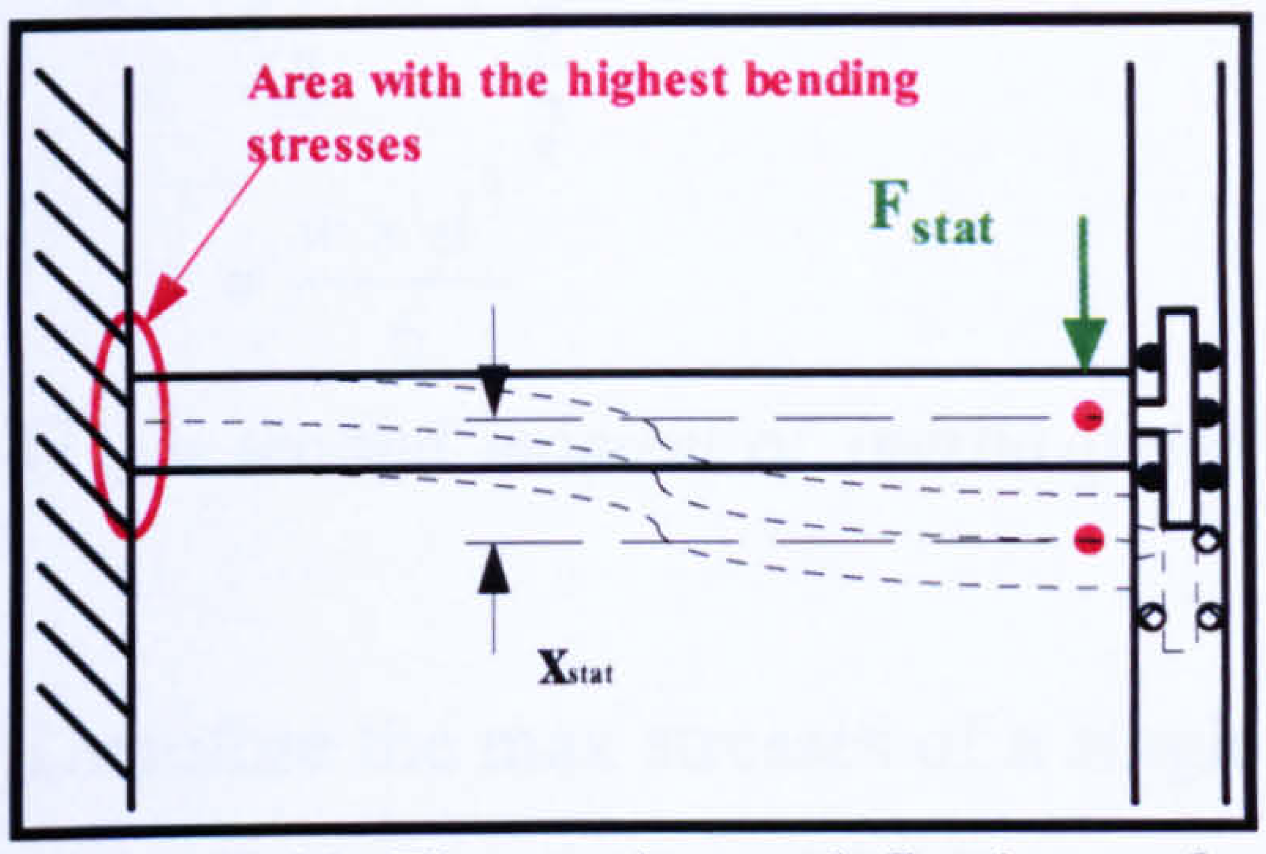

Figure 7.11: The maximum deflection and stress in a single cantilever flexure bridge

First the force component acting on each individual cantilever bridge was calculated.

$$
\begin{aligned}
F_{Stat_{GS}} &= k_{GS} \times x_{Stat} \\
&= 55\frac{N}{\mu m} \times 2.94\mu m \\
F_{Stat_{GS}} &= 161.7\ N
\end{aligned}
$$

Eq. 7.12: Static force component on a single flexure

$$
\begin{aligned}
F_{Stat_{CB}} &= \frac{F_{Stat_{GS}}}{4} \\
&= \frac{161.7}{4} \\
F_{Stat_{CB}} &= 40.43\ N
\end{aligned}
$$

The maximum stress level due to bending of a cantilever beam is:

$$\sigma_{b_{\max}} = \frac{M_{b_{\max}}}{W_b}$$

Eq. 7.13: The maximum bending stresses

(W_b = section modulus of a cantilever beam due to bending [mm^3])
($M_{b_{max}}$ = Maximum bending torque of a cantilever beam [Nm])

The section modulus of a single cantilever bridge can be calculated as:

$$W_b = \frac{I}{d/2}$$

Eq. 7.14: The section modulus

For a solid rectangular cross section of the bridge with the neutral axis in the centre of this cross section, the section modulus of our cantilever bridges can be calculated (using equation 7.9 and 7.14) to be:

$$W_{bx} = \frac{I_{xx}}{d/2} = \frac{\frac{w \times d^3}{12}}{\frac{d}{2}} = \frac{w \times d^2}{6}$$

Eq. 7.15: The section modulus of a single flexure

$(I_{xx} = second\ moment\ of\ inertia\ of\ the\ cantilever\ bridge\ [mm^4])$

Therefore the max stresses of a single bridge under the static cutting forces can be calculated (using equation 7.13 and 7.15) to:

$$\sigma_{b_{max}} = \frac{M_{Stat_{b_{max}}}}{W_{bx}} = \frac{F_{Stat_{CB}} \times l}{\frac{w \times d^2}{6}} = \frac{40.43N \times 30mm \times 6}{45mm \times 3.4^2\ mm^2}$$

$$\underline{\underline{\sigma_{Stat_{b_{max}}} = 13.99 \frac{N}{mm^2}}}$$

Eq. 7.16: The maximum bending stresses due to the static cutting force

Apart from the bending stresses there will also be shearing stresses, which compensates for the shearing forces in the cantilever bridges. In this case these shearing stresses have a maximum at the neutral axis. For a rectangular cross section the maximum shearing stress can be calculated as [151]:

$$\tau_{q_{max}} \approx \frac{3}{2} \times \frac{F_q}{A} \qquad (A = cross\,section \quad ; \quad F_q = shear\ forces)$$

$$\left|\tau_q\right|_{max} = 1.5 \times \frac{40.43N}{45mm \times 3.4mm}$$

$$\left|\tau_q\right|_{max} = 0.396 \frac{N}{mm^2}$$

Eq. 7.17: The estimated shearing stresses

This is approximately 2.8% of the maximum bending stresses, which means that the shearing stresses for our configuration can be neglected. More commonly it can be said that the shearing stress can always be neglected if the length *l* is substantially greater then the transverse dimensions [151]. The dynamic stresses were calculated in exactly the same way. Figure 7.12 shows the predicted deflection and stresses of a single flexure due to the chatter vibration at 450Hz on the machine.

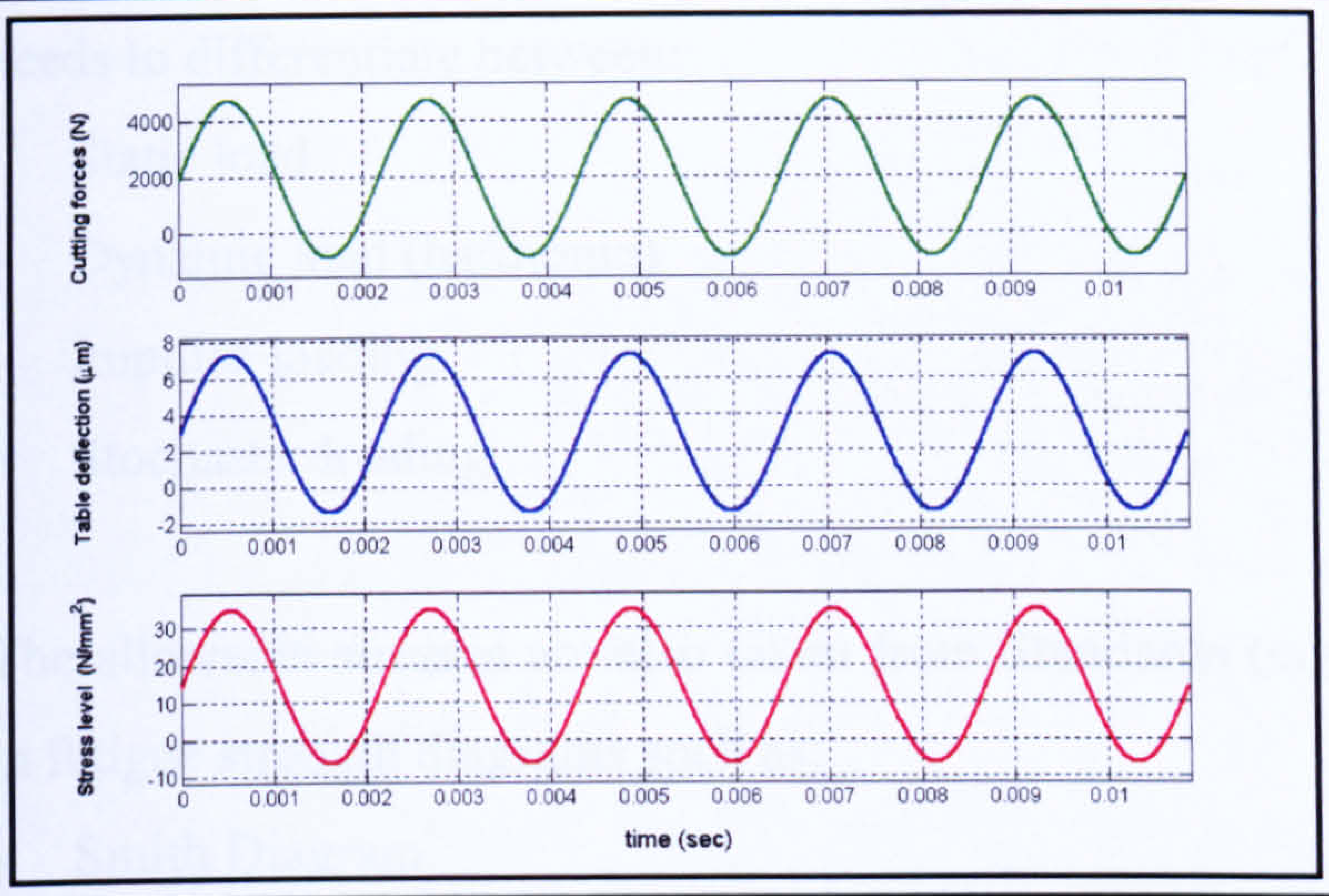

STATIC:

$F_{Stat} = 1900N$

$x_{Stat_{max}} = 2.94\ \mu m$

$\sigma_{Stat_{max}} = 13.99\ \dfrac{N}{mm^2}$

DYNAMIC:

$F_{Dyn} = {}^{+}\!/_{-}\,2800N$

$x_{Dyn_{max}} = {}^{+}\!/_{-}\,4.34\mu m$

$\sigma_{Dyn_{max}} = {}^{+}\!/_{-}\,20.65\dfrac{N}{mm^2}$

Figure 7.12: The predicted deflection and stresses due to the 450Hz chatter forces on the milling machine

7.4.1.3 The predicted factor of safety for the flexure guide system

For the design of the flexure guiding system it is important to include a safety factor for the fatigue limit. In general this, is a security index to make sure that the predicated stresses do not exceed the maximum allowable stresses of the material and give enough confidence that a design still works, not just under operational conditions but also over time and with extreme loads, which may occur. Other factors, which result in design tolerances are, for example poor, or not well-specified materials, material tolerances, dimension tolerances and poor surfaces.

In general:

$$\sigma_{calculated} \leq \sigma_{allowed} = \frac{K}{S}$$

Eq. 7.18: The allowed stresses including safety factor

where:

$\sigma_{calculated}$ = The calculated stresses of the design (analytically or numerically using FEM)

$\sigma_{allowed}$ = The guaranteed allowed stresses for the applied loading case

K = Material characteristics including form factors and surface quality factors found in mechanical handbooks

S = Safety factor depending on the loading case for the particular design (e.g. static and dynamic bending). S can be found in the appropriate standard (e.g. for bridges, buildings, aeroplanes etc.)

The allowed stresses are dependent on the kind of load the component has to withstand. It needs to differentiate between:

- Static load
- Dynamic load (harmonic)
- Impulse loading
- Stochastic loading

The allowable stresses are also taken from Standards (e.g. DIN10025) and can be illustrated in fatigue strength diagrams such as:

- Smith Diagram
- Haigh Diagram
- Wöhler Digram

Figure 7.13, for example, shows the *Smith Diagram* [154].

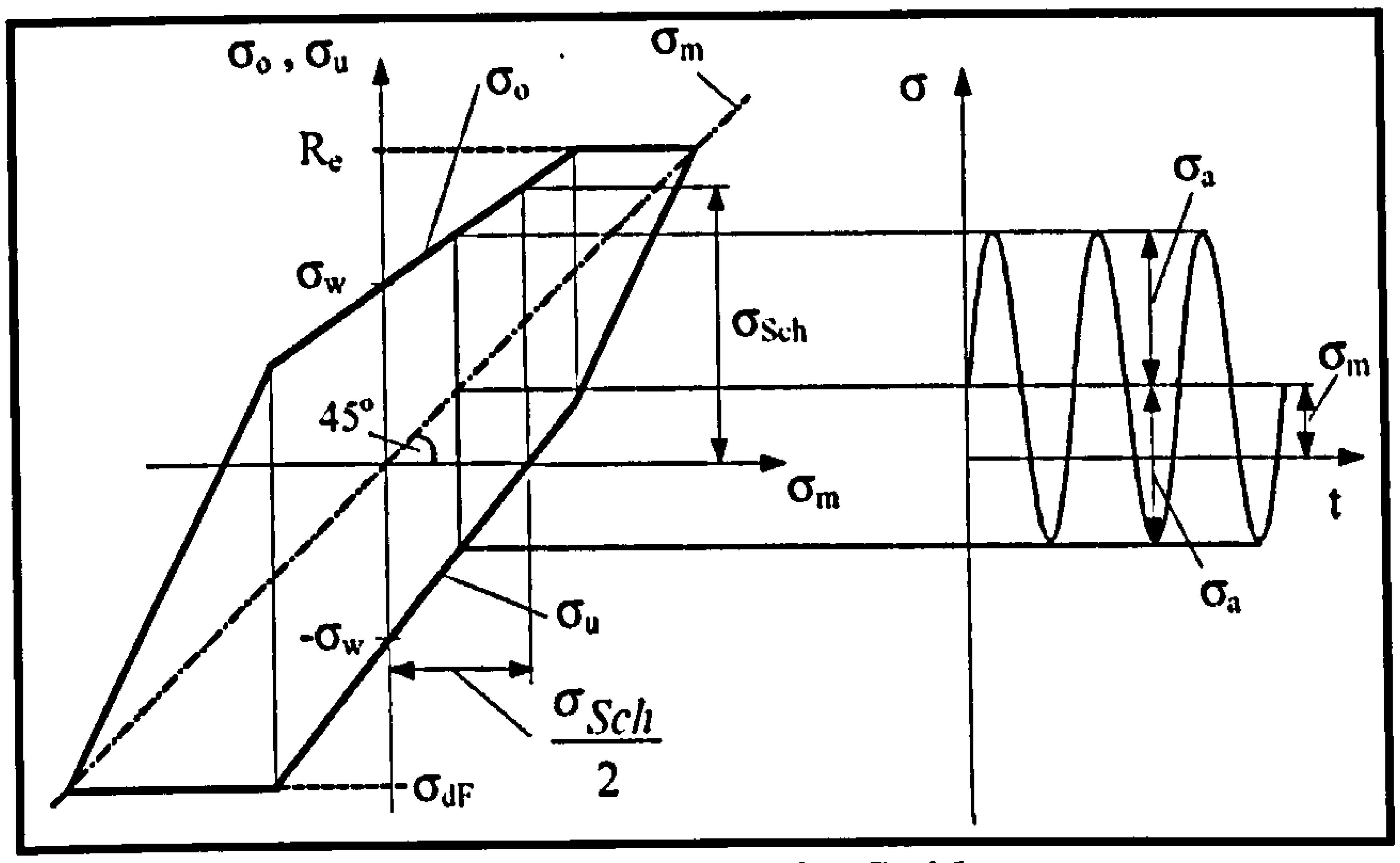

Figure 7.13: Fatigue strength diagram after Smith

Each material will have 3 different diagrams depending on the test:

- Axial load fatigue testing
- Bending load fatigue testing
- Torsion load fatigue testing

These diagrams are the results of intensive experiments on standard probes and recorded in databases and handbooks. To predict the allowable stresses for the flexure guiding system the DIN EN 10025 standard was used.

Here the static and dynamic material strengths of S235JR or St37 (mild steel) were:

General:	*Axial loading*:	*Bending loading*:	*Torsional loading*:
$R_e = 235 \, N/mm^2$	$\sigma_{zdF} = R_e$	$\sigma_{bF} = 330 \, N/mm^2$	$\sigma_{tF} = 135 \, N/mm^2$
$R_m = 340 \, N/mm^2$	$\sigma_{zdW} = 140 \, N/mm^2$	$\sigma_{bW} = 170 \, N/mm^2$	$\sigma_{tW} = 100 \, N/mm^2$
	$\sigma_{zdSch} = 225 \, N/mm^2$	$\sigma_{bSch} = 305 \, N/mm^2$	$\sigma_{tSch} = 135 \, N/mm^2$

In order to compare the calculated stresses with the allowable stresses from the DIN norm, the Smith Diagram was used. The calculated maximum stresses from the last section:

$$\sigma_m = \sigma_{Stat_{\max}} = 13.99 \, N/mm^2$$

$$\sigma_a = \sigma_{Dyn_{\max}} = +/- \, 20.65 \, N/mm^2$$

These values can now be used in order to construct the Smith Diagram to illustrate the safety factor. The construction is best done through commercially available material database software, which uses calculated stress values and the material parameters (given by the DIN norm) as input parameters. Figure 7.14 shows the constructed diagram of WST1 [155]. Unfortunately they are in German, but it shows the Smith-Diagram for bending (Smith-Diagram Biegung). Other Diagrams of the software include the Stress-strain graph, Smith-Diagram for axial loading and Smith-Diagram for torsional loading.

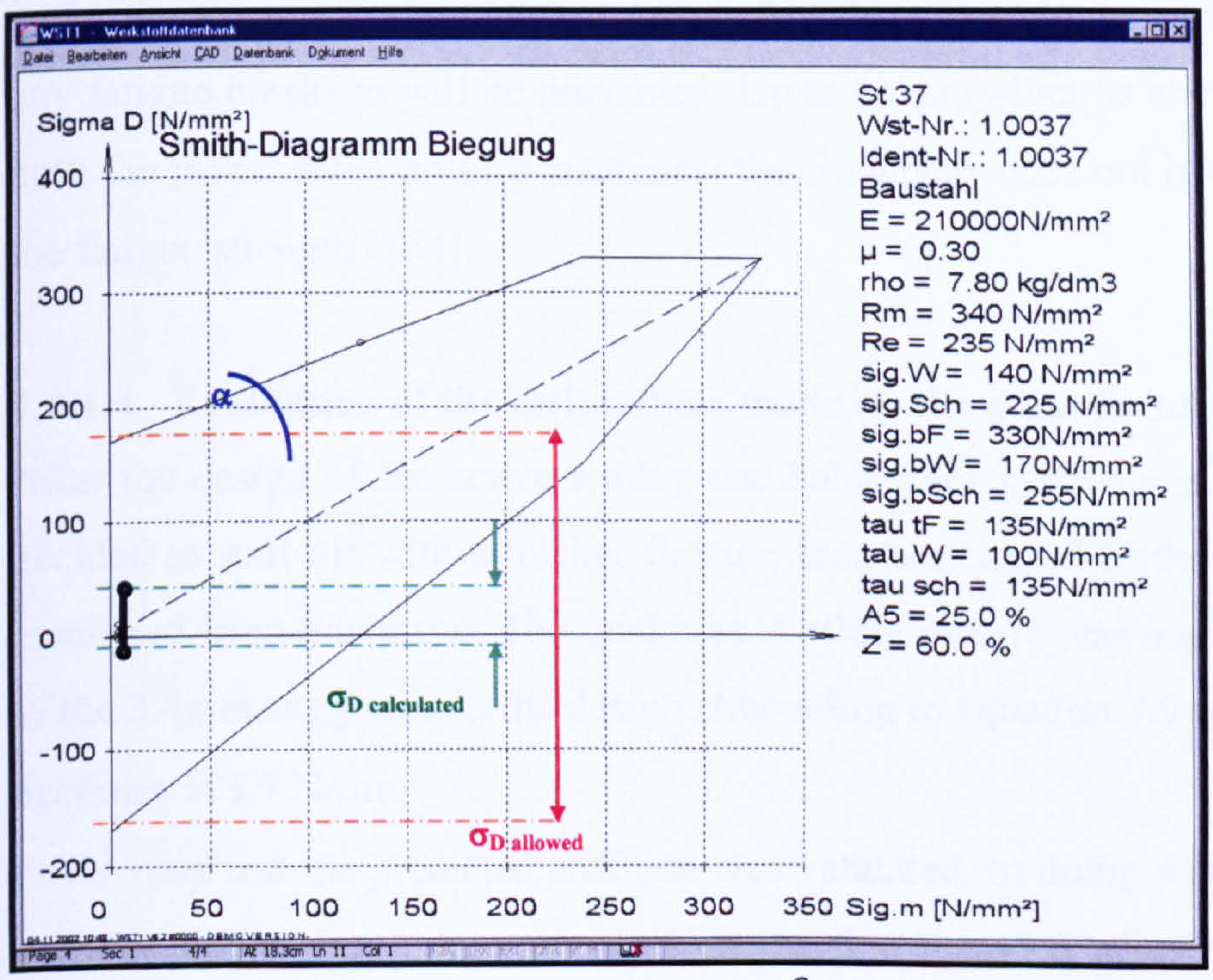

***Figure 7.14:** The graphical user interface of WST1©, showing the Smith Diagram of St 37 (mild steel) for bending loads [155]*

The diagram illustrates the safety factor between the maximum allowed and predicted bending stresses. The exact safety number can be calculated using simple geometry:

$$\tan\alpha = \frac{\sigma_{Sch} - \sigma_W}{\frac{\sigma_{Sch}}{2}}$$

Eq. 7.19: Estimation of the maximum allowed stress

$$\alpha = arc\tan\frac{(255-170)\,N/mm^2}{0.5\times 255\,N/mm^2}$$

$$\alpha = 33.69°$$

$$\sigma_D = 2\times(\tan\alpha\times\sigma_m + \sigma_W)$$

$$\sigma_D = 2\times(\tan 33.69°\times 4.18\,N/mm^2 + 170\,N/mm^2)$$

$$\sigma_D = \sigma_{allowed} = 358.65\,N/mm^2$$

Therefore the predicted safety factor S becomes:

$$S_{Guide\,System} = \frac{\sigma_D}{\sigma_{D_{calculated}}} = \frac{358.65\,N/mm^2}{2\times 20.65\,N/mm^2}$$

Eq. 7.20: The predicted safety factor of the guiding system

$$\underline{\underline{S_{GS} = 8.7}}$$

The usual dynamic safety factor is between 2 and 4 [154]. Choosing a safety factor of almost 9, for the flexure guiding system means that these is enough security for any tolerances and any fatigue breakage will be prevented. Up to 1kHz (which is above the chatter frequency of both the investigated milling machines) the frequency does not have any significant effect on the fatigue strength [154].

7.4.1.4 Evaluation of the estimations made on the manufactured system

After the design of the active work-piece holder, the system was built (figure 7.8.b). It was decided to start off with a thicker flexure, than anticipated in the design, since the base was machined from one piece. The thickness *d* of the flexure was machined to 3.7mm, compared to the 3.4mm suggested in the design. According to equation 7.9 the guide way stiffness (k_{GS}) becomes 103.7 N/µm.

In the next test the predicted stiffness was validated. In doing so the flexure guiding system, without disc springs, was moved using the fine threaded adjustment screw. The force was measured using the KISTLER load washers and the displacement with a Laser interferometer.

Figure 7.15 shows the experimental set up.

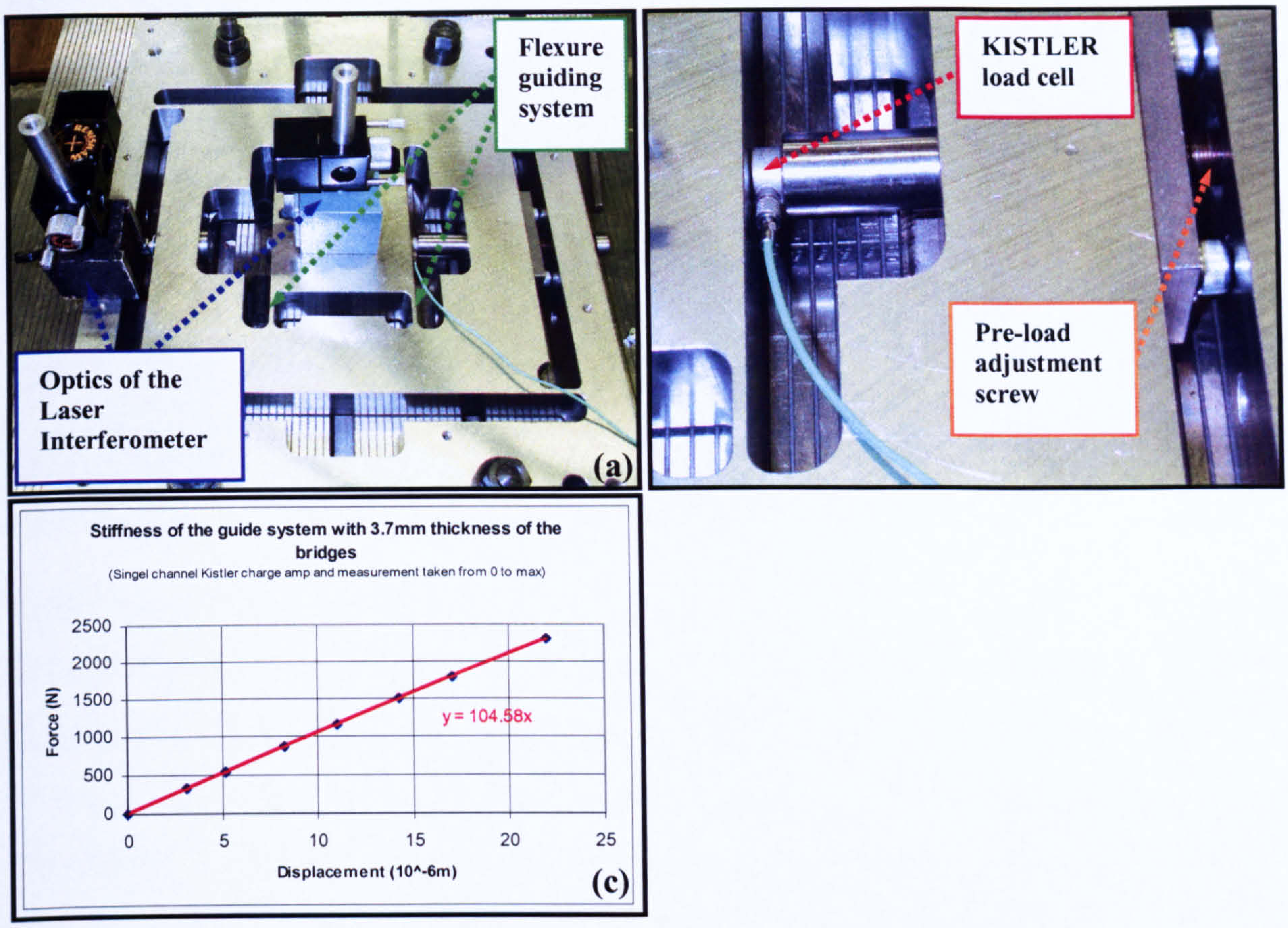

Figure 7.15: Validation of the flexure guiding system stiffness:
- ***Experimental set up (a,b)***
- ***The determined stiffness value (c)***

The measured stiffness of the flexure guiding system was approximately 104 N/μm. This is about +32% off the predicted stiffness from the analytical model. The main explanation for this is that the flexure is not machined rectangular. To distribute the stress more evenly it was machined with a 3mm radius (see figure 7.15.b). The actual pre-load factor *PF* (equation 7.7) has therefore increased to 18.8% and the theoretical maximum displacement of the axis is 8.1μm (equation 7.8). In order to evaluate the maximum axis movement, the PZT actuators and the preload arrangement with the disc springs needed to be assembled. A special screw arrangement was developed to help with the fitting of the PZT ceramics. The gap between actuator and base was closed with a washer, which was ground so that the initial deflection of the flexure was exactly zero (zero stress). If for example after releasing the pre-load of the flexure, the washer was only 1μm too thin, over 10% of the maximum PZT stroke would have been lost. Apart from grinder and sandpaper, a special Fuller gage (1 thousandth of an inch – thinnest one available) and again the laser interferometer were used.

Figure 7.16 illustrates the Y-axis assembly.

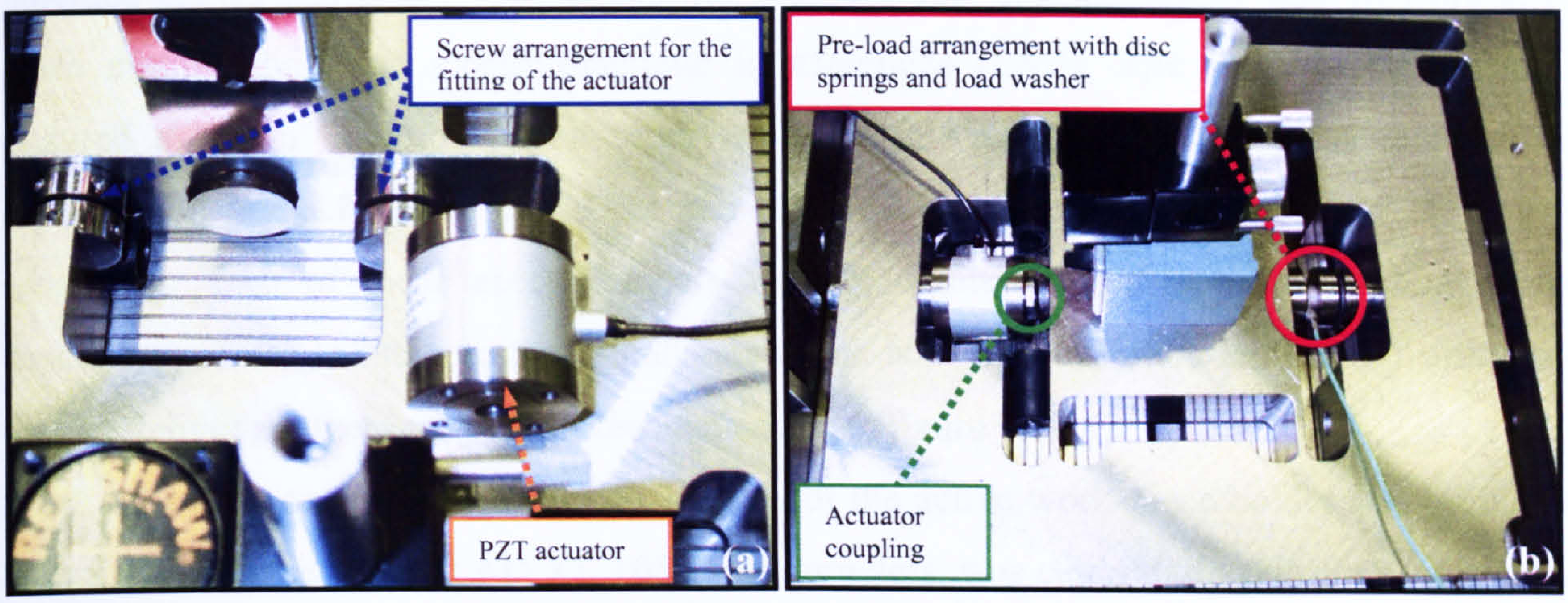

Figure 7.16: Before the assembling of the Y-axis (a) and after (b)

After fitting the PZT actuators the maximum displacement of the Y-axis was measured to be 5.3μm and X-axis to 5.8μm. The control input voltage of the HVPZT amplifier ranges between 0-10V, which corresponds to 0-1000V as the output voltage for the PZT ceramics. However the measured maximum displacement was about 35% (X-axis) and 28% (Y-axis) of the predicted value. According to PI® the main reason for that was the Hertzian contact at the ball tip of the PZT actuator coupling, which also acts as a stiffness. Therefore it is normal to lose a few microns with this coupling. The only way to reduce this effect is to use a flat or a flexure contact for the coupling, which was not an option since the flat contact may break the ceramic and the flexure would take too much space [90].

7.4.2 The integrated sensors

An important feature of the design is the integration of 4 sensors, which are not only used for condition monitoring, but also for the feedback controller. With these, the *active work-piece holder* is able to measure:

- The direct acceleration in 2 axes using MEM accelerometers
- The cutting force in 2 axes using load washers
- The position of the high resolution guide way system (direct displacement of the 2 axes) using strain gauges
- The humidity inside the enclosure, using humidity sensors

7.4.2.1 Accelerometer

The MEM sensor from Analog Devices (AD XL 105) was introduced in chapter 5.3. This sensor was optimised for the active vibration control system, by using a special housing, shielded cables and battery power supply. This ensured that the sensor unit was protected from cutting fluid and electro-magnetic interferences (EMI). The battery power supply ensured a "clean" and low noise supply voltage. It was shown that these improvements reduced the noise floor of the MEM sensor by 30% and therefore improved the sensor resolution. Two of these accelerometers were integrated to the spindle housing of the machining centre in order to better understand the actively controlled cutting dynamics and also to deliver another option for a feedback sensor (figure 7.17.a).

Next a 2-axis accelerometer for the inner table of the active work-piece holder was built. The sensor, which consists of 2 AD XL 105 accelerometers, was calibrated against a piezoelectric electric sensor (ICP type - Techni Measure®) using the back-to-back method, discussed in chapter 5.3.2 (figure 7.17.b). The aluminium housing (appendix B.5) of the sensor can be screwed to the inner table, so that it is located under the work-piece (figure 7.17.c and d).

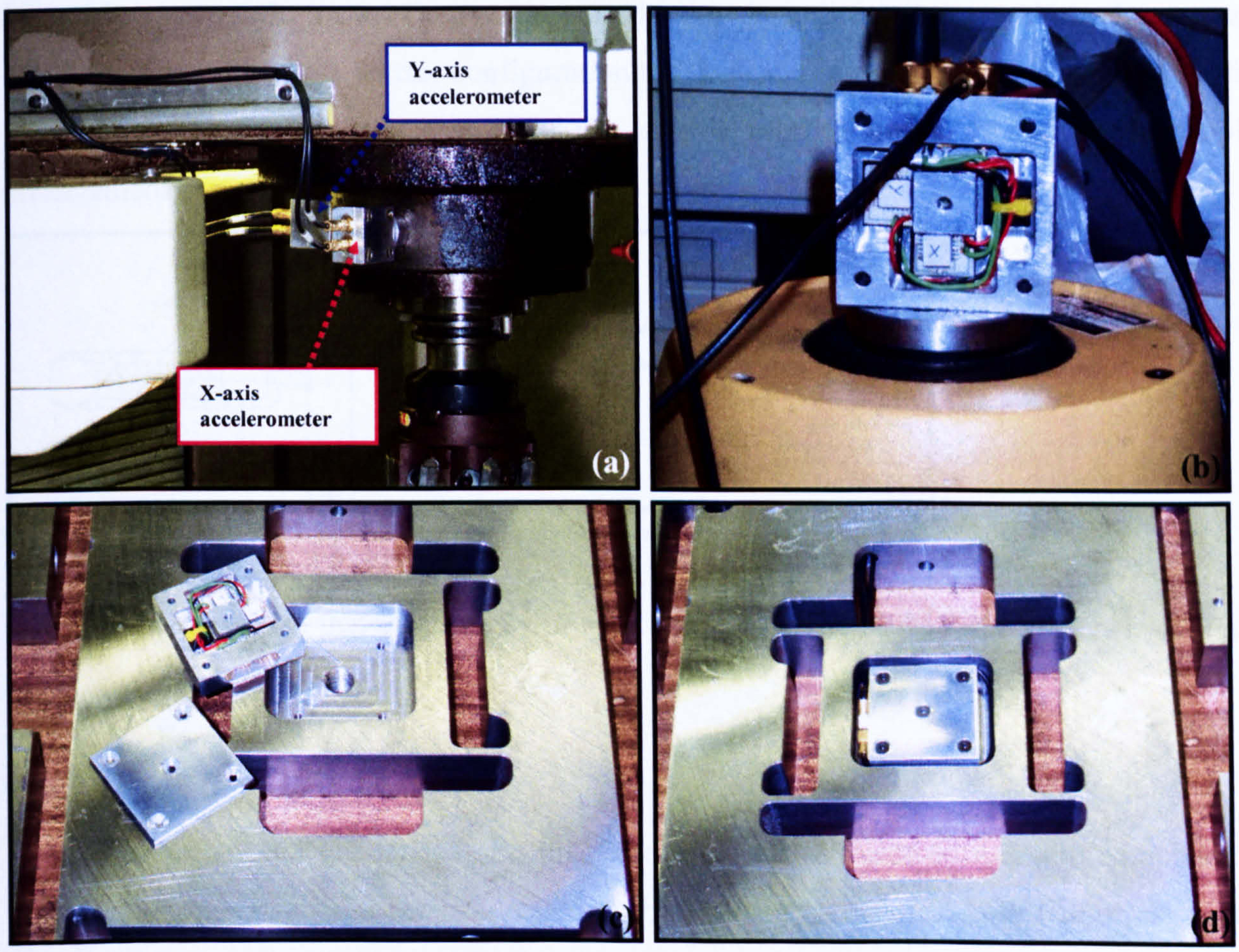

Figure 7.17: The integration of the designed accelerometers units :
- ***Two sensors integrated to the spindle housing of the machining centre***
- ***Sensor calibration***
- ***The integration of the 2 axis MEM sensor into the active work-piece holder (c and d)***

7.4.2.2 Piezoelectric force sensor

Piezoelectric transducers are the most widely used vibration sensors. As already mentioned, ceramic piezoelectric elements produce an electrical charge when being strained or pressured (direct piezoelectric effect – opposite to the inverse piezoelectric effect used in PZT actuators). Because of the high impedance of these sensors a charge amplifier is used as a buffer in order to obtain a usable low impedance output voltage. Therefore the sensitivity of the piezoelectric sensor (*pC* / Mechanical unit) and charge amplifier (Mechanical unit / Output Voltage) needs to be taken into account. The piezo crystals acts like active springs, where the strain or displacement of the crystals is directly proportional to the applied force. The proportional factor is the very high stiffness of the crystals themself, typically around several thousand $N\mu m^{-1}$ [91]. This small deformation of the piezo crystals results in a charge, which is dependent on the type of crystals being used. This direct piezo effect is used in force (figure 7.18 a) and pressure sensors (e.g. microphone). Another very common application is in accelerometers. In an accelerometer, transduction is indirect and is achieved using an auxiliary or seismic mass. In this configuration the measured force on the crystal is the inertia force (*Newton's second law: F=ma*) of the seismic mass. Figure 7.18.b shows a simple arrangement of a piezo-electric accelerometer.

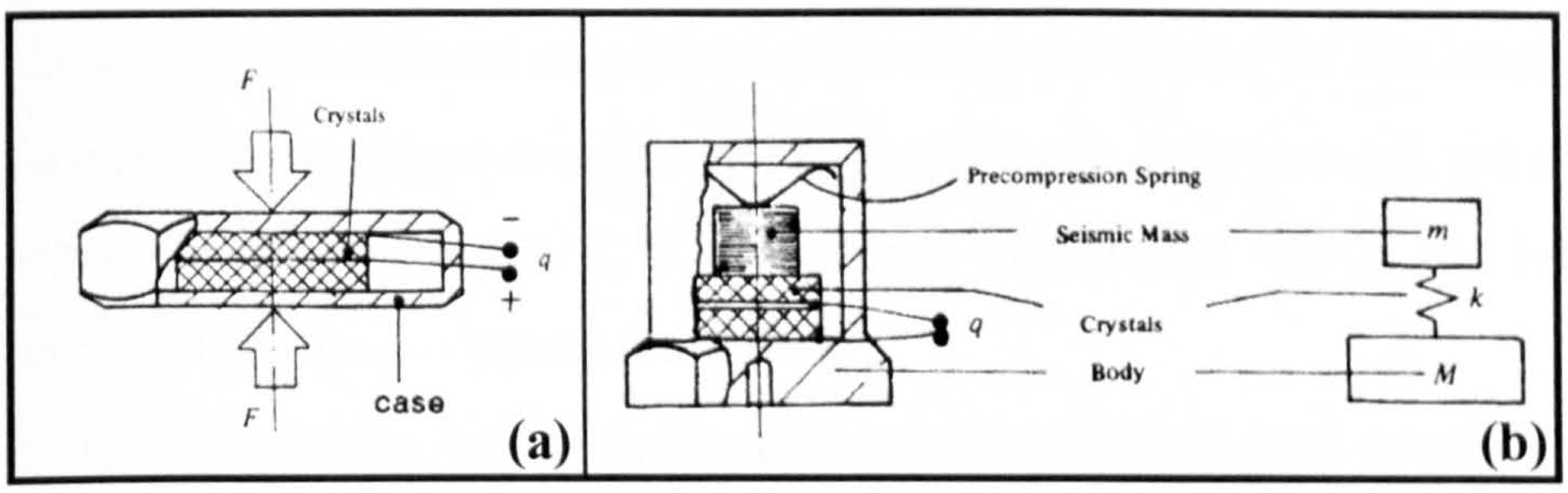

Figure 7.18:Piezoelectric- load washers and accelerometer

It is important to know that there are 2 different types of piezoelectric force sensors available:

- Load washers
- Force links

Load washers are not pre-loaded and therefore, only can be used to measure compression forces, whereas force links are pre-loaded enabling them to measure both compression and tension. The principle is the same for transducers as it is for actuators (discussed in 7.3, figure 7.7).

Figure 7.19 illustrates the effect of this pre-load.

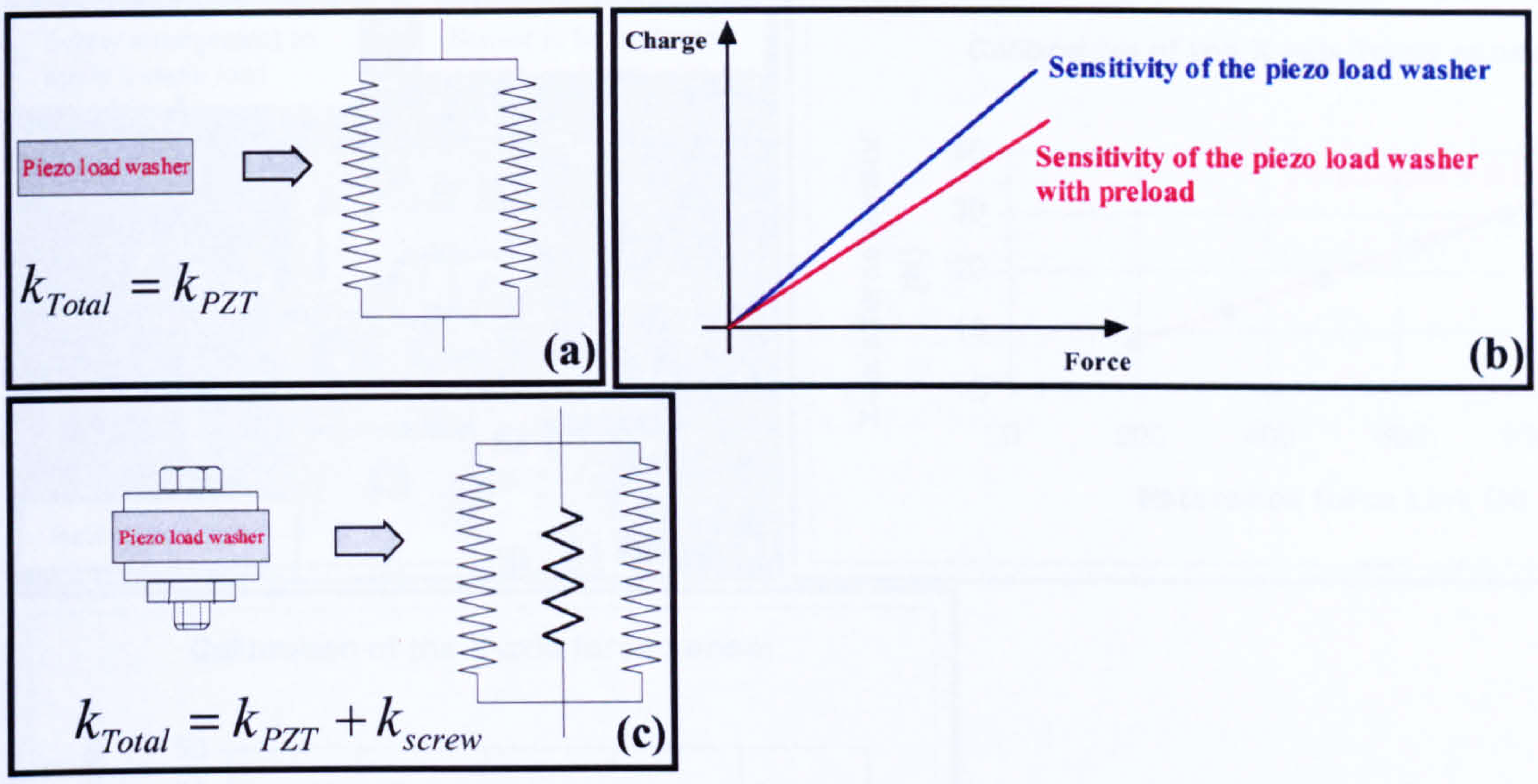

Figure 7.19: The difference between a load washer and a preloaded washer or force link
- ***Load washer (a)***
- ***Force link (b)***
- ***Effect of the pre-load on the sensor sensitivity (c)***

The stiffness of the pre-load screw (about 10% of the stiffness of the piezo ceramic), parallel to the stiffness of the piezo ceramic (about 1000-1800N/µm) of the load washer, acts as a force shunt. The resulting, higher, stiffness changes the sensitivity factor of the sensor by the same amount the stiffness has changed. Usually a re-calibration of the pre-loaded sensor is necessary. The amount of preload-force does not matter for the sensitivity of the sensor but if the screw is stretched over the yield point (plastic deformation), the stiffness and therefore the sensor becomes non-linear. The sensor is only linear within the linear region of the screw (constant stiffness – young modulus).

It was decided to use high impedance piezoelectric load washers from KISTLER in this project. The advantage is that compared to the low impedance load washer (ICP type – direct voltage output), it can measure "quasi-static" forces [139], because of the very long time constant of the required charge amplifier. This means that the integrated force sensors will not only be able to measure the dynamic but also the static cutting force (experimental tests have shown that the KISTLER charge amplifier was able to hold the charge of a static force for a few hours).

After the assembly of the *active work-piece* holder, the load washers needed to be re-calibrated, since the pre-load stiffness of the flexure guiding system and disc springs increased the sensors sensitivity factor. The load washers were calibrated against a KISTLER force link and the static force applied by a screw arrangement (figure 7.20).

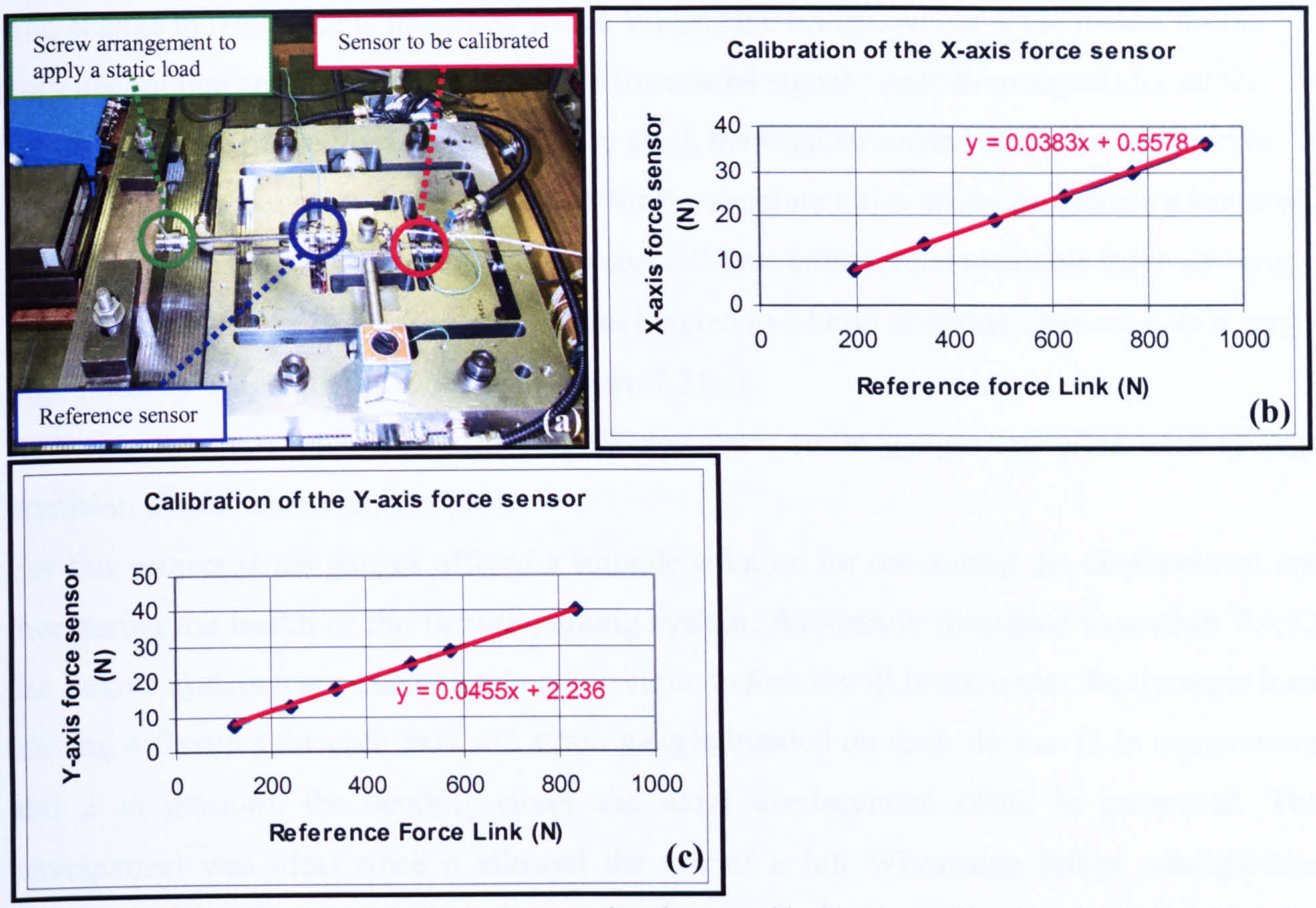

Figure 7.20: Re-calibration of the load washers after the assembly: X axis - calibration chart of pre-loaded load washer (b) and Y axis - calibration chart of pre-loaded load washer (c)

The additional gain factors for the sensors sensitivity were 22.0 for the Y-axis and 26.2 for the X-axis (figure 7.20.a and b).

7.4.2.3 Strain gauges

Strain gauges as the name suggests measure strain. They are therefore a particular form of relative displacement and vibration sensor (DC to several kHz) [87]. A very fine wire or foil is wound onto a plastic backing which is then bonded onto the surface on which strain should be detected. The principle is based on the variation in wire length and corresponding Poisson reduction in diameter giving a change in electrical resistance, when being strained. The longer the wire the bigger the change and the bigger the measured signal (Figure 7.21 a,b and d).

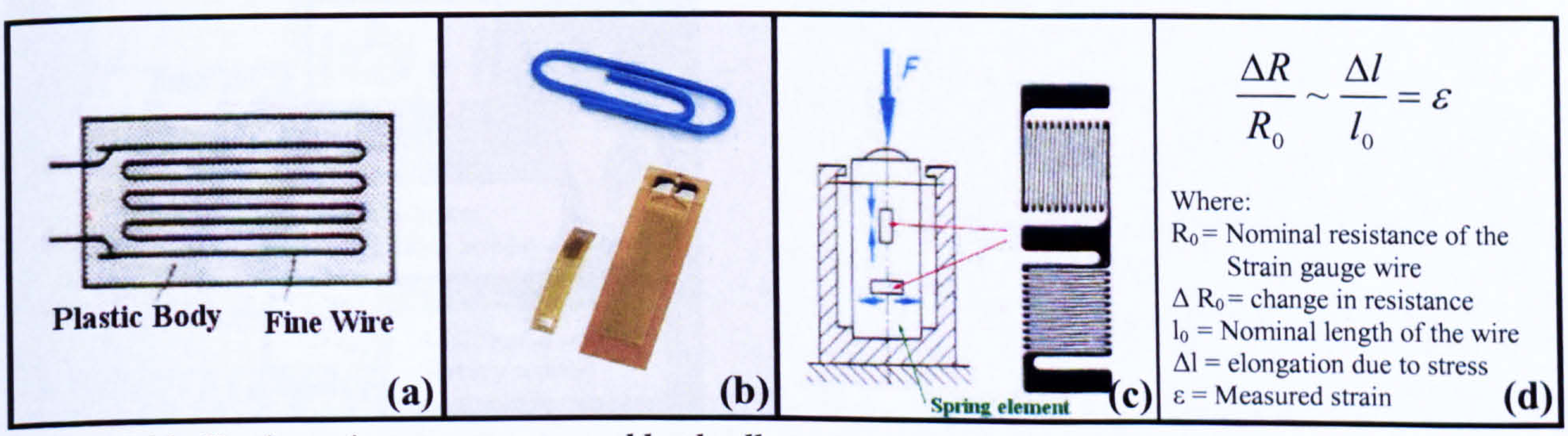

Figure 7.21: Single strain gauge sensor and load cell

The change in resistance is measured with a Wheatsone bridge, which is the reason for the very uncommon sensitivity factor of mV/V (measured signal / excitation signal) for strain gauges. Because of the linear relationship in steel, between stress and strain for the specific units (Young modulus) or force and length for the absolute units, strain gauges are often used not only to measure displacement, but also force. These commercial available force sensors, often referred as *load cells*, are strain gauges bonded to a body or spring element with a very high linearity (high quality tool steel – figure 7.21.c).

Referring to smart materials, such as PZT actuators, strain gauges are often used as high precision displacement sensors [90].

For this project strain gauges offered a suitable solution for measuring the displacement and monitoring the health of the flexure guiding system. As already discussed in section 7.4.1.3 the flexure system has a maximum bending strain before it will break under the dynamic load. Having 4 flexures for each axis and strain gauges bonded on each flexure (2 in compression and 2 in tension), the bending strain and axial displacement could be measured. This arrangement was ideal since it allowed the use of a full Wheatsone bridge configuration where the change of all 4 resistances of the strain gauges are detected making it more sensitive and temperature stable [156]. Figure 7.22 shows the integrated strain gauges bonded onto each flexure and the calibration set up.

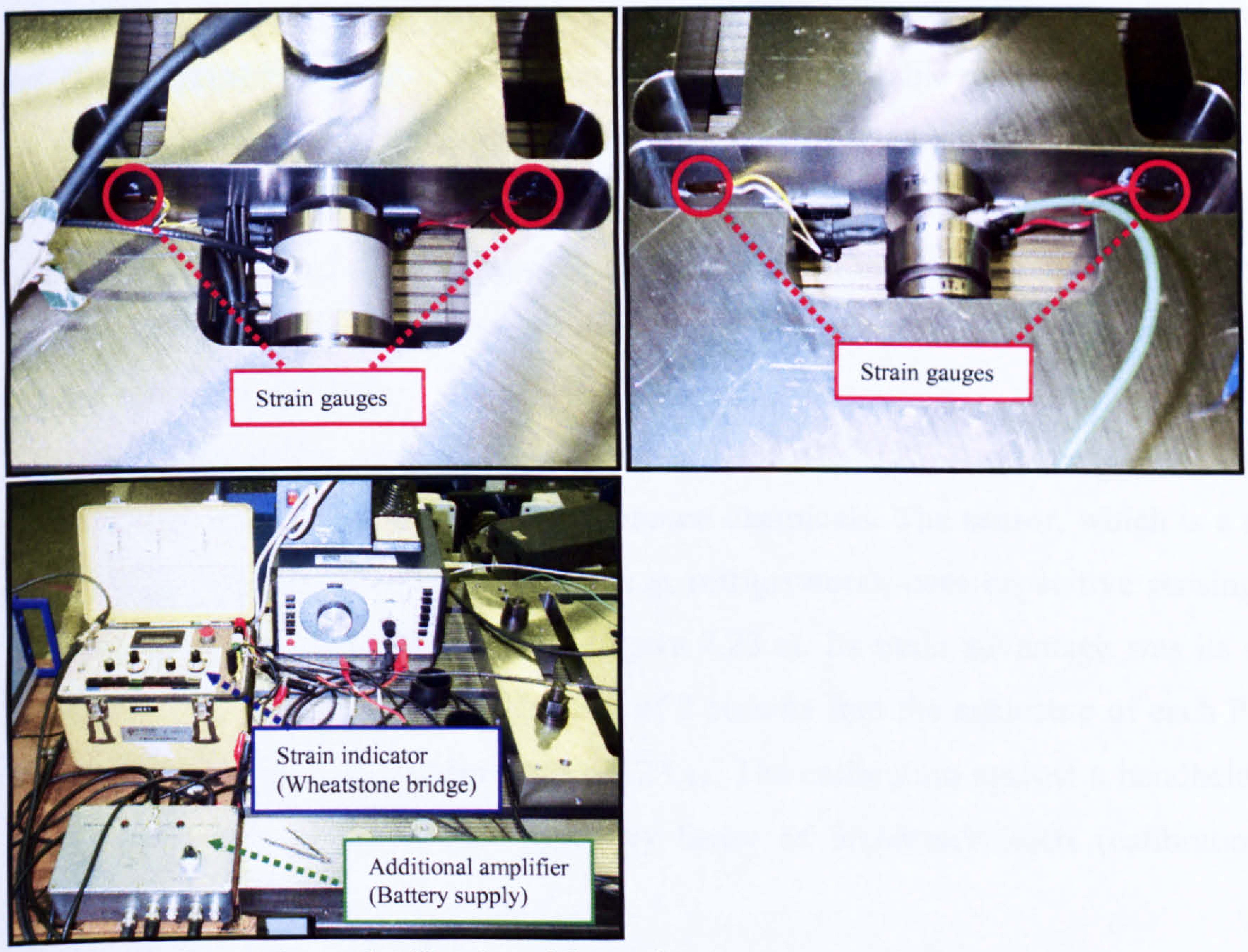

Figure 7.22: Integration and calibration of the strain gauges

The axial calibration was carried out using a Laser Interferometer and revealed a calibration factor of the new positioning sensor of 1mV/µm. This was increased to 10mV/µm using additional amplification, with low pass filtering to attenuate the increased noise level. A better sensor resolution could be achieved by reducing the thickness (*d* in figure 7.9.a) of the flexure. According to equation 7.13 this would increase the stress, and as long as thus is within the linear region of the stress strain graph with the Young's modulus as proportional factor, also the strain. This linear relationship is:

Eq. 7.21: Young's modulus

$$\varepsilon = \frac{\sigma}{E} \times 100\,[\%] \quad (\textit{where } E \textit{ is the Young's modulus and } \varepsilon \textit{ the strain})$$

Unfortunately thinner flexures with a higher strain, reduce the safety factor and therefore increase the danger of breakage. The best way of increasing the accuracy of the positioning system, for future work, would be to use an additional flexure made from stainless or tool steel (better linearity than mild steel) with the sole purpose of measuring the guide way deflection.

7.4.2.4 Humidity sensor

Initially it was not intended to integrate a humidity sensor into the design, but the first cutting tests with coolant revealed that it was necessary. The perspex enclosure, where the HVPZT are placed, started to show condensation. The highest allowable relative humidity is quoted to be 60% [90], since the insulation between the HVPZT ceramics (1000V !) for the stacked design, would otherwise result in a dielectric breakdown (discharge). The solution was better sealing, silica gel, and monitoring of the humidity. For long-term operation the integration of an air-ventilation system may be required or the use of special PZT systems with enclosed stacks, offered by PI [90].

The chosen humidity sensors (Honeywell HIH-3610 – [157]) are resistant to application hazards such as wetting, dirt, oils and common chemicals. The sensor, which is a monolithic IC for high volume OEM applications (e.g. refrigerators), uses capacitive sensing elements and has on-board signal conditioning (figure 7.23.c). Its main advantage was its small size, which allowed the permanent integration of 2 sensors into the enclosure of each PZT-pocket of the *active work-piece holder* (figure 7.23.a). The calibration against a handheld industrial humidity sensor confirmed the sensitivity factor of 30.680mV/%RH (calibration chart in figure 7.23.b).

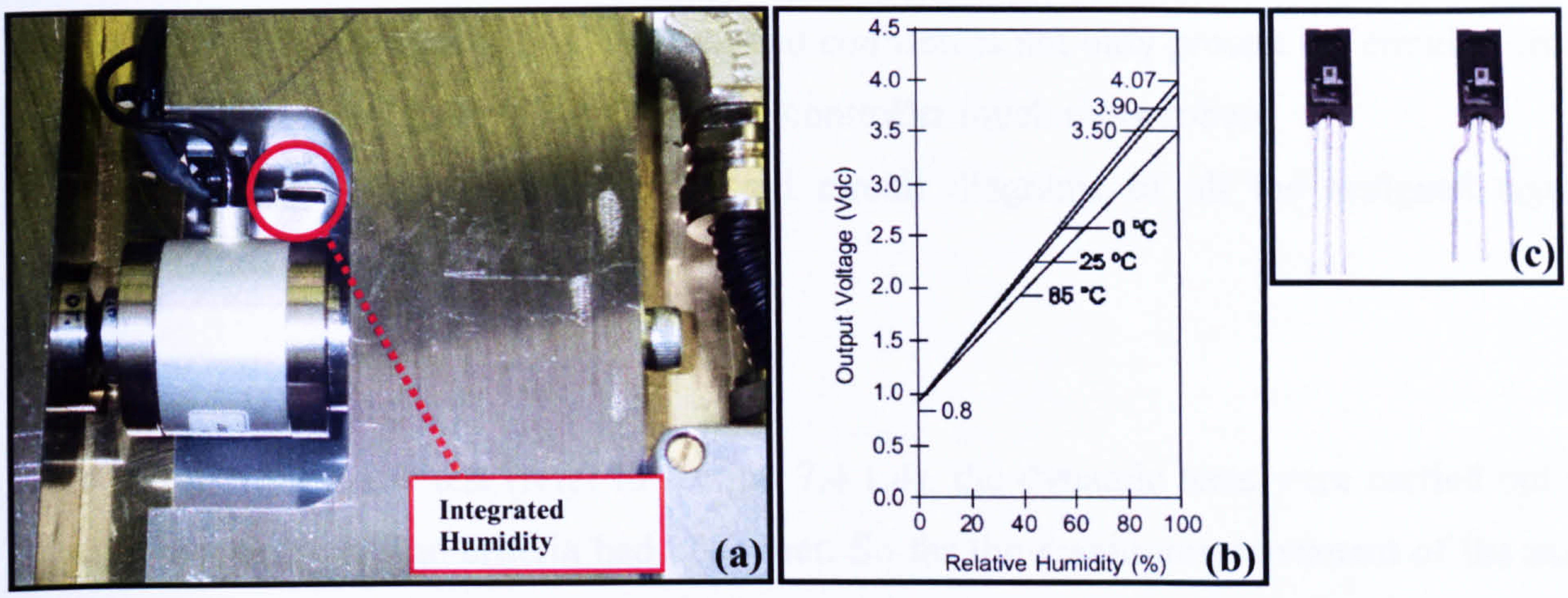

Figure 7.23: The integrated humidity sensor, Y-axis sensor (a), Calibration (b) and Honeywell HIH-3610 (c)

7.4.3 Signal conditioning

Analogue signal conditioning is necessary to process and re-shape the feedback and control signals. All the signal conditioning required for this project was built into 5 discrete units:

- The main signal conditioning unit
- Amplifier and attenuator unit for the controller (proportional gain controller)
- Precision 3rd order all-pass filter unit
- Over-voltage protection unit for the HVPZT amplifier
- Adapter cards for the data acquisition system

These units are battery supplied in order to minimise noise levels, since as experience has shown, there is a great deal of electromagnetic interference on the main power supply of the machine workshop (mainly due to the thyristor driven motor drives of the machine tools).

The noise can affect the low signal levels (mV), but not the relatively high dynamic control signals of the HVPZT amplifier, which was between +/-5V and +/-6V. To ensure that the control signals were not saturating a positive and negative supply voltage for the operational amplifiers of at least +/- 7V was required. It was decided to use two 9V block batteries connected in series to produce an 18V positive supply, and a second set connected in the opposite polarity for the negative 18V supply.

The battery supply also ensures portability, whereas the added low battery detection system always ensures a safe control operation. To recognise a low voltage a window detector was used [118]. The measured positive and negative current of the units confirmed the estimated battery life of several hours. After the successful design of the prototypes this could be improved further using low power surface mount components for all the electronics. The

diecast aluminium enclosures and BNC coaxial connectors not only protect the circuitry from dust and EMI, but also make the whole active controller much more robust.
More information such as functionality and circuit diagrams of all the designed signal conditions units are attached to appendix C.

7.5 Dynamic testing

Together with the static test (refer to section 7.4.1.4), the dynamic tests were carried out to reveal whether the design criteria had been met. So far the maximum movement of the axes were about 5.8μm, which is less than the expected 8μm. Nevertheless there was still the option to reduce the stiffness of the flexure guiding system, which would then increase the maximum stroke but increase also the risk of breakage.
The dynamic tests were designed so as to judge the sensor quality for dynamic loading and to measure the bandwidth of each axis. So far, both the static sensors (strain gauges and load washer), accurately measured the static displacement and force and the PZT actuator allowed the very fine positioning, claimed by PI [90].
Figure 7.24.a shows the experimental set up of the dynamic testing and figure 7.24.b and c the measured FRF of each axis using the force sensor for the response. The excitation was applied by the HVPZT actuator and the signals recorded with the spectrum analyser.

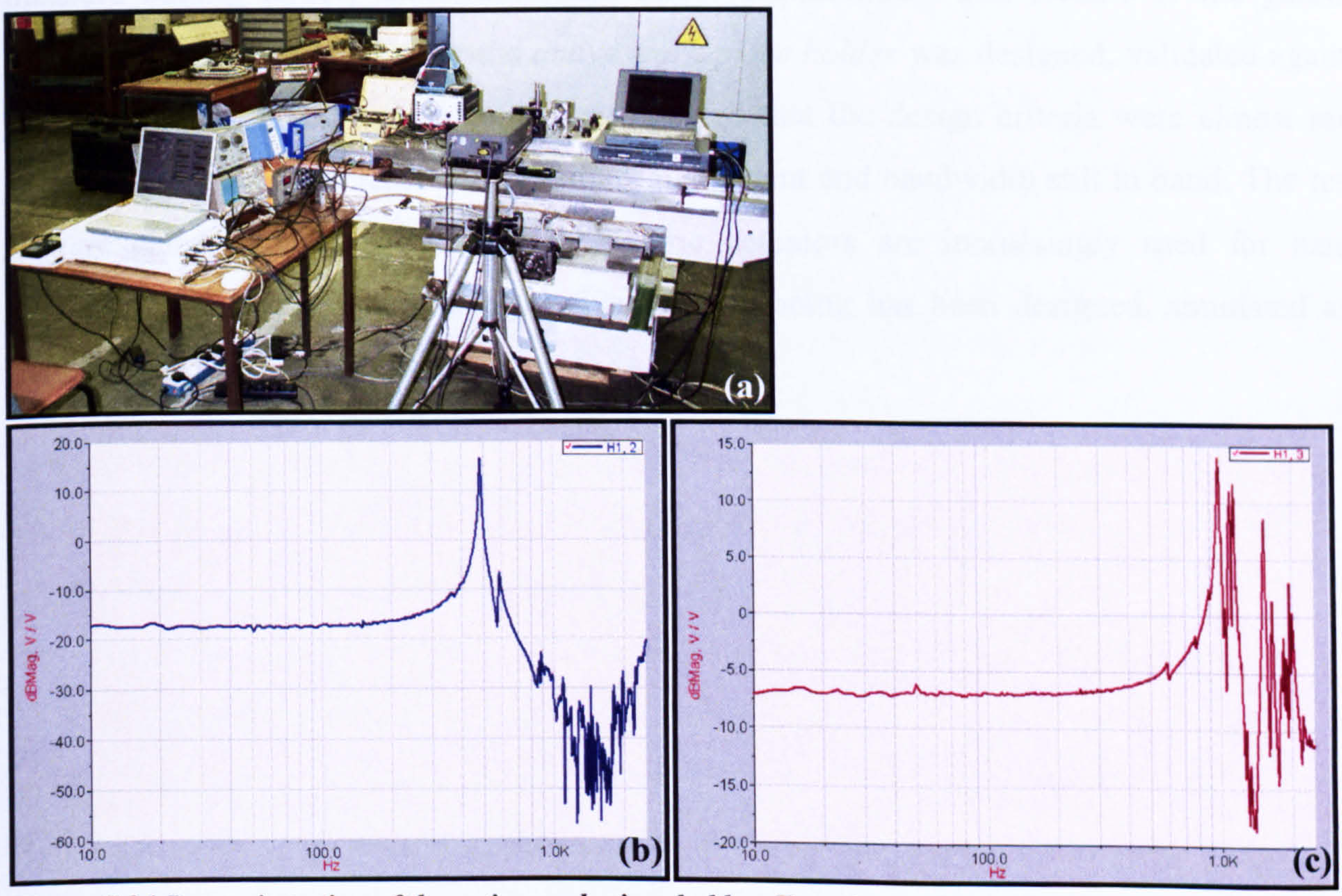

Figure 7.24:Dynamic testing of the active work-piece holder: Experimental set up (a), the measured FRF of the X- axis (b) and the measured FRF of the Y-axis (c)

Harmonic excitation showed that all the integrated sensors had a good response at various excitation frequencies. The measured resonant frequency was 500Hz for the X-axis and 1kHz for the Y-axis, which confirmed the estimation using equation 7.6. It meant that for the chatter frequency (450Hz) both axes produced a controllable work-piece movement. Nevertheless, there was also still the option of machining pockets into the frame to reduce its weight, which especially for the X-axis would increase the usable bandwidth.

7.6 Summary

A universal active vibration control system for vertical milling machines has been designed. The system adds another 2 degrees of freedom to the machine not only to analyse the cutting process, but also to modify it by reducing any static or dynamic deflection generated.

The cutting forces of an unstable machining operation have been modelled and validated through cutting tests. This and the estimated tool defection at the cutting point helped in the selection of the actuators and set the design boundaries. After a comparison with other actuator types it was decided to use piezo-electric based actuators to modify the work-piece position. The fundamental theory of this actuator type has been discussed and according to the design specifications a special high voltage PZT stack actuator was selected.

The design also features a high-resolution flexure guiding system and integrated sensors to measure cutting forces, acceleration and direct displacement. The flexure of the guiding system was modelled and, after the *active work-piece holder* was designed, validated against the real system. Static and dynamic tests showed that the design criteria were almost met, with the potential to increase the maximum movement and bandwidth still in hand. The tests also revealed, the reason why piezo electric actuators are increasingly used for nano-positioning. The additional analogue signal conditioning has been designed, simulated and built to be robust and user friendly.

Chapter 8

Active vibration control of a machine tool

8.1 Introduction

Following the development of the universal active vibration control system for vertical milling machines described in the previous chapter, this chapter presents the results of how this technique helped to improve the performance of a machine tool. Initial static and dynamic testing on the system had already validated the design specifications, but it still needed to be tested against a machine tool under cutting conditions. Only these tests would verify and validate the thesis that it is possible to control the vibration of the time varying multipoint tool operation of the intermittent milling cutting process. So far the proposed adaptive control techniques have only been tested on a simple test rig, which is a good representation for a single point continuous cutting operation (e.g. turning operation). Although these tests were promising they did not prove if the system would be effective in a milling operation where the excitation forces and also the system changes with time.

In the first section of the chapter, the usable bandwidth of a traditional ballsrew axis servo drive is estimated. In order to make a correct and overall judgment, this measurement was carried out on 2 different small sized machine tools. These tests showed to what extent it would be possible to use the standard axis drive as an actuator for machine tool vibration control. In the next section the advantages of having a piezo driven axis in addition to a standard axis drive system are further demonstrated. It is shown that vibration introduced by the servo drive can be reduced with the developed piezo actuator system. The simulation also included the identification of the characteristics of the servo axis drive system using adaptive filters and again revealed the powerful alternative techniques of modelling mechanical and electrical structures in real time using digital filters.

Next the active control system was used to control the vibration of the cutting process. In doing so, the proper secondary path for the adaptive controller needed to be found. A light face milling cutting operation was superimposed with controlled vibration through the piezo actuator system to prove that it would affect the cutting process itself. Eventually it was shown that it is possible to reduce the vibration level and improve the surface finish of a stable and unstable cutting operation by using the adaptive controller with acceleration and dynamic cutting force feedback.

8.2 Identification of the usable bandwidth of a standard axis drive system

The question, "why not simply use an adaptive controller in conjunction with the standard axis drive, as actuator, to reduce the vibrations?", was repeatedly asked during the project. Previous tests on a single axis of a machine tool have shown the machine table responded to signals over 100Hz, although its bandwidth was thought to be less than 100Hz. If the command signal to the axis drive was sufficiently high, this movement at a few hundred Hertz may still be in the micrometre region, which would be enough to compensate for vibration on the tool tip. However, the fact that the weight of common machine tool tables is a few hundred kilos and the coupling often via pulley and timing belt is relatively flexible, made this difficult to believe. It is believed that the more direct and stiff the coupling of the actuator system to the cutting process is, the easier it would be to transmit the control forces. These initial tests also showed that at high frequency excitation through the axis drive system, the whole machine tool appeared to vibrate, rather then just the axis under control. The following test procedure therefore aimed to estimate a usable bandwidth for a machine tool axis. This could be used as a measure between the capabilities of individual machines to judge to what extent the axis drive can be used for active vibration control. The measurements identified the frequency limit of each axis, when the controlled axis movement in one direction was overshadowed by uncontrolled structural vibration in all 3 directions. The general data logger developed by Freeman [145] was used to excite the axis drive. The advantage of using this system was that it is not necessary to open the servo loop since it allows the injection of pre-defined signals into the closed loop using digital scaler cards. It therefore made it possible to alter and offset the feedback signals from either the rotary or linear encoders.

8.2.1 Single axis Bridgeport Ballscrew rig

The first machine to be tested was a single axis test rig from Bridgeport (VMC 800) shown in figure 8.1.a. It only has one axis (linear guide ways) with no covers to guarantee easy access to all structural parts. The rig is part of a current EPSRC project and fitted with both rotary and linear encoders. The controller is a Heidenhain TNC 46 with Siemens axis drive.

The servo drive was excited with both harmonic signals at different frequencies and white noise using the signal injection technique developed by Freeman [145]. The resulting table movement was measured in 3 axes with eddy current NCDTs, accelerometers and a linear feedback encoder. Figure 8.1.b-d shows the experimental set up for this test.

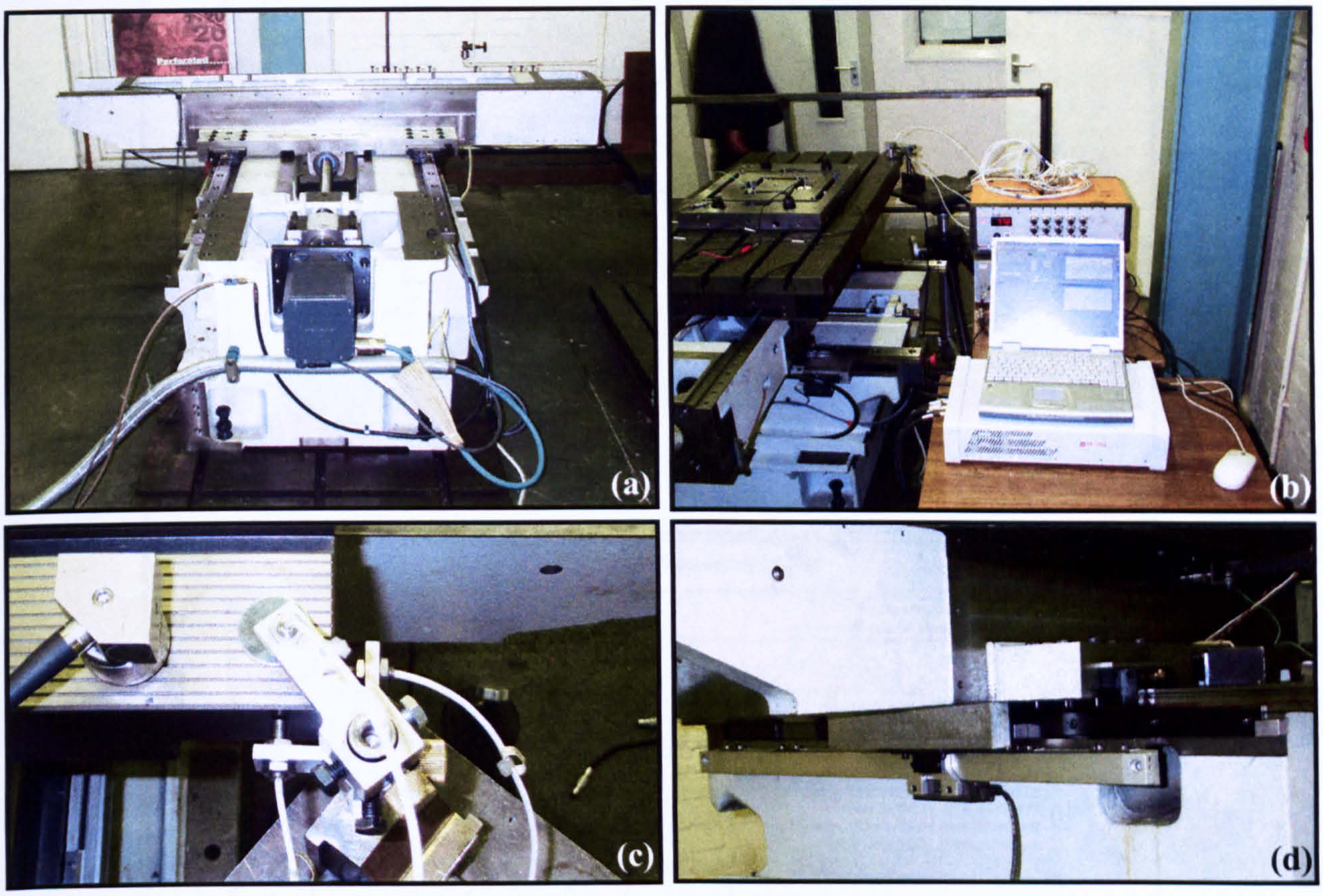

Figure 8.1: Experimental tests on the single axis ballscrew test rig:
- ***The Bridgeport VMC 800 single axis rig (a)***
- ***Experimental test set up for the dynamic tests on the axis drive (b)***
- ***Linear encoder (c)***
- ***Tri-axis accelerometer and NCDT (d)***

The NCDT's were mounted onto a rigid tri-pod, whereas the accelerometers, unlike the NCDT's do not need a reference point, were positioned directly on the machine table.

First harmonic signals with 100μm peak-peak and frequencies between 1Hz and 100Hz were injected into the position loop.

Figure 8.2.a-c shows the response on the encoder output, NCDT and accelerometer in 3 axes. The results illustrate clearly that at 10Hz already the axis not only moves on the commanded direction, but also in the other 2 directions. Between 20Hz and 50Hz the movement in the X- and Z-axis is as big as that in the Y-axis, which is the direction of the driving system of the single axis rig. This can be seen as the frequency limit of the system, where the structural vibration in 3 axes suppresses the controlled movement of the table in 1 axis.

The figures also show again the reason why accelerometers do not work well at low frequencies (refer to chapter 6.2.1).

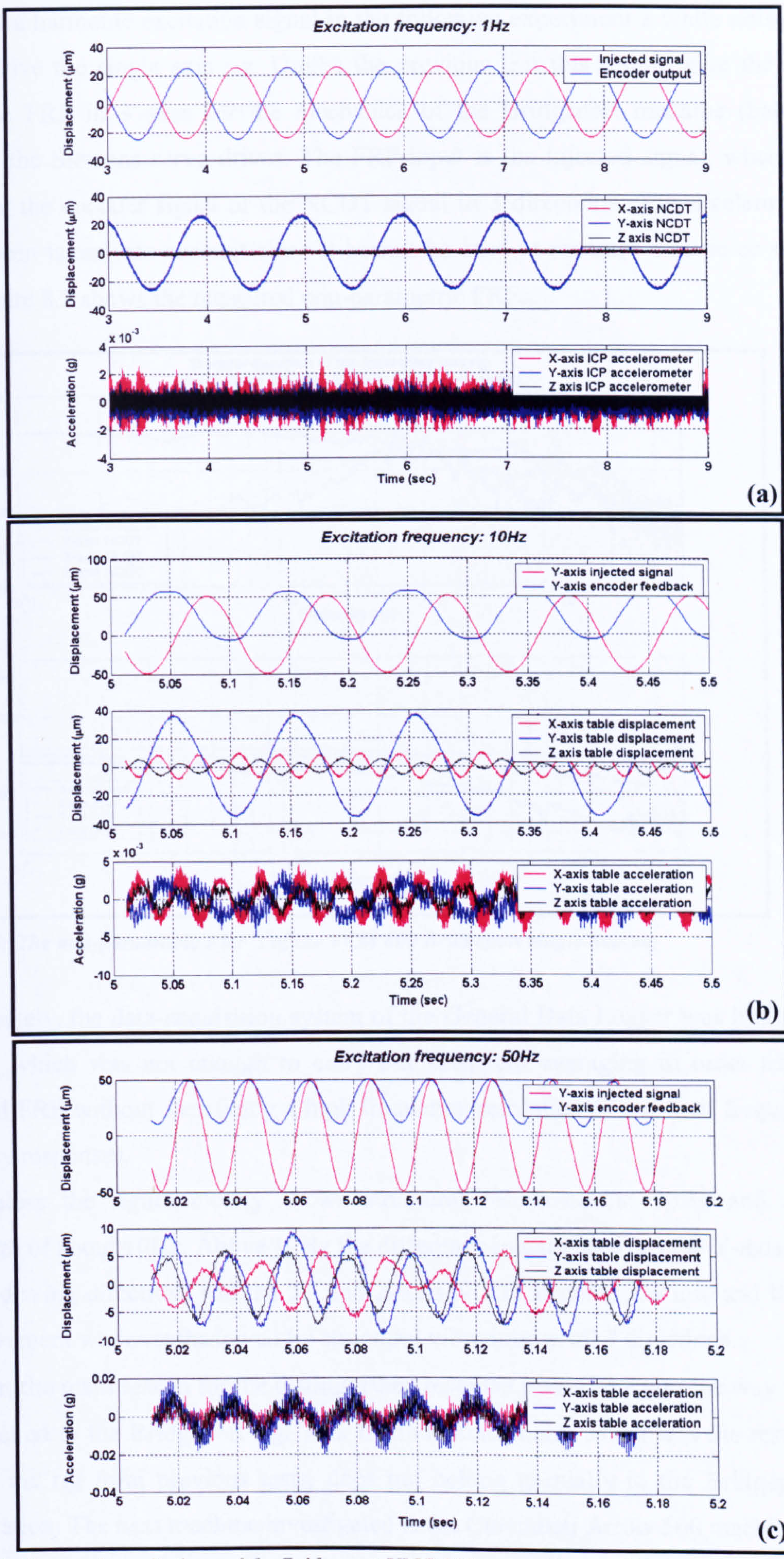

Figure 8.2: Harmonic excitations of the Bridgeport VMC 800 servo drive at: 1Hz (a), 10Hz (b) and 50Hz (c)

Instead of a harmonic excitation signal in the following experiment a white noise signal was used to drive the single axis rig. Unlike the previous test this should give the whole non-parametric FRF in 3 axes for the mechanics of the Bridgeport machine (ballscrew etc.) including the Siemens servo drives. The FRF input is the injected signal, where the output was either the encoder signal or the NCDT signal in 3 directions. The accelerometer signal has not been taken into account since it cannot be used to measure a static or slow moving table. Figure 8.3 shows the measured non-parametric FRFs.

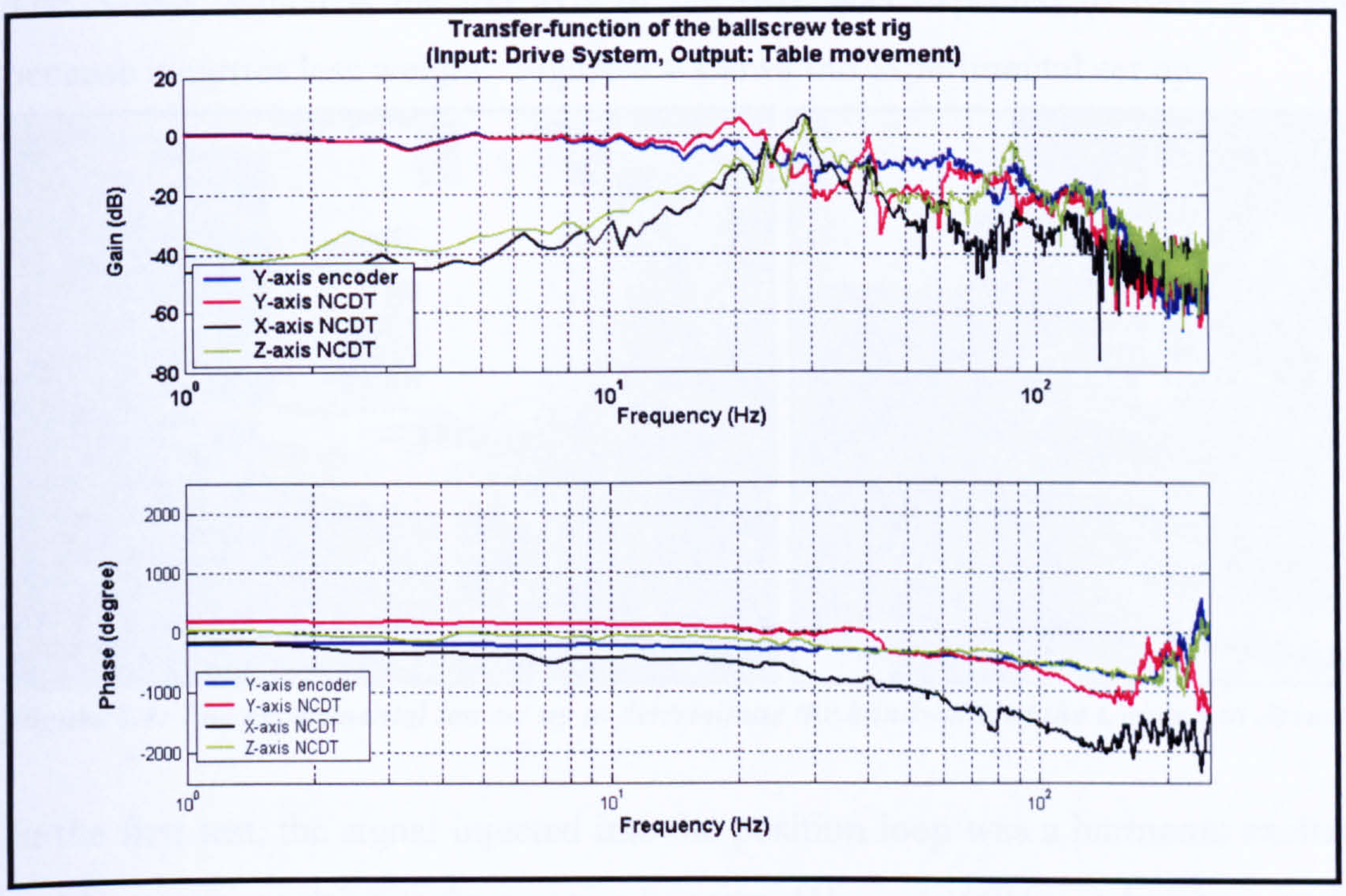

Figure 8.3: The non-parametric FRF's of the VCM 800 Bridgeport single axis rig

Unfortunately, the data-acquisition system of the General Data Logger was limited to 10.000 samples, which was not enough to carry out sufficient averaging in order to smooth the measured FRF without sacrificing a high frequency resolution (number of frequency lines in frequency response).

Nevertheless the figure clearly shows structural resonances at 30Hz and a maximum bandwidth of about 10Hz. Above 10Hz the difference in gain between the Y-axis encoder and NCDT (driving direction) and the X- and Z-axis NCDT become too low and the controlled axis movement was overshadowed by structural vibrations in all 3 directions.

However, the main reason for the distinguished resonant peaks here was the way that the table was attached to the Bridgeport rig. This flexible attachment, which was the result of adding mass to the rig from previous tests, does not belong normally to the Bridgeport machine configuration. The next machine investigated is the Cincinnati Arrow 500 machining centre.

8.2.2 3 axis Cincinnati vertical machining centre

Unlike the Bridgeport single axis rig this is a fully assembled vertical milling machining centre. The Arrow 500 has Siemens axis drives and controller (840D). The test procedure was the same as in the previous section. Harmonic and white noise signals were injected in the position loop of the controller using the data logger and the table movement measured using the linear positioning encoder, tri-axial accelerometers and NCDT's. The measurement was carried out for the X- and Y-axes, which represent the direction of the movement of the table. The X-axis, which is the top axis of the two, was expected to have a higher bandwidth because it carries less weight. Figure 8.4 shows the experimental set up.

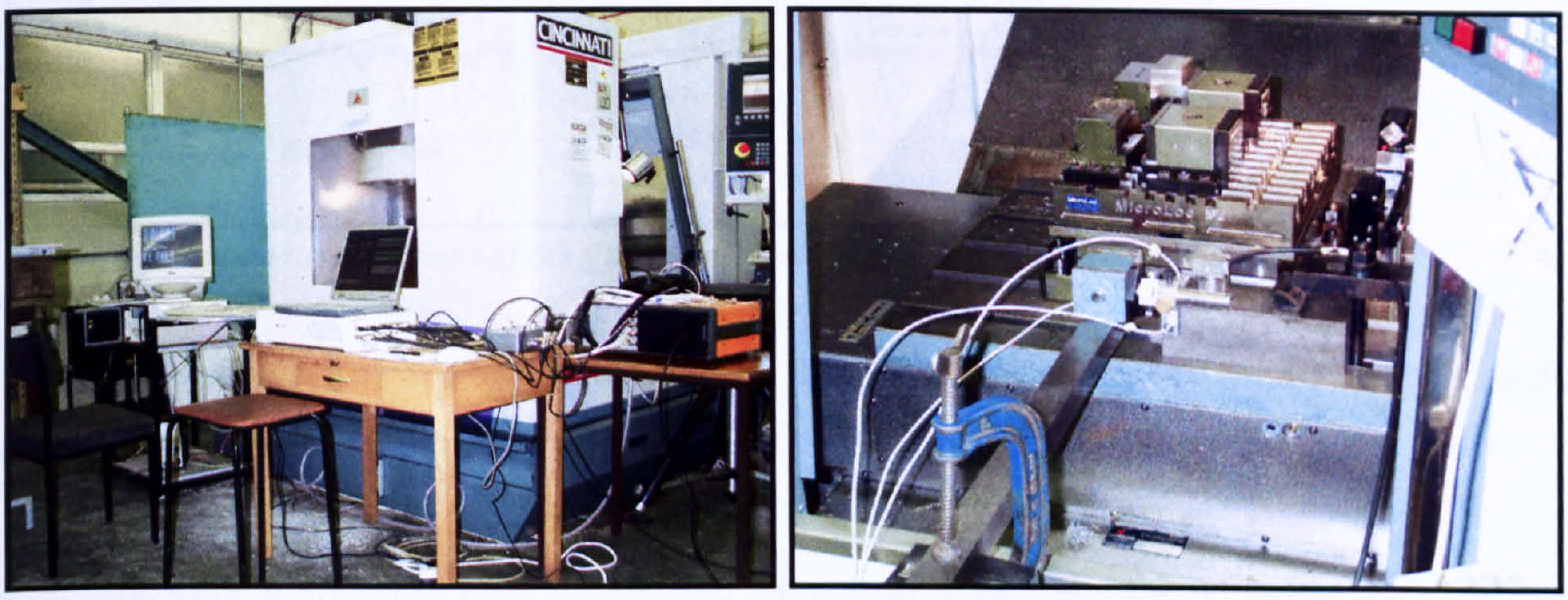

Figure 8.4: The experimental test set up to determinate the bandwidth of the Cincinnati Arrow 500

In the first test, the signal injected into the position loop was a harmonic excitation of the X- and Y-axis servo drive at frequencies between 1Hz and 100Hz, and 100μm peak to peak. The response again was measured in all 3 axis using accelerometers and NCDTs (figure 8.5).

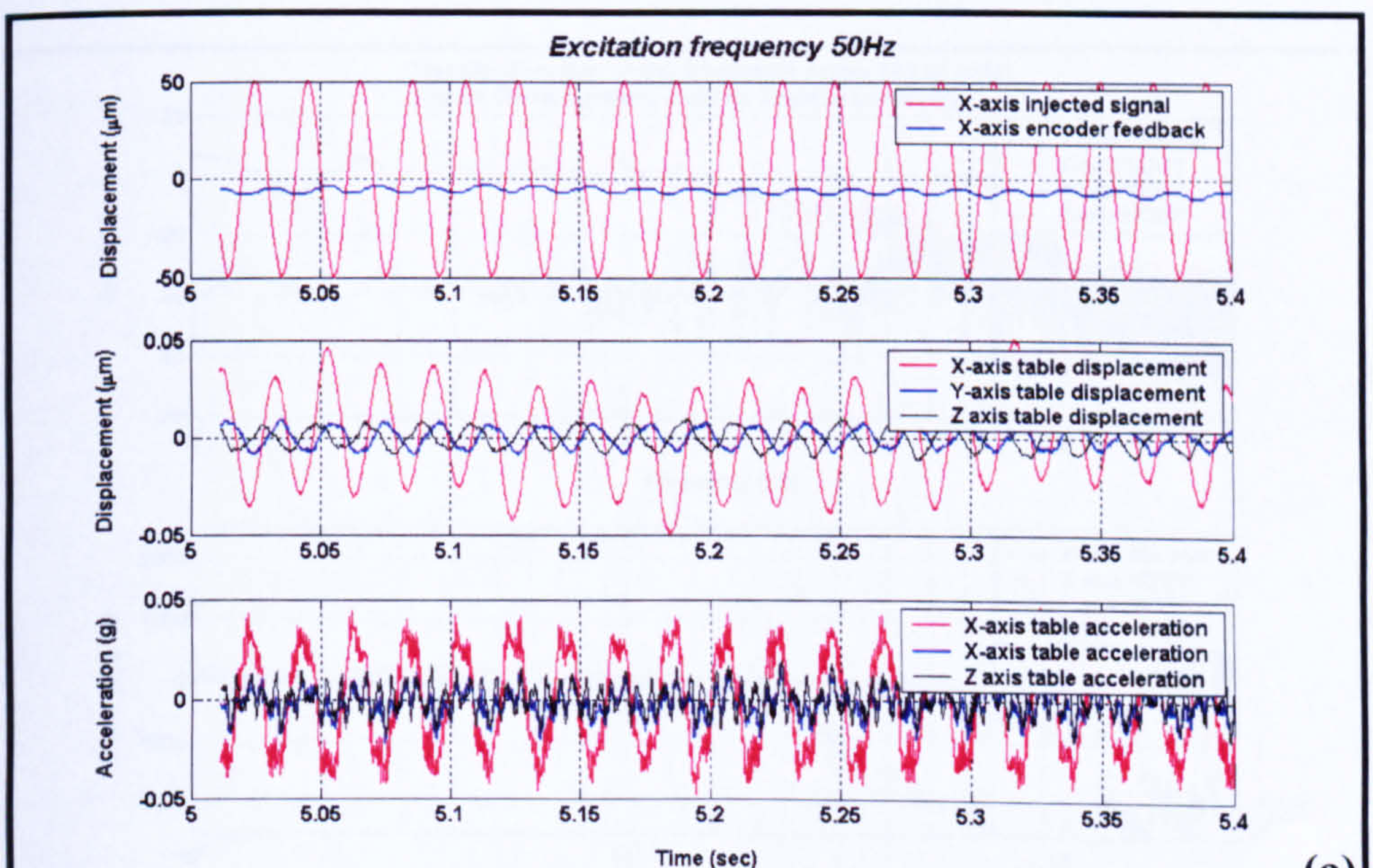

(a)

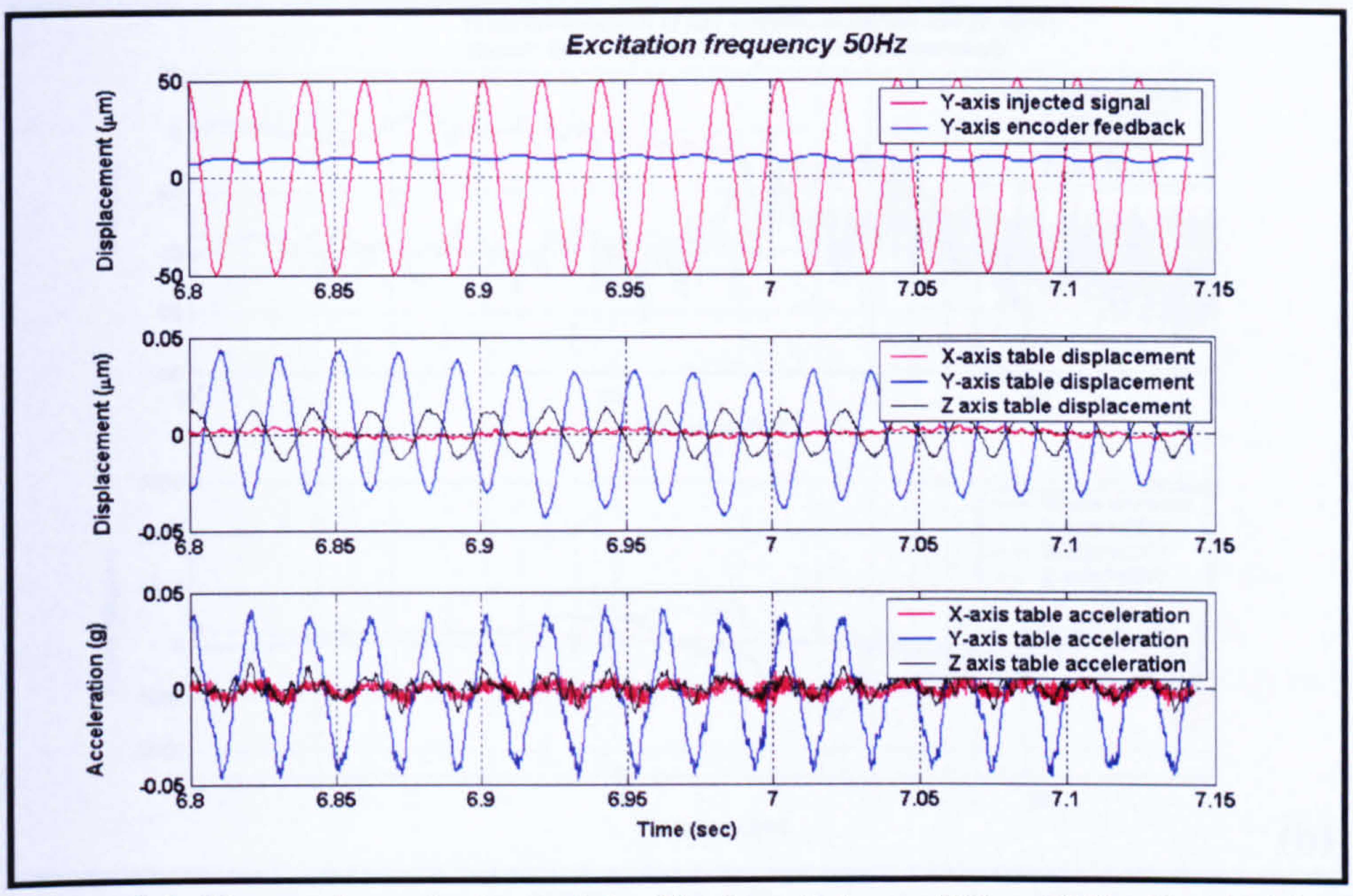

Figure 8.5: Harmonic excitations of the Cincinnati Arrow 500 at 50Hz: X-axis (a) and Y-axis (b)

The figure shows that at 50Hz excitation of the driving axes, the tri-axial sensors already revealed structural vibrations all three axes.

The following white noise tests (figure 8.6) were used to estimate the non-parametric FRF in both axes and therefore give more exact information of the maximum bandwidth on the servo drive of this machine. The figures show that at about 25Hz for the Y-axis and 50Hz for the X-axis, the controlled movement of the excited single axis starts to be overshadowed by structural vibration in all 3-axis.

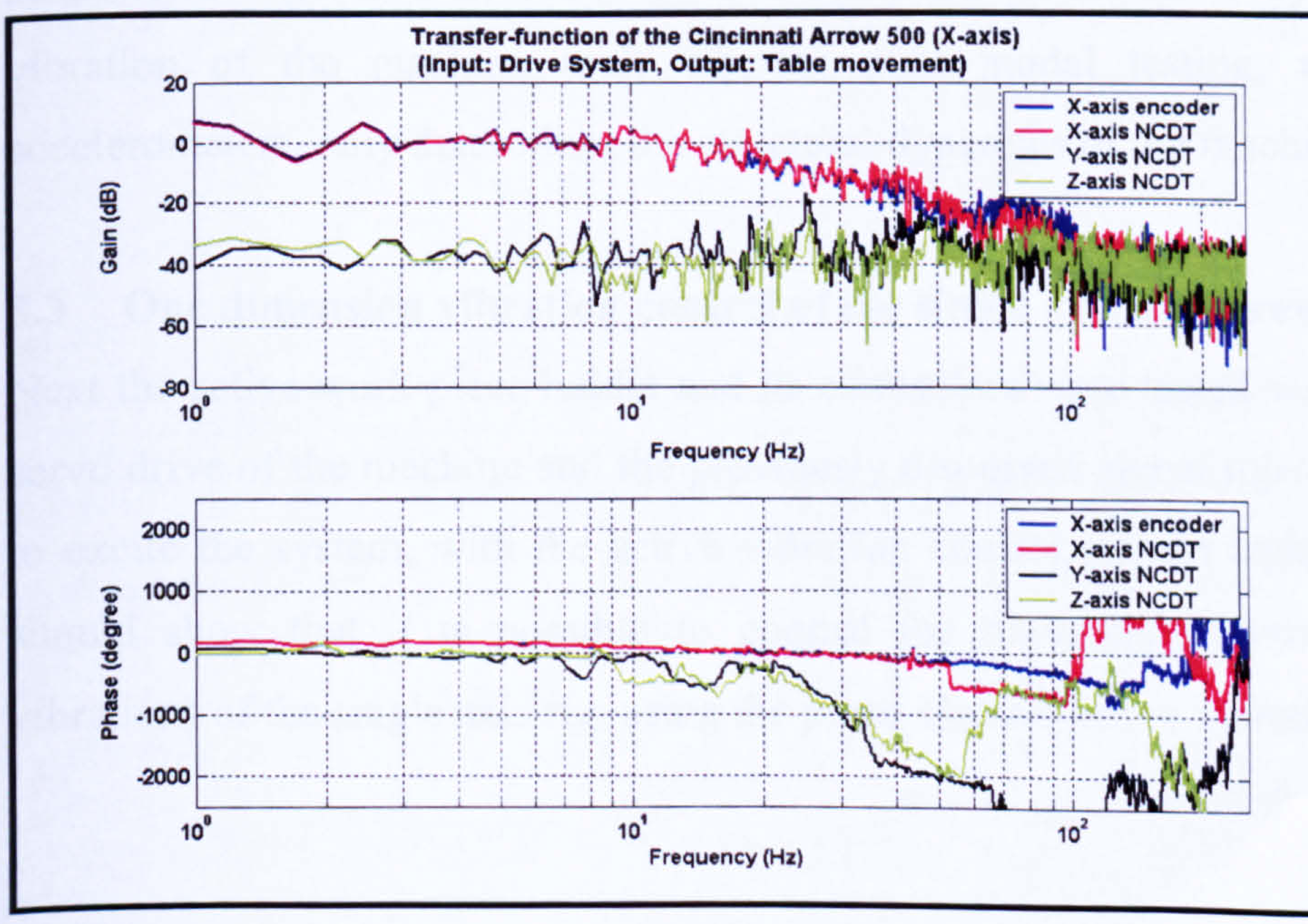

(a)

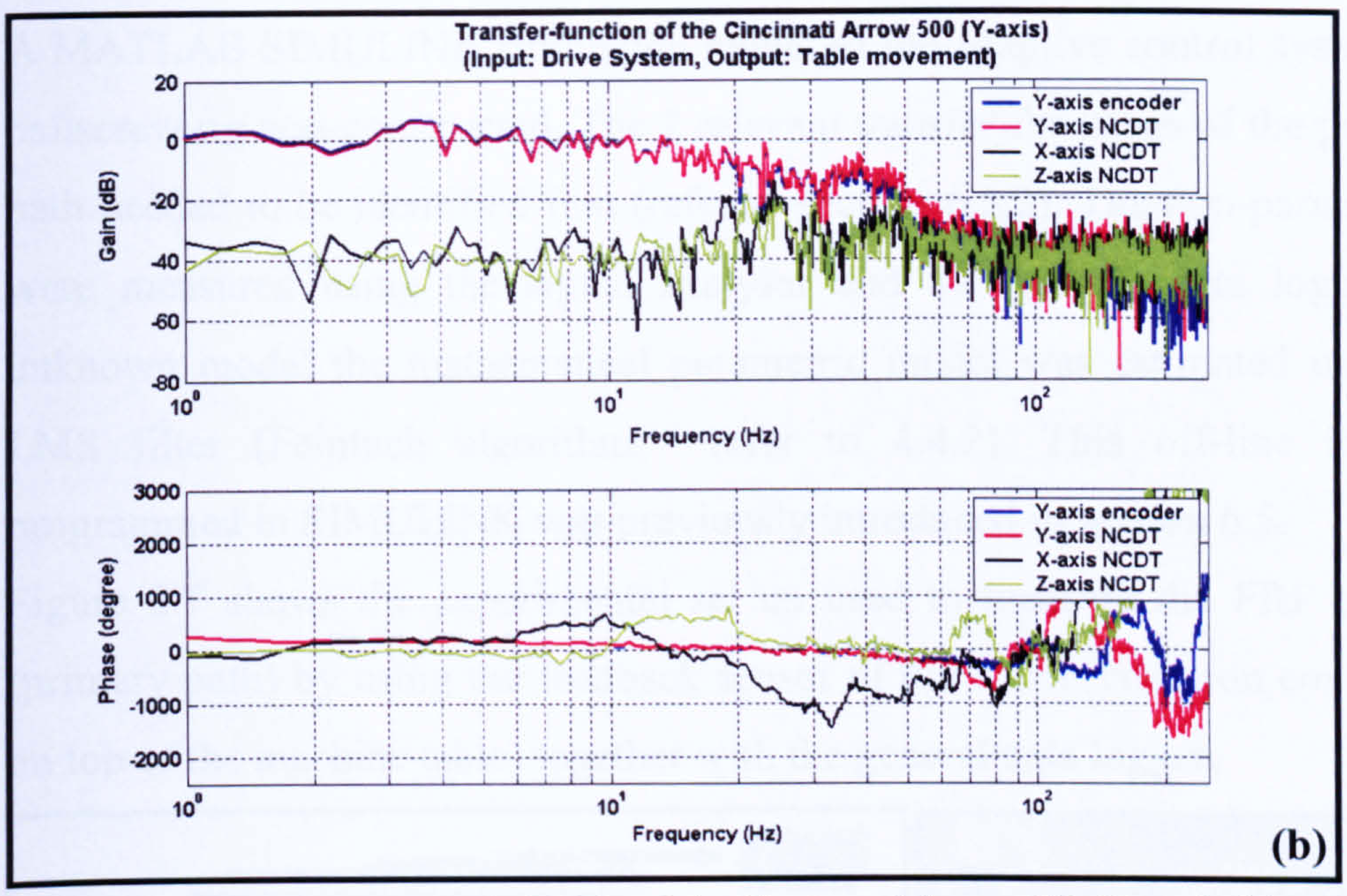

Figure 8.6: The non-parametric FRF's of the Cincinnati Arrow 500: X - axis (a) and Y- axis (b)

This is much better than on the previous ballscrew rig with the improvisational table attachment, since not only the bandwidth is higher, but also resonant peaks are not apparent. It should be mentioned that usually the low pass filter of the drive system is adjusted to filter any mechanical resonances of the machine structure out in any case, since these are highly undesirable. As expected the bandwidth of the Y-axis was lower since it not only has to carry its own weight but also the weight of the X-axis.

The tests have shown that the test procedure of injecting an excitation signal into the servo drive of one axis and measuring the resulting table response in 3 direction using displacement sensors, is a good method to link the dynamics of the drive system with the structural vibration of the machine tool, whereas pure modal testing, usually only done with accelerometers, only determines the structural dynamics of the machine.

8.3 One dimension vibration control of the single axis ballscrew rig

Next the active work-piece holder and its controllers were tested without cutting. Instead the servo drive of the machine and the previously discussed signal injection technique were used to excite the system, with the active vibration control system trying to reduce it. The tests should show that it is possible to control the previously investigated 3 axis structural vibrations of the single axis rig, using the piezo electric active vibration system.

8.3.1 Simulation

A MATLAB SIMULINK simulation model of the adaptive control system on the single axis ballscrew rig was constructed. The 2 relevant transfer-functions of the primary and secondary path needed to be identified first (refer to section 6.5.2). The non-parametric models (FRFs) were measured using the signal analyser and the general data logger [145]. From this unknown model the mathematical parametric model was estimated using the adaptive IIR LMS filter (Feintuch algorithm - refer to 4.4.2). This off-line identification routine, programmed in SIMULINK was previously introduced in section 6.5.

Figure 8.7 shows the experimental set up used to measure the FRF of the single axis rig (primary path) by using the feedback sensor of the active vibration control system (mounted on top of the machine table) together with the general data logger.

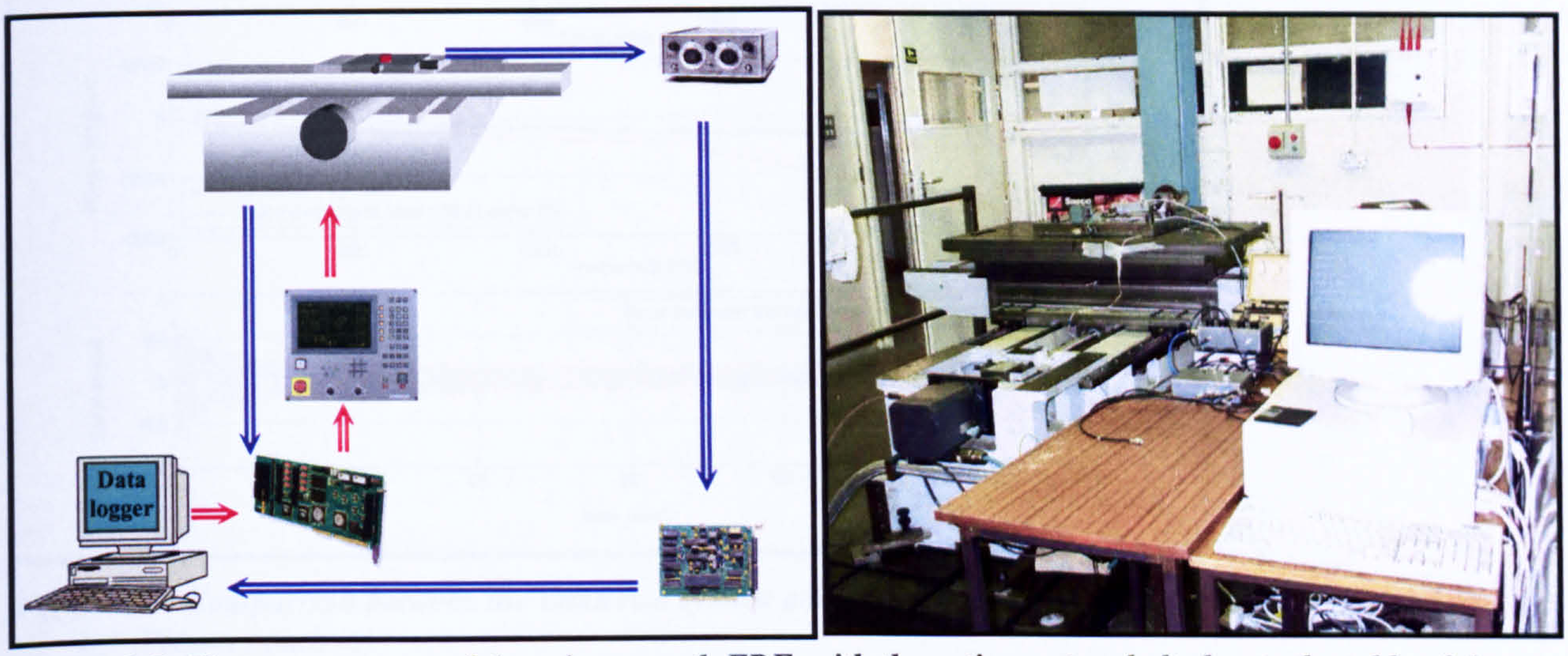

Figure 8.7: The measurement of the primary path FRF, with the active system bolted onto the table of the single axis Bridgeport rig

The feedback sensor for the controller was the accelerometer, whose output was integrated twice to obtain the displacement of the inner table of the active work-piece holder. The measurement of the FRF of the secondary path used the same sensor as the primary path but the excitation this time was introduced through the piezo actuator of the control system. The table displacement was monitored using NCDTs.

Both the mathematical models of the secondary path and primary path were obtained off-line using the SIMULINK identification routine. The secondary path model was also compared with the estimated model produced by the optional calibration routine of the digital controller (refer to 6.6.2).

Figure 8.8 shows the comparison between the unknown primary- (a) and secondary path (b) and their estimated digital models for the Y-axis.

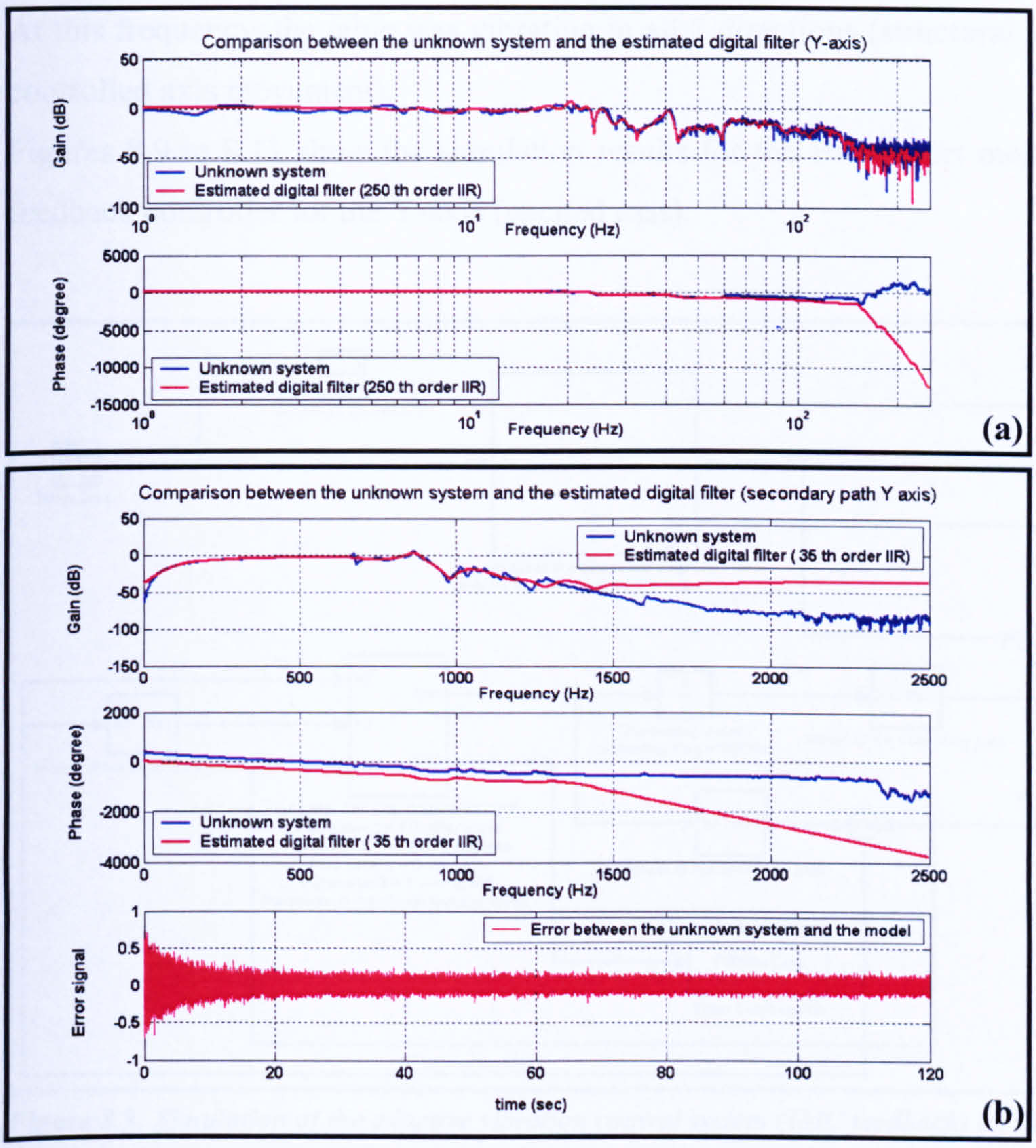

Figure 8.8: Comparison between the unknown system and the estimated digital models for:
- ***Primary path (a)***
- ***secondary path (b)***

The X- and Z-axis of the primary path were identified so that the system could be simulated in all 3 axes. The collected data of the primary path needed to be re-sampled in order to match the sampling frequency of the secondary path. This was necessary since the sampling frequency of the general data logger (500Hz) was 10 times lower than the sampling frequency of the spectrum analyser (5000Hz). The model order of the primary path was relatively high (250^{th} order) compared to the secondary path (35^{th} order). The reason for this was the limitation of the general data logger to collect only 10000 samples at high sampling frequency (the spectrum analyser has no such restriction). This meant that the noise of the FRF could not be averaged out, which led to a higher order of the model (figure 8.8.a).

Having identified all the relevant transfer-functions, the performance of the adaptive control system in reducing the vibration of the single axis rig was simulated. The 3-axis model of the Bridgeport rig was excited through the servo drive with a 10 μm peak injected signal at 80Hz.

At this frequency, the table was vibrating in all 3 directions (structural vibration rather than a controlled axis movement).

Figures 8.9 to 8.11 show the simulation results for the Bridgeport model using the adaptive feedback controller for the Y-axis (excited axis).

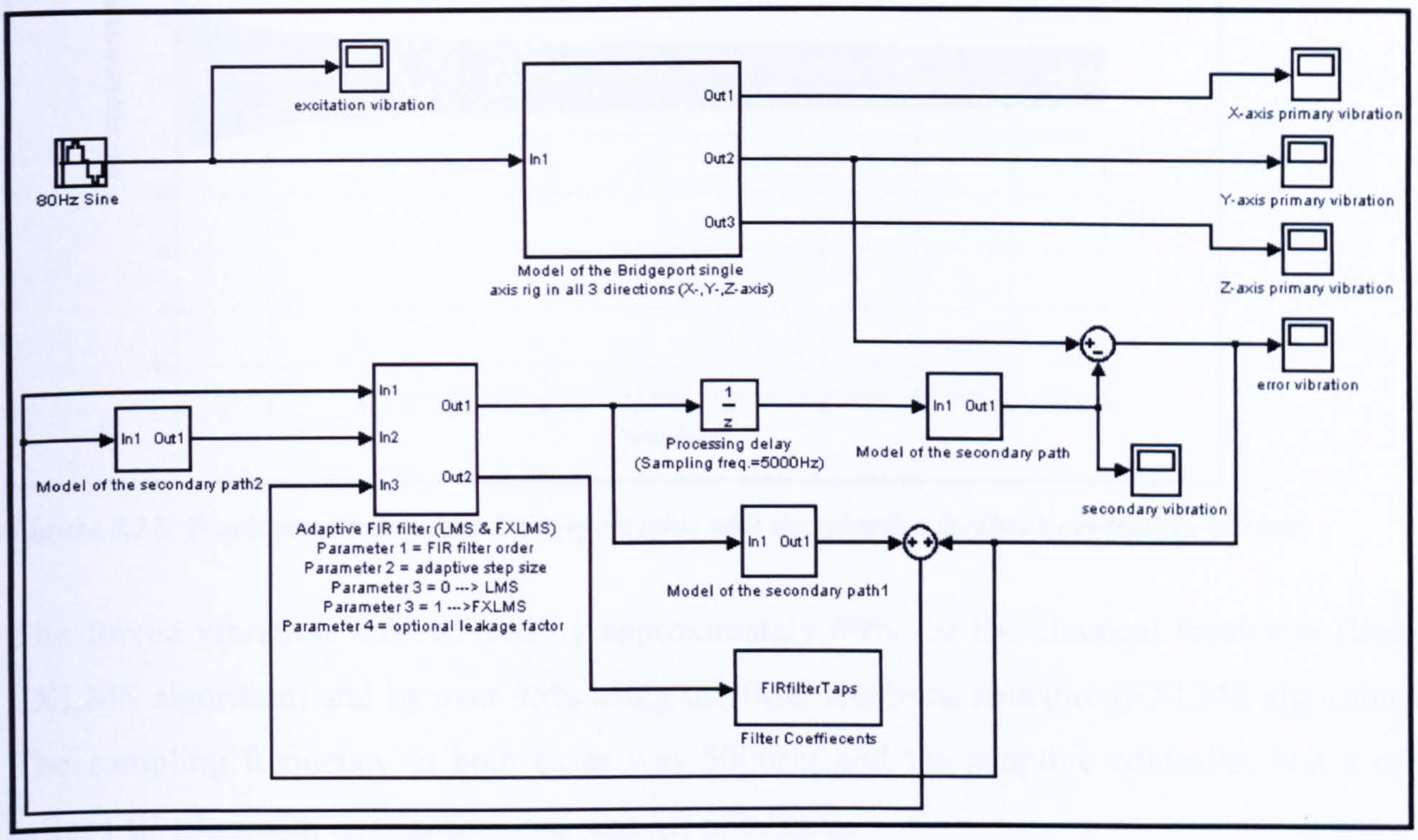

Figure 8.9: Simulation of the adaptive vibration control system (IMC feedback) on the Bridgeport rig

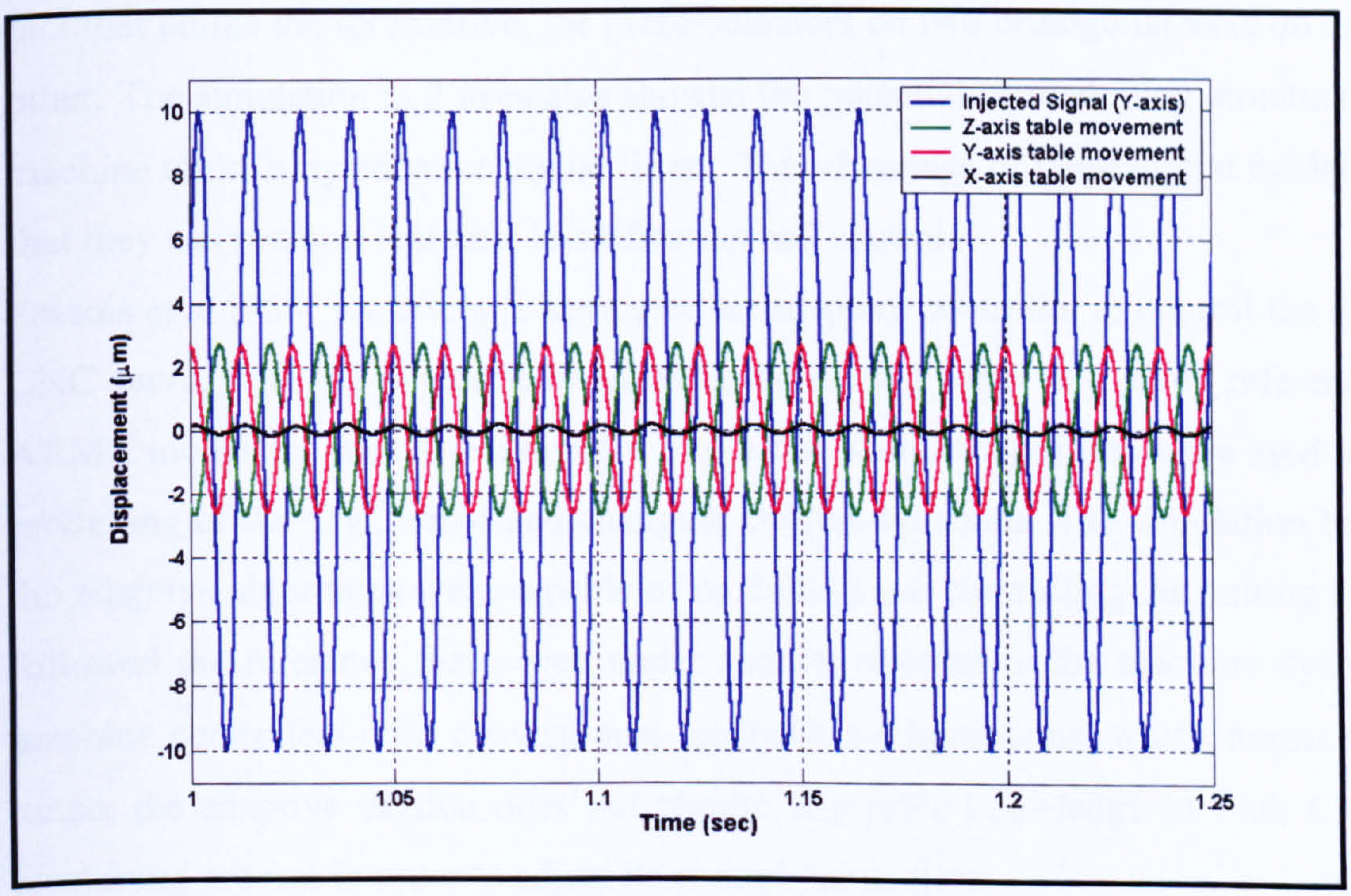

Figure 8.10: Simulation of the table movement of the Bridgeport rig at 80Hz with the Y-axis controller off

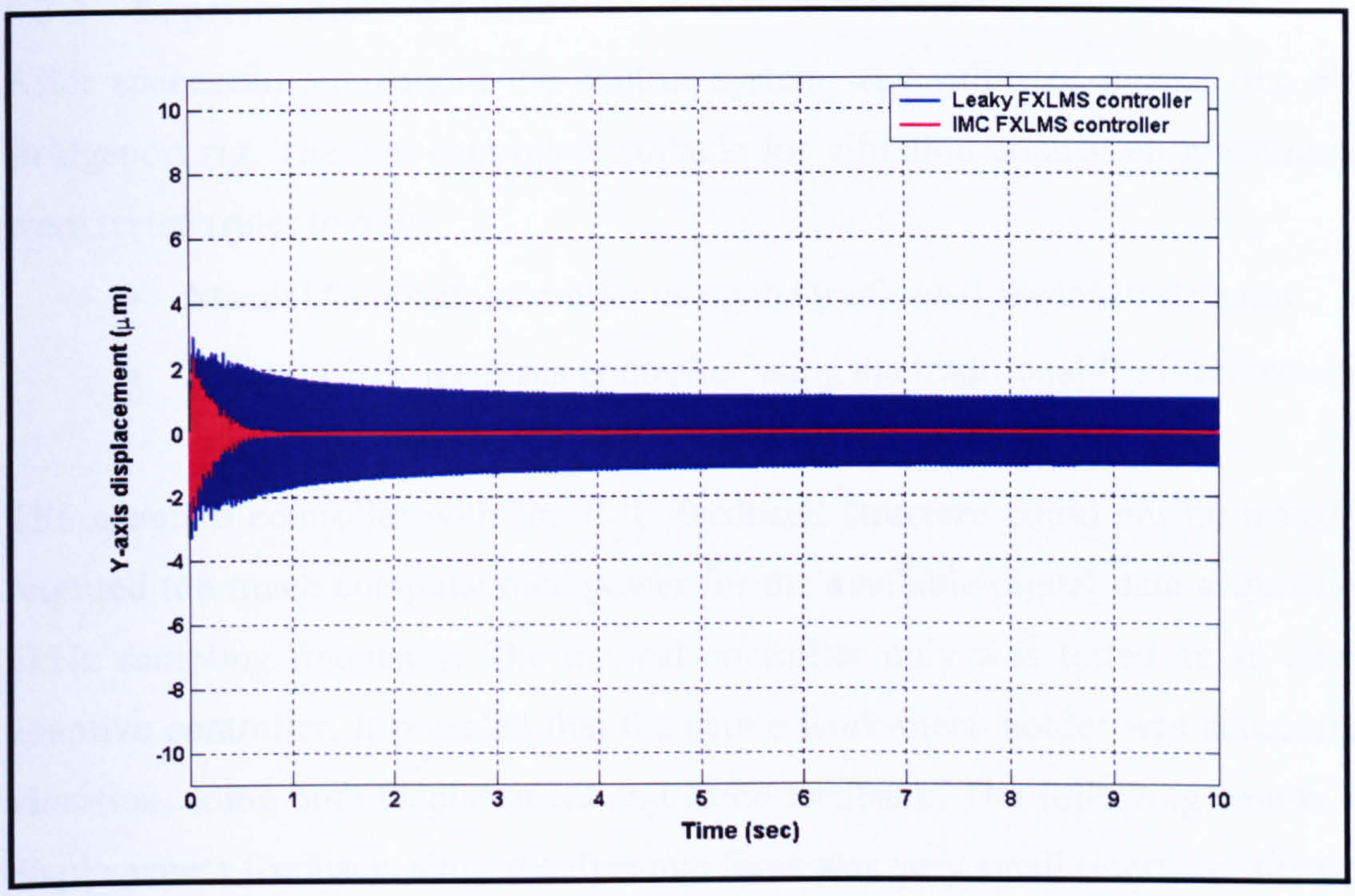

Figure 8.11: Y-axis movement of the Bridgeport table with the adaptive feedback controllers activate

The forced vibration was reduced by approximately 60% for the classical feedback- (leaky FXLMS algorithm) and by over 95% using the IMC feedback-structure (FXLMS algorithm). The sampling frequency in both cases was 5000Hz and the adaptive controller had a 65[th] order FIR filter with an adaptive step size (μ) of 0.0002.

The following experiments on the real rig validated this simulation and also confirmed the fact that unlike the servo-drive, the piezo-actuators on two orthogonal axes do not affect each other. The simulation in 3 axes also showed the potential of modelling structural elements of machine tools using adaptive digital filters. The advantage of these digital model estimators is that they can perform real time identification and control.

Fassois et al [158] for example have used an adaptive controller to control the feedrate of the CNC servo, with the objective of tracking the cutting force to a given reference signal. An ARMA model and recursive estimator plus a fast Kalman algorithm were used for the on-line modelling of the CNC servo and changing cutting dynamics. The simulation has shown that the adaptive algorithms were capable of modelling and controlling the cutting force so that it followed the reference force even under sudden changes in the machine dynamics. Unlike machine controllers with conventional feedback configurations, which normally need to be tuned, the adaptive version does not require any prior knowledge of both CNC servo and machining process in order to adjust its control parameters.

8.3.2 Experimental validation

After successful simulation, the control system was validated against the real single axis Bridgeport rig. The two controllers suitable for vibration control on machine tool structures were tested (refer to 6.9):

- Manual feedback controller using the traditional feedback structure
- Adaptive FIR feedback controller using the traditional feedback structure

The adaptive controller with the IMC feedback structure could not be tested here, since it required too much computational power for the available digital data acquisition platform at 5kHz sampling frequency. The manual controller only was tested as an alternative to the adaptive controller. It revealed that the active work-piece holder was successful in reducing vibration, using both displacement and force feedback. The following results only show the displacement feedback, since the dynamic force was very small (inertia of the weight from the inner table of the active work-piece holder).

Figure 8.12 shows the experimental set up for the adaptive digital controller, whereas figure 8.13 represents the manual electronic controller.

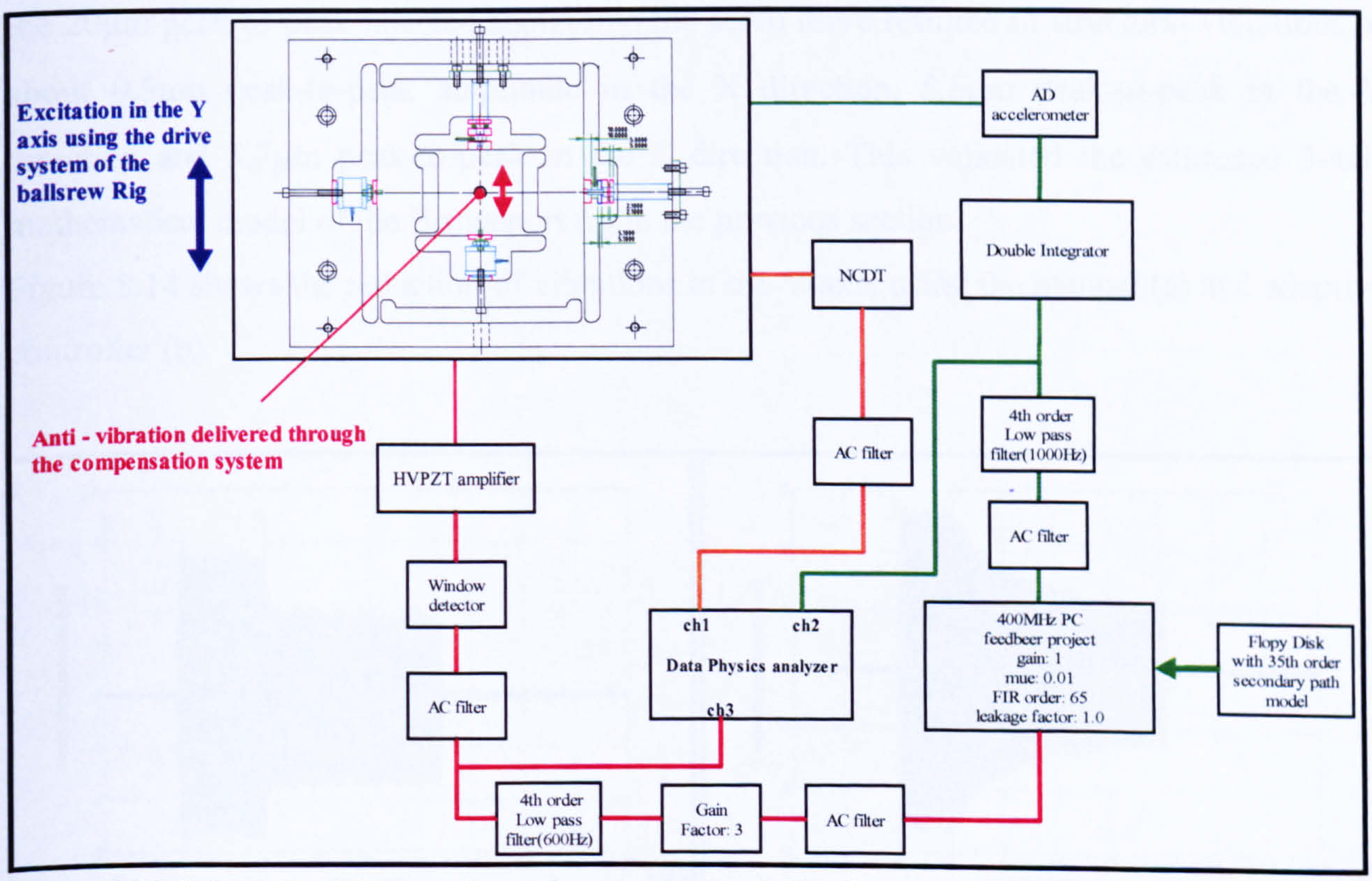

Figure 8.12: Schematic of the experimental set up to control vibrations on the single axis Bridgeport rig using the digital adaptive controller

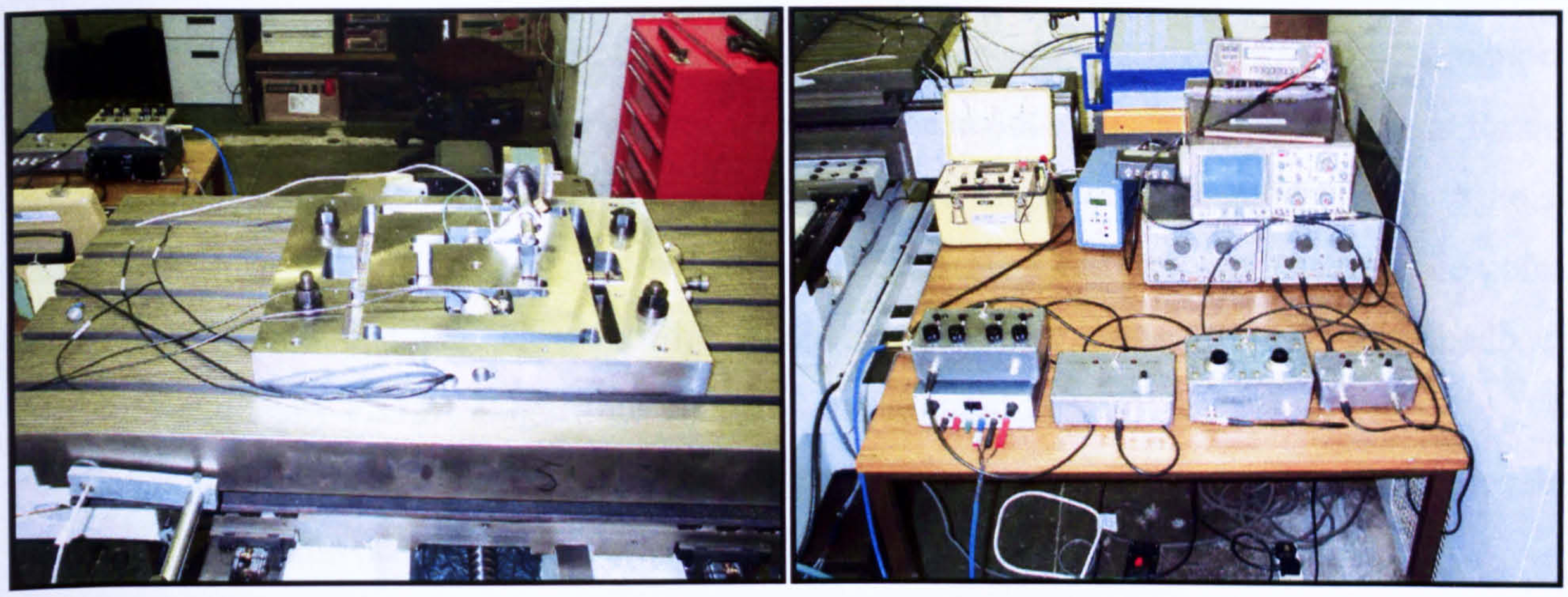

Figure 8.13: Experimental set up to control vibrations on the single axis Bridgeport rig using the manual electronic controller

The identification of the secondary path for the adaptive controller was done with the optional on-line calibration routine. It was found that the estimated model was just as good as with the designed off-line identification routine using SIMULINK.

As already discussed, the feedback sensor was the double integrated Y-axis accelerometer output, whereas the resulting 3-axes vibrations were monitored using the NCDT's. At 80Hz, the 20μm peak-to-peak injected signal into the servo drive resulted in structural vibrations of about 0.5μm peak-to-peak amplitude in the X direction, 5.6μm peak-to-peak in the Y direction and 5.7μm peak-to-peak in the Z direction. This validated the estimated 3-axis mathematical model of the Bridgeport rig in the previous section.

Figure 8.14 shows the reduction of vibrations in the Y-axis using the manual (a) and adaptive controller (b).

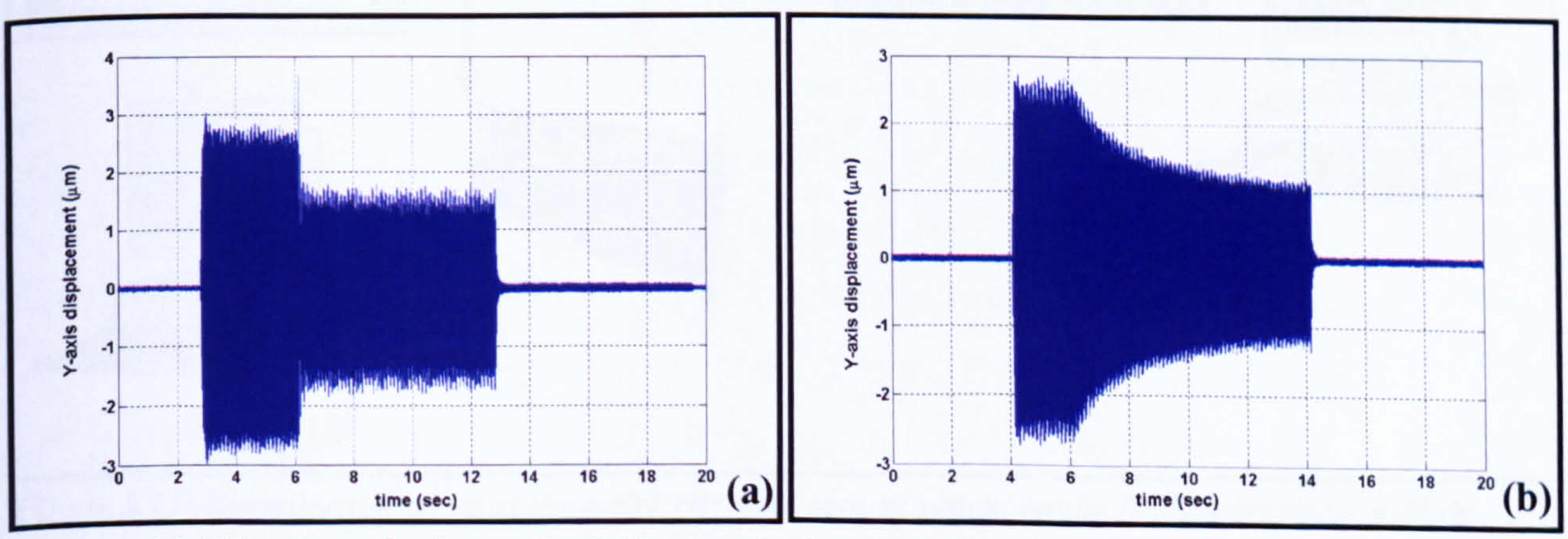

Figure 8.14: Vibration reduction on the Bridgeport single axis rig using the manual (a) and adaptive controller (b)

The vibration was reduced by about 60% for the adaptive controller and 40% for the manual controller. The major advantage for the adaptive controller was that the vibration was reduced automatically without tuning whereas time needed to be spent adjusting the parameters for the manual controller. The double integrated accelerometer signal had a good signal to noise ratio, and unlike the NCDTs, against which it was calibrated, did not need a reference point. The results show that the adaptive FIR feedback controller using the classical feedback structure and leaky FXLMS algorithm validated the simulation results.

As a conclusion for these static tests on the single axis ballscrew rig, figure 8.15 illustrates the whole experimental procedure using the adaptive controller.

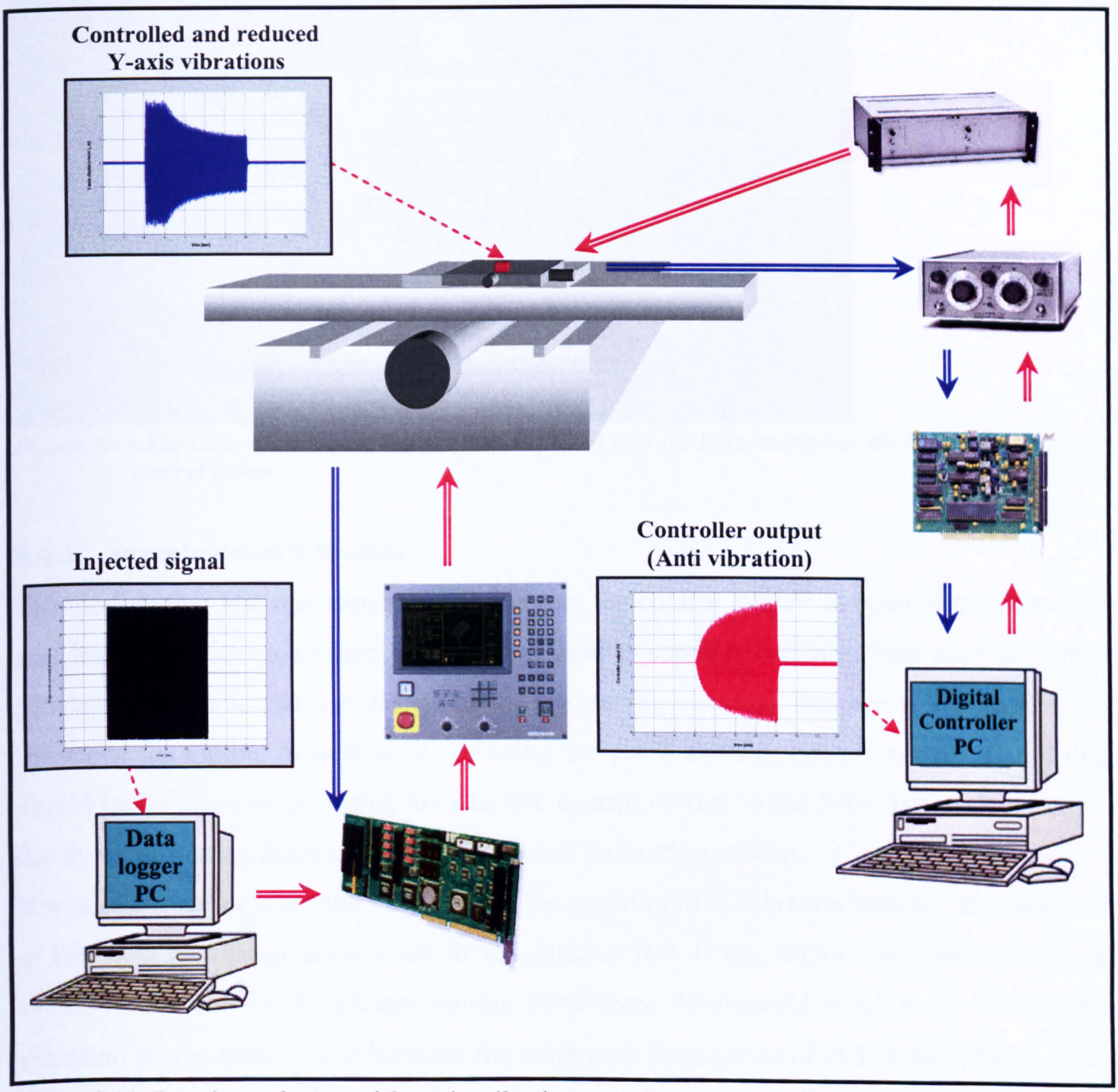

Figure 8.15: Experimental set up of the active vibration control system on the Bridgeport single axis rig

Next the active control system is tested on a machine tool under cutting conditions.

8.4 Cutting tests on a 3-axis machining centre with integrated active vibration system

The active vibration control system was integrated onto the same vertical machining centre used earlier for the first cutting test (Beaver VC 35 – refer to chapter 5). This allowed the improvement that the vibration control system has made to the machine tool performance to be revealed. Just as before, a 100 mm face mill cutter was used.

Figure 8.16 shows the integrated piezoelectric active vibration control system mounted on the machining table of the Beaver VC 35.

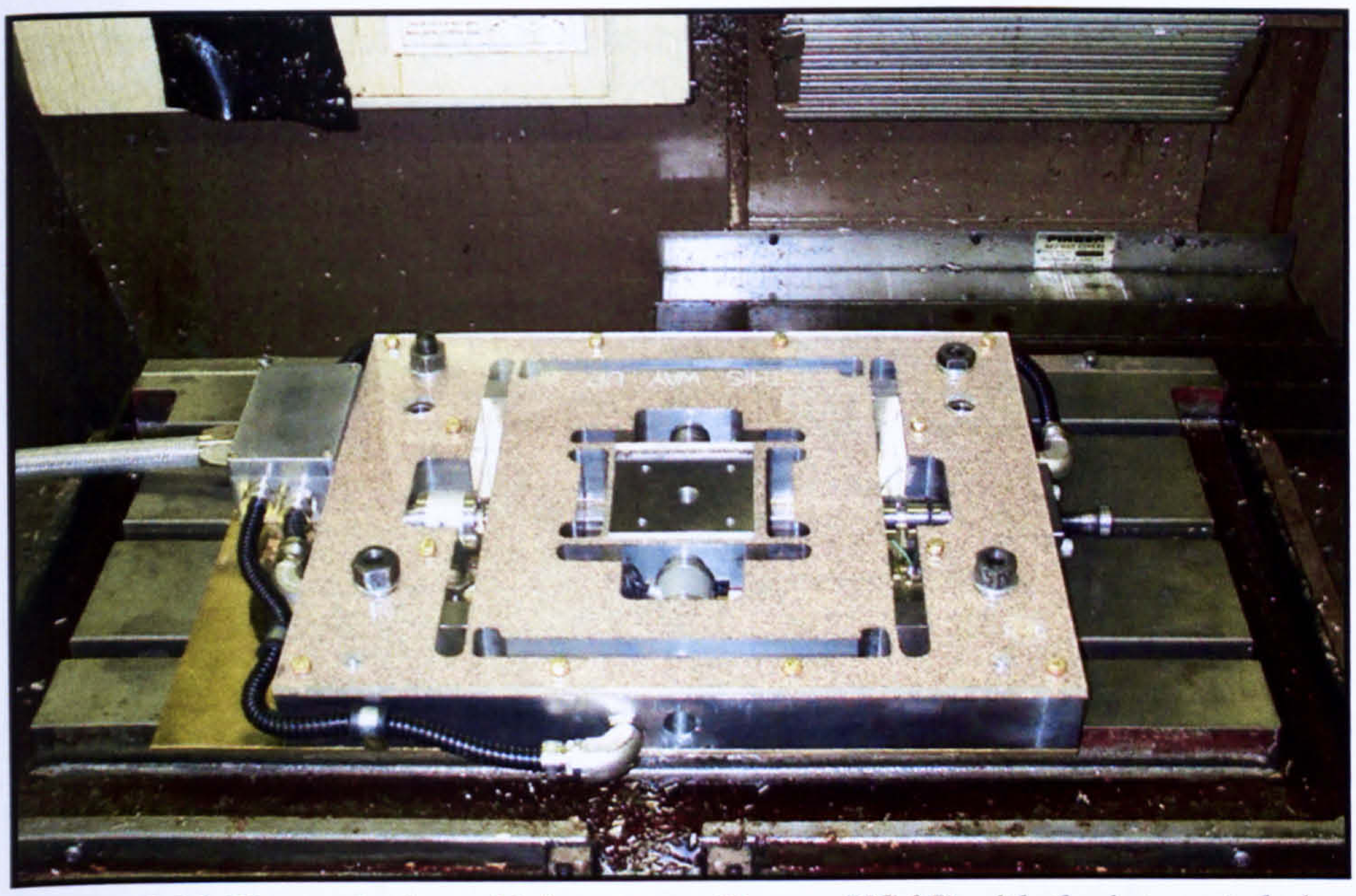

Figure 8.16: The vertical machining centre (Beaver VC 35) with the integrated piezo-electric active vibration control system

8.4.1 Superimposed vibration

The first cutting test was carried out by driving the control system in open loop. This meant that the active vibration control system was used to superimpose vibrations onto the cutting process. This validated the design of the system by showing whether it was possible to influence the cutting process at all by using the piezo actuator control system. If not there would be no sense in activating the adaptive control system in the hope that it would reduce the dynamic cutting force and vibration level of the cutting process.

It was important to select the frequency of the superimposed vibration between the harmonics of the tooth pass frequencies to see its maximum effect. It was decided to excite the actuator system at 330Hz for the chosen cutting conditions. This would result in an independent vibration source since it is in between the tooth pass frequencies of 295Hz and 354Hz. It was also unaffected by the 300Hz vibrations of the spindle thyristor drive. Both axes were excited separately in order to see whether there was any cross-talk between them. As already mentioned in the section 8.2 it was important, from a control point of view, that the actuator only modified the vibration in its own direction without influencing the other 2 axes.

The 330Hz vibration was first superimposed onto the cutting process via the X-axis of the piezo-electric actuator system. During this cut the actuator was switched off in order to see the difference it made. The cutting process was recorded using all the sensors of the active vibration platform, including the accelerometer on the spindle housing.

As an example, figure 8.17 shows the measured cutting force, with superimposed vibrations into the X-axis. The spectral density of each section of the cut shows the significant difference the piezo-electric actuator system made to the cutting process.

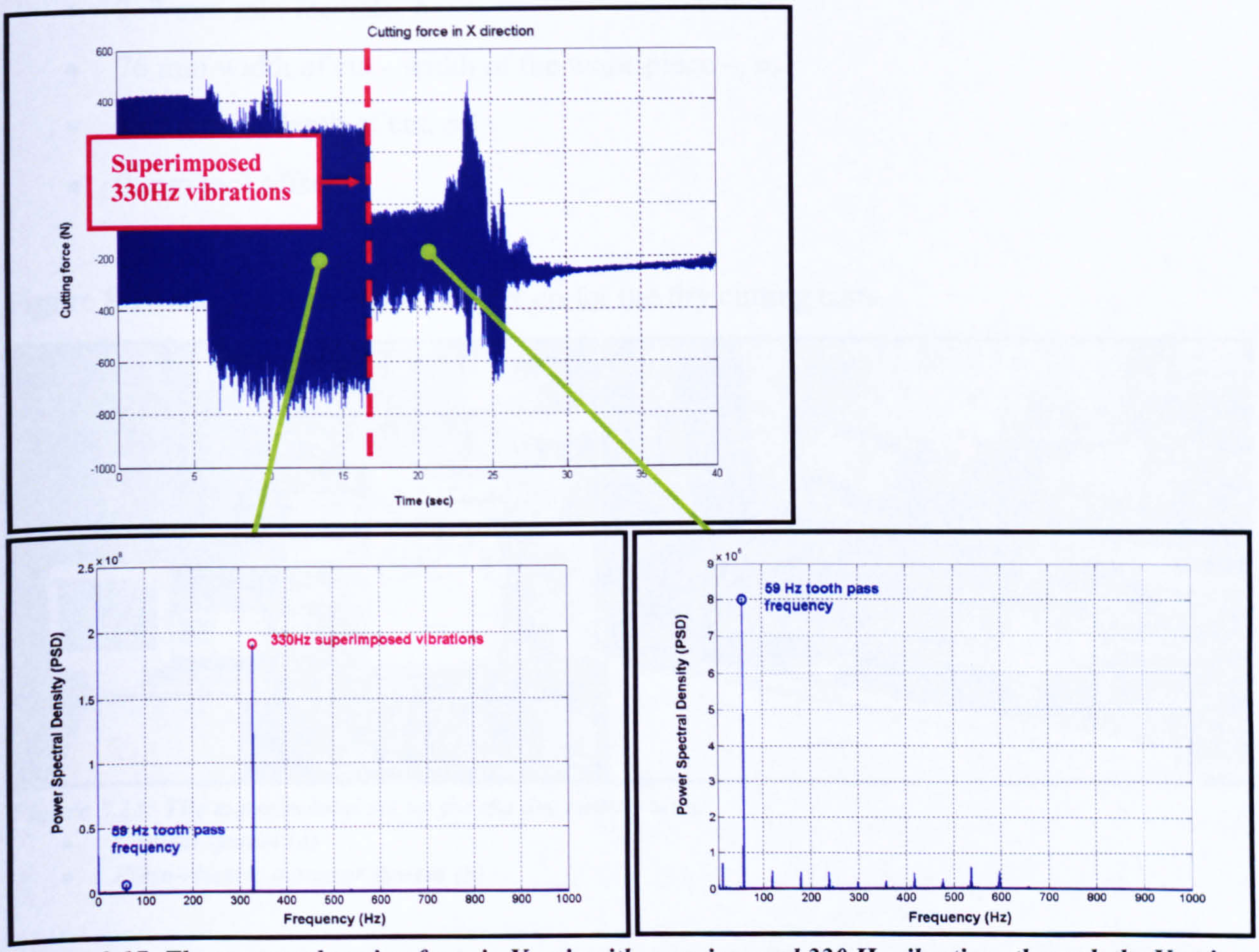

Figure 8.17: The measured cutting force in X-axis with superimposed 330 Hz vibrations through the X-axis actuator

It was found that it was possible to influence the cutting process significantly. There was also very little cross talk between the X- and Y-axis, which makes the piezo-electric actuator system ideal for the control purposes. Furthermore the open loop tests validated the mechanics and design of the piezo-electric actuator system. The next series of tests show how the system can be used to control the cutting process of a light and stable cutting operation.

8.4.2 Active vibration control of a light and stable cutting operation

Before the control system was used under heavy unstable cutting conditions, all the available controllers were tested on a light cutting operation without any coolant. The system should be able to control and reduce the dynamic cutting forces and the vibration levels of the cutting process and improve surface finish.

The cutting conditions for all the following tests were:

- 100 mm face mill, D_c
- 8 inserts, m
- 477 RPM spindle speed, n
- 267 mm/min feedrate, f
- 76 mm width of cut - width of the work-piece –, a_r
- 1 mm axial depth of cut, a_a
- 0 mm tool offset

Figure 8.18 shows the experimental set up for the dry cutting tests.

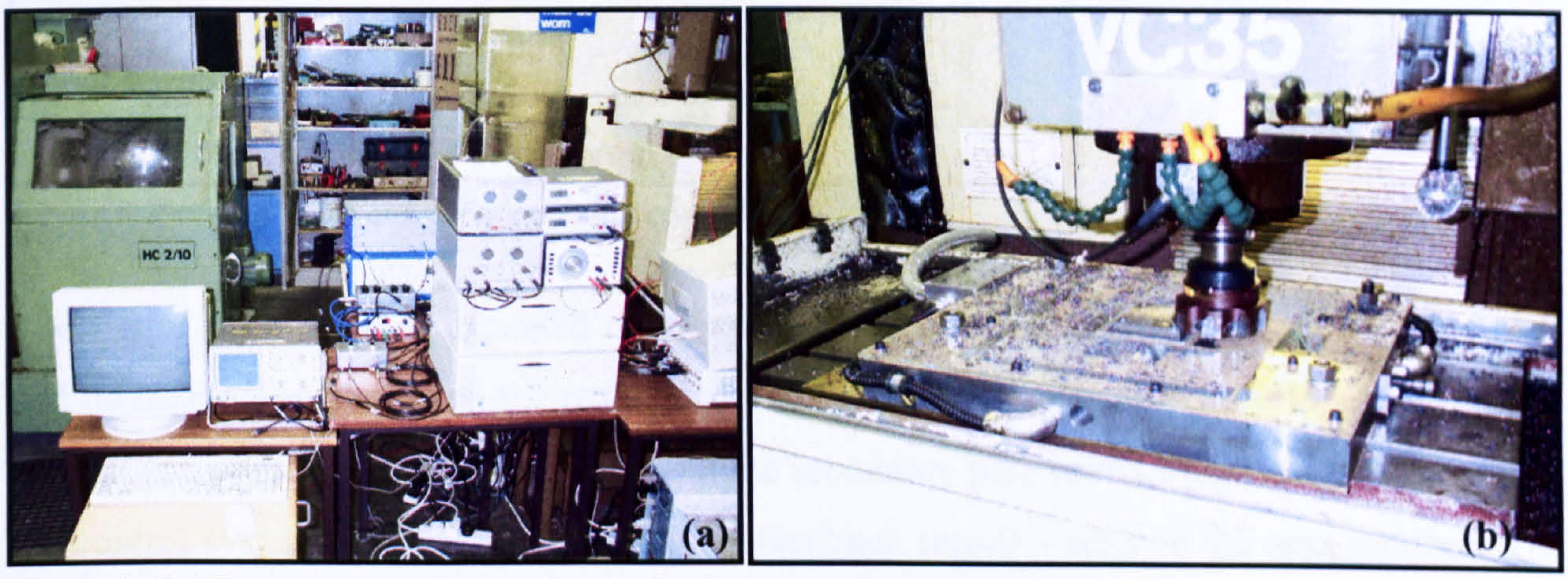

Figure 8.18: The experimental set up for the dry cutting tests:
- *Control system (a)*
- *Piezo-electric actuator system (b)*

8.4.2.1 Active vibration control using the manual feedback controller

The first controller to be tested was the manual feedback controller, with traditional feedback structure (refer to chapter 6.3, 6.8.2 and 6.9). This controller can be used to control a single frequency in the vibration spectrum, by manually adjusting the gain and phase of the feedback signal so that it is 180° out of phase with the vibration signal.

In this test it was used to reduce the 300Hz vibrations caused by the thyristor drive of the spindle motor. As already mentioned in chapter 5, this forced vibration is amplified significantly by a structural resonance in the spindle housing also at around 300Hz (refer to chapter 5.4 and 5.5 – figure 5.8b). The accelerometers on the spindle housing are therefore used as feedback sensors for the controller. Although the structural dynamics of the spindle housing acts as a bandpass filter for the 300Hz vibration, the additional bandpass filter for the manual controller made sure that the feedback signal was a pure harmonic signal with only varying amplitude. After the modification of the gain and phase through the controller, the control signal was fed to the piezo-electric actuator signal.

Figure 8.19 shows the difference of the spectral density with the controller on and off.

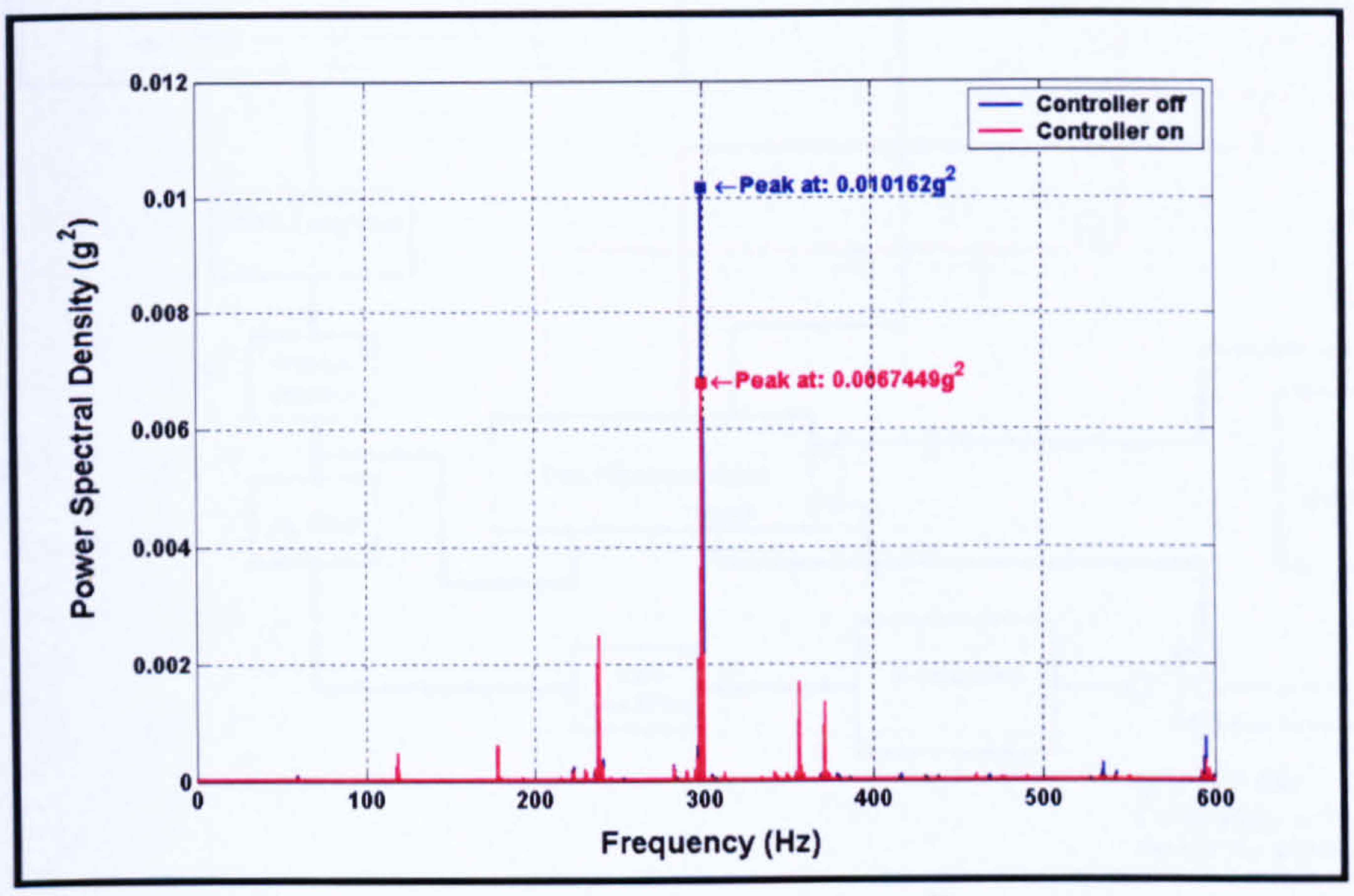

Figure 8.19: The performance of the manual controller

The figure shows that as expected the controller successfully modified the 300Hz vibration and its harmonics. However, the reduction of the 300Hz vibration was only 19%. The reason for that is a poor transfer-function between the secondary path (open-loop transfer-function of the control system between the actuator and feedback sensor – refer to the next section). The next test with the adaptive controller showed that the force sensor and work-piece accelerometer, which are closer to the actuator system, are much more suitable as feedback sensors.

8.4.2.2 Active vibration control using the adaptive feedback controller

In this test the adaptive feedback controller with the traditional feedback structure (refer to chapter 6.8 and 6.9) was used. The feedback sensor was either the work-piece accelerometer or the force sensor located on the piezo-electric active work-piece holder. The advantage of the adaptive controller is that it will not only control a single vibration frequency, but depending on the size of the adaptive filters, the whole region of the dominant frequencies (modal frequencies). Furthermore it does not require any complicated and time consuming tuning like many other control techniques. Figure 8.20 shows the schematics of the experimental test set up for both feedback options (dynamic cutting force and work-piece acceleration).

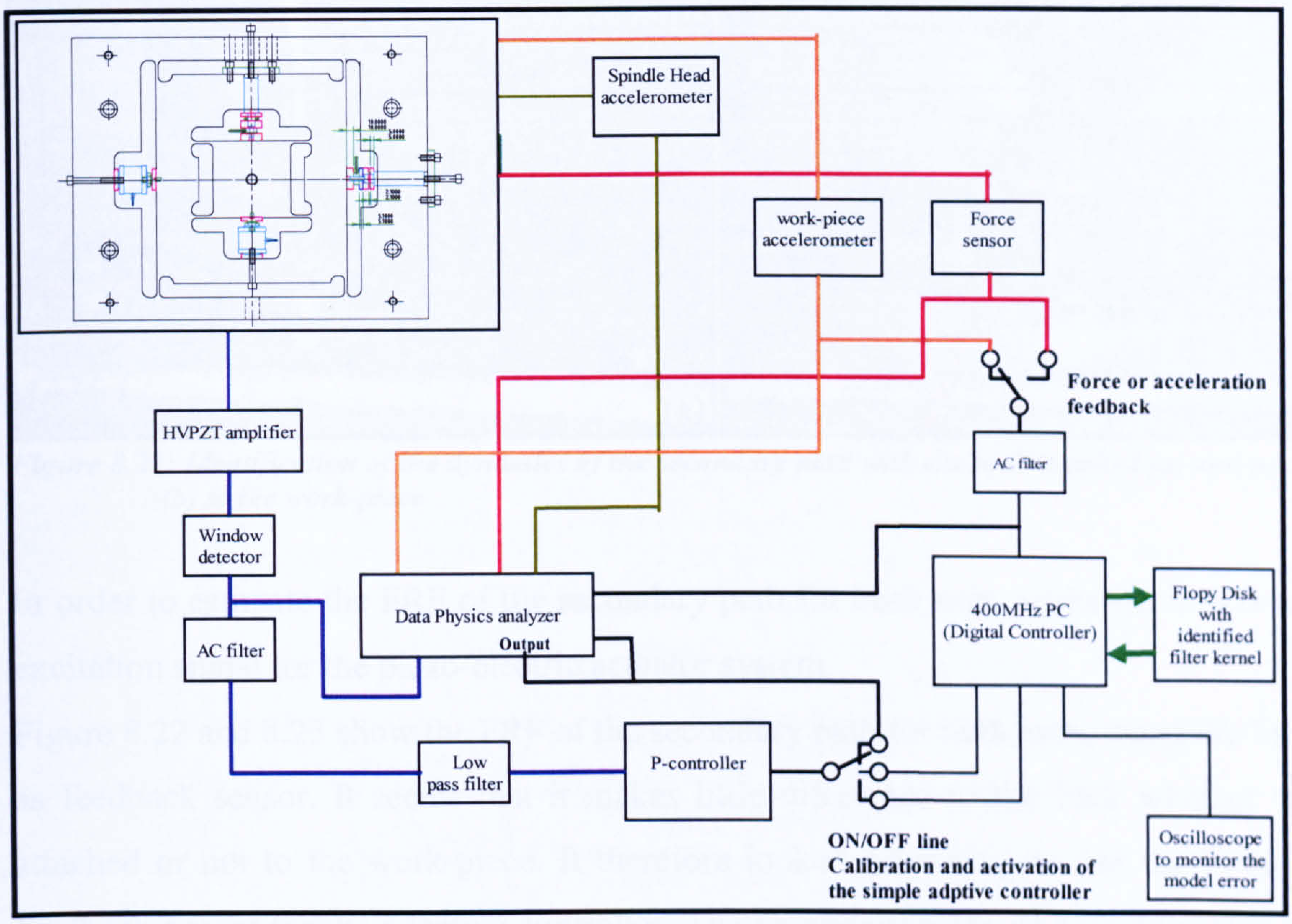

Figure 8.20: The schematics of the experimental set up for the adaptive controller

8.4.2.2.a Identification of the secondary path

Before the adaptive controller could be used, the secondary path needed to be calibrated (refer to chapter 6.7). Since the secondary path is the transfer-function of the open loop for a traditional feedback control system it can be used as an indication for the closed loop performance of the controller and the most suitable feedback sensor. The identification of the secondary path was carried out with all the available sensors as possible feedback sensors for the control system. The identifications were carried out off-line, and on-line using the calibration routine of the adaptive controller on-line (refer to chapter 6.6.2).

Apart from the right choice of feedback sensor, there was also the question to be asked, whether the proper secondary path is the one with the tool attached or not attached to the work-piece. This would depend on the physical connection of the cutting tool inserts to the work-piece. The idea was to measure both secondary path transfer functions and, if very different, to use both of them for the adaptive controller and compare their performance. The advantage of the manual controller was that it did not require any knowledge of the dynamics of the open loop or secondary path transfer function. Figure 8.21 shows the set up for both the experiments, with the tool attached and not attached to the work-piece.

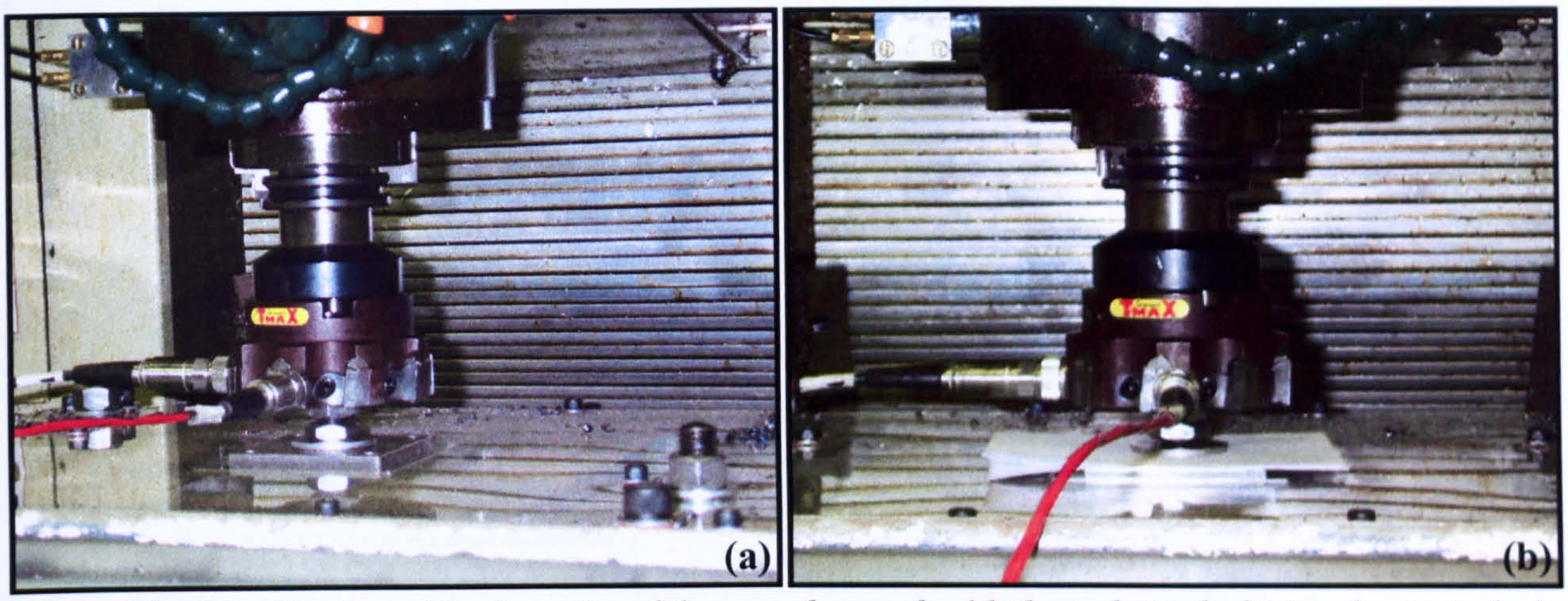

Figure 8.21: Identification of the dynamics of the secondary path with the tool attached (a) and not attached (b) to the work-piece

In order to estimate the FRF of the secondary path for both axes, white noise was used as an excitation signal for the piezo-electric actuator system.

Figure 8.22 and 8.23 show the FRF of the secondary path for both axes, using the force sensor as feedback sensor. It seems that it makes little difference to the FRF whether the tool is attached or not to the work-piece. It therefore looked promising to use the force sensor as feedback sensor for the adaptive controller. The secondary paths of both axes also seemed to be very direct, without affecting each other (25dB difference for the X-axis and 39dB for the Y-axis). Another advantage in using the force sensor is the effective bandwidth, from almost 0Hz to over 1000Hz for the Y-axis (500Hz for the X-axis).

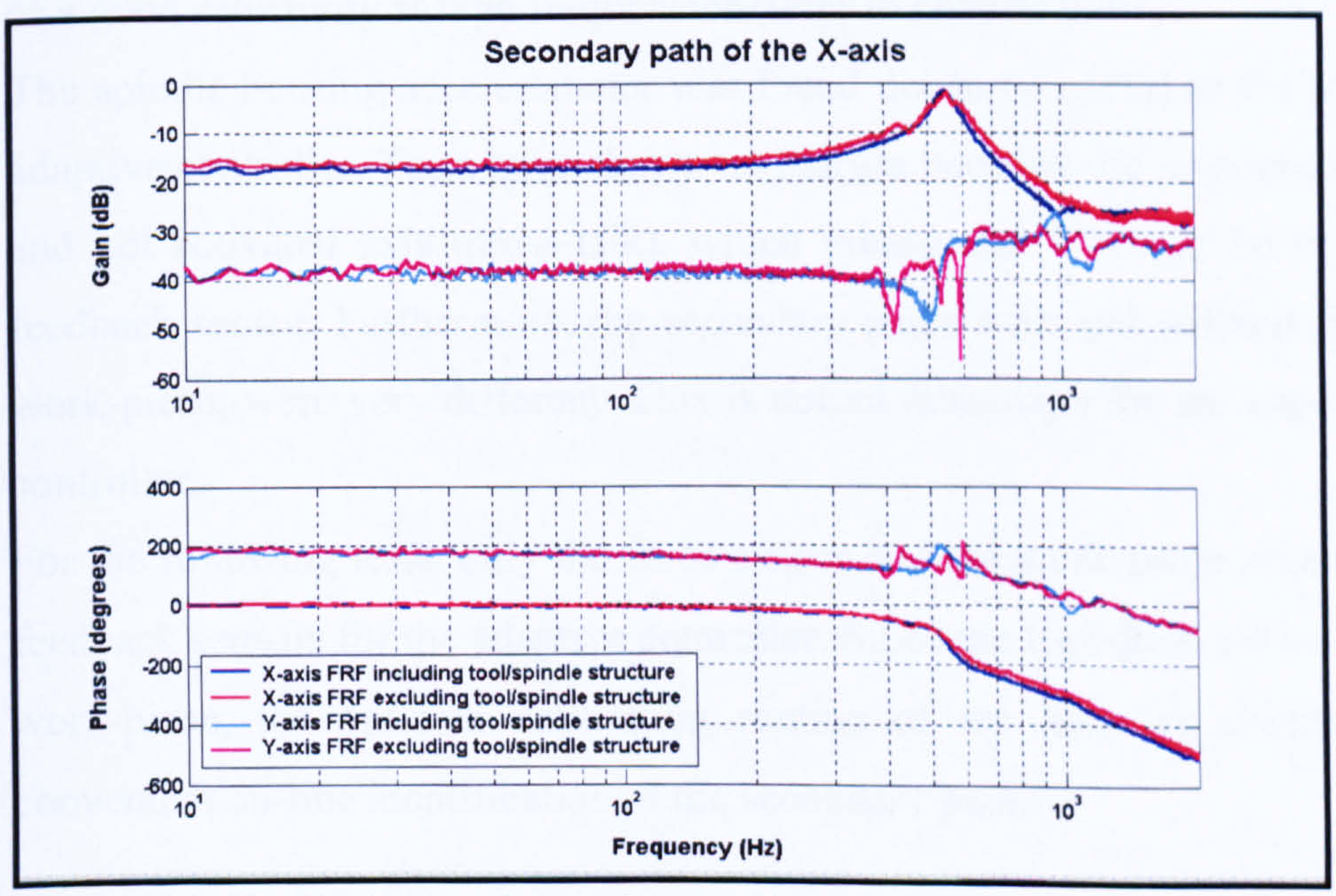

Figure 8.22: The X-axis secondary path using the force sensor as feedback or error sensor

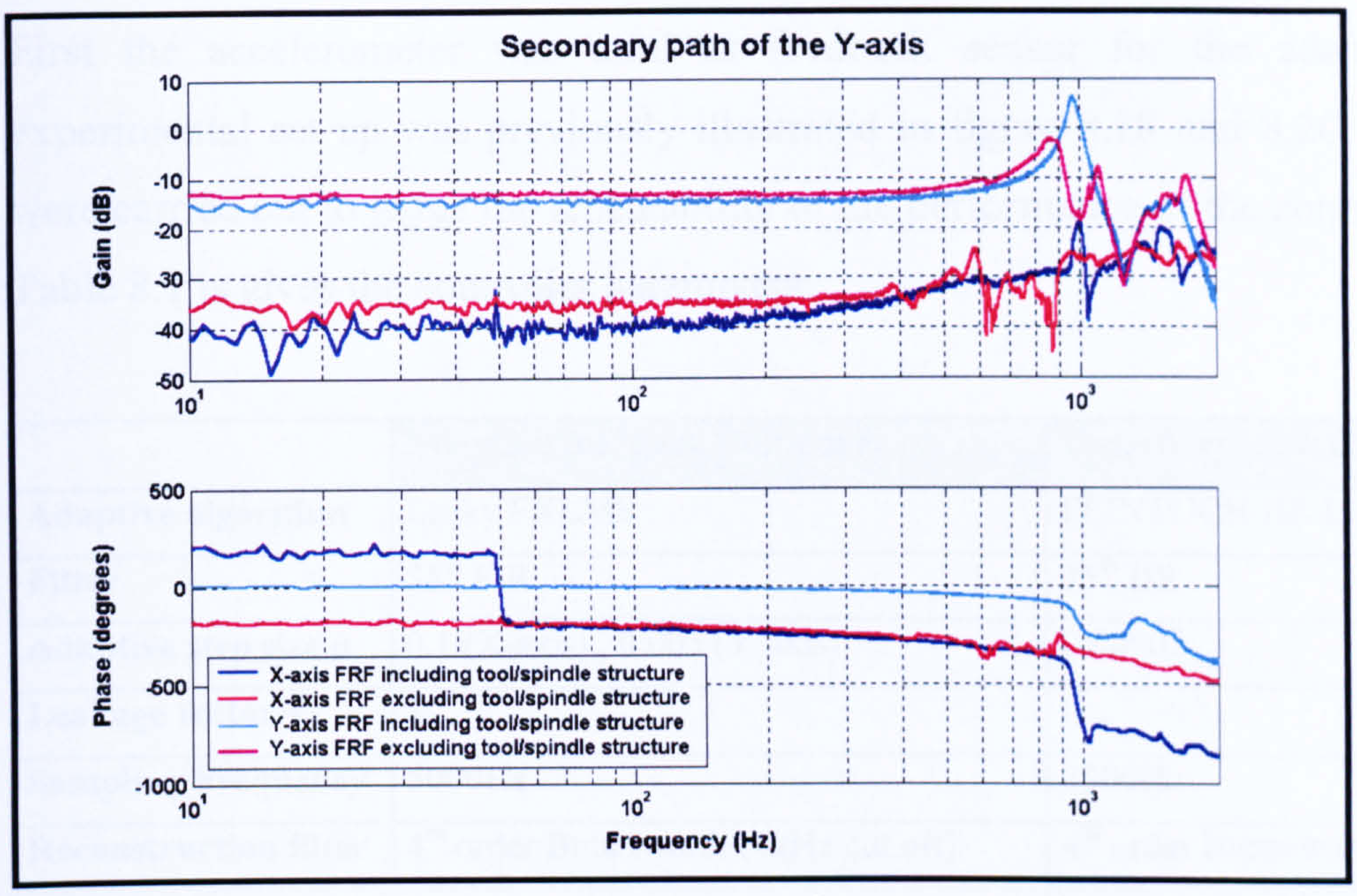

Figure 8.23: The Y-axis secondary path using the force sensor as feedback or error sensor

The other suitable feedback sensor is the work-piece accelerometer. Just as with the force sensor before the secondary path was not much different, whether the tool was attached to the work-piece or not. The measured cross talk here was also very small (about 20dB). The only thing to keep in mind was that an accelerometer is not very suitable for measuring low frequencies. For measuring chatter however, an accelerometer is usually ideal, since the frequency is typically over 100Hz. If, for some machines the chatter frequency or the modal frequency to control is low, the accelerometer signal can be integrated once or even twice, to obtain the velocity or displacement of the vibrations, although this again would be at the cost of a good sensitivity at high frequencies (refer to chapter 6.2.1).

The spindle housing accelerometer was found not to be useful as the feedback sensor for the adaptive controller. Tests have shown no margin between the response sensor of the activated and not activated axis (cross-talk), which means that it would be difficult to use them as feedback sensor. Furthermore, the secondary paths with and without the tool attached to the work-piece, were very different. This is not an advantage for the experimental testing of the controller.

For the following tests, only the force sensor and the work-piece accelerometer were used as feedback sensors for the adaptive controller. Since the tool does not have to be attached to the work-piece, the optional calibration routine of the adaptive controller can be used for convenient on-line identification of the secondary path.

8.4.2.2.b Acceleration feedback

First the accelerometer was used as feedback sensor for the adaptive controller. The experimental set up was previously illustrated in figure 8.18 and 8.20. Several cutting tests were carried out to judge the repeatability of the performance of the controller.

Table 8.1 is gives the controller parameters.

	Adaptive feedback Controller	Secondary path identification
Adaptive algorithm	Leaky FXLMS	FEINTUCH IIR LMS
Filter	35^{th} FIR	35^{th} IIR
Adaptive step size μ	0.1 (X-axis) , 0.005 (Y-axis)	0.00005
Leakage factor γ	1	-
Sampling Frequency	5000Hz	5000Hz
Reconstruction filter	4^{th} order Butterworth (4kHz cut off)	4^{th} order Butterworth (4kHz cut off)
Digital Gain	1	3.0 (X-axis), 1.0 (Y-axis)
Analogue Gain	4.5 (X-axis) , 3.0 (Y-axis)	1.0

Table 8.1: The parameter settings of the adaptive acceleration feedback controller

The higher the controller and filter order at the highest possible sampling frequency the better the performance of the controller (refer to chapter 6.9).

Figure 8.24 shows the performance of the adaptive piezo-electric control system using the measured vibrations (acceleration) as feedback signal on the stable cutting process.

The figure shows that the controller was able to reduce the vibration level significantly. The reduction was mainly achieved around the system resonance (as on the beam test rig).

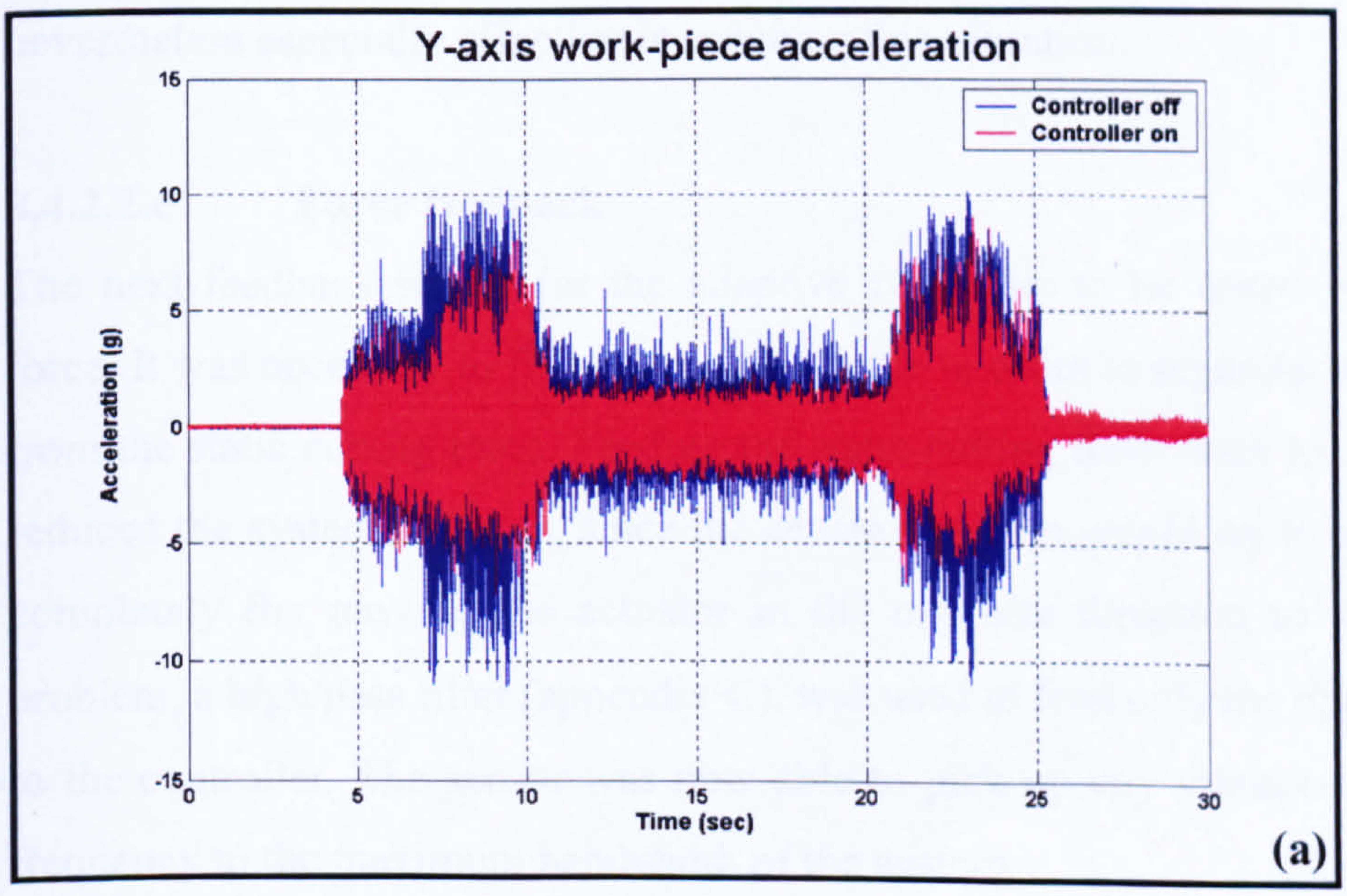

(a)

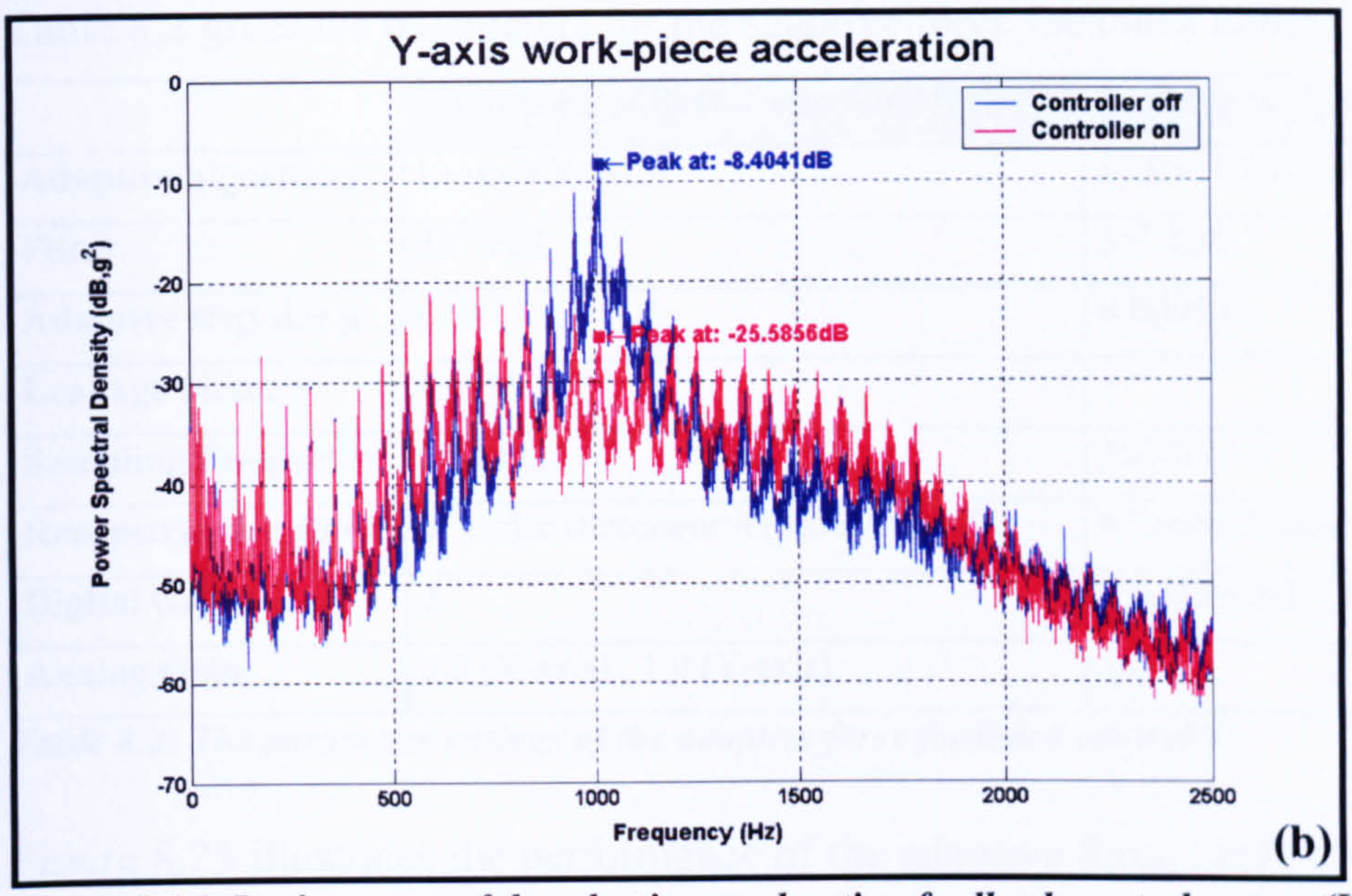

Figure 8.24: Performance of the adaptive acceleration feedback control system (Y-axis) on a stable cutting operation: Time response (a) and Power spectral density (b)

For the X-axis the system reduced the vibration level by 10-11dB (70%) at around 600Hz. For the Y-axis it was 16-17dB (85%) at around 1000Hz. This can be explained by the good sensitivity of the accelerometer around the resonance, which results in a strong feedback signal for the controller and actuator.

For the run-in and run-out of the cutter (refer to chapter 5.6), where the vibration level is much higher, the reduction was higher compared to the middle section of the cut (figure 8.24.a). The other reason, why the vibration level at the beginning and end of the cut are higher is because of the holes for the screws holding the work-piece, which lead to strong forced vibrations at the tooth pass frequency (and its harmonics). The control system was nevertheless especially effective in reducing this vibration.

8.4.2.2.c Force feedback

The next feedback sensor for the adaptive controller to be tested was the dynamic cutting force. It was necessary to filter the cutting force in order to separate the dynamic cutting force from the static cutting force. Feeding the static cutting force back to the controller effectively reduced the system stiffness, since the actuator system would try to avoid the cutting process completely (by moving the actuator in the opposite direction to the feed). To avoid this problem, a high pass filter (appendix C), was used to feed only the dynamic cutting force back to the controller. The sensor was now able to pick up any vibration from the cutter run-out frequency to the maximum bandwidth of the system.

Table 8.2 gives the parameters for the adaptive force feedback controller.

	Adaptive feedback Controller	Secondary path identification
Adaptive algorithm	Leaky FXLMS	FEINTUCH IIR LMS
Filter	35th FIR	35th IIR
Adaptive step size μ	0.001	0.00005
Leakage factor γ	0.9999	-
Sampling Frequency	5000Hz	5000Hz
Reconstruction filter	4th order Butterworth (2kHz cut off)	4th order Butterworth (2kHz cut off)
Digital Gain	1	3.0 (X-axis), 1.0 (Y-axis)
Analog Gain	2.5 (X-axis) , 1.0 (Y-axis)	1.0

Table 8.2: The parameter settings of the adaptive force feedback controller

Figure 8.25 illustrates the performance of the adaptive force feedback controller on the stable face milling operation.

The reduction using the dynamic force as feedback signal was about 6 -7dB (55%) at the spindle run out frequency of 7.4Hz (imbalance) and also for the tooth pass frequency of 59Hz. It is interesting that, compared to the acceleration feedback, the reduction of the dynamic cutting force, was the same for both axes, at the same low frequencies. This was expected since in contrast to the accelerometers, the low frequencies were not filtered out. The fact that the performance of both axes was almost the same compared to accelerometer feedback may be explained by the location of the sensor itself. The force sensors were located in a direct line with the piezo-electric actuators, and therefore picked up any movement or force generated. The accelerometer of the X-axis was much further away from the actuator than the one on the Y-axis, and the coupling was not as direct as with the force sensors (refer to chapter 7.4).

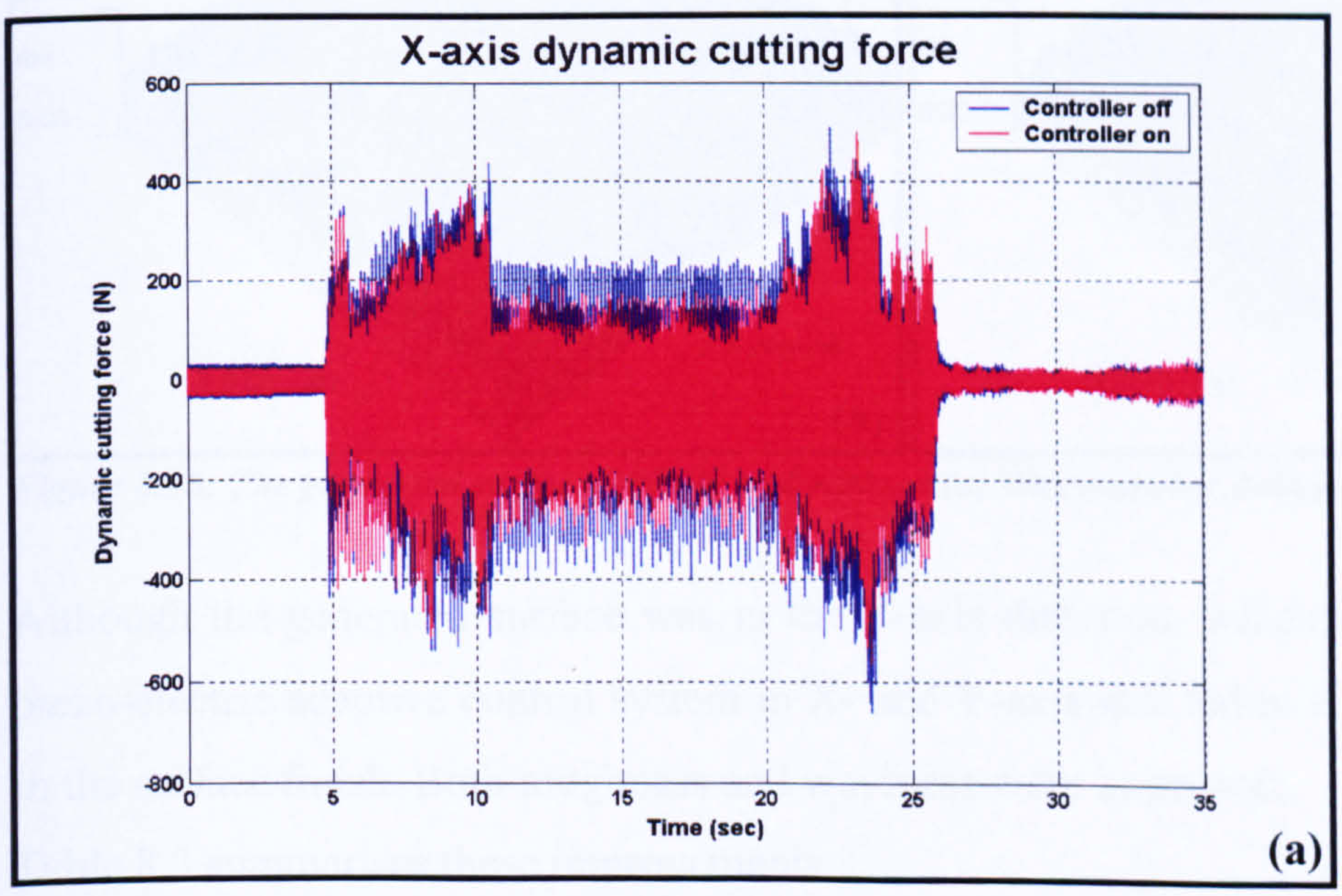

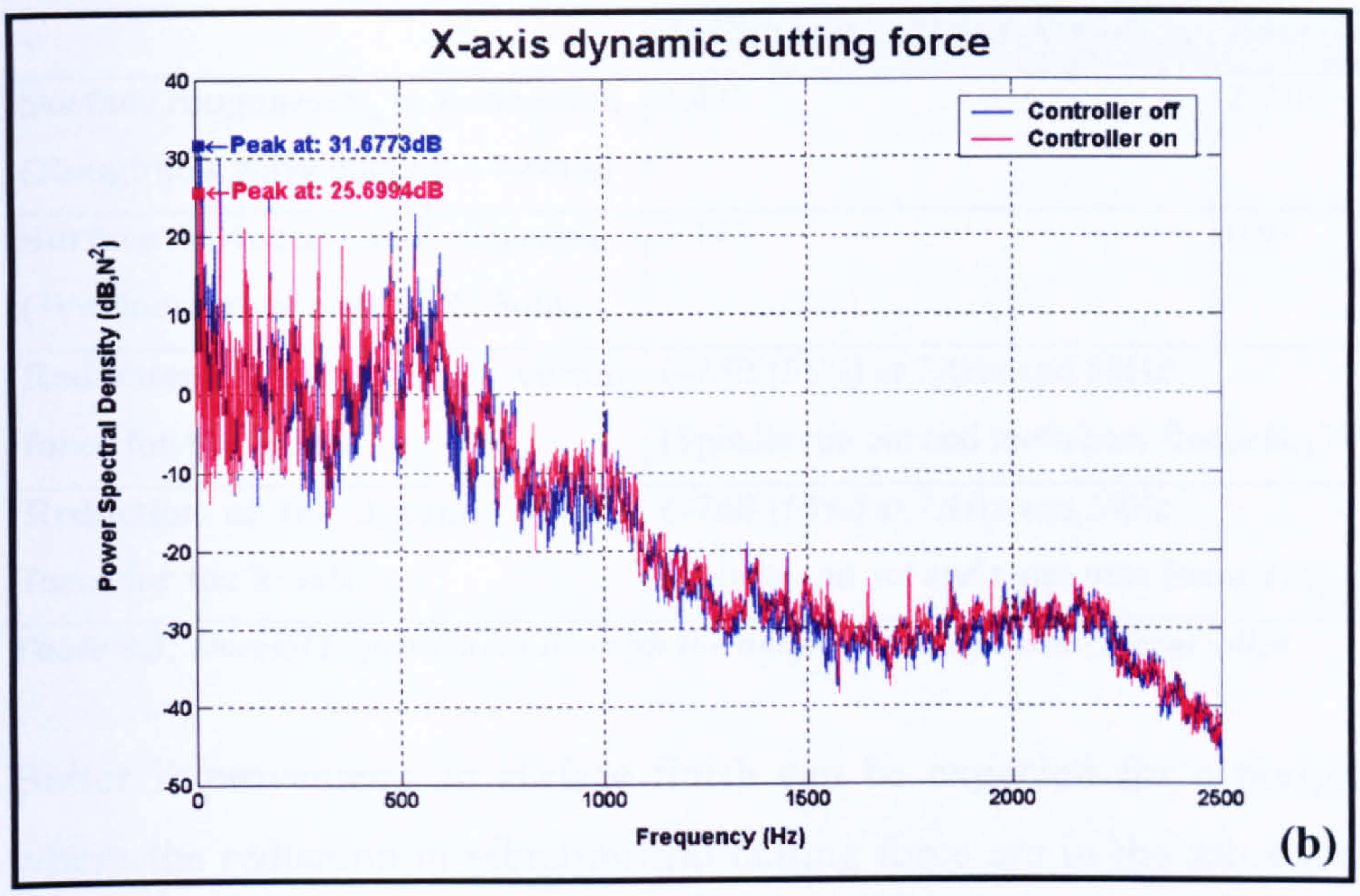

Figure 8.25: Performance of the adaptive dynamic force feedback control system (X-axis) on a stable cutting operation: Time response (a) and Power spectral density (b)

Although the overall reduction in vibration seemed to be less than with the accelerometers, from the generated surface point of view the dynamic cutting force feedback performed better as the following results show.

Figure 8.26 compares the surface just before and after the adaptive force feedback controller was activated. More information about the characterisation of surface topography used in this project are given by Jiang and Blunt [130,131].

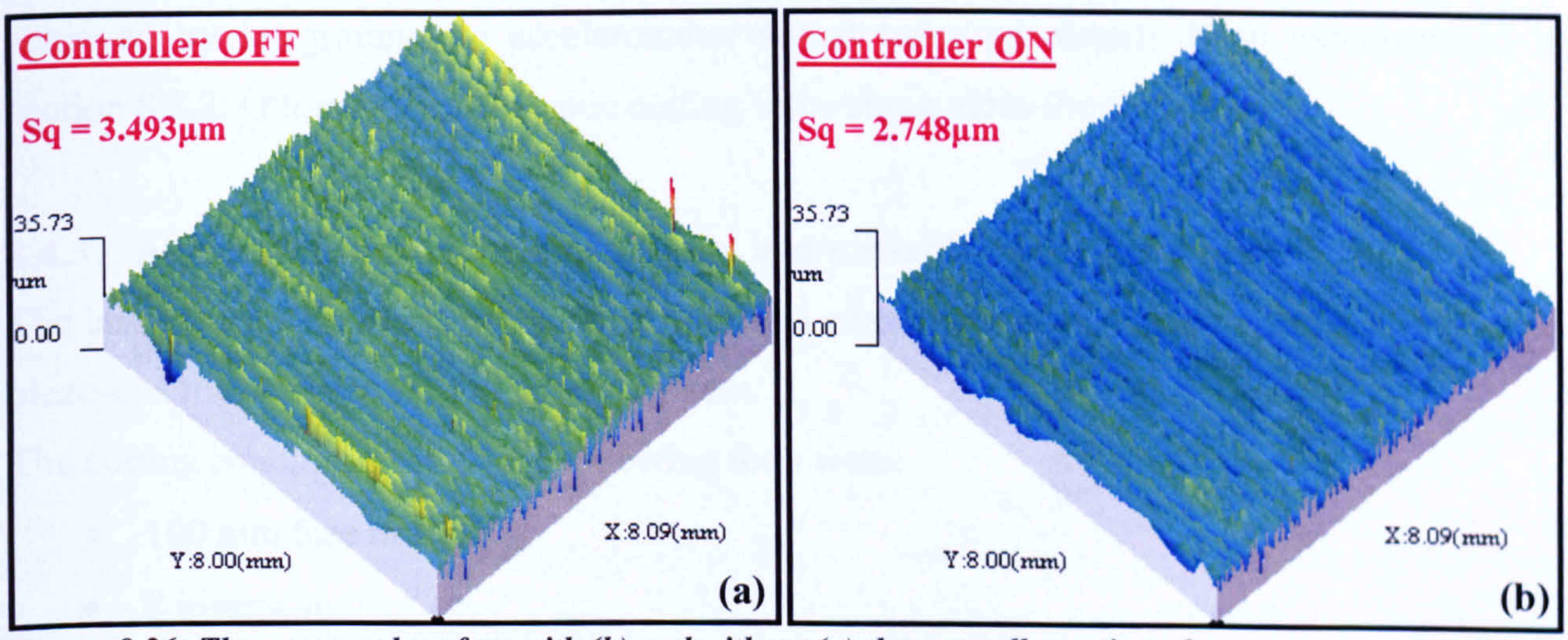

Figure 8.26: The generated surface with (b) and without (a) the controller activated

Although the generated surface was in the Z-axis direction, which is not under control, the piezo-electric adaptive control system in X- and Y-axis still led to a significant improvement in the surface finish. Both roughness and waviness were improved.

Table 8.3 summarises these improvements.

	Adaptive force Controller off	Adaptive force Controller on
Surface roughness S_q in Z-direction (Roughness wavelength 0 – 0.8mm)	3.493	2.748
Surface waviness S_q in Z-direction (Waviness wavelength 0.8 - 5mm)	1.148	0.93
Reduction of the dynamic cutting force for the X-axis	6-7dB (55%) at 7.4Hz and 59Hz (Spindle run out and tooth pass frequency)	
Reduction of the dynamic cutting force for the Y-axis	6-7dB (55%) at 7.4Hz and 59Hz (Spindle run out and tooth pass frequency)	

Table 8.3: Overall improvement through the adaptive force feedback controller

Better improvements in surface finish can be expected for a peripheral milling operation, where the reduction in vibration and cutting force are in the same direction as the generated surface finish.

The surface finish of the acceleration feedback system was also analysed, but since the main reduction in vibration was at high frequency (500Hz for the X-axis and 1kHz for the Y-axis), which appeared to be higher than the bandwidth of the discrete surface texture instrument, it has not been taken into account. It can therefore be concluded that the type of feedback sensor is important for the control objectives. The surface finish of a stable cutting operation is at very low frequencies, where the sensitivity of the accelerometer is very poor. If a vibration sensor is used then the displacement signal would be much more appropriate. This can be achieved by integrating the accelerometer signal twice as already been demonstrated in section 8.3.2. Otherwise the dynamic cutting force signal does the same job.

8.4.3 Active vibration control of a heavy and unstable cutting operation

The last experimental tests of the project were to control chatter vibration using the developed piezo-electric active vibration control system.

The cutting conditions for all the following tests were:

- 100 mm face mill, D_c
- 8 inserts, m
- 477 RPM spindle speed, n
- 133 mm/min feedrate, f
- 76 mm width of cut - width of the work-piece –, a_r
- 2-3 mm axial depth of cut, a_a
- 0-8mm tool offset

Before any heavy cutting could be done, the system was checked to make sure it would be liquid tight. Unlike the light cutting tests, which were done dry without cutting fluid, the heavy cutting operations, needed coolant in order to dissipate the thermal energy generated through the cutting process, so that the tool, work-piece and instrumentation of the piezo-electric system were kept cool. This was important especially for the piezoelectric actuator [90]. The humidity sensors showed that the humidity still exceeded 60% RH (refer to 7.4.2.4) over a period of time flushing the system with coolant. In order to keep the pockets of the PZT actuators dry, a pneumatic air supply was used to create dry air pockets, by injecting air at a few mbar higher than the atmospheric pressure (the regulation was done by a pressure control valve).

Figure 8.27 shows part of the pneumatic circuit and initial experiments to judge its performance.

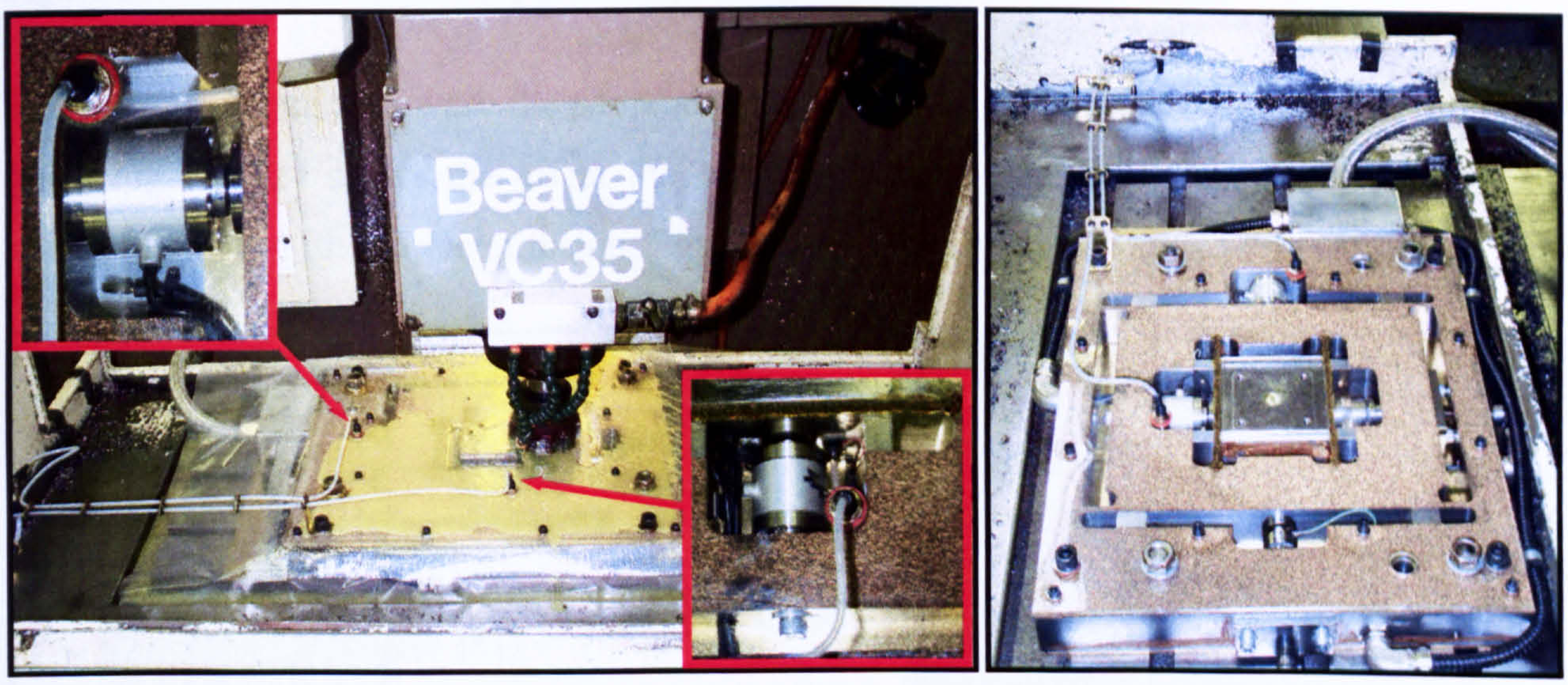

Figure 8.27: The pneumatic air supply for keeping the PZT actuators dry

The experiments showed that the humidity was stable and never increased over 10% RH, even over a long period of cutting trails. This was an ideal solution, since the humidity in the workshop had fluctuations, between 20- and 55% RH depending on the weather.

The first wet cutting operation was to increase the axial depth of cut until the cutting process became unstable and on the brink of chatter.

It was mentioned earlier that force or displacement feedback are the better feedback option to improve the surface finish of a stable cutting operation. For an unstable cutting process, however, the accelerometer may be the better solution. The main chatter frequency of this machine using the same face mill was about 450-460Hz, which is the ideal frequency for an accelerometer (refer to chapter 5.6 and 5.7). Therefore the accelerometer was used as feedback sensor for trying to control unstable cutting operations (chatter).

Figure 8.28 shows the experimental set up for the heavy cutting tests (see also figure 8.20).

Figure 8.28: The experimental set up for the dry cutting tests:

The control parameters were the same as shown in table 8.1 except for a reduced analogue gain. Figure 8.29 shows the effect the adaptive control system has made for an unstable cutting operation (the surface finish in figure 8.29.b was captured with a digital camera)

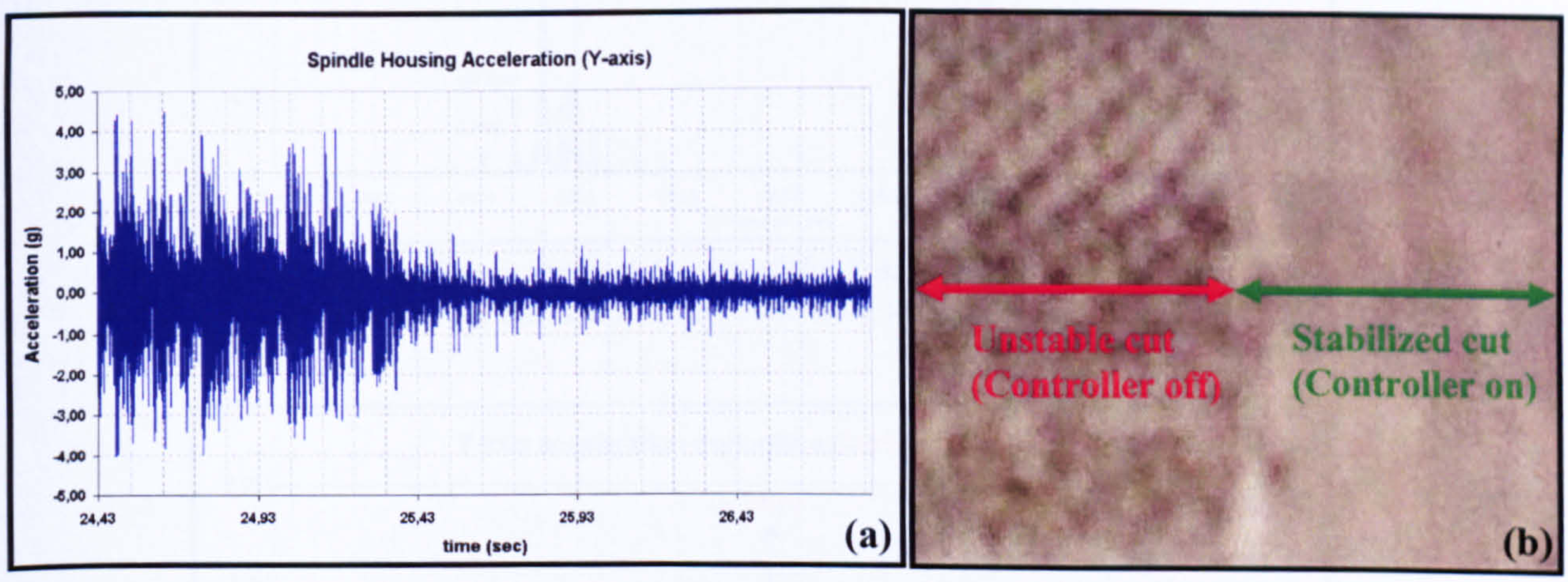

Figure 8.29: Control of chatter vibrations using the adaptive active vibration control system. Reduction in vibrations (a) and the improved surface finish (b)

The figures show that the system successfully controlled chatter vibration with the result that both the vibration level and the generated surface were improved significantly (no chatter marks).

Figure 8.30 to 8.33 confirm the results by showing the spectral density of all the sensors before and after the controller was activated.

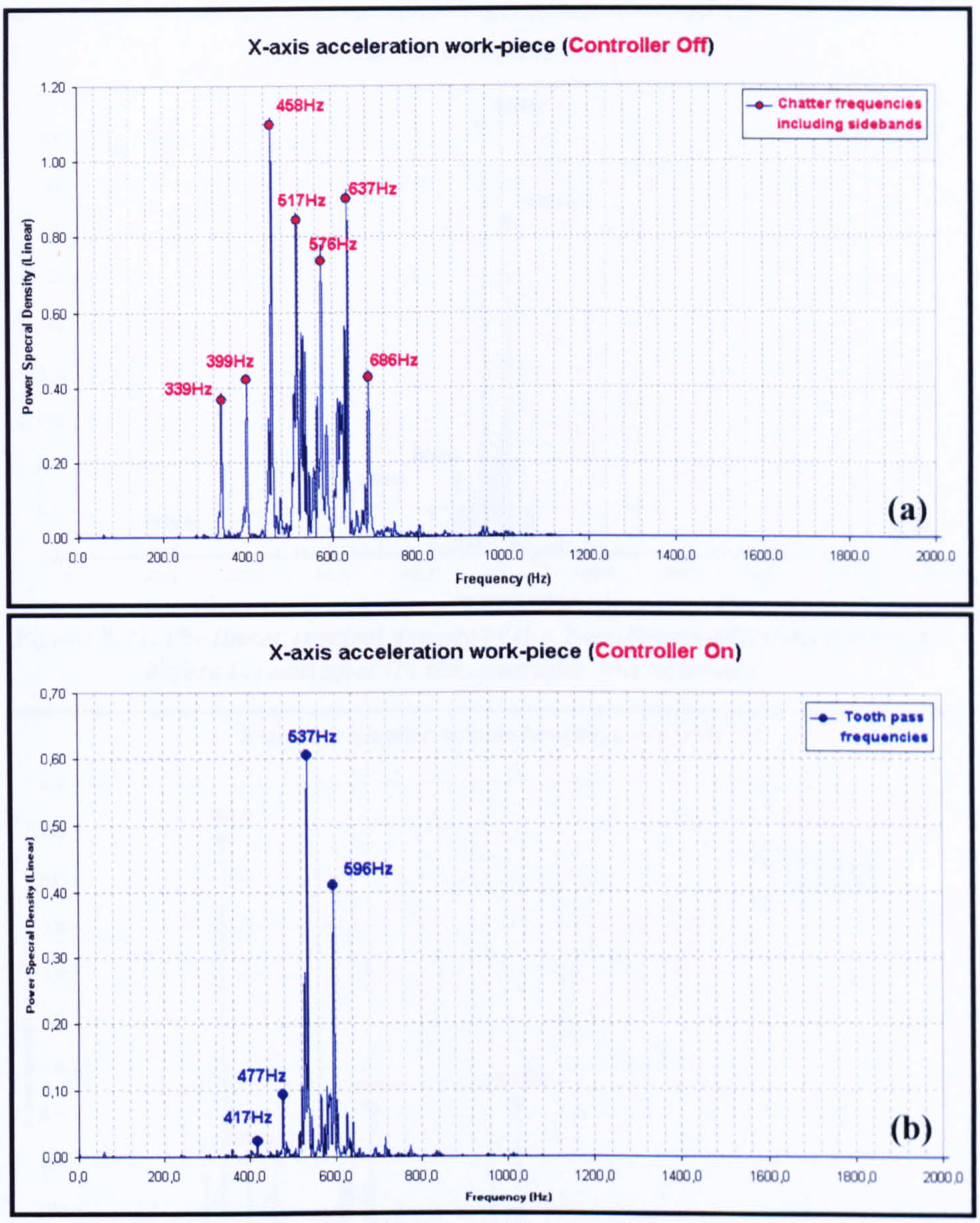

Figure 8.30:The linear spectral density of the X-axis work-piece accelerometer before (a) and after (b) the controller was activated

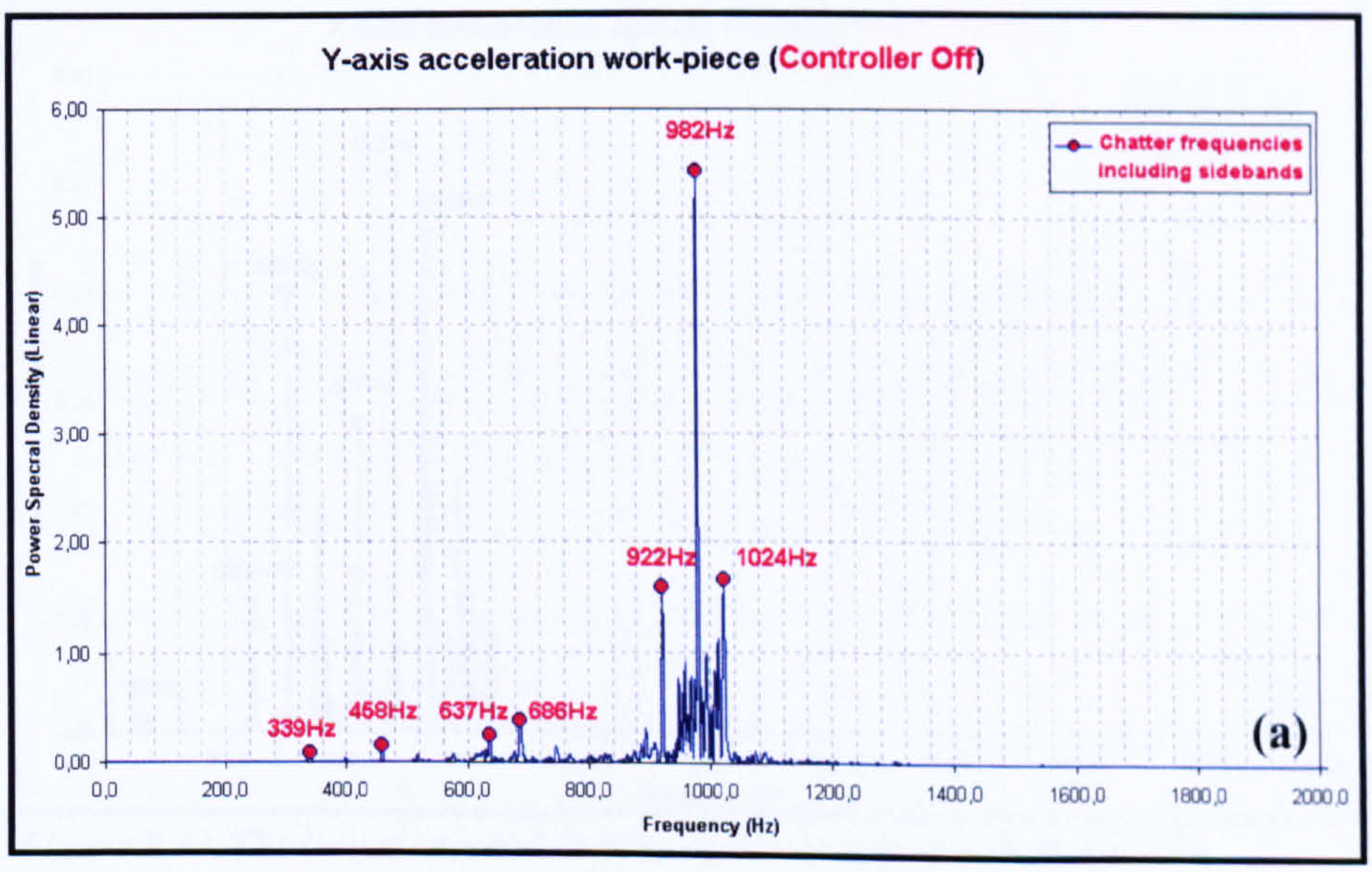

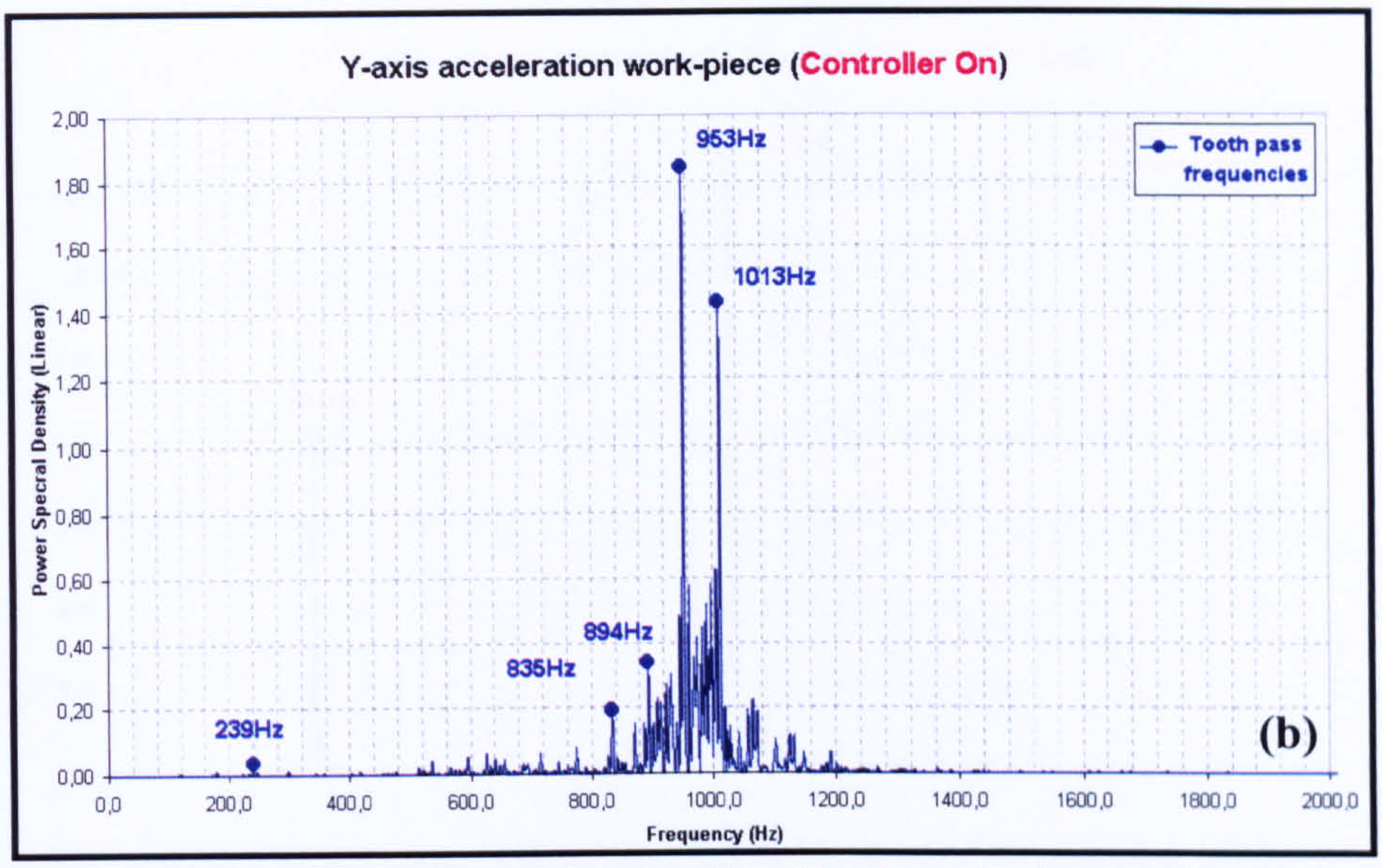

Figure 8.31: The linear spectral density of the Y-axis work-piece accelerometer before (a) and after (b) the controller was activated

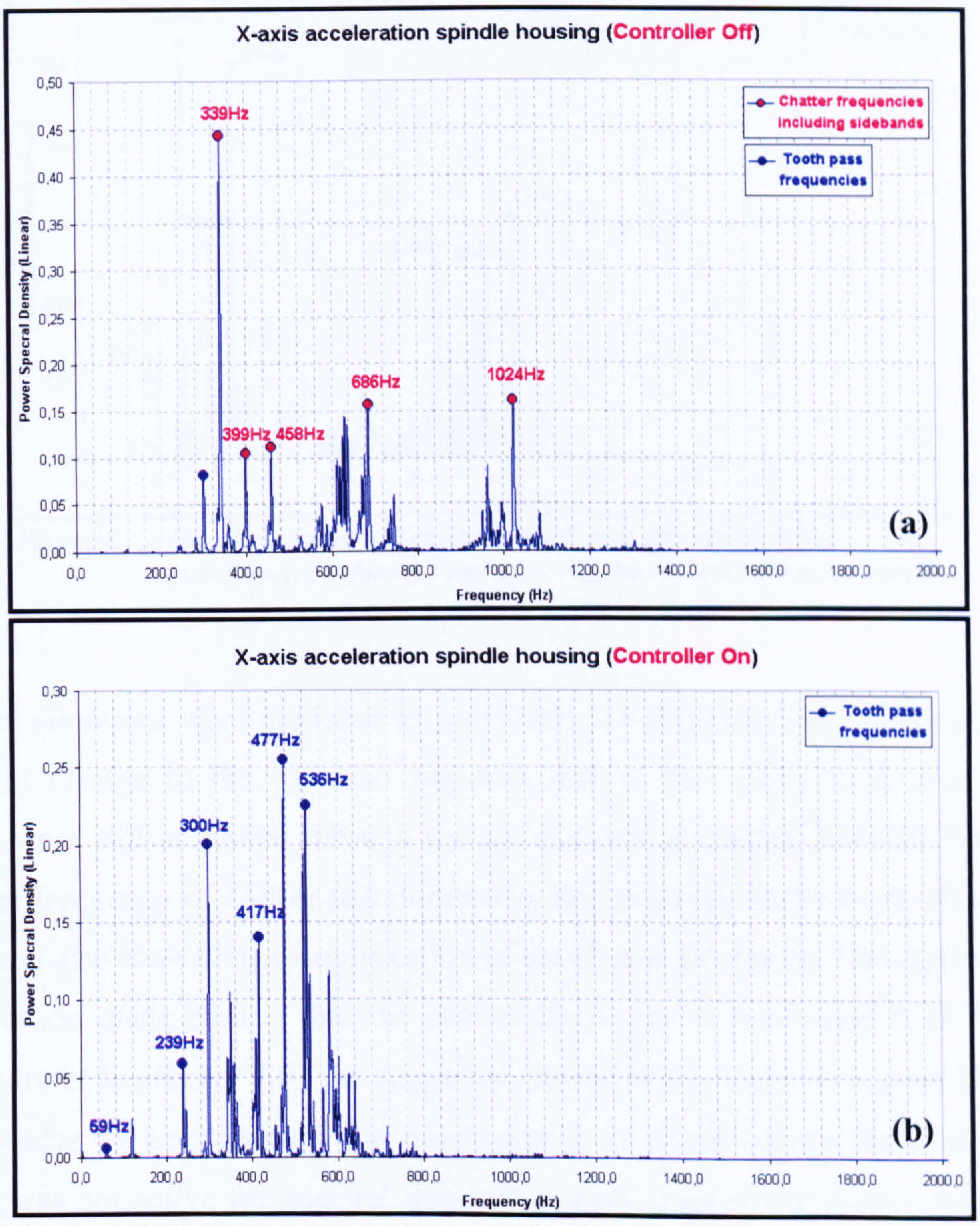

Figure 8.32: The linear spectral density of the X-axis spindle housing accelerometer before (a) and after (b) the controller was activated

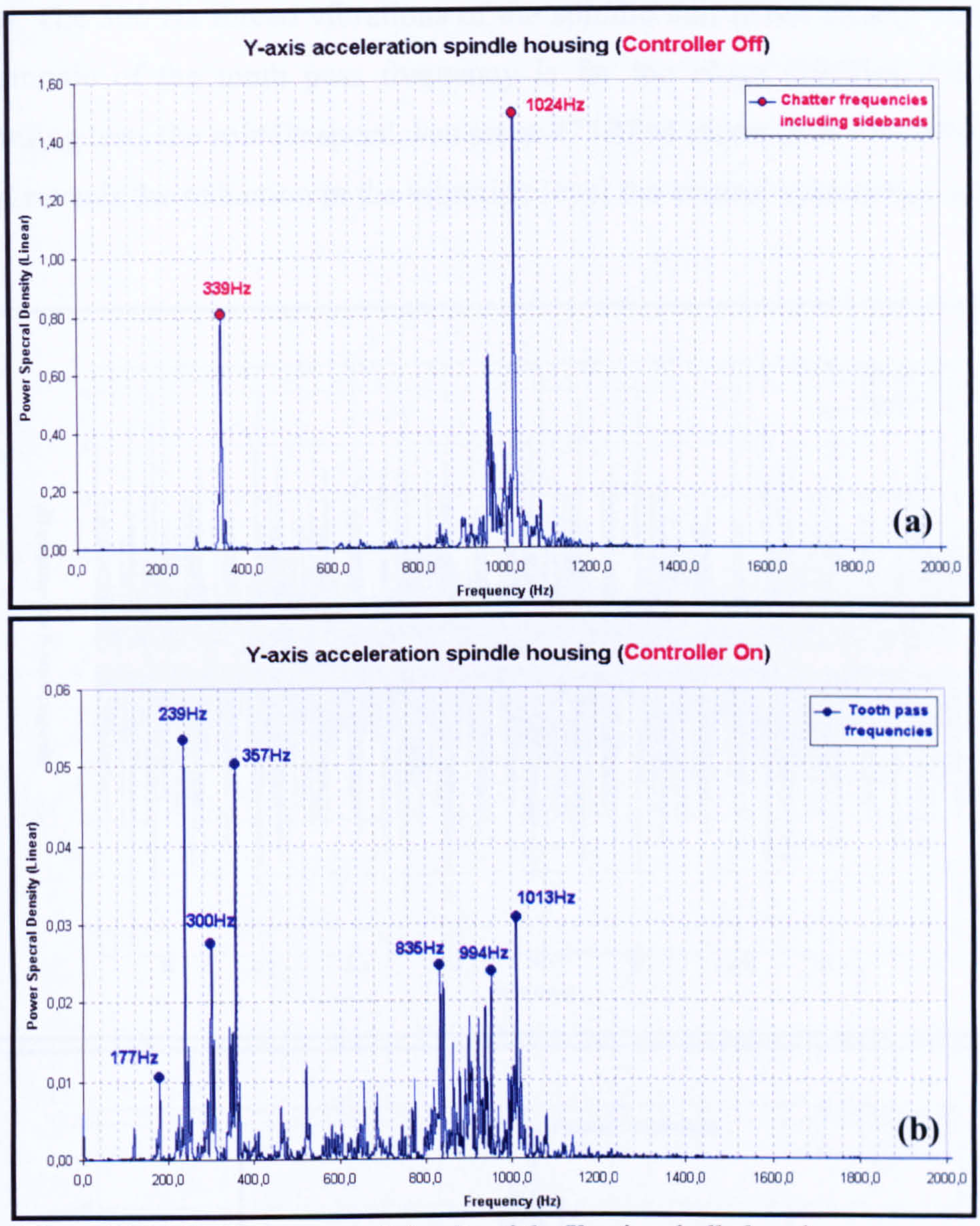

Figure 8.33:The linear spectral density of the Y-axis spindle housing accelerometer before (a) and after (b) the controller was activated

The chatter vibrations were the same as previously investigated (refer to chapter 5.6) except for a slight change in the dynamic response due to the active work-piece holder. The vibrations were still amplified through the spindle unit at around 300-500 Hz and 900 Hz. The chatter frequency of 458Hz still dominated the spectrum of the work-piece acceleration (X-axis), and also shows huge amplification of the chatter sidebands. The figures also confirm the observation made earlier, that the chatter frequency is modulated with the tooth pass frequency (refer to chapter 5.6). As suggested earlier, there might be a great benefit in using this knowledge to help identify the development of chatter at an early stage. When the controller was not active the spectral densities mainly showed the chatter frequency and its sidebands, whereas after the controller was activated they mainly consisted of the tooth pass frequencies. The 300 Hz forced vibrations of the spindle unit is not clearly visible here since the 5^{th} harmonic of the tooth pass frequency is far too close (295Hz). Compared to the previous cutting tests the spindle speed was set at 477RPM rather than 410RPM.

Figure 8.34 reveals the reduction in the vibration level the control system has achieved.

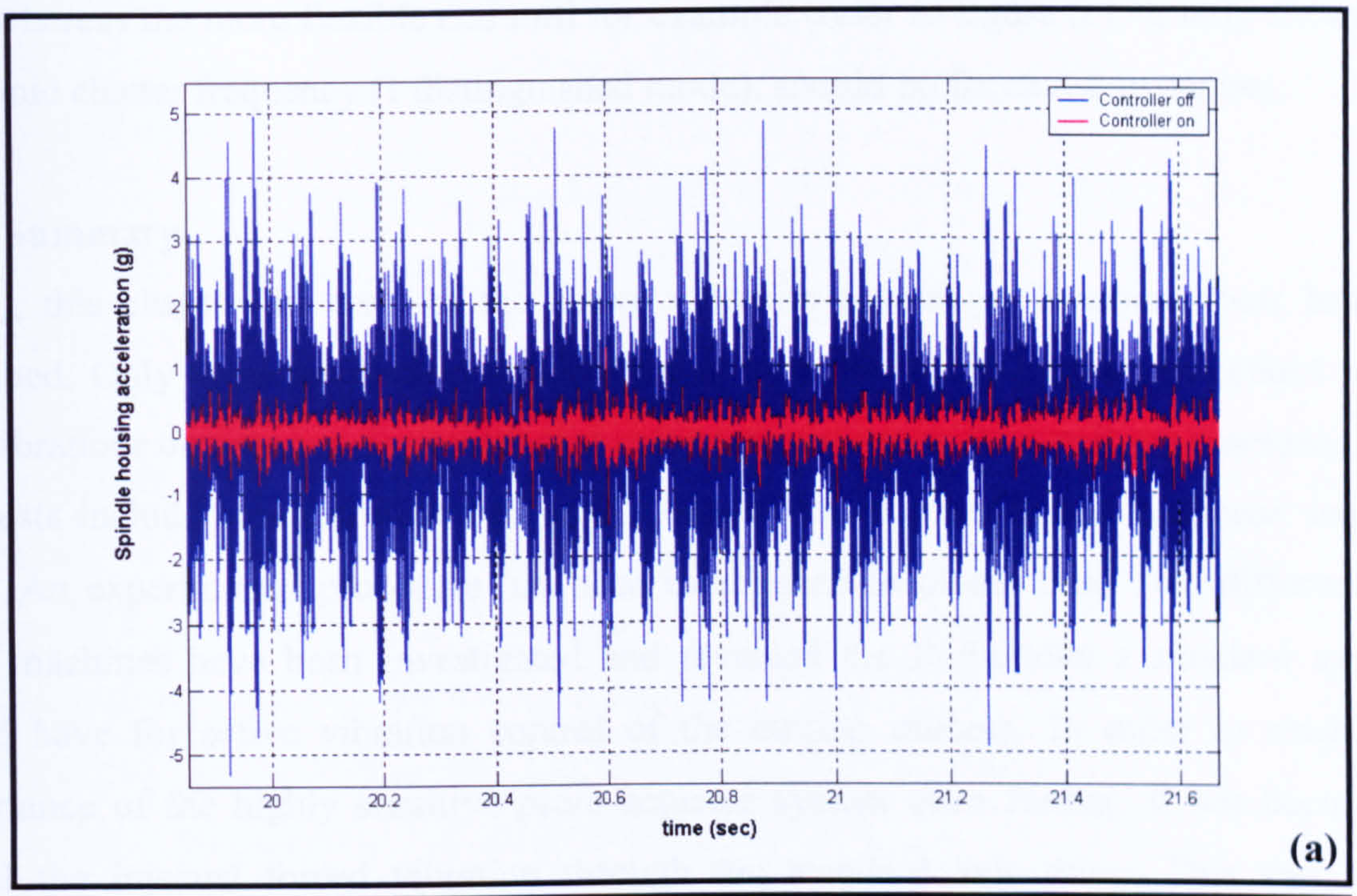

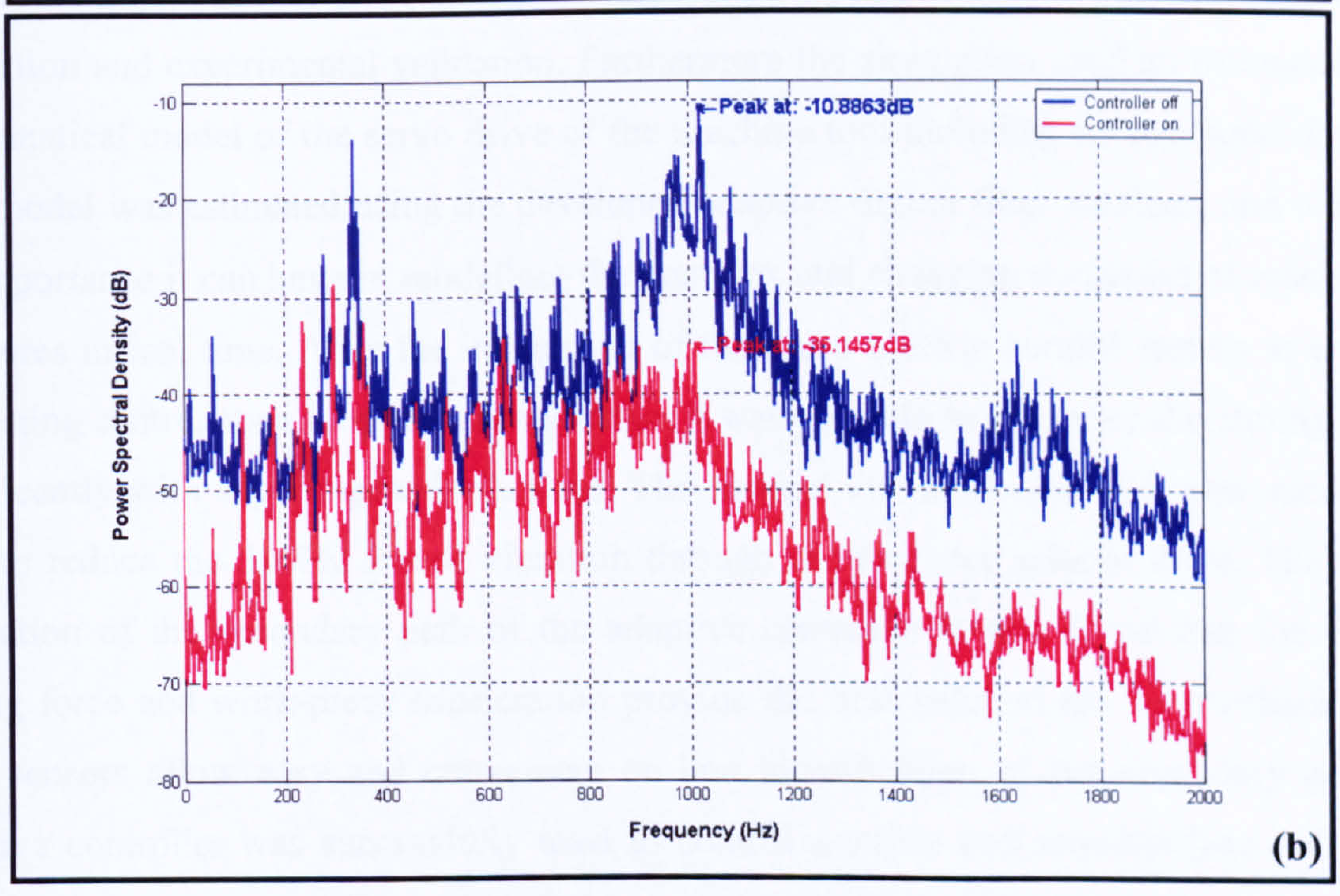

Figure 8.34: Improvement of the vibration level through the active chatter control system:

- ***Time response (a)***
- ***Power spectral density (b)***

The controller has significantly reduced the vibration level and the reductions are mainly at the system modal frequencies. The vibration level at around 339Hz was reduced by 23dB, whereas at 1024 Hz it was 24.5dB. This means that the adaptive controller is ideal, since it is not only capable of controlling one frequency, but all the relevant modal frequencies (refer to chapter 6.8.2). This is especially important for relatively stiff cutting tools, such as the face mill, whereas the more flexible end mill for example (refer to figure 5.17), only showing one harmonic chatter frequency (1 distinguished mode), should be far easier to control.

8.5 Summary

During this chapter the tests of the active vibration system on machine tools have been described. Only these tests could validate the aim of the whole project, to control machine tool vibrations on time varying multipoint cutting operations such as milling machines.

The tests included the estimation of usable bandwidth of a traditional ballscrew axis servo drive. An experimental procedure has been established to obtain this. Two different small-sized machines have been investigated and revealed the limitations a standard axis drive would have for active vibration control of the cutting process. In order to establish the importance of the highly sensitive piezo-actuator system even further, it has been used to cancel the injected forced vibration through the standard axis drive. This test included simulation and experimental validation. Furthermore the simulation used an estimated 3-axis mathematical model of the servo drive of the machine tool including its structural dynamics. This model was estimated using the developed adaptive digital filter routines, and confirmed the importance it can have in modelling the complex and changing dynamics of machine tool structures in real time. After the integration of the piezo-electric control system to a vertical machining centre, open loop tests showed that it was possible to influence the cutting process significantly with superimposed vibration. The manual vibration controller was successfully used to reduce the 300Hz forced vibration through the thyristor spindle drive. Through the estimation of the secondary path of the adaptive controller it was found that the dynamic cutting force and work-piece acceleration provide the best solution for the feedback sensor. Both sensors allow easy and convenient on-line identification of the secondary path. The adaptive controller was successfully used to control a stable and unstable face mill cutting operation. The vibration and surface finish were improved significantly and showed that the adaptive controller was an ideal control solution.

Chapter 9

Conclusions and suggestions for further work

9.1 Conclusions

The main aim of this project, to develop and build a universal adaptive, active vibration control system for reducing the vibrations of an intermittent cutting process (milling), has been achieved.

The work presented has shown that machine tool vibrations, in particular machine tool chatter, play a vital role in its performance. The value of machine tools today is directly proportional to this performance (e.g. Maximum Metal Removal Rate and surface finish).
Previous research work on improving the performance due to machine tool vibrations was mainly focused on process control (not vibration control). This involves the variation and optimisation of the parameters of the cutting process such as spindle speed and feedrate. It has been shown to be very successful and there are a number of commercial systems available to do this on- or off line, which both have their advantages and disadvantages. However it was also pointed out that this method of controlling vibrations does not improve the dynamics of a machine tool and therefore not its MMRR capability. It is simply a method of optimising and controlling the machine tool parameters for a particular cutting process.
Vibration control on the other hand changes the dynamics of a machine tool. It was shown that traditional passive methods, which have already been applied to their full extent are only popular for troubleshooting and that examples of promising active vibration control methods are only relatively few. Furthermore most of the research using active vibration control was concentrated on the turning operation only, mainly due to the fact that only a single point cutting operation has to be controlled. The simple integration of the instrumentation to the non-rotating cutting tool is also an advantage.
The decision to apply active vibration control to a milling machine and to control the time varying cutting process by using digital adaptive controllers is not only novel, but also has the potential for significantly improving the machine's performance.

The following points summarise the achievements and conclusions of this work:

1. The need for increasing the machine tool performance using active vibration control has been shown.
2. A vibration analysis on a vertical machining centre has helped to concentrate and to put focus on the project. This included light and heavy cutting tests, modal testing and the investigation of other possible vibration sources. The surface finish has been successfully correlated to the vibration signal. The use of process parameters (e.g. feedrate and spindle speed) to control chatter vibrations has been studied. Possible methods of identifying chatter at an early stage have been developed and results shown on two different machines.
3. New types of silicon accelerometers (MEM technology) have successfully been used to measure machine tool vibration. Their small size and price make them an extremely attractive alternative to traditional piezo-electric accelerometers.
4. The theory of active vibration control has been studied. This included an overview of the actuators and sensors required and the theoretical basis for adaptive control algorithms. The whole new concept of using energy to replace mass is often referred to as being a discipline of smart structures or adaptronic structures.
5. The advantages of the strategy of concentrating on discrete rather than continuous control methods have been demonstrated on a beam test rig.
6. Adaptive filter routines have been written in MATLAB/SIMULINK and C. These routines have successfully been used to estimate and fit, off and on line, mathematical models to a Frequency Response Function from a modal tests. The identified structural models for the beam test rig have helped to develop a simulation program for the adaptive vibration controller.
7. It was found, that compared to continuous methods, the discrete adaptive models are able to track and adjust in real time to changing structural dynamics. This makes them an ideal solution for modelling complex vibrating structures.
8. The user-friendly simulation routines can be applied to any mechanical structure and help to find the ideal control solution. All the adaptive control and identification routines used here have been added to the standard MATLAB/SIMULINK library at the University of Huddersfield.

9. The simulation results on the beam structure have been validated using a DOS based digital control platform. All the necessary analogue signal conditioning has been designed and built.
10. A comparison between traditional active vibration control (e.g. active damping), and digital adaptive control has been done. It was found that the traditional PID control methods are not always suitable for controlling machine tool vibrations, since they rely on a collocated sensor/actuator pair. A very practical estimation of the optimal sensor/actuator position has been done as a result of this.
11. The adaptive controller was able to increase the damping of the structural modes of the beam test rig significantly. Chatter vibrations, recorded from an unstable cutting process of the investigated milling machine, have been used to excite the beam structure. The adaptive controller was able to reduce the main chatter frequency by 16.5dB (85%).
12. A novel, universal prototype and demonstration system for active vibration control on vertical milling machines has been designed and built. The 2-axis system uses a novel high- resolution flexure guiding system and its integrated sensors are able to measure the cutting force (Kistler load washers), direct acceleration (MEM accelerometers) and direct displacement (Strain gauges). Piezo-ceramic based actuators are able to move each axis by about $6\mu m$ with *nm* resolution. The system is protected from cutting fluid and hot chips and can withstand cutting forces over 12.5kN.
13. Implemented onto a single axis ballscrew rig, which was excited through the servo-drive, the system was able to reduce the vibrations by about 50%. A measurement strategy has been established to estimate the usable bandwidth of the machine tool servo drive. The results on 2 small-sized CNC milling machines have shown that the axis servo drives of machine tools generally have limitations for active vibration control.
14. Adaptive filters have successfully been used to estimate a mathematical model of a single axis ballsrew rig in all three directions (single input, 3 directional output). This 3-axis model not only included the dynamics of the servo drive, but also the structural dynamics of the machine tool. The measurement and modelling strategy therefore may be a useful alternative to pure modal testing, which only measures and identifies the structural dynamics of a machine.

15. The developed active vibration control system has successfully been used to influence the cutting process of a stable face milling operation. Pre-defined harmonic excitation forces have been added to existing cutting forces of the milling operation, and therefore changed the vibration response in a defined way.
16. The developed active vibration control system has successfully been used to control and reduce the vibration of a stable face milling operation by up to 16-17dB (85%). Although only the 2 axes in the plane perpendicular to the rotating spindle axis were under control, the adaptive dynamic cutting force feedback control system has improved the surface finish, leaving the even more promising peripheral cutting operations open to future work.
17. The developed active vibration control system has successfully been used to control and reduce the vibration of an unstable face milling operation. The system was able to stabilize the cut and eliminate chatter vibration. The vibration level at the modal frequencies has been reduced significantly (23dB or 92.9% at 339Hz and 24.5dB or 93.9% at 1024Hz), and as a result a significant improvement in the surface finish has been achieved.

9.2 Suggestions for further work

These promising results on the demonstration rig leave much potential for future work. The fact that active vibration control can be used for controlling the cutting process for even very stiff face mill cutting tools, opens the door for design engineers to reconsider the mechanical design of milling machines. Depending on the cutting tool and work-piece, active vibration control can increase the performance and cutting speed even on relatively low cost machine tools.

For the developed system there are a few simple and low cost improvements that could be made. First reducing the guide way stiffness and therefore increasing the maximum stroke of each axis up to 8-10μm could optimise the existing 2-axis system relatively easily. Secondly the cutting trials could be extended to peripheral cutting operations. This should show even better results, since the generated surface finish has the same direction as the axes under control. Also the normally relatively flexible and lightly damped peripheral mill would be the main cause for mechanical instabilities (chatter) and therefore an ideal show case for the active vibration control system.

Other improvements are listed below:

1. A faster and more up to date, DSP based, digital controller platform could be used. More computational power would make it possible to increase the sampling frequency, model order and to use other recursive adaptive algorithms.
2. A faster digital controller may also allow for the on-line identification of the secondary path during cutting. The identification routine could continuously run and the secondary path could be updated periodically. Also no white noise excitation signal would be required, since the multipoint cutting operation excites the system adequately. This is one advantage of the intermittent cutting operation compared to a single point operation.
3. A major improvement would be the integration of the whole actuator system into the spindle head of the machine. Although this would mean that the system could only be used for one machine, it would have the advantage of controlling the spindle and tool directly. This would mean that the table would be free to mount a work-piece of any size, which is not possible on the current system.

Chapter 10

References

1. Weck M., Schulze O., Michels F., Bonse R., "Optimization of Machine Tool Performance and Accuracy", Manufacturing Science and Engineering Volume 2, ASME 1994
2. The engineer report, "Drilled for accuracy", The Engineer, 24 July 1998
3. Andrén L., Håkansson L.,Claesson I., Olsson O., Adaptive control of machine-tool vibration based on an active tool holder shank with an embedded piezo ceramic actuator, Proceedings of the 30th International Congress in Exhibition on Noise Control Engineering, 2001
4. Tlusty G., "Manufacturing Processes and Equipment", Prentice Hall, 2000
5. Postlethwaite, S.R., Ford D.G., "Dynamic calibration of CNC machine tools", In Proceedings of LAMADAMAP 1997 on Laser Metrology and Machine Performances III, 1997, pp. 305-315
6. Weck M., "Wekzeugmachinen Konstruktion und Berechnung", Springer Verlag, 1997
7. Ford D.G, Postlethwaite S.R., Blake M.D.,"The identification of Non-rigid Geometric Errors in a Vertical Machining Centre", published Proc. ImechE Vol. 213, Part B pp 555-566 1999
8. Altintas, Y., "Manufacturing Automation", Cambridge University Press, 2000
9. Koenigsberger, F. and Tlusty, J. "Machine tool Structures", Pergamon Press, Volume 1, 1970
10. Ford D.G.,"Machining to mircrons – error avoidance or compensation", In Proceedings of LAMADAMAP 1995 on Laser Metrology and Machine Performances II, 1995, pp. 41-52
11. Ford D.G., Postlethwaite S.R., Allen J.P., Blake M.D., "Compensation Algorithms for the Real-Time Correction of Time and Spatial Errors in a Vertical Machining Centre", Proceedings of ImechE, journal of Engineering Manufacture, Vol. 214. pp221-234, 2000

12. Postlethwaite S.R., "Electronic Based Accuracy Enhancement of CNC Machine Tools", PhD Thesis 1992, University of Huddersfield
13. White A., "Experimental thermal error analysis and correction applied to CNC machine tools", PhD Thesis 2000, University of Huddersfield
14. Weck M., "Meßtechnische Untersuchung und Beurteilung", Springer Verlag, 1997
15. Snyder P., M.A. Davies, J. R. Pratt, S. Smith," New device for stable speed determination in machining", Radical Departures (Advanced Technique in aerospace manufactures), magazine report
16. Tlusty J.,"High speed machining", Annals of the CIRP,Vol 42, page 733-738, 1993
17. Smith S., Tlusty J.," Update on High-Speed Milling Dynamics",Journal of engineering for industry, transactions of the ASME, Vol. 112, 1990
18. Pan G., Xu H., Kwan C.M., Liang C., Haynes L., Geng Z., "Modelling and intelligent chatter control strategies for a lathe machine", Control Engineering practice, Vol 4, No 12, page 1647-1658, 1996
19. Tlusty J., Polacek M., "The stability of the machine tool against self-excited vibration in machining", Prod. Eng. Res. Conf. ASME, Pittsburgh 1963
20. Merrit H.E., "Theory of self-excited machine tool chatter", Transactions of the ASME Journal of Engineering for Industry, Vol. 87, 447-454, 1965
21. Tlusty J., Ismail F., "Basic non-linearity in machining chatter", Annals of the CIRP, Vol 30/1/1981
22. Tobias S.A., "Machine tool vibration", Blackie & Son, Glasgow 1965
23. Naterwalla U., "Chatter Theory Fundamentals", Feature article of the Modern Machine Shop magazine, 2000
24. Engin S., Altintas Y., "Mechanics and dynamics of general milling cutters Part I: helical end mills", International Journal of machine tools and manufacturing, Vol. 41, No 15, pp 2195-2212, 2001
25. Engin S., Altintas Y., "Mechanics and dynamics of general milling cutters Part II: inserted cutters", International Journal of machine tools and manufacturing, Vol 41, No 15, pp 2213-2231, 2001
26. MAL (Manufacturing Automation Laboratories Inc.) on line, www.malinc.com
27. MLI Manufacturing Laboratories Inc., www.mfg-labs.com
28. Albert M., "Sweet, Sweet Spot", Feature article of the Modern Machine Shop magazine, 2001

29. West D., "High performance aluminium and titanium machining", High speed machining seminar 2002
30. Badrawy S., "Cutting dynamics of high speed machining", WolfTracks magazine (Cincinnati), Vol. 8, Issue 1, 2001
31. Weck M., Verhagg E., Gather M., "Adaptive Control of Face Milling Operations with Strategies for avoiding chatter-vibrations for automatic cut distribution", annals of the CIRP, 24(1):405-409, 1975
32. Weck M., "Automatisierung und Steuerungstechnik 1 and 2", Springer Verlag, 1997
33. Manufacturing Laboratories Incorporated, "The most reliable way to select chatter free spindle speeds", Handbook of the Harmonizer®
34. Smith S., Delio T., "Sensor based chatter detection and avoidance by the spindle speed selection", Journal of dynamic and control system, Transactions of the ASME, Vol. 114, 1992
35. Smith S., Tlusty J., "Stabilizing Chatter by Automatic Spindle Speed Regulation", Annals of the CIRP Vol. 41/1/1992
36. "Chatter Control in a box", online article in modern machine shop, Nov. 2001
37. Liao Y., Young Y., "A new on-line spindle speed regulation strategy for chatter control", International Journal Machine Tool Manufacturing, Vol 36, No. 5, pp 651-660, 1996
38. Sim W.M., Dewes R.C., Aspinwall D.K., "An integrated approach to the high-speed machining of moulds and dies involving both a knowledge-based system and a chatter detection and control system", Proc. Instn. Mech. Engrs., Vol 216, Part B: J Engineering Manufacture, 2002
39. Zelinski P., "Maximum aluminium", Feature article of the Modern Machine Shop magazine, Nov. 2001
40. Zelinski P., "The overhang effect", Feature article of the Modern Machine Shop magazine, Nov. 2001
41. Schmitz T., Davis M., "Tool point frequency response prediction for high speed machining by RCSA", Journal of Manufacturing Science and Engineering, Vol. 123, pp 700-707, November 2001
42. Choudhury S.K., Mathew J., "Investigations of the effect of non-uniform inserted pitch on vibration during face milling" International Journal of Machine tool manufacturing, Vol. 35, No. 10, pp. 1435-1444, 1995

43. Batrakov S.V., Tkhomirov B.K., "Insert lathe tools with vibration damping holder", Machining Tools, Vol. 61, No 12, 1990
44. Juneja B.L., "Fundamentals of Metal Cutting and Machine Tools", John Wiley & Son, 1987
45. Hardwick B., "Identification and solution of machine too chatter problems", In Proceedings of LAMADAMAP 1995 on Laser Metrology and Machine Performances I, 1993, pp. 123-139
46. Tarng Y.S., Kao J.Y., Lee E.C., "Chatter suppression in turining operations with a tuned vibration absorber", Journal of Materials Processing Technology, Vol. 105, pp. 55-60, 2000
47. Rojas J., Liang C., "Experimental Investigation of Active Machine Tool Vibration Control", SPIE Vol. 2721 / 373, 1996
48. Pan G., Xu H., Kwan C.M., Liang C., Haynes L., Geng Z., „Modelling and intelligent chatter control strategies for a lathe machine", Control eng. Practise, No. 12, pp. 1647-1658, 1996
49. Pan G., "MDSP-200 and its application in vibration isolation", Technical report, Intelligent Automation Inc., 1995
50. O'Reagan S., Miesner J., Aiken R., Packman A., Unver E., Akerley S., "Machine Tool Chatter Reduction Via Active Structural Control", Second European Conference on Smart Structures and Materials, 1994
51. Browning D., "Pro-Active Chatter Reduction", Article of the Modern Machine Shop magazine, 1998
52. Håkansson L., Claesson I. , Sturesson P.O.H., "Adaptive feedback control of machine tool vibration based on the filtered-x LMS algorithm", Journal of low frequency noise, vibration and active control, Vol. 17, No. 4, 1998
53. Håkansson L., "Adaptive active control of machine tool vibration in a lathe", Doctoral Thesis, Lund University (Sweden), 1999
54. Kuo S.M., Morgan D.R., "Active Noise Control Systems", John Wiley & Sons, 1996
55. Lagö T., Olsson S., Håkansson L., Claesson I., "Performance of a chatter control system for turning and boring application", GRACM Congress on Computational Mechanics, GRACM 2002, June 2002

56. Olgac N., Holm-Hansen B.T., "Tuneable active vibration absorber : The Delayed Resonator", Journal dymanic systems, measurement and control, Vol. 117, pp 513-519, 1995

57. Dold G.R., "Design of a microprocessor based adaptive control system for active vibration compensation using PMN actuators", Master's thesis, University of Maryland, 1996

58. Ko W.F., "A systems engineering approach to design a smart tool post structure", Master's thesis, University of Maryland, 1995

59. Eshete Z., "In process machine tool vibration cancellation using electrostrictive actuators", Doctorial thesis, University of Maryland, 1996

60. Hood A., "Control system design for active vibration control of a turning process using PMN actuators", Master's thesis, University of Maryland, 1996

61. Jang J.L., Tarng Y.S., "A study of the active vibration control of a cutting tool", Journal of materials and processing technology, Vol. 95, 1999

62. Ehmann C., Schönhoff U., Nordmann R., „Aktive Schwingungsdämpfung bei Portalfräsmachinen", Technical report, University of Darmstadt, Germany, 2001

63. The MathWorks, "Robust Control Toolbox", User Guide Version 2, the MathWorks Inc., 2001

64. Dohner J.L., Lauffer J.P., Hinnerichs T.D., Shankar N. , Regelbruegge M.E., Kwan C.M., Xu R., Winterbauer B., Bridger K., "Mitigation of Chatter Instabilities in Milling by Active Structural Control", Sandia National Laboratories, Technical report SAND2001-3031, December 2001

65. Lauffner J.P., Hinnerichs T., Kuo C.P., Wada B., Ewaldz D., Winfough B., Shankar N., "Milling Machine for the 21st Century – Goals, Approaches, Characterisation and Modelling", Proc. SPIE Smart Structures & Material Symposium 1996, Vol. 2721, 1996

66. Dohner J.L., Hinnerichs T.D., Lauffer J.P., Kwan C.M., Regelbruegge M.E., Shankar N., "Active chatter control in a miling machine: A design study", SPIE Smart Structures and Material, March 1997

67. Shankar N., Bridger K., Regelbruegge M., Winfought B., "A Smart Spindle Unit for Active Chatter Suppression of a Milling Machine Part 1: Overview, Fabrication and Assembly", SPIE Smart Structures and Material, 1998

68. Lauffner J.P., Regelbruegge M., Kwan C., Lin Y., Xu R., Dohner J., Hinnerichs T., "A Smart Spindle Unit for Active Chatter Suppression of a Milling Machine Part 2: Overview, Fabrication and Assembly", SPIE Smart Structures and Material, 1998
69. Vaccaro R.J., "Digital Control – A State-Space Approach", McGraw-Hill Inc.,1995
70. A. Preumont, "Vibration Control of Active Structures", Kluwer Academic Publishers, 1997
71. Trent E.M., "Metal Cutting", Butterworth & Co Ltd, 2000
72. Bruins D.H., Dräger H.J., „ Werkzeuge und Werkzeugmaschinen für die spanende Metallverarbeitung Teil 1", Hanser Verlag, 1984
73. Hirsch A., "Werkzeugmaschinen - Grundlagen", Viehweg Verlag 2000
74. Lambert B.K., " Milling – Methods and Machines", Published by the society of manufacturing engineers, 1982
75. Merchant M.E., "Basic mechanics of the metal cutting process", Journal of applied mechanics, Vol. 11, Transactions of the ASME, Vol. 66, 1940
76. Sweeney G., "Vibration of Machine Tools", The Machinery Publishing Co. Ltd., 1971
77. Koenigsberger F., Tlusty J., "Machine tool Structures", Pergamon Press, Volume 1, 1970
78. Ogata K., "Modern Control Engineering", Prentice HALL Inc., 1997
79. Lutz H., Wendt W., "Taschenbuch der Regelungstechnik", Verlag Harri Deutsch, 1995
80. Hansen C. H., Snyder S. D., "Active Control of Sound and Vibration", Chapman & Hall, 1997
81. Janocha H., "Adaptronics and Smart Structures", Springer Verlag, 1999
82. Cao W., Cudney H., Waser R., "Smart Material and Structures", Proc. Natl. Acd. Sci. USA, Vol 96, pp 8330-8331, 1999
83. Gandhi M.V., Thomson B.S., "Smart Materials and Structures", Chapman & Hall, 1992
84. Black J., "Adaptive Aircraft: No flight of Fantasy", Special report: Military technology, BusinessWeek magazine, 2003
85. Weismüller J., Viswanathz R.N., Kramer D., Zimmer P., Würschum R., Gleiter H., "Charge-Inducede Reversible Strain in a Metal", The Science, Vol. 300, April 2003
86. Serridge M., Licht T., "Piezoelectric Accelerometers and Vibration Preamplifiers – Theory and Application Handbook, Brüel & Kjær, 1987

87. Springer G., "Fachkunde Electrotechnik", Europa Verlag, 1993

88. Bolton W., "Mechatronics - electronic control system in mechanical and electrical engineering", Longman Ltd, 1999

89. Vishay Measurement Group, " Strain Gage Based Transeducers" Vishay Handbook, 2001

90. Vorndran S., "Micro Positioning, Nano Positioning, Nano Automation – Solutions for Cutting edge Technologies", Physik Instrumente (PI) GmbH & Co., 2001

91. Bentley J.P., "Measurement System", Longman Ltd, 1995

92. Evans D.J., "Modal Testing: Theory and Practice", Research Studies Press Ltd, 1984

93. Maluf N., "An Introduction to Mircoelectronical System Engineering", Artech House Inc., 2000

94. Weinberg H., "Dual Axis, Low g, Fully Integrated Accelerometers", Analog Device Application Note, 1999

95. Smith S., "The Scientist and Engineer's Guide to Digital Signal Processing", California Technical Publishing, 1997

96. Shinners S.M., "Modern Control System Theory and Design", John Wiley & Sons Inc., 1998

97. Fuller C.R., Elliott S.J., Nelson P.A., "Active Control of Vibration", Academic Press Inc., 1996

98. Morani M., Zafiriou E., "Robust Process Control", Prectice-Hall Inc., 1989

99. Lockwood S., Haase F., Ford D.G., "Active Vibration Control of Machine Tool Structures - Part 1: DSP Algorithms", In Proceedings of LAMADAMAP 2003 on Laser Metrology and Machine Performances VI, 2003, pp. 441-451

100. Inmann D., "Engineering Vibration", Prentice Hall, second edition, 2001

101. Benaroya H., "Mechanical Vibration", Prentice Hall, 1998

102. Richardson M., " Measurement and Analysis of the Dynamics of Mechanical Structures", Hewlett Packard Conference for Automotive and related Industries, Detroit, MI, 1978

103. Richardson M., "Global Curve Fitting of Frequency Response Measurements using the Rational Fraction Polynomial Method", 3rd IMAC Conference, 1985

104. Haykin S, Van Veen B., "Signals ans Systems", John Wiley & Sons Inc., 1999

105. Jervis B. W., "Digital Signal Processing", Addison Wesley, 1997

106. Mulgrew B., Grant P. Thomson J., "Digital Signal Processing", Macmillan Press Ltd, 1999

107. Cavicchi T.J.," Digital Signal Processing", John Wiley & Son Inc., 2000

108. Widrow B., Stearns S. D., "Adaptive Signal Processing", Prentice Hall, 1985

109. Hayes M.H., "Statistical Digital Signal Processing and Modelling", John Wiley & Sons Inc, 1996

110. Dutton K., Thomson S., Barraclough B., "The Art of Control Engineering", Addison-Wesley Ltd, 1997

111. Boucher C.C., Elliott S.J., Nelson P.A., "Effects of errors in the plant model on the performance of algorithms for adaptive feedforward control", Proceedings of the institution of electrical engineers, Vol. 138, pp 313-319, 1991

112. Elliott S., "Signal Processing for Active Control", Academic Press, 2001

113. Stothers I,M., Saunders T.J., McDonald A.M., Elliott S.J., "Adaptive feedback control of sun roof flow oscillations", Proceedings of the Institute of Acoustics, part 15, page 383-393, 1993

114. Morani, M., "Implications for Internal Modal Control for PID controllers", American Control Conference, Vol. 2, page 661-666, 1992

115. AMTRI Project report 1999, "Modal Analysis & Frequency Response Measurements of a Beaver Milling machine"

116. Haase F., Lockwood S., Ford D.G., "Vibration modelling of machine tool structures", In Proceedings of LAMADAMAP 2001 on Laser Metrology and Machine Performances V, 2001, pp. 451-460

117. Pitter F., Thomas J., Feldmann K., "A Silicon Vibration Sensor for State Monitoring Machine Tools in High Acceleration Range", mstnews 5/2000

118. Franco S., "Design with Operational amplifiers and Analog Integrated Circuits", McGraw Hill, 1997

119. Døssing O., "Strukturen prüfen - Teil 1: Mechanische Beweglichkeits- Messungen", Brüel & Kjær Handbook, K. Larsen & Søn A/S Glostrup Denmark, December 1989

120. Døssing O., "Strukturen prüfen - Teil 2: Modalanalyse und Simulation", Brüel & Kjær Handbook, K. Larsen & Søn A/S Glostrup Denmark, December 1989

121. Shepherd W.,"Power electronics and motor control", Cambridge University Press, 1995

122. Manual, "Contraves Varidyn Compact Spindle Drive", Contraves Antriebstechnik AG

123. Datasheet, "LEM current transducer Module LTA 50P/SP1" , Heme International Limited

124. Miller G., "Modern electronic communications", Prentice Hall Inc., 1996

125. Jemielniak K., Widota A., "The Development of frequency and amplitude of chatter vibration", Intentional Journal of Machine Tool and Manufacturing , Vol 29, Part 2, pp 249-256, 1989

126. Tarng Y.S., Lee E.C., "A critical investigation of the phase shift between the inner and outer modulation for the control of machine tool chatter" , International Journal of Machine Tool and Manufacturing, Vol 37, No 12, pp 1661-1672, 1997

127. Courrech J., "Envelope analysis for effective rolling-element fault detection – fact or fiction", UPTIME Magazine, Vol.8, 2000

128. SKF Conditioning Monitoring, "Early warning fault detection in rolling element bearings using microlog enveloping" Application Note CM3021

129. Shaw M.C., Metal cutting Principles, Oxford series on Advanced Manufacturing, 1984

130. Jiang X. Blunt L., Stout K.J., "Development of a lifting wavelet representation for characterisation of surface topography", Proc. Royal Soc. Lond. A (2000) 456, pp 1-31, 2000

131. Jiang X.-Q, Blunt L., "Surface analysis techniques to optimise the performance of CNC machine tools", In Proceedings of LAMADAMAP 2003 on Laser Metrology and Machine Performances VI, 2003, pp. 107-117

132. Haase F., Lockwood S., Ford D.G., "Active Vibration Control of Machine Tool Structures - Part 2: An experimental active vibration control system", In Proceedings of LAMADAMAP 2003 on Laser Metrology and Machine Performances VI, 2003, pp. 451-460

133. Freeman M., "The application of the continuous wavelet transform and wavelet denoising to modal analysis", University of Huddersfield, 2002

134. The MathWorks Inc.., "SIMULINK – Writing S-Functions", MATLAB Handbook, 1998

135. Krauss T, Shure L, Little J, "Signal Processing Toolbox", MATLAB handbook, 1994

136. Krakosch H.-J., Preumont A., "Recent advances in active damping and vibration control", ACTUATOR 2002, 8th International Conference on New Actuators, June 2002

137. Preumont A., Francois F., Bossens F., Abu-Hanieh A., "Force feedback versus acceleration feedback in active vibration isolation", Journal of Sound and Vibration, Vol. 257(4), page 605-613, 2002

138. Enterprise Edition, "SpectraLAB Software ", www.soundtechnology.com

139. Datasheet, "6-component Dynamometer 9255B", KISTLER, No. 6.9255B, 1997

140. International Organisation for Standardization, "Additional Japanese contribution for vibration tests", Ref ISO 230-8 and ISO/TC39/SC2/N1449, Oct. 2003

141. The Technical Author, "Beaver VC35 Operators and Maintenance Manual", Beaver Machine Tool Ltd., 1983

142. P. Bach," Milling machine tool stability and performance", In Proceedings of LAMADAMAP 2003 on Laser Metrology and Machine Performances VI, 2003, pp. 25-33

143. PRESTO Cutting Tool Handbook, "PRESTO Engineering Cutting Tools", Counsellor publication PC3/C, PRESTO Engineering Cutting Tools Ltd.

144. Etter D.M., "Engineering Problems Solving with MATLAB®", Second Edition, Prentice Hall International Inc., 1997

145. Freeman J.M., "General Data Logging Hardware and Software – User Guide", University of Huddersfield, 2004

146. Pinsopon U., Larson G., Nakajima S., Cetinkunt S., "Design, fabrication and real time neural network control of a piezo electric actuated tool post", International Journal of Intelegent Control and Systems, Vol. 2, No. 1, page 59-72, 1998

147. Woronko A., Huang J., Altintas Y., "Piezoelectric tool actuator for precision machining on conventional CNC turning centres", Precision engineering, No. 27, page 335-345, 2003

148. Golz H.U., Weule H., "Vorspannungsregelung im Kugelgewindetrieb – ein neuer Ansatz für den Werkzeugmachinenbau", wt Werkstattechnik 80, page 366-368, Springer Verlag, 1990

149. Chen J.S., Dwang I.C., "A ballscrew drive mechanism with piezo-electric nut for preload and motion control", International Journal of Machine Tools & Manufacture, No. 40, page 513526, 2000

150. Fischer U., "Fachkunde Metall", Europa Verlag, 1996

151. Mayr. M., "Technische Mechanik", Hanser Verlag, 1999

152. Fischer K.F., "Taschenbuch der technischen Formeln", Fachbuchverlag Leipzig, 1996

153. Leonhardt, ., "Disc Spring , Data sheet, Part 180003", MUBEA Tellerfedern und Spannelemente GmbH, 1999
154. Dubbel H., Beitz W., Küttner K.-H., "Dubbel – Taschenbuch für den Maschinenbau", Springer Verlag 1994
155. HEXAGON, "WST1 für Windows© – Werkstoffdatenbank", HEXAGON Industriesoftware GmbH, 1997
156. Instruction Manual, "Digital Strain Indicator P-3500", Vishay Measurement Group
157. Datasheet, "Humidity sensor HIH-3610 Series", Sensing and Control Honeywell
158. Fassois S.D., Eman K.F., Wu S.M., "A fast algorithm for on-line machining process modelling and adaptive control", Journal of Engineering Industry, Vol 111, page 133-139, 1989

Appendix A

A selection of the adaptive control program code

A.1 The secondary path calibration program

The following key code is taken of the sec_cali.cpp program

```
/////////////////////////////////////////////////////////////////////////////////////
// Section 3
// Start the CONVERSION LOOP for the calibration process
/////////////////////////////////////////////////////////////////////////////////////
 printf("THIS PROGRAM CALIBRATES THE SECONDARY PATH USING AN ADAPTIVE IIR FILTER
\n");
printf("IT IS THE X - AXIS OF THE ACTIVE VIBRATION PLATFORM (100Hex) \n\n\n");
printf("Press the keyboard in order to enable the X-axis calibration process\n\n");
if (!kbhit());
        getch(); // The key needs to be thrown away, otherwise the program stops altogether
printf("Press the keyboard to disable the calibration process\n\n");
while(!kbhit())
        {

        /////////////////////////////////////////////////////////////////////////////////////
        // Section 3.1
        // Chechs the digital input until a the trigger has occured
        /////////////////////////////////////////////////////////////////////////////////////
        while (IO_bit == MASK_DIGITAL_C7)
                {
                IOinput = inportb(base1+10);
                // Reads, because the PIO register or port (base+11) is set to 155, means that all I/O
                // (Port A,B,C) are set to Input. So port C (base+10) and its 8 bits are going to be read in

                IO_bit = IOinput & MASK_DIGITAL_C7;
                // We read in the 1 bit (I/O C7) and map it with 1000 0000 (80 Hex). Means that we logically
                // (AND) connect each bit from PORT C with
                // 1000 0000. Means if the digital input C7 is high 1, IO_bit is 1, if it is 0 IO_bit is 0.
                }

        while (IO_bit == 0)
                {
                IOinput = inportb(base1+10);
                IO_bit = IOinput & MASK_DIGITAL_C7;
                }
        ///////////////////////////////////////////////////////////////////////
        // End of section 3.1
        ///////////////////////////////////////////////////////////////////////

        /////////////////////////////////////////////////////////////////////////////////////////////
        // Section 3.2
        // Reads in the error and reference signal over channel ADC15 (100Hex)
        // Range settings: +/- 2.5V
        /////////////////////////////////////////////////////////////////////////////////////////////
```

```
outportb(base1+12,channel1);
// Select Mux channel
a1=inportb(base1+2);
// Start conversion and write the lower byte already into the memory (variable a1)
while(!(inportb(base1+0) >= 128))
// Conversion takes 10 micro sec or so long until ADC bit 7 busy flag goes high (read base+0)
        {
        };
a1=inportb(base1+1);            // Reads the high byte
b1=inportb(base1+2);            // Reads the low byte and starts another conversion
sanalog_inbit1=(a1*256)+b1;     // Combine the results

// The next comand calibrates the value from bit's into voltage
// First we need to substract 2047 (half range -> 4095 full range)
// Because at 2047 we have 0 Volt and then -2045 = -2.5V
// and +2045 = +2.5V
// The calibrated numbers of the ADC15 (100Hex) are slightly diffrent
sanalog_involt1=(float) (sanalog_inbit1-2046)*0.00126f;
////////////////////////////////////////////////////////////////////
//  End of section 3.2
////////////////////////////////////////////////////////////////////

////////////////////////////////////////////////////////////////////////////////////////////////////////////////////
//  Section 3.3:
//  The algorithm must be entered here
//  This section applies the filter to the input samples and calculates the
//  filtered output samples
////////////////////////////////////////////////////////////////////////////////////////////////////////////////////
sinput_sample = gain_factor_input*sanalog_involt1;
error_signal = sinput_sample;

////////////////////////////////////////////////////////////////////////////////////////////////////////////////////
// Section 3.3.1:
// This section creates white noise or a gaussion random number with
// its input parameters mean and standard deviation
////////////////////////////////////////////////////////////////////////////////////////////////////////////////////
white_sample = 0.0;
sum = 0.0;
for (i=0; i != 12; i++)
        {
        floatrand = (float) rand();
        sum = sum + (floatrand / 32767);
        white_sample = ((sum - 6) * sd) + mean;
        }
white_sample =  white_sample;
////////////////////////////////////////////////////////////////////////////////////////////////////////////////////
// END of section 3.3.1
////////////////////////////////////////////////////////////////////////////////////////////////////////////////////

////////////////////////////////////////////////////////////////////////////////////////////////////////////////////
// Section 3.3.2:
// This section does the LMS algorithm for the IIR filter (Nominator and Denominator)
// The estimated or calibrated IIR filter can then be used as model
// of the secondary path for the FXLMS
////////////////////////////////////////////////////////////////////////////////////////////////////////////////////

/////////////////////////////////////////////////////////////
// LMS algorithm for the nominator
/////////////////////////////////////////////////////////////
for(int zn = IIRORDER; zn < (IIRORDER*2) ; zn++)
```

```
        {
        vIIR_taps_cali[zn] = vIIR_taps_cali[zn] + (mue_IIR_num *
        error_of_secondary_path_model * vIIR_signal_cali[zn]);
        }
//////////////////////////////////////////////////////
// END of the LMS for the nominator
//////////////////////////////////////////////////////

//////////////////////////////////////////////////////
// LMS algorithm for the denominator
//////////////////////////////////////////////////////
for(int zd = 1; zd < (IIRORDER) ; zd++)
        {
        vIIR_taps_cali[zd] = vIIR_taps_cali[zd] + (mue_IIR_den *
        error_of_secondary_path_model * vIIR_signal_cali[zd]);
        77 The first coefficient of the denuminator remains 0
        77 (This is the 1 in the z-transform of the ARMA model)
        vIIR_taps_cali[0] = 0.0;
        }
//////////////////////////////////////////////////////
// END of the LMS for the denominator
//////////////////////////////////////////////////////
IIR_cali();
// Summation point for model error of secondary path
error_of_secondary_path_model = error_signal - sIIR_filtered_output_sample_cali;
//////////////////////////////////////////////////////
// END of section 3.3.2
//////////////////////////////////////////////////////
sanalog_outvolt1 = white_sample;
sanalog_outvolt2 = error_of_secondary_path_model;
////////////////////////////////////////////////////////////////////////////////////////////////////////
// END of section 3.3 (Applying the algorithm for the secondary path identification)
////////////////////////////////////////////////////////////////////////////////////////////////////////

////////////////////////////////////////////////////////////////////////////////////////////////////////
// Section 3.4
// Reads out the first signal to DAC A (0x100)
// (Filtered output signal or anti vibration in controller program)
// In the calibration program it is the secondary path input (white noise)
////////////////////////////////////////////////////////////////////////////////////////////////////////
sanalog_outvolt1=sanalog_outvolt1+5.0f;
// Because the DAC is unipolar (0-10V) but the input was (-5V - +5V),
// the input voltage needs to have an 5Volt offset. Since the range of
// both is 10Volt we just need an AC filter at the output e.g AC on
// ocilloscope to filter the DAC out again
sanalog_outbit1=sanalog_outvolt1*400;
// The resolution of the board is 10V/2^12 = 2.44mV/bit
// This means a calibration factor of 409.6 bit/volt.
// The entered value is now in bit !!!
// After calibrating the DAC A of this board a factor of
// 2.5mV/bit was identified. This means 400bits/volt.
// The offset was less than 1 bit (0.44bits)
high1 = sanalog_outbit1/256;
low1  = sanalog_outbit1-256*high1;
outportb(base1+4,low1);
outportb(base1+5,high1);
outportb(base1+3,0);
////////////////////////////////////////////////////////////////////////////////////////////////////////
// End of section 3.4
////////////////////////////////////////////////////////////////////////////////////////////////////////
```

```
        ////////////////////////////////////////////////////////////////////////////////////////////
        // Section 3.5
        // Reads out the second signal (model error of the secondary path)
        // to DAC B (0x100)
        ////////////////////////////////////////////////////////////////////////////////////////////
        sanalog_outvolt2=sanalog_outvolt2+5.0f;
        // Because the DAC is unipolar (0-10V) but the input was (-5V - +5V),
        // the input voltage needs to have an 5Volt offset. Since the range of
        // both is 10Volt we just need an AC filter at the output e.g AC on
        // ocilloscope to filter the DAC out again
        sanalog_outbit2=sanalog_outvolt2*400;
        // The resolution of the board is 10V/2^12 = 2.44mV/bit
        // This means a calibration factor of 409.6 bit/volt.
        // The entered value is now in bit !!!
        // After calibrating the DAC A of this board a factor of
        // 2.5mV/bit was identified. This means 400bits/volt.
        // The offset was less than 1 bit (0.44bits)
        high2 = sanalog_outbit2/256;
        low2  = sanalog_outbit2-256*high2;
        outportb(base1+6,low2);
        outportb(base1+7,high2);
        outportb(base1+3,0);
        ////////////////////////////////////////////////////////////////////////////////////////////
        // End of section 3.5
        ////////////////////////////////////////////////////////////////////////////////////////////
        }
getch(); // The key from the while loop needs to thrwn away otherwise the program stops altogether

////////////////////////////////////////////////////////////////////////////////////////////
// END of section 3 (CONVERSION LOOP FOR THE CALIBRATION PROCESS)
////////////////////////////////////////////////////////////////////////////////////////////
```

A.2 The Adaptive FIR feedback/feed forward controller (LMS or FXLMS algorithm)

The following key code is taken of the fxlms.cpp program

```
//////////////////////////////////////////////////////////////////////////////
// Section 5:
//          START OF THE CONVERSION LOOP
//////////////////////////////////////////////////////////////////////////////
if (!kbhit());
        {
        getch(); // The key needs to be thrown away, otherwise the program stops altogether
        }
printf("<Press the keyboard in order to disable the adaptive filter>\n\n");

while(!kbhit())
        {
        //////////////////////////////////////////////////////////////////////////////
        // Section 5.1
        // Checks the digital input until a the trigger has occurred
        //////////////////////////////////////////////////////////////////////////////
        while (IO_bit == MASK_DIGITAL_C7)
                {
```

```
        IOinput = inportb(base1+10);
        // Reads, because the PIO register or port (base+11) is set to 155, means that all I/O
        // (Port A,B,C) are set to Input. So port C (base+10) and its 8 bits are going to be read in

        IO_bit = IOinput & MASK_DIGITAL_C7;
        // We read in the 1 bit (I/O C7) and map it with 1000 0000 (80 Hex). Means that we logically
        // (AND) connect each bit from PORT C with
        // 1000 0000. Means if the digital input C7 is high 1, IO_bit is 1, if it is 0 IO_bit is 0.
        }

 while (IO_bit == 0)
        {
        IOinput = inportb(base1+10);
        IO_bit = IOinput & MASK_DIGITAL_C7;
        }
////////////////////////////////////////////////////////////////////
// End of section 5.1
////////////////////////////////////////////////////////////////////

//////////////////////////////////////////////////////////////////////////////////////////////////
// Section 5.2
// Reads in the error and reference signal over channel ADC15 (100Hex)
// Range settings: +/- 2.5V
//////////////////////////////////////////////////////////////////////////////////////////////////
outportb(base1+12,channel1);
//Select Mux channel
a1=inportb(base1+2);
// Start conversion and write the lower byte already into the memory (variable a1)
while(!(inportb(base1+0) >= 128))
// Conversion takes 10 micro sec or so long until ADC bit 7 busy flag goes high (read base+0)
        {
        };
a1=inportb(base1+1);            // Reads the high byte
b1=inportb(base1+2);            // Reads the low byte and starts another conversion
sanalog_inbit1=(a1*256)+b1;     // Combine the results

// The next comand calibrates the value from bit's into voltage
// First we need to substract 2047 (half range -> 4095 full range)
// Because at 2047 we have 0 Volt and then -2045 = -2.5V
// and +2045 = +2.5V
// The calibrated numbers of the ADC15 (100Hex) are slightly diffrent
sanalog_involt1=(float) (sanalog_inbit1-2046)*0.00126f;
////////////////////////////////////////////////////////////////////
//  End of section 5.2
////////////////////////////////////////////////////////////////////

//////////////////////////////////////////////////////////////////////////////////////////////////
//  Section 5.3:
//  The algorithm must be entered here
//  This section applies the filter to the input samples and calculates the
//  filtered output samples
//////////////////////////////////////////////////////////////////////////////////////////////////
sinput_sample = gain_factor_input * sanalog_involt1;
error_signal = sinput_sample;
reference_signal = sinput_sample;

IIR_fxlms();  // Applying the filter model about the secondary path dynamics

for (int z=1 ; z < FIRORDER ; z++)
// shifting the output signal buffer with the filtered reference for the LMS algorithm (it is then
```

```
        // called FXLMS algorithm)
                {
                v_fxlms_buffer[FIRORDER-z] = v_fxlms_buffer[FIRORDER-z-1];
                }
        v_fxlms_buffer[0] = sIIR_filtered_output_sample_fxlms;
        // Fills the elemnt of the signal or input buffer with the current input sample
        // LMS or FXLMS algorithm
        for (i = 0; i < FIRORDER ; i++)
                {
                vFIR_taps[i] = (leakage_factor * vFIR_taps[i]) + (error_signal * v_fxlms_buffer[i] *
                mue); 77 XLMS
                // vFIR_taps[i] = (leakage_factor * vFIR_taps[i]) + (error_signal * vFIR_signal[i] *
                mue); 77 LMS
                }
        FIR();
        sanalog_outvolt1 = sFIR_filtered_output_sample;


        ////////////////////////////////////////////////////////////////////////
        // End of section 5.4
        ////////////////////////////////////////////////////////////////////////

        //////////////////////////////////////////////////////////////////////////////////
        // Section 5.5
        // Reads out the filtered samples to DAC A (100Hex)
        //////////////////////////////////////////////////////////////////////////////////
        sanalog_outvolt1=sanalog_outvolt1+5.0f;
        // Because the DAC is unipolar (0-10V) but the input was (-5V - +5V),
        // the input voltage needs to have an 5Volt offset. Since the range of
        // both is 10Volt we just need an AC filter at the output e.g AC on
        // ocilloscope to filter the DAC out again
        sanalog_outbit1=sanalog_outvolt1*400;
        // The resolution of the board is 10V/2^12 = 2.44mV/bit
        // This means a calibration factor of 409.6 bit/volt.
        // The entered value is now in bit !!!
        // After calibrating the DAC A of this board a factor of
        // 2.5mV/bit was identified. This means 400bits/volt.
        // The offset was less than 1 bit (0.44bits)
        high1 = sanalog_outbit1/256;
        low1  = sanalog_outbit1-256*high1;
        outportb(base1+4,low1);
        outportb(base1+5,high1);
        outportb(base1+3,0);
        ////////////////////////////////////////////////////////////////////////
        // End of section 5.5
        ////////////////////////////////////////////////////////////////////////
        }
getch(); 77 The key from the while loop needs to thrown away otherwise the program stops altogether

////////////////////////////////////////////////////////////////////////////////
// END of section 5 (THE CONVERSION LOOP)
////////////////////////////////////////////////////////////////////////////////
```

A.3 The Adaptive FIR feedback controller using IMC (FXLMS algorithm)

The following key code is taken of the imc.cpp program

```
/////////////////////////////////////////////////////////////////////////////////
// Section 5:
//          START OF THE CONVERSION LOOP
/////////////////////////////////////////////////////////////////////////////////
if (!kbhit());
        {
        getch(); // The key needs to be thrown away, otherwise the program stoppes altogether
        }
printf("<Press the keyboard in order to disable the adaptive filter>\n\n");

while(!kbhit())
        {
        /////////////////////////////////////////////////////////////////////////////////
        // Section 5.1
        // Checks the digital input until a the trigger has occurred
        /////////////////////////////////////////////////////////////////////////////////
        while (IO_bit == MASK_DIGITAL_C7)
                {
                IOinput = inportb(base1+10);
                // Reads, because the PIO register or port (base+11) is set to 155, means that all I/O
                // (Port A,B,C) are set to Input. So port C (base+10) and its 8 bits are going to be read in

                IO_bit = IOinput & MASK_DIGITAL_C7;
                // We read in the 1 bit (I/O C7) and map it with 1000 0000 (80 Hex). Means that we logically
                // (AND) connect each bit from PORT C with
                // 1000 0000. Means if the digital input C7 is high 1, IO_bit is 1, if it is 0 IO_bit is 0.
                }

        while (IO_bit == 0)
                {
                IOinput = inportb(base1+10);
                IO_bit = IOinput & MASK_DIGITAL_C7;
                }
        /////////////////////////////////////////////////////////////////////////
        // End of section 5.1
        /////////////////////////////////////////////////////////////////////////

        ///////////////////////////////////////////////////////////////////////////////////////////
        // Section 5.2
        // Reads in the error and reference signal over channel ADC15 (100Hex)
        // Range settings: +/- 2.5V
        ///////////////////////////////////////////////////////////////////////////////////////////
        outportb(base1+12,channel1);
        // Select Mux channel
        a1=inportb(base1+2);
        // Start conversion and write the lower byte already into the memory (variable a1)
        while(!(inportb(base1+0) >= 128))
        // Conversion takes 10 micro sec or so long until ADC bit 7 busy flag goes high (read base+0)
                {
                };
        a1=inportb(base1+1);            // Reads the high byte
        b1=inportb(base1+2);            // Reads the low byte and starts another conversion
        sanalog_inbit1=(a1*256)+b1;     // Combine the results
```

```
// The next command calibrates the value from bit's into voltage
// First we need to subtract 2047 (half range -> 4095 full range)
// Because at 2047 we have 0 Volt and then -2045 = -2.5V
// and +2045 = +2.5V
// The calibrated numbers of the ADC15 (100Hex) are slightly different
sanalog_involt1=(float) (sanalog_inbit1-2046)*0.00126f;
//////////////////////////////////////////////////////////////////////
// End of section 5.2
//////////////////////////////////////////////////////////////////////


////////////////////////////////////////////////////////////////////////////////////////////////////
// Section 5.3:
// The algorithm must be entered here
// This section applies the filter to the input samples and calculates the
// filtered output samples
////////////////////////////////////////////////////////////////////////////////////////////////////
sinput_sample = gain_factor_input * sanalog_involt1;
error_signal = sinput_sample;

IIR_IMC(); // Applying the filter model about the secondary path dynamics
reference_signal = sIIR_filtered_output_sample_IMC + error_signal;

IIR_fxlms(); // Applying the filter model about the secondary path dynamics


for (int z=1 ; z < FIRORDER ; z++)
        // shifting the output signal buffer with the filtered reference
        // for the LMS algorithm (it is then called FXLMS algorithm)
        {
        v_fxlms_buffer[FIRORDER-z] = v_fxlms_buffer[FIRORDER-z-1];
        }
v_fxlms_buffer[0] = sIIR_filtered_output_sample_fxlms;
// Fills the element of the signal or input buffer with the current input sample
for (i = 0; i < FIRORDER ; i++)
        {
        vFIR_taps[i] = (leakage_factor * vFIR_taps[i]) + (error_signal * v_fxlms_buffer[i] *
        mue);
        }
FIR();
sanalog_outvolt1 = sFIR_filtered_output_sample;

//////////////////////////////////////////////////////////////////////
// End of section 5.4
//////////////////////////////////////////////////////////////////////

//////////////////////////////////////////////////////////////////////////////////
// Section 5.5
// Reads out the filtered samples to DAC A (100Hex)
//////////////////////////////////////////////////////////////////////////////////
sanalog_outvolt1=sanalog_outvolt1+5.0f;
// Because the DAC is unipolar (0-10V) but the input was (-5V - +5V),
// the input voltage needs to have an 5Volt offset. Since the range of
// both is 10Volt we just need an AC filter at the output e.g AC on
// ocilloscope to filter the DAC out again
sanalog_outbit1=sanalog_outvolt1*400;
// The resolution of the board is 10V/2^12 = 2.44mV/bit
// This means a calibration factor of 409.6 bit/volt.
// The entered value is now in bit !!!
// After calibrating the DAC A of this board a factor of
// 2.5mV/bit was identified. This means 400bits/volt.
```

```
        // The offset was less than 1 bit (0.44bits)
        high1 = sanalog_outbit1/256;
        low1  = sanalog_outbit1-256*high1;
        outportb(base1+4,low1);
        outportb(base1+5,high1);
        outportb(base1+3,0);
        ////////////////////////////////////////////////////////////////////
        // End of section 5.5
        ////////////////////////////////////////////////////////////////////
        }
getch(); // The key from the while loop needs to thrown away otherwise the program stops altogether

////////////////////////////////////////////////////////////////////////////////
// END of section 5 (THE CONVERSION LOOP)
////////////////////////////////////////////////////////////////////////////////
```

Appendix B

Mechanical drawings of the active work-piece holder

B.1 Universal active work-piece holder produced for vertical machining centres

The prototype system for active vibration control is be designed to universal for a variety of vertical milling machines. The 2 axes of the flexure guiding system are moved about 6μm by piezoelectric actuators. Compared to ballscrew servo systems the design offers high resolution since it does not contain any moving parts. The integrated sensors allow measurement of the cutting force, direct axis movement, direct acceleration and relative humidity. The system is protected from cutting fluid and hot chips.

Figure B1 shows the active work-piece holder integrated onto the Beaver machine (3-axis vertical machining centre).

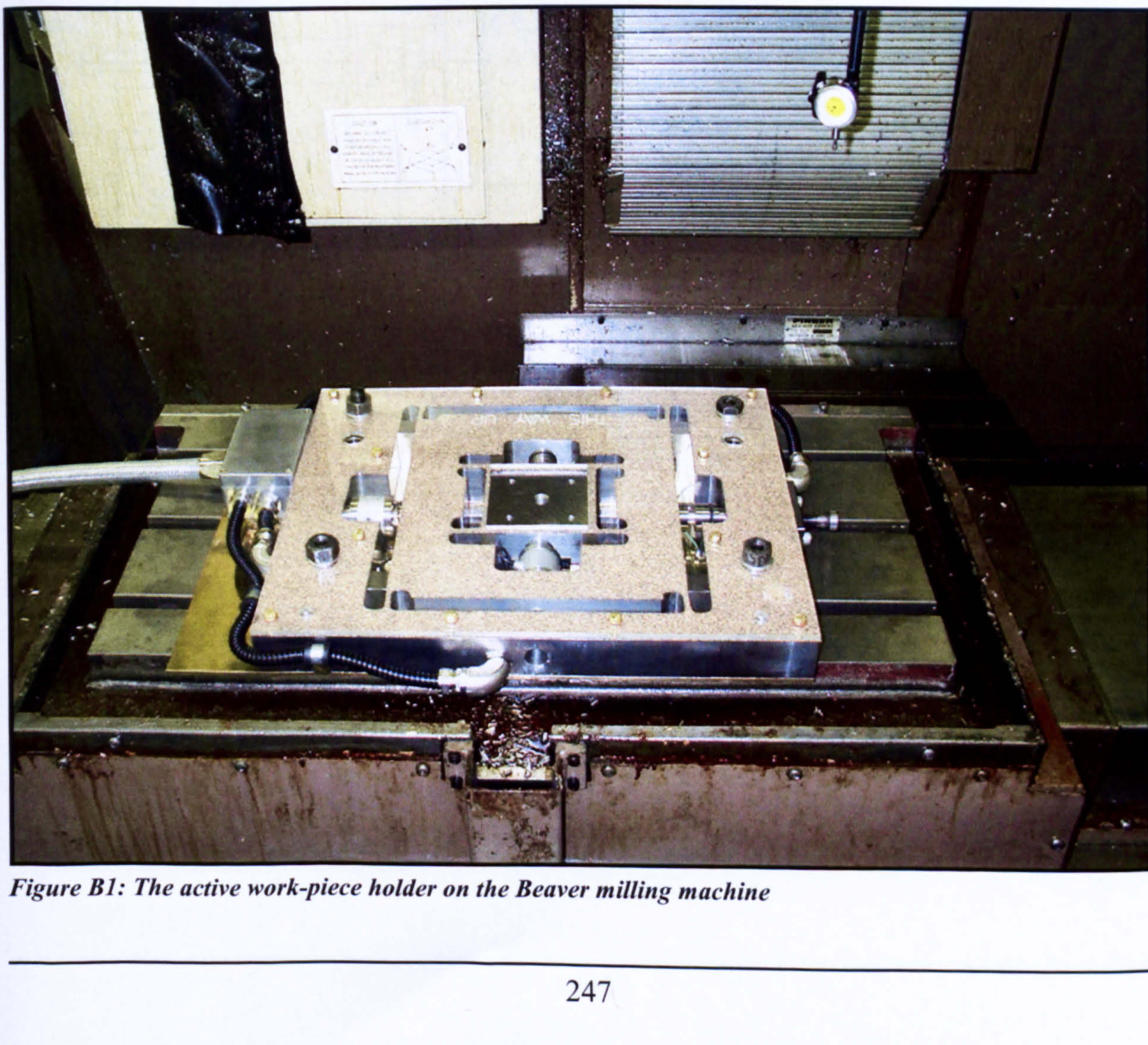

Figure B1: The active work-piece holder on the Beaver milling machine

B.2 Active work-piece holder Lay Out

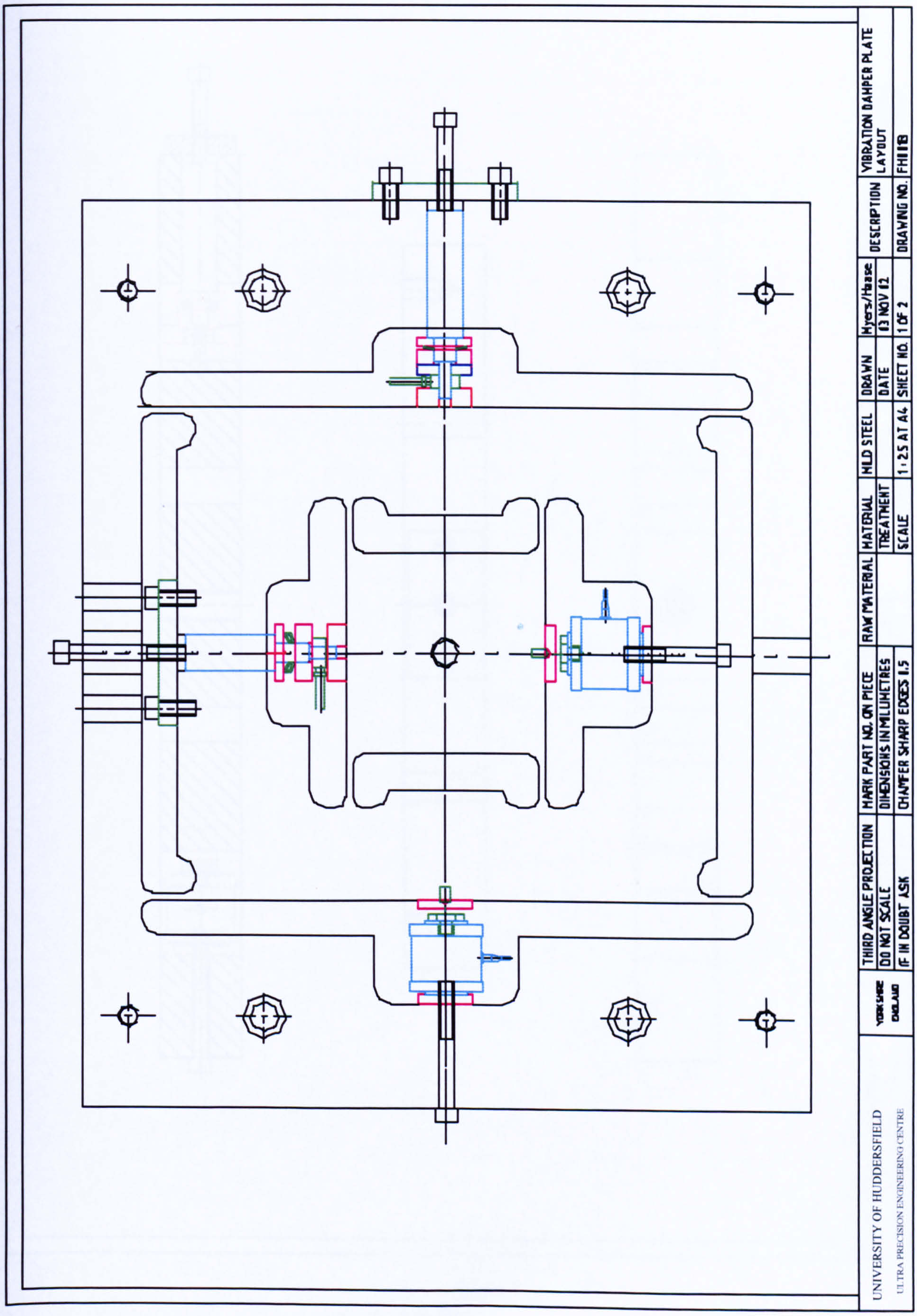

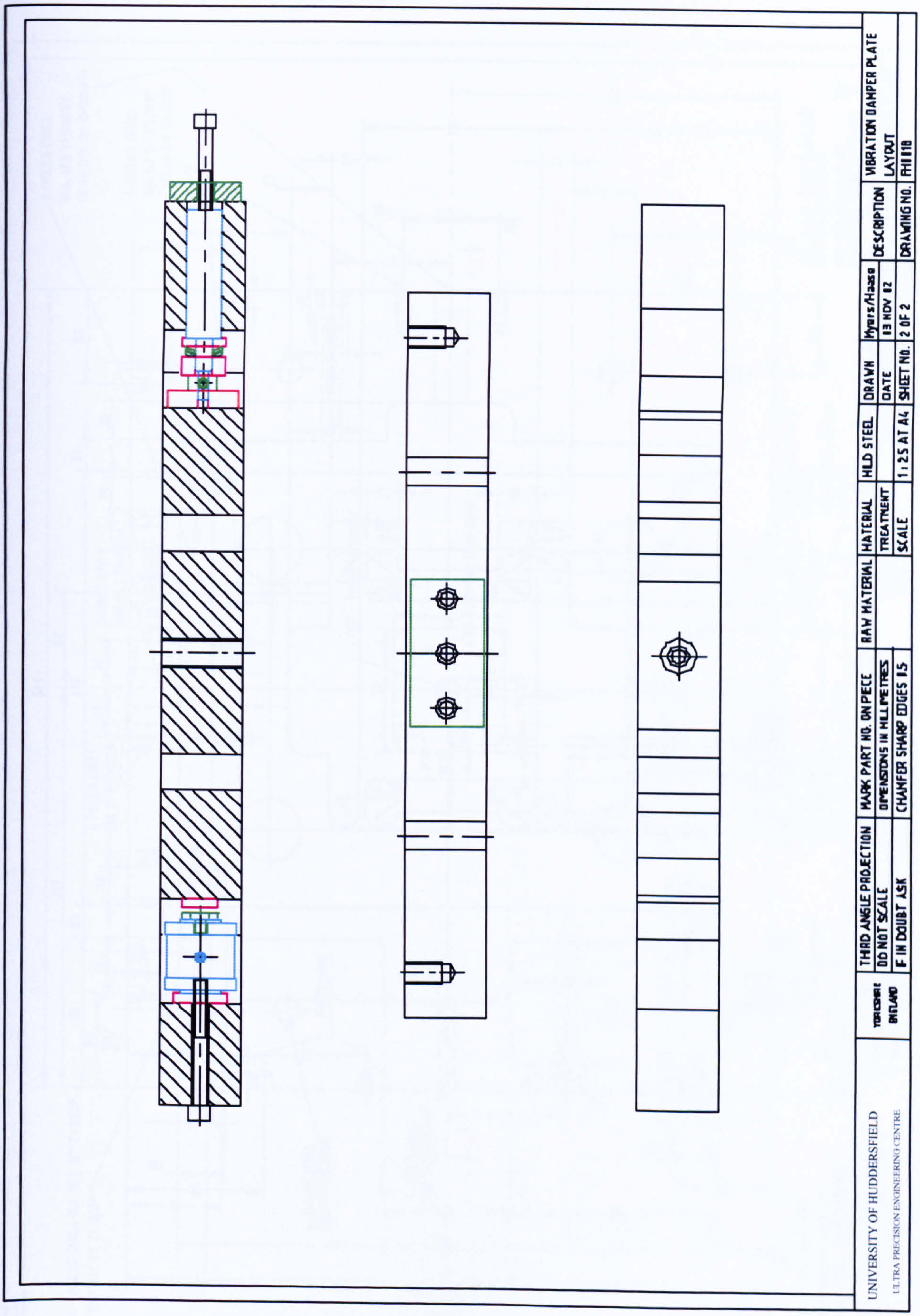

UNIVERSITY OF HUDDERSFIELD
ULTRA PRECISION ENGINEERING CENTRE
YORKSHIRE ENGLAND
THIRD ANGLE PROJECTION
DO NOT SCALE
IF IN DOUBT ASK
MARK PART NO. ON PIECE
DIMENSIONS IN MILLIMETRES
CHAMFER SHARP EDGES 0.5
RAW MATERIAL
MATERIAL
MILD STEEL
TREATMENT
SCALE
1:2.5 AT A4
DRAWN
Myers/Haase
DATE
13 NOV 02
SHEET NO.
2 OF 2
DESCRIPTION
VIBRATION DAMPER PLATE LAYOUT
DRAWING NO.
FH11B

B.3 Active work-piece holder details

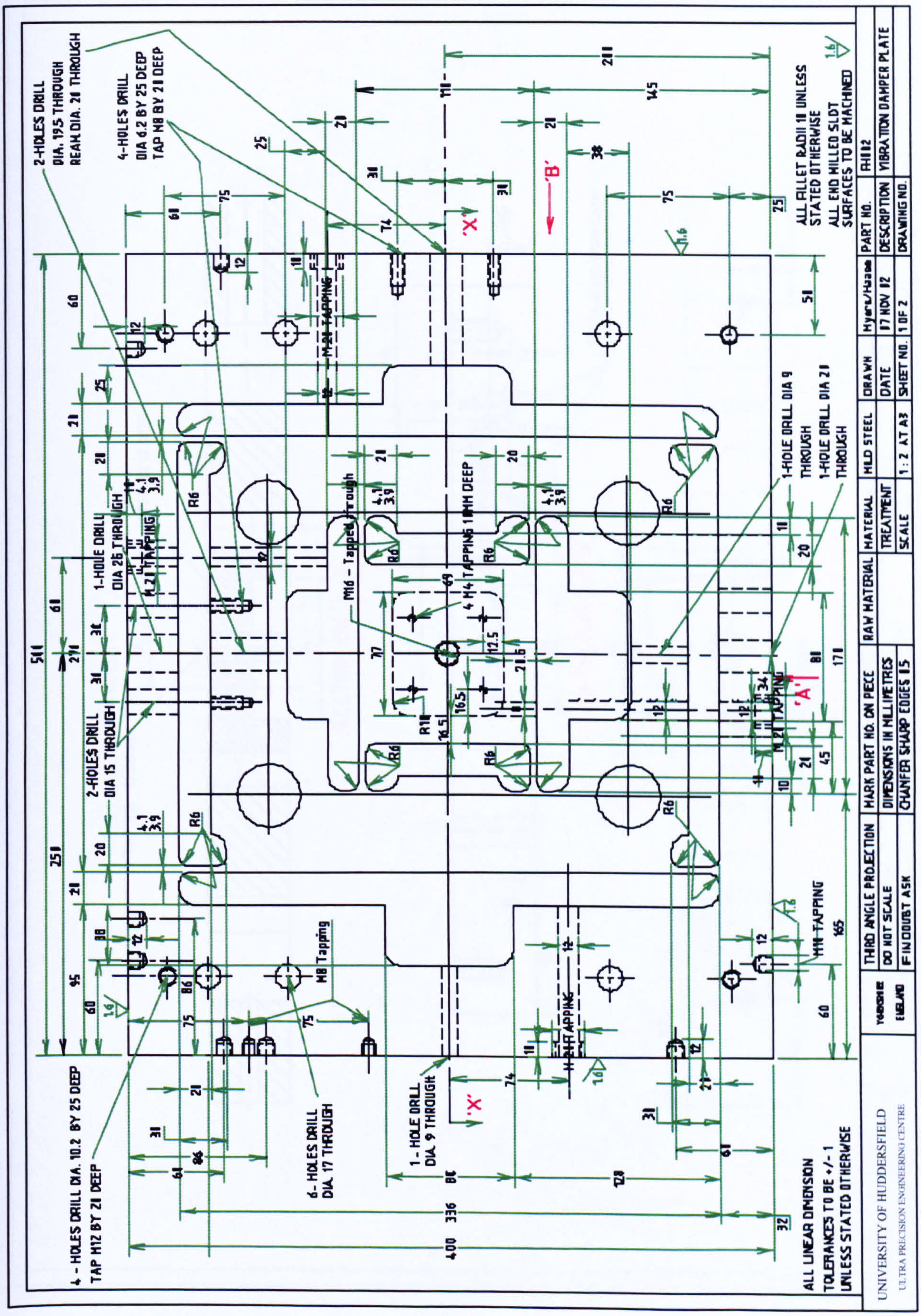

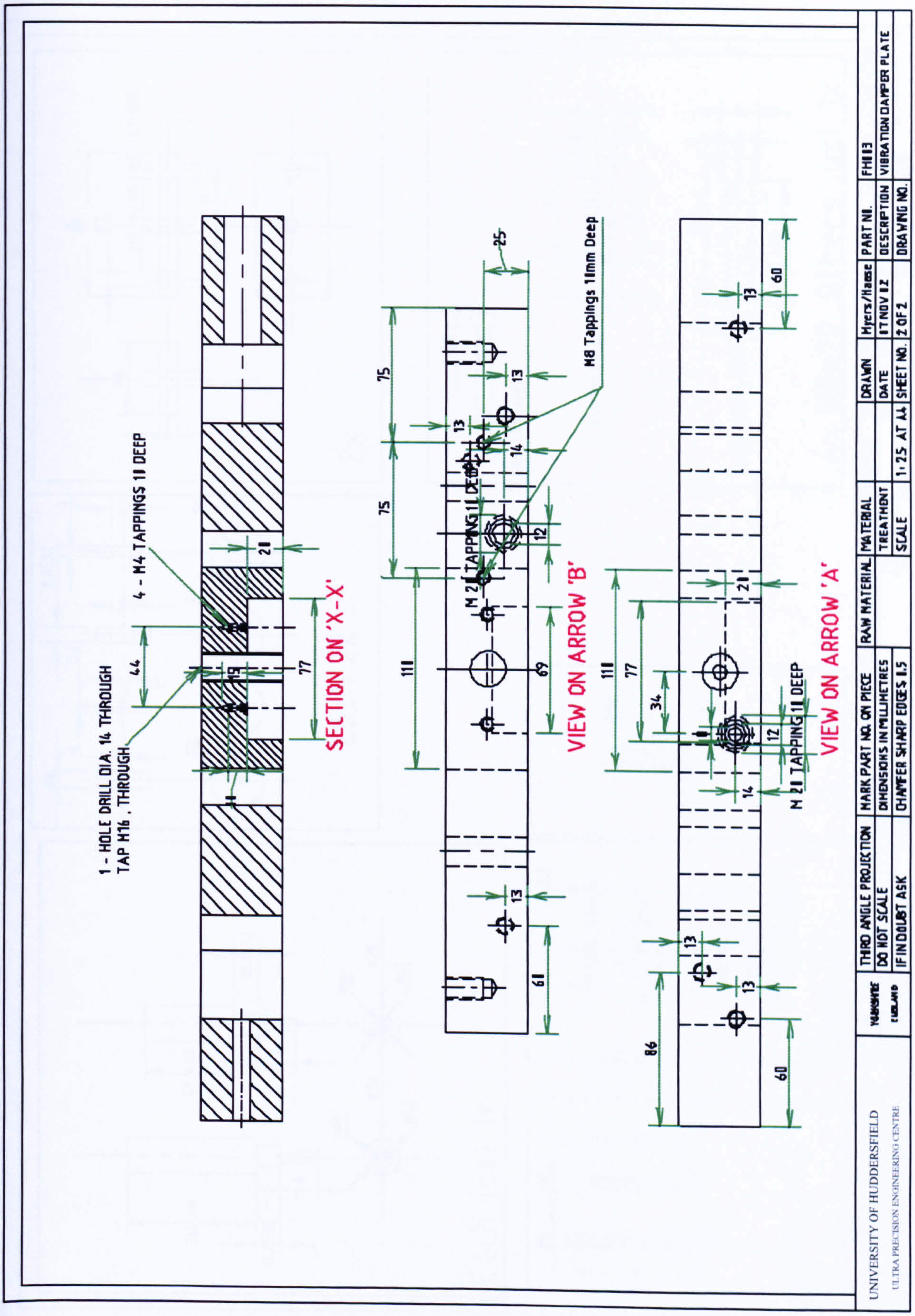
1 - HOLE DRILL DIA. 14 THROUGH
TAP M16 , THROUGH
4 - M4 TAPPINGS 11 DEEP
SECTION ON 'X-X'
M8 Tappings 11mm Deep
VIEW ON ARROW 'B'
VIEW ON ARROW 'A'
UNIVERSITY OF HUDDERSFIELD
ULTRA PRECISION ENGINEERING CENTRE
THIRD ANGLE PROJECTION
DO NOT SCALE
IF IN DOUBT ASK
MARK PART NO. ON PIECE
DIMENSIONS IN MILLIMETRES
RAW MATERIAL
MATERIAL
TREATMENT
SCALE
1:2.5 AT A4
DRAWN
Myers/Haese
DATE
SHEET NO.
2 OF 2
PART NO.
FH113
DESCRIPTION
VIBRATION DAMPER PLATE
DRAWING NO.

B.4 Active work-piece holder small parts

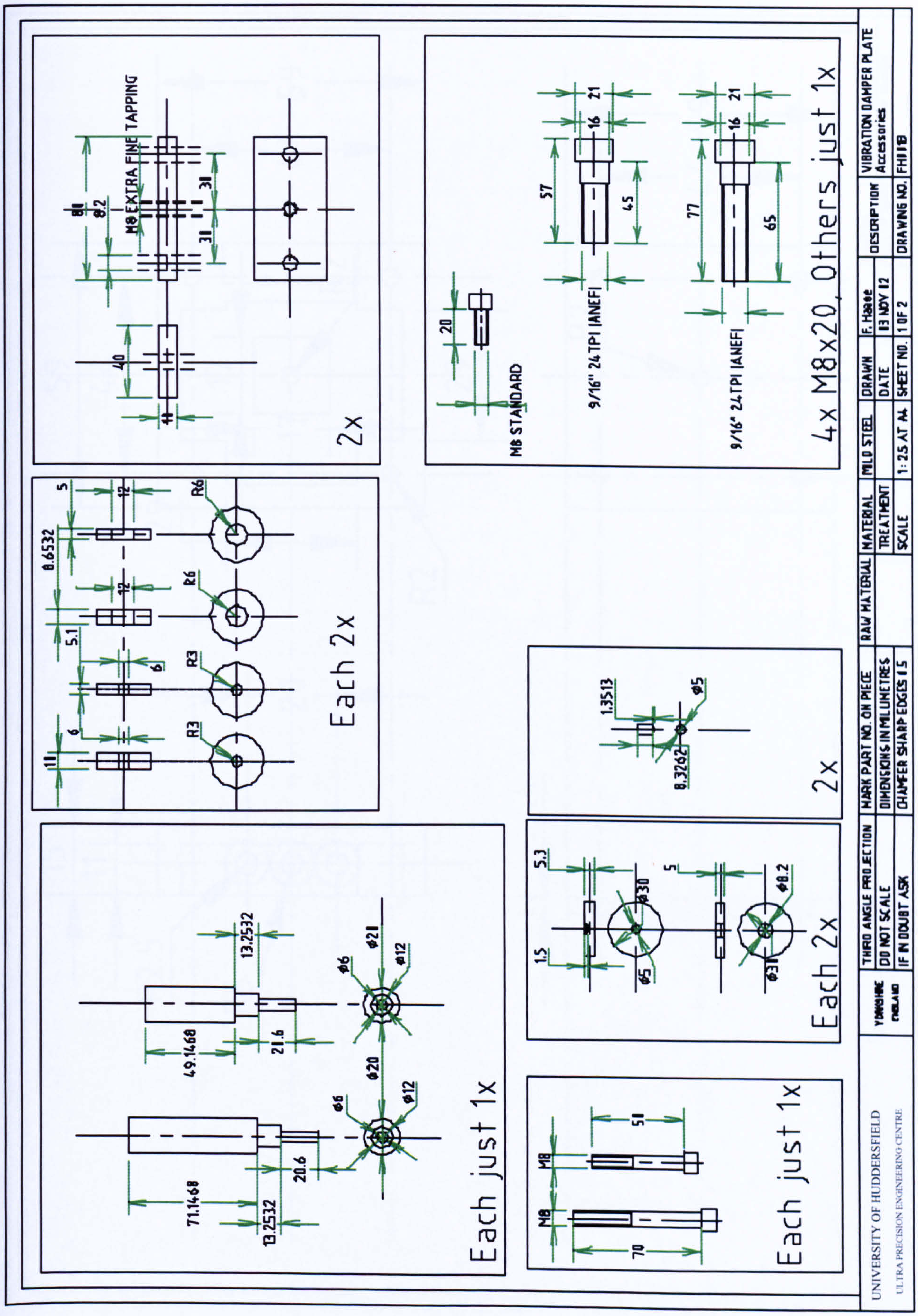

B.5 Active work-piece holder 2 axis acceleration aluminium housing

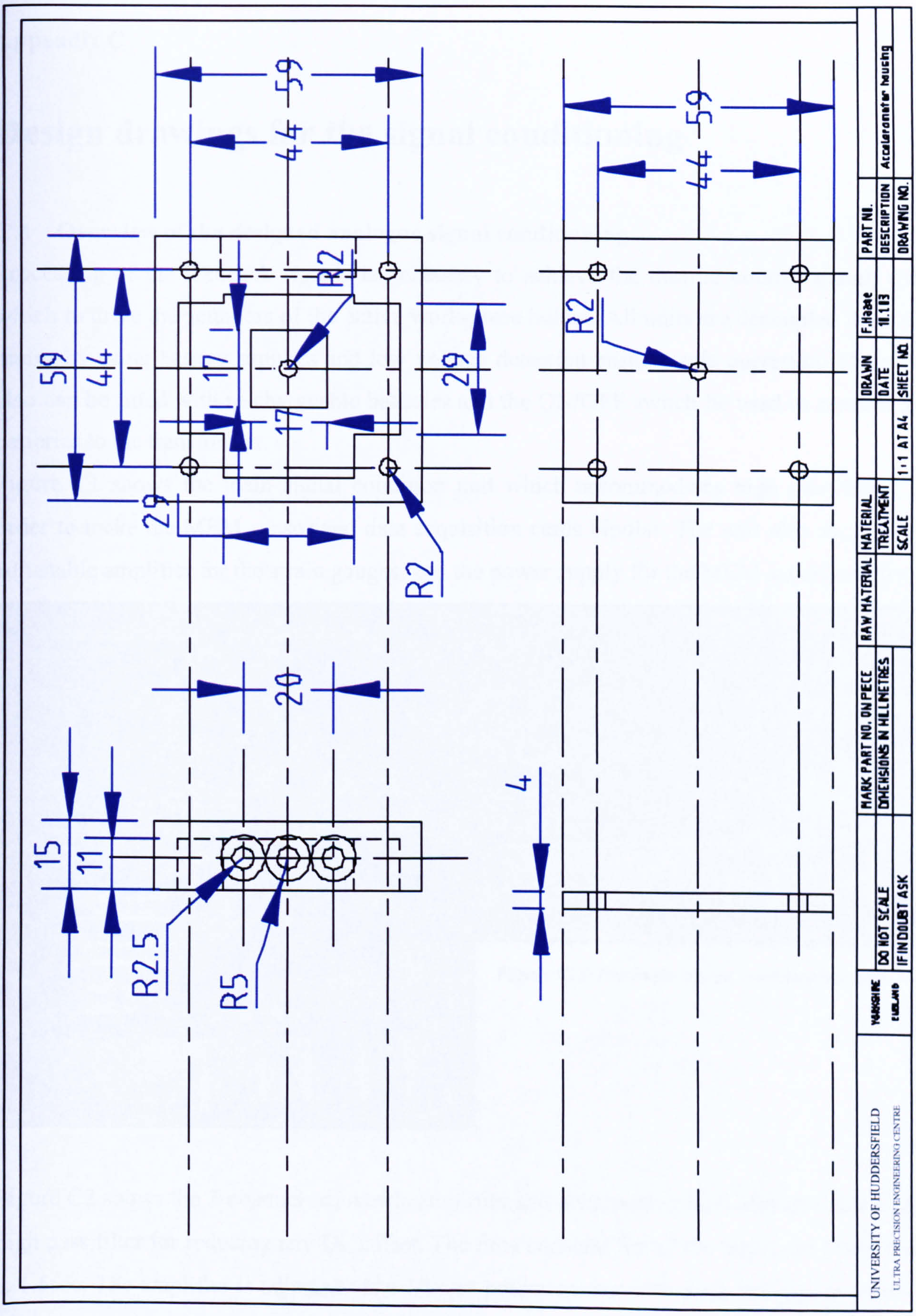

Appendix C

Design drawings for the signal conditioning

C.1 Overview of the designed analogue signal conditioning

Processing of the feedback signals is necessary to achieve the desired control signal, with which to drive the actuators of the active work-piece holder. All units are decoupled from the mains by using battery supplies and low voltage detection ensures safe operation. The units also can be fitted with re-chargeable batteries and the ON/OFF switch be used to connect the batteries to the transformer.

Figure C1 shows the main signal condition unit which accommodates high pass filters in order to make the MEM sensor and data acquisition cards bipolar. The unit also includes an adjustable amplifier for the strain gauges, and the power supply for the MEM accelerometers.

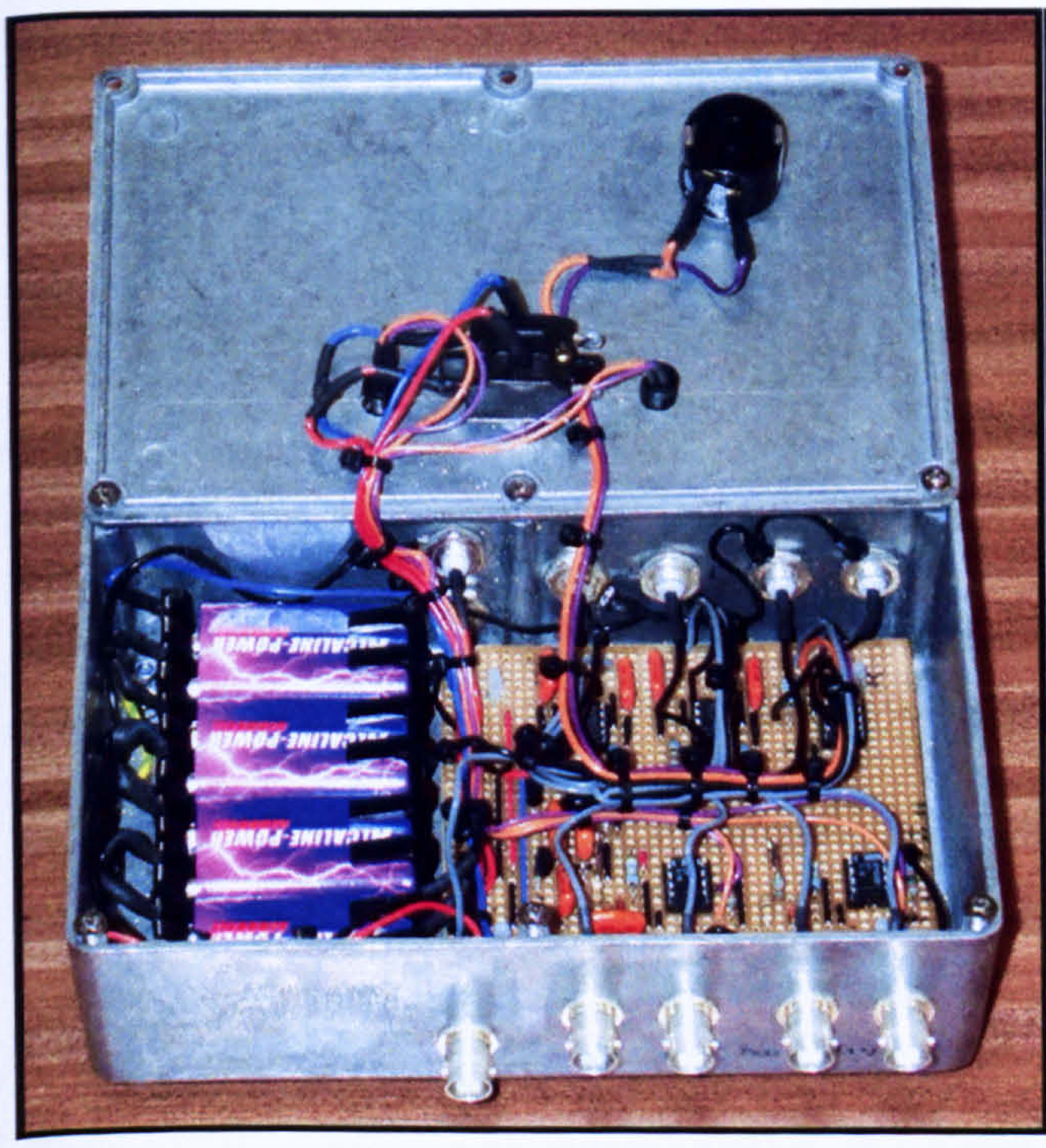

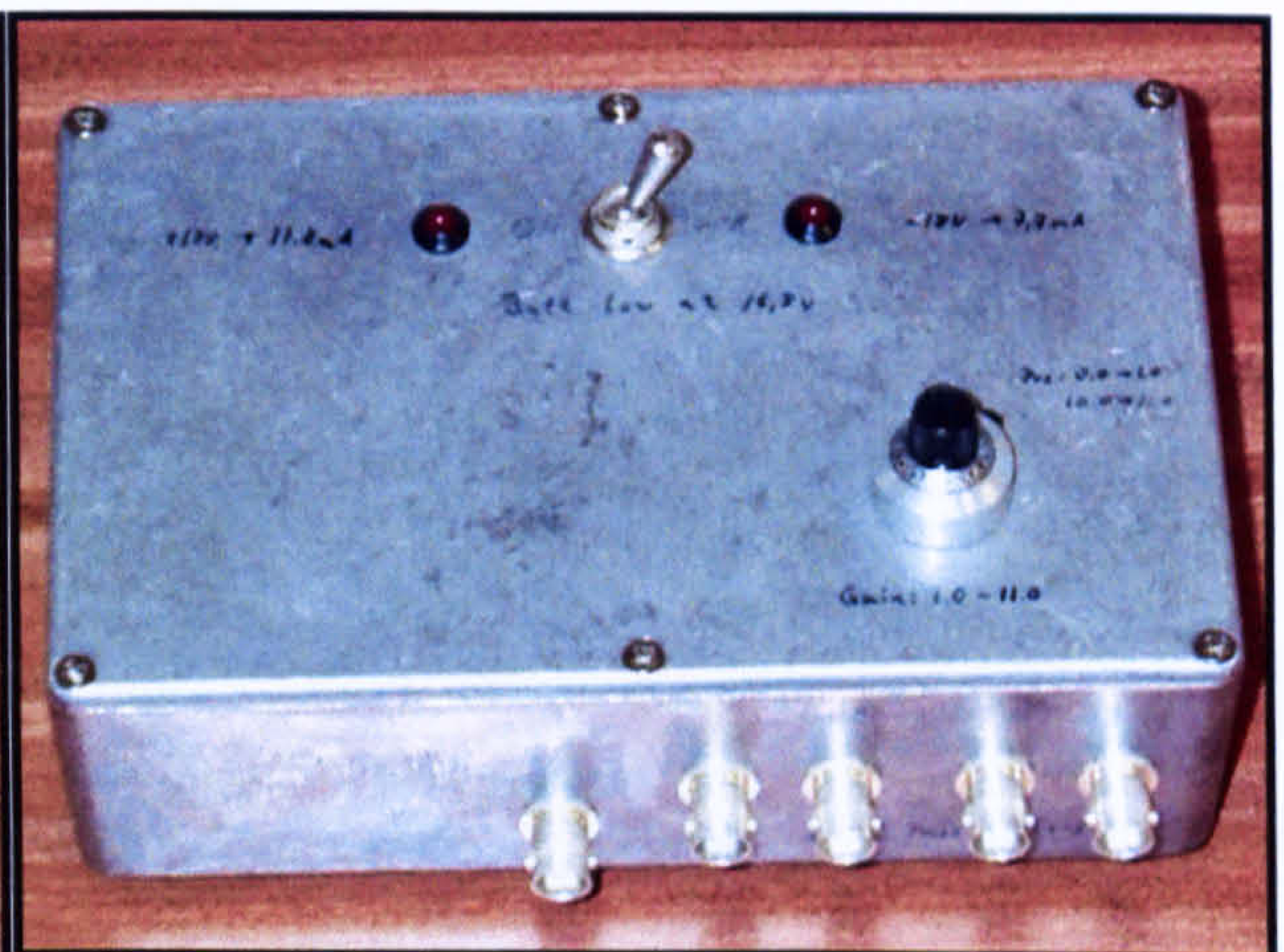

Figure C.1:The main signal conditioning unit

Figure C2 shows the 2-channel adjustable amplifier and attenuator, which also includes a pre-high pass filter for reducing any DC offset. The time constant for all the high pass filters used is 1.5sec. The amplifier is adjusted via a 10-turn potentiometer with scale settings, to insure a precise and defined analog gain for the control signal. This unit is the main analogue control unit, since it is not only a proportional gain controller, but also has the option to switch between open loop and positive or negative feedback closed loop systems.

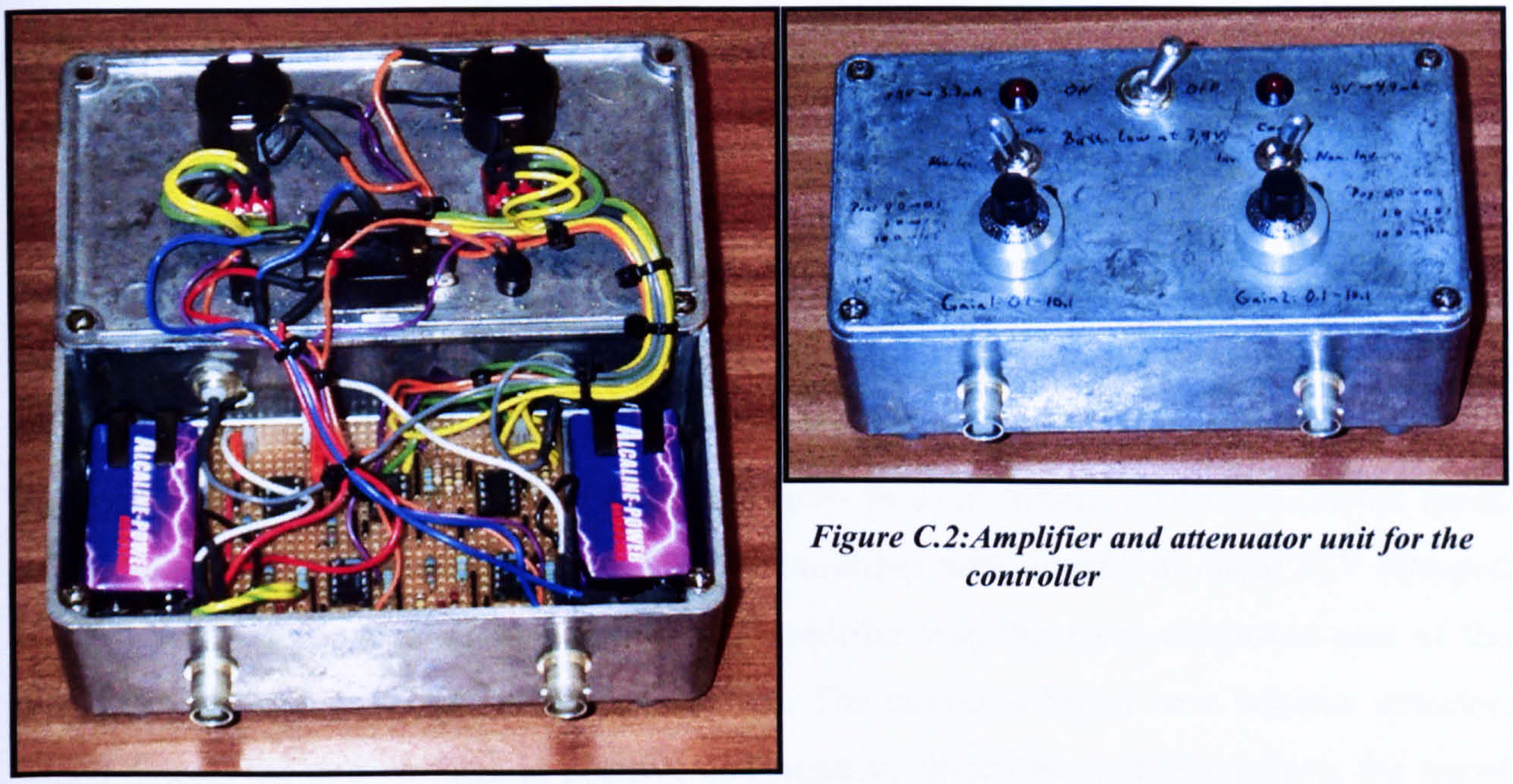

Figure C.2:Amplifier and attenuator unit for the controller

Figure C3 shows the precision 3rd order all pass filter unit. It allows the phase of the control signal to be changed without affecting its gain.

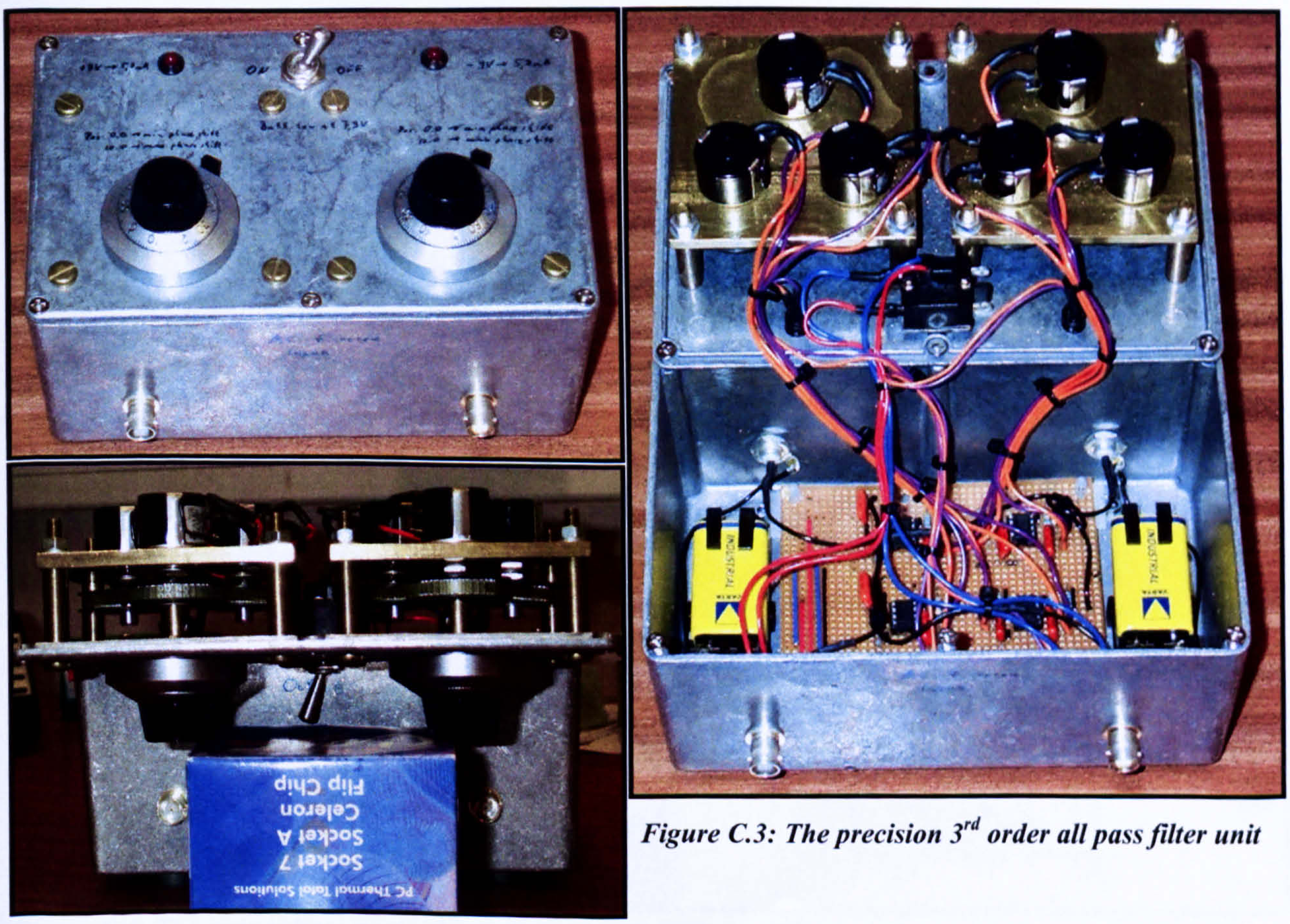

Figure C.3: The precision 3rd order all pass filter unit

This unit can be seen as a manual controller since the error or feedback signal can be adjusted to produce a control signal, which is 180° out of phase with the disturbance signal so that it cancels it. An additional bandpass filter is necessary for the case when the error signal is not of a harmonic nature. The filter allows for sufficient phase adjustment up to a bandwidth of 1kHz. The controlled phase can be precise adjusted by three 10-turn potentiometers coupled using pulleys and a timing belt.

Figure C4 shows the 2-channel over-voltage protection unit for the HVPZT amplifier. Since feedback systems are always in danger of becoming unstable the unit presents the limit switch once the control signal exceeds a defined voltage level. Normally the PZT translators are used for positioning and therefore do not have any built- in over-voltage protection for the input. According to PI the input stage of the HVPZT amplifier will saturate at about 12V (Output: 1200V) and fail above that limit. Since this amplifier was the most expensive part of the whole project, this protection was implemented. The circuit is based on a window detector, which detects the over-voltage in positive and negative directions and disconnects the signal from the HVPZT amplifier once a pre-defined level is reached. It was decided to have a selection between the following detection levels (sizes of the detection windows):

- +/- 4V
- +/- 5V
- +/- 5.5V
- +/- 6V

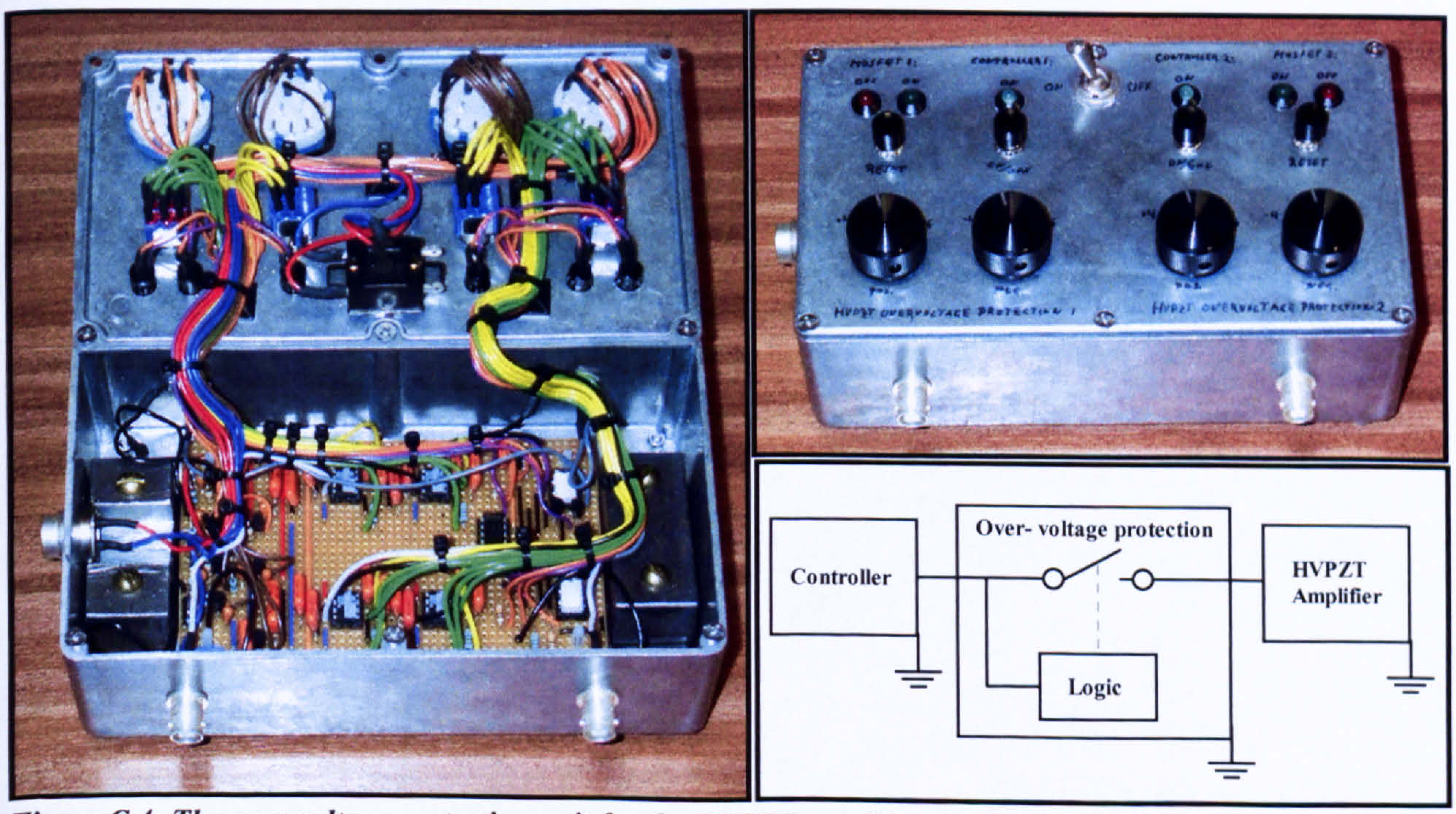

Figure C.4: The over-voltage protection unit for the HVPZT amplifier

The switch itself is a PhotoMOSFET relay ensuring a fast response time and decoupling of the control signal from the mains which supplies the logic. Once an over voltage is detected the relay is locked until the RESET button is pressed. A second button also allows the relay to be activated manually and the control loop to be opened or closed (controller ON/OFF switched).

All the circuits were soldered onto vero board, since this allowed additional alterations of the circuit design in the prototype stage. However all the following electrical drawings were done using an electronic-CAD package to ensure a fast design of the PCB layouts in future. CadSoft computer GmbH supplied the CAD software.

C.2 Electrical drawing for the main signal conditioning unit

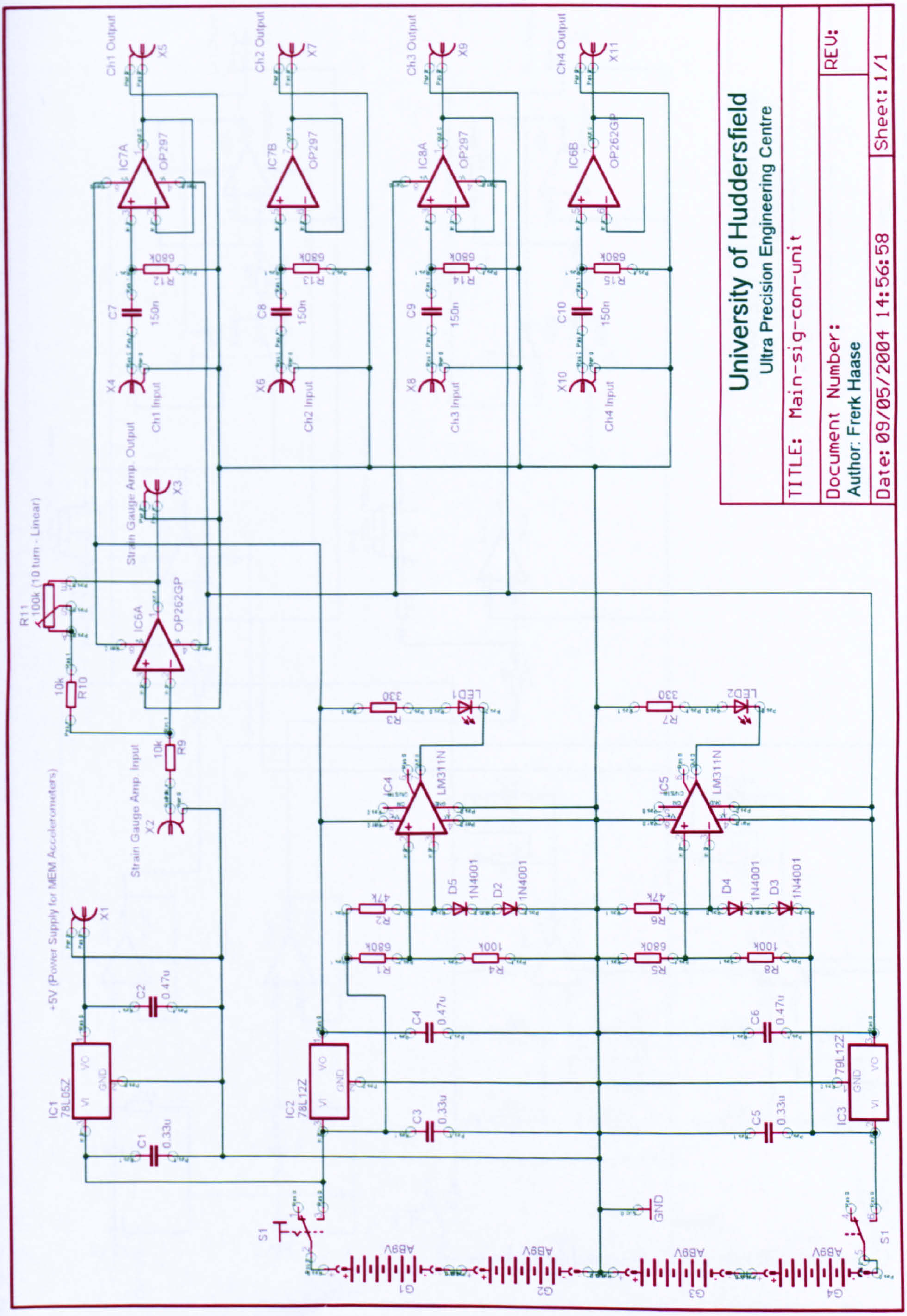

C.3 Electrical drawing for the Amplifier and attenuator unit for the controller

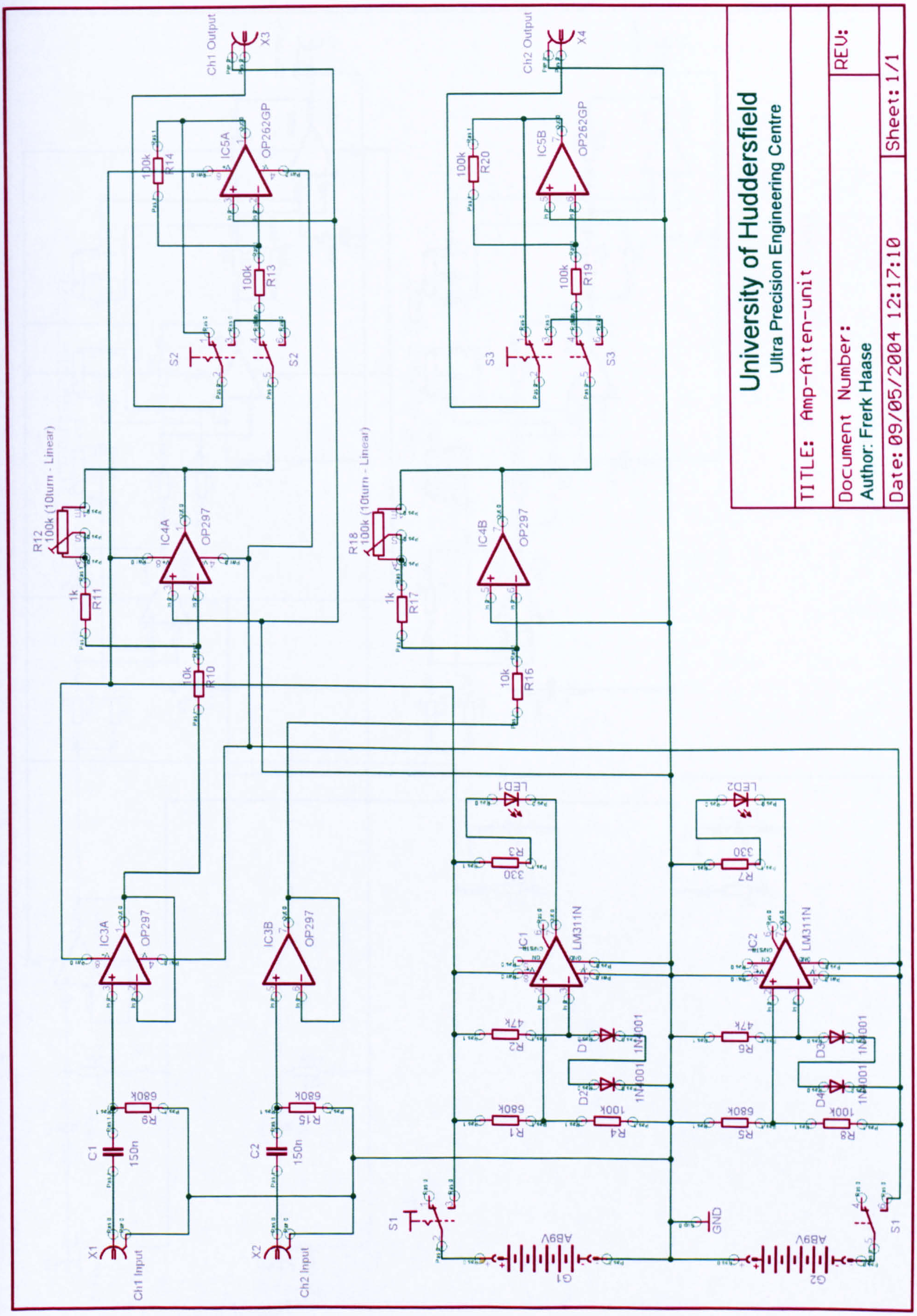

C.4 Electrical drawing for the precision 3rd order all-pass filter unit

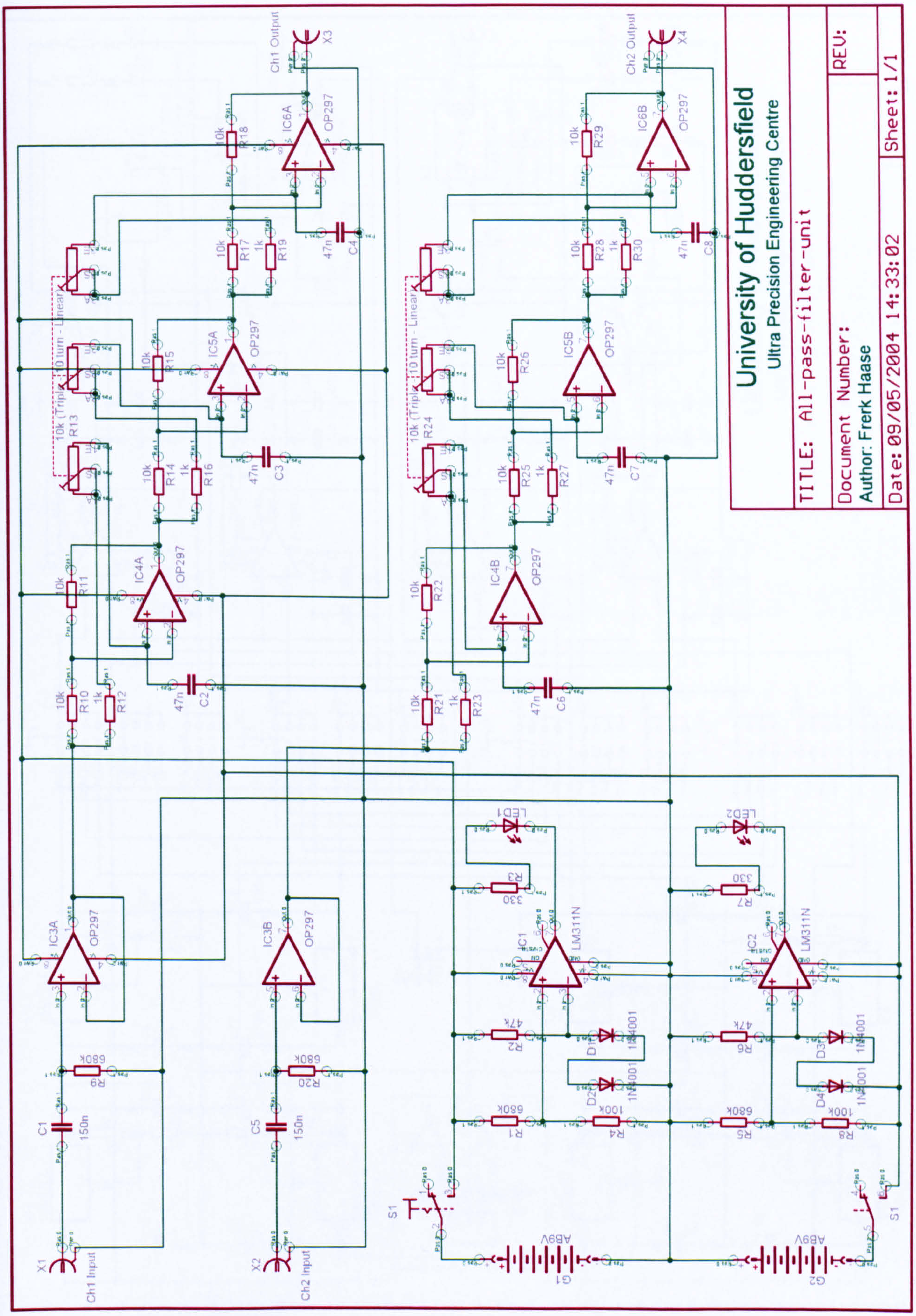

C.5 Electrical drawing for the over-voltage protection unit for the HVPZT amplifier

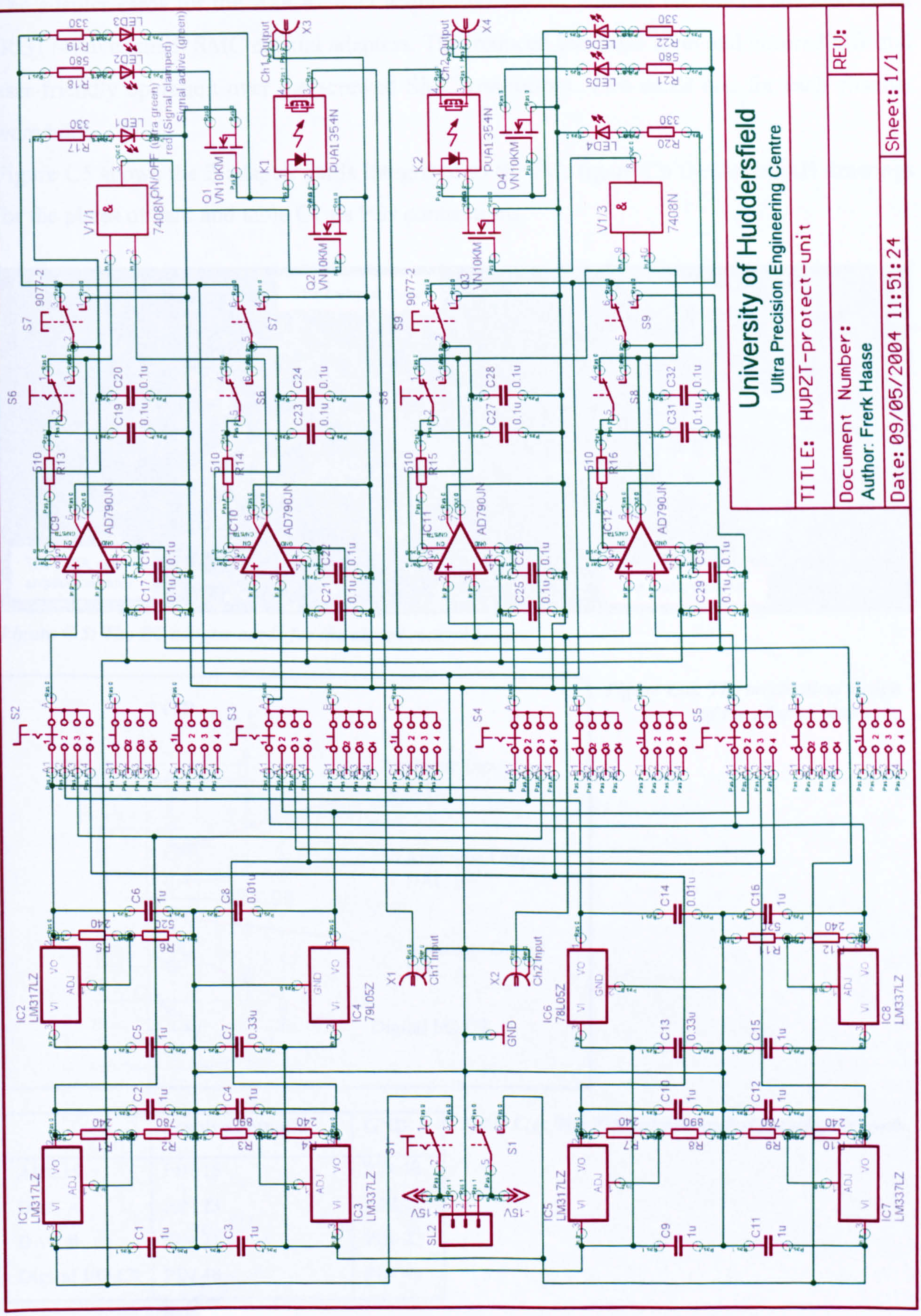

C.6 Adapter cards for the data acquisition system

The adapter cards for the ADC42 data acquisition system allowed the use of shielded cable (RG174) over small SMC coaxial adapters. This reduced the noise level and ensured safe and user-friendly operation over the screwed SMC connectors. Two cards one for each channel were built.

Figure C5 shows the 2 adapter cards integrated to the PC, figure C6 the AutoCAD drawings for the plates of card and table C1 its PIN connections.

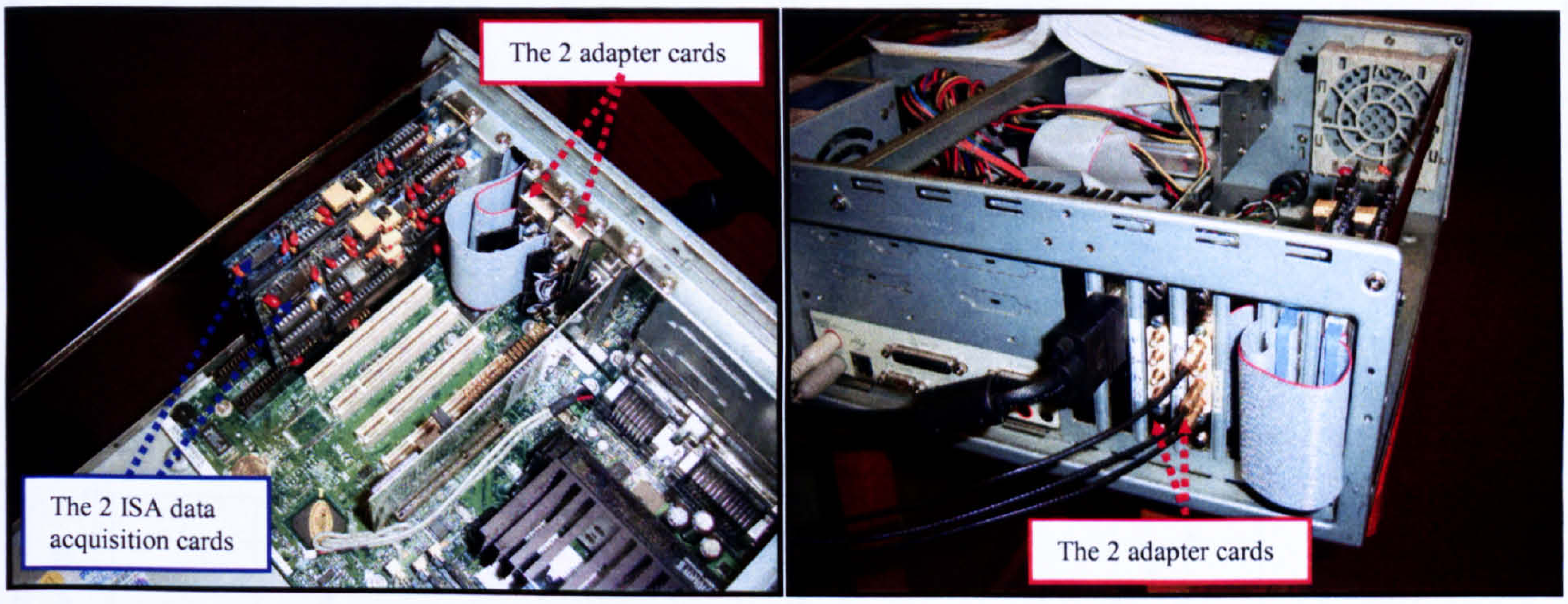

Figure C.5: The PC adapter cards for the digital control system

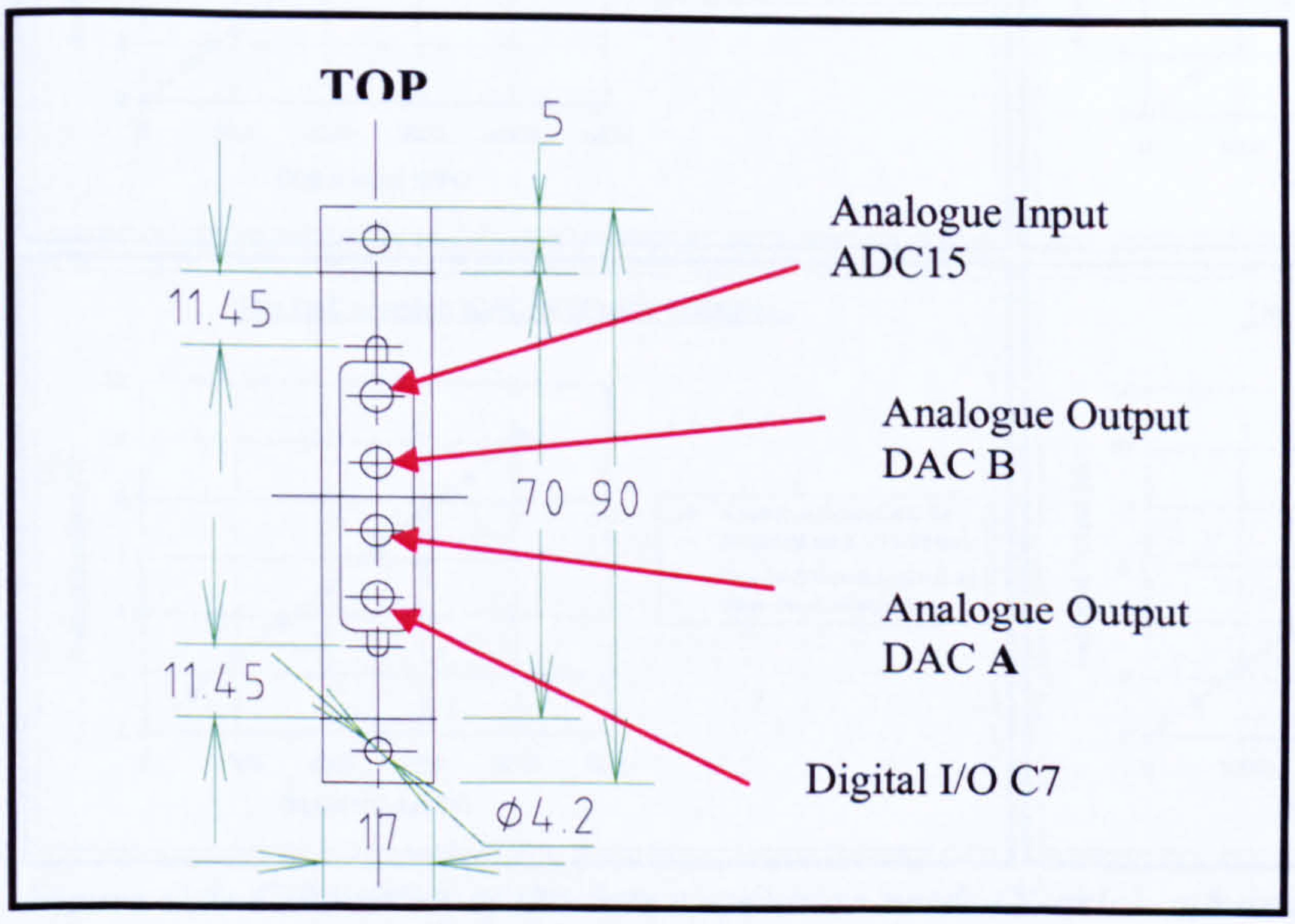

Figure C.6: The mechanical design of the adapter plates

	Positive Potential	GND
ADC15	PIN 16	PIN 18
DAC A	PIN 23	PIN 24
DAC B	PIN 21	PIN 22
Digital I/O C7	PIN 48	PIN 49

Table C.1: The PIN connections of the adapter cards

C.7 Calibrating the DAC and ADC of the data acquisition system

The digital controller cards were calibrated using a DC power supply and precision multimeter. A special calibration routine for the data acquisition card was written, allowing a comfortable identification of the ADC and DAC gain.

Figures C7 (a-c) show the calibration charts for the X-axis data acquisition card (Address 100Hex) and figures C7 (d-f) the calibration charts for card Y-axis (Address 200Hex).

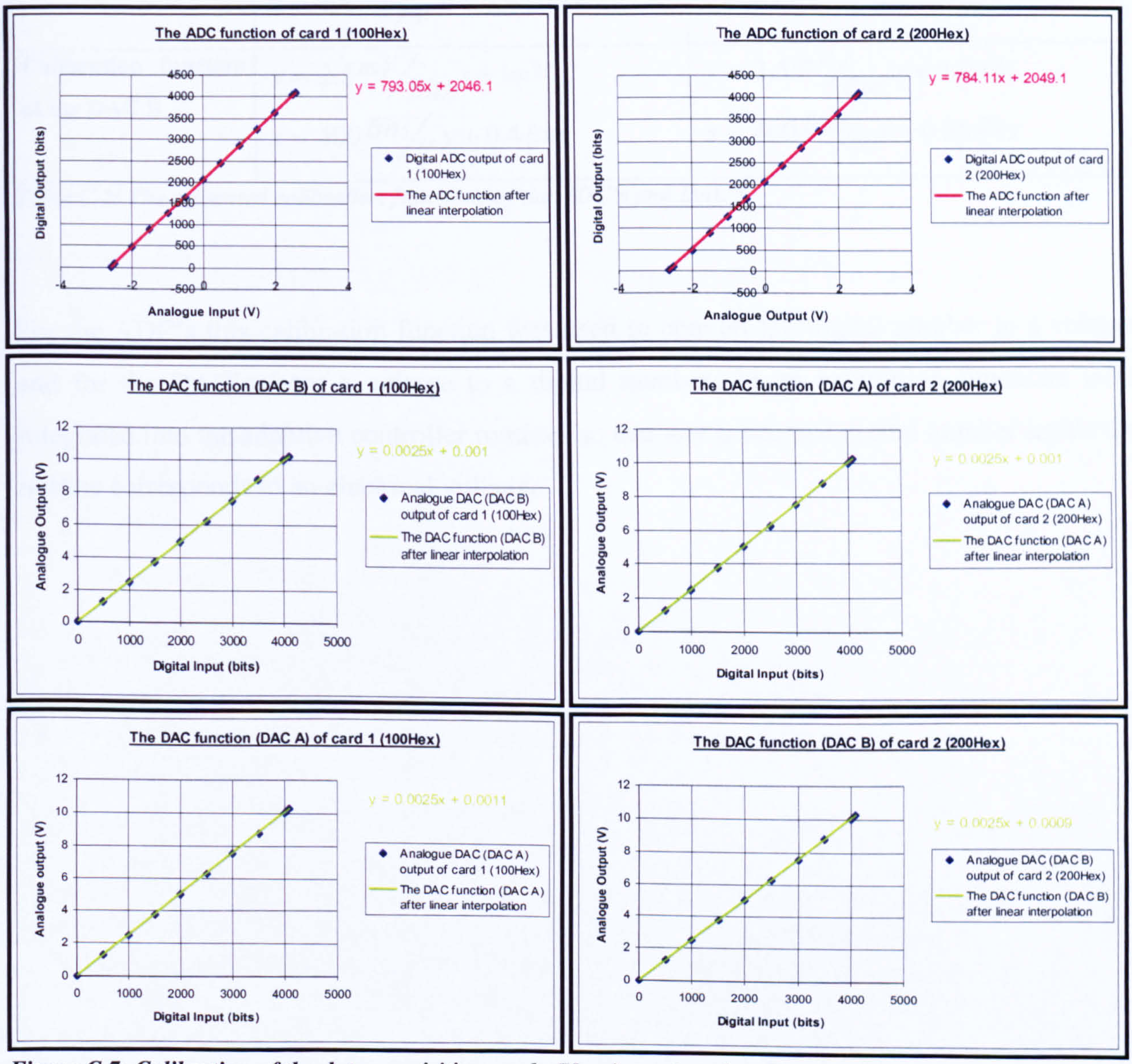

Figure C.7: Calibration of the data acquisition cards (X-axis – a,b and c ; Y-axis card d,e and f)

The calibration procedure also reveals the linearity of both ADC and DAC. A linear interpolation was therefore used to estimate the calibration factor.

Table C2 shows the calibration factor, which can be obtained by inverting the estimated linear functions.

	X-axis digital controller card (Address: 100Hex)	Y-axis digital controller card (Address: 200Hex)
Calibration function of the ADC	$y = 793.05 \,{}^{Bits}\!/_{V}\, x + 2046.1$ $x = 1.261 \,{}^{mV}\!/_{Bits}\, y + 2.58V$	$y = 784.11 \,{}^{Bits}\!/_{V}\, x + 2049.1$ $x = 1.28 \,{}^{mV}\!/_{Bits}\, y + 2.613V$
Calibration function of the DAC A	$y = 2.5 \,{}^{mV}\!/_{Bits}\, x + 1.1mV$ $x = 400 \,{}^{Bits}\!/_{V}\, y + 0.44Bits$	$y = 2.5 \,{}^{mV}\!/_{Bits}\, x + 1mV$ $x = 400 \,{}^{Bits}\!/_{V}\, y + 0.4Bits$
Calibration function of the DAC B	$y = 2.5 \,{}^{mV}\!/_{Bits}\, x + 1mV$ $x = 400 \,{}^{Bits}\!/_{V}\, y + 0.4Bits$	$y = 2.5 \,{}^{mV}\!/_{Bits}\, x + 0.9mV$ $x = 400 \,{}^{Bits}\!/_{V}\, y + 0.36Bits$

Table C.2: The estimated calibration functions of the ADC's and DAC's

For the ADC's this calibration function was used to convert the digital number to a voltage and for the DAC's from a voltage to a digital number. These calibration functions were integrated into the adaptive controller routines so that any processed digital number inside the routine corresponds to an electrical voltage.